Supplementary Table 1

antibody	code	host	manufacturer
CENPV	HPA042616	R	Sigma
AURKA	3092	R	Cell Signaling
PARN	3894	R	Cell Signaling
NSUN2	52901	R	Cell Signaling
GAPDH	9545	R	Sigma
α-TUBULIN	2125	R	Cell Signaling
ac-TUBULIN	T6793	M	Sigma
primer	**5'-3' sequence**		
18S rRNA F	CGCTCCACCAACTAAGAACG		
18S rRNA R	CTCAACACGGGAAACCTCAC		
28S rRNA F	CTAAATACCGGCACGAGACC		
28S rRNA R	TTCACGCCCTCTTGAACTCT		

Supplementary Table 2

GO term	IVM COC – IVO DE Genes (Names) P value ≤ 0.005
0022904	Afg1l, Cox7c, Dld, Sdhaf2, Uqcr11, mt-Co1, mt-Co2, mt-Co3, mt-Nd1, mt-Nd2
0022900	Afg1l, Cox7c, Dld, Sdhaf2, Uqcr11, mt-Co1, mt-Co2, mt-Co3, mt-Nd1, mt-Nd2
0006139	Ada, Atic, Bcas2, Brca1, Brip1, Cwf19l1, Dis3l2, Dld, Eloa, Gm42421, Hnrnpa2b1, Hormad1, Iho1, Klf4, Larp7, Meiob, Msh4, Mterf4, Nme2, Noc3l, Npm1, Nsun2, Nucks1, Parg, Polk, Polr2i, Prpf40a, Rad23a, Rpl10a, Rpl35, Rps17, Rrm1, Rtraf, Sf3b1, Smc5, Smg8, Snrpb2, Snrpd2, Snrpg, Tent2, Terf2, Tfam, Trmt13, Tsnax, Ttf2, Wrn, Zfyve26, mt-Atp6, mt-Nd1, mt-Nd2
0006123	Afg1l, Cox7c, mt-Co1, mt-Co3
0090304	Bcas2, Brca1, Brip1, Cwf19l1, Dis3l2, Eloa, Gm42421, Hnrnpa2b1, Hormad1, Iho1, Klf4, Larp7, Meiob, Msh4, Mterf4, Noc3l, Npm1, Nsun2, Nucks1, Polk, Polr2i, Prpf40a, Rad23a, Rpl10a, Rpl35, Rps17, Rrm1, Rtraf, Sf3b1, Smc5, Smg8, Snrpb2, Snrpd2, Snrpg, Tent2, Terf2, Tfam, Trmt13, Tsnax, Ttf2, Wrn, Zfyve26
0140236	Rpl10a, Rpl15, Rpl28, Rpl35, Rpl38, Rpl6
0140242	Rpl10a, Rpl15, Rpl28, Rpl35, Rpl38, Rpl6
0046483	Ada, Atic, Bcas2, Brca1, Brip1, Cwf19l1, Dis3l2, Dld, Eloa, Gm42421, Hnrnpa2b1, Hormad1, Iho1, Klf4, Larp7, Meiob, Msh4, Mterf4, Nme2, Noc3l, Npm1, Nsun2, Nucks1, Parg, Polk, Polr2i, Prpf40a, Rad23a, Rpl10a, Rpl35, Rps17, Rrm1, Rtraf, Sf3b1, Smc5, Smg8, Snrpb2, Snrpd2, Snrpg, Tent2, Terf2, Tfam, Trmt13, Tsnax, Ttf2, Wrn, Zfyve26, mt-Atp6, mt-Nd1, mt-Nd2
0034641	Ada, Adam10, Atic, Bcas2, Brca1, Brip1, Cwf19l1, Dis3l2, Dld, Eloa, Gm42421, Hnrnpa2b1, Hormad1, Iho1, Klf4, Larp7, Meiob, Mrpl15, Msh4, Mterf4, Nme2, Noc3l, Npm1, Nsun2, Nucks1, Parg, Polk, Polr2i, Prpf40a, Rad23a, Rpl10a, Rpl15, Rpl28, Rpl35, Rpl38, Rpl6, Rps17, Rrm1, Rtraf, Sf3b1, Smc5, Smg8, Snrpb2, Snrpd2, Snrpg, Tent2, Terf2, Tfam, Trmt13, Tsnax, Ttf2, Wrn, Zfyve26, mt-Atp6, mt-Nd1, mt-Nd2
0006725	Ada, Atic, Bcas2, Brca1, Brip1, Cwf19l1, Dis3l2, Dld, Eloa, Gm42421, Hnrnpa2b1, Hormad1, Iho1, Klf4, Larp7, Meiob, Msh4, Mterf4, Nme2, Noc3l, Npm1, Nsun2,

	Nucks1, Parg, Polk, Polr2i, Prpf40a, Rad23a, Rpl10a, Rpl35, Rps17, Rrm1, Rtraf, Sf3b1, Smc5, Smg8, Snrpb2, Snrpd2, Snrpg, Tent2, Terf2, Tfam, Trmt13, Tsnax, Ttf2, Wrn, Zfyve26, mt-Atp6, mt-Nd1, mt-Nd2
0006281	Brca1, Brip1, Gm42421, Meiob, Npm1, Nucks1, Polk, Polr2i, Rad23a, Rrm1, Smc5, Ttf2, Wrn, Zfyve26
0022402	Abcb1b, Bnip2, Brca1, Brip1, C2cd3, Ccng2, Ckap2, Dis3l2, Esrrb, Hormad1, Iho1, Ing2, Meiob, Msh4, Npm1, Nsfl1c, Nsun2, Smc5, Spag5, Stag1, Tbce, Ube2l3, Zwilch
0007129	Brip1, Hormad1, Iho1, Meiob, Msh4
0060629	Hormad1, Iho1
1901360	Ada, Atic, Bcas2, Brca1, Brip1, Cwf19l1, Dis3l2, Dld, Eloa, Gm42421, Hnrnpa2b1, Hormad1, Hsd17b7, Iho1, Klf4, Larp7, Meiob, Msh4, Mterf4, Nme2, Noc3l, Npm1, Nsun2, Nucks1, Parg, Polk, Polr2i, Prpf40a, Rad23a, Rpl10a, Rpl35, Rps17, Rrm1, Rtraf, Sf3b1, Smc5, Smg8, Snrpb2, Snrpd2, Snrpg, Tent2, Terf2, Tfam, Trmt13, Tsnax, Ttf2, Wrn, Zfyve26, mt-Atp6, mt-Nd1, mt-Nd2
0006974	Brca1, Brip1, Gm42421, Grb2, Meiob, Npm1, Nucks1, Parg, Polk, Polr2i, Rad23a, Rrm1, Sirt4, Slf1, Smc5, Terf2, Ttf2, Wrn, Zfyve26
0034622	Acad9, Cadps2, Cenpv, Gemin5, Gemin8, H2bc14, H4c14, Luc7l2, Mterf4, Npm1, Rpl38, Rpl6, Sdhaf2, Sf3b1, Snrpd2, Snrpg, Tbce, Tfam, mt-Co3, mt-Nd1, mt-Nd2
0006259	Brca1, Brip1, Gm42421, Hnrnpa2b1, Meiob, Msh4, Noc3l, Npm1, Nucks1, Polk, Polr2i, Rad23a, Rrm1, Smc5, Terf2, Ttf2, Wrn, Zfyve26
0006807	Ada, Adam10, Atic, Bcas2, Brca1, Brip1, Cwf19l1, Dis3l2, Dld, Eloa, Elovl5, Gm42421, Hnrnpa2b1, Hormad1, Iho1, Klf4, Larp7, Meiob, Mrpl15, Msh4, Mterf4, Nme2, Noc3l, Npm1, Nsun2, Nucks1, Parg, Polk, Polr2i, Prpf40a, Rad23a, Rpl10a, Rpl15, Rpl28, Rpl35, Rpl38, Rpl6, Rps17, Rrm1, Rtraf, Sf3b1, Sirt4, Smc5, Smg8, Snrpb2, Snrpd2, Snrpg, Tent2, Terf2, Tfam, Trmt13, Tsnax, Ttf2, Wrn, Zfyve26, mt-Atp6, mt-Nd1, mt-Nd2
0051726	Aatf, Brca1, Ccng2, Ccsap, Cenpv, Cited2, Entr1, Hormad1, Iho1, Klf4, Larp7, Npm1, Nsfl1c, Nsun2, Prpf40a, Rad23a, Rrm1, Slf1, Smc5, Spag5, Ttll12, Uba3, Uhmk1, Zfyve26, Zwilch
0065003	Acad9, Adam10, Add2, Atl2, Cadps2, Cenpv, Comp, Gemin5, Gemin8, H2bc14, H4c14, Luc7l2, Mterf4, Npm1, Rpl38, Rpl6, Rrm1, Sdhaf2, Sf3b1, Snrpd2, Snrpg, Tbce, Tfam, mt-Co3, mt-Nd1, mt-Nd2
0000387	Gemin5, Gemin8, Snrpd2, Snrpg
0002181	Rpl10a, Rpl15, Rpl28, Rpl38, Rpl6, Rps17
0051301	Aatf, Brip1, Esrrb, Fut10, Ing2, Tial1
0051276	Brip1, Cenpv, Hnrnpa2b1, Hormad1, Iho1, Meiob, Msh4, Smc5, Spag5, Stag1, Terf2, Wrn
0006091	Afg1l, Cox7c, Dld, Sdhaf2, Uqcr11, mt-Co1, mt-Co2, mt-Co3, mt-Nd1, mt-Nd2
0008380	Bcas2, Cwf19l1, Hnrnpa2b1, Prpf40a, Rtraf, Sf3b1, Snrpb2, Snrpd2, Snrpg
0006996	Afg1l, Akt3, Atl2, Bnip2, Brca1, Brip1, C2cd3, Ccsap, Cenpv, Cfap58, Cilk1, Cog3, Dync1li2, Gm20695, Grb2, Hnrnpa2b1, Hormad1, Ift172, Iho1, Ing2, Meiob, Mrpl15, Msh4, Mterf4, Npm1, Nsfl1c, Ppp1r9b, Prpf40a, Rab18, Ranbp10, Serbp1, Shank2, Smap1, Smc5, Spag5, Stag1, Syt7, Tbce, Terf2, Tfam, Timd4, Tmed7, Tmem38b, Vta1, Wdr47, Wrn, Zfyve26
0006396	Bcas2, Cwf19l1, Hnrnpa2b1, Larp7, Nsun2, Prpf40a, Rpl10a, Rpl35, Rps17, Rtraf, Sf3b1, Snrpb2, Snrpd2, Snrpg, Tent2, Trmt13, Tsnax
0022618	Gemin5, Gemin8, Luc7l2, Mterf4, Rpl38, Rpl6, Sf3b1, Snrpd2, Snrpg
0001841	Cited2, Ift172, Stk3
1901070	Ada, Atic, Nme2

0017145	Esrrb, Fut10, Ing2, Tial1
0034184	Slf1, Smc5
0044806	Hnrnpa2b1, Wrn
0000377	Bcas2, Cwf19l1, Hnrnpa2b1, Prpf40a, Sf3b1, Snrpb2, Snrpd2, Snrpg
0000398	Bcas2, Cwf19l1, Hnrnpa2b1, Prpf40a, Sf3b1, Snrpb2, Snrpd2, Snrpg
0000375	Bcas2, Cwf19l1, Hnrnpa2b1, Prpf40a, Sf3b1, Snrpb2, Snrpd2, Snrpg
0006310	Brca1, Brip1, Meiob, Msh4, Nucks1, Smc5, Wrn, Zfyve26
0000724	Brca1, Meiob, Nucks1, Smc5, Wrn, Zfyve26
0000725	Brca1, Meiob, Nucks1, Smc5, Wrn, Zfyve26
0006120	Dld, mt-Nd1, mt-Nd2
0034093	Slf1, Smc5
0042138	Hormad1, Iho1
0071826	Gemin5, Gemin8, Luc7l2, Mterf4, Rpl38, Rpl6, Sf3b1, Snrpd2, Snrpg
0010564	Aurka, Brca1, Ccsap, Cenpv, Entr1, Hormad1, Iho1, Klf4, Larp7, Npm1, Nsfl1c, Prpf40a, Rrm1, Slf1, Smc5, Spag5, Zfyve26, Zwilch
0016071	Bcas2, Cwf19l1, Dis3l2, Hnrnpa2b1, Nsun2, Prpf40a, Sf3b1, Smg8, Snrpb2, Snrpd2, Snrpg, Tent2
0070192	Brip1, Hormad1, Iho1, Meiob, Msh4
0006397	Bcas2, Cwf19l1, Hnrnpa2b1, Prpf40a, Sf3b1, Snrpb2, Snrpd2, Snrpg, Tent2
0042451	Ada, Atic, Nme2, mt-Atp6, mt-Nd1, mt-Nd2
0046129	Ada, Atic, Nme2, mt-Atp6, mt-Nd1, mt-Nd2
0033313	Hormad1, Nsun2
0071840	Aatf, Abcb1b, Acad9, Adam10, Add2, Afg1l, Akt3, Arpc2, Atl2, Bnip2, Brca1, Brip1, C2cd3, Cadps2, Ccsap, Cenpv, Cfap58, Cilk1, Cog3, Comp, Dync1li2, Esrrb, Gemin5, Gemin8, Gm20695, Gm49378, Grb2, H2bc14, H4c14, Hnrnpa2b1, Hormad1, Ift172, Iho1, Ing2, Luc7l2, Meiob, Mrpl15, Msh4, Mterf4, Npm1, Nsfl1c, Nucks1, Pecam1, Phf20l1, Ppp1r9b, Prpf40a, Rab18, Ranbp10, Rap1a, Rcor1, Rpl38, Rpl6, Rps17, Rrm1, Rybp, Sdhaf2, Serbp1, Sf3b1, Shank2, Slc9a3r2, Smap1, Smc5, Snrpd2, Snrpg, Spag5, Stag1, Syt7, Tbce, Terf2, Tfam, Timd4, Tmed7, Tmem38b, Uhmk1, Vta1, Wdr47, Wrn, Zfyve26, mt-Co3, mt-Nd1, mt-Nd2
0009124	Ada, Atic, Nme2, mt-Atp6, mt-Nd1, mt-Nd2
0044260	Adam10, Afg1l, Akt3, Ankrd26, Bcas2, Brap, Brca1, Brip1, Cilk1, Cog3, Cwf19l1, Dis3l2, Eloa, Erp44, Flt1, Gm42421, Gm49325, Grb2, Hnrnpa2b1, Kif16b, Klf4, Larp7, Meiob, Mrpl15, Msh4, Mterf4, Nme2, Noc3l, Npm1, Nsfl1c, Nsun2, Nucks1, Otulin, Phf20l1, Polk, Polr2i, Ppp1cb, Prpf40a, Rad23a, Rcor1, Rpl10a, Rpl15, Rpl28, Rpl35, Rpl38, Rpl6, Rps17, Rrm1, Rtraf, Rybp, Sdhaf2, Sf3b1, Sirt4, Smc5, Smg8, Snrpb2, Snrpd2, Snrpg, Stk3, Tbk1, Tent2, Terf2, Tfam, Trmt13, Tsnax, Ttf2, Uba3, Ube2l3, Uhmk1, Wrn, Zfyve26
0045333	Uqcr11, mt-Co1, mt-Co3, mt-Nd1, mt-Nd2
0003416	Bnc2, Comp
0034182	Slf1, Smc5
0090119	Syt7, Vps53
0043170	Adam10, Afg1l, Akt3, Ankrd26, Bcas2, Brap, Brca1, Brip1, C2cd3, Cilk1, Cog3, Comp, Cwf19l1, Dis3l2, Dld, Eloa, Erp44, Flt1, Gm42421, Gm49325, Grb2, Hnrnpa2b1, Hormad1, Ift172, Iho1, Kif16b, Klf4, Larp7, Meiob, Mrpl15, Msh4, Mterf4, Nme2, Noc3l, Npm1, Nsfl1c, Nsun2, Nucks1, Otulin, Parg, Phf20l1, Polk, Polr2i, Ppp1cb, Prpf40a, Rad23a, Rcor1, Rpl10a, Rpl15, Rpl28, Rpl35, Rpl38, Rpl6, Rps17, Rrm1,

	Rtraf, Rybp, Sdhaf2, Sf3b1, Sirt4, Smc5, Smg8, Snrpb2, Snrpd2, Snrpg, Stk3, Tbk1, Tent2, Terf2, Tfam, Trmt13, Tsnax, Ttf2, Uba3, Ube2l3, Uhmk1, Wrn, Zfyve26
0061028	Abcb1b, Pecam1, Rap1a
0042455	Ada, Atic, Nme2, mt-Atp6, mt-Nd1, mt-Nd2
0009163	Ada, Atic, Nme2, mt-Atp6, mt-Nd1, mt-Nd2
0022607	Acad9, Adam10, Add2, Atl2, Brip1, C2cd3, Cadps2, Cenpv, Cfap58, Cilk1, Comp, Gemin5, Gemin8, Gm20695, H2bc14, H4c14, Hormad1, Ift172, Luc7l2, Mterf4, Npm1, Nsfl1c, Pecam1, Ppp1r9b, Rpl38, Rpl6, Rrm1, Sdhaf2, Sf3b1, Shank2, Snrpd2, Snrpg, Stag1, Tbce, Tfam, mt-Co3, mt-Nd1, mt-Nd2
0034091	Slf1, Smc5
0045876	Slf1, Smc5
0061820	Terf2, Wrn
1901659	Ada, Atic, Nme2, mt-Atp6, mt-Nd1, mt-Nd2
0044085	Aatf, Acad9, Npm1, Rps17, Sdhaf2, mt-Nd1, mt-Nd2

GO term	**IVM DO – IVO DE Genes (Names) P value ≤ 0.005**
0022904	Ndufa10, Sdhaf2, mt-Co1, mt-Co2, mt-Co3, mt-Cytb, mt-Nd1, mt-Nd2
0022900	Ndufa10, Sdhaf2, mt-Co1, mt-Co2, mt-Co3, mt-Cytb, mt-Nd1, mt-Nd2
0033108	Aifm1, Coa5, Ndufa10, Oma1, Sdhaf2, Taco1, mt-Nd1, mt-Nd2
0006818	Ndufa10, Slc36a1, mt-Atp6, mt-Atp8, mt-Co1, mt-Cytb, mt-Nd1, mt-Nd2
0015992	Ndufa10, Slc36a1, mt-Atp6, mt-Atp8, mt-Co1, mt-Cytb, mt-Nd1, mt-Nd2
1902600	Ndufa10, Slc36a1, mt-Atp6, mt-Atp8, mt-Co1, mt-Cytb, mt-Nd1, mt-Nd2
0070271	Aifm1, Coa5, Ndufa10, Sdhaf2, Taco1, mt-Nd1, mt-Nd2
0044085	Aifm1, Coa5, Gtf3a, Ndufa10, Pak1ip1, Sdhaf2, Taco1, mt-Nd1, mt-Nd2
0043623	Aifm1, Cadps2, Ccdc65, Coa5, Diaph3, Drc1, Ndufa10, Oma1, Sdhaf2, Taco1, mt-Co3, mt-Nd1, mt-Nd2
0015980	Agl, Lepr, Ndufa10, mt-Co1, mt-Co3, mt-Cytb, mt-Nd1, mt-Nd2
0034622	Aifm1, Bdp1, Cadps2, Ccdc65, Cenpv, Coa5, Diaph3, Drc1, Dync1h1, Ndufa10, Oma1, Rad51c, Sdhaf2, Sec24d, Setx, Taco1, mt-Co3, mt-Nd1, mt-Nd2
0006091	Agl, Lepr, Ndufa10, Sdhaf2, mt-Co1, mt-Co2, mt-Co3, mt-Cytb, mt-Nd1, mt-Nd2
0045333	Ndufa10, mt-Co1, mt-Co3, mt-Cytb, mt-Nd1, mt-Nd2
0006139	Aff1, Ahcyl2, Arrb2, Ash1l, Casc3, Ccnb1ip1, Cwc15, Ddx10, Ddx21, Dkc1, Fastkd5, Gm21992, Henmt1, Hprt, Ighmbp2, Irf2bp1, Klf4, Mnd1, Morc1, Nbn, Ndufa10, Nsmce2, Pdhb, Polb, Rad51c, Rpa3, Setx, Smarcal1, Snrpb2, Sp1, Sympk, Taf1c, Wdhd1, Yju2, mt-Atp6, mt-Atp8, mt-Nd1, mt-Nd2
0035825	Ccnb1ip1, Mnd1, Nbn, Rad51c
0065003	Aifm1, Bdp1, Cadps2, Ccdc65, Cenpv, Coa5, Diaph3, Dnajb12, Drc1, Dync1h1, Ehd3, Hprt, Ndufa10, Oma1, Rad51c, Sdhaf2, Sec24d, Setx, Taco1, Zfp148, mt-Co3, mt-Nd1, mt-Nd2
0042776	Ndufa10, mt-Atp6, mt-Atp8, mt-Nd1, mt-Nd2
0009060	Ndufa10, mt-Co1, mt-Co3, mt-Nd1, mt-Nd2
0046483	Aff1, Ahcyl2, Alpl, Arrb2, Ash1l, Casc3, Ccnb1ip1, Cwc15, Ddx10, Ddx21, Dkc1, Fastkd5, Gm21992, Henmt1, Hprt, Ighmbp2, Irf2bp1, Klf4, Mnd1, Morc1, Nbn,

	Ndufa10, Nsmce2, Pdhb, Polb, Rad51c, Rpa3, Setx, Smarcal1, Snrpb2, Sp1, Sympk, Taf1c, Wdhd1, Yju2, mt-Atp6, mt-Atp8, mt-Nd1, mt-Nd2
0009127	Hprt, Ndufa10, mt-Atp6, mt-Atp8, mt-Nd1, mt-Nd2
0009168	Hprt, Ndufa10, mt-Atp6, mt-Atp8, mt-Nd1, mt-Nd2
0015985	Ndufa10, mt-Atp6, mt-Atp8, mt-Nd1, mt-Nd2
0015986	Ndufa10, mt-Atp6, mt-Atp8, mt-Nd1, mt-Nd2
0043933	Aifm1, Ash1l, Bdp1, Cadps2, Cbx5, Ccdc65, Cenpv, Coa5, Ddx21, Diaph3, Dnajb12, Dpf2, Drc1, Dync1h1, Ehd3, Hprt, Mbip, Ndufa10, Oma1, Rad51c, Rybp, Sdhaf2, Sec24d, Setx, Taco1, Tada2a, Zfp148, mt-Co3, mt-Nd1, mt-Nd2
0006461	Aifm1, Cadps2, Ccdc65, Coa5, Diaph3, Drc1, Ehd3, Hprt, Ndufa10, Oma1, Sdhaf2, Taco1, mt-Co3, mt-Nd1, mt-Nd2
0009156	Hprt, Ndufa10, mt-Atp6, mt-Atp8, mt-Nd1, mt-Nd2
0006725	Aff1, Ahcyl2, Alpl, Arrb2, Ash1l, Casc3, Ccnb1ip1, Cwc15, Ddx10, Ddx21, Dkc1, Fastkd5, Gm21992, Henmt1, Hprt, Ighmbp2, Irf2bp1, Klf4, Mnd1, Morc1, Nbn, Ndufa10, Nsmce2, Pdhb, Polb, Rad51c, Rpa3, Setx, Smarcal1, Snrpb2, Sp1, Sympk, Taf1c, Wdhd1, Yju2, mt-Atp6, mt-Atp8, mt-Nd1, mt-Nd2
0006754	Ndufa10, mt-Atp6, mt-Atp8, mt-Nd1, mt-Nd2
0015988	mt-Co1, mt-Cytb
0015990	mt-Co1, mt-Cytb
0042451	Hprt, Ndufa10, mt-Atp6, mt-Atp8, mt-Nd1, mt-Nd2
0046129	Hprt, Ndufa10, mt-Atp6, mt-Atp8, mt-Nd1, mt-Nd2
0006120	Ndufa10, mt-Nd1, mt-Nd2
0009124	Hprt, Ndufa10, mt-Atp6, mt-Atp8, mt-Nd1, mt-Nd2
0009206	Ndufa10, mt-Atp6, mt-Atp8, mt-Nd1, mt-Nd2
0009145	Ndufa10, mt-Atp6, mt-Atp8, mt-Nd1, mt-Nd2
1901360	Aff1, Ahcyl2, Alpl, Arrb2, Ash1l, Casc3, Ccnb1ip1, Cwc15, Ddx10, Ddx21, Dkc1, Fastkd5, Gm21992, Henmt1, Hprt, Ighmbp2, Irf2bp1, Klf4, Lepr, Mnd1, Morc1, Nbn, Ndufa10, Nsmce2, Pdhb, Polb, Rad51c, Rpa3, Setx, Smarcal1, Snrpb2, Sp1, Sympk, Taf1c, Wdhd1, Yju2, mt-Atp6, mt-Atp8, mt-Nd1, mt-Nd2
1990542	Aifm1, Ndufa10, mt-Atp6, mt-Atp8, mt-Nd1, mt-Nd2
0009201	Ndufa10, mt-Atp6, mt-Atp8, mt-Nd1, mt-Nd2
0042455	Hprt, Ndufa10, mt-Atp6, mt-Atp8, mt-Nd1, mt-Nd2
0090304	Aff1, Arrb2, Ash1l, Casc3, Ccnb1ip1, Cwc15, Ddx10, Ddx21, Dkc1, Fastkd5, Gm21992, Henmt1, Ighmbp2, Irf2bp1, Klf4, Mnd1, Morc1, Nbn, Nsmce2, Polb, Rad51c, Rpa3, Setx, Smarcal1, Snrpb2, Sp1, Sympk, Taf1c, Wdhd1, Yju2
0009163	Hprt, Ndufa10, mt-Atp6, mt-Atp8, mt-Nd1, mt-Nd2
1901659	Hprt, Ndufa10, mt-Atp6, mt-Atp8, mt-Nd1, mt-Nd2
0006310	Ccnb1ip1, Mnd1, Nbn, Nsmce2, Polb, Rad51c, Rpa3
0055114	Agl, Lepr, Ndufa10, Sdhaf2, mt-Co1, mt-Co2, mt-Co3, mt-Cytb, mt-Nd1, mt-Nd2
0034654	Aff1, Arrb2, Ash1l, Ddx21, Dkc1, Hprt, Irf2bp1, Klf4, Ndufa10, Setx, Sp1, Taf1c, mt-Atp6, mt-Atp8, mt-Nd1, mt-Nd2
0007131	Ccnb1ip1, Mnd1, Rad51c
0043353	Mb, Sp1
0009152	Hprt, Ndufa10, mt-Atp6, mt-Atp8, mt-Nd1, mt-Nd2
0008535	Coa5, Taco1, mt-Co3
0006302	Nbn, Nsmce2, Polb, Rad51c, Rpa3, Setx, Smarcal1
0061743	C1ql1, Taco1

0009142	Ndufa10, mt-Atp6, mt-Atp8, mt-Nd1, mt-Nd2
0051085	Dnajb12, Hspa14, Hspa2
0010257	Aifm1, Ndufa10, mt-Nd1, mt-Nd2
0032981	Aifm1, Ndufa10, mt-Nd1, mt-Nd2
0097031	Aifm1, Ndufa10, mt-Nd1, mt-Nd2
0006164	Hprt, Ndufa10, mt-Atp6, mt-Atp8, mt-Nd1, mt-Nd2
1902582	Aifm1, Bicdl1, Dst, Dync1h1, Ift43, Ndufa10, Sec24d, Syne2, Yif1b, mt-Atp6, mt-Atp8, mt-Nd1, mt-Nd2
0009260	Hprt, Ndufa10, mt-Atp6, mt-Atp8, mt-Nd1, mt-Nd2
0032456	Btbd8, Cmtm6, Ehd3, Stx16
0072522	Hprt, Ndufa10, mt-Atp6, mt-Atp8, mt-Nd1, mt-Nd2
0071822	Aifm1, Cadps2, Ccdc65, Coa5, Diaph3, Drc1, Ehd3, Hprt, Ndufa10, Oma1, Sdhaf2, Taco1, mt-Co3, mt-Nd1, mt-Nd2
0035967	Dnajb12, Hspa14, Hspa2
0018130	Aff1, Arrb2, Ash1l, Ddx21, Dkc1, Hprt, Irf2bp1, Klf4, Ndufa10, Setx, Sp1, Taf1c, mt-Atp6, mt-Atp8, mt-Nd1, mt-Nd2
0001539	Ccdc65, Drc1
0060285	Ccdc65, Drc1
0051084	Dnajb12, Hspa14, Hspa2
1901990	Cdc14a, Dpf2, Hspa2, Klf4, Nbn, Nsmce2, Pdpn, Rad51c, Zwilch
0046390	Hprt, Ndufa10, mt-Atp6, mt-Atp8, mt-Nd1, mt-Nd2
0006458	Dnajb12, Hspa14, Hspa2
0019438	Aff1, Arrb2, Ash1l, Ddx21, Dkc1, Hprt, Irf2bp1, Klf4, Ndufa10, Setx, Sp1, Taf1c, mt-Atp6, mt-Atp8, mt-Nd1, mt-Nd2
0071840	Aifm1, Arfgef2, Arl5c, Ash1l, Atp11b, Bdp1, Bicdl1, Btbd8, C1ql1, Cadps2, Cbx5, Ccdc65, Ccnb1ip1, Cdc14a, Cenpv, Cep20, Coa5, Cog3, Ddx21, Diaph3, Dkc1, Dnajb12, Dpf2, Drc1, Dst, Dync1h1, Ehd3, Epb41l4a, Fastkd5, Gcc2, Gtf3a, Hey1, Hprt, Hspa2, Ift43, Ighmbp2, Marco, Mbip, Mbtps1, Mnd1, Nbn, Ndufa10, Nsmce2, Oma1, Pak1ip1, Pdpn, Pdzd8, Rad51c, Rybp, Sdhaf2, Sec24d, Setx, Stpg1, Stx16, Taco1, Tada2a, Timd4, Ubxn2a, Uhmk1, Wdr45b, Yif1b, Zcwpw1, Zfp148, mt-Co3, mt-Nd1, mt-Nd2
0017004	Coa5, Taco1, mt-Co3
0000722	Nsmce2, Rad51c

GO term	**IMZ – IVZ DE Genes (Names) P value ≤ 0.005**
0016071	Aurkaip1, Cwc25, Dcp1a, Eftud2, Exosc10, Fip1l1, Hnrnpab, Hnrnpc, Magoh, Nudt16l1, Parn, Prpf38a, Prpf40a, Rbm17, Sf3a3, Smu1, Snrnp70, Snrpb2, Snrpd1, Snrpf, Syf2, Tut7, Upf3b, Ythdc1, Zcrb1, Zrsr1
0000377	Cwc25, Eftud2, Hnrnpc, Prpf38a, Prpf40a, Rbm17, Sf3a3, Smu1, Snrnp70, Snrpb2, Snrpd1, Snrpf, Syf2, Ythdc1, Zcrb1, Zrsr1
0000398	Cwc25, Eftud2, Hnrnpc, Prpf38a, Prpf40a, Rbm17, Sf3a3, Smu1, Snrnp70, Snrpb2, Snrpd1, Snrpf, Syf2, Ythdc1, Zcrb1, Zrsr1
0000375	Cwc25, Eftud2, Hnrnpc, Prpf38a, Prpf40a, Rbm17, Sf3a3, Smu1, Snrnp70, Snrpb2, Snrpd1, Snrpf, Syf2, Ythdc1, Zcrb1, Zrsr1

0008380	Cwc25, Eftud2, Hnrnpc, Magoh, Prpf38a, Prpf40a, Rbm17, Sf3a3, Smu1, Snrnp70, Snrpb2, Snrpd1, Snrpf, Syf2, Ythdc1, Zcrb1, Zrsr1
0006397	Aurkaip1, Cwc25, Eftud2, Fip1l1, Hnrnpc, Prpf38a, Prpf40a, Rbm17, Sf3a3, Smu1, Snrnp70, Snrpb2, Snrpd1, Snrpf, Syf2, Ythdc1, Zcrb1, Zrsr1
0022402	Anp32b, Bub1b, Calm2, Ccdc57, Ccnb1ip1, Cdc7, Cdk15, Cenps, Cenpx, Cep120, Ddx11, Dscc1, Ercc4, Fzr1, Golga2, Haus8, Ist1, Khdc3, Kif20a, Klhdc8b, Mad2l1, Map9, Mcm6, Mos, Npm1, Nudc, Poldip2, Pttg1, Rhob, Rps6, Sde2, Spc25, Spg20, Stk11, Syf2, Tubgcp5
2001251	Bub1b, Ercc4, Exosc10, Hnrnpc, Khdc3, Mad2l1, Pttg1, Spc25, Sub1
0010564	Anp32b, Bub1b, Calm2, Ccsap, Cdc7, Cep120, Cep76, Chmp3, Ddx3x, Ecd, Fzr1, Igf1r, Khdc3, Kif20a, Mad2l1, Map9, Mos, Myo19, Nek10, Npm1, Pdgfb, Pebp1, Poldip2, Ppp2ca, Prpf40a, Pttg1, Sde2, Spc25, Syf2, Zfyve26
0032465	Calm2, Chmp3, Igf1r, Kif20a, Map9, Myo19, Poldip2, Prpf40a, Zfyve26
0048008	Pdap1, Pdgfb, Plekha1, Rapgef1, Txnip, Zfand5
0051898	Cib1, Igf1r, Otud3, Plekha1, Ppp2ca, Rapgef1
0006396	Aurkaip1, Cwc25, Ddx3x, Eftud2, Exosc10, Fip1l1, Hnrnpc, Magoh, Mphosph6, Parn, Prpf38a, Prpf40a, Rbm17, Rps6, Sf3a3, Smu1, Snrnp70, Snrpb2, Snrpd1, Snrpf, Syf2, Trmt112, Trmu, Tut7, Ythdc1, Zcrb1, Zrsr1
1904872	Cct2, Exosc10, Parn
0051302	Calm2, Chmp3, Cib1, Igf1r, Kif20a, Map9, Myo19, Poldip2, Prpf40a, Txnip, Zfyve26
0022605	Rps6, Ythdc1
0032485	Ralgps1, Rgl2
1905552	Ddrgk1, Rtn4
0051985	Bub1b, Khdc3, Mad2l1, Mos, Pttg1, Spc25
0051347	Cct2, Cib1, Dcun1d1, Ddr1, Ddx3x, Dscc1, Fzr1, Igf1r, Il34, Mertk, Nek10, Nod2, Npm1, Parn, Pdgfb, Pim1, Ppp2ca, Psmd10, Reln, Sesn2, Stk11, Tcl1b5, Vav2
1902916	Ddx3x, Marchf7, Nod2, Rnf40
0051726	Anp32b, Bub1b, Calm2, Ccdc57, Ccsap, Cdc7, Cep120, Cep76, Chmp3, Ddx3x, Ecd, Fzr1, Igf1r, Khdc3, Kif20a, Mad2l1, Map9, Mapk14, Mos, Myo19, Nek10, Npm1, Pdgfb, Pebp1, Pim1, Poldip2, Ppp2ca, Prpf40a, Psmd10, Pttg1, Rhob, Rps6, Sde2, Spc25, Syf2, Thoc1, Wfs1, Zfyve26
0010639	Bub1b, Cib1, Clec16a, Dlc1, Ercc4, Exosc10, Hnrnpc, Khdc3, Mad2l1, Map2, Mos, Npm1, Psmd10, Pttg1, Spc25, Sub1, Tchp, Tesk1
2000816	Bub1b, Khdc3, Mad2l1, Pttg1, Spc25
1902100	Bub1b, Khdc3, Mad2l1, Mos, Spc25
0022904	Afg1l, Ndufa7, Sco2, Uqcr10, Uqcrb, mt-Nd1, mt-Nd6
0006139	1700066M21Rik, Aip, Atf4, Atp5e, Atp5g2, Aurkaip1, Ccnb1ip1, Cdc7, Cenps, Cenpx, Cwc25, Dcp1a, Dcxr, Ddx3x, Eftud2, Ercc4, Exd2, Exosc10, Fip1l1, Flad1, Gnpnat1, Hnrnpab, Hnrnpc, Khdc3, Magoh, Mapk14, Mcm6, Mphosph6, Naxe, Ndufa7, Npm1, Nudt16l1, Parn, Parp4, Pgls, Pias2, Poldip2, Prpf38a, Prpf40a, Pycrl, Rbm17, Rnaseh2a, Rnaseh2c, Rps6, Sesn2, Sf3a3, Smc6, Smu1, Snrnp70, Snrpb2, Snrpd1, Snrpf, Ssbp1, Sub1, Syf2, Thoc1, Tk1, Trmt112, Trmu, Tut7, Upf3b, Upp1, Ythdc1, Zcrb1, Zfyve26, Zrsr1, mt-Nd1, mt-Nd6
1903047	Anp32b, Bub1b, Calm2, Ccdc57, Cdk15, Dscc1, Fzr1, Golga2, Khdc3, Kif20a, Klhdc8b, Mad2l1, Map9, Mcm6, Nudc, Poldip2, Pttg1, Rhob, Rps6, Sde2, Spc25, Syf2
0048585	Apoe, Atf4, Brms1l, Calm2, Cib1, Ddrgk1, Ddx3x, Derl3, Dlc1, Dlg5, Dnaja1, Esr2, Faim, Fzr1, Gpc1, Grina, Igbp1, Igf1r, Limd1, Lmbr1l, Lpl, Mapk14, Marchf7, Ncoa5, Nenf, Nod2, Nudt16l1, Otud3, Parpbp, Pdgfb, Pebp1, Phf14, Pias2, Pid1, Plekha1,

	Ppp2ca, Psmd10, Ptger4, Ptgis, Ptprt, Rapgef1, Rtn4, Sap30, Sema4c, Sesn2, Sinhcaf, Spg20, Stk11, Thoc1, Trim59, Ubac2, Wfs1, Zfp653
0034641	1700066M21Rik, Aip, Atf4, Atp5e, Atp5g2, Aurkaip1, Ccnb1ip1, Cdc7, Cenps, Cenpx, Cwc25, Dcp1a, Dcxr, Ddx3x, Eftud2, Eif2s1, Ercc4, Exd2, Exosc10, Fip1l1, Flad1, Fpgs, Furin, Gnpnat1, Hnrnpab, Hnrnpc, Khdc3, Magoh, Mapk14, Mcm6, Mphosph6, Mrpl14, Mrpl38, Mrps22, Naxe, Ndufa7, Nod2, Npm1, Nudt16l1, Odc1, Paox, Parn, Parp4, Pgls, Pias2, Plpp3, Poldip2, Prpf38a, Prpf40a, Pycrl, Rbm17, Rnaseh2a, Rnaseh2c, Rpl18, Rplp1, Rps12, Rps6, Sesn2, Sf3a3, Smc6, Smu1, Snrnp70, Snrpb2, Snrpd1, Snrpf, Sptlc2, Ssbp1, Sub1, Syf2, Thoc1, Tk1, Trmt112, Trmu, Tut7, Upf3b, Upp1, Ythdc1, Zcrb1, Zfyve26, Zrsr1, mt-Nd1, mt-Nd6
0007051	Cep120, Golga2, Haus8, Khdc3, Map9, Mos, Nudc, Poldip2, Spc25, Tubgcp5
0031297	Cenps, Cenpx, Exd2, Khdc3, Thoc1
0035331	Dlg5, Limd1, Mapk14
0033048	Bub1b, Khdc3, Mad2l1, Pttg1, Spc25
1902532	Apoe, Calm2, Cib1, Ddx3x, Dlc1, Dlg5, Dnaja1, Grina, Igf1r, Limd1, Mapk14, Marchf7, Otud3, Pebp1, Plekha1, Ppp2ca, Psmd10, Ptprt, Rapgef1, Sesn2, Stk11, Trim59, Wfs1
1902455	Brms1l, Hnf1b, Sap30, Sinhcaf
0051784	Bub1b, Khdc3, Mad2l1, Mos, Pttg1, Spc25
0044260	Afg1l, Aip, Akirin2, Ap2s1, Apoe, Atf4, Aurkaip1, Brms1l, Cacng7, Ccnb1ip1, Cdc7, Cdk15, Cenps, Cenpx, Clec16a, Clk2, Cwc25, Dcp1a, Dcun1d1, Ddr1, Ddrgk1, Ddx3x, Derl3, Dscc1, Eftud2, Eif2s1, Ercc4, Exd2, Exosc10, Fip1l1, Furin, Fzr1, Golga2, Gpc1, Hnrnpab, Hnrnpc, Igf1r, Kbtbd6, Khdc3, Klhdc2, Kmt5a, Lmf1, Magoh, Mapk14, Mapkapk2, Marchf7, Mast3, Mcm6, Med6, Mertk, Mgat4a, Mphosph6, Mrpl14, Mrpl38, Mrps22, Ndufa7, Nek10, Nenf, Nod2, Npm1, Nudt16l1, Otud3, Parn, Parp4, Pdgfb, Pebp1, Pias2, Pim1, Poldip2, Ppme1, Ppp2ca, Prpf38a, Prpf40a, Prpf4b, Prr5l, Ptger4, Ptprt, Rabggta, Rala, Rapgef1, Rbm17, Rce1, Reln, Rnaseh2a, Rnaseh2c, Rnf40, Rpl18, Rplp1, Rps12, Rps6, Sde2, Sesn2, Sf3a3, Smc6, Smu1, Snrnp70, Snrpb2, Snrpd1, Snrpf, Ssbp1, Stk11, Sub1, Syf2, Tbk1, Thoc1, Timm50, Tpst2, Trmt112, Trmu, Tut7, Ubap1, Ube3c, Ubqln2, Ubxn2a, Upf3b, Wfs1, Ythdc1, Zcrb1, Zfyve26, Zrsr1
0051053	Dffa, Dppa3, Ercc4, Exosc10, Hnrnpc, Mphosph8, Nudt16l1, Parpbp, Sub1, Thoc1
0033046	Bub1b, Khdc3, Mad2l1, Pttg1, Spc25
0022900	Afg1l, Ndufa7, Sco2, Uqcr10, Uqcrb, mt-Nd1, mt-Nd6
0031952	Ddx3x, Nek10, Pdgfb, Ppp2ca, Tesk1
0009446	Odc1, Paox
0016077	Exosc10, Nudt16l1
0034382	Apoe, Lmf1
0051665	Naxe, Rala
0071830	Apoe, Lmf1
0072639	Ptger4, Rbbp9
1905550	Ddrgk1, Rtn4
0031396	Bub1b, Dcun1d1, Ddx3x, Dnaja1, Fzr1, Mad2l1, Marchf7, Nod2, Npm1, Psmd10, Rnf40, Ubxn2a, Wfs1
0031398	Dcun1d1, Ddx3x, Fzr1, Marchf7, Nod2, Npm1, Psmd10, Rnf40, Wfs1
2000622	Hnrnpab, Magoh, Upf3a
0045005	Cenps, Cenpx, Exd2, Khdc3, Thoc1

0000226	Ccdc57, Ccsap, Cep120, Cib1, Gas2l3, Golga2, Haus8, Khdc3, Kif20a, Mad2l1, Map2, Map9, Mos, Nudc, Poldip2, Spc25, Tuba1c, Tubgcp5, Vamp4
1902914	Ddx3x, Marchf7, Nod2, Rnf40
0006996	Afg1l, Apoe, Armc1, Atad3a, Aurkaip1, Bscl2, Bub1b, Ccdc57, Ccsap, Cep120, Cfap298, Chmp3, Cib1, Ddrgk1, Ddx11, Ddx3x, Dlc1, Eif2s1, Ercc4, Fam161b, Gas2l3, Ggct, Golga2, Golga5, Haus8, Khdc3, Kif20a, Limd1, Mad2l1, Map2, Map9, Mast3, Mcm6, Mos, Mrpl14, Mrpl38, Mrps22, Myo9a, Ndufa7, Nos1ap, Npm1, Nudc, Odf2, Parp4, Pdgfb, Pid1, Poldip2, Prpf40a, Pttg1, Rala, Reln, Rhob, Rtn4, Selenof, Sesn2, Smc6, Snap47, Spc25, Spg20, Ssbp1, Tesk1, Timm50, Tln1, Tmem216, Trappc2, Trappc6a, Tuba1c, Tubgcp5, Ubqln2, Ubxn2a, Vamp4, Yif1b, Zfyve26
0046483	1700066M21Rik, Aip, Atf4, Atp5e, Atp5g2, Aurkaip1, Ccnb1ip1, Cdc7, Cenps, Cenpx, Cwc25, Dcp1a, Dcxr, Ddx3x, Eftud2, Ercc4, Exd2, Exosc10, Fip1l1, Flad1, Fpgs, Gnpnat1, Hnrnpab, Hnrnpc, Khdc3, Magoh, Mapk14, Mcm6, Mphosph6, Naxe, Ndufa7, Npm1, Nudt16l1, Parn, Parp4, Pgls, Pias2, Poldip2, Prpf38a, Prpf40a, Pycrl, Rbm17, Rnaseh2a, Rnaseh2c, Rps6, Sesn2, Sf3a3, Smc6, Smu1, Snrnp70, Snrpb2, Snrpd1, Snrpf, Ssbp1, Sub1, Syf2, Thoc1, Tk1, Trmt112, Trmu, Tut7, Upf3b, Upp1, Ythdc1, Zcrb1, Zfyve26, Zrsr1, mt-Nd1, mt-Nd6
0033044	Bub1b, Cct2, Ercc4, Exosc10, Hnrnpc, Khdc3, Mad2l1, Mos, Parn, Pttg1, Spc25, Sub1
0044237	1700066M21Rik, Afg1l, Aip, Akirin2, Ap2s1, Apoe, Atf4, Atp5e, Atp5g2, Aurkaip1, Brms1l, Bscl2, Cacng7, Car9, Ccnb1ip1, Cdc7, Cdk15, Cenps, Cenpx, Clec16a, Clk2, Crabp2, Cwc25, Dbil5, Dcp1a, Dcun1d1, Dcxr, Ddr1, Ddrgk1, Ddx3x, Derl3, Dscc1, Eftud2, Eif2s1, Ercc4, Exd2, Exosc10, Fasn, Fip1l1, Flad1, Fmo3, Fpgs, Furin, Fzr1, Gk, Glrx3, Gnpnat1, Golga2, Gpc1, Hnrnpab, Hnrnpc, Igf1r, Kbtbd6, Khdc3, Klhdc2, Kmt5a, Limd1, Lmf1, Lpcat4, Lpl, Magoh, Mapk14, Mapkapk2, Marchf7, Mast3, Mcm6, Med6, Mertk, Mgat4a, Mphosph6, Mrpl14, Mrpl38, Mrps22, Naxe, Ndufa7, Nek10, Nenf, Nod2, Npm1, Nudt16l1, Odc1, Otud3, Paox, Parn, Parp4, Pdgfb, Pebp1, Pgls, Pias2, Pim1, Plcb3, Plekha1, Plpp3, Poldip2, Ppa1, Ppme1, Ppp2ca, Prdx1, Prpf38a, Prpf40a, Prpf4b, Prr5l, Ptger4, Ptgis, Ptprt, Pycrl, Rabggta, Rala, Rapgef1, Rbm17, Rce1, Reln, Rnaseh2a, Rnaseh2c, Rnf40, Rpl18, Rplp1, Rps12, Rps6, Sco2, Sde2, Sesn2, Sf3a3, Smc6, Smu1, Snrnp70, Snrpb2, Snrpd1, Snrpf, Sptlc2, Ssbp1, Stk11, Sub1, Syf2, Tbk1, Tecr, Thoc1, Timm50, Tk1, Tmem150a, Tpst2, Trmt112, Trmu, Tut7, Ubap1, Ube3c, Ubqln2, Ubxn2a, Upf3b, Upp1, Uqcr10, Uqcrb, Wfs1, Ythdc1, Zcrb1, Zfyve26, Zrsr1, mt-Nd1, mt-Nd6
0000075	Bub1b, Fzr1, Khdc3, Mad2l1, Mapk14, Rps6, Sde2, Spc25, Syf2
0043043	Aurkaip1, Eif2s1, Furin, Mrpl14, Mrpl38, Mrps22, Ndufa7, Nod2, Rpl18, Rplp1, Rps12, Rps6
0009624	Ptger4, Rbbp9
0009838	Ist1, Spg20
0034370	Apoe, Lpl
0034372	Apoe, Lpl
0060468	Astl, Tpst2
1900127	Pdgfb, Ptger4
1901610	Map2, Stk11
1904502	Sesn2, Sptlc2
1904504	Sesn2, Sptlc2
0007093	Bub1b, Fzr1, Khdc3, Mad2l1, Rps6, Sde2, Spc25, Syf2
0007094	Bub1b, Khdc3, Mad2l1, Spc25
0071173	Bub1b, Khdc3, Mad2l1, Spc25
0006401	Dcp1a, Exosc10, Magoh, Nudt16l1, Parn, Rnaseh2a, Rnaseh2c, Tut7, Upf3b

0033674	Cib1, Ddr1, Ddx3x, Igf1r, Il34, Mertk, Nek10, Nod2, Npm1, Pdgfb, Pim1, Ppp2ca, Psmd10, Reln, Sesn2, Stk11, Tcl1b5, Vav2
0090304	Aip, Atf4, Aurkaip1, Ccnb1ip1, Cdc7, Cenps, Cenpx, Cwc25, Dcp1a, Ddx3x, Eftud2, Ercc4, Exd2, Exosc10, Fip1l1, Hnrnpab, Hnrnpc, Khdc3, Magoh, Mapk14, Mcm6, Mphosph6, Npm1, Nudt16l1, Parn, Parp4, Pias2, Poldip2, Prpf38a, Prpf40a, Rbm17, Rnaseh2a, Rnaseh2c, Rps6, Sesn2, Sf3a3, Smc6, Smu1, Snrnp70, Snrpb2, Snrpd1, Snrpf, Ssbp1, Sub1, Syf2, Thoc1, Trmt112, Trmu, Tut7, Upf3b, Ythdc1, Zcrb1, Zfyve26, Zrsr1
0051338	Apoe, Bub1b, Cct2, Cib1, Dcun1d1, Ddr1, Ddx3x, Dnaja1, Dscc1, Fzr1, Igf1r, Il34, Mad2l1, Mertk, Nek10, Nod2, Npm1, Parn, Parp4, Pdgfb, Pim1, Ppp2ca, Psmd10, Reln, Sesn2, Stk11, Tcl1b5, Tesk1, Vav2
0009894	Apoe, Bscl2, Clec16a, Ddrgk1, Derl3, Dffa, E330034G19Rik, Furin, Hnrnpab, Mad2l1, Magoh, Marchf7, Odc1, Ppp2ca, Prr5l, Psmd10, Rnf40, Sesn2, Sptlc2, Ubac2, Ubqln2, Ubxn2a, Upf3a
0051129	Apoe, Bub1b, Cib1, Clec16a, Ddx3x, Dffa, Dlc1, Ercc4, Exosc10, Hnrnpc, Itm2c, Khdc3, Mad2l1, Map2, Mos, Npm1, Pid1, Psmd10, Ptger4, Pttg1, Rps6, Rtn4, Sema4c, Spc25, Spg20, Sub1, Tchp, Tesk1, Ubqln2
0051783	Bub1b, Ccsap, Fzr1, Igf1r, Khdc3, Mad2l1, Map9, Mos, Pdgfb, Pebp1, Pttg1, Spc25
0009968	Apoe, Brms1l, Calm2, Cib1, Ddrgk1, Ddx3x, Dlc1, Dlg5, Dnaja1, Esr2, Faim, Gpc1, Grina, Igbp1, Igf1r, Limd1, Lmbr1l, Mapk14, Marchf7, Ncoa5, Nod2, Otud3, Pebp1, Phf14, Pias2, Pid1, Plekha1, Ppp2ca, Psmd10, Ptprt, Rapgef1, Sap30, Sesn2, Sinhcaf, Spg20, Stk11, Trim59, Ubac2, Wfs1, Zfp653
0006725	1700066M21Rik, Aip, Atf4, Atp5e, Atp5g2, Aurkaip1, Ccnb1ip1, Cdc7, Cenps, Cenpx, Cwc25, Dcp1a, Dcxr, Ddx3x, Eftud2, Ercc4, Exd2, Exosc10, Fip1l1, Flad1, Fpgs, Gnpnat1, Hnrnpab, Hnrnpc, Khdc3, Magoh, Mapk14, Mcm6, Mphosph6, Naxe, Ndufa7, Npm1, Nudt16l1, Parn, Parp4, Pgls, Pias2, Poldip2, Prpf38a, Prpf40a, Pycrl, Rbm17, Reln, Rnaseh2a, Rnaseh2c, Rps6, Sesn2, Sf3a3, Smc6, Smu1, Snrnp70, Snrpb2, Snrpd1, Snrpf, Ssbp1, Sub1, Syf2, Thoc1, Tk1, Trmt112, Trmu, Tut7, Upf3b, Upp1, Ythdc1, Zcrb1, Zfyve26, Zrsr1, mt-Nd1, mt-Nd6
0045839	Bub1b, Khdc3, Mad2l1, Pttg1, Spc25
1903573	Ddrgk1, Derl3, Grina, Ubac2, Wfs1
0009895	Bscl2, Clec16a, Ddrgk1, Derl3, Dffa, Furin, Hnrnpab, Mad2l1, Marchf7, Ubac2, Upf3a
0043085	Akirin2, Anp32b, Apoe, Calm2, Cct2, Cib1, Dcun1d1, Ddr1, Ddrgk1, Ddx3x, Dlc1, Dscc1, Fzr1, Igf1r, Il34, Lmf1, Mapk14, Mertk, Nek10, Nod2, Npm1, Parn, Pdgfb, Pim1, Ppp2ca, Psmd10, Ralgps1, Rapgef1, Reln, Rgl2, Sesn2, Ssbp1, Stk11, Tbc1d15, Tcl1b5, Vav2
0000712	Cenps, Cenpx, Ercc4
0030521	Dnaja1, Esr2, Pias2
0032606	Ifnar1, Ppme1, Tbk1
0043555	Ddx3x, Eif2s1, Sesn2

Title

The Impact of ART-relevant *In Vitro* Maturation on Active Translation in Oocytes and Zygotes.

Authors

Michal Dvoran* (ORCID - 0000-0002-0131-5878), Rajan Iyyappan, Tomas Masek, Martin Pospisek, Michal Kubelka, Andrej Susor*.

Affiliations

M. Dvoran (dvoran@iapg.cas.cz), R. Iyyappan (iyyappan@iapg.cas.cz), M. Kubelka (kubelka@iapg.cas.cz), A. Susor (susor@iapg.cas.cz) - Institute of Animal Physiology and Genetics, Czech Academy of Sciences, Rumburska 89, 277 21, Libechov (www.iapg.cas.cz)

T. Masek (masek@natur.cuni.cz), M. Pospisek (martin.pospisek@natur.cuni.cz) – Faculty of Science, Albertov 6, 128 00, Praha 2 (www.natur.cuni.cz)

Keywords

maturation, oocyte, embryo, ART, reproduction, mouse, human

Abstract

Assisted reproductive technology (ART) has become an indispensable tool in fertility treatment. Most ART patients respond normally to controlled ovarian stimulation, in which ovulation is induced by the administration of human chorionic gonadotropin. However, a subset of patients suffering from polycystic ovarian syndrome or ovarian hyper-stimulation syndrome often experience complications in the production of developmentally competent oocytes. These people could benefit from the alternative method of oocyte *in vitro* maturation (IVM), a recognized but still underdeveloped method providing limited results. As oocytes undergo the transcriptionally silent phase of meiosis, properly regulated translation of stored maternal transcripts becomes a crucial factor for their successful development. This work evaluated clinically relevant IVM against *in vivo* conditions from the perspective of active translation in mouse oocytes and zygotes. Our findings uncovered significant differences in global transcriptome as well as alterations in translation of specific transcripts encoding components of energy production, cell cycle regulation, and protein synthesis in oocytes and RNA metabolism in zygotes. Highlighted importance of proper translational regulation in IVM is to prompt further investigation into clinical IVM optimisation in context of translation.

Introduction

Assisted reproduction technology (ART) is becoming essential for our society as we are confronted with delayed parenthood and a polluted living environment. Since the birth of Louise Brown in 1975, the first baby conceived by *in vitro* fertilization (IVF), ART has developed diagnostic techniques capable of advanced oocyte and early embryo screening. However, the quality and quantity of collected fully grown MII oocytes vary greatly due to the complexity of underlying factors, for example: the selected approach to controlled ovarian stimulation (COS), maternal age, genetic and social background, previous surgeries, lifestyle, associated diseases, and others.

The *in vitro* oocyte maturation (IVM) technique was developed with the intention of increasing the amount of developmentally competent MII oocytes and therefore maximizing the chances for a successful pregnancy. The potential of the IVM technique had been previously explored in mammalian species such as mice (1,2), rats (3) and eventually humans (4). In due time it was tested for its potential clinical application (5–8). However, the proper IVM comparison with *in vivo* conditions was and still is limited to certain mammalian models, particularly if ART relevance is sought. The bovine model, although possibly more suitable for correlation with humans, is almost impossible to synchronize properly *in vivo*. Human *in vivo* samples are out of the question for obvious ethical reasons, which points towards the mouse model, which can be easily synchronized *in vivo*. (9).

IVM has found its place in the management of infertility due to anovulation in patients suffering from polycystic ovary syndrome (PCOS). PCOS has been diagnosed in about 5 – 20 % of females, varying among people of different origin (10). The first clinical application of IVM in 19 PCOS patients resulted in just one live birth (11) and ended up with a live birth rate of over 20% when fertilized by ICSI (12).

Alternatively, the 1 – 5 % of ART patients suffering from ovarian hyperstimulation syndrome (OHSS) can also benefit from IVM technology (13). Severe OHSS is triggered by the administration of hCG, which increases vascular permeability via the vascular endothelial factor (VEGF). The resulting hypovolemic hyponatremia is a life-threatening condition, which can be avoided by oocyte IVM (14). In 2020 the IVM technique was officially declared safe for clinical use (15).

IVM itself is based on the collection of cumulus oocyte complexes (COC) from patients in COS cycles and has two main variants. Either the conventional approach is applied with *in vitro* COC culture in media supplemented with human serum albumin, amino acids, vitamins, rFSH (recombinant follicle-stimulating hormone) and rLH (recombinant luteinizing hormone) (15), or the rescue IVM (R-IVM) approach, in which immature GV oocytes from COS are denuded (DO) with

hyaluronidase and cultured *in vitro* without gonadotropins (16). In both IVM techniques, it is challenging to assess the quality of nuclear and cytoplasmic maturation as the oocyte progresses through meiosis. (17–19).

Oocytes store maternal transcripts within their cytoplasm as they mature within follicles. Consequently, efficient spatiotemporal utilization of these transcripts is vital for the success of meiotic maturation and the acquisition of oocyte developmental competence (20). Translation-associated processes and their regulation are key, as transcription is stopped throughout meiosis (21).

Polysomal occupancy reflects the extent of a particular transcript's "active" translation based on how many ribosomes translate the transcript at one time. This phenomenon can be detected by the method of scarce-sample profiling (SSP), in which the acquisition of 18S and 28S rRNA qPCR data is indicative of the large and small ribosomal subunits respectively, and hence the polysomal bound RNA presence in a particular fraction (22). Previously, SSP identified significant differences in the translation of cell cycle and cytokinesis factors in oocytes from aged females (23,24).

Here we aim to identify genome-wide translatomes of oocytes and zygotes produced by various cultivation techniques that mimic the production of oocytes and zygotes used in human assisted reproduction techniques. We found significant differences when MII oocytes produced in this way were compared to those obtained *in vivo* in the translation of transcripts related to energy production, the cell cycle or RNA metabolism.

Results

Mouse model comparing *in vitro* maturation of denuded, cumulus-enclosed oocytes and pronuclear zygotes with respect to *in vivo* conditions.

To determine the differences in actively translated transcripts *in vitro* and *in vivo*, we applied the mouse model, as its genome is well mapped and *in vivo* samples can be easily synchronized and collected (Fig. 1). We set two different IVM conditions related to human IVM: one with denuded oocytes (IVM DO) (Supp. Fig. 1A), and the other with cumulus-oocyte complexes (IVM COC) in the presence of the gonadotropins rFSH and rhCG (recombinant human chorionic gonadotropin) (Supp. Fig. 1B). Our IVM media composition mimicked clinical ones, conventionally used in human assisted reproduction, which are supplemented with human serum albumin, amino acids, and vitamins.

To synchronize the timing of oocyte maturation between *in vitro* and in *vivo* conditions, we set the completion of nuclear maturation as a reference point. In IVM DO we employed the live-cell imaging of sir-tubulin labelled IVM DO matured from the MI to MII stage (Supp. Fig. 1A). We found that nuclear maturation is completed 90 minutes after PBE occurred (Supp. Fig. 1A).

To analyse the maturity of GV oocytes selected for IVM COC samples (Fig.1), we stripped COCs and visualized DNA by DAPI, which clearly showed the exclusive presence of fully grown GV oocytes with surrounded nucleolus (SN) chromatin architecture (Supp. Fig. 1C). The duration of meiotic IVM was optimized based on the timing of nuclear envelope breakdown (NEBD) to 1st polar body extrusion (PBE) (Supp. Fig. 1D). Bright-field live-cell imaging showed delayed NEBD, but shorter NEBD-PBE timing in the IVM COC samples than in the IVM DO. However, the time from IBMX release to PBE was not significantly different (Supp. Fig. 1D).

IVO collection timing modelled the clinical ovum pick-up, which is routinely performed by puncturing follicles and retrieving oocytes *in vivo* from stimulated ovaries. Thus, the IVO collection was optimized for the moment shortly before follicles ovulate, which happens between 11 - 12 hours post hCG administration (Supp. Fig. 1E). Moreover, the completion of nuclear maturation was assessed at specific time-points post hCG administration by the immunocytochemical staining of the MII spindle (Supp. Fig. 1F). Importantly, we not only confirmed the completion of nuclear maturation at 11 hours post hCG, but also the progressive MII spindle instability during oocyte post-ovulatory aging.

We also evaluated the cessation of gap-junctional communication in IVO samples to assess the potential supportive effect of cumulus cells via transzonal projections (TZPs). We observed fluorescent Calcein-AM dye accumulation that positively correlated with terminated oocyte-cumulus cells communication via gap-junctions 5-10 hours post hCG administration *in vivo* (Supp. Fig. 1G). In contrast, GV denuded oocytes terminated gap-junctional communications instantly (Supp. Fig. 1G).

To elucidate the homogeneity of the zygotic samples we performed time—lapse imaging to analyse the timing of pronuclei (PN) formation between *in vitro* fertilized IVM DO (IMZ) and i*n vivo* zygotes (IVZ) which showed a similarity in PN formation (Supp. Fig. 2).

As the exact timing of *in vivo* fertilization is impossible to optimize, we assumed the sperm was already present in the oviduct by the time oocytes ovulated IVO, and hence IVF occurred about 12-13 hours post hCG administration. Since we synchronized fertilization timings *in vitro* and *in vivo* with respect to pronuclear zygote nuclear envelope break-down (NEBD) (Supp. Fig. 2B), IMZ and IVZ collection was set for 8 hours post fertilization.

We optimized the timing of both *in vitro* and *in vivo* meiotic maturation conditions in the ICR mouse strain with culture conditions relevant to the clinical environment to extrapolate our findings.

Transcriptome and translatome is significantly influenced in differentially derived oocytes and zygotes.

To distinguish maternal transcripts that are differentially expressed (DGE) in MII oocytes and pronuclear zygotes under *in vitro* and *in vivo* conditions, the SSP profiling (Scarce Sample Polysome Profiling) approach was applied. Each analysed sample was separated by ultracentrifugation on a sucrose gradient and collected into 10 distinct fractions. Because the very low material input made reading absorbance impossible, we visualised polysome profiles indirectly by qPCR of the 18S and 28S rRNA content in each fraction (Supp. Fig. 3; (22), (25)). The qPCR analyses of fractionated samples confirmed the presence of free 40S ribosomal subunits preferentially in fractions F2 - F3; 60S subunits in F3 - F4 and monosomes in F4 - F5. Fractions F6 – F10 then clearly corresponded to low- to high-molecular weight polysomes (Supp. Fig. 3). As we wanted to distinguish mRNAs actively engaged in translation from those ones that were either not translated at all or with a very low rate of translation (e.g. mRNAs associated with monosomes), we pooled the RNA isolated from fractions F1 - F5 (reflecting the non-translated pool of mRNAs; regarded as NP (non-polysomal)) and F6-F10 (corresponding to mRNAs actively translated, regarded as P (polysomal)), respectively. RNA-seq of the P (polysomal) and the NP (non-polysomal) samples from IVM DO, IVM COC, IVO, IMZ and IVZ were performed in quadruplicates (Fig. 2). In addition, RNA-seq datasets of global transcriptomes (T; total RNA) were produced as a further comparison to fractionated samples (Fig.2).

The principal component analysis (PCA) of RNA-seq datasets showed a clear clustering of fractionated and total transcriptome samples (Supp. Fig. 4). Upon the distribution of PCA data, first the replicates of IVM DO and IVZ samples were excluded from further DGE analysis, due to their low similarity to the other three replicates (Supp. Fig. 4). To exclude the possibility of oocyte and zygote sample contamination by cumulus cells, we verified the absence of cumulus specific EGF-like transcripts (*Areg, Ereg, Btc*) in our datasets (Supp. Fig. 5).

The differential gene expression (DGE) analysis was performed between IVM DO, IVM COC and IVO conditions, as well as between IMZ and IVZ shortlisted transcripts with reads per kilobase million (RPKM) ≥ 0.2. The pool of differently expressed transcripts for IVM DO – IVO consisted of 5093 transcripts, IVM COC – IVO of 7527 transcripts, IVM DO – IVM COC of 5018 transcripts and IMZ – IVZ of 6336 transcripts (GSE241633).

Initially, we explored the overall sample distribution by determining the value of log2 fold change as a function of max group mean RPKM. This highlights the upregulated and downregulated

transcripts in non-polysomal and polysomal fractions, as well as in total transcriptomes. Minor differences in fold change were found among non-polysomal transcripts (Fig. 2), in contrast to the polysome-bound transcripts with more profound fold changes (Fig. 2). In the most striking comparison of IVM DO *vs.* IVO and IVM COC *vs.* IVO, the majority of polysomal transcripts were downregulated when *in vitro* conditions were compared to *in vivo* (Fig. 2AB), however, these differences were not reflected in the total transcriptome (Fig. 2A). Surprisingly, the IVM DO *vs.* IVM COC comparison gave highly similar RNA-seq data for both the fractionated and total transcriptome with very few transcripts showing more than a 2-fold difference (Fig. 2C). IVM COC *vs.* IVO DGE comparison data showed no preference in distribution towards up- or downregulated polysomal transcripts. However, in the total transcriptome there were only a few transcripts with DE (Fig. 2B). A similar trend of analysed IVM COC *vs.* IVO differences data was observed in the comparison of IMZ *vs.* IVZ pronuclear zygotes (Fig. 2D). To further investigate the overall degree of similarity between polysome-derived and transcriptomic RNA-seq datasets, the Spearman's correlation coefficient was calculated using transcript $\log_2$ fold change for the compared samples. The resulting analysis showed only an approximately 10% correlation between the transcriptome and translatome in IVM DO *vs.* IVO and IVM COC vs. IVO pairs (Supp. Fig. 6A). In IMZ *vs.* IVZ, the correlation increased to about 20% (Supp. Fig. 6B).

In summary, we obtained genome-wide snapshots of cellular transcriptomes and translatomes that mirror the influence of various cultivation techniques relevant to human assisted reproduction.

Biological processes and cellular components are influenced by the way in which the oocytes and zygotes are derived.

To determine which processes are influenced by various cultivation techniques, the significant DE transcripts of IVM DO *vs.* IVO, IVM COC *vs.* IVO, IVM DO *vs.* IVM COC and IMZ *vs.* IVZ with RPKM ≥ 0.2 in every replicate and $P \leq 0.005$ were further included in the gene ontology enrichment (GO) analysis. GO clustering was performed either towards biological processes or cellular components.

The GO analysis between IVM DO - IVO (Fig. 3A) revealed the most significant DE of transcripts involved in biological processes associated with chromosome organization (e.g., *Cenp-v, Dkc1, Dpf2, Nbn;* Supp. File 1) and energy production (e.g., *Ndufa10, mt-Atp6, mt-Atp8, mt-Nd1, mt-Nd2;* Supp. File 1). The GO analysis of cellular components (Fig. 3B) highlighted respiratory chain complex- and mitochondria-related transcripts (e.g., *Ndufa10, mt-Atp6, mt-Atp8, mt-Nd1, mt-Nd2;* Supp. File 1).

The most significant of the performed GO analyses was the comparison of IVM COC *vs.* IVO (Fig. 3A), demonstrating the impact of IVM COC culture in the presence of rFSH and rhCG on cell cycle regulation (e.g., *Aurka, Cenp-v, Spag5, Terf2*; Supp. File 1), energy production (e.g., *mt-Atp6, mt-Atp8, mt-Nd1, mt-Nd2;* Supp. Fig. 8; Supp. File 1), protein synthesis (*Rps14, Rpl15, Rpl35, Rpl38*) and DNA

repair (e.g., *Brca1, Ttf2, Brip1*; Supp. File 1). The GO analysis for cellular components (Fig. 3B) identified ribonucleoprotein complexes (RNP), chromosomes, microtubule organizing centers and mitochondria.

In contrast, the only significant GO term in IVM DO *vs.* IVM COC was protein synthesis (Fig. 3A). All the detected transcripts (*Rpl10a, Rpl18, Rpl8, Rps13, Rps17, Rps21, Rps23, Rps26)* were downregulated in IVM COC, however with less than a 2-fold difference (Supp. Fig. 9A).

The GO analysis of biological processes in IMZ *vs.* IVZ also detected transcripts involved in the cell cycle (e.g., *Pttg1, Birc5, Mos;* Fig. 3C; Supp. File 1) as in oocytes, but in contrast others were related to RNA metabolism (e.g., *Parn, Nsun2*, *Exosc10;* Fig. 3C; Supp. File 1), microtubule organization (e.g., *Bub1b, Khdc3;* Fig. 3C; Supp. File 1) or the spindle assembly checkpoint (e.g., *Aurkaip1, Furin;* Fig. 3B; Supp. File 1), and were specific to changes between *in vitro* and i*n vivo* zygotes (Fig. 3C). Cellular component GO analysis in IMZ vs. IVZ clustered transcripts related to RNPs, chromosomes, spindle, or microtubules (Fig. 3D).

Thus, the GO analyses pointed at the *in vitro* deregulated biological processes related to cell cycle regulation, energy production, DNA repair and protein synthesis in MII oocytes. The *in vitro* conditions in pronuclear zygotes similarly affected the cell cycle, but also influenced RNA metabolism or microtubule organization.

Significantly enriched GO clusters demonstrated the impact of COC *in vitro* maturation conditions in the presence of rFSH and rhCG on the regulation of the cell cycle, chromosome organization, DNA repair and energy metabolism.

Actively translated mRNAs are employed in essential processes for oocyte and early embryo development.

The transcripts detected at polysomes should be actively translated into proteins to maintain oocyte and early embryo development. We clustered DE mRNAs bound by polysomes (Fig. 2) according to their GO terms (Fig. 3; Supp. File 1). To validate the acquired datasets, we selected candidate transcripts employed in the cell cycle (Aurora kinase A, AURKA; Centromere protein V, CENPV; Fig. 4A) and energy metabolism (Adenosine deaminase, ADA; Fig. 4D) in MII oocytes as well as candidate transcripts engaged in RNA metabolism (Poly(A)-Specific Ribonuclease, PARN; NOP2/Sun RNA Methyltransferase; NSUN2) in pronuclear zygotes (Fig. 4H).

The data from our normalized RNA-seq expression analysis indicate changes in *Aurka* transcript polysomal occupancy, which showed a 2-fold increase in IVM COC samples compared to IVO (Fig. 4A). AURKA, is a serine/threonine kinase required for spindle assembly (26). The Western blot validation (Fig. 4B) confirmed an approx 20% increase in protein level in IVM COC compared to IVO (Fig. 4C).

Another protein, differentially present at polysomes *in vitro* and *in vivo* conditions (Fig. 4A), CENPV, is crucial for oocyte spindle stability (27). Its expression is decreased to 75% in IVM DO (Fig. 4A) compared to IVO (Fig. 4BC).

Oocyte fertilization capability and further embryo developmental competence is strongly dependent on its ability to produce energy for underlying molecular processes (28). Our data suggest that IVM compromises oocyte energy metabolism. To justify this observation, we initially shortlisted mitochondrially encoded transcripts (Supp. Fig. 8A) and investigated their relative polysome occupancy by calculating the ratio of polysomal to non-polysomal transcript abundance between all the studied *in vitro* and *in vivo* conditions in both oocytes and zygotes. We detected a highly significant increase in polysome occupancy in IVO samples compared to IVM DO and IVM COC. However, no significant difference was found between pronuclear IMZ and IVZ (Fig. 4D). Heat maps were prepared depicting the polysome recruitment of each of 13 mt-protein-coding transcripts (Supp. Fig. 8B), as well as the relative abundance of these mt-RNAs in respective transcriptomes (Supp. Fig. 8C). This was to evaluate the active translation in IVO samples (Supp. Fig. 8B), which was undetectable in the transcriptome (Supp. Fig. 8C), as there was an increase in transcript abundance with respect to *in vitro* maturation conditions. As we wanted to have a clear indication of the changes in energy metabolism between MII oocytes matured *in vitro* and *in vivo* , we performed CMXRos Mitotracker Red staining of the oocyte's mitochondria. A clear clustering of labelled mitochondria was detected in IVO samples compared to IVM COC, which appeared to be much smoother and with an even signal within the oocyte's cytoplasm (Supp. Fig. 8D).

The *Ada* transcript, coding for Adenosine deaminase, was identified as an additional candidate with DE in the polysomes. ADA is a crucial protein for purine metabolism, in particular, it has an important role in converting free adenosine to inosine (29). Protein abundance determined by western blotting confirmed the RNA-seq results (Fig. 4E), demonstrating decreased ADA protein abundance (Fig. 4F) to about 75% in IVM COC compared to IVO (Fig. 4FG). This fully correlated with the obtained RNA-seq data that showed increased transcript abundance in IVO (Fig. 4E).

For the pronuclear zygote samples, IMZ and IVZ, we additionally selected two mRNA candidates with differential polysome occupancy for WB validation (Fig. 4H): NSUN2, involved in m^5C methylation and m^5C introduction on mitochondrial tRNAs (30), and PARN, which is employed in maternal mRNA deadenylation (31) (Fig. 4H). Our results (Fig. 4I) showed decreased protein levels of NSUN2 to 75% in IMZ (Fig. 4IJ) and PARN to about 60% (Fig. 4IJ) with respect to IVZ.

Immunoblotting results clearly demonstrated that the identified differential polysome occupancy of selected candidate transcripts positively correlated with the resulting protein levels, thus supporting

our results that indicated a significant influence of various culture conditions and nature of the samples on the translatomes/proteomes.

The decrease in global protein synthesis in *in vitro*-matured oocytes correlates with the decreased developmental competency.

The performed genome-wide analyses showed considerable differences in the translatomes of the analysed samples produced under *in vitro* and *in vivo* maturation conditions (Fig.1 and Fig. 2). To further extend this observation, we utilized the ^{35}S-methionine labelling of actively synthetized proteins to quantify global translation. The acquired ^{35}S-Met signal intensity decreased by about 20 % in IVM DO and COC samples in comparison to IVO (Fig. 5A), however, without significant difference between IVM DO and COC samples (Fig. 5A). The ^{35}S -methionine data did correlate with differentially expressed polysome-bound transcripts enriched more than 2-fold between compared samples (Fig. 5B). Based on the DGE comparison of IVM DO *vs.* IVO, IVM COC *vs.* IVO and IVM DO *vs.* IVM COC pairs, we detected 150 IVM DO enriched transcripts versus 203 IVO enriched transcripts, 118 IVM COC enriched transcripts over 511 IVO enriched transcripts and eventually 141 IVM DO enriched transcripts compared to 43 IVM COC transcripts with P≤0.005 (Supp. File 2).

In zygotes, ^{35}S methionine labelling produced similar signal intensity between IMZ and IVZ samples, with a non-significant minor increase under *in vivo* conditions (Fig. 5C). Again, a similar pattern was obtained when IMZ *vs.* IVZ differentially expressed polysome-bound transcripts with a more than 2-fold difference were compared (Fig. 5D). 352 IVZ transcripts were shortlisted, compared to 289 IMZ transcripts (Supp. File 2).

To answer the question of how the studied *in vitro* maturation conditions affect early embryo development, we performed IVF experiments with *in vitro* cultivation up to the blastocyst stage. Data from bright-field live-cell imaging monitored IVM DO, IVM COC and IVO developmental competence. The IVF rate decreased gradually from 90% in IVO, 65% in IVM COC to 50% in IVM DO. (Fig. 5E). Extended *in vitro* embryo cultivation to the blastocyst stage mirrored the IVF rate with a progressive decline in embryo survival, with the largest difference being between *in vivo* and *in vitro* maturation conditions. IVM DO developmental competence gradually decreased with respect to IVM COC beyond the embryo 4-cell stage, ending up with about 25% and 40% of fertilized embryos developing into blastocysts, respectively (Fig. 5F).

In summary, we connected genome-wide snapshots of transcriptomes and translatomes highlighting major changes in the translation of mRNAs encoding cell cycle and energy production components and a decrease in global translation i.e., with decreasing fertilization capability and developmental competence of IVM oocytes or produced zygotes.

Discussion

IVM technology has been utilized in animal as well as human reproduction strategies (32). This study is to discover changes in translated transcripts between *in vitro* and *in vivo* maturation conditions in MII oocytes and the respective fertilized pronuclear zygotes. Meiotic maturation conditions were tailored to fit the conventional IVM technology in ART with the aim of drawing transferable conclusions for further validation in other animal or human IVM systems. It is extremely complicated to achieve IVO consistency in animal model systems such as porcine or bovine (33). To achieve a high reproducibility of *in vivo* stimulations, the ICR mouse model was selected to precisely set and monitor the culture. Importantly, the differences between the mouse and human model (34) were taken into consideration upon careful interpretation of our findings with regard to ART. This study is the first to compare a subset of transcripts actively employed in the translation of *in vitro*- and *in vivo*-maturated oocytes and the respective fertilized zygotes.

Experimental IVM culture medium was supplemented with bovine serum albumin, amino acids and vitamins. In addition, the IVM COC culture was supplemented with gonadotropins, recombinant FSH and hCG in order to mimic conventional clinical medium (15). In contrast, for the DOs culture, the same IVM medium was devoid of gonadotropins to simulate R-IVM conditions according to the published ART protocols (16).

The IVM COC culture setting had a significantly delayed NEBD with respect to IVM DOs, but the overall time from IBMX release to PBE remained equal. The underlying mechanism behind this could be the communication between oocytes and cumulus cells in COC via TZP. The delay in cGMP efflux and consequent drop in cAMP within an oocyte (35) can be responsible for the delayed NEBD onset. Moreover, it has recently been shown that TZPs cease *in vivo* at 8 hours post hCG administration (36), so the communication between oocyte and cumulus cells still persists at the time when NEBD occurs. The kinetics of translational regulation in the IVM COC and IVO system is complex due to the persistence and variations in the cessation of communication via TZP. It has been previously demonstrated by autoradiographic RNA labelling in bovine COC that RNAs can travel via TZP in RNA-containing granules (37). Our gap-junctional assay data confirmed the presence of TZP communication halfway through maturation in IVO, as well as demonstrating that upon denudation in IVM DOs, TZPs are closed. However, recently other means of oocyte-environment communication have been described and can increase the complexity of the process. For instance, the emerging role of extracellular vesicles in IVM, described in porcine oocytes (38) that perhaps originated from follicular or oviductal fluid, are currently under investigation.

Furthermore, correctly determining the time of the hidden process of *in vivo* fertilization was particularly difficult. We confirmed that *in vivo* ovulation occurs about 12 hours post hCG administration. The pronuclei NEBD in IVZ was set as the reference point to calculate probable *in vivo* fertilization time retrospectively. Assuming the presence of sperm in an oviduct, the earliest possible *in vivo* fertilization time is 12-13 hours post hCG administration. The IVZ collection was set for 20 hrs post hCG, i.e., 8 hours post IVF provided that the developmental speed was equal. Previous *in vitro* experiments with a marker of transcription (bromouridine), have revealed that 12 hours post IVF, a minor zygotic genome transcription is activated (ZGA) (39). This clearly implies that the analysed zygotic transcriptomes and translatomes are of maternal origin.

The DGE analysis of acquired polysome-derived RNA-seq data revealed significant changes in translation between *in vitro* and *in vivo* matured oocytes and subsequent fertilization in zygotes, but surprisingly, the overall changes were more subtle than we expected. As the IVM culture media in our study were supplemented with amino acids and vitamins, including vitamin C, to support IVM, the latter could have potentially suppressed the negative effect of reactive oxygen species (40,41).

In vitro vs. *in vivo* studies conducted on clinical samples in the past only compared changes in total transcriptomes or proteomes. A microarray gene expression study on human oocytes (42) observed extensive overlap between the IVM and IVO groups, which is in good agreement with our data. In contrast, in the same year, another microarray study reported more than 2 000 upregulated transcripts in human IVM compared to IVO (43). Specifically, the GO terms showed correlation with our data, i.e. cell cycle, DNA damage response, or RNA metabolism. Almost a decade later, with the advent of single-cell RNA-seq technology (44), a study on mouse IVM oocytes reported significant alterations to mitochondrial metabolism (45). This finding not only supports our data, but also GO data from previous microarray-based publications (42,43). Changes in mitochondrial translation were also detected in a recent sc-RNAseq comparison between the R-IVM and IVO maturation of human oocytes. However, the ambiguity in findings may be caused by oocyte maturation under hypoxic conditions (46). The group of (47) claimed high proteome heterogeneity between *in vitro* and *in vivo* oocytes, however, the IVM culture protocol corresponded to R-IVM with GV oocytes of inferior quality.

The GO analysis of DE IVM DO - IVM COC indicated changes in protein synthesis. The detected decrease in protein synthesis-related transcripts of IVM DO *vs.* IVM COC was in accordance with the decreased, but not significantly so, level of incorporation of radioactive ^{35}S methionine labelling, which was indicative of changes in global translation. In general, the decreased protein synthesis in IVM COC in comparison with IVO or IVM DO could be attributed to either the presence of cumulus cells or rFSH and hCG administration. Based on the statistical significance of the difference between IVM COC and

IVO, decreased protein synthesis is more likely to be linked to gonadotropin administration. Our previous findings confirmed the effect of rFSH on decreased global translation across various mammalian species, including humans (48).

The minor but significant increase in AURKA expression may be attributed to destabilized IVM oocyte spindle integrity, because it is a serine/threonine kinase required for proper spindle pole focusing, the formation of a liquid-like spindle domain and for the regulation of Transforming Acidic Coiled-Coil Containing Protein 3 (TACC3) (26). A recent publication on mouse oocytes found the presence of TACC3 to be essential for the nucleation of human microtubule organizing centres (49). The second studied protein, CENPV, has been recently shown to be important for proper chromosome segregation, as it connects them to microtubules and its deficiency can lead to a weakening of the spindle assembly checkpoint (27). Our Western Blot data showed a significantly decreased level of IVM DO CENPV, which is about 75% of IVO. However the functional role of this decrease is still uncertain, it may contribute to the multifactorial decrease in spindle stability in MII and become a basis for aneuploidy. A similar pattern can be observed in SPAG5/Astrin. This protein, although not validated here, has previously been reported to be involved in spindle pole integrity and may interact with AURKA and PLK1 (50). SPAG5 may be connected with the well-known phenomenon of barrel-shaped spindles in IVM oocytes (48).

The transcripts that exhibited significantly different association with polysomes in both IVM DO and IVM COC were related to energy production. For validation purposes, ADA was selected as the enzyme converting adenosine to inosine and also linked to PCOS in humans (29). The significantly decreased expression of ADA in IVM COC could point to a higher demand for adenosine to produce ATP, i.e., suggesting energy deprivation in both IVM COC as well as IVM DO. Indeed, mtRNA transcripts encoding proteins employed in energy production were more translated in IVO than in IVM COC or IVM DO. Moreover, increased mitochondrial clustering in IVO compared to IVM DO was indicative of increased ATP production, as previously published for mouse oocytes (51).

Two DE transcripts, *Parn* and *Nsun2* were selected for IMZ *vs.* IVZ validation, as they represent significant DET in IMZ *vs.* IVZ, also based on enriched GO categories “RNA metabolism” and “Cell cycle”. PARN protein activity has a clear impact on the zygote function, as it has recently been found to play a role in embryogenesis, cell-cycle regulation, telomere function, etc. (31). Our validation experiments by Western Blot showed a decreased protein level in IMZ to about 60% of IVZ, which also correlated with the RNA-seq data. The next one, NSUN2, has recently been shown to stabilize mRNAs via m^5C modification in Plasmodium (52). Our RNA-seq data showed a difference between IMZ and IVZ; a difference that was also confirmed by Western Blot results. A significant decrease in NSUN2 protein

level by 25% in IMZ relative to the compared *in vivo* condition was observed. Here, we could hypothesize that NSUN2 could be crucial for the stabilization of particular mRNA transcripts as MII oocytes progress through the maternal - zygotic transition. NSUN2 deficiency may well be the cause of some key mRNA transcripts being degraded.

In conclusion, our findings revealed important insights that explain the compromised developmental competence of embryos made from IVM COC by conventional IVM technology. The DGE analysis, most importantly IVM COC vs. IVO, revealed significant differences in "actively" translated transcripts related to cell cycle regulation, chromosome organisation, protein synthesis and energy production. However, the sole effect of the cumulus cells contribution could not be addressed by comparing IVM COC vs. IVM DO, because the IVM DO were matured without gonadotropin supplementation. The DGE analysis of IVM DO vs. IVO did demonstrate that the clinical rescue IVM approach, where IVM DO are utilized, could impact similar actively translated transcripts, particularly related to cell cycle regulation, chromosome organisation and energy production. Moreover, the DGE analysis of pronuclear zygotes, IMZ *vs.* IVZ, from the respective fertilized oocytes revealed that IVM coupled with IVF compromises IMZ RNA metabolism, cell cycle regulation, chromosome organisation as well as spindle assembly. In summary, our findings confirm the inferiority of conventional IVM technology versus the IVO approach, and pinpointed the compromised biological processes in MII oocytes and pronuclear zygotes employed in the critical translational regulation processes for meiotic maturation and the achievement of developmental competence.

Materials & Methods

Isolation and maturation of mouse oocytes

8-week-old female ICR mice bred in-house (12 hrs day-night cycle) were stimulated with 5IU pregnant mare serum gonadotropin (PMSG) 46 hrs before sacrifice by cervical dislocation. Fully grown germinal vesicle stage oocytes were harvested as IVM DO or IVM COC by ovum pick-up in 0,1% (v/v) isobutylmetylxanthine (IBMX, ProSpec) supplemented transfer media. After washing in IBMX free transfer media, the collected DOs were transferred for *in vitro* maturation into aMEM (M0200, Merck) media supplemented with 4 g/L BioXtra BSA (A3311, Merck) with 280 mOsm/kg osmolality. COC maturation medium was additionally supplemented with 5 ng/mL rFSH (Gonal, Merck) and 5 ng/mL rhCG (Ovitrelle, Merck). MII oocytes with an extruded 1st polar body were collected after 10 hrs of *in vitro* culture following nuclear envelope breakdown (NEBD).

8-week-old female ICR mice destined for *in vivo* oocyte collection were stimulated with 5 IU PMSG 46 hrs prior to the administration of 5 IU rhCG (Ovitrelle, Merck). *In vivo* oocytes (IVO) were collected from isolated ovaries by ovum pick-up 11 hrs post rhCG application. Collected IVM COC and IVO oocytes were denuded prior to freezing by 15-min treatment in media supplemented with 20 ug/mL hyaluronidase (H3506, Merck) for 15 min followed by mechanical denudation. Samples designed for SSP profiling were incubated for 10 minutes in culture media supplemented with 0.1 g/L cycloheximide prior to freezing at -80°C.

Scarce Sample Profiling

Cycloheximide-treated samples (200 oocytes or zygotes/sample) collected in quadruplicates and stored at -80°C were subjected to SSP profiling (22). All sample handling was performed on ice. Briefly, cells were lysed in 350 µl of polysome extraction buffer containing 1% (v/v) Triton X-100, RNAse inhibitor (Ribolock, Thermo), and protease inhibitor cocktail (Complete EDTA-free, Roche). To ensure complete disruption of the zona pellucida, zirconia-silica beads were added to tubes containing samples. Prepared samples were loaded into a mixer mill (MM301, Retsch GmbH) and shaken 3 times for 1 min at 30 Hz with intermittent cooling on ice. Meanwhile, a sucrose gradient (10 – 50%) was prepared in SW55Ti tubes (Beckman Coulter) in a Gradient Master 108 ™ (BioComp) from individual 10% and 50% sucrose solutions containing the same components as the lysis buffer, except for the Triton X-100. Sample lysates were cleared by centrifugation at 10 000x g, 4°C for 10 min. The supernatants were loaded onto the prepared sucrose gradients and subjected to ultracentrifugation at 45 000 RPM, 4°C for 65 min in an Optima L-90 ultracentrifuge (Beckman Coulter). The ultracentrifugation samples were then fractionated into 10 equal fractions by pumping 60% sucrose solution into SW55Ti tubes with the fractionated samples. The absorbance of the outlet was continuously monitored with a UA-5 detector and UV absorbance reader (Teledyne, ISCO) to determine the beginning and the end of the fractionation process. The overall quality of polysome profiling was monitored by the parallel fractionation of HEK293 cell lysate. The fractionation profile itself was determined by qPCR.

RNA isolation and qPCR

Each fraction was collected into a 2-ml tube containing 1 µl of GenElute LPA (56575, Merck). Immediately after fractionation, 900 µl of TRI Reagent (T9424, Merck) was added into each tube followed by 3 min of vortexing, then 350 µl of chloroform was added and again vortexed vigorously for 3 min. After centrifugation for 10 min at 13 000 RPM, 4°C the upper phase was transferred into a new tube and mixed with an equal volume of 100% ice-cold isopropanol. After overnight precipitation at -20°C, samples were centrifuged for 40 min at 13 000 RPM, 4°C. The supernatant was

removed, and the pellet was washed with 1 ml of 75% (v/v) ice-cold ethanol. Samples were vortexed briefly and centrifuged for 5 min at 13 000 RPM, 4°C. After repeated ethanol washes, the sample pellet was quickly air-dried and resuspended in 12 µl of RNAse-free water. 2 µl of isolated RNA were used for cDNA synthesis to backtrack polysome profiles.

cDNA was synthesized from total RNA with a qPCRBIO cDNA synthesis kit containing a mix of oligo dT and random primers (PCR Biosystems) according to the manufacturer's protocol. For 18S and 28S rRNA qPCR, 5 ul of LightCycler480® SYBR Green I Master mix (Roche) was mixed with 2 µL of cDNA and 2 ul of the respective 2,5uM gene-specific primer pair (Supp. Table 1) in a total reaction volume of 10 µL. Each reaction was performed in triplicates. For the absolute quantification, recombinant pCR™4-Topo™ plasmids (Invitrogen) containing 18S and 28S rRNA amplicons were prepared to calculate a standard curve.

Library preparation & NGS RNA sequencing

Quadruplicate samples were pooled into non-polysomal (NP; fractions 1-5) and polysomal (P; fractions 6-10) samples, and accompanied by an unfractionated total RNA sample (T). RNA was dissolved in RNAse-free water at a minimal concentration of 250 pg total RNA per sample. Sample Quality Assessment was performed with a RNA 6000 Pico Chip (Agilent) using a Bioanalyzer 2100 instrument (Agilent). cDNA libraries were prepared with a SMARTer Stranded Total RNA-Seq Kit v2 Kit - Pico Input Mammalian (Takara Bio) according to the manufacturer's instructions. Library quantification was performed using a Qubit™ DNA HS Assay Kit (Thermo). To perform cDNA library QC, the pre-sequencing of libraries was done in an iSeq 100 (Illumina) with the following settings (number of reads: 4 million, 150 bp read length, base call quality > Q30). The NGS RNA-seq was done on NovaSeq 6000 (Illumina) in an S4 Flow Cell with the following settings (number of reads/sample: 100 million; 150 bp read length, Paired End). The output sequencing data were in FASTQ format.

Bioinformatic analysis

Reads were quality checked with FastQC (v. 0.11.9) followed by read alignment to the mouse genome (build GRCm39); transcript quantification and the detection of probable gene fusions was performed with the DRAGEN (Dynamic Read Analysis for GENomics) Bio-IT Platform (Illumina) RNA pipeline (3.7.5). Further RNA-Seq, PCA, DGE and GO analyses were performed with the software CLC Genomics Workbench 22.0.1 (Qiagen). Transcripts with a cutoff at 0.2 RPKM were considered in the DGE analysis.

Western blot

MII oocytes and pronuclear embryos were lysed with 6 µl of Millipore H_2O and 2.5 µl of 4X NuPAGE Lysis buffer (NP007, Thermo), and 1 µl reduction buffer (NP 0004, Thermo) at 100 °C for 5 min. Lysates were separated using a 4–12% gradient precast SDS-PAGE gels (NP323BOX, Life Technologies) and transferred to a PVDF membrane (Immobilon-P, Merck) with a semidry blotting system (TurboBlot, BioRad). Membranes were blocked for 1 h in a blocking buffer (Azure Biosystems) or if needed in 5% BSA diluted in Tween-Tris- buffer saline (TTBS, pH 7.4). Membranes were incubated at 4°C overnight in primary antibodies diluted at an optimized ratio. After the 3×10 min wash in TTBS buffer, membranes were incubated for 1 h in a secondary antibody HRP peroxidase conjugated anti-rabbit produced in donkey (711-035-152, Jackson Immunoresearch) at 1:10 000 in TTBS for 1 hr at room temperature. The specific antibody signal was visualized by chemiluminescent ECL reagent (Amersham, Cytiva). Signal detection was performed on Azure 600 (Azure Biosystems). Signal quantification was done with AzureSpot software 2.1 (Azure Biosystems).

In vitro fertilization

Motile sperm was collected from the cauda epididymis of 12-month-old ICR mouse males by needle puncture. Sperm capacitation for 1 hr as well as subsequent IVF was performed under IVF-grade paraffin oil (Vitrolife) in 100 µL of equilibrated HTF medium (Merck) supplemented with 4 g/L BioXtra BSA (A3311, Merck) and 1mM BioXtra GSH (G6529, Merck) 30 min before the IVF; matured MII oocytes were added into the HTF media. The IVF itself was performed by adding 4 µL of capacitated motile sperm to the HTF media containing IVM DO MII oocytes. After 4 hours of co-culture with capacitated sperm, zygotes were transferred into 100 µL of equilibrated fresh advanced KSOM medium (MR-101-D, Merck) under IVF grade paraffin oil (Vitrolife) for an additional 4 hrs. Next, pronuclear zygotes with both maternal and paternal pronuclei present were selected and washed three times in transfer medium and once in PVA/PBS medium prior to freezing at -80°C.

Immunofluorescent labelling

For protein visualization, oocytes and embryos were fixed for 15 min in 4% PFA (Merck) in PBS. Fixed oocytes were permeabilized in 0.1% Triton X-100 for 10 min, washed in PBS supplemented with PVA (Merck) and then incubated with primary antibodies overnight at 4 °C (Supp. Table 2). Oocytes were then washed 3X for 15 min in PVA/PBS, and the detection of primary antibodies was performed using relevant Alexa Fluor 488 or 647 conjugates (Invitrogen) diluted 1:500 and incubated for 1 h at room temperature. Washed oocytes (3X 15 min in PVA/PBS) were subsequently mounted on a slide in Vectashield Mounting Medium containing DAPI (Vector Laboratories) and solidified for at least an hour prior to imaging in a Leica SP5 confocal microscope (Leica). Images were processed with LasX software (Leica).

Live cell imaging

Oocyte *in vitro* maturation and early embryo development was live-cell imaged (LCI) in a DMI 6000B epi-fluorescent microscope (Leica) in a controlled and humidified atmosphere at 37°C, 5% CO_2. LCI was performed in a 30 µL drop of respective media overlaid with 800 µL of an IVF-grade paraffin oil (Ovoil, Vitrolife) in a 4-well chamber (Sarstedt). The chamber with media and oil was preheated and equilibrated over 4 hours prior to introducing experimental samples. Oocytes and embryos were imaged every 10 minutes (bright-field imaging) or shortly before and after the first polar body extrusion under green fluorescence (SiR-tubulin, SC002, Spirochrome).

Gap-junctional assay

Calcein-acetoxymethyl ester (AM) dye (56496, Merck) 1 mM-stock solution was freshly prepared in 0.1% DMSO. The respective matured oocytes were incubated in culture media with 1 µM Calcein-AM for 25 minutes to facilitate dye exchange between oocytes and cumulus cells and to allow time for the conversion of non-fluorescent Calcein-AM to fluorescent Calcein (permeable only via gap junctions) by intracellular esterases. After the incubation, oocytes were washed 3X in Transfer media and immediately imaged in the DMI 6000B epi-fluorescent microscope (Leica) using a filter for green fluorescence.

Mitotracker labelling

Matured oocytes were incubated in freshly prepared media (M0200, Merck) supplemented with 4 g/L BioXtra BSA (A3311, Merck) and 100 nM Mt-CMXRos for 30 minutes. After a quick wash in transfer medium (TM), oocytes were transferred into pre-warmed 4% paraformaldehyde and incubated at room temperature for 30 min. After three consecutive washes in PVA/PBS buffer, oocytes were mounted in Vectashield HardSet mounting medium with DAPI (Vector Laboratories) and hardened for 1 hr prior to imaging. Images were acquired in a TCS SP5 confocal microscope (Leica) with a DPSS 561 nm laser.

Radioactive methionine labelling

In order to determine *de novo* protein synthesis in MII oocytes and pronuclear zygotes cultured *in vitro* and *in vivo*, the ^{35}S-methionine incorporation assay was applied according to a previously published approach (53). Briefly, after maturation in the respective culture conditions, samples were denuded by treatment with 6 ug/ml hyaluronidase for 15 minutes if applicable and treated with 25 µCi/ml of ^{35}S-methionine (Hartmann analytics) for 1 hour. After incubation, samples were washed in polyvinylalcohol (PVA)-supplemented phosphate-buffered saline (PBS) and stored for Western

blotting at -80°C. Following the SDS-PAGE Western blotting protocol as described above, samples were transferred to the PVDF membrane (Immobilon-P, Merck) by semidry transfer for 25 min at 5 mA/cm^2 (TurboBlot, BioRad). Blotted radioactive samples were then exposed in a cassette with a FujiFilm autoradiographical membrane for 7 days. The signal was recorded with a BAS-2500 Photo Scanner (FujiFilm Life Sciences) and quantified with the software ImageJ. Normalization between samples was done using GAPDH.

Statistics

The software Prism (GraphPad, 9.5.1.) was employed for statistical analyses. Differences between multiple variables were assessed by either one- or two-way ANOVA test. Differences between two groups were assessed by paired or unpaired t-test. Statistically significant values ($p<0.05$) are indicated by an asterisk.

Acknowledgement & Funding statement

We wish to thank Dr. Helena Fulkova for advice on IVF; Jaroslava Supolikova and Marketa Hancova for technical assistance; and the Institute for Applied Biotechnologies in Olomouc for their help with NGS RNA-seq processing. This work was supported by the Czech Grant Agency (22-27301S), the Charles University Grant Agency (project No. 372621),
MSMT (EXCELLENCECZ.02.1.01/0.0/0.0/15_003/0000460 OP RDE) and Institutional Research Concept RVO67985904.

Data availability statement

The data discussed in this publication have been deposited in NCBI's Gene Expression Omnibus and are accessible through GEO Series accession number GSE241633 (https://www.ncbi.nlm.nih.gov/geo/query/acc.cgi?acc=GSE241633)

Ethics approval statement

Legal permission for animal experimentation (no. MZE-24154/2021-18134) was obtained from the Ministry of Agriculture of the Czech Republic.

Conflict of interest disclosure

I hereby declare that all authors of this manuscript have no financial/commercial conflict of interest.

References

1. Donahue RP. Maturation of the mouse oocyte in vitro. I. Sequence and timing of nuclear progression. J Exp Zool [Internet]. 1968 [cited 2023 Mar 14];169(2):237–49. Available from: https://pubmed.ncbi.nlm.nih.gov/5750655/

2. Schroeder AC, Eppig JJ. The developmental capacity of mouse oocytes that matured spontaneously in vitro is normal. Dev Biol [Internet]. 1984 [cited 2023 Mar 14];102(2):493–7. Available from: https://pubmed.ncbi.nlm.nih.gov/6706011/

3. Merker HJ, Zimmermann B. Electron microscopic studies on the oocyte maturation in cultures of juvenile rat ovaries. Z Zellforsch Mikrosk Anat [Internet]. 1970 Sep [cited 2023 Mar 14];111(3):364–78. Available from: https://pubmed.ncbi.nlm.nih.gov/5495354/

4. Edwards RG. Maturation in vitro of human ovarian oöcytes. Lancet (London, England) [Internet]. 1965 Nov 6 [cited 2023 Mar 14];2(7419):926–9. Available from: https://pubmed.ncbi.nlm.nih.gov/4165802/

5. Zamboni L, Thompson RS, Smith DM. Fine Morphology of Human Oocyte Maturation In Vitro. Biol Reprod [Internet]. 1972 Dec 1 [cited 2023 Mar 14];7(3):425–57. Available from: https://academic.oup.com/biolreprod/article/7/3/425/2768762

6. Veeck LL, Wortham JWE, Witmyer J, Sandow BA, Acosta AA, Garcia JE, et al. Maturation and fertilization of morphologically immature human oocytes in a program of in vitro fertilization. Fertil Steril [Internet]. 1983 [cited 2023 Mar 14];39(5):594–602. Available from: https://pubmed.ncbi.nlm.nih.gov/6404659/

7. Fishel SB. Oocyte maturation and fertilization in vitro. Acta Eur Fertil [Internet]. 1985 [cited 2023 Mar 14];16(1):13–9. Available from: https://pubmed.ncbi.nlm.nih.gov/4013616/

8. Lefèvre B, Gougeon A, Testart J. In-vitro oocyte maturation: some questions concerning the initiation and prevention of this process in humans. Hum Reprod [Internet]. 1987 [cited 2023 Mar 14];2(6):495–7. Available from: https://pubmed.ncbi.nlm.nih.gov/3667906/

9. Madissoon E, Töhönen V, Vesterlund L, Katayama S, Unneberg P, Inzunza J, et al. Differences in Gene Expression between Mouse and Human for Dynamically Regulated Genes in Early Embryo. PLoS One [Internet]. 2014 Aug 4 [cited 2023 Mar 20];9(8). Available from: /pmc/articles/PMC4121084/

10. Ding T, Hardiman PJ, Petersen I, Wang FF, Qu F, Baio G. The prevalence of polycystic ovary

syndrome in reproductive-aged women of different ethnicity: a systematic review and meta-analysis. Oncotarget [Internet]. 2017 [cited 2023 Mar 15];8(56):96351–8. Available from: https://pubmed.ncbi.nlm.nih.gov/29221211/

11. Trounson A, Wood C, Kausche A. In vitro maturation and the fertilization and developmental competence of oocytes recovered from untreated polycystic ovarian patients. Fertil Steril [Internet]. 1994 [cited 2023 Mar 14];62(2):353–62. Available from: https://pubmed.ncbi.nlm.nih.gov/8034085/

12. Shalom-Paz E, Holzer H, Young Son W, Levin I, Tan SL, Almog B. PCOS patients can benefit from in vitro maturation (IVM) of oocytes. Eur J Obstet Gynecol Reprod Biol [Internet]. 2012 [cited 2023 Mar 20];165(1):53–6. Available from: https://pubmed.ncbi.nlm.nih.gov/22819571/

13. Nastri CO, Ferriani RA, Rocha IA, Martins WP. Ovarian hyperstimulation syndrome: pathophysiology and prevention. J Assist Reprod Genet [Internet]. 2010 Feb [cited 2023 Jun 26];27(2–3):121–8. Available from: https://pubmed.ncbi.nlm.nih.gov/20140640/

14. Pfeifer S, Butts S, Dumesic D, Fossum G, Gracia C, La Barbera A, et al. Prevention and treatment of moderate and severe ovarian hyperstimulation syndrome: a guideline. Fertil Steril [Internet]. 2016 Dec 1 [cited 2023 Mar 14];106(7):1634–47. Available from: https://pubmed.ncbi.nlm.nih.gov/27678032/

15. In vitro maturation: a committee opinion. Fertil Steril. 2021 Feb 1;115(2):298–304.

16. Lee HJ, Barad DH, Kushnir VA, Shohat-Tal A, Lazzaroni-Tealdi E, Wu YG, et al. Rescue in vitro maturation (IVM) of immature oocytes in stimulated cycles in women with low functional ovarian reserve (LFOR). Endocrine [Internet]. 2016 Apr 1 [cited 2023 Jun 26];52(1):165–71. Available from: https://pubmed.ncbi.nlm.nih.gov/26419849/

17. Coticchio G, Dal Canto M, Renzini MM, Guglielmo MC, Brambillasca F, Turchi D, et al. Oocyte maturation: Gamete-somatic cells interactions, meiotic resumption, cytoskeletal dynamics and cytoplasmic reorganization. Hum Reprod Update. 2014;21(4):427–54.

18. Sánchez F, Lolicato F, Romero S, De Vos M, Van Ranst H, Verheyen G, et al. An improved IVM method for cumulus-oocyte complexes from small follicles in polycystic ovary syndrome patients enhances oocyte competence and embryo yield. Hum Reprod. 2017;32(10):2056–68.

19. De Vos M, Grynberg M, Ho TM, Yuan Y, Albertini DF, Gilchrist RB. Perspectives on the development and future of oocyte IVM in clinical practice. J Assist Reprod Genet.

2021;38(6):1265–80.

20. Curtis D, Lehmann R, Zamore PD. Translational regulation in development. Cell [Internet]. 1995 Apr 21 [cited 2023 Mar 14];81(2):171–8. Available from: https://pubmed.ncbi.nlm.nih.gov/7736569/

21. De La Fuente R, Viveiros MM, Burns KH, Adashi EY, Matzuk MM, Eppig JJ. Major chromatin remodeling in the germinal vesicle (GV) of mammalian oocytes is dispensable for global transcriptional silencing but required for centromeric heterochromatin function. Dev Biol [Internet]. 2004 Nov 15 [cited 2023 Mar 14];275(2):447–58. Available from: https://pubmed.ncbi.nlm.nih.gov/15501230/

22. Masek T, Del Llano E, Gahurova L, Kubelka M, Susor A, Roucova K, et al. Identifying the Translatome of Mouse NEBD-Stage Oocytes via SSP-Profiling; A Novel Polysome Fractionation Method. Int J Mol Sci [Internet]. 2020 Feb 1 [cited 2022 Jun 17];21(4). Available from: https://pubmed.ncbi.nlm.nih.gov/32070012/

23. del Llano E, Masek T, Gahurova L, Pospisek M, Koncicka M, Jindrova A, et al. Age-related differences in the translational landscape of mammalian oocytes. Aging Cell [Internet]. 2020 Oct 1 [cited 2023 Mar 16];19(10). Available from: https://pubmed.ncbi.nlm.nih.gov/32951297/

24. del Llano E, Iyyappan R, Aleshkina D, Masek T, Dvoran M, Jiang Z, et al. SGK1 is essential for meiotic resumption in mammalian oocytes. Eur J Cell Biol [Internet]. 2022 Apr 1 [cited 2023 Jun 26];101(2). Available from: https://pubmed.ncbi.nlm.nih.gov/35240557/

25. Zhu L, Zhou T, Iyyappan R, Ming H, Dvoran M, Wang Y, et al. High-resolution ribosome profiling reveals translational selectivity for transcripts in bovine preimplantation embryo development. Development [Internet]. 2022 Nov 1 [cited 2023 Jun 26];149(21). Available from: https://pubmed.ncbi.nlm.nih.gov/36227586/

26. Blengini CS, Ibrahimian P, Vaskovicova M, Drutovic D, Solc P, Schindler K. Aurora kinase A is essential for meiosis in mouse oocytes. PLoS Genet [Internet]. 2021 Apr 26 [cited 2023 Apr 20];17(4). Available from: https://pubmed.ncbi.nlm.nih.gov/33901174/

27. Nabi D, Drechsler H, Pschirer J, Korn F, Schuler N, Diez S, et al. CENP-V is required for proper chromosome segregation through interaction with spindle microtubules in mouse oocytes. Nat Commun. 2021;12(1).

28. van der Reest J, Nardini Cecchino G, Haigis MC, Kordowitzki P. Mitochondria: Their relevance

during oocyte ageing. Ageing Res Rev [Internet]. 2021 Sep 1 [cited 2023 Jun 26];70. Available from: https://pubmed.ncbi.nlm.nih.gov/34091076/

29. Salehabadi M, Farimani M, Tavilani H, Ghorbani M, Poormonsefi F, Poorolajal J, et al. Association of G22A and A4223C ADA1 gene polymorphisms and ADA activity with PCOS. Syst Biol Reprod Med [Internet]. 2016 May 3 [cited 2023 Jun 26];62(3):213–22. Available from: https://pubmed.ncbi.nlm.nih.gov/26980102/

30. Van Haute L, Lee SY, McCann BJ, Powell CA, Bansal D, Vasiliauskaitė L, et al. NSUN2 introduces 5-methylcytosines in mammalian mitochondrial tRNAs. Nucleic Acids Res [Internet]. 2019 Sep 19 [cited 2023 Jun 26];47(16):8720–33. Available from: https://pubmed.ncbi.nlm.nih.gov/31276587/

31. Nanjappa DP, Babu N, Khanna-Gupta A, O'Donohue MF, Sips P, Chakraborty A. Poly (A)-specific ribonuclease (PARN): More than just "mRNA stock clearing." Life Sci [Internet]. 2021 Nov 15 [cited 2023 Jun 26];285. Available from: https://pubmed.ncbi.nlm.nih.gov/34520768/

32. Albertini DF. Prospects for new oocyte-based assisted reproduction in animals and humans. Reprod Fertil Dev [Internet]. 2019 Dec 2 [cited 2023 Jun 26];32(2):7–10. Available from: https://pubmed.ncbi.nlm.nih.gov/32188554/

33. Katz-Jaffe MG, McCallie BR, Preis KA, Filipovits J, Gardner DK. Transcriptome analysis of in vivo and in vitro matured bovine MII oocytes. Theriogenology. 2009;71(6):939–46.

34. Zhao ZH, Meng TG, Li A, Schatten H, Wang ZB, Sun QY. RNA-Seq transcriptome reveals different molecular responses during human and mouse oocyte maturation and fertilization. BMC Genomics [Internet]. 2020 Jul 10 [cited 2023 Jun 26];21(1). Available from: https://pubmed.ncbi.nlm.nih.gov/32650721/

35. Shuhaibar LC, Egbert JR, Norris RP, Lampe PD, Nikolaev VO, Thunemann M, et al. Intercellular signaling via cyclic GMP diffusion through gap junctions restarts meiosis in mouse ovarian follicles. Proc Natl Acad Sci U S A. 2015;112(17):5527–32.

36. Abbassi L, El-Hayek S, Carvalho KF, Wang W, Yang Q, Granados-Aparici S, et al. Epidermal growth factor receptor signaling uncouples germ cells from the somatic follicular compartment at ovulation. Nat Commun. 2021;12(1):1–13.

37. Macaulay AD, Gilbert I, Scantland S, Fournier E, Ashkar F, Bastien A, et al. Cumulus cell transcripts transit to the bovine oocyte in preparation for maturation. Biol Reprod [Internet]. 2016 Jan 1 [cited 2022 Sep 1];94(1):16–7. Available from:

https://academic.oup.com/biolreprod/article/94/1/16, 1-11/2434435

38. Han Y, Qu X, Chen X, Lv Y, Zhang Y, Jin Y. Effects of follicular fluid exosomes on in vitro maturation of porcine oocytes. Anim Biotechnol [Internet]. 2022 [cited 2023 Jun 26]; Available from: https://pubmed.ncbi.nlm.nih.gov/36036234/

39. Abe K ichiro, Funaya S, Tsukioka D, Kawamura M, Suzuki Y, Suzuki MG, et al. Minor zygotic gene activation is essential for mouse preimplantation development. Proc Natl Acad Sci U S A. 2018;115(29):E6780–8.

40. Rakha SI, Elmetwally MA, El-Sheikh Ali H, Balboula A, Mahmoud AM, Zaabel SM. Importance of Antioxidant Supplementation during In Vitro Maturation of Mammalian Oocytes. Vet Sci [Internet]. 2022 Aug 1 [cited 2023 Jun 26];9(8). Available from: https://pubmed.ncbi.nlm.nih.gov/36006354/

41. Qin H, Qu Y, Li R, Qiao J. In Vivo and In Vitro Matured Oocytes From Mice of Advanced Reproductive Age Exhibit Alternative Splicing Processes for Mitochondrial Oxidative Phosphorylation. Front Endocrinol (Lausanne) [Internet]. 2022 Jan 26 [cited 2023 Jun 26];13. Available from: https://pubmed.ncbi.nlm.nih.gov/35154017/

42. Wells D, Patrizio P. Gene expression profiling of human oocytes at different maturational stages and after in vitro maturation. Am J Obstet Gynecol [Internet]. 2008 [cited 2023 Jun 26];198(4):455.e1-455.e11. Available from: https://pubmed.ncbi.nlm.nih.gov/18395038/

43. Jones GM, Cram DS, Song B, Magli MC, Gianaroli L, Lacham-Kaplan O, et al. Gene expression profiling of human oocytes following in vivo or in vitro maturation. Hum Reprod [Internet]. 2008 [cited 2023 Jun 26];23(5):1138–44. Available from: https://pubmed.ncbi.nlm.nih.gov/18346995/

44. Borensztein M, Syx L, Servant N, Heard E. Transcriptome Profiling of Single Mouse Oocytes. Methods Mol Biol [Internet]. 2018 [cited 2023 Jun 26];1818:51–65. Available from: https://pubmed.ncbi.nlm.nih.gov/29961255/

45. Gao L, Jia G, Li A, Ma H, Huang Z, Zhu S, et al. RNA-Seq transcriptome profiling of mouse oocytes after in vitro maturation and/or vitrification. Sci Rep. 2017;7(1):1–10.

46. Lee AWT, Ng JKW, Liao J, Luk AC, Suen AHC, Chan TTH, et al. Single-cell RNA sequencing identifies molecular targets associated with poor in vitro maturation performance of oocytes collected from ovarian stimulation. Hum Reprod [Internet]. 2021 [cited 2023 Jun 26];36(7):1907–21. Available from: https://pubmed.ncbi.nlm.nih.gov/34052851/

47. Guo Y, Cai L, Liu X, Ma L, Zhang H, Wang B, et al. Single-Cell Quantitative Proteomic Analysis of Human Oocyte Maturation Revealed High Heterogeneity in In Vitro–Matured Oocytes. Mol Cell Proteomics [Internet]. 2022 Aug 1 [cited 2022 Aug 31];21(8):100267. Available from: https://linkinghub.elsevier.com/retrieve/pii/S1535947622000755

48. Tetkova A, Susor A, Kubelka M, Nemcova L, Jansova D, Dvoran M, et al. Follicle-stimulating hormone administration affects amino acid metabolism in mammalian oocytes†. Biol Reprod [Internet]. 2019 Oct 25 [cited 2022 Apr 28];101(4):719–32. Available from: https://pubmed.ncbi.nlm.nih.gov/31290535/

49. Wu T, Dong J, Fu J, Kuang Y, Chen B, Gu H, et al. The mechanism of acentrosomal spindle assembly in human oocytes. Science [Internet]. 2022 Nov 18 [cited 2023 Jun 26];378(6621). Available from: https://pubmed.ncbi.nlm.nih.gov/36395215/

50. Yuan J, Li M, Wei L, Yin S, Xiong B, Li S, et al. Astrin regulates meiotic spindle organization, spindle pole tethering and cell cycle progression in mouse oocytes. Cell Cycle. 2009;8(20):3384–95.

51. Yu Y, Dumollard R, Rossbach A, Lai FA, Swann K. Redistribution of mitochondria leads to bursts of ATP production during spontaneous mouse oocyte maturation. J Cell Physiol. 2010;224(3):672–80.

52. Liu M, Guo G, Qian P, Mu J, Lu B, He X, et al. 5-methylcytosine modification by Plasmodium NSUN2 stabilizes mRNA and mediates the development of gametocytes. Proc Natl Acad Sci U S A [Internet]. 2022 Mar 1 [cited 2023 Jun 26];119(9). Available from: https://pubmed.ncbi.nlm.nih.gov/35210361/

53. Šušor A, Jelínková L, Karabínová P, Torner H, Tomek W, Kovářová H, et al. Regulation of cap-dependent translation initiation in the early stage porcine parthenotes. Mol Reprod Dev [Internet]. 2008 Dec [cited 2023 Aug 4];75(12):1716–25. Available from: https://pubmed.ncbi.nlm.nih.gov/18386287/

Table of contents

Since protein synthesis is a key driver of oocyte and embryo development, we assessed mouse oocyte and zygote translation in clinically relevant *in vitro* and *in vivo* maturation conditions.

Our findings uncovered differences in the selective translational recruitment of stored maternal transcripts related to critical molecular pathways that lead to decreased oocyte quality and compromise its developmental potential.

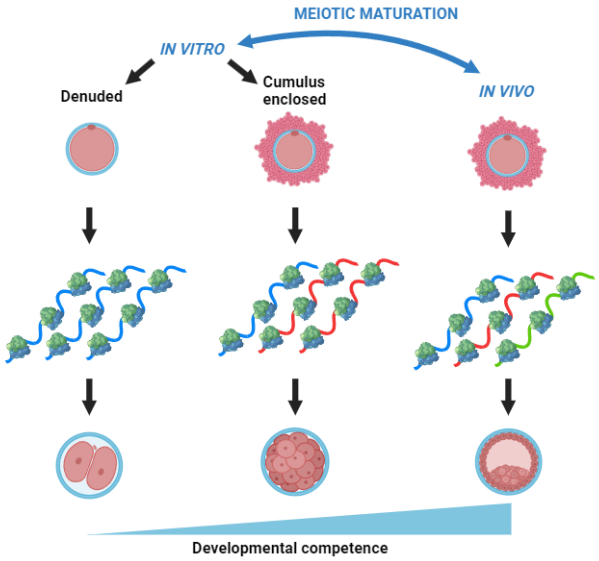

Figure legends

Fig. 1 Mouse model comparing *in vitro* maturation of denuded, cumulus-enclosed oocytes and pronuclear zygotes with respect to *in vivo* conditions.

The scheme of collected sample variants for the SSP profiling and total transcriptome analysis. GV oocytes were matured in vitro to the MII stage as denuded (IVM DO) or as cumulus-oocyte complexes in the presence of 0.075 IU/ml rFSH and 0.075 IU/ml rhCG (IVM COC). To simulate the conventional clinical IVM medium, the experimental IVM medium was enriched with amino acids, vitamins, and bovine serum albumin. Accordingly, pronuclear zygotes were generated by *in vitro* fertilization (IVF) of IVM DO (IMZ) or by 5 IU rhCG administration and male mating followed by collection of *in vivo* zygotes (IVZ) 20 hours later (related to Suppl. Figs. 1. and 2.)

Fig. 2 Transcriptome and translatome is significantly influenced in differentially derived oocytes and zygotes.

A. Differential expression analysis of mRNA from non-polysomal and polysomal fractions of SSP-profiles and total transcriptomes between *in vitro* denuded oocytes (IVM DO) and *in vivo* oocytes (IVO).

B. Differential expression analysis of mRNA from non-polysomal and polysomal fractions of SSP-profiles and total transcriptomes between *in vitro* cumulus-enclosed oocytes (IVM COC) and *in vivo* oocytes (IVO).

C. Differential expression analysis of mRNA from non-polysomal and polysomal fractions of SSP-profiles and total transcriptomes between *in vitro* denuded oocytes (IVM DO) and *in vitro* cumulus-enclosed oocytes (IVM COC).

D. Differential expression analysis of mRNA from non-polysomal and polysomal fractions of SSP-profiles and total transcriptomes between pronuclear zygotes generated by *in vitro* fertilization of IVM DO (IMZ) and *in vivo* by hCG administration and mating (IVZ).

Max group means (RPKM >= 0.2) vs. log2 fold change (log2FC) (>=1) from RNA-seq data analysis.

See Suppl. Figs. 4 – 6.

Fig. 3 Biological processes and cellular components are influenced by nature of the oocyte and zygote derivation.

A. Gene ontology (GO) analysis of differentially expressed polysome occupied transcripts (DET) from *in vitro* matured oocytes linked biological processes to energy production, DNA repair or cell cycle compared to *in vivo* conditions. *In vitro* matured cumulus-enclosed oocytes (IVM COCs) vs. *in vitro* matured denuded oocytes (IVM DO) showed highest significance compared to protein synthesis transcripts. See **Suppl. File 1.**

B. GO analysis of DET from *in vitro* matured oocytes. The most significant cellular components were linked to ribonucleoprotein complexes, chromosomes, mitochondria, etc., compared to *in vivo* conditions. See **Suppl. File 1.**

C. GO analysis of DET from IVM DO in vitro fertilized pronuclear zygotes (IMZ) linked biological processes to the cell cycle, RNA metabolism or spindle assembly checkpoint compared to *in vivo* conditions. See **Suppl. File 1.**

D. GO analysis of DET from IMZ linked cellular components to ribonucleoprotein complexes, chromosomes, splieceosomes or spindle compared to *in vivo* conditions. See **Suppl. File 1.**

See Suppl. Figs. 7 – 10.

Fig. 4 Actively translated mRNAs are employed in essential processes for oocyte and early embryo development.

A. Cell cycle regulation players *Aurka, Cenpv* show differential polysome occupancy in MII oocyte RNA-seq datasets. See **Supp. Fig. 7.**

B. Representative image from immunoblot (WB) analysis of AURKA and CENPV protein. GAPDH was used as a loading control.

C. Normalized densitometric values from WB analysis **B.** Data are presented as mean±s.d.; *P<0.1; **P<0.01 according to Student's *t*-test; from at least three independent experiments.

D. Mitochondrially-enconded mRNA transcripts from RNA-seq datasets involved in energy production exhibit higher polysomal/non-polysomal (P/NP) ratio between *in vivo* and *in vitro* oocytes, but not zygotes. Data are presented as the mean±s.d. of each mtRNA transcript P/NP ratio; *ns*, non-significant; ****P<0.0001 according to Student's *t*-test; from four independent experiments. See **Supp. Fig. 8.**

E. Energy production participant *Ada* exhibit differential polysome occupancy in RNA-seq datasets.

F. Representative image from immunoblot (WB) analysis of ADA protein. GAPDH was used as a loading control.

G. Normalized densitometric values from WB analysis. Data are presented as mean±s.d.; *P<0.1 according to Student's *t*-test; from three independent experiments.

H. **RNA metabolism** participants *Parn* and *Nsun2* exhibit differential polysome occupancy in pronuclear zygote based on RNA-seq datasets. See **Suppl. Fig. 9B.**

I. Representative image from immunoblot (WB) analysis of PARN & NSUN2 protein. TUBULIN was used as a loading control.

J. Normalized densitometric values from WB analysis **I.** Data are presented as mean±s.d.; *P<0.1, **P<0.01 according to Student's *t*-test; from three independent experiments.

For additional DET see Suppl. Figs 9-10

Fig. 5 The decrease in global protein synthesis in *in vitro* matured oocytes correlate with decreased developmental competency.

A. Comparison of *de novo* global protein synthesis via incorporation of ^{35}S-Methionine between *in vitro* denuded (IVM DO) and *in vivo* (IVO) matured oocytes;. cumulus-enclosed MII oocytes (IVM COC) and IVO;. IVM COC and IVM DO. Data are presented as the mean±s.d.; *ns*, non-significant, *P<0.1, **P<0.01 according to Student's *t*-test; three independent experiments.

B. Number of significantly enriched differentially expressed polysome occupied transcripts (DET) with fold change ≥ 2 in IVM DO *vs.* IVO, IVM COC *vs.* IVO; and IVM DO *vs.* IVM COC groups. Number of DET in IVO was set to 100%. Data are presented as the mean DET; **P<0.01, according to One-way ANOVA test; four independent experiments. See **Suppl. File 2.**

C. Comparison of *de novo* global protein synthesis via incorporation of ^{35}S-Methionine between *in vitro* fertilized (IMZ) and *in vivo* (IVZ) zygotes. Data are presented as the mean ± s.d.; *ns*, non-significant according to Student's *t*-test; from three independent experiments.

D. Significantly enriched differentially expressed polysome occupied transcripts (DET) (fold change ≥ 2) in IMZ *vs.* IVZ. The number of DET in IVZ was set to 100%. Data are presented as the mean DET; **P<0.01, according to One-way ANOVA test; from four independent experiments. See **Suppl. File 2.**

E. The IVF fertilization rates of IVM DO; *P<0.1, IVM COC; *P<0.1 and IVO. Data are presented as the mean±s.d.; *P<0.1, according to Student's *t*-test; from three independent experiments, *n*≥90.

F. Preimplantation development analysis of *in vitro* fertilized oocytes derived from IVM DO, IVM COC and IVO. Data are presented as the mean±s.d.; ****P<0.001 according to Two-way ANOVA test; from three independent experiments, *n*≥48.

Supplementary figure legends

Supp. Fig. 1 Analysis of quality and timing of oocyte samples.

A. Live cell imaging of spindle formation timing in *in vitro* matured denuded (IVM DO) MII oocytes by sir-tubulin staining (green) and bright-field. Data are representative of two independent experiments, *n*≥25. Scale bar, 20 µm.

B. Representative bright-field images of *in vitro* cumulus-oocyte complex (IVM COC) morphology at the onset (GV) and completion (MII) of *in vitro* maturation. Data are representative of three independent experiments, *n*≥30. Scale bar, 180 µm.

C. Immunocytochemical assessment (DAPI) of selected IVM COC for chromatin configuration upon collection from ovarian follicles. Fully-grown oocyte, surrounded nucleolus (SN) vs. growing oocyte, non-surrounded nucleolus (NSN). Data are presented as the mean±s.d., ****P<0.0001, according to Student's *t*-test; from two independent experiments, *n*≥29.

D. Time-lapse imaging assessment (bright field) of nuclear envelope breakdown (NEBD) timing and 1st polar body extrusion (PBE) in IVM DO and IVM COC samples. Data are presented as the mean±s.d.; ****P<0.0001, according to Student's *t*-test; from three independent experiments, *n*≥30

E. Representative bright-field images of PMSG-stimulated mouse ovary 11 hrs post hCG administration. Scale bar: 3 and 0,5 mm respectively.

F. Immunocytochemical (acetylated tubulin+DAPI) assessment of selected IVO MII with PBE for spindle configuration, i.e. oocyte nuclear maturation upon collection from ovarian follicles or infundibulum. Spindle morphology was categorized as dynamic (MII spindle is forming), matured (MII spindle was properly formed), aging (MII spindle became prolonged) and destabilized (MII spindle 2nd polar body was formed irrespective of fertilization). Data are presented as the mean±s.d.; from two independent experiments, *n*≥29

G. Assessment of gap-junctional permeability by gap junctional assay (Calcein AM, green) of *in vivo* oocyte maturation at 0 hrs (denuded), 5 hrs, 10 hrs and 20 hrs post hCG administration. Data are representative of two independent experiments, *n*≥20. Scale bar, 80 μm.

Supp. Fig. 2 Time from fertilization to zygote pronuclei NEBD is equal *in vitro* and *in vivo*.

A. Representative bright-field images of *in vitro* fertilized IVM DO (IMZ) and *in vivo* (IVZ) zygotes. Scale bar, 80 μm.

B. Timing of zygotic pronuclei NEBD with respect to fertilization. IMZ fertilization was set to 0 hrs. IVZ fertilization was set for 13 hrs post hCG administration assuming the presence of capacitated sperm in infundibulum. Data are presented as the mean±s.d.; *ns*, non-significant, according to Student's *t*-test; from two independent experiments, *n*≥46.

Supp. Fig. 3 Validation of ribosomal fractionation by Scarce sample profiling (SSP).

Quantitative PCR analysis of 18S and 28S rRNAs from each collected SSP fraction of *in vitro* matured denuded MII oocytes (IVM DO), *in vitro* matured cumulus-enclosed MII oocytes (IVM COC), *in vivo* oocytes (IVO), pronuclear zygotes *in vitro* fertilized IVM DO (IMZ) and *in vivo* pronuclear zygotes (IVZ). Presented as mean ± s.d.; from four independent experiments.

Supp. Fig. 4 Principal component analysis (PCA) of in vitro and in vivo conditions in unclear, however the difference between fractionated and total transcriptome is obvious.

A. PCA analysis of mRNA transcripts mapped against GRCm39 mouse genome reference from *in vitro* matured denuded MII oocytes (IVM DO), *in vitro* matured cumulus-enclosed MII oocytes (IVM COC) and *in vivo* oocytes (IVO). Analyzed RNA-seq data were sequenced from pooled non-polysomal fractions (NP), polysomal fractions (P) and total transcriptome (T). PCA analysis was performed with the software GraphPad Prism software (9.5.1).

B. PCA analysis of mRNA transcripts mapped against GRCm39 mouse genome reference from pronuclear zygotes *in vitro* fertilized IVM DO (IMZ) and *in vivo* pronuclear zygotes (IVZ). Analyzed RNA-seq data were sequenced from pooled non-polysomal fractions (NP), polysomal fractions (P) and total transcriptome (T). PCA analysis was performed with the software GraphPad Prism software (9.5.1).

Supp. Fig. 5 Oocyte samples shows absence of transcripts specific for cumulus cells.

Analysis of abundance of mRNAs coding for cumulus cell specific proteins AREG, EREG, BTC in RNA-seq datasets. NP, non-polysomal; P, polysomal; T, total transcriptome.

Supp. Fig. 6 Polysomal occupancy and total mRNA expression show low correlation.

A. Spearman's correlation of polysome occupied transcripts and total transcriptome; (RPKM >=0.2) of *in vitro* matured denuded MII oocytes (IVM DO); ρ=0.107), *in vitro* matured cumulus-enclosed MII oocytes (IVM COC); ρ=0.099 with respect to *in vivo* MII oocytes (IVO); ρ=0.107. Data are presented as the $\log_2$ fold change. The correlation was analyzed according to Spearmans correlation test; from four independent experiments

B. Spearman's correlation of polysome occupied transcripts and total transcriptome; (RPKM >=0.2) between pronuclear zygotes obtained by *in vitro* fertilization of IVM DO (IMZ) and *in vivo* pronuclear zygotes (IVZ); ρ=0.218). The correlation was analyzed according to Spearmans correlation test; from four independent experiments.

Supp. Fig. 7 Cell cycle related mRNAs with differential polysome occupancy.

A. Candidate mRNAs coding for cell cycle regulators with differential polysome occupancy in the oocyte samples.

B. Candidate mRNAs coding for cell cycle regulators with differential polysome occupancy in the zygote samples.

See Supp. File 1.

Supp. Fig. 8 Energy production related mRNAs with differential polysomal occupancy.

A. Candidate mRNAs coding for energy production components with differential polysome occupancy in the *in vitro* and the *in vivo* matured oocytes.

B. Heat map of relative polysome recruitment (non-polysomal fraction/polysome fraction ratio) for selected mt-mRNAs associated with energy production components

C. Heat map of relative abundancy of selected mt-mRNAs employed in energy production in transcriptome normalized to *in vivo* conditions (IVO).

D. Confocal image of Mitotracker CMXRos labelled mitochondria within *in vivo* matured and *in vitro* matured cumulus-oocyte complexes (denuded), respectively, with detail on mitochondrial clustering associated with increased ATP production. Scale bar, 20 µm.

See Suppl. File 1.

Supp. Fig. 9 Protein synthesis regulators & RNA metabolism related mRNAs with differential polysome occupancy.

A. Candidate mRNAs coding for RNA protein synthesis regulators with differential polysome occupancy in the oocyte samples.

B. Candidate mRNAs coding for RNA metabolism regulators with differential polysome occupancy in the zygote samples.

See Supp. File 1.

Supp. Fig. 10 DNA repair & Spindle Assembly Checkpoint related mRNAs with differential polysome occupancy.

A. Candidate mRNAs coding for DNA repair components with differential polysome occupancy in the oocyte samples.

B. Candidate mRNAs coding for Spindle Assembly Checkpoint components with differential polysome occupancy in the zygote samples.

See Supp. File 1.

Fig. 1

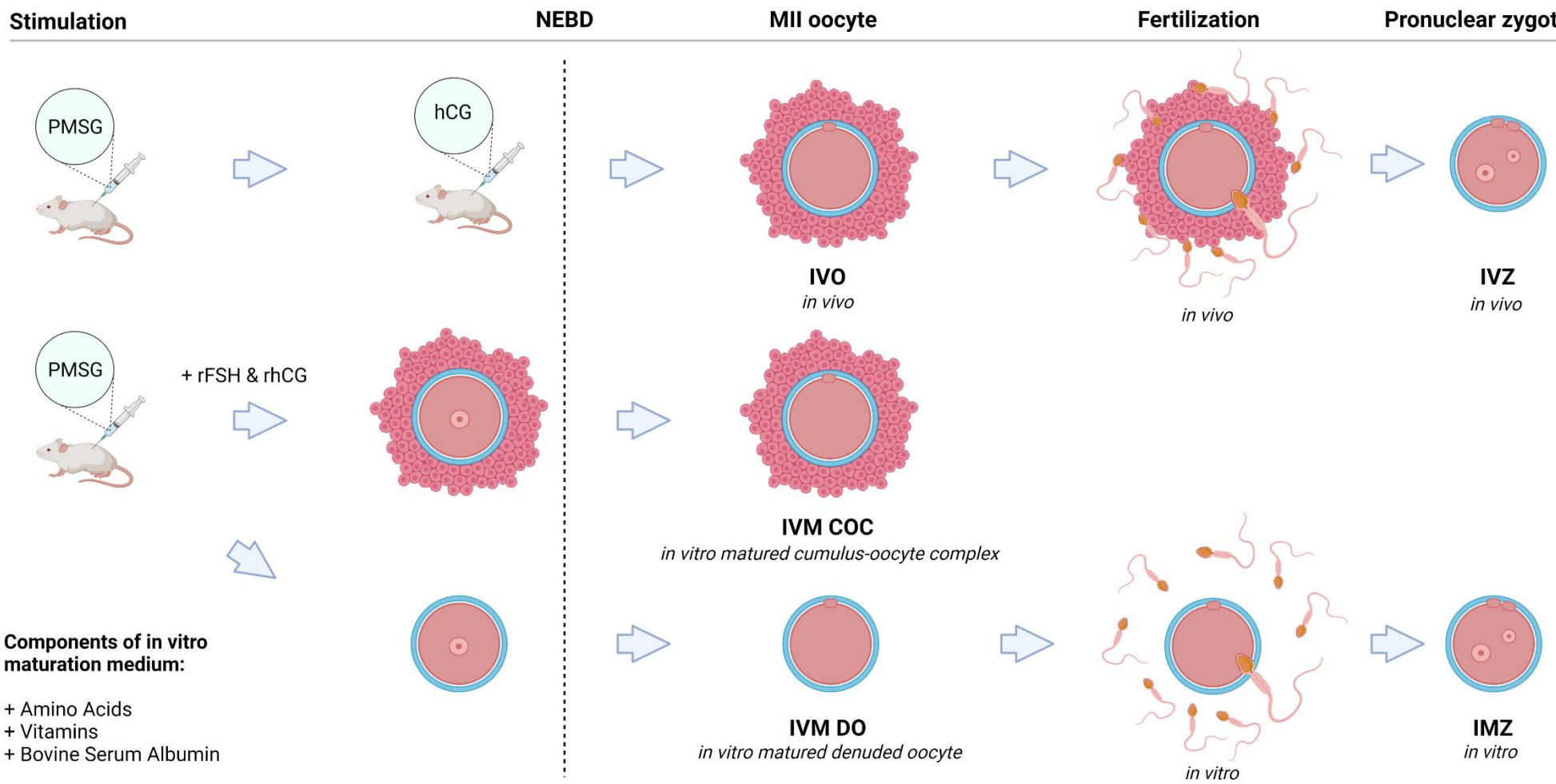
Stimulation
NEBD
MII oocyte
Fertilization
Pronuclear zygote
PMSG
hCG
IVO
in vivo
in vivo
IVZ
in vivo
PMSG
+ rFSH & rhCG
IVM COC
in vitro matured cumulus-oocyte complex
Components of in vitro maturation medium:
+ Amino Acids
+ Vitamins
+ Bovine Serum Albumin
IVM DO
in vitro matured denuded oocyte
in vitro
IMZ
in vitro

Fig. 2

A

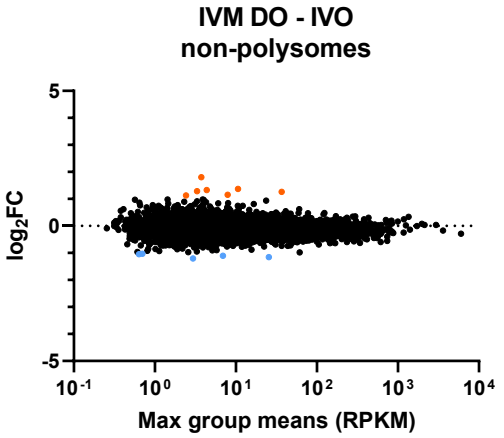

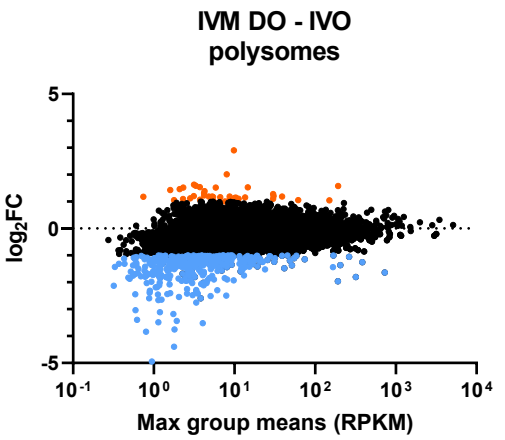

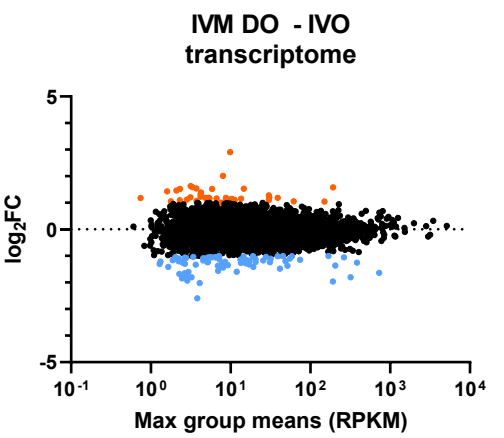

B

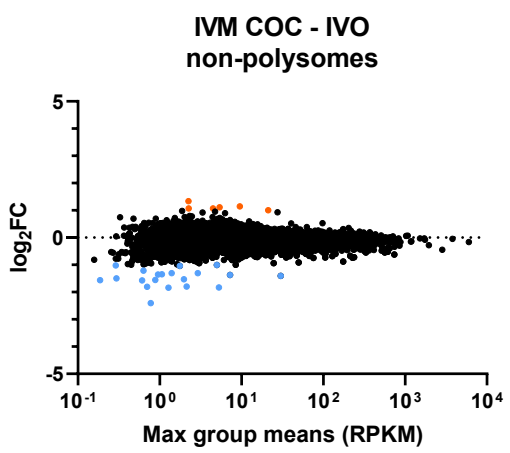

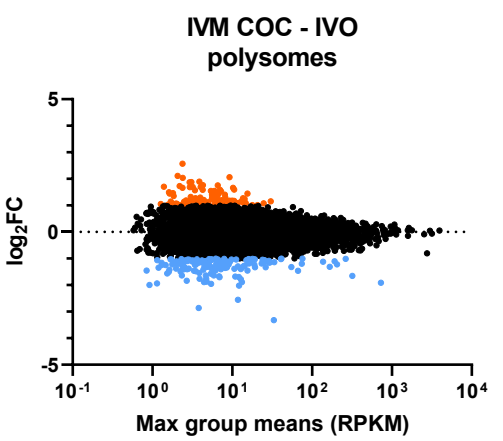

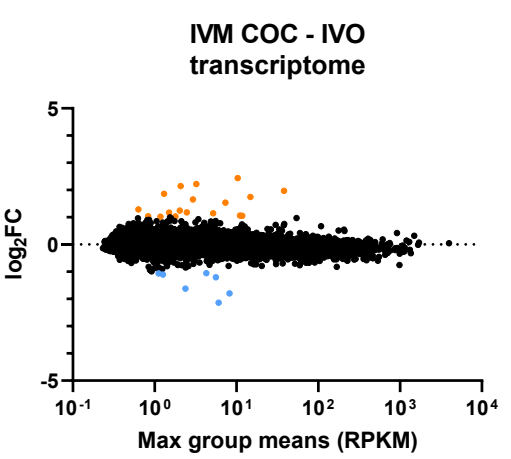

C

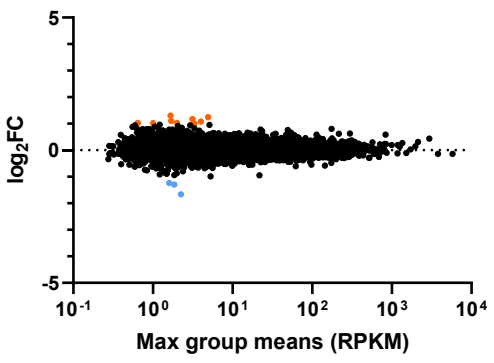

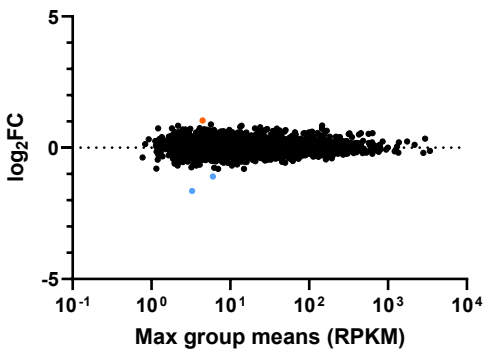

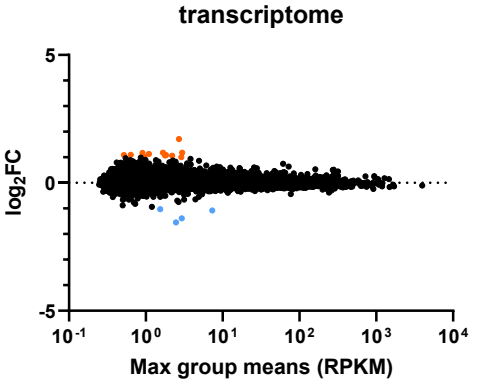

D

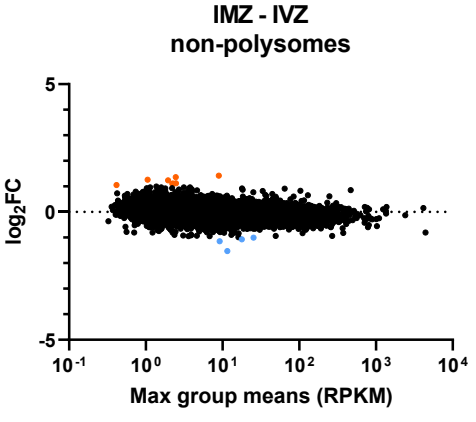

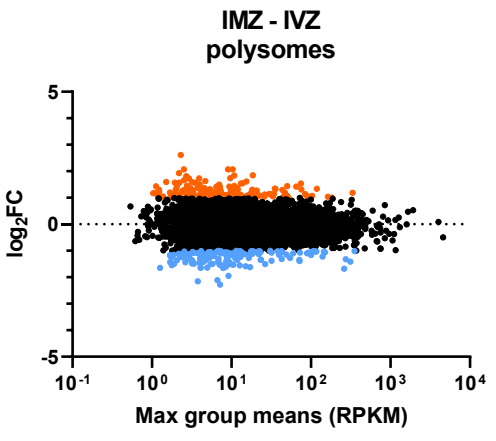

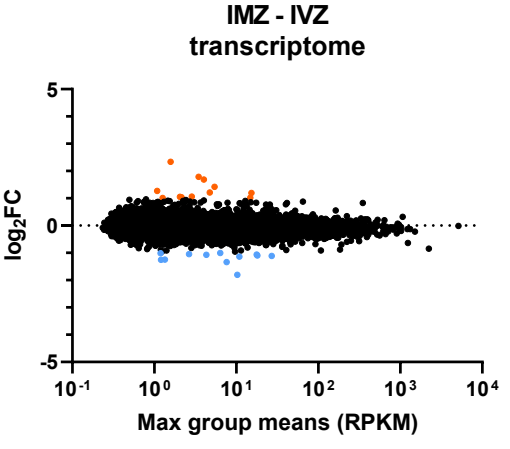

In colour: fold change >= 2 ; upregulated / downregulated

Fig. 3

A

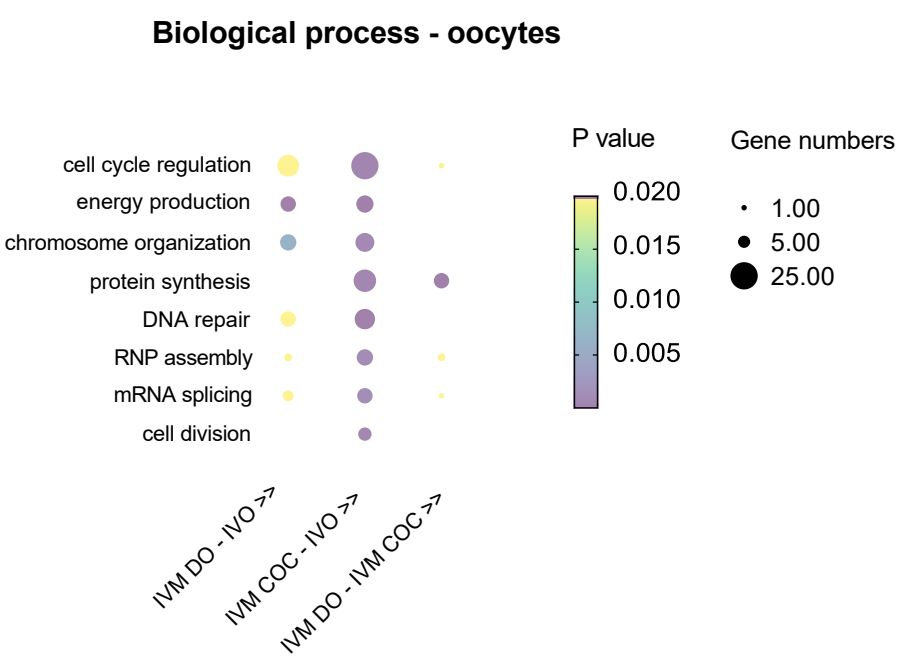
Biological process - oocytes
cell cycle regulation
energy production
chromosome organization
protein synthesis
DNA repair
RNP assembly
mRNA splicing
cell division
IVM DO - IVO >>
IVM COC - IVO >>
IVM DO - IVM COC >>
P value
0.020
0.015
0.010
0.005
Gene numbers
1.00
5.00
25.00

B

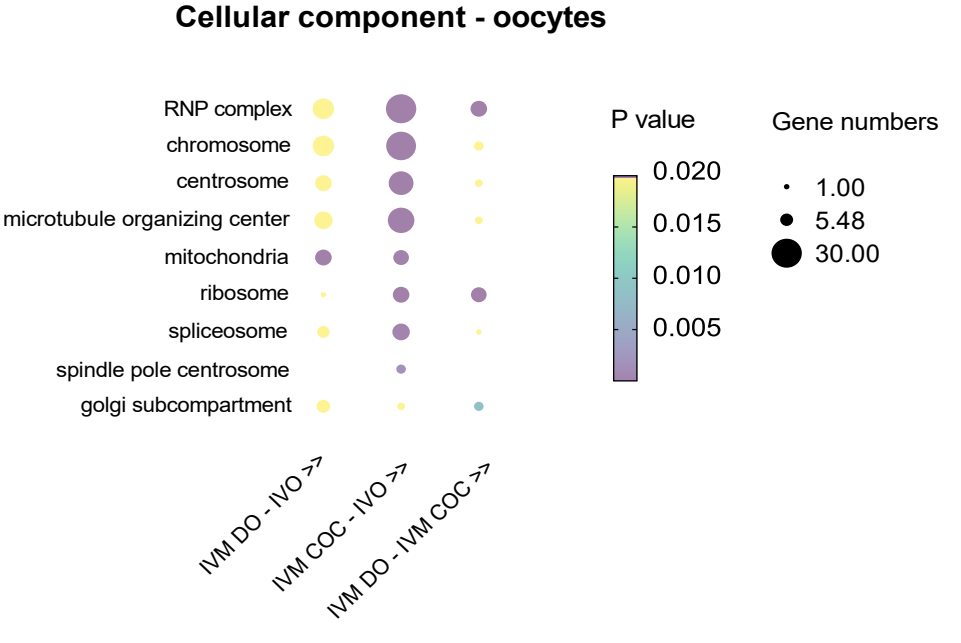
Cellular component - oocytes
RNP complex
chromosome
centrosome
microtubule organizing center
mitochondria
ribosome
spliceosome
spindle pole centrosome
golgi subcompartment
IVM DO - IVO >>
IVM COC - IVO >>
IVM DO - IVM COC >>
P value
0.020
0.015
0.010
0.005
Gene numbers
1.00
5.48
30.00

C

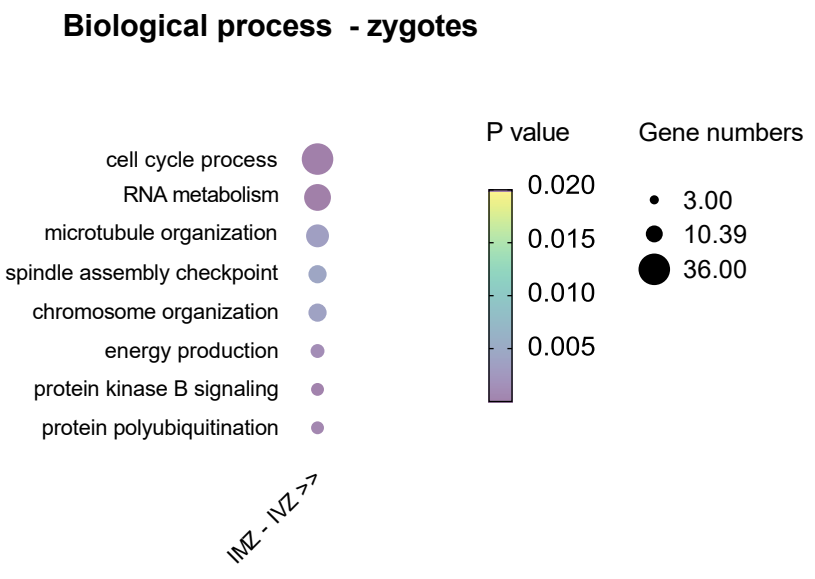
Biological process - zygotes
cell cycle process
RNA metabolism
microtubule organization
spindle assembly checkpoint
chromosome organization
energy production
protein kinase B signaling
protein polyubiquitination
IMZ - IVZ >>
P value
0.020
0.015
0.010
0.005
Gene numbers
3.00
10.39
36.00

D

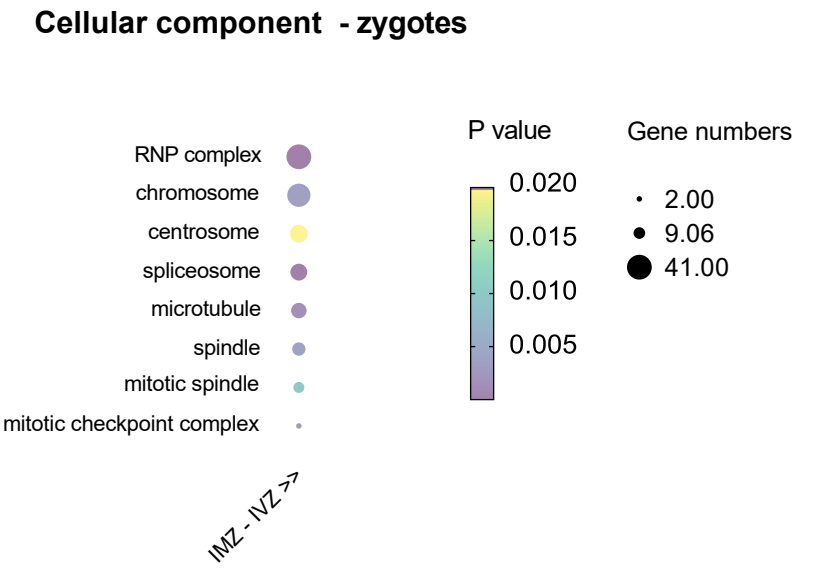
Cellular component - zygotes
RNP complex
chromosome
centrosome
spliceosome
microtubule
spindle
mitotic spindle
mitotic checkpoint complex
IMZ - IVZ >>
P value
0.020
0.015
0.010
0.005
Gene numbers
2.00
9.06
41.00

Fig. 4

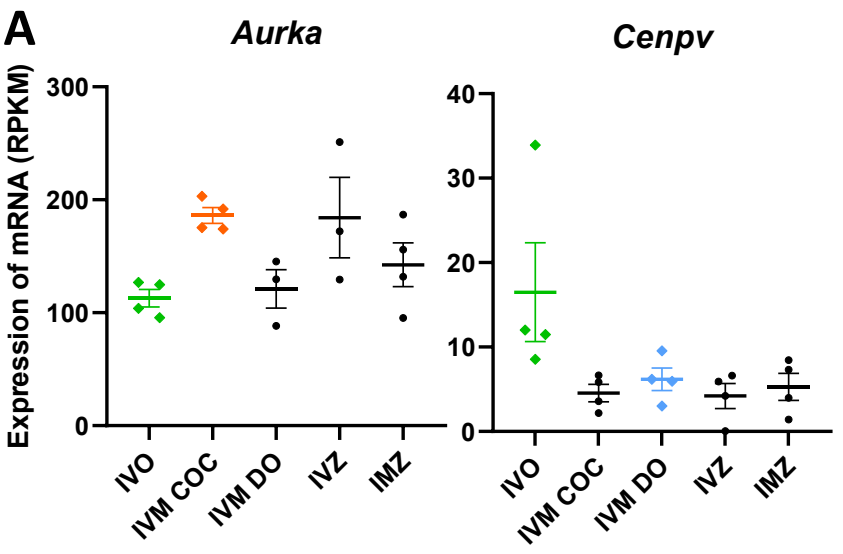
A
Aurka
Cenpv
Expression of mRNA (RPKM)
300
200
100
0
40
30
20
10
0
IVO
IVM COC
IVM DO
IVZ
IMZ

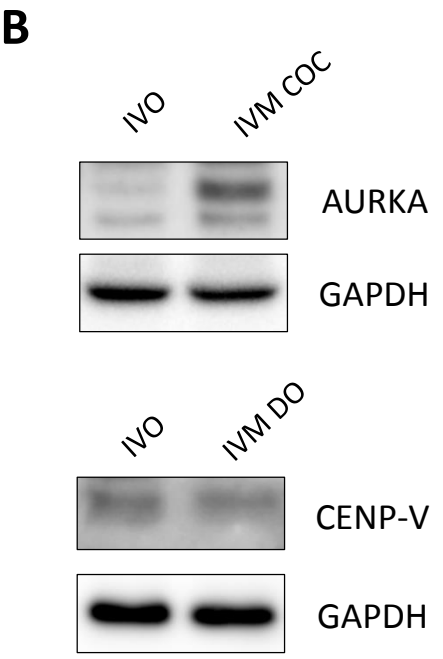
B
IVO
IVM COC
AURKA
GAPDH
IVO
IVM DO
CENP-V
GAPDH

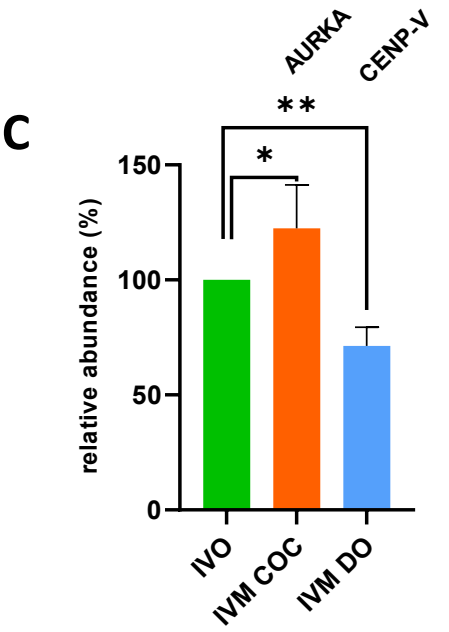
C
AURKA
CENP-V
**
*
relative abundance (%)
150
100
50
0
IVO
IVM COC
IVM DO

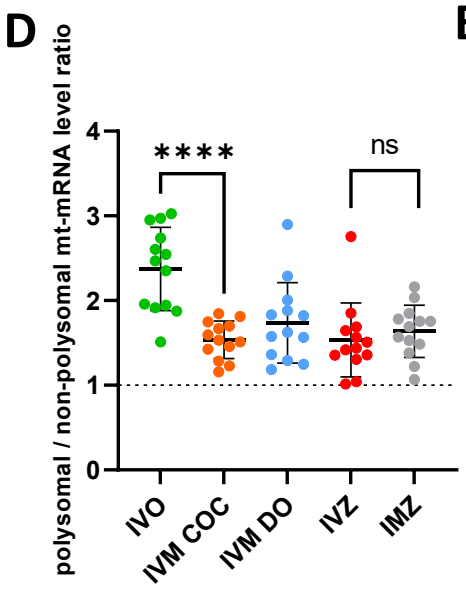
D
polysomal / non-polysomal mt-mRNA level ratio
4
3
2
1
0
****
ns
IVO
IVM COC
IVM DO
IVZ
IMZ

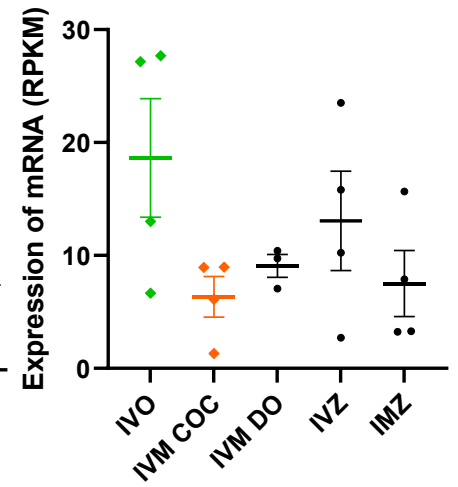
E
Ada
Expression of mRNA (RPKM)
30
20
10
0
IVO
IVM COC
IVM DO
IVZ
IMZ

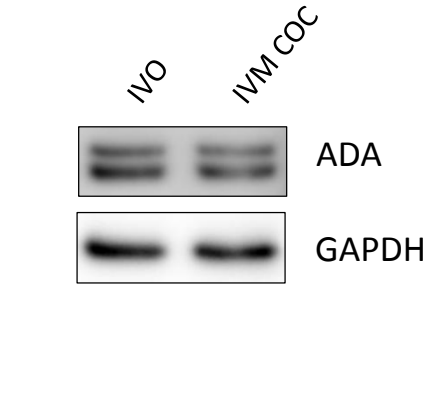
F
IVO
IVM COC
ADA
GAPDH

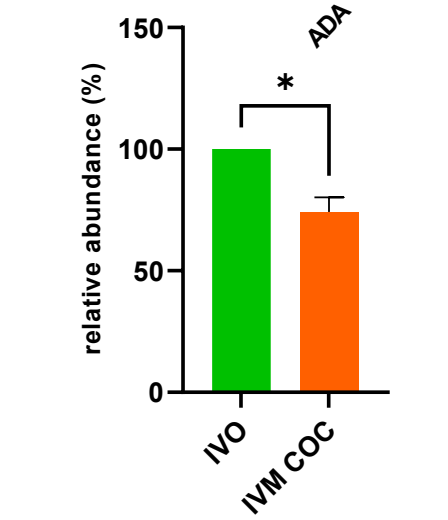
G
ADA
*
relative abundance (%)
150
100
50
0
IVO
IVM COC

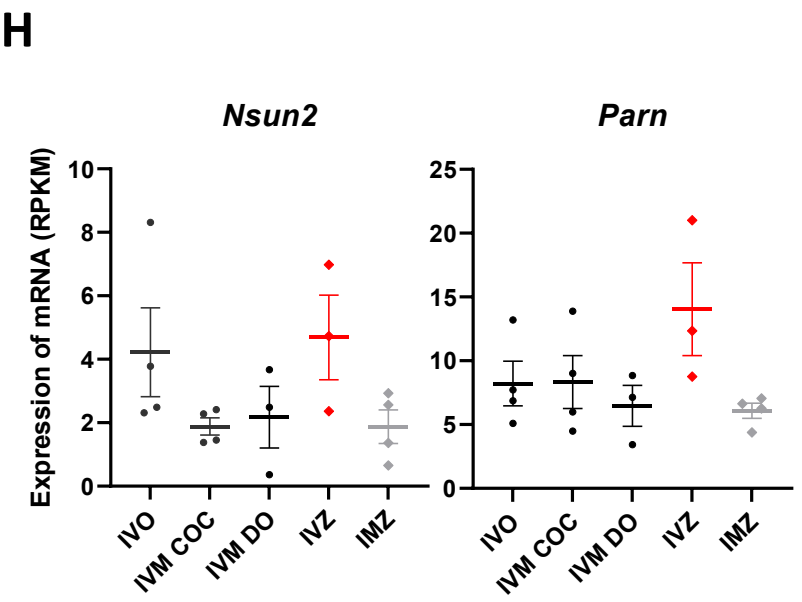
H
Nsun2
Parn
Expression of mRNA (RPKM)
10
8
6
4
2
0
25
20
15
10
5
0
IVO
IVM COC
IVM DO
IVZ
IMZ

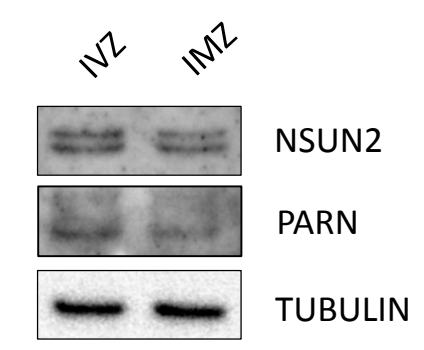
I
IVZ
IMZ
NSUN2
PARN
TUBULIN

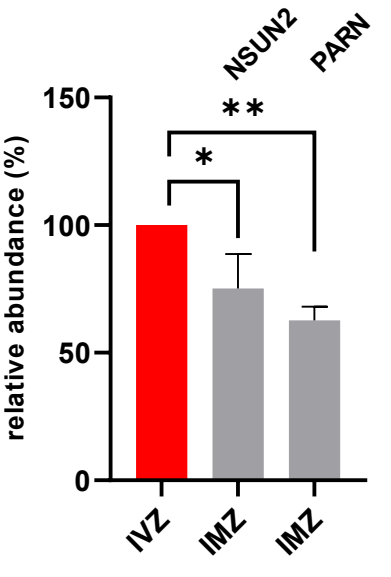
J
NSUN2
PARN
**
*
relative abundance (%)
150
100
50
0
IVZ
IMZ
IMZ

Fig. 5

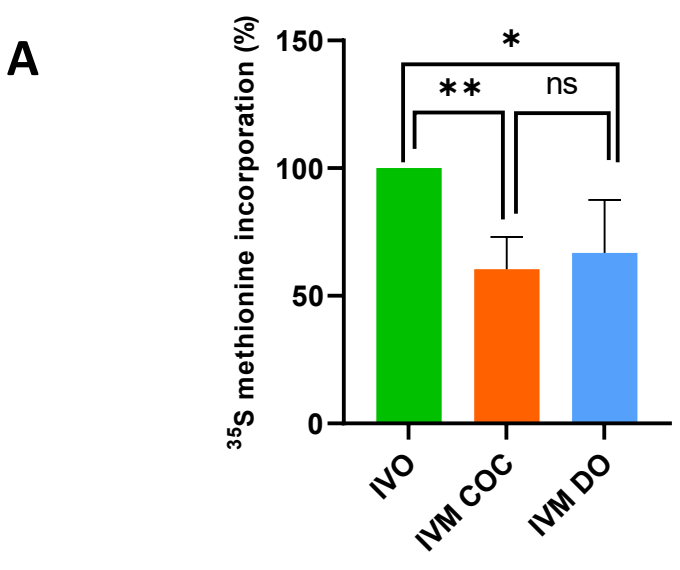
A
^{35}S methionine incorporation (%)
150
100
50
0
*
**
ns
IVO
IVM COC
IVM DO

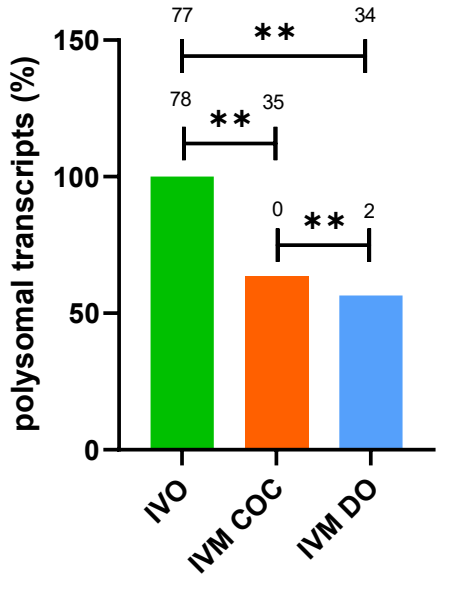
B
polysomal transcripts (%)
150
100
50
0
77
**
34
78
**
35
0
**
2
IVO
IVM COC
IVM DO

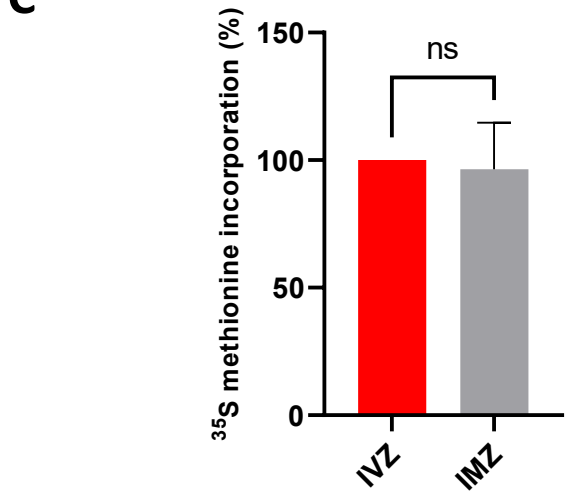
C
^{35}S methionine incorporation (%)
150
100
50
0
ns
IVZ
IMZ

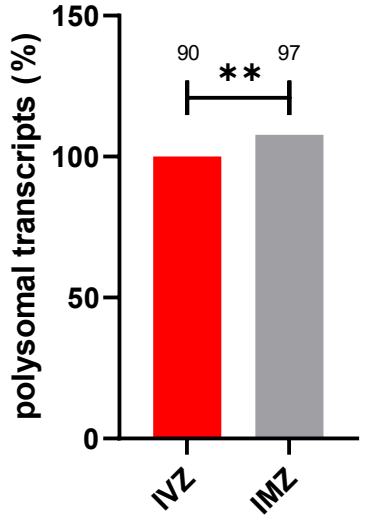
D
polysomal transcripts (%)
150
100
50
0
90
**
97
IVZ
IMZ

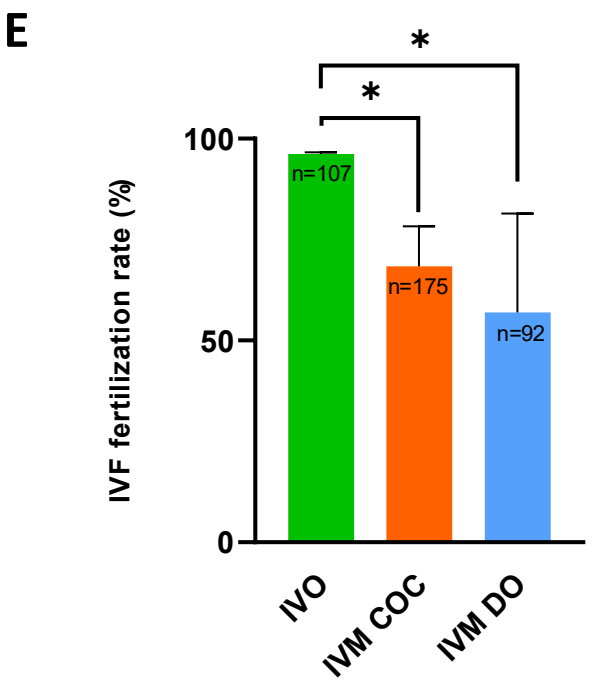
E
IVF fertilization rate (%)
100
50
0
*
*
n=107
n=175
n=92
IVO
IVM COC
IVM DO

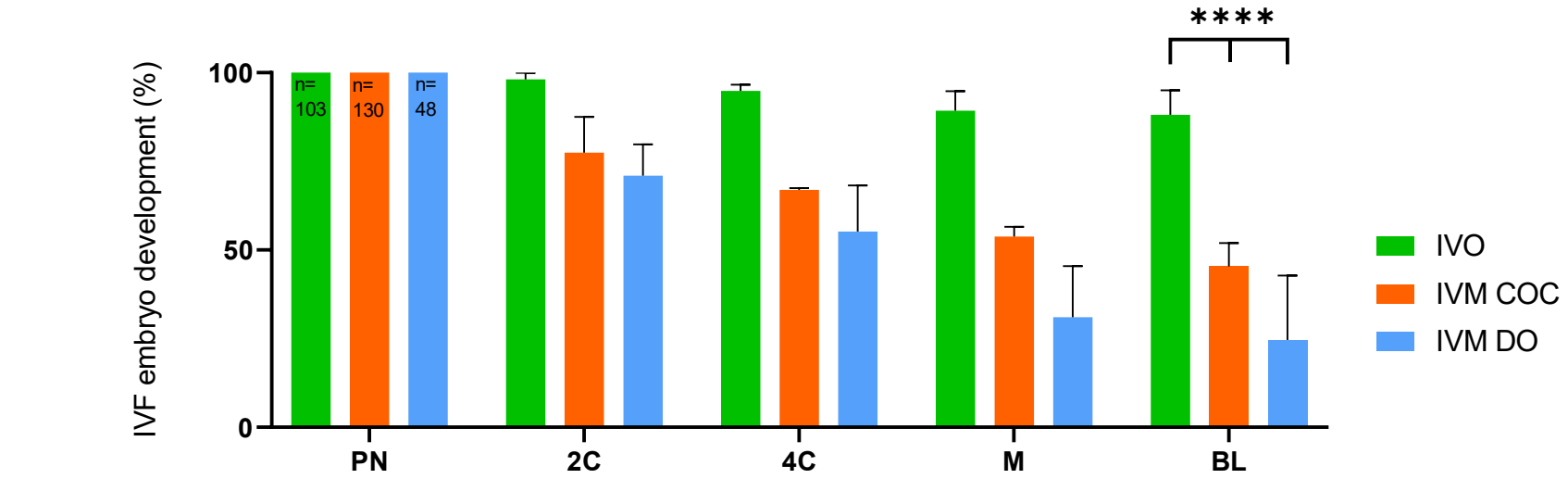
F
IVF embryo development (%)
100
50
0
****
n= 103
n= 130
n= 48
PN
2C
4C
M
BL
IVO
IVM COC
IVM DO

Supp. Fig. 1

A

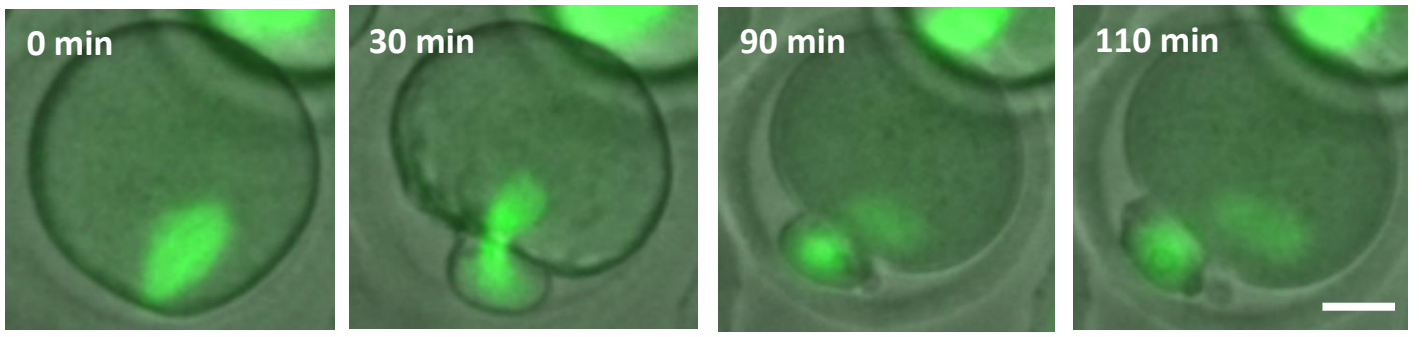

B

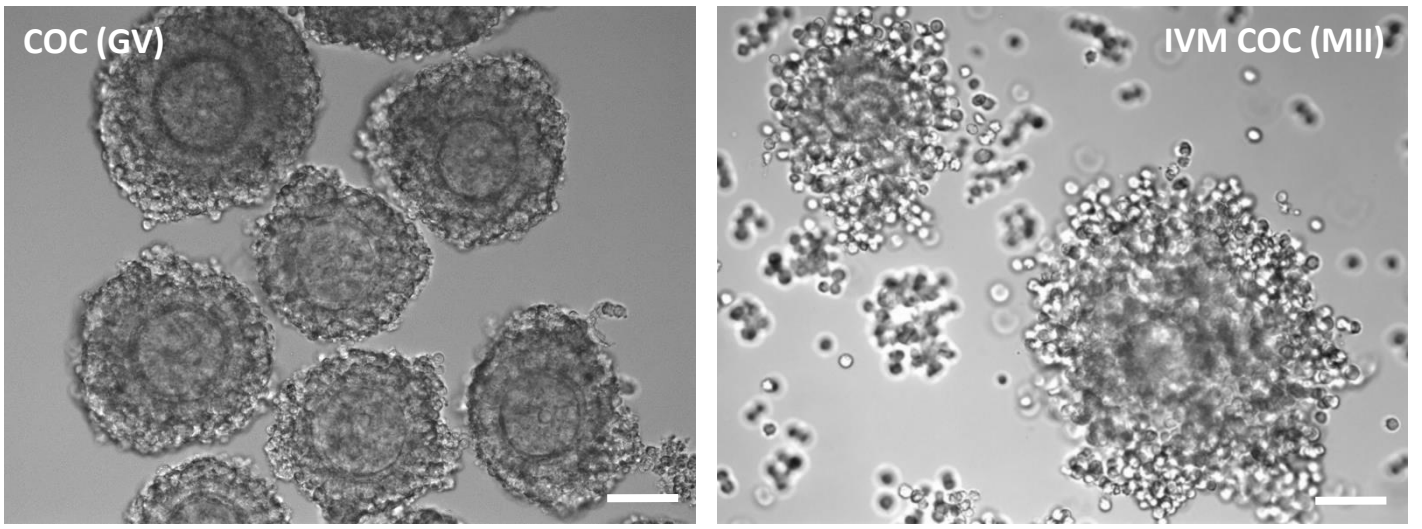

C

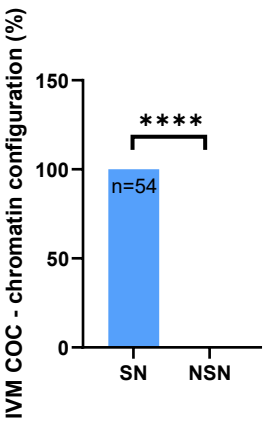

D

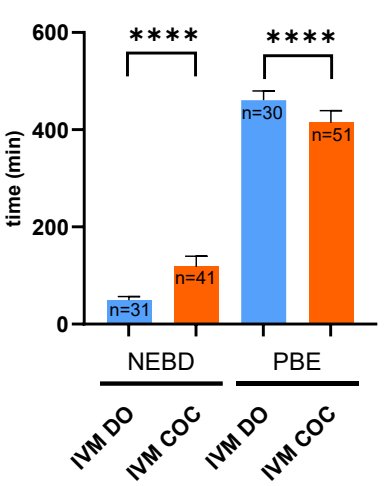

E

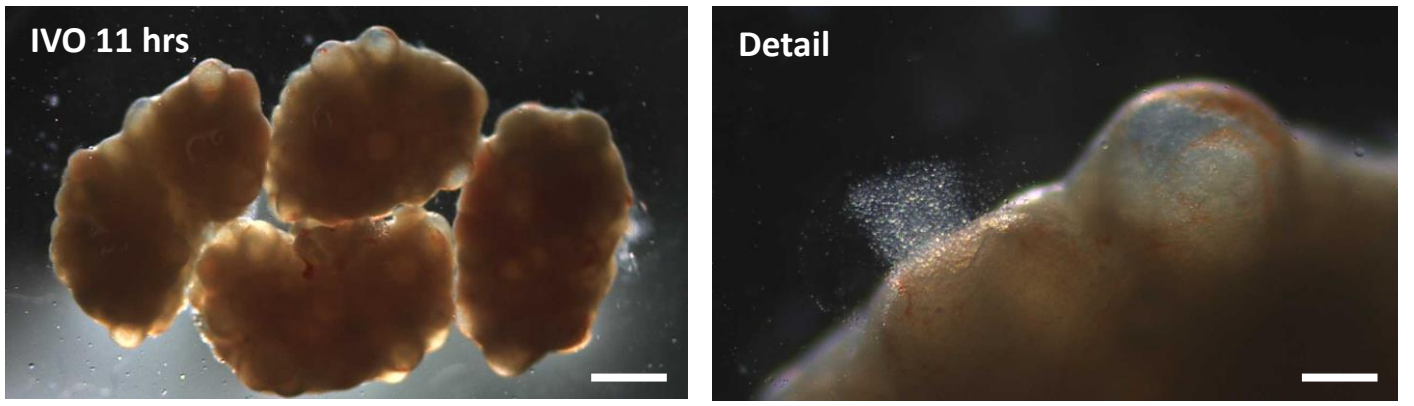

F

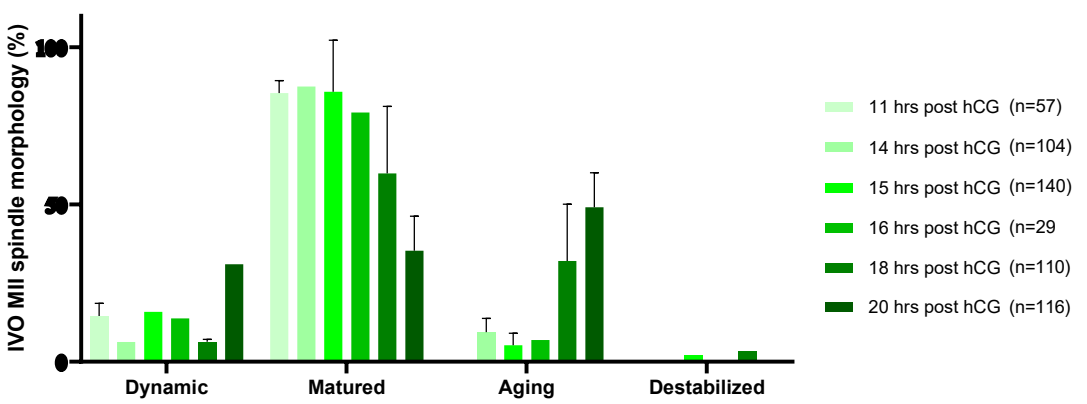

G

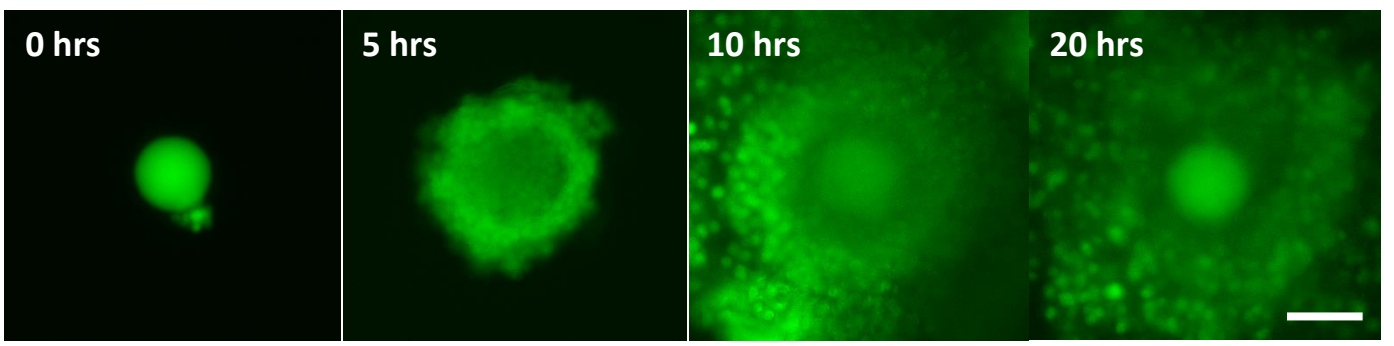

Suppl. Fig. 2

A

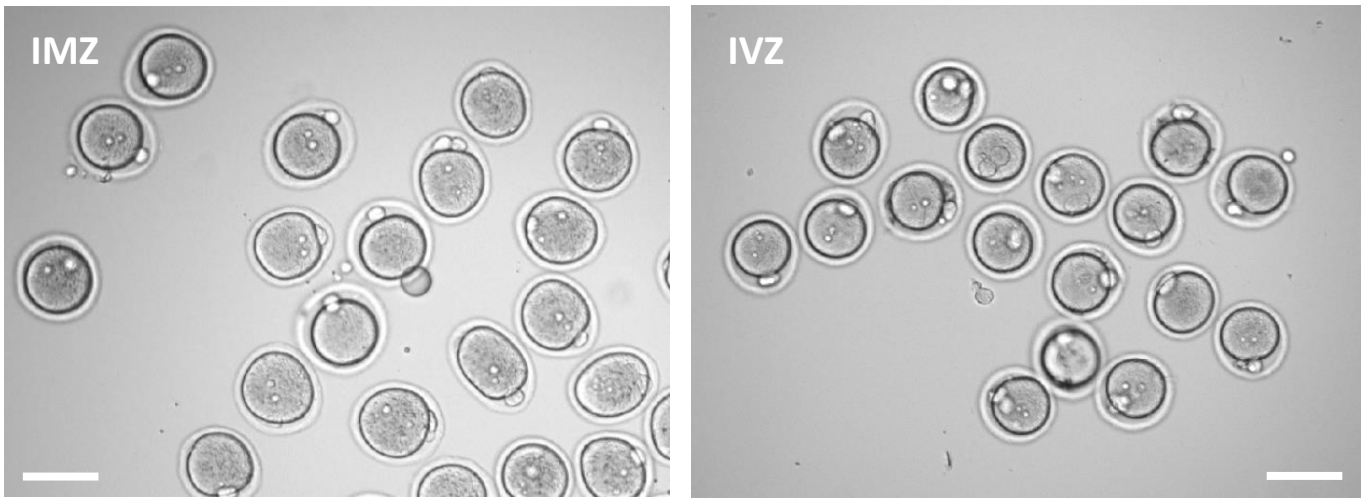

B

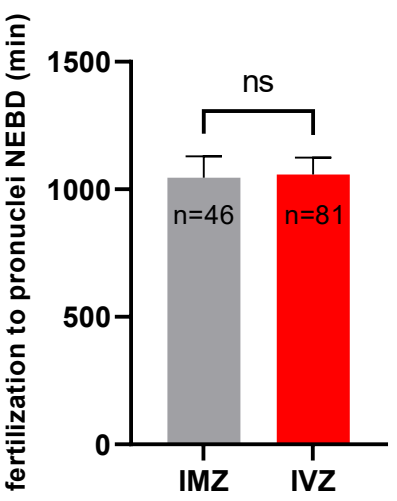

Supp. Fig. 3

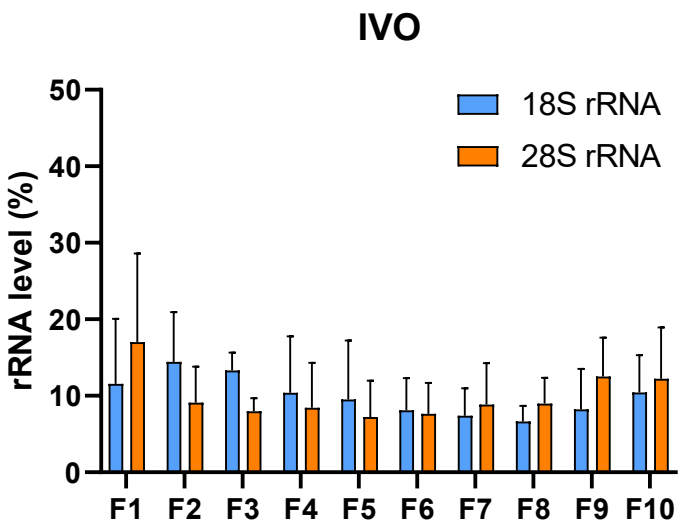
IVO
18S rRNA
28S rRNA
rRNA level (%)
0
10
20
30
40
50
F1 F2 F3 F4 F5 F6 F7 F8 F9 F10

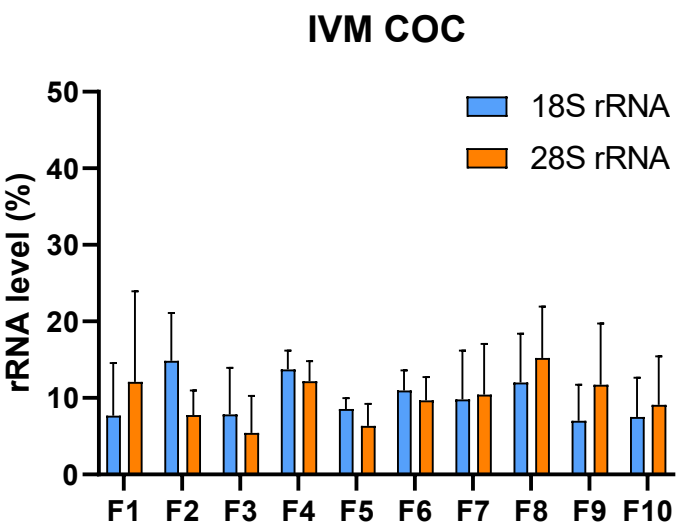
IVM COC
18S rRNA
28S rRNA
rRNA level (%)
0
10
20
30
40
50
F1 F2 F3 F4 F5 F6 F7 F8 F9 F10

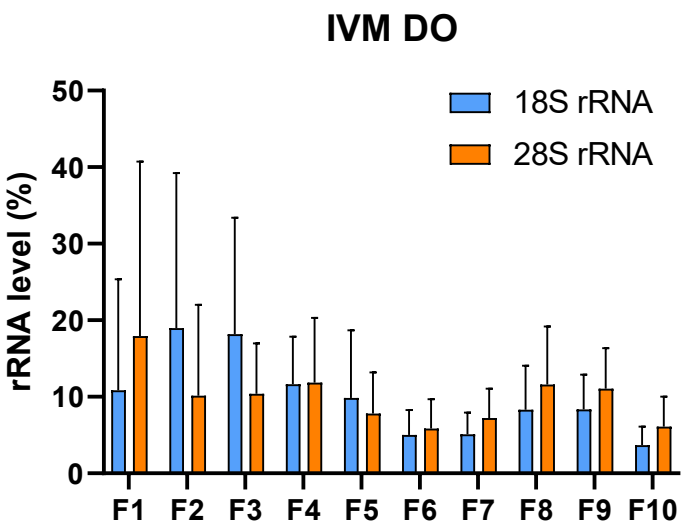
IVM DO
18S rRNA
28S rRNA
rRNA level (%)
0
10
20
30
40
50
F1 F2 F3 F4 F5 F6 F7 F8 F9 F10

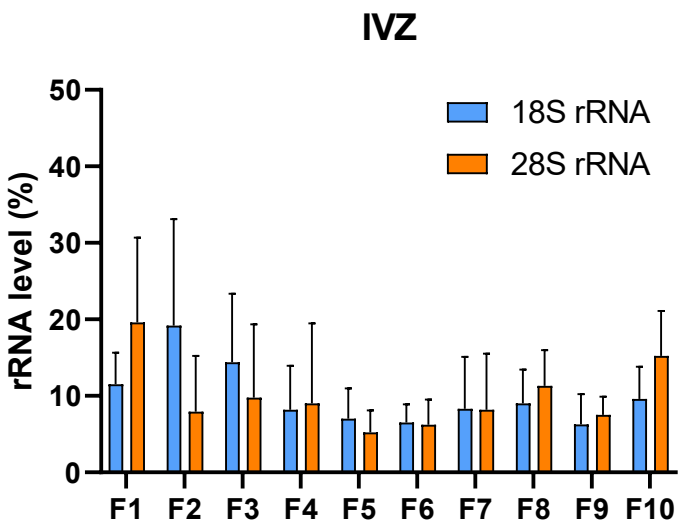
IVZ
18S rRNA
28S rRNA
rRNA level (%)
0
10
20
30
40
50
F1 F2 F3 F4 F5 F6 F7 F8 F9 F10

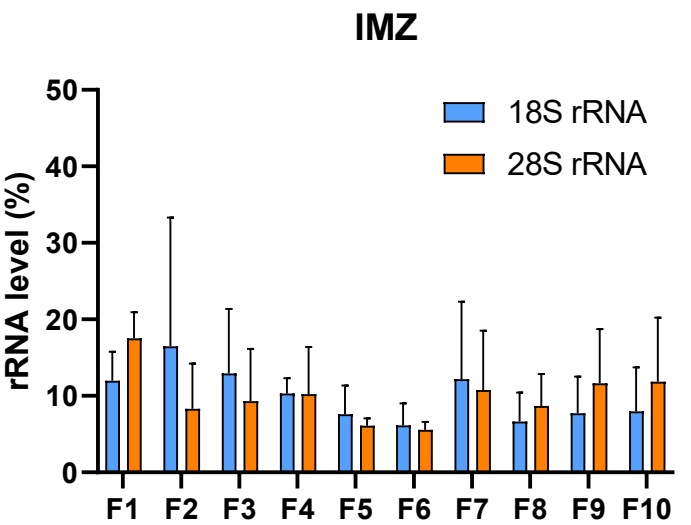
IMZ
18S rRNA
28S rRNA
rRNA level (%)
0
10
20
30
40
50
F1 F2 F3 F4 F5 F6 F7 F8 F9 F10

Supp. Fig. 4

A

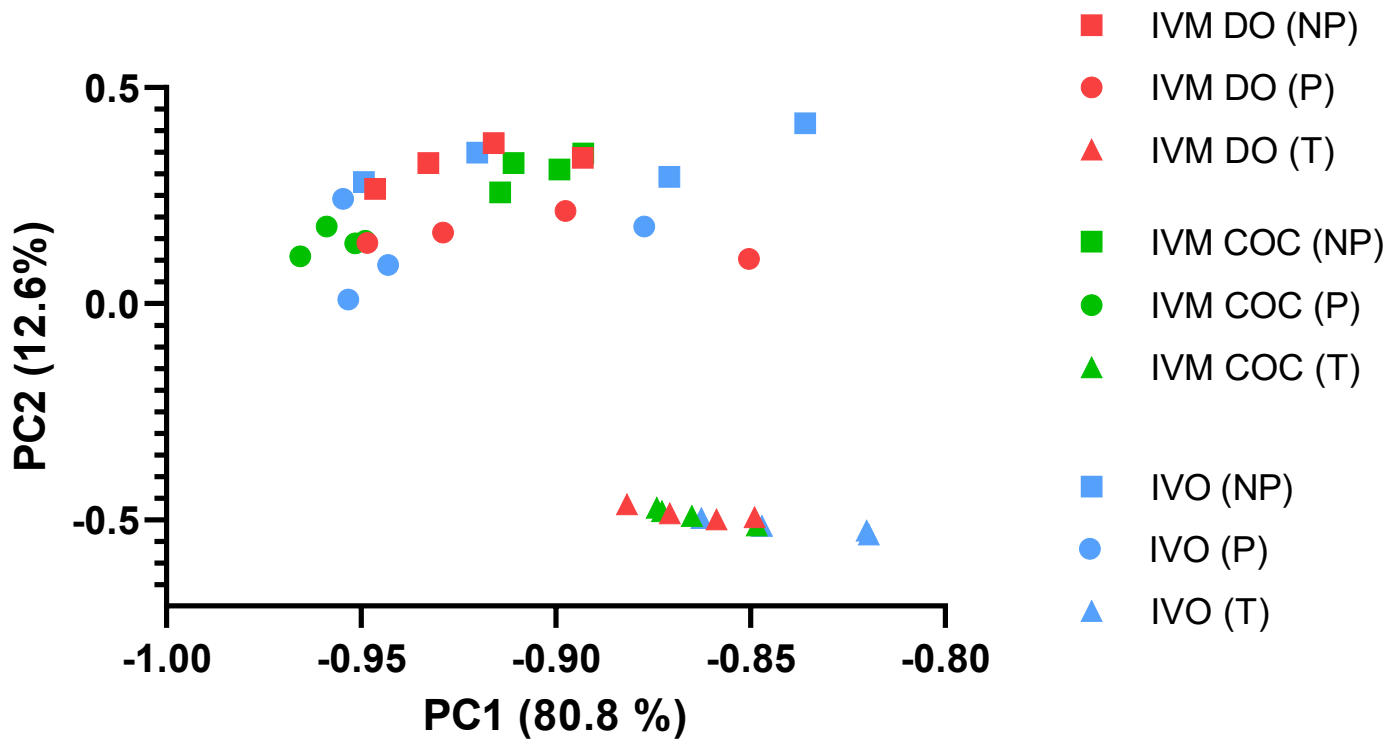
0.5
0.0
-0.5
PC2 (12.6%)
-1.00
-0.95
-0.90
-0.85
-0.80
PC1 (80.8 %)
IVM DO (NP)
IVM DO (P)
IVM DO (T)
IVM COC (NP)
IVM COC (P)
IVM COC (T)
IVO (NP)
IVO (P)
IVO (T)

B

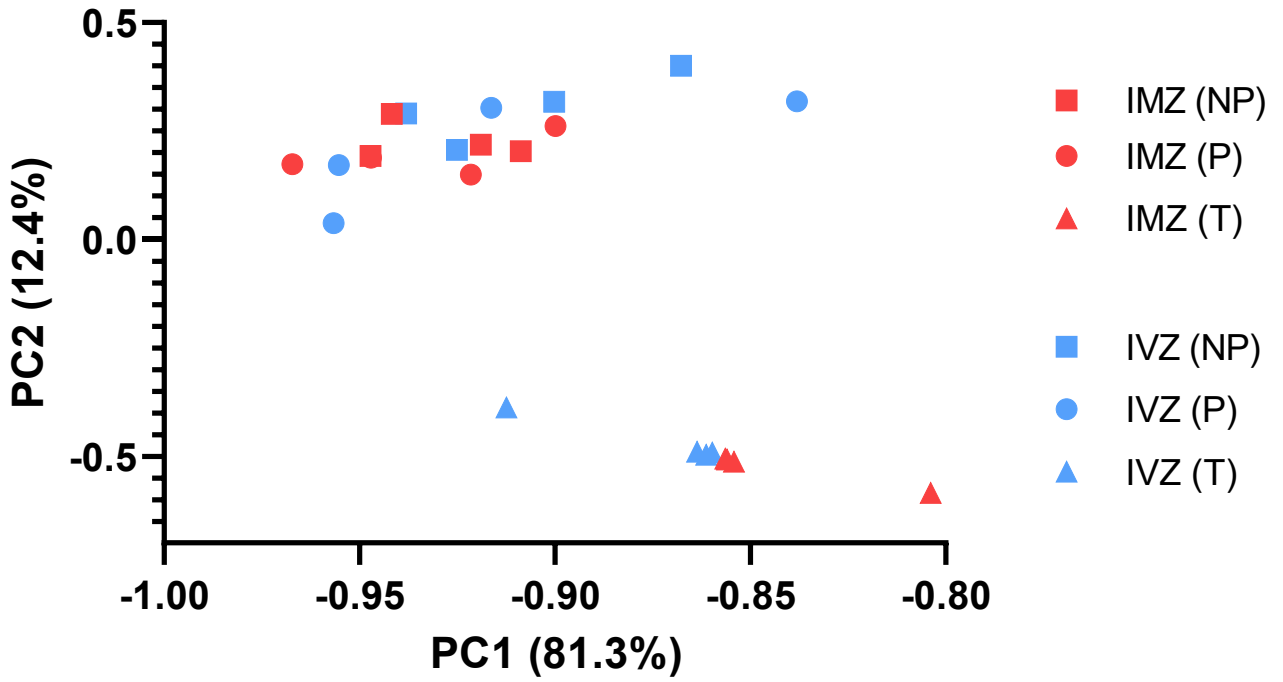
0.5
0.0
-0.5
PC2 (12.4%)
-1.00
-0.95
-0.90
-0.85
-0.80
PC1 (81.3%)
IMZ (NP)
IMZ (P)
IMZ (T)
IVZ (NP)
IVZ (P)
IVZ (T)

Supp. Fig. 5

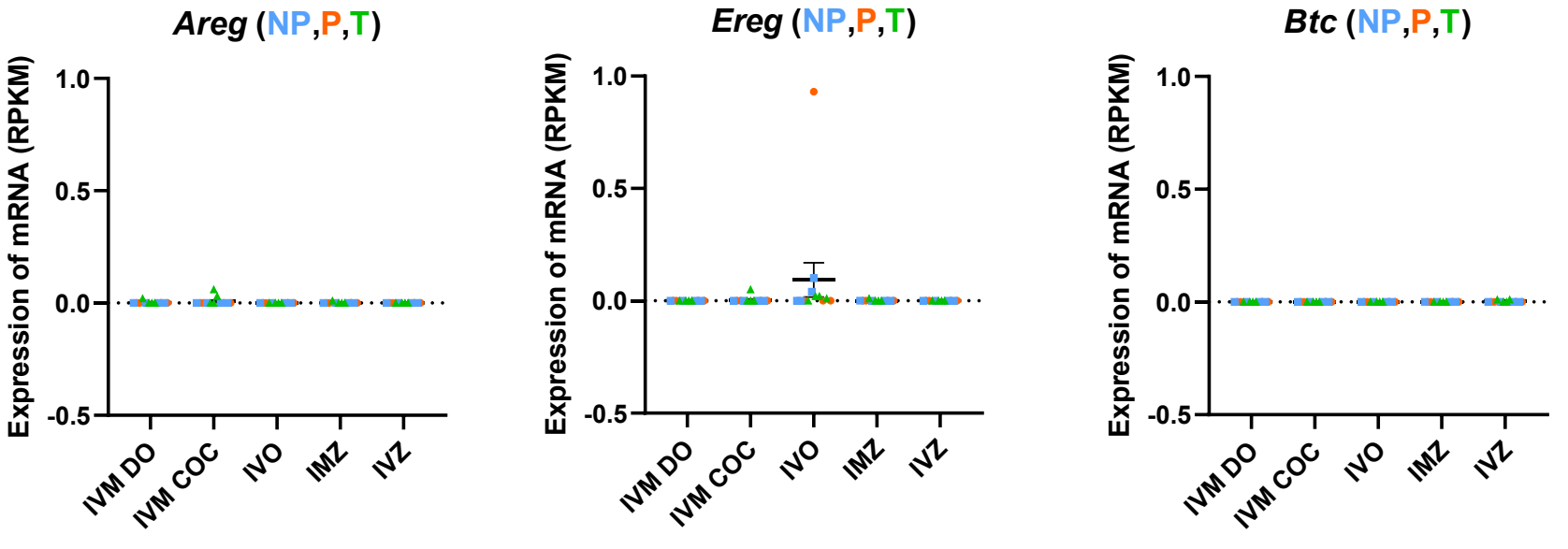
Areg (NP,P,T)
Ereg (NP,P,T)
Btc (NP,P,T)
Expression of mRNA (RPKM)
1.0
0.5
0.0
-0.5
IVM DO
IVM COC
IVO
IMZ
IVZ

Supp. Fig. 6

A

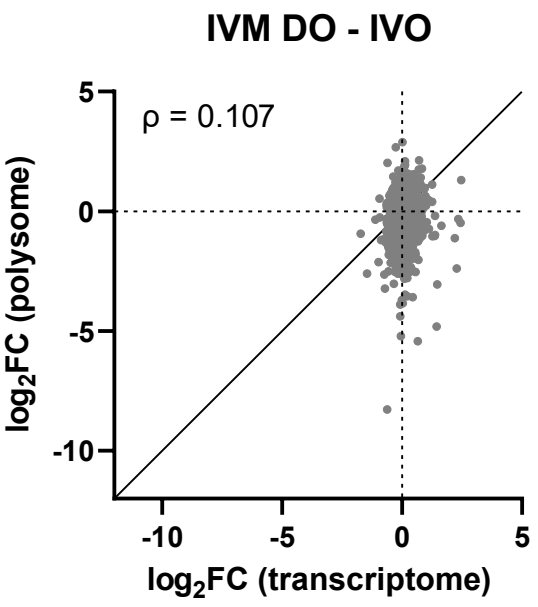
IVM DO - IVO
ρ = 0.107
log2FC (polysome)
log2FC (transcriptome)
5
0
-5
-10
-10
-5
0
5

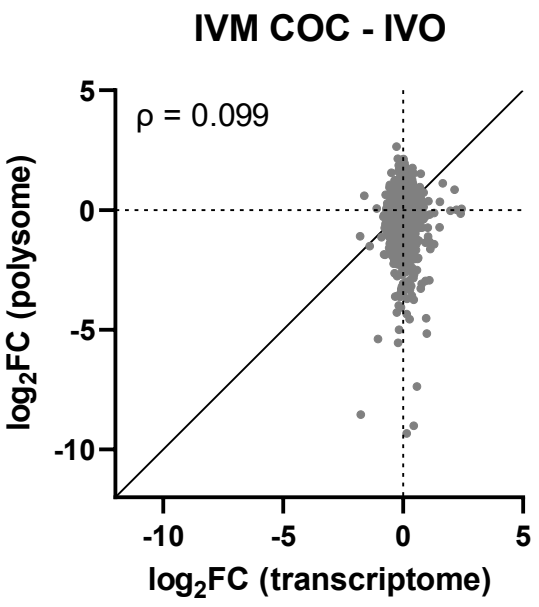
IVM COC - IVO
ρ = 0.099
log2FC (polysome)
log2FC (transcriptome)
5
0
-5
-10
-10
-5
0
5

B

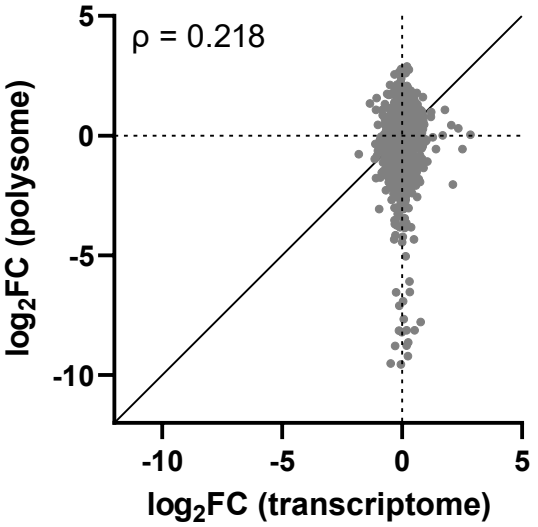
IMZ - IVZ
ρ = 0.218
log2FC (polysome)
log2FC (transcriptome)
5
0
-5
-10
-10
-5
0
5

Supp. Fig. 7

A

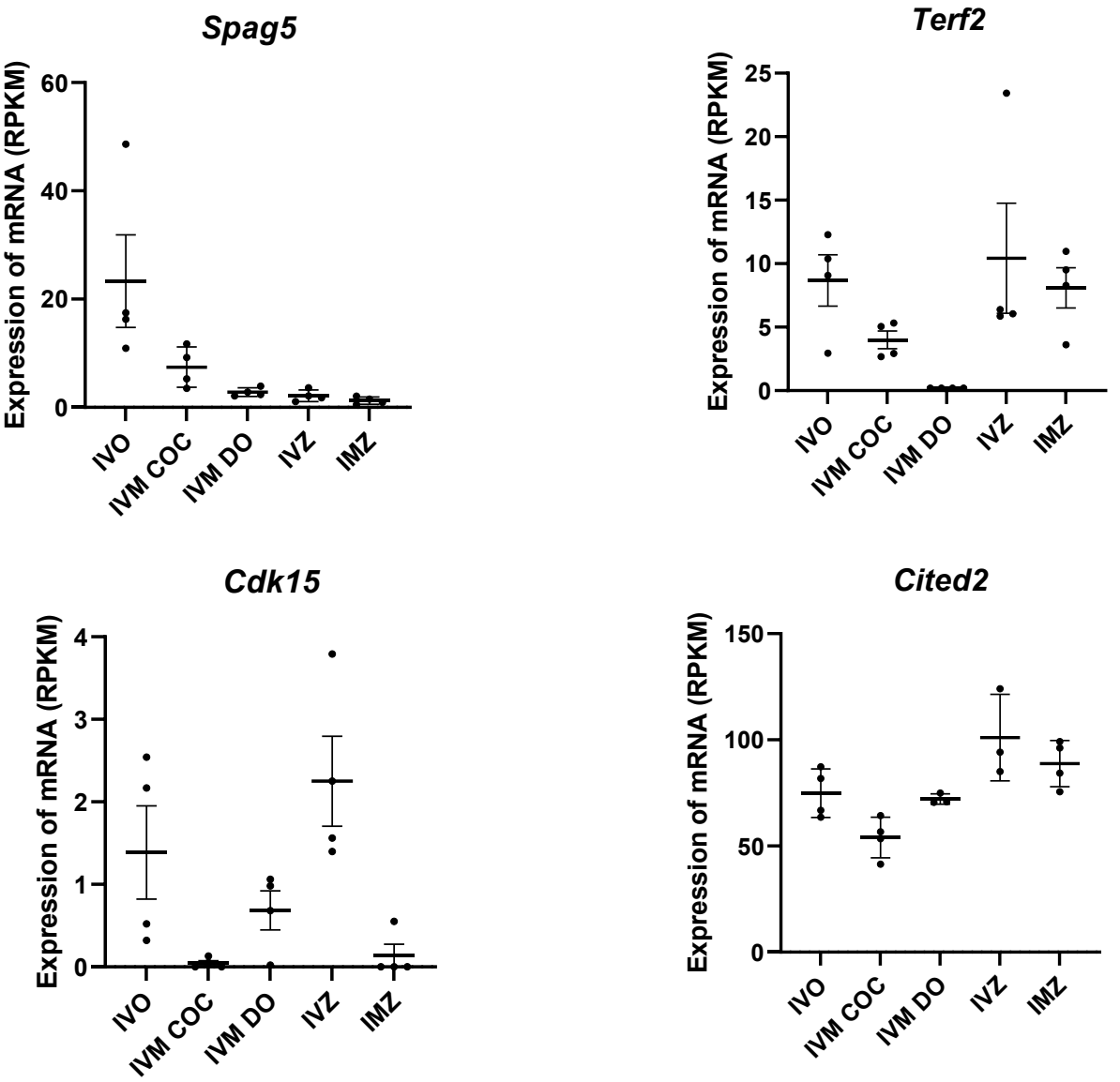
Spag5
Expression of mRNA (RPKM)
60
40
20
0
IVO
IVM COC
IVM DO
IVZ
IMZ
Terf2
Expression of mRNA (RPKM)
25
20
15
10
5
0
IVO
IVM COC
IVM DO
IVZ
IMZ
Cdk15
Expression of mRNA (RPKM)
4
3
2
1
0
IVO
IVM COC
IVM DO
IVZ
IMZ
Cited2
Expression of mRNA (RPKM)
150
100
50
0
IVO
IVM COC
IVM DO
IVZ
IMZ

B

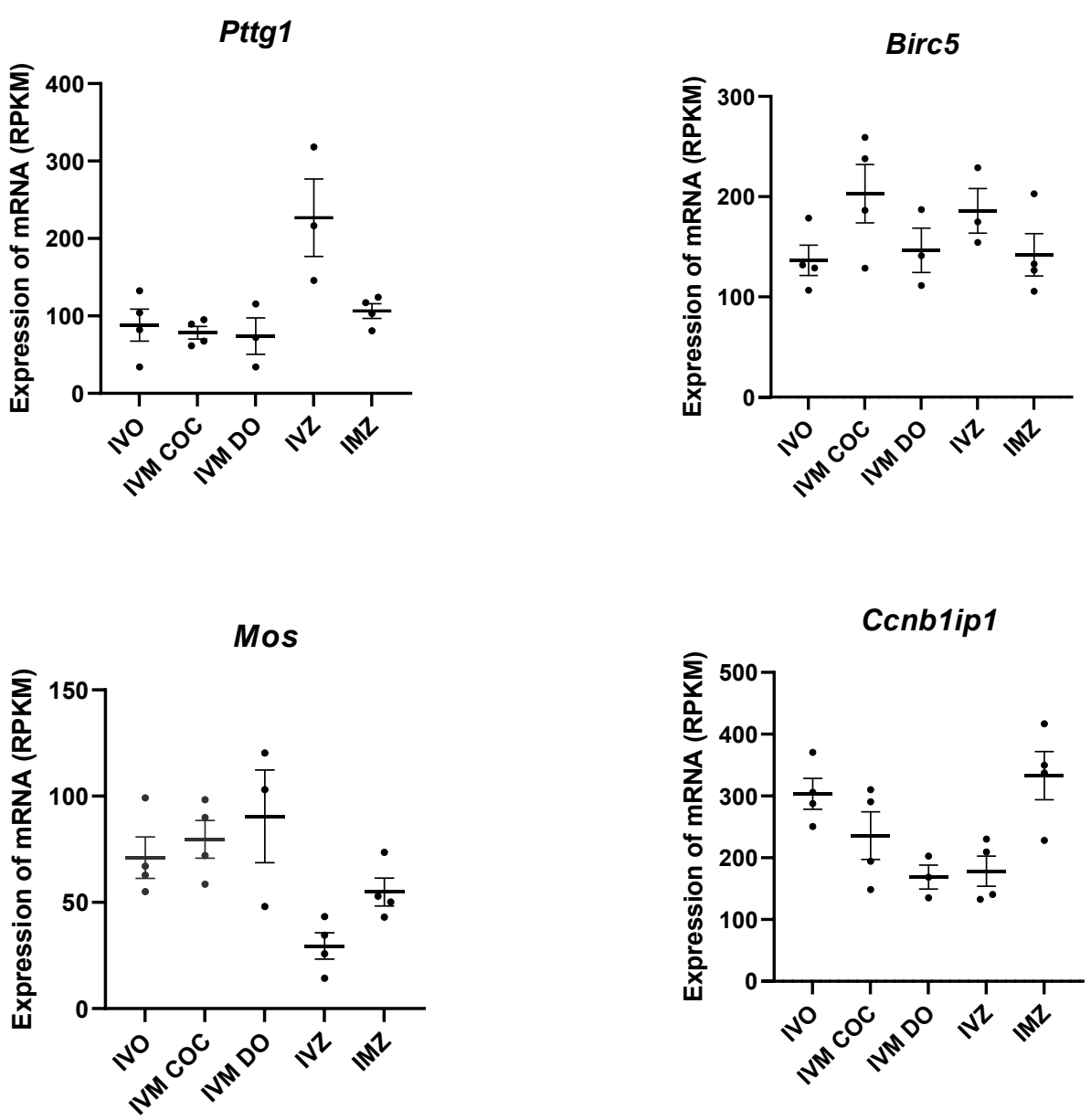
Pttg1
Expression of mRNA (RPKM)
400
300
200
100
0
IVO
IVM COC
IVM DO
IVZ
IMZ
Birc5
Expression of mRNA (RPKM)
300
200
100
0
IVO
IVM COC
IVM DO
IVZ
IMZ
Mos
Expression of mRNA (RPKM)
150
100
50
0
IVO
IVM COC
IVM DO
IVZ
IMZ
Ccnb1ip1
Expression of mRNA (RPKM)
500
400
300
200
100
0
IVO
IVM COC
IVM DO
IVZ
IMZ

Supp. Fig. 8

A

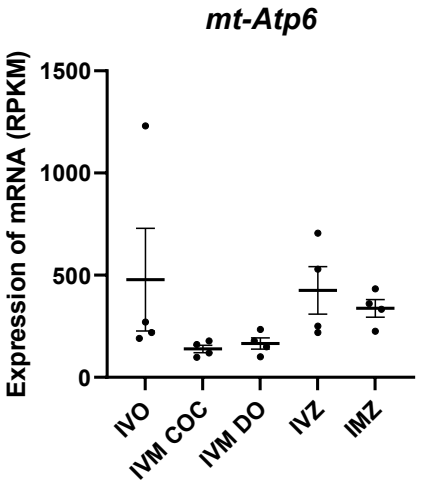

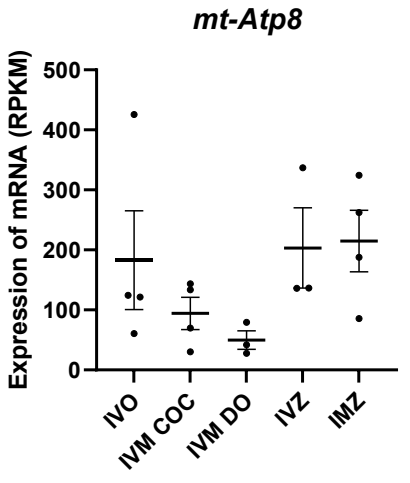

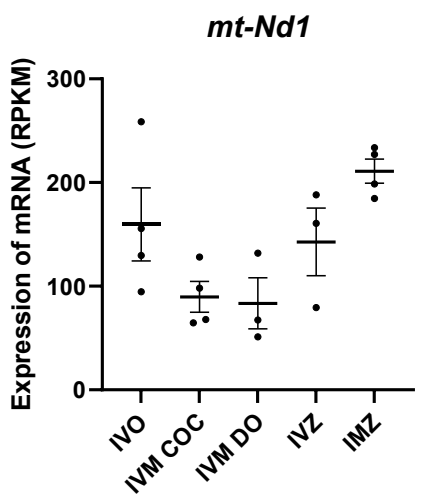

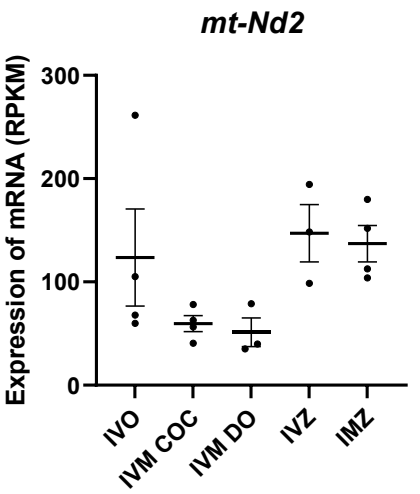

B

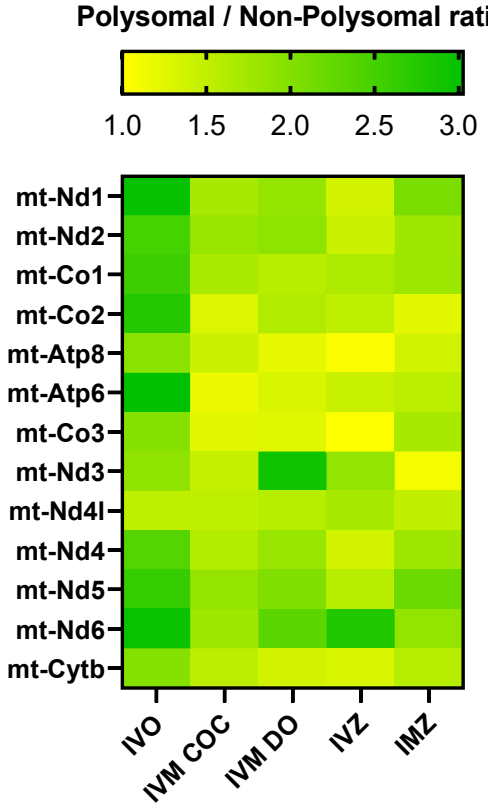

C

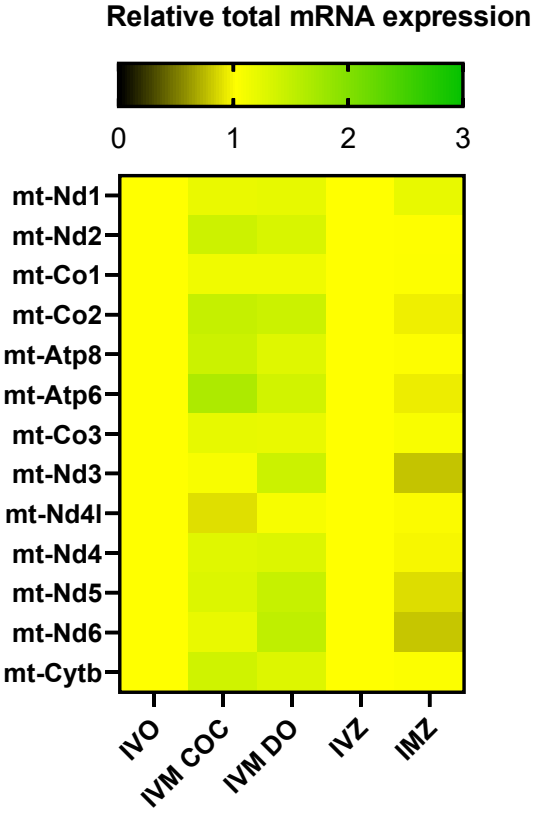

D

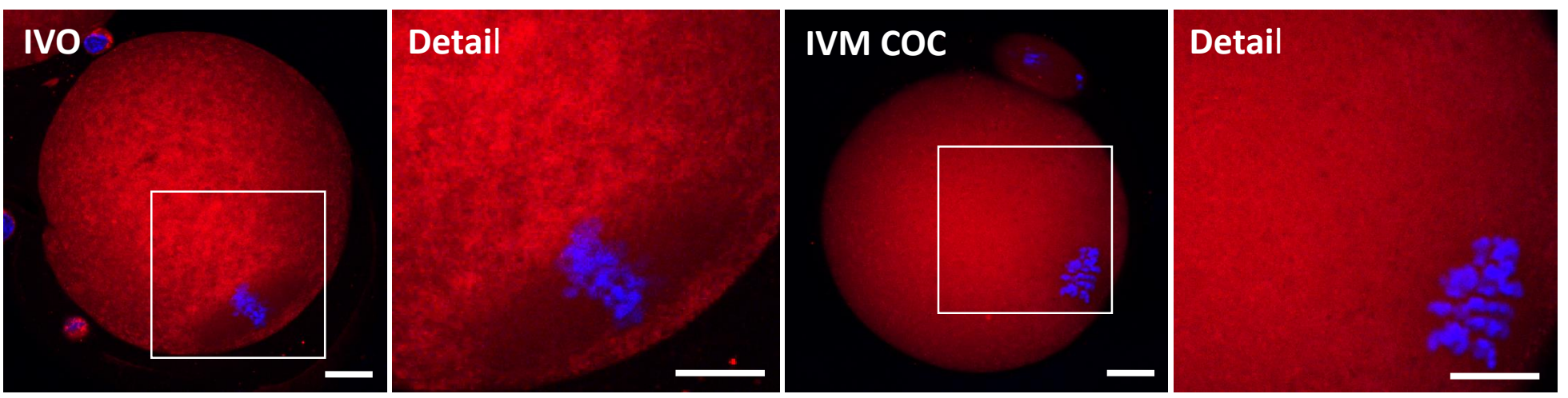

Suppl. Fig. 9

A

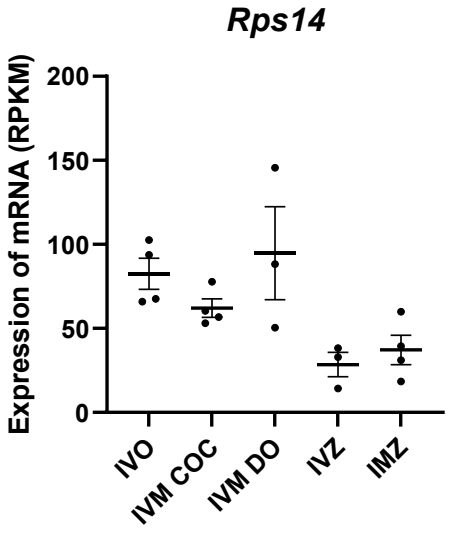

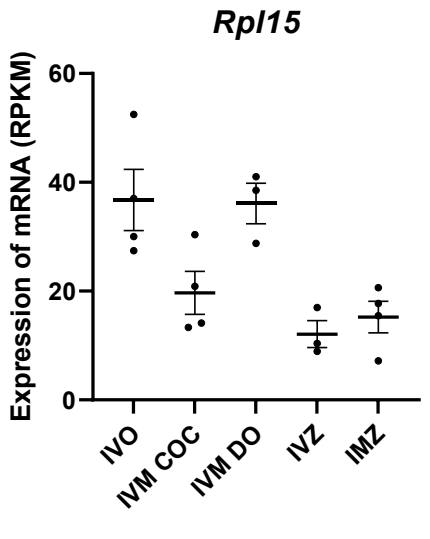

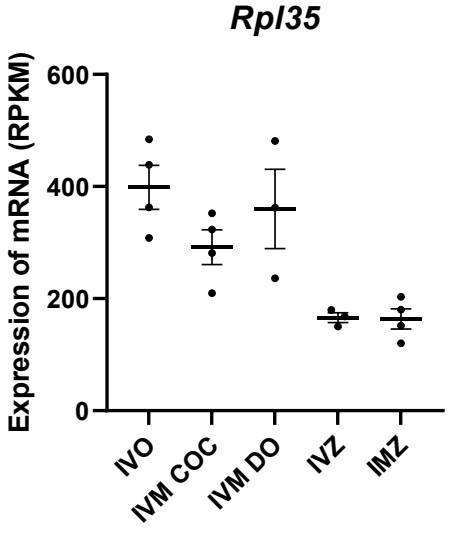

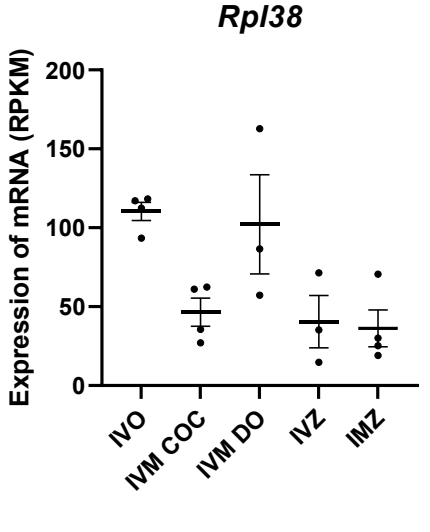

B

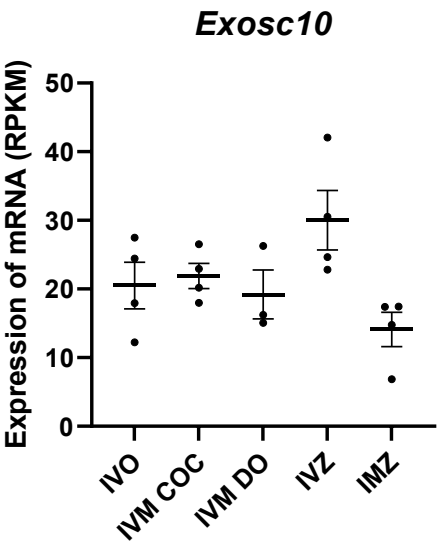

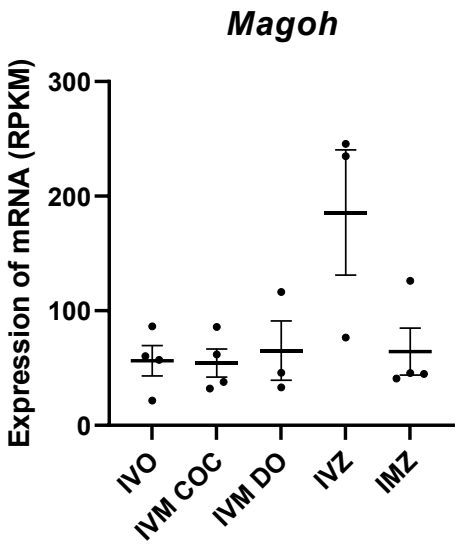

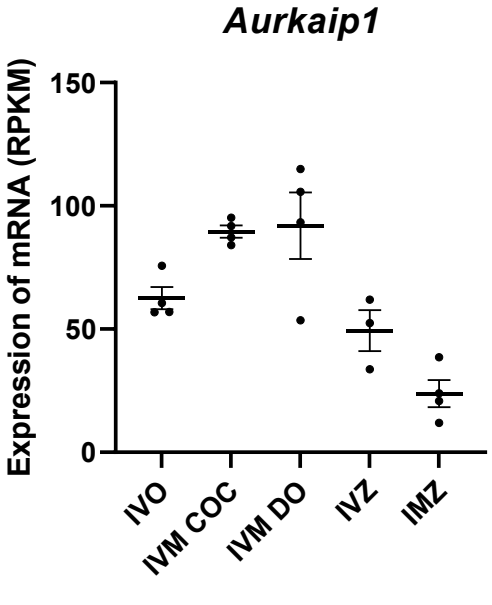

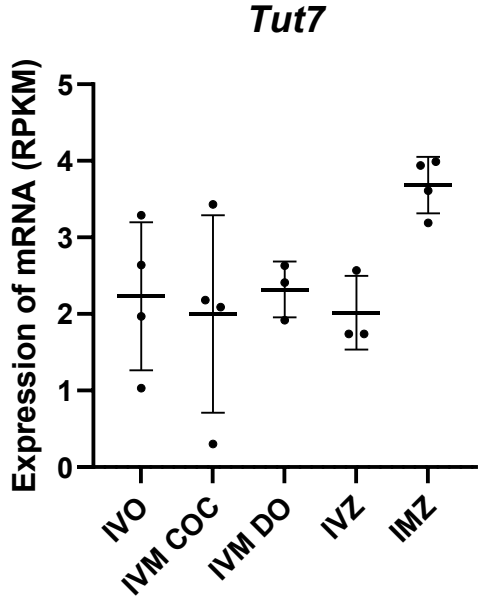

Suppl. Fig. 10

A

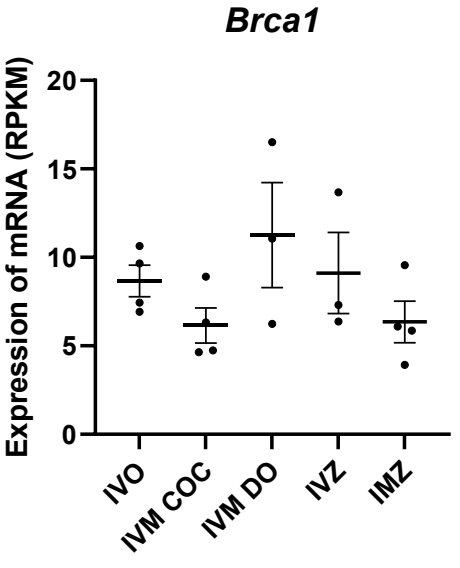

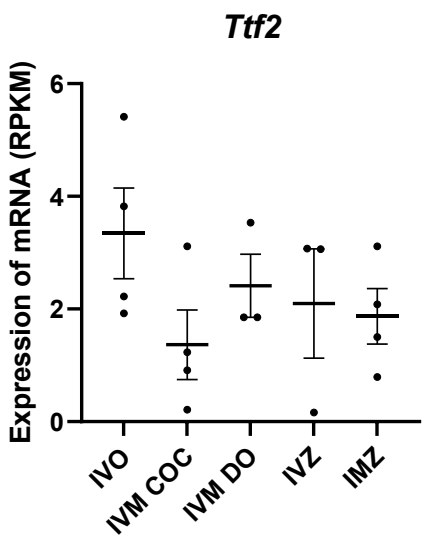

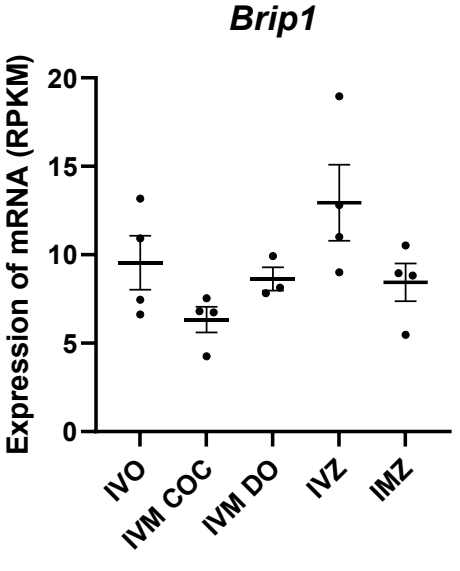

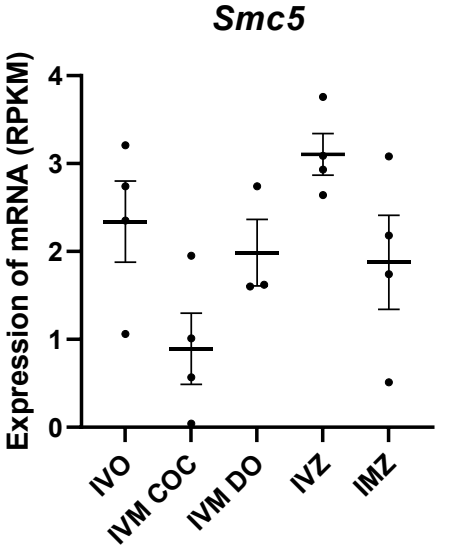

B

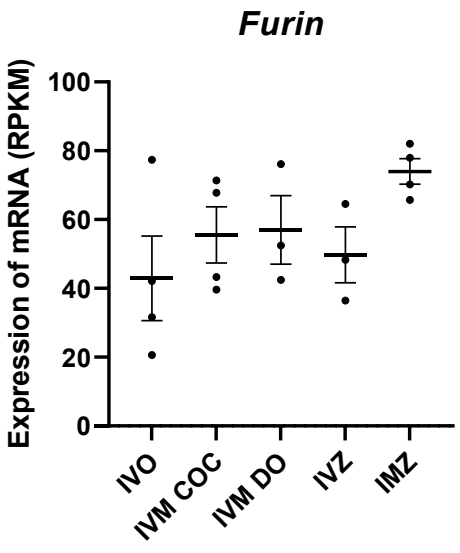

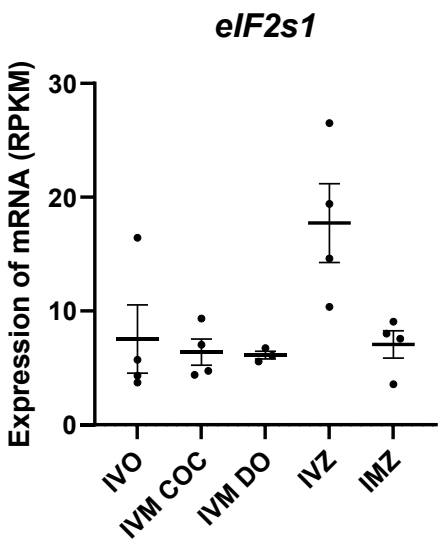

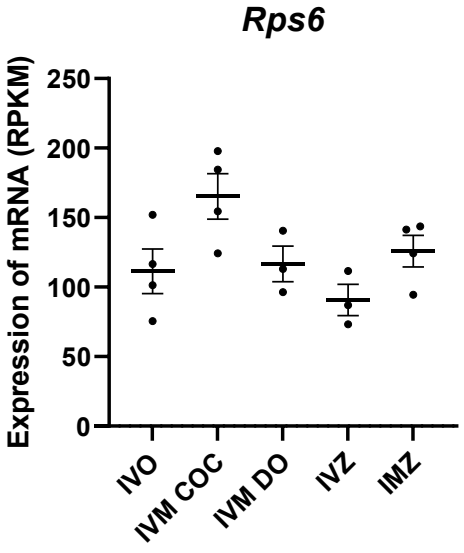

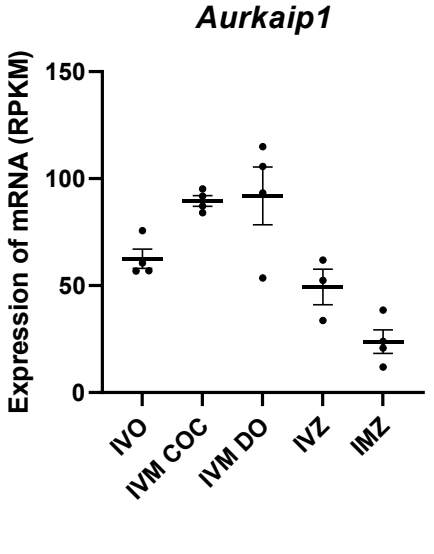

Absence of CPEB3 in the oocyte leads to early embryo lethality

Lucia Lamacova[1], Denisa Jansova[1], Zongliang Jiang[2], Michal Dvoran[1], Daria Aleshkina[1], Rajan Iyyappan[1], Anna Jindrova[1], Heng-Yu Fan[3], Yuxuan Gao[3], Andrej Susor[1]*

[1] Laboratory of Biochemistry and Molecular Biology of Germ Cells, IAPG CAS, Rumburska 89, 277 21 Libechov, Czech Republic

[2] Department of Animal Sciences, Genetics Institute, University of Florida, Gainesville, FL 32610, United States

[3] Life Sciences Institute, Zhejiang University, China

*susor@iapg.cas.cz

Abstract

Mammalian oocyte development is dependent on the temporally controlled translation of maternal transcripts, most importantly to coordinate meiotic and early embryonic development when transcription has ceased. The translation of mRNA is regulated via various RNA-binding proteins. We show that the absence of cytoplasmic polyadenylation element-binding protein 3 (CPEB3) negatively affects female reproductive fitness. CPEB3-depleted oocytes undergo meiosis normally, but they experience early embryonic arrest due to an impaired transcriptome, leading to aberrant protein expression and subsequent failure to commence embryonic transcription. We found that CPEB3 stabilises a subset of mRNAs with significantly longer 3'UTR enriched by cytoplasmic polyadenylation elements in their distal region. Taken together, our results reveal a key maternal factor that regulates the stability and translation of a subclass of mRNAs essential for the initiation of embryonic transcription and thus for embryonic development.

Introduction

The growing oocyte is transcriptionally active, accumulating large amounts of mRNA to meet a substantial proteomic demand during a long period of transcriptional quiescence between maturation and the 2cell stage in mice and at the 8cell stage in humans (Brandhorst 1985; De La Fuente et al. 2004; Clarke 2012). However, multiple consecutive events such as meiotic maturation, MII arrest, fertilisation, the completion of meiosis, and the oocyte-to-embryo transition require a different pool of proteins (Hamatani et al. 2004; Cao et al. 2012; Wang et al. 2010). In the absence of transcription, these changes are mainly coordinated by the translational regulation and stability of maternally stored mRNAs in a spatiotemporal manner (de Vantéry et al. 1997; Susor et al. 2015; Richter 1999; Sha et al. 2019).

The precise timing of a transcript's translation or degradation is controlled by the intrinsic properties of mRNAs in which various sequence motifs are present in their 5´ or 3´UTR, providing binding sites for RNA-binding proteins (Kuersten and Goodwin 2003; Leppek et al. 2018). The formed RNA-protein complex can increase/decrease the affinity of mRNA for translation-initiation machinery, recruit degradation enzymes, spatially localise the mRNA within a cell, or regulate posttranscriptional modifications such as splicing, RNA methylation, uridylation, and polyadenylation (Dominguez et al. 2018; Hentze et al. 2018; Susor et al. 2016; Morgan et al. 2017).

Polyadenylation plays a key role in the control of transcript stability and translation (Morgan et al. 2017; Vassalli et al. 1989). Almost all eukaryotic mRNAs are polyadenylated, except for replication-dependent histone mRNAs (Colgan and Manley 1997; Dávila López and Samuelsson 2008). PolyA-binding proteins bind to the tail and facilitate cap-dependent translation by bridging the 3' and 5' ends by interaction with the initiation factor eIF4G or by other recently discovered mechanisms (Tarun et al. 1997; Zhao and Fan 2021). Sequential waves of polyadenylation and deadenylation occur during oocyte and embryo development, and by affecting mRNA turnover, they drive meiotic maturation or future developmental progress (Morgan et al. 2017; Paynton et al. 1988).

The decrease in female fertility is mainly due to poor quality oocytes that are unable to sustain preimplantation development. Here, we found that the maternal effect polyadenylation factor CPEB3, which is responsible for the metabolism of a subset of maternal transcripts in oocytes, influences early embryonic development.

Results

CPEB3 is actively translated during oocyte maturation

To analyse CPEB3 translation in the mouse oocyte and early embryo, we performed polysomal fractionation, which showed that CPEB3 has a comparatively higher polysomal abundance at the MII oocyte stage relative to the CPEB family member CPEB1, which is active in the GV oocyte (Sha et al. 2017; Komrskova et al. 2014). This observation indicated a higher CPEB3 translation (Fig. 1A). Further CPEB3 immunoblotting analysis revealed a significantly higher CPEB3 expression in the MII oocyte, which gradually decreased as the 2cell stage of the embryo approached (Fig. 1B, C).

Our data demonstrated that CPEB3 is actively translated and expressed in the MII oocyte.

Significantly decreased CPEB3 in the oocytes, leading to subfertility

By combining the CreLox system with the ZP3 promoter, we bred mice with oocyte conditional knockout (cKO) for CPEB3 (Chao et al. 2013). cKO oocytes (*conditional knock-out, CPEB3$^{LoxP/LoxP}$, ZP3$^{Cre\ +/-}$;* CPEB3$^{-/-}$) exhibited the absence of mRNA coding for CPEB3 in the oocyte (Fig. S1A). Immunoblot analysis showed a significant reduction of CPEB3 protein in the oocyte (CPEB3$^{-/-}$, Fig. 2A, B). Breeding females with cKO oocytes for CPEB3 with wild-type males gave a significantly decreased litter size (Fig. 2C). The presence of a single wildtype allele (CPEB3$^{+/-}$) did not exhibit a reduction in litter size (Fig. 2C), indicating no CPEB3 haploinsuifiency in the oocyte. Additional morphological analysis of wild-type and cKO genotypes showed physiologically normal folliculogenesis and ovaries (Fig. S1B) with no difference in the length of intrauterine development (Fig. S1C).

We generated an experimental model for CPEB3 deficiency which leads to female subfertility.

Oocytes with downregulated CPEB3 are not able to sustain preimplantation embryo development

Firstly, to unveil compromised CPEB3 cKO female fertility, we isolated MII oocytes and zygotes from CPEB3$^{+/+}$ and CPEB3$^{-/-}$ mice. Both genotypes produced a similar quantity and quality of collected oocytes as well as fertilised zygotes (Fig. 3A; Fig. S2). Next, we cultured *in vitro* zygotes until the blastocyst stage. A significant reduction in embryo development was observed post 2cell stage in embryos derived from CPEB3$^{-/-}$ oocytes fertilized by wild-type males (Fig. 3B, C). The first embryonic cleavage from the zygote to 2cell stage exhibited no significant difference in timing (Fig. S2B).

By utilizing breeding experiments together with the examination of isolated oocytes and zygotes, we demonstrated that the impaired female fertility in our experimental model for CPEB3 deficiency is caused by a developmental incompetency of CPEB3$^{-/-}$ oocytes.

CPEB3 depletion results in decreased global protein synthesis and transcriptional activity of the 2cell embryo

Because CPEBs are involved in mRNA metabolism and translation, we analysed ^{35}S-methionine uptake, which serves as a marker of translational activity, in oocytes and embryos. CPEB3 cKO oocytes or derived 2cell embryos have a slightly but significantly decreased global translational rate (Fig. 4A, B). Further transcriptional activity analysis in the 2-cell embryo by 5-ethynyl uridine (EU) labelling showed a significant decrease in the embryos derived from CPEB3$^{-/-}$ oocytes (Fig. 4C, D). Next, to assess the transcriptomes of CPEB3$^{+/-}$ and CPEB3$^{-/-}$ oocytes and their consequent 2cell embryos, we performed RNA sequencing (Fig. S3). The acquired datasets showed significantly differentially expressed (DE) transcripts, with more than 1.5-fold difference in 356 mRNAs in the MII CPEB3$^{-/-}$ oocyte, and 1,269 mRNAs in the 2cell embryo derived from the CPEB3$^{-/-}$ oocyte (Fig. 5A). Gene ontology analysis showed that DE mRNAs coding mostly for genes involved in RNA expression, translation and transcription (Fig. 5B and Supplementary File 1) in both oocytes and embryos. We selected candidate transcripts from the DE mRNA datasets related to the decreased developmental competence of MII CPEB3$^{-/-}$ oocytes and 2cell embryos: *Cnot7*, *Zscan4*, *Histone 1.4*, *Obox5*, *Cbfa2t3*, *Zfp770*, *Spi-C*, *Eif1a.* The subsequent validation of candidate mRNAs by qPCR showed consistency with RNA-seq datasets (Fig. 5C).

CPEB3 absence influences translation of specific mRNAs via polyadenylation

Our previous results showed that the absence of CPEB3 in MII oocytes leads to decreased global translation (Fig. 4A, B) and the destabilization of particular transcripts within the oocyte (Fig. 5). Moreover, by immunoblotting we confirmed the protein expression of RNA-seq candidate mRNAs that were up- or downregulated in the CPEB3$^{-/-}$ oocytes (CNOT7, ZSCAN4, CBFA2T3) and in the resulting 2cell embryos (SPI-C). We observed that mRNA expression positively correlates with protein expression (Fig. 6A, B).

CPEBs are also involved in the polyadenylation of mRNAs and their translation (Stebbins-Boaz et al. 1996) thus we performed Poly(A) Tail-Length Assay (PAT) in the CPEB3$^{+/+}$ and CPEB3$^{-/-}$ oocytes to investigate the difference in the polyA tail lengths. The polyadenylation of 3'UTR mRNA coding for Cyclin B1 (*Ccnb1*), which is not DE in the CPEB3$^{-/-}$ oocyte, is equal between genotypes (Fig. 6C), however selected candidate mRNA 3'UTRs were differentially polyadenylated (Fig. 6C). In all the analysed candidates, we found significant differences in the size of polyadenylated tails Fig. 6C). To experimentally substitute for absent endogenous CPEB3 protein in the CPEB3$^{-/-}$ oocytes, we injected CPEB3 protein into GV oocytes (Fig. S4) and subsequently analysed the expression of selected candidate proteins, ZSCAN4 and CBFA2T3, in the MII oocytes. We detected levels of candidate proteins similar to CPEB3$^{+/+}$ MII oocytes after the injection of CPEB3 protein in the CPEB3$^{-/-}$ oocyte (Fig. 6D, E).

Our data show aberrant protein expression of differentially expressed mRNAs in the CPEB3$^{-/-}$ oocytes during the meiotic progression to MII, which is linked to the difference in the polyA tail length of 3'UTR termini.

CPEB3 regulates translation of specific mRNAs via 3'UTR

The bioinformatic analysis of the DE transcripts in the CPEB3$^{-/-}$ oocytes addressed their 3'UTR composition. The 3'UTR length, density and spatial distribution of the polyadenylation signal (PAS) and cytoplasmic polyadenylation elements (CPE) motives were investigated. Downregulated mRNAs had significantly longer 3'UTRs compared to stable or upregulated transcripts (Fig. 7A). The quantification of CPEs and PAS motifs showed a significant enrichment of PAS and CPEs in the downregulated mRNAs (Fig. 7B, C), but the number of CEPs and PAS was equal to the stable mRNAs (Fig. 7B, C). The spatial distribution of CEP and PAS motifs showed a more distal localization of downregulated transcripts than with the stable or upregulated mRNAs (Fig. 7D, E).

Our results show that CPEB3 regulates the fate of mRNAs containing long 3'UTRs with CPEs and PAS domains in the distant part of the mRNA transcripts.

Discussion

The RNA-binding protein CPEB3 mediates the fate of several identified mRNA targets (Huang et al. 2006; Lu et al. 2021). Although the highest expression of CPEB3 has been reported in the oocyte and zygote (Potireddy et al. 2006; Boroviak et al. 2018), the specific role of this maternal factor has not yet been elucidated. To gain insight into the function of CPEB3 in oocyte and early embryo development, we performed a specific downregulation of CPEB3 in the oocyte to characterize its importance for female reproductive outcome.

Despite the presence of approximately 20% CPEB3 protein in the cKO oocytes, we observed a decreased number of pups in the litter. The residual presence of CPEB3 protein was likely due to its synthesis in the growing oocyte prior to ZP3-Cre activation. Its high stability across stages could be attributed to its prion-like nature, the CPEB3 belongs to the prion-like class of proteins. (Fioriti et al. 2015; Hervás et al. 2021; Stephan et al. 2015). We may speculate that the total absence of CPEB3 would lead towards female sterility due to impaired oocyte developmental competence.

In contrast to the appearance of CPEB3 in later developmental stages, the CPEB family member CPEB1 is abundant in the GV; however, upon oocyte meiotic resumption, ERK1/2 is activated by upstream kinases and triggers CPEB1 for degradation (Sha et al. 2017; Komrskova et al. 2014). In Xenopus oocytes, CPEB4 has been identified as the protein that takes over from CPEB1 and regulates the expression of cytostatic factors in MII (Igea and Méndez 2010). However, the downregulation of CPEB4 in mouse oocytes did not affect oocyte meiosis (Chen et al. 2011) or fertility (Tsai et al. 2013), indicating the existence of a different mechanism in mammals. It appears that CPEB3 replaces the role of CPEB1 for a specific subclass of mRNAs' post nuclear envelope breakdown (NEBD). We discovered that CPEB3 downregulation influences a subclass of RNAs, e.g. *Cnot7* mRNA, in which polyA tail elongation and translation in MII is negatively affected. CNOT7 is critical for the deadenylation of maternal transcripts (Ma et al. 2015), and inhibiting the maturation-

associated increase in CNOT7 leads to phenocopy due to transcriptional decrease in 2cell embryos (Ma et al. 2015). The results presented here also demonstrate that the absence of CPEB3 leads to mRNA stabilization and impaired deadenylation of specific candidate mRNAs, resulting in overexpression at the protein level in the MII oocyte (ZSCAN4, CBFA2T3, H1.4.). Importantly, ZSCAN4d is a unique 2cell-specific transcription factor (Falco et al. 2007), that when expressed in MII oocytes results in a loss of developmental competence (Smith et al. 2022). Similarly CBFA2T3, another transcriptional factor responsible for the recruitment of a large number of corepressors and histone-modifying enzymes (Davis et al. 2003), is stabilized in both the CPEB3-downregulated oocyte and embryo. On the other hand, the level of early embryonic transcription factor SPI-C, essential for preimplantation development and the regulation of eIF-1A (Kageyama et al. 2006) expression, is significantly decreased in the absence of CPEB3 in the 2cell embryo. However physiologically, SPI-C should be increased (Kageyama et al. 2006).

Interestingly, one of the most overexpressed genes at both developmental stages was replication-dependent histones, of which *Hist1h1e* coding for H1.4 was one of the candidate genes validated by qPCR. H1.4 is related to a more compact chromatin structure (Willcockson et al. 2021), leading us to speculate that its premature incorporation instead of the oocyte linker variant (*h1foo*) could prevent proper loosening of the chromatin (Wu et al. 2016) in pronuclei and sterically block binding sites for TFs. Additionally, unbalanced histone stoichiometry could significantly affect EGA, as reported in *Drosophilla* embryos (Chari et al. 2019). Given that somatic histones usually have a stem loop instead of a polyA tail at the 3' UTR, the function of CPE found in H1.4 3' UTR and the possible switch to polyadenylation, as reported in other cell types (Pirngruber and Johnsen 2010; Lyons et al. 2016), remains unexplained.

Generally, CPEB3 downregulation leads to 356 DE transcripts in the MII and 1164 DE mRNAs in the 2cell embryo. Our findings demonstrate that the deregulation of particular maternal mRNAs in the oocyte results in aberrant embryonic transcription, which mirrors decreased transcriptional activity in the 2cell embryo, significantly altering its developmental potential beyond the 2cell stage. In contrast to a study conducted by Fang et al. (Fang et al. 2021) using whole-organism *Cpeb3*-null mice, we did not observe impaired oocyte development or folliculogenesis. This difference is likely attributed to the different *Cpeb3*-depletion strategies.

As has been reported, different tissues exhibit a global tendency to favour certain mRNA isoforms (Zhang et al. 2005) for example, neuronal tissues favour isoforms that utilize distal PASs in 3' UTRs, while the use of proximal PASs is more prominent in blood cells and testis tissue (Zhang et al. 2005; Liu et al. 2007). It appears that CPEB3 tends to favour the polyadenylation of distal PAS of mRNAs that are translationally dormant at the onset of oocyte meiosis. This is in accordance with a study by Zhang et al. (2021) demonstrating that CPEB3 affects the fate of mRNA in lung cancer cells by influencing the choice of PAS, and its depletion leads to 3´UTR shortening, allowing transcripts to escape from the miRNA degradation pathway (Zhang et al. 2021). As demonstrated by our results, the CPEB3 expression in the oocyte is accompanied by the stabilization and translation of factors employed in the terminal part of oocyte meiosis (e.g. MOS, CNOT7) or transcriptional factors (e.g. ZSCAN4, SPI-C, CBFA2T3, OBOX5) essential for embryonic genome activation.

In summary, here we demonstrated that CPEB3 plays a crucial role in maintaining oocyte developmental competence, allowing for sustained development towards the blastocyst stage by shaping its transcriptome and consequently proteome at the end of meiotic maturation. While CPEB3 is not essential for meiotic progression itself, it is vital for the proper activation of embryonic transcription and subsequent embryonic development.

Material and Methods

Oocyte isolation and cultivation

6-10-week-old BL6 females were superovulated by the intraperitoneal injection of 5 IU of pregnant mare serum gonadotropin (PMSG). GV oocytes were obtained from dissected ovaries 46 h after stimulation. Collected oocytes were handled in prewarmed M2 transfer medium (Merck) supplemented with 100 µM of IBMX (3-isobutyl-1-methylxanthine, phosphodiesterase inhibitor; Sigma) to prevent NEBD. For *in vitro* maturation, selected oocytes were denuded, washed twice in TM, and cultured in M16 medium (Millipore) without IBMX at 37 °C, 5% CO_2 for another 13-16h. After 70 minutes, oocytes that had progressed through NEBD were selected. To obtain MII oocytes *in vivo*, 5 IU hCG (ProSpec) was administered 48 h post PMSG. Zygotes were obtained from PMSG-primed females mated with males 17 h post hCG and cultured *in vitro* in M16 medium under paraffin oil (Ovoil, Vitrolife). 2cell embryos were

collected 37 h post hCG administration. For subfertility studies, zygotes were cultivated up to the blastocyst stage and the number of arrested 2cell embryos and blastocyst rates were counted and compared with the control. For further processing, the samples were washed (3x) in a 0,1% solution of polyvinyl alcohol (PVA; Sigma) in phosphate-buffered saline (PBS) and frozen according to the Tetkova and Hancova (2016) protocol (Tetkova and Hancova 2016). Recombinant CPEB3 protein (H00022849-P01, Bio-Techne) was injected into the GV oocyte at a final concentration of 40 ng/µl using an Eppendorf microinjection system. The PBS-injected CPEB3$^{+/+}$ and CPEB3$^{-/-}$ oocytes were used as controls. *CPEB3* $^{LoxP/-}$*; ZP3* $^{Cre+/-}$ represents WT oocyte/genotype or CPEB3$^{+/+}$ and *CPEB3* $^{LoxP/LoxP}$*; ZP3* $^{Cre+/-}$ represents cKO or CPEB3 $^{-/-}$ oocyte/genotype. All animal work was conducted according to Act No. 246/1992 on the protection of animals against cruelty.

RNA-sequencing

Polysome fractionation followed by RNA isolation was carried out according to the Scarce Sample Polysome profiling (SSP-profiling) method by Masek et al. (Masek et al. 2020). Briefly, cycloheximide-treated oocytes were lysed and loaded onto a 10–50% sucrose gradient. Samples were ultracentrifuged in an SW55Ti rotor (Beckman Coulter) at 45,000 RPM (246,078 x g) for 65 min at 4°C (Optima L-90 ultracentrifuge, Beckman Coulter). Ten equal fractions were collected from each polysomal profile and subjected to RNA isolation with Trizol reagent (Merck). The qPCR-based quantification of 18S and 28S rRNAs in each fraction was done to reconstitute polysomal profiles (Masek et al. 2020). cDNA libraries were prepared using a SMART-seq v4 ultra low input RNA kit (Takara Bio). The RNA sequencing was performed by NovaSeq v4 (Illumina) with a 150-bp read length, paired-end. Acquired reads were trimmed using Trim Galore v0.4.1 and mapped onto the mouse reference genome assembly GRCm38 using Hisat2 v2.0.5. RNA expression was quantified as fragments per kilobase per million (FPKM) values in Seqmonk v1.40.0. Polysomal data were used from Rajan et al. 2023. Global transcriptome data have been submitted to NCBI: GSE239545 at: https://www.ncbi.nlm.nih.gov/geo/query/acc.cgi?acc=GSE239545.

RNA isolation and cDNA synthesis

RNA was isolated from 10-100 oocytes/embryos at the indicated stages. To avoid the loss of scarce material, the entire procedure was performed in a single tube without any sample transfer, using a TATAA CelluLyser Micro Lysis and DNA Synthesis Kit. The cells were lysed in 5 µl of CelluLyser™ buffer added directly to the sample tubes and kept on ice for 10 min to perform lysis. cDNA synthesis was carried out by RT-PCR using both oligo-dT primers and random hexamers with the following conditions: 5 min at 22°C, 30 min at 42°C, 5 min at 85°C for enzyme inactivation. To exclude potential bias caused by the single-tube RNA isolation, we performed simultaneous RNA isolation by spin column extraction with an RNeasy Plus Micro Kit (Qiagen). cDNA from column-isolated RNA was synthesized with a qPCRbio cDNA synthesis kit (PCR Biosystems). The obtained results showed no differences in transcript levels between both methodological approaches.

PCR and qPCR

Real-time quantitative PCR (qPCR) assays were performed using QuantStudio 3® (Applied Biosystems). To perform qPCR, Luna® Universal qPCR master mix (New England Biolabs) was used according to the manufacturer's instructions, supplemented with sample cDNA and 0.5 µl of the forward and reverse primers (Supplementary Table 1). Each qPCR run was done in technical duplicates. mRNA levels were normalized to the *Gapdh* reference gene, using the *ΔΔCt* calculation method (Livak and Schmittegen, 2001) for relative quantification. General PCR experiments for the purpose of primer validation and mouse genotyping were conducted with PPP master mix (TOP-Bio), under the following PCR conditions: 1 min at 94 °C, 18 secs at 94 °C, 18 secs at 58 °C, 15 secs at 72 °C. Products were separated on 1.2% agarose gel with GelRed (41003, Biotinum) and developed in an Azure 600 imaging system (Azure Biosystems). Full images of selected segments are shown in Suppl. Fig. 5.

Poly-A-tail length assay

The experimental procedure was based on the protocol by Sallés and Strickland (Sallés and Strickland 1999), with the following modifications. To keep the entire length of the polyA tail of each transcript, the total RNA was extracted by the phenol-chloroform method. Isolated RNA was incubated with 1 µl of 50µM oligo-dT per sample for 5 min at 65°C. The ligation mix was prepared from the following components: T4 ligase (1µl), Superscript IV 5x buffer (5 µl), 20U/µl RNAse inhibitor (1µl), 10mM dNTP (1 µl), 10mM ATP (1 µl), 1M MgCl2 (0.1 µl), 0,1M DTT (2 µl), and RNAse-free water (2 µl). Each sample was processed in 10 µl of the mixture and incubated for 30 min at 42°C to allow T4-mediated oligo-dT ligation. Anchoring was carried out by incubating with 1 µl of oligo-dT anchor (*5´-GCGAGCTCCGCGGCCGCGT-3´*) for

1 h at 12°C, followed by 2 min of incubation at 42°C. cDNA synthesis was done by the addition of 1 µl of Superscript II Reverse Transcriptase with the following setup: 45 min at 45°C, 10 min at 80°C, hold at 4°C. Prepared cDNA was subjected to PCR with gene-specific forward primers and anchoring reverse primer (Supplementary Table 1). Images were developed in an Azure 600 (Azure Biosystems). Each experiment was carried out in technical triplicates.

Transcription assay

The 5-EU was added to the M16 medium and incubated with zygotes overnight. The resulting 2cell embryos were fixed in 4% paraformaldehyde/PBS for 15 min, permeabilized with 0.1% Triton X-100/PBS for 10 min at room temperature, and incubated with the Click-iT reaction cocktail for 1 h at room temperature in the dark. After incubation, oocytes were washed once with the PBS, and mounted onto slides with Vectashield (H-1500, Vector laboratories). Images were scanned in a Leica SP5 confocal laser-scanning microscope (Leica Microsystems, Wetzlar, Germany).

Western Blotting

Lysed oocytes or embryos were subjected to 4–12% SDS–polyacrylamide gel electrophoresis. Samples were transferred to a polyvinylidene fluoride membrane (Immobilon P; Merckmillipore) using a blotting system (Biometra GmbH) at 5 mA/cm2 over 25 min. Membranes were blocked for 1 h at room temperature, and incubated at 4 °C overnight with the primary antibodies (Supplementary Table 1) with 1% milk/TTBS (Tween-Tris-buffer saline; NaCl, Tween 20, 2M; Tris pH 7,6; dH_2O). After 3 cycles of 10 min of washing in 0,05% TTBS, the membrane was incubated at room temperature for 1 h in 3% milk with secondary antibody conjugated with peroxidase (Jackson Immunoresearch). After the washing step with 0,05% TTBS, proteins were visualized by chemiluminescence (Amersham, GE Healthecare Life Science) according to the manufacturer's instructions.

Measurement of overall protein synthesis

To measure the overall protein synthesis, 50 µCi of ^{35}S-methionine (Susor et al. 2008) (Perkin Elmer) was added to methionine-free culture medium for 12 h, then lysed in SDS-buffer and subjected to SDS–polyacrylamide gel electrophoresis. Radioactively labelled proteins were developed on a film by autoradiography and imaged in a BasReader (FujiFilm). Signal quantification was done with the software ImageJ/FiJi. GAPDH was used as a loading control.

Motive analysis

The 3'UTR sequences of each group were mapped against the GRCm39 mouse reference genome (http://genome.ucsc.edu/cgi-bin/hgTables). The 3' UTR length and motif number were calculated with the R package Biostring (PAS motifs include "UUUUAU", "UUUUAAAU", "UUUUAAGU", "UUUUACU" and "UUUUCAU", and CPE motifs include "AAUAA" and "AUUAAA"). The violin diagrams were plotted with https://www.bioinformatics.com.cn, a free online platform for data analysis and visualization. The relative positions of motifs in transcripts and the corresponding distribution maps were calculated and plotted with the software MS Excel (Microsoft). The total motif number at each position was plotted with OriginPro8.5.

Statistical analysis

Mean and standard error values were calculated in MS Excel. Student's t-test was calculated in the software GraphPad 5 (Prism) to determine statistical significance between groups. *$P < 0.05$ was considered to be statistically significant (labelled with an asterisk). **$P < 0.01$ and ***$P < 0.001$.

Declaration of interests

The authors declare no competing interests.

Acknowledgements

We thank to Jaroslava Supolikova and Marketa Hancova for assistance with experiments. We thank to Dr. Yi-Shuian Huang (Institute of Biomedical Sciences at Academia Sinica, Taipei, Taiwan) for providing the modified mouse line.

Author contributions

Conceptualization, AS; Methodology, AS, LL, ZJ, MD, DA, DJ, HF, YG; Validation, LL, AS, RI, ZJ, MD, DA, AJ; Investigation, AS, LL, MD, RI, DA, DJ, HF, YG; Resources, AS, ZJ; Data Curation, ZJ, AS, RI, HF; Writing – Original Draft, AS, LL; Writing – Review & Editing, all authors; Visualization, AS, LL, ZJ, HF, AJ; Supervision, AS; Project Administration, AS; Funding Acquisition, AS.

Data Availability

The data included in this article are available in the article and in its online supplementary material. All data are available from the authors upon reasonable request. RNA-seq data were deposited the GEO repository https://www.ncbi.nlm.nih.gov/geo/query/acc.cgi?acc=GSE239545.

Funding

The project was funded by Institutional Research Concept RVO67985904 and The Czech Science Foundation (22-27301S) and Institutional Research Concept RVO67985904. Z. J was supported by the NIH Eunice Kennedy Shriver National Institute of Child Health and Human Development (R01HD102533) and USDA National Institute of Food and Agriculture (2019-67016-29863).

References

Boroviak T, Stirparo GG, Dietmann S, Hernando-Herraez I, Mohammed H, Reik W, Smith A, Sasaki E, Nichols J, Bertone P. 2018. Single cell transcriptome analysis of human, marmoset and mouse embryos reveals common and divergent features of preimplantation development. *Dev Camb Engl* **145**: dev167833.

Brandhorst BP. 1985. Informational content of the echinoderm egg. *Dev Biol N Y N 1985* **1**: 525–576.

Cao S, Guo X, Zhou Z, Sha J. 2012. Comparative proteomic analysis of proteins involved in oocyte meiotic maturation in mice. *Mol Reprod Dev* **79**: 413–422.

Chao H-W, Tsai L-Y, Lu Y-L, Lin P-Y, Huang W-H, Chou H-J, Lu W-H, Lin H-C, Lee P-T, Huang Y-S. 2013. Deletion of CPEB3 Enhances Hippocampus-Dependent Memory via Increasing Expressions of PSD95 and NMDA Receptors. *J Neurosci* **33**: 17008–17022.

Chari S, Wilky H, Govindan J, Amodeo AA. 2019. Histone concentration regulates the cell cycle and transcription in early development. *Dev Camb Engl* **146**: dev177402.

Chen J, Melton C, Suh N, Oh JS, Horner K, Xie F, Sette C, Blelloch R, Conti M. 2011. Genome-wide analysis of translation reveals a critical role for deleted in azoospermia-like (Dazl) at the oocyte-to-zygote transition. *Genes Dev* **25**: 755–766.

Clarke HJ. 2012. Post-transcriptional control of gene expression during mouse oogenesis. *Results Probl Cell Differ* **55**: 1–21.

Colgan DF, Manley JL. 1997. Mechanism and regulation of mRNA polyadenylation. *Genes Dev* **11**: 2755–2766.

Dávila López M, Samuelsson T. 2008. Early evolution of histone mRNA 3' end processing. *RNA* **14**: 1–10.

Davis JN, McGhee L, Meyers S. 2003. The ETO (MTG8) gene family. *Gene* **303**: 1–10.

De La Fuente R, Viveiros MM, Burns KH, Adashi EY, Matzuk MM, Eppig JJ. 2004. Major chromatin remodeling in the germinal vesicle (GV) of mammalian oocytes is dispensable for global transcriptional silencing but required for centromeric heterochromatin function. *Dev Biol* **275**: 447–458.

de Vantéry C, Stutz A, Vassalli JD, Schorderet-Slatkine S. 1997. Acquisition of meiotic competence in growing mouse oocytes is controlled at both translational and posttranslational levels. *Dev Biol* **187**: 43–54.

Dominguez D, Freese P, Alexis MS, Su A, Hochman M, Palden T, Bazile C, Lambert NJ, Van Nostrand EL, Pratt GA, et al. 2018. Sequence, Structure, and Context Preferences of Human RNA Binding Proteins. *Mol Cell* **70**: 854-867.e9.

E F, Zhang H, Yin W, Wang C, Liu Y, Li Y, Wang L, Wu Y, Zhang R, Zou C, et al. 2021. CPEB3 deficiency in mice affect ovarian follicle development and causes premature ovarian insufficiency. *Cell Death Dis* **13**: 21.

Falco G, Lee S-L, Stanghellini I, Bassey UC, Hamatani T, Ko MSH. 2007. Zscan4: a novel gene expressed exclusively in late 2-cell embryos and embryonic stem cells. *Dev Biol* **307**: 539–550.

Fioriti L, Myers C, Huang Y-Y, Li X, Stephan JS, Trifilieff P, Colnaghi L, Kosmidis S, Drisaldi B, Pavlopoulos E, et al. 2015. The Persistence of Hippocampal-Based Memory Requires Protein Synthesis Mediated by the Prion-like Protein CPEB3. *Neuron* **86**: 1433–1448.

Hamatani T, Carter MG, Sharov AA, Ko MSH. 2004. Dynamics of global gene expression changes during mouse preimplantation development. *Dev Cell* **6**: 117–131.

Hentze MW, Castello A, Schwarzl T, Preiss T. 2018. A brave new world of RNA-binding proteins. *Nat Rev Mol Cell Biol* **19**: 327–341.

Hervás R, del Carmen Fernández-Ramírez M, Galera-Prat A, Suzuki M, Nagai Y, Bruix M, Menéndez M, Laurents DV, Carrión-Vázquez M. 2021. Divergent CPEB prion-like domains reveal different assembly mechanisms for a generic amyloid-like fold. *BMC Biol* **19**: 43.

Huang Y-S, Kan M-C, Lin C-L, Richter JD. 2006. CPEB3 and CPEB4 in neurons: analysis of RNA-binding specificity and translational control of AMPA receptor GluR2 mRNA. *EMBO J* **25**: 4865–4876.

Igea A, Méndez R. 2010. Meiosis requires a translational positive loop where CPEB1 ensues its replacement by CPEB4. *EMBO J* **29**: 2182–2193.

Kageyama S, Liu H, Nagata M, Aoki F. 2006. The role of ETS transcription factors in transcription and development of mouse preimplantation embryos. *Biochem Biophys Res Commun* **344**: 675–679.

Komrskova P, Susor A, Malik R, Prochazkova B, Liskova L, Supolikova J, Hladky S, Kubelka M. 2014. Aurora Kinase A Is Not Involved in CPEB1 Phosphorylation and cyclin B1 mRNA Polyadenylation during Meiotic Maturation of Porcine Oocytes. *PLoS ONE* **9**: e101222.

Kuersten S, Goodwin EB. 2003. The power of the 3' UTR: translational control and development. *Nat Rev Genet* **4**: 626–637.

Leppek K, Das R, Barna M. 2018. Functional 5' UTR mRNA structures in eukaryotic translation regulation and how to find them. *Nat Rev Mol Cell Biol* **19**: 158–174.

Liu D, Brockman JM, Dass B, Hutchins LN, Singh P, McCarrey JR, MacDonald CC, Graber JH. 2007. Systematic variation in mRNA 3'-processing signals during mouse spermatogenesis. *Nucleic Acids Res* **35**: 234–246.

Lu W-H, Chao H-W, Lin P-Y, Lin S-H, Liu T-H, Chen H-W, Huang Y-S. 2021. CPEB3-dowregulated Nr3c1 mRNA translation confers resilience to developing posttraumatic stress disorder-like behavior in fear-conditioned mice. *Neuropsychopharmacol Off Publ Am Coll Neuropsychopharmacol* **46**: 1669–1679.

Lyons SM, Cunningham CH, Welch JD, Groh B, Guo AY, Wei B, Whitfield ML, Xiong Y, Marzluff WF. 2016. A subset of replication-dependent histone mRNAs are expressed as polyadenylated RNAs in terminally differentiated tissues. *Nucleic Acids Res* **44**: 9190–9205.

Ma J, Fukuda Y, Schultz RM. 2015. Mobilization of Dormant Cnot7 mRNA Promotes Deadenylation of Maternal Transcripts During Mouse Oocyte Maturation. *Biol Reprod* **93**: 48.

Masek T, Del Llano E, Gahurova L, Kubelka M, Susor A, Roucova K, Lin C-J, Bruce AW, Pospisek M. 2020. Identifying the Translatome of Mouse NEBD-Stage Oocytes via SSP-Profiling; A Novel Polysome Fractionation Method. *Int J Mol Sci* **21**: 1254.

Morgan M, Much C, DiGiacomo M, Azzi C, Ivanova I, Vitsios DM, Pistolic J, Collier P, Moreira PN, Benes V, et al. 2017. mRNA 3' uridylation and poly(A) tail length sculpt the mammalian maternal transcriptome. *Nature* **548**: 347–351.

Paynton BV, Rempel R, Bachvarova R. 1988. Changes in state of adenylation and time course of degradation of maternal mRNAs during oocyte maturation and early embryonic development in the mouse. *Dev Biol* **129**: 304–314.

Pirngruber J, Johnsen SA. 2010. Induced G1 cell-cycle arrest controls replication-dependent histone mRNA 3' end processing through p21, NPAT and CDK9. *Oncogene* **29**: 2853–2863.

Potireddy S, Vassena R, Patel BG, Latham KE. 2006. Analysis of polysomal mRNA populations of mouse oocytes and zygotes: dynamic changes in maternal mRNA utilization and function. *Dev Biol* **298**: 155–166.

Richter JD. 1999. Cytoplasmic Polyadenylation in Development and Beyond. *Microbiol Mol Biol Rev* **63**: 446–456.

Sallés FJ, Strickland S. 1999. Analysis of poly(A) tail lengths by PCR: the PAT assay. *Methods Mol Biol Clifton NJ* **118**: 441–448.

Sha Q-Q, Dai X-X, Dang Y, Tang F, Liu J, Zhang Y-L, Fan H-Y. 2017. A MAPK cascade couples maternal mRNA translation and degradation to meiotic cell cycle progression in mouse oocytes. *Dev Camb Engl* **144**: 452–463.

Sha Q-Q, Zhang J, Fan H-Y. 2019. A story of birth and death: mRNA translation and clearance at the onset of maternal-to-zygotic transition in mammals†. *Biol Reprod* **101**: 579–590.

Smith R, Susor A, Ming H, Tait J, Conti M, Jiang Z, Lin C-J. 2022. The H3.3 chaperone Hira complex orchestrates oocyte developmental competence. *Dev Camb Engl* **149**: dev200044.

Stebbins-Boaz B, Hake LE, Richter JD. 1996. CPEB controls the cytoplasmic polyadenylation of cyclin, Cdk2 and c-mos mRNAs and is necessary for oocyte maturation in Xenopus. *EMBO J* **15**: 2582–2592.

Stephan JS, Fioriti L, Lamba N, Colnaghi L, Karl K, Derkatch IL, Kandel ER. 2015. The CPEB3 Protein Is a Functional Prion that Interacts with the Actin Cytoskeleton. *Cell Rep* **11**: 1772–1785.

Susor A, Jansova D, Anger M, Kubelka M. 2016. Translation in the mammalian oocyte in space and time. *Cell Tissue Res* **363**: 69–84.

Susor A, Jansova D, Cerna R, Danylevska A, Anger M, Toralova T, Malik R, Supolikova J, Cook MS, Oh JS, et al. 2015. Temporal and spatial regulation of translation in the mammalian oocyte via the mTOR-eIF4F pathway. *Nat Commun* **6**: 6078.

Susor A, Jelínková L, Karabínová P, Torner H, Tomek W, Kovárová H, Kubelka M. 2008. Regulation of cap-dependent translation initiation in the early stage porcine parthenotes. *Mol Reprod Dev* **75**: 1716–1725.

Tarun SZ, Wells SE, Deardorff JA, Sachs AB. 1997. Translation initiation factor eIF4G mediates in vitro poly(A) tail-dependent translation. *Proc Natl Acad Sci U S A* **94**: 9046–9051.

Tetkova A, Hancova M. 2016. Mouse Oocyte Isolation, Cultivation and RNA Microinjection. *Bio-Protoc* **6**: e1729.

Tsai L-Y, Chang Y-W, Lin P-Y, Chou H-J, Liu T-J, Lee P-T, Huang W-H, Tsou Y-L, Huang Y-S. 2013. CPEB4 knockout mice exhibit normal hippocampus-related synaptic plasticity and memory. *PloS One* **8**: e84978.

Vassalli JD, Huarte J, Belin D, Gubler P, Vassalli A, O'Connell ML, Parton LA, Rickles RJ, Strickland S. 1989. Regulated polyadenylation controls mRNA translation during meiotic maturation of mouse oocytes. *Genes Dev* **3**: 2163–2171.

Wang S, Kou Z, Jing Z, Zhang Y, Guo X, Dong M, Wilmut I, Gao S. 2010. Proteome of mouse oocytes at different developmental stages. *Proc Natl Acad Sci* **107**: 17639–17644.

Willcockson MA, Healton SE, Weiss CN, Bartholdy BA, Botbol Y, Mishra LN, Sidhwani DS, Wilson TJ, Pinto HB, Maron MI, et al. 2021. H1 histones control the epigenetic landscape by local chromatin compaction. *Nature* **589**: 293–298.

Wu J, Huang B, Chen H, Yin Q, Liu Y, Xiang Y, Zhang B, Liu B, Wang Q, Xia W, et al. 2016. The landscape of accessible chromatin in mammalian preimplantation embryos. *Nature* **534**: 652–657.

Zhang H, Lee JY, Tian B. 2005. Biased alternative polyadenylation in human tissues. *Genome Biol* **6**: R100.

Zhang Y, Shen L, Shi Q, Zhao G, Wang F. 2021. Comprehensive Analysis of APA Events and Their Association With Tumor Microenvironment in Lung Adenocarcinoma. *Front Genet* **12**: 645360.

Zhao L-W, Fan H-Y. 2021. Revisiting poly(A)-binding proteins: Multifaceted regulators during gametogenesis and early embryogenesis. *BioEssays News Rev Mol Cell Dev Biol* **43**: e2000335.

Fig. 1

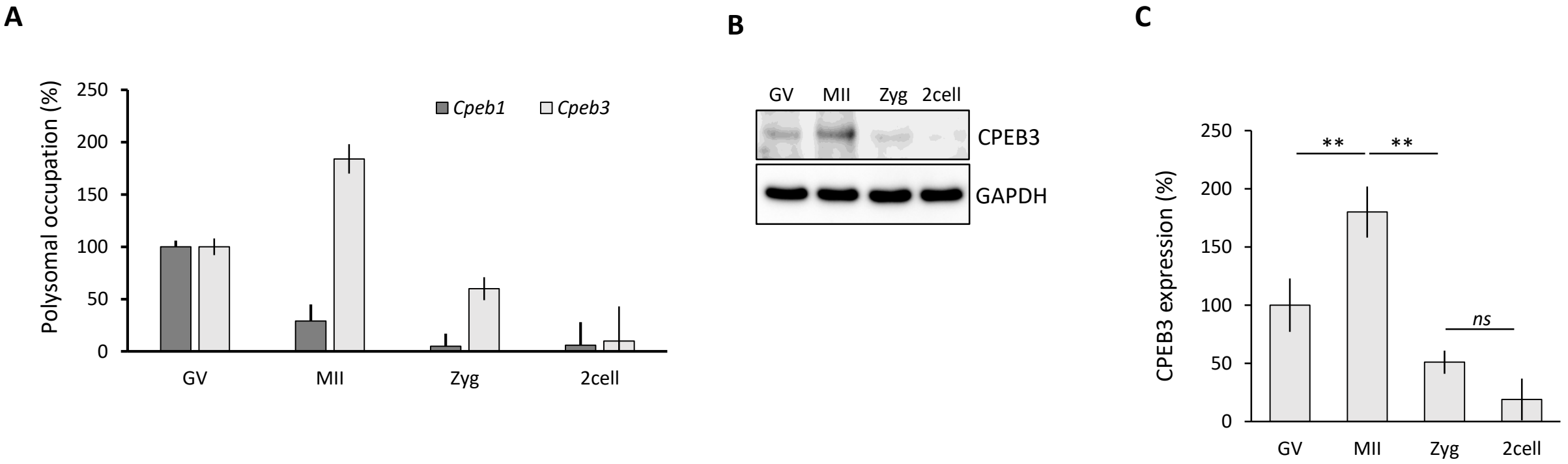

Fig. 1: CPEB3 is actively translated during oocyte maturation. A) Quantification of polysomal occupation of *Cpeb1* and *Cpeb3* mRNAs in oocyte and early embryo. **B**) CPEB3 protein expression in oocyte and early embryo. The images are representative from three biological replicates. **C**) Quantification of CPEB3 protein expression. Data are represented as the mean ± SEM of at least three independent experiments; *ns*, not significant; **$p < 0.01$ according to One-way ANOVA.

Fig. 2

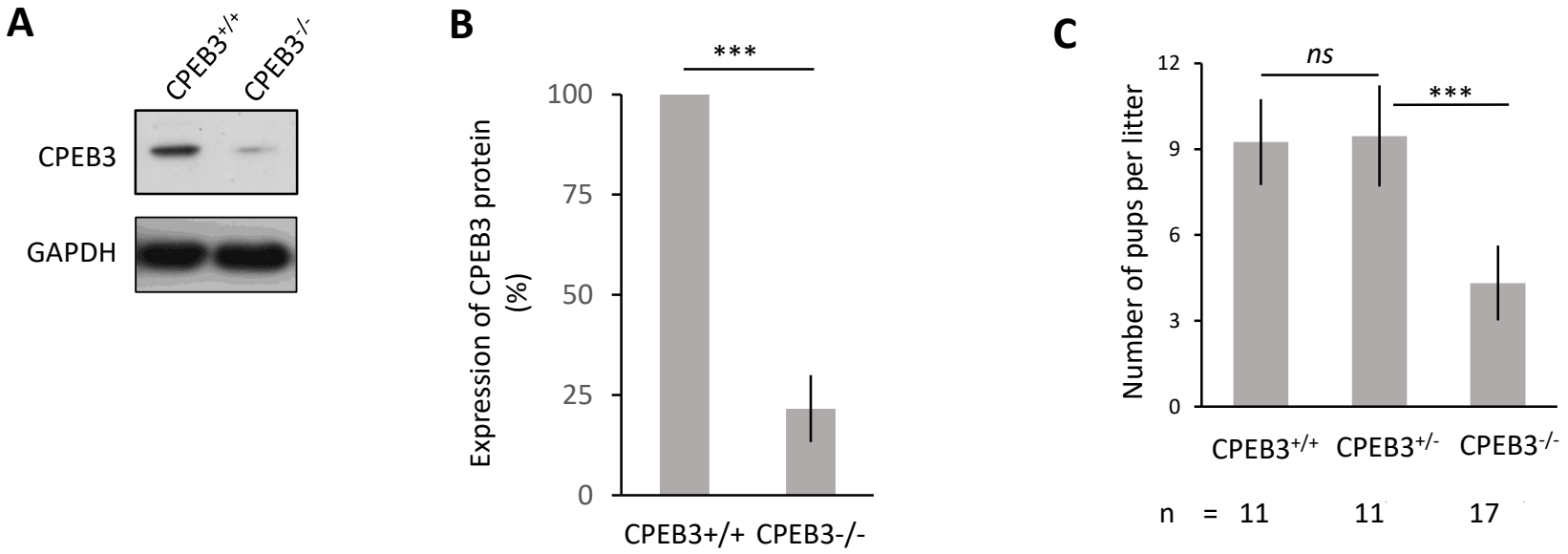

Fig. 2: Significantly decreased CPEB3 in the oocytes, leading to subfertility. A) CPEB3 protein expression in wild-type ($CPEB3^{+/+}$ and cKO ($CPEB3^{-/-}$) oocytes. The images are representative from six biological replicates. For CPEB3 mRNA expression, see **Fig. S1. B**) Quantification of CPEB3 protein expression in **A**). Data are represented as the mean ± SEM of six independent experiments; *** $p < 0.001$ according to one-way ANOVA. **C**) Quantification of number of pups per litter for females with specific genotype. Data are represented as the mean ± SEM; the number of breeding pairs is depicted below; *ns*, non-significant; *** $p < 0.001$ according to one-way ANOVA. For additional analyses of reproductive fitness, see **Fig. S1.**

Fig. 3

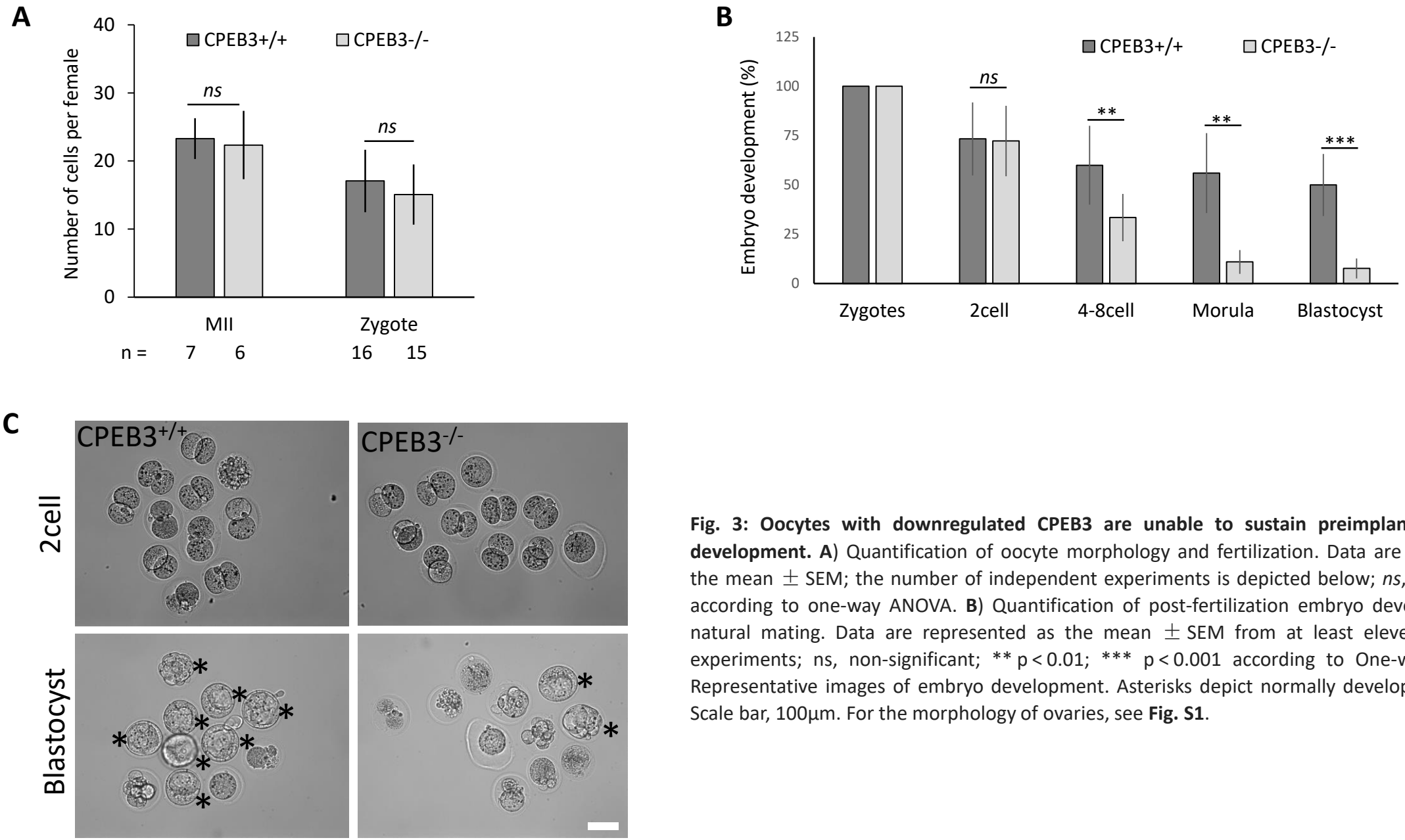

Fig. 3: Oocytes with downregulated CPEB3 are unable to sustain preimplantation embryo development. A) Quantification of oocyte morphology and fertilization. Data are represented as the mean ± SEM; the number of independent experiments is depicted below; *ns*, non-significant according to one-way ANOVA. **B**) Quantification of post-fertilization embryo development using natural mating. Data are represented as the mean ± SEM from at least eleven independent experiments; ns, non-significant; ** $p < 0.01$; *** $p < 0.001$ according to One-way ANOVA. **C**) Representative images of embryo development. Asterisks depict normally developed blastocysts. Scale bar, 100µm. For the morphology of ovaries, see **Fig. S1**.

Fig. 4

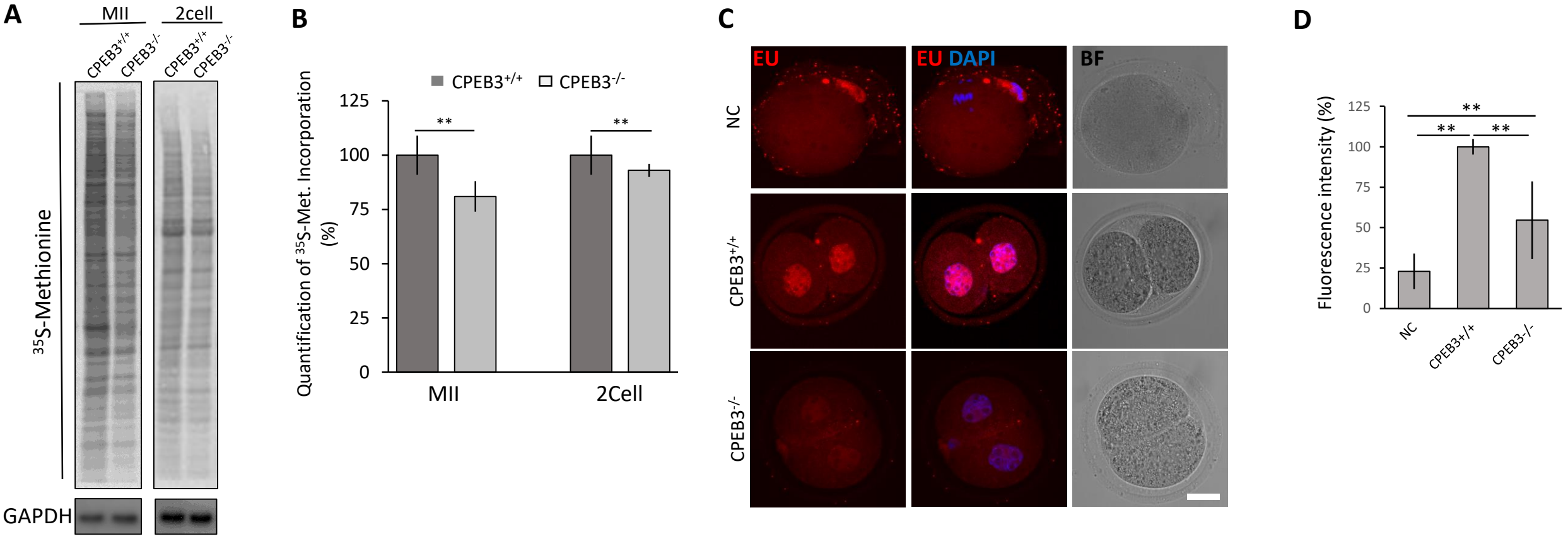

Fig. 4: CPEB3 depletion results in decreased global protein synthesis and transcriptional activity of the 2-cell embryo. A) Visualization of ^{35}S-Methionine incorporation into nascently synthetized proteins. N≥4 of biological replicates, GAPDH was used as a loading control. **B**) Quantification of Visualization of ^{35}S-Methionine incorporation. Data are represented as the mean ± SEM from at least flour independent experiments; ** $p < 0.01$ according to one-way ANOVA. **C**) Fluorescent labelling of newly transcribed RNA via 5-ethynyluridine (EU, red) in 2cell embryo. Transcriptionally inactive MII oocytes were used as a negative control (NC); n≥30, DNA blue; BF, bright field. For the timing of embryo cleavage, see **Fig. S2**. **D**) Quantification of EU fluorescence intensity. Data are represented as the mean ± SEM; the value from CPEB3$^{+/+}$ was set as 100%; ** $p < 0.01$ according to one-way ANOVA.

Fig. 5

A

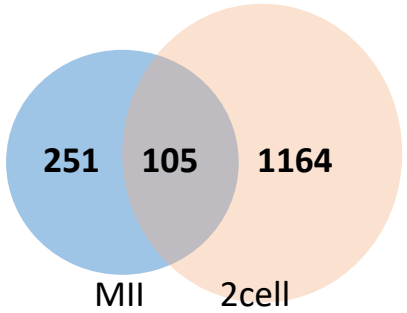

B

	Categories	Functions Annotation	p-Value	# of genes
MII	Nervous System Development	Abnormal morph. of subventricular zone	8,34E-06	5
	Gene Expression	***Expression of RNA***	***0,0000111***	***50***
	Gene Expression, Protein Synthesis	***Translation of mRNA***	***0,0000554***	***9***
	Cell Death and Survival	Apoptosis of neurons	0,000107	15
	Cell Death and Survival	Neuronal cell death	0,000127	20
	Cell Death and Survival	Cell death of T lymphocytes	0,000128	12
	Gene Expression	Expression of mRNA	0,00016	10
	Cell Cycle	**Arrest in M phase of oocytes**	**0,000191**	**2**
2cell	***Gene Expression***	***Transcription of DNA***	***3,41E-26***	***169***
	Gene Expression	***Transcription of RNA***	***3,22E-25***	***190***
	Gene Expression	***Transcription***	***3,67E-25***	***211***
	Gene Expression	***Activation of DNA endogenous***	***2,81E-24***	***142***
	Gene Expression	***Expression of RNA***	***1,64E-22***	***213***
	Embryonic Development	Development of body axis	8,30E-11	102
	Embryonic Development	Patterning of rostrocaudal axis	8,94E-11	21
	Developmental Disorder, Embr. Dev.	Abnormal morph. of embryonic tissue	1,26E-10	63

C

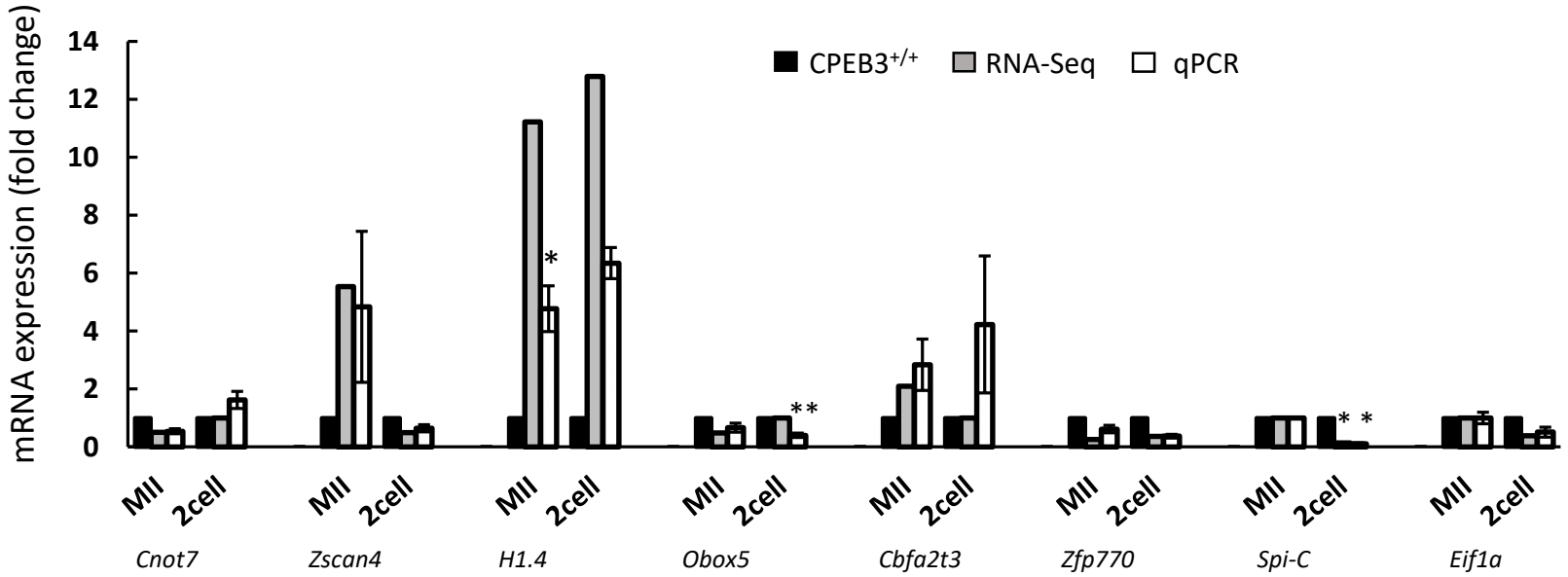

Fig. 5: Absence of CPEB3 affects specific mRNAs in the oocyte and embryo. A) Venn diagram shows number of differentially expressed RNAs, detected by RNA-sequencing. Intersection depicts overlapping genes between two stages. Also see Supplementary File 1. **B**) Top 8 GO cluster enrichment of genes that are differentially expressed in CPEB3$^{-/-}$ MII oocytes and 2cell embryos compared to CPEB3$^{+/-}$. Also see Supplementary File 1. **C**) Validation of candidate genes from RNA-sequencing datasets (grey columns) by qPCR (white columns). Data are represented as the mean ± SEM; the value from CPEB3$^{+/-}$ was set as 1; *p < 0.05, ** p < 0.01 according to one-way ANOVA.

Fig. 6

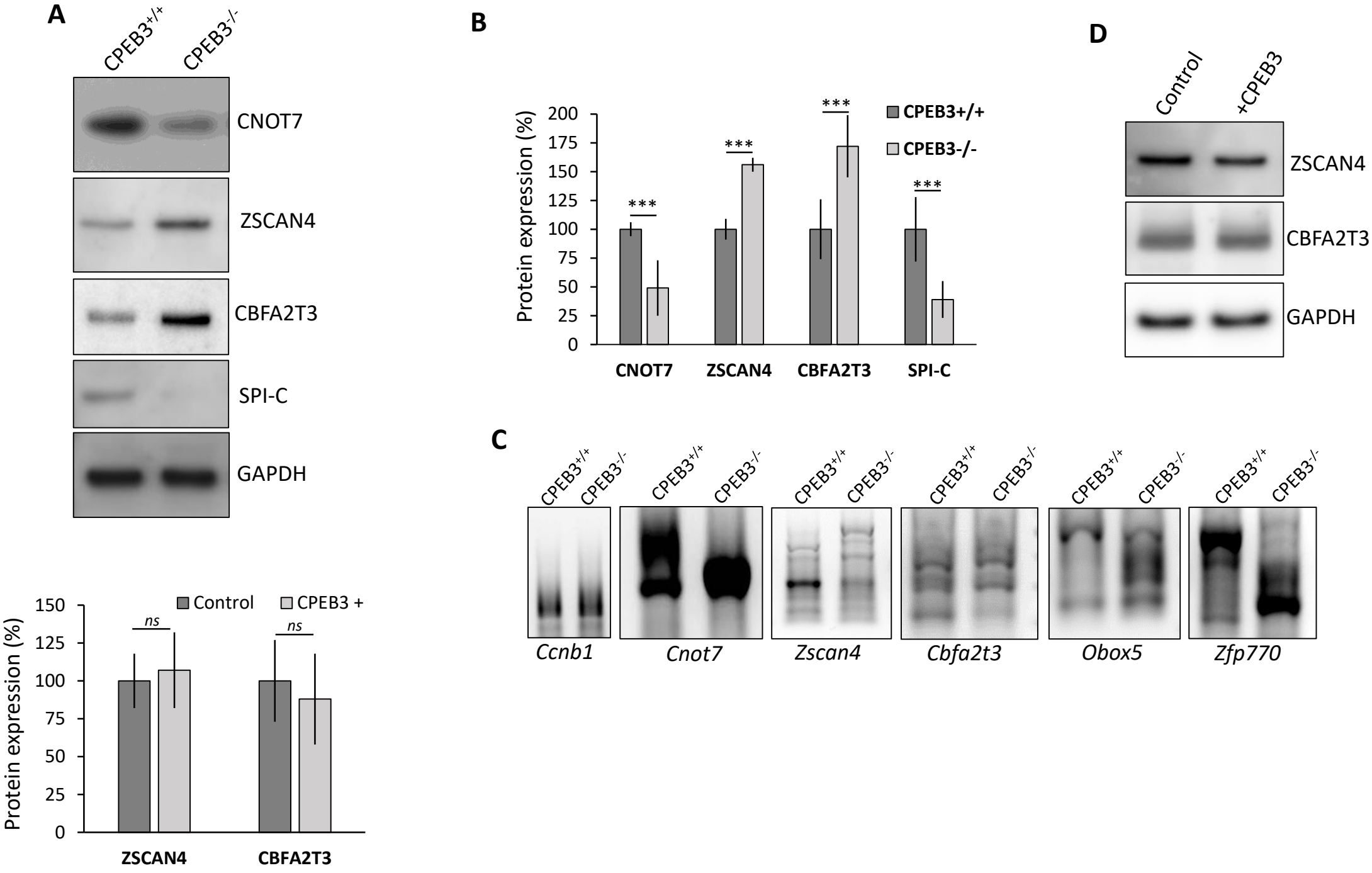
A
CPEB3+/+
CPEB3-/-
CNOT7
ZSCAN4
CBFA2T3
SPI-C
GAPDH
B
Protein expression (%)
200
175
150
125
100
75
50
25
0
***
CPEB3+/+
CPEB3-/-
CNOT7
ZSCAN4
CBFA2T3
SPI-C
D
Control
+CPEB3
ZSCAN4
CBFA2T3
GAPDH
C
CPEB3+/+
CPEB3-/-
Ccnb1
Cnot7
Zscan4
Cbfa2t3
Obox5
Zfp770
E
Protein expression (%)
150
125
100
75
50
25
0
Control
CPEB3 +
ns
ZSCAN4
CBFA2T3

Fig.6: Absence of CPEB3 influences translation of specific mRNAs via polyadenylation. A) Immunoblot analysis of expression of candidate proteins in oocytes (CNOT7, ZSCAN4, CBFA2T3) and embryos (SPI-C). The images are representative from at least three biological replicates. **B**) Quantification of protein expression. Data are represented as the mean ± SEM of at least three independent experiments; *** $p < 0.001$ according to one-way ANOVA. **C**) Polyadenylation assay (PAT) of candidate proteins. *Cyclin B1* mRNA (*Ccnb1*) was used as a negative control. The images are representative from at least three biological replicates. **D**) Microinjection of CPEB3 protein into CPEB3$^{-/-}$ GV oocytes normalizes specific protein expression similarly to that in the CPEB3$^{+/+}$ MII oocyte. Representative images from at least three biological replicates. For analysis of CPEB3 expression see **Fig. S4. E**) Quantification of the protein expression from **D**). Data are represented as the mean ± SEM of at least three independent experiments; *ns*, non-significant according to one-way ANOVA. CPEB3$^{+/+}$ MII oocytes were used as a control and set as 100%.

Fig. 7

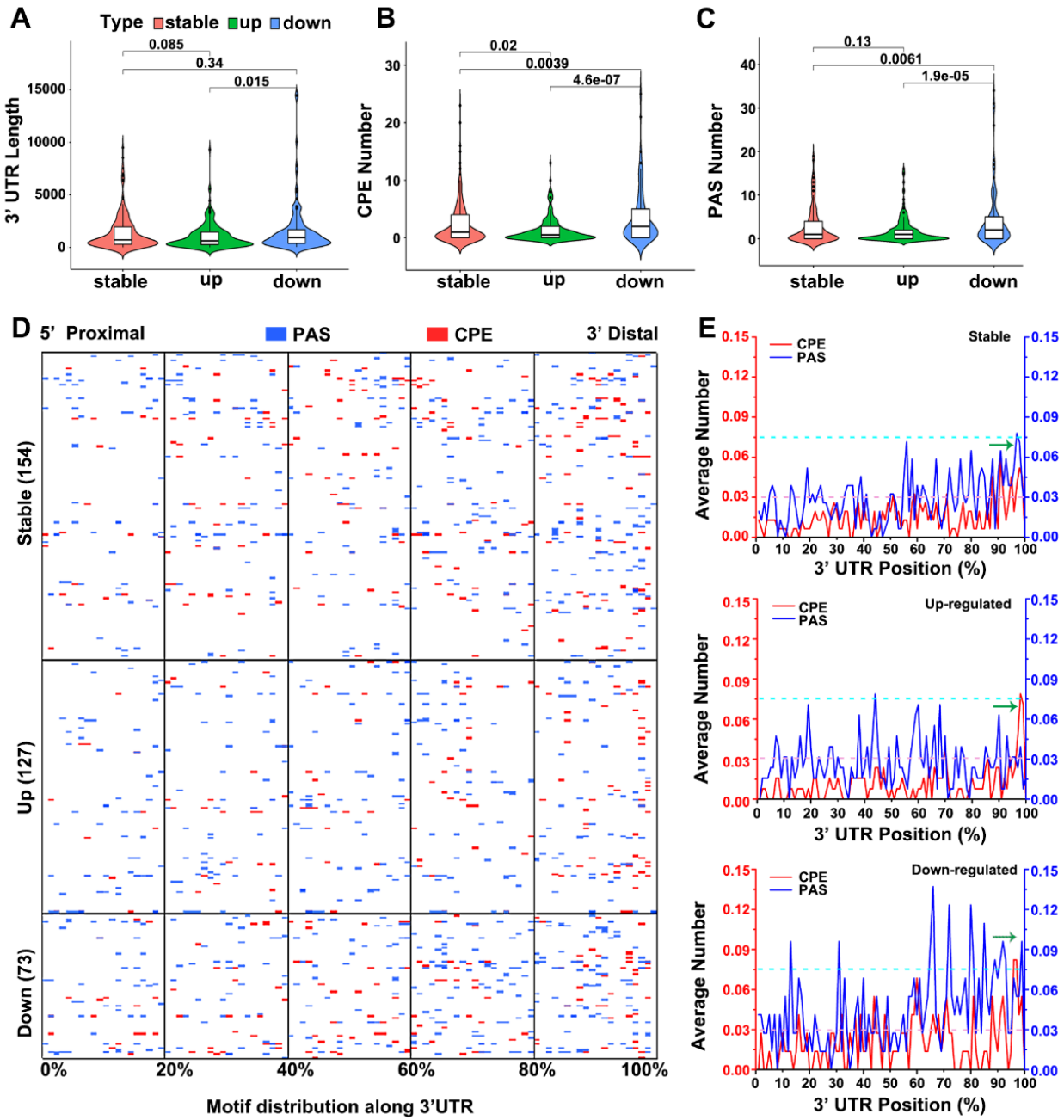

Fig. 7: CPEB3 regulates translation of specific mRNAs via 3'UTR. Computational analysis of differentially expressed transcripts in CPEB3-depleted oocytes. **A**) 3'UTR length. **B**) Number of Cytoplasmic Polyadenylation Element (CPE) motifs. **C**) Number of Polyadenylation Signal (PAS) motifs. **Data are represented in Fig. S1.; stat values according to Wilcoxon test. D**) CPE (red) and PAS (blue) motif distribution in differentially expressed mRNAs in CPEB3-depleted MII oocytes. **E**) CPE (red) and PAS (blue) motif distribution in differentially expressed subclass of transcripts in CPEB3 depleted MII oocytes.

OXFORD UNIVERSITY PRESS | Nucleic Acids Research

The translational oscillation in oocyte and early embryo development

Journal:	*Nucleic Acids Research*
Manuscript ID	NAR-01157-J-2023.R1
Manuscript Type:	1 Standard Article
Key Words:	translation, cell cycle, meiosis, embryogenesis, translational initiation

DATA AVAILABILITY

Does the manuscript use or report the following? If so, please provide details in a Data Availability statement below and in the manuscript.	
New genome expression or sequencing data (ChIP-seq, RNA-seq…) - Must comply with ENCODE Guidelines. - All datasets must be validated via biological replicates. - Must deposit data in GEO or an equivalent publicly available depository and provide accession numbers, private tokens, reviewer login details and/or private URLs for Referees. - Excluding RNA-Seq, data must be viewable on the UCSC (eukaryotes) or other suitable genome browsers; must provide genome browser session links (even if GEO entries are publicly available).	**Yes**
Novel nucleic acid sequences - Must deposit in EMBL / GenBank / DDBJ. - Must provide sequence names and accession numbers.	**No**
Illumina-type sequencing data - Must submit data to BioProject/SRA, ArrayExpress or GEO. - Must provide link for reviewers (BioProject/SRA), login details (ArrayExpress) or accession numbers and private tokens (GEO).	**No**
Novel protein sequences - Must deposit UniProt using the interactive tool SPIN. - Must provide sequence names and accession number.	**No**
Novel molecular structures determined by X-ray crystallography, NMR and/or CryoEM/EM - Must deposit to a member site of the Worldwide Protein Data Bank (RCSB PDB, PDBe, PDBj) and provide the accession numbers. - If structures are unreleased (i.e. status HPUB), **MUST** upload: - the validation reports (.pdf) - molecular coordinates (.pdb or .mmcif). - one of the following: • X-ray data (.mtz, .cif) • NMR restraints and chemical shift files (.mr, .tbl or .str) • CryoEM map files (.map).	**No**
Novel molecular models based on SAXS, computational modeling, or other combinations of strategies that are generally not appropriate for deposition in the PDB - Must deposit coordinates and all underlying data in appropriate databases (including but not limited to the Small Angle Scattering Database and PDB-Dev). - Must report on validation of the structure against experimental data (if available) or report on statistical validation of the structure by model quality assessment programs. If applicable, these should be uploaded as a Data file.	**No**
Molecular behaviour studies derived from biological NMR spectroscopy data (not necessarily leading to new structures)	**No**

- Must deposit NMR spectral data, including assigned chemical shifts, coupling constants, relaxation parameters (T1, T2, and NOE values), dipolar couplings, in BMRB.	
Novel nucleic acids structure - Must deposit to NDB (via PDB if possible) and provide accession numbers.	**No**
Structures of nucleosides, nucleotides, other small molecules - Must deposit in the Cambridge Crystallographic Data Centre (CCDC) and provide the structure identifiers.	**No**
Mass spectrometry proteomics - Must deposit to ProteomeXchange consortium and provide Dataset Identifier and reviewer account details. If appropriate, data and corresponding details can also be deposited in the Panorama repository for targeted mass spec assays and workflows.	**No**
Microarray data - Must comply with the MIAME Guidelines - Must deposit the data to GEO or Array Express, and provide accession numbers and private tokens (GEO) or login details (ArrayExpress).	**No**
Quantitative PCR - Must comply with the MIQE Guidelines. - Details should be supplied in Materials and Methods section of manuscript.	**Yes**
Synthetic nucleic acid oligonucleotides including siRNAs or shRNAs - The manuscript should include controls to rule out off-target effects, such as use of multiple siRNA/shRNAs or inclusion of cDNA rescue data. - Manuscript should provide exact sequences, exact details of chemical modifications at any position, and source of reagent or precise methods for creation. These can be included in the main text or in Supplementary Material.	**Yes**
Software and source codes - Must deposit in FigShare and provide link to code and/or DOI or upload source code as Data file.	**No**
Gel images, micrographs, graphs, and tables - Optionally, may deposit in a general-purpose repository such as Zenodo or Dryad. If applicable, provide access details.	**Yes**

REFEREES – you will find data deposition details below
To review GEO accession GSE230016: Go to https://www.ncbi.nlm.nih.gov/geo/query/acc.cgi?acc=GSE230016. Enter token ufydyqaybnuflwz into the box

KEY POINTS

(3 bullet points summarizing the manuscript's contribution to the field)

â€¢	Uniform activation of translational initiation and elongation axes in M-phases of oocyte & embryo.
â€¢	Translational regulation is significantly enriched in meiosis and 2nd embryonic mitosis.
â€¢	The activity of eEF2K/eEF2 axis is essential for preimplantation development.

The translational oscillation in oocyte and early embryo development

Rajan Iyyappan[1*], Daria Aleshkina[1], Hao Ming[2], Michal Dvoran[1], Kianoush Kakavand[1], Denisa Jansova[1], Edgar del Llano[1], Lenka Gahurova[1], Alexander W. Bruce[3], Tomas Masek[4], Martin Pospisek[4], Filip Horvat[5,6], Michal Kubelka[1], Zongliang Jiang[2], Andrej Susor[1*]

[1]Laboratory of Biochemistry and Molecular Biology of Germ Cells, Institute of Animal Physiology and Genetics of the Czech Academy of Sciences, Rumburska 89, 277 21 Libechov, Czech Republic

[2]Department of Animal Sciences, Genetics Institute, University of Florida, Gainesville, FL, 32610, United States

[3]Laboratory of Early Mammalian Developmental Biology, Department of Molecular Biology & Genetics, Faculty of Science, University of South Bohemia in České Budějovice, Branisovská 31a, České Budějovice, Czech Republic

[4]Laboratory of RNA Biochemistry, Department of Genetics and Microbiology, Faculty of Science, Charles University, Viničná 5, 128 44 Prague 2, Czech Republic

[5]Laboratory of Epigenetic Regulations, Institute of Molecular Genetics of the Czech Academy of Sciences, Videnska 1083, 142 20 Prague 4, Czech Republic

[6]Bioinformatics Group, Division of Molecular Biology, Department of Biology, Faculty of Science, University of Zagreb, 10000, Zagreb, Croatia

ABSTRACT

Translation is critical for development as transcription in the oocyte and early embryo is silenced. To illustrate the translational changes during meiosis and consecutive two mitoses of the oocyte and early embryo, we performed a genome-wide translatome analysis. Acquired data showed significant and uniform activation of key translational initiation and elongation axes specific to M-phases. Although global protein synthesis decreases in M-phases, translation initiation and elongation activity increases in a uniformly fluctuating manner, leading to qualitative changes in translation regulation via the mTOR1/4F/eEF2 axis. Overall, we have uncovered a highly dynamic and oscillatory pattern of translational reprogramming that contributes to the translational regulation of specific mRNAs with different modes of polysomal occupancy/translation that are important for oocyte and embryo developmental competence. Our results provide new insights into the regulation of gene expression during oocyte meiosis as well as the first two embryonic mitoses and show how temporal translation can be optimized. This study is the first step towards a comprehensive analysis of the molecular mechanisms that not only control translation during early development, but also regulate translation-related networks employed in the oocyte-to-embryo transition and embryonic genome activation.

INTRODUCTION

The regulation of gene expression and protein synthesis is a complex and dynamic process that involves translational control, modulating the translation of mRNA into protein. Although mRNA levels are an important measure of gene expression, they may not always correspond directly to protein levels due to various molecular mechanisms that can influence translation. Thus, translational control plays a critical role in maintaining a dynamic system of gene expression and protein synthesis in cells (1). Protein synthesis is especially important for mature mammalian oocytes, that rely solely on pre-synthesised maternal mRNAs, translation and its regulation (2, 3). Once the oocyte reaches its fully grown state, referred to as the "germinal vesicle stage" (GV-stage, GV), meiosis is halted during prophase I and transcription is silenced (4). After two asymmetric meiotic divisions with two polar body extrusions (MI and MII) and fertilization, the zygote forms male and female interphase pronuclei. As the pronuclei come together during syngamy, a metaphase plate is established, which triggers the first mitotic division (5). In contrast to non-mammalian vertebrates, zygotic genome activation in mouse occurs at the 2cell stage, however, the first mitotic cleavage is completed relatively late (24 hours after fertilization) (6). Once meiosis is resumed, degradation of maternal mRNAs begins and firmly continues until the major genome activation at the 2cell stage (7).

Many mRNAs in the GV oocyte are stored within ribonucleoproteins (RNPs) to prevent their degradation (8). Selective polyadenylation and de-capping are major controlling mechanisms leading to translation regulation, storage or degradation (9, 10). After nuclear envelope breakdown (NEBD), the oocyte relies mainly on cap-dependent translation, however, global protein synthesis is downregulated (11). Cap-dependent translation is regulated by binding of the translation repressor eIF4E binding protein 1 (4E-BP1) to the eukaryotic translation initiation factor 4E (eIF4E), preventing translation initiation (12). In addition, translation is controlled by the eukaryotic elongation factor 2 kinase (eEF2K), which phosphorylates and inhibits eEF2 (T56), slowing down the translation elongation step (13). The mammalian oocyte is a large cell and therefore has to control its translation spatially, *e.g.* several active chromosomal translation hotspots are controlled by mammalian target of rapamycin (mTOR)–eIF4F activity (the mTOR/4F axis) (14).

It is generally accepted that global translation is less active during M-phase in comparison to interphase as a result of translation initiation factor phosphorylation states (reviewed in 15). Despite a significant reduction of translation in both in mitosis (16) and meiosis (17), translation of a subset of mRNAs is upregulated during the M-phase progression, compared to interphase, via upregulation of the mTOR/4F axis (14, 18, 19). In somatic cells, terminal oligopyrimidine tract (TOP) containing mRNAs are actively translated in mitotic M-phase (20). In mammalian oocytes, there is a unique opportunity to compare the expression of various proteins in the meiotic M-phase or early embryo mitoses and identify specific actively translated mRNAs. The roles of such upregulated mRNAs during M-phase are not well understood and studying their expression in oocytes and early embryos may provide valuable insights into their functions.

Here we present the patterns of translational regulation in oocyte and early embryo development, with emphasis on the cell cycle. We show highly dynamic quantitative and qualitative changes of translatomes in interphases and M-phases, related to the regulation of cell physiology that orchestrates developmental processes. In addition, our results reveal several candidate genes that may be important for meiotic maturation and early embryonic development.

MATERIAL AND METHODS

Oocyte and embryo isolation and cultivation

Oocytes were acquired from ICR mice of a minimum of 6 weeks old. The females were stimulated 46 h prior to oocyte isolation using 5 IU of pregnant mare serum gonadotropin (PMSG; Folligon; Merck Animal Health) per mouse. Fully grown GV oocytes were isolated into transfer medium (TM) supplemented with 100 µM 3-isobutyl-1-methylxanthine (IBMX, Sigma Aldrich) to prevent spontaneous meiotic resumption. Selected oocytes were denuded and cultivated in M16 medium (Merck Millipore) without IBMX at 37°C, 5% CO_2 for 0 (GV) or 12 hours (MII). For embryo collection, the PMSG stimulated mice were injected with 5 IU hCG before being mated overnight with males of the same strain. After 16 hours, zygotes were recovered from the excised oviducts and cultured in KSOM medium (Merck Millipore) until 2cell stage. Interphase pronuclei zygotes were collected at the time point of isolation; metaphase zygotes and 2cell embryos were treated with nocodazole (10uM; M1404, Sigma Aldrich). Embryos were treated with 0.5 mM sodium arsenite in KSOM medium (21). The expected developmental results of the treated cells were normalized to the controls, which were set at 100%. All animal experiments were performed in accordance to guidelines and protocols approved by Laboratory of Biochemistry and Molecular Biology of Germ Cells at the Institute of Animal Physiology and Genetics in Czech Republic (22). All animal work was conducted according to Act No. 246/1992 on the protection of animals against cruelty, issued by experimental project #67756/2020MZE-18134, issued by the Ministry of Agriculture.

In vitro fertilization (IVF)

4-week old female ICR mice were injected with 5IU of PMSG (ProSpec) 46 hours prior to hCG (ProSpec) administration (12-12-day/night cycle). For *in vivo* MII collection, mice were sacrificed 14 hours post-hCG injection. Cumulus-oocyte complexes for *in vitro* fertilization (IVF) were collected from ampulla into preheated and equilibrated KSOM medium (Merck). In *vitro* matured denuded MII oocytes were subjected to IVF following 15 hours culture in a MEM medium (M0200, Sigma Aldrich). Sperm were retrieved from cauda epididymis of 12-week old males and capacitated for a 1 hour in HTF medium (Merck) supplemented with BSA (BioXtra, Sigma Aldrich) and GSH (BioXtra, Sigma Aldrich). The IVF itself was performed for 4 hours in the same media as sperm capacitation followed by switching into KSOM media.

Inhibitor treatment

Oocytes were treated with selective p70 ribosomal S6 kinase (S6K1) inhibitor p70KI (5μM; PF-4708671, Selleckchem) or Exotoxin A (72nM, ETA; P0184, Merck) from 0 (GV) to 16 hours (MII) in M16 medium. Zygotes were treated with p70KI or ETA, 0 (Zygote) 20 hour (2cell) then washed and cultured until the blastocyst stage in M16 medium under mineral oil. IVF embryos were treated with p70KI prior to fertilization during oocyte progression from 0 (GV) to 16 hours (MII) in M16 medium.

RNA isolation and qPCR

TRIzol reagent (Invitrogen) was used for RNA extraction following the manufacturer's instructions. Reverse transcription was performed with qPCRBIO cDNA Synthesis Kit (PCR Biosystems). qPCR was then carried out using the QuantStudio 3 (Applied Biosystems) and the Luna® Universal qPCR Master Mix (New England BioLabs) according to manufacturer's protocols with an annealing temperature of 60˚C. Primers are listed in Supplementary Table S1A.

Immunoblotting

An exact number of cells (15–30 oocytes) were washed in PVA/PBS and frozen to −80°C. Prepared samples were lysed in NuPAGE LDS Sample Buffer (NP0007, Thermo Fisher Scientific) and NuPAGE Sample Reducing Agent (NP0004, Thermo Fisher Scientific) and heated at 100°C for 5 minutes. Proteins were separated on precast gradient 4–12% SDS–PAGE gel (Thermo Fisher Scientific) and blotted to Immobilon P membrane (Millipore) in a semidry blotting system (Biometra GmbH) at 5 mA cm^2 for 25 minutes. Membranes were then blocked in 5% skimmed milk dissolved in 0.05 % Tween-Tris buffer saline (TTBS), pH 7.4 for 1 hour. Membranes were incubated overnight at 4°C with relevant primary antibodies (Supplementary Table S1B) diluted in 1% milk/TTBS. Appropriate Peroxidase conjugated secondary antibodies were used (711-035-152 Anti-Rabbit Donkey, or 715-035-151 Anti-Mouse Donkey, both Jackson Immunoresearch) at a 1:7500 dilution in 1% milk/TTBS for 1 hour at room temperature. ECL (Amersham) was used for visualization of immunodetected proteins on X-ray films. The films were scanned by calibrated densitometer (GS- 800, Bio-Rad Laboratories) and quantified in ImageJ. Presented images were cropped from membranes, contrast and brightness was adjusted using Adobe Photoshop CS3.

Immunocytochemistry

Fixed oocytes (15 minutes in 4% PFA, Sigma Aldrich) were permeabilized in 0.1% Triton X-100 for 10 minutes, washed in PBS supplemented with polyvinyl alcohol (PVA, Sigma Aldrich) and incubated with primary antibodies (Supplementary Table S1B), diluted in PVA/PBS and incubated overnight at 4°C. Oocytes were then washed 2 × 15 minutes in PVA/PBS and antigen-associated primary antibodies were detected using relevant Alexa Fluor 488/594/647 conjugates (Invitrogen), diluted to 1:250 for 1 hour at room temperature. One drop of ActinGreen 488 ReadyProbes Reagent (R37110, Invitrogen) per 10 minute was then used for labelling filamentous actin in each sample (20–30 oocytes per group). Washed oocytes (2 × 15 minutes in PVA/PBS) were mounted onto slides using ProLong Mounting Medium with DAPI. An inverted confocal microscope (Leica SP5) was used for sample visualization. Image quantification and assembly were performed using ImageJ and Adobe Photoshop CS3. Experiments were repeated three time, with 20–30 oocytes per group/experiment.

Measurement of overall protein synthesis

To measure the overall protein synthesis, 50 mCi of ^{35}S-methionine (Perkin Elmer) was added to methionine- free culture medium. Exact number of oocytes per sample (5-10) were labelled for 12 hours, then lysed in SDS-buffer and subjected to SDS–polyacrylamide gel electrophoresis (PAGE). The labelled proteins were visualized by autoradiography on a BasReader (Fuji) and quantified by Aida software (RayTest). GAPDH (G9545, Sigma Aldrich) was used as a loading control.

***In situ* proximity ligation assay (PLA)**

Proximity ligation assays were performed according to manual instructions of the PLA Duolink kit (Sigma Aldrich). Oocytes and embryos were fixed for 15 minutes in 4% paraformaldehyde in PBS and permeabilized for 10 minutes in 0.1% Triton X-100 in PBS; PLA Duolink kit blocking solution was added to each sample. Oocytes were incubated with primary antibodies; rabbit anti-RPL24 (PA562450, Thermo Fisher) and mouse anti-RPS6 (74459, Santa Cruz) at 4°C overnight. The samples were washed in PBS and then in Wash Buffer A (Sigma Aldrich). The samples were incubated with 40 μL reaction mixtures (8 μL PLA probe MINUS stock, 8 μL PLA probe PLUS stock and 24 μL PBS) in a chamber for

1 hour at 37°C. The slides were then washed in 1x Wash Buffer A for 6x2 minutes and ligation was performed in 40 µL reaction: 1 µL of ligase to 39 µL of ligation solution. Samples were incubated in ligation reaction mixture for 30 minutes at 37°C then washed 6x2 min in Wash Buffer A. 40 µL of amplification reaction (0.5 µL polymerase and 39.5 µL amplification solution) was added to each sample before incubation at 37°C for 100 minutes. Next, the samples were washed in Wash Buffer B (Sigma Aldrich) for 3x5 minutes and in 0.01% Wash Buffer B for 2 minutes. The samples were mounted in Vectashield Mounting Medium containing DAPI (Vector Laboratories). Quantification of interaction foci was performed using ImageJ/FIJI. 3 experiments with 70 oocytes/embryos each were performed.

SSP-profiling

Polysome fractionation followed by RNA isolation was carried out according to Scarce Sample Polysome profiling (SSP-profiling) method by (23). Briefly, cycloheximide - treated oocytes (CHX, Sigma Aldrich) were lysed and resulting samples were loaded onto 10–50% sucrose gradients. Centrifugation was performed in the SW55Ti rotor (Beckman Coulter) at 45,000 RPM (246,078 x g) for 65 minutes at 4°C (Optima L-90 ultracentrifuge, Beckman Coulter). Ten equal fractions were collected from each polysome profile and subjected to RNA isolation by Trizol reagent (Sigma Aldrich). qRT-PCR-based (QuantStudio 3, Applied Biosystems) quantification of 18S and 28S rRNAs in each fraction was applied to visualize individual polysome profiles (23). Sequencing libraries were prepared using SMART-seq v4 ultra low input RNA kit (Takara Bio). Sequencing was performed with Novaseq 6000 (Illumina) as 150-bp paired-end reads. Reads were trimmed using Trim Galore v0.4.1 and mapped onto the mouse GRCm38 genome assembly using STAR (2.5.3a) with default parameters. Individual mapped reads were quantified as fragments per kilobase of exon model per million mapped fragments (FPKM) values with RefSeq genes as reference. Differential expression analysis was performed by a Partek Flow GSA algorithm with default parameters. The genes were deemed differentially expressed if they provided a false discovery rate of < 0.05 and fold change > 2. Webgestalt (https://www.webgestalt.org/) was used to reveal the Gene Ontology (GO).

Statistical analysis and data visualization

For the statistical analysis and data visualization (column charts) GraphPad Prism 8.3 was used. Statistical analysis included Student's t tests to determine if the difference between the groups is statistically significant. All experiments were repeated at least three times. The analysis and visual representation of RNA-seq data were done via R studio and PrismaGraph9 software (volcano plots, heatmaps, Vienna diagrams, dot-plots, PCA; box-plots).

RESULTS

Global translation is decreased in the M-phase of meiosis and the two subsequent mitoses

Due to transcriptional silencing in oocytes and early embryos, mRNA translation is the dominant regulator of oocyte and preimplantation embryo development. To better understand active translation during oocyte (GV and MII) and early embryo development (Zygote and 2cell) we performed a systematic analysis and compared active translation, with emphasis on two major cell cycle phases, interphase and metaphase (M). Timing and sample collection were standardized based on the morphology and immunostaining with an antibody against a nuclear marker (Lamin A/C) and metaphase marker (Histone H3 phosphorylated at Ser130) (Figure 1A), plus the chromosomal and nuclear morphology (Supplementary Figure 1A). Firstly, we performed a ^{35}S-Methionine incorporation assay to analyse global translation in GV (meiotic prophase) and MII (meiotic M-phase) oocytes, as well as early embryos in the zygote (Zyg), zygote in the first mitotic M-phase (Zyg M), 2cell (2cell) and 2cell in the second mitotic M-phase (2cell M) stages. Consistent with previously published results (15, 17), we observed a global decrease in protein synthesis during oocyte and embryo development with a significant decrease during M-phases (Figure 1B, C). To further confirm this finding, we performed proximity ligation assays (PLA) using RPL24 and RPS6 ribosome assembly markers (3). Similarly, ribosome assembly showed decreases from oocyte to embryo stages, with subsequent increases in the zygote and the 2cell stage, yet with concomitant and significant decreases at all M-phases examined (Figure 1D, E). To exclude the possibility that our experimental approach influenced translation, we analysed the activity of the stress marker eIF2α (Ser51) (24), that showed no increase in our samples (Supplementary Figure 1B,C), despite our observation that global translation was significantly decreased (Figure 1B-E). Additionally, we analysed the effect of our synchronisation protocol using nocodazole in the naturally occurring oocyte M-phase. We found no effect of nocodazole on the activity of the stress marker eIF2α (Ser51), phosphorylation of translation initiation and elongation regulators; 4E-BP1 and

eEF2K, respectively (Supplementary Figure 1D), suggesting that such treatment does not induce a translational stress response. Additionally, we analyzed phosphorylation of 4E-BP1, eEF2 and eIF2a in the absence or presence of a cellular stressor (sodium arsenite, 22) which shows clear influence in the M-phases on the translational players via dephosphorylation of 4E-BP1 and phosphorylation of eEF2 and eIF2a (Supplementary Figure 1E). Correspondingly, the Gene Ontology (GO) profiles do not show processes related to the stress response or apoptosis (Figure 5F). The results indicate similar trends for active translation at the global scale with significant decrease in the M-phases (Figure 1B-E). Overall, these results suggest that significant translational changes occur in the oocyte and early embryo depending on the cell cycle stage.

Dynamics of polysome bound mRNAs coding for components of specific biological processes in the oocyte and early embryo development

To decipher the pattern of protein synthesis and its regulation, we conducted Scarce Sample Polysome Profiling (SSP-profiling) to analyse active translation of mRNAs at the genome-wide level (23). An improved SSP-profiling protocol was followed by RNA sequencing (RNA-seq), which allowed us to analyse mRNA translational profiles of mouse oocytes at the GV and MII stages, as well as Zyg, Zyg M, 2cell, and 2cell M stages. A total of 10 fractions were separated by polysomal fractionation, from which the first 5 fractions were pooled and labelled as non-polysome (NP) fractions and the heavier 5 fractions were pooled and labelled as polysome (P) associated fractions. qRT-PCR analysis quantification of 18S and 28S rRNA (the amount of 18S and 28S rRNA provided an assessment of the reproducibility of collected fractions, Supplementary Figure 2) content confirmed the successful separation of polysome occupied RNA (23). Additionally, principal component analysis (PCA) and clustering analysis of polysome and non-polysome RNA-seq profiles demonstrated the reproducibility of sample preparation and RNA-seq profiles between biological replicates in each group and across the assayed developmental stages (Supplementary Figure 3A-E).

We next sought to investigate the regulation of global translation during various stages of oocyte and early embryo development, with a particular emphasis on interphases, meiosis, and the first two embryonic mitoses. First, we characterized the behavior of actively translating mRNAs by analysing the patterns of translational changes between the different stages. A total of 12 distinct clusters exhibiting a specific pattern of mRNAs associated with polysomes were uncovered to statistical significance ($P < 0.05$) (Figure 2A and Supplementary File 2; where genes of each cluster are listed) across all analysed stages. The results clearly show that the translation of maternal mRNAs is highly dynamic and falls into different subgroups representing mRNAs that are important for particular stages. For example, genes falling under clusters 1 and 8 are essential for meiosis and the second mitosis of the embryo. Genes in cluster 10 are mostly expressed in M-phases of meiosis and the first and second embryonic mitoses. Cluster 6 genes are actively translated during the second meiosis of oocyte and the first mitosis in the zygote. Cluster 7 shows a strong association with polysomes only in the first embryonic mitosis. Conversely, cluster 11 is important only for the second meiotic division without a role in earlier development. Translation of mRNAs from clusters 5, 9, and 12 are involved in post-fertilization processes and are necessary for the second embryonic meiosis.

Next, we performed Gene Ontology analysis (GO; Figure 2B) to understand the biological function of each gene cluster. Overall, GO analysis showed that most of the polysome occupied mRNAs belong to biological processes linked to translation, RNA metabolism, proteasome, post-translational modification, apoptosis and cell cycle (Figure 2B and Supplementary File 3).

Differential perturbations of the translatome depending on developmental and cell cycle stage

We next performed comparative analyses of differential mRNA translation based on developmental stage and cell cycle in connection to Figure 1 B-E. For validation we selected candidate genes coding for a key meiotic and mitotic cell cycle factor *Cdc20* (25), Oocyte- And Embryo-Specific Protein 19 (OOEP), 60S Ribosomal Protein L35 (RPL35), MOS Proto-Oncogene, Serine/Threonine Kinase (Mos) and RNA Polymerase II Subunit I (POLR2I) (Supplementary Figure 4). Total mRNA coding for CDC20 is equally expressed in oocytes and embryos except for 2cell stage (2-fold change between 2cell M vs. 2cell) (Supplementary Figure 4A), however, in the polysomal fractions its mRNA is significantly elevated during the M-phases (Supplementary Figure 4B, C), positively correlating with the CDC20 protein expression profile (Supplementary Figure 4D). Similarly, the additional candidate mRNAs showed similar polysomal occupancy measured by qPCR (Supplementary Figure 4) and positively correlated with protein expression (Supplementary Figure 4).

Our comparative analyses of GV oocytes with early embryos in interphase (Figure 3A) consistently showed (with respect to Figure 1B-E) that the number of actively translating mRNAs in GV oocytes was significantly higher than in the zygote, with the highest difference being observed in the comparison with the 2cell stage (569 genes) (Figure 3B-E and Supplementary File 4). Translation of 49 and 100 genes were constitutively down- and upregulated, respectively, in zygotes compared to GV oocytes (Figure 3B-E and Supplementary File 4). GO analysis showed that the translation of genes involved in translational processes was significantly higher in GV oocytes when compared to the zygote and 2cell stages (Figure 3F and Supplementary File 5).

When we compared active translation between meiotic metaphase MII and mitotic metaphases (Figure 4A), as expected from Figure 1B, the number of actively translating mRNAs in meiosis was significantly higher than first and second embryonic mitoses (Figure 4B, C). Out of 1,838 identified genes in 2cell M and 539 genes in zygote M, only 180 genes were constitutively upregulated; similarly, out of 427 genes in 2cell M and 215 genes in zygote M, only 97 were constitutively downregulated when compared to meiosis (Figure 4C-E and Supplementary File 6). GO analysis showed that the translation of genes involved in translational processes were significantly higher in the MII stage (Figure 4F and Supplementary File 7).

We then asked how mRNA translation behaves in M-phases in connection to relevant interphases of the oocyte and embryo. To answer this question, we compared the polysome bound mRNA of M-phase with its corresponding interphase stage (Figure 5A). The highest difference among translatomes of M-phase and corresponding interphases was found between 2cell M and 2cell (Figure 5B-D and Supplementary File 8). Next, we analysed if specific genes were uniformly translated in the interphases or M-phases, however, we found that only *Cdc20, CenpA, H2afz, and Nip7* mRNAs were constitutively translated and *Ooep, Elob1* mRNAs suppressed in translation in the M-phase (Figure 5B). Gene ontology analysis showed that translation of mRNAs coding for proteins involved in protein synthesis were highly enriched in M-phases of meiosis and the second mitosis (Figure 5F, G and Supplementary File 8&9). Conversely, the translation of genes involved in the cell cycle regulation were highest in the GV and 2cell interphases (Figure 5F, G and Supplementary File 8&9).

Collectively, our analysis indicates that translation of maternally stored mRNAs is significantly higher in GV and MII stage compared to the zygote and 2cell stages. Additionally, we show that translation of the subset of mRNAs is highly dynamic, stage specific and higher in oocytes than in early embryos. The most significant translatome dynamic occurs in meiosis and the second embryonic mitosis. Our data clearly indicate that the translation of maternal mRNAs is temporally regulated in connection to the cell cycle and developmental stage.

Increased activity of eEF2, 4E-BP1 and mTOR translational pathways during M-phase

The phosphorylation of 4E-BP1 by mTOR results in the release of eIF4E, enabling its interaction with eIF4G and the formation of the eIF4F complex, thereby facilitating cap-dependent translation initiation. To examine the relationship between mTOR signaling and translation during oocyte and embryo development, we conducted immunoblotting (IB) to assess the status of key translational regulators, including 4E-BP1, eukaryotic elongation factor kinase (eEF2K), and its downstream substrate, elongation factor eEF2. We showed that 4E-BP1 was uniformly hyper-phosphorylated during the M-phases, independent of developmental stage, leading to its inability to suppress initiation eIF4F complex formation. (Figure 6A-C). Additionally, the translational and elongation axis consistently exhibited higher activity during the M-phases across all developmental stages. (Figure 6A-C). Our current data also showed that specific mRNAs were actively translated during the M-phase (Figure 5B). Further IB analysis of the additional translational regulators mTOR, RPS6, ERK and translation initiation factors (14, 26) showed the highest activity in the MII oocyte (Figure 6D, E, F and Supplementary Figure 5), correlating with a higher number of mRNAs being translated during this stage (Figure 4). Similarly, we observed that mRNA coding for components of the mTOR pathway (AKT, RPS6) and a number of eukaryotic initiation factors, abundantly occupied polysomes in MII oocytes, with a decreasing trend towards the 2cell M embryo stage (Supplementary Figure 5). To our knowledge, these results provide the first evidence of a uniform activation pattern of the key translation initiation and elongation factors linked to early developmental and cell cycle stages. Furthermore, the obtained data indicate variability of translation and activity of the key translational factors throughout meiotic maturation and early embryo development.

Modulation of eEF2K/ eEF2 axis negatively influences embryo development

Based on the results indicating the activation of eEF2 in oocytes and embryos during M-phase (Figure 6A-C), we investigated whether inactivation of eEF2 would affect the meiotic or developmental competence of oocytes and embryos, respectively. To achieve eEF2 inhibition, we employed continuous activation of eEF2K via inhibition of S6K1 using a selective p70 ribosomal S6 kinase (S6K1) inhibitor (p70KI) and eEF2 inhibitor, ETA compound, (27, 28); leading to increased eIF2 phosphorylation at Ser56 (Supplementary Figure 6A, B and Supplementary Figure 7A, B). Thus, resulting in eEF2 inhibition (29). Our findings revealed no discernible inhibitor effect on meiotic progression nor fertilization (Figure 7A, B and Supplementary Figure 6C and Supplementary Figure 7C, D, F). However, the induced change in eEF2 activity negatively impacted the ability of *in vitro* fertilized oocytes to accomplish preimplantation embryo development to the blastocyst stage (Figure 7C, D). Additionally, we treated zygotes with p70KI and analyzed developmental competence up to the 2cell stage. We found no visible effect of eEF2 inhibition on development to the 2cell stage (Supplementary Figure 6D and Supplementary Figure 7E, G), however, blastocyst development rates were decreased significantly (Figure 7E, F and Supplementary Figure 7E, G).

Collectively, our data clearly suggest that altering the activity of translation elongation during the earliest stages of development (during oocyte meiotic maturation and during the oocyte-embryo transition) has a detrimental effect on the preimplantation developmental potential of oocytes and zygotes.

DISCUSSION

In this study, we used a genome-wide approach to identify cell cycle-dependent translation of maternal mRNAs. In the absence of transcription, translation is the major regulator of oocyte and early embryonic development (7, 30, 31). Our results reveal that global translation varies throughout the cell cycle, specifically during the studied interphases and M-phases, independently of oocyte meiosis or embryonic mitoses. Although translation is globally decreased in M-phases, our analysis of M-phase translatomes reveal surprising uniformity in the activation of translation initiation and elongation players, that promote the translation of a subclass of maternal mRNAs. Throughout the cell cycle, it is critical that certain proteins are synthesized rapidly and in sufficient quantities to ensure an intact continuum of developmental progression (32). Our findings support the importance of translational regulation in this process and suggest that specific subsets of maternal mRNAs are selectively translated during M-phases.

Our study also reveals that certain subsets of mRNAs are part of highly dynamic translational clusters, with the translational rate of 12 observed clusters changing significantly during development and promoting the synthesis of specific proteins essential for the current or subsequent stage. Interestingly, subclasses of mRNAs belonging to different biological processes were expressed in temporally coordinated patterns, exhibiting a few dominant biological processes at specific stages. For example, translation of mRNAs encoding translation factors were most active in the MII oocyte and the 2cell M embryo, positively correlating with increased translation of specific mRNAs associated with the completion of meiosis and the maternal-zygotic transition (MZT) (7). Interestingly, translation of mRNAs encoding cell cycle regulatory factors decreased from the GV oocyte to the MII oocyte and peaked in their translational activity at the 2cell stage, with minimal translation in the MII oocyte or 2cell M embryo. To our surprise, we found only six uniformly translating mRNAs in the M-phases, indicating specific translation in each metaphase. We also observed that a large number of mRNAs were not commonly translated in the M-phases, as in interphases, indicating differential contribution to the meiotic and the first two mitotic M-phases. However, mRNAs encoding essential cell division factors such as CDC20, CENP A, and H2AFZ (33–35), were significantly translated in all three M-phases examined, as were the downregulated oocyte-specific transcripts OOEP and ELOBL (36). Importantly, GO profiles associated with apoptosis showed a decreasing trend, indicating no negative effects of *in vitro* manipulation.

The observed increase in the number of gene transcripts at the 2cell stage could be due to onset of the major genome activation. In mice, the maternal-zygotic transition (MZT) occurs at the late 2cell stage, where developmental control is transferred to the zygotic genome (reviewed in (37). This is accompanied by a significant increase in mRNAs encoding factors involved in translation processes. Interestingly, translation of protein synthesis associated factors are significantly reprogrammed in the MII oocyte and post-2cell stage embryo. Our study also revealed that the most robust translational changes were detected in the second mitotic M-phase, suggesting that transcriptional reprogramming in the second embryonic interphase is reflected by accompanying and related translational changes. This finding is consistent with observations in the bovine model, where MZT occurs at the 8-cell stage (38). Consistently, the post 2cell stage embryo is significantly affected by the downregulation of the eIF2K/eIEF2 signalling axis. Taken

together, our results provide new insights into the dynamic regulation of translation during oocyte and early embryonic development, highlighting the importance of translational control in ensuring the timely and germane progression of the early developmental stages.

Additionally, the study showed significant quantitative changes in the translatomes during oocyte and embryonic development with uniform oscillations observed in the activity of the translational machinery components, including translation initiation and elongation factors. This suggests that the protein synthesis machinery may adapt to optimize the translation of specific mRNAs. Similarly, Smith and Proud, 2008 have reported low phosphorylation status of eEF2 by the inactivation of eEF2K due to elevated calcium levels (40), controlled by the cyclin-dependent kinase (CDK1) in mitotic cells. This is consistent with our finding that eEF2 is dephosphorylated and active during the M-phases of meiosis and mitosis, while the mTOR-eIF4F translation pathway is highly activated during NEBD (14). Such activation disappears post-fertilization and reactivates in the 8- to 16-cell stage mouse embryo (41). Moreover, the dominant activity of mTOR1, RPS6, eIF4E, and ERK1/2 occurs in the oocyte, which correlates with the highest observed levels of global translation. It has been shown that mTOR1 and RPS6 phosphorylation play a role in translational control of a subclass of mRNAs containing the 5'-tract oligopyrimidine sequence (5' TOP) and this level of regulation may confer greater specificity to the ribosome (12, 14, 42, 43). Similarly, ERK1/2 triggers meiosis-dependent mRNA translation. In addition to the uniform mode of increased translational initiation/elongation activity in M-phases, the mTOR1 signaling pathway is unique to oocyte development, which could distinguish meiotic from mitotic translation and represents cell type-specific translation.

Inhibition of the mTOR pathway differentially affects polysomal recruitment of newly translated mRNAs, which are either mTOR-dependent (44) or mTOR-independent (21, 45–49). Similarly, ERK1/2 triggers meiosis-dependent mRNA translation (26). Our results highlight the possibility of translation being reprogrammed to promote translation in a cell type- and cell cycle-dependent manner. This may explain the observed discrepancy between the decrease in global translation and the activation of translation initiation and elongation in meiotic and mitotic M-phases.

In summary, our work sheds light on mRNA translation encoding components of metabolic pathways whose periodic expression has not been previously demonstrated. It is tempting to speculate that the discovered mRNAs and encoded proteins play, as yet, unknown roles in the progression or regulation of the mammalian cell cycle and early development. Along with the observation that temporal patterns are present at the level of translation and oscillatory activity of specific translational players simultaneously ensures the transition of different cell types, cell cycles, and developmental stages.

DATA AVAILABILITY

The raw FASTQ files and normalized gene expression profiles (FPKM) are available at Gene Expression Omnibus (GEO) (https://www.ncbi.nlm.nih.gov/geo/) under the accession number GSE230016.

To review GEO accession GSE230016:

Go to https://www.ncbi.nlm.nih.gov/geo/query/acc.cgi?acc=GSE230016.

Enter token ufydyqaybnuflwz into the box

FUNDING

The project was funded by The Institutional Research Concept RVO67985904 and The Czech Science Foundation (22-27301S) and EXCELLENCE CZ.02.1.01/0.0/0.0/15_003/0000460 OP RDE. Z. J was supported by the NIH Eunice Kennedy Shriver National Institute of Child Health and Human Development (R01HD102533) and USDA National Institute of Food and Agriculture (2019-67016-29863).

DECLARATION OF INTERESTS

The authors declare no competing interests.

ACKNOWLEDGEMENTS

We thank Jaroslava Supolikova and Marketa Hancova for technical assistance with experiments and Petr Svoboda for helpful discussions.

AUTHOR CONTRIBUTIONS

Conceptualization, AS and RI; Methodology, AS, RI, HM, ZJ, TM, MD, DJ, LG, MP, EL, AWB; Validation, AS, RI, ZJ; Investigation, AS, RI, DA; Resources, AS, MK, ZJ; Data Curation, HM, ZJ, AS, RI, LG, KK, FH; Writing – Original Draft, AS, RI, DA; Writing – Review & Editing, all authors; Visualization, RI, AS, DA; ZJ; Supervision, AS, ZJ; Project Administration, AS; Funding Acquisition, AS, MK, ZJ.

REFERENCES

1. Buccitelli,C. and Selbach,M. (2020) mRNAs, proteins and the emerging principles of gene expression control. *Nat Rev Genet*, **21**, 630–644.

2. Hu,W., Zeng,H., Shi,Y., Zhou,C., Huang,J., Jia,L., Xu,S., Feng,X., Zeng,Y., Xiong,T., *et al.* (2022) Single-cell transcriptome and translatome dual-omics reveals potential mechanisms of human oocyte maturation. *Nat Commun*, **13**, 5114.

3. Jansova,D., Tetkova,A., Koncicka,M., Kubelka,M. and Susor,A. (2018) Localization of RNA and translation in the mammalian oocyte and embryo. *PLoS One*, **13**, e0192544.

4. De La Fuente,R. (2006) Chromatin modifications in the germinal vesicle (GV) of mammalian oocytes. *Developmental Biology*, **292**, 1–12.

5. Li,L., Zheng,P. and Dean,J. (2010) Maternal control of early mouse development. *Development*, **137**, 859–870.

6. Svoboda,P. (2018) Mammalian zygotic genome activation. *Semin Cell Dev Biol*, **84**, 118–126.

7. Sha,Q.-Q., Zhang,J. and Fan,H.-Y. (2019) A story of birth and death: mRNA translation and clearance at the onset of maternal-to-zygotic transition in mammals†. *Biology of Reproduction*, **101**, 579–590.

8. Christou-Kent,M., Dhellemmes,M., Lambert,E., Ray,P.F. and Arnoult,C. (2020) Diversity of RNA-Binding Proteins Modulating Post-Transcriptional Regulation of Protein Expression in the Maturing Mammalian Oocyte. *Cells*, **9**, E662.

9. Reyes,J.M. and Ross,P.J. (2016) Cytoplasmic polyadenylation in mammalian oocyte maturation. *Wiley Interdiscip Rev RNA*, **7**, 71–89.

10. Susor,A., Jansova,D., Anger,M. and Kubelka,M. (2016) Translation in the mammalian oocyte in space and time. *Cell Tissue Res*, **363**, 69–84.

11. Susor,A. and Kubelka,M. (2017) Translational Regulation in the Mammalian Oocyte. *Results Probl Cell Differ*, **63**, 257–295.

12. Kalous,J., Tetkova,A., Kubelka,M. and Susor,A. (2018) Importance of ERK1/2 in Regulation of Protein Translation during Oocyte Meiosis. *Int J Mol Sci*, **19**, 698.

13. Hizli,A.A., Chi,Y., Swanger,J., Carter,J.H., Liao,Y., Welcker,M., Ryazanov,A.G. and Clurman,B.E. (2013) Phosphorylation of Eukaryotic Elongation Factor 2 (eEF2) by Cyclin A–Cyclin-Dependent Kinase 2 Regulates Its Inhibition by eEF2 Kinase. *Mol Cell Biol*, **33**, 596–604.

14. Susor,A., Jansova,D., Cerna,R., Danylevska,A., Anger,M., Toralova,T., Malik,R., Supolikova,J., Cook,M.S., Oh,J.S., *et al.* (2015) Temporal and spatial regulation of translation in the mammalian oocyte via the mTOR-eIF4F pathway. *Nat Commun*, **6**, 6078.

15. Sivan,G. and Elroy-Stein,O. (2008) Regulation of mRNA Translation during cellular division. *Cell Cycle*, **7**, 741–744.

16. Tanenbaum,M.E., Stern-Ginossar,N., Weissman,J.S. and Vale,R.D. (2015) Regulation of mRNA translation during mitosis. *eLife*, **4**, e07957.

17. Susor,A., Jelínková,L., Karabínová,P., Torner,H., Tomek,W., Kovárová,H. and Kubelka,M. (2008) Regulation of cap-dependent translation initiation in the early stage porcine parthenotes. *Mol Reprod Dev*, **75**, 1716–1725.

18. Jansova,D., Koncicka,M., Tetkova,A., Cerna,R., Malik,R., del Llano,E., Kubelka,M. and Susor,A. (2017) Regulation of 4E-BP1 activity in the mammalian oocyte. *Cell Cycle*, **16**, 927–939.

19. Tomek,W., Melo Sterza,F.A., Kubelka,M., Wollenhaupt,K., Torner,H., Anger,M. and Kanitz,W. (2002) Regulation of translation during in vitro maturation of bovine oocytes: the role of MAP kinase, eIF4E (cap binding protein) phosphorylation, and eIF4E-BP1. *Biol Reprod*, **66**, 1274–1282.

20. Park,J.-E., Yi,H., Kim,Y., Chang,H. and Kim,V.N. (2016) Regulation of Poly(A) Tail and Translation during the Somatic Cell Cycle. *Mol Cell*, **62**, 462–471.

21. Aleshkina,D., Iyyappan,R., Lin,C.J., Masek,T., Pospisek,M. and Susor,A. (2021) ncRNA BC1 influences translation in the oocyte. *RNA Biol*, **18**, 1893–1904.

22. Tetkova,A. and Hancova,M. (2016) Mouse Oocyte Isolation, Cultivation and RNA Microinjection. *Bio-protocol*, **6**, e1729–e1729.

23. Masek,T., Del Llano,E., Gahurova,L., Kubelka,M., Susor,A., Roucova,K., Lin,C.-J., Bruce,A.W. and Pospisek,M. (2020) Identifying the Translatome of Mouse NEBD-Stage Oocytes via SSP-Profiling; A Novel Polysome Fractionation Method. *Int J Mol Sci*, **21**, E1254.

24. Oyadomari,S., Harding,H.P., Zhang,Y., Oyadomari,M. and Ron,D. (2008) Dephosphorylation of translation initiation factor 2alpha enhances glucose tolerance and attenuates hepatosteatosis in mice. *Cell Metab*, **7**, 520–532.

25. Cooper,K.F. and Strich,R. (2011) Meiotic control of the APC/C: similarities & differences from mitosis. *Cell Division*, **6**, 16.

26. Sha,Q.-Q., Dai,X.-X., Dang,Y., Tang,F., Liu,J., Zhang,Y.-L. and Fan,H.-Y. (2017) A MAPK cascade couples maternal mRNA translation and degradation to meiotic cell cycle progression in mouse oocytes. *Development*, **144**, 452–463.

27. Pearce,L.R., Alton,G.R., Richter,D.T., Kath,J.C., Lingardo,L., Chapman,J., Hwang,C. and Alessi,D.R. (2010) Characterization of PF-4708671, a novel and highly specific inhibitor of p70 ribosomal S6 kinase (S6K1). *Biochem J*, **431**, 245–255.

28. Gholami,A., Minai-Tehrani,D., Mahdizadeh,S.J., Saenz-Mendez,P. and Eriksson,L.A. (2023) Structural Insights into Pseudomonas aeruginosa Exotoxin A–Elongation Factor 2 Interactions: A Molecular Dynamics Study. *J Chem Inf Model*, **63**, 1578–1591.

29. Zhu,H., Yang,X., Liu,J., Zhou,L., Zhang,C., Xu,L., Qin,Q., Zhan,L., Lu,J., Cheng,H., *et al.* (2015) Eukaryotic elongation factor 2 kinase confers tolerance to stress conditions in cancer cells. *Cell Stress and Chaperones*, **20**, 217–220.

30. Hashimoto,N. and Kishimoto,T. (1988) Regulation of meiotic metaphase by a cytoplasmic maturation-promoting factor during mouse oocyte maturation. *Dev Biol*, **126**, 242–252.

31. Wang,Q. and Latham,K.E. (1997) Requirement for protein synthesis during embryonic genome activation in mice. *Mol Reprod Dev*, **47**, 265–270.

32. Barrett,T., Wilhite,S.E., Ledoux,P., Evangelista,C., Kim,I.F., Tomashevsky,M., Marshall,K.A., Phillippy,K.H., Sherman,P.M., Holko,M., *et al.* (2013) NCBI GEO: archive for functional genomics data sets--update. *Nucleic Acids Res*, **41**, D991-995.

33. Dong,M., Chen,J., Deng,Y., Zhang,D., Dong,L. and Sun,D. (2021) H2AFZ Is a Prognostic Biomarker Correlated to TP53 Mutation and Immune Infiltration in Hepatocellular Carcinoma. *Frontiers in Oncology*, **11**.

34. Kapanidou,M., Curtis,N.L. and Bolanos-Garcia,V.M. (2017) Cdc20: At the Crossroads between Chromosome Segregation and Mitotic Exit. *Trends in Biochemical Sciences*, **42**, 193–205.

35. Régnier,V., Vagnarelli,P., Fukagawa,T., Zerjal,T., Burns,E., Trouche,D., Earnshaw,W. and Brown,W. (2005) CENP-A Is Required for Accurate Chromosome Segregation and Sustained Kinetochore Association of BubR1. *Molecular and Cellular Biology*, **25**, 3967–3981.

36. Ganesh,S., Horvat,F., Drutovic,D., Efenberkova,M., Pinkas,D., Jindrova,A., Pasulka,J., Iyyappan,R., Malik,R., Susor,A., *et al.* (2020) The most abundant maternal lncRNA Sirena1 acts post-transcriptionally and impacts mitochondrial distribution. *Nucleic Acids Res*, **48**, 3211–3227.

37. Vastenhouw,N.L., Cao,W.X. and Lipshitz,H.D. (2019) The maternal-to-zygotic transition revisited. *Development*, **146**, dev161471.

38. Zhu,L., Zhou,T., Iyyappan,R., Ming,H., Dvoran,M., Wang,Y., Chen,Q., Roberts,R.M., Susor,A. and Jiang,Z. (2022) High-resolution ribosome profiling reveals translational selectivity for transcripts in bovine preimplantation embryo development. *Development*, **149**, dev200819.

39. Smith,E.M. and Proud,C.G. (2008) cdc2-cyclin B regulates eEF2 kinase activity in a cell cycle- and amino acid-dependent manner. *EMBO J*, **27**, 1005–1016.

40. Nygård,O., Nilsson,A., Carlberg,U., Nilsson,L. and Amons,R. (1991) Phosphorylation regulates the activity of the eEF-2-specific Ca(2+)- and calmodulin-dependent protein kinase III. *Journal of Biological Chemistry*, **266**, 16425–16430.

41. Gahurova,L., Tomankova,J., Cerna,P., Bora,P., Kubickova,M., Virnicchi,G., Kovacicova,K., Potesil,D., Hruska,P., Zdrahal,Z., *et al.* (2023) Spatial positioning of preimplantation mouse embryo blastomeres is regulated by mTORC1 and 7mG-cap dependent translation at the 8- to 16-cell transition. 10.1101/2023.03.07.531473.

42. Meyuhas,O. and Dreazen,A. (2009) Ribosomal protein S6 kinase from TOP mRNAs to cell size. *Prog Mol Biol Transl Sci*, **90**, 109–153.

43. Thoreen,C.C., Chantranupong,L., Keys,H.R., Wang,T., Gray,N.S. and Sabatini,D.M. (2012) A unifying model for mTORC1-mediated regulation of mRNA translation. *Nature*, **485**, 109–113.

44. Sabatini,D.M. (2006) mTOR and cancer: insights into a complex relationship. *Nat Rev Cancer*, **6**, 729–734.

45. Dai,X.-X., Pi,S.-B., Zhao,L.-W., Wu,Y.-W., Shen,J.-L., Zhang,S.-Y., Sha,Q.-Q. and Fan,H.-Y. (2022) PABPN1 functions as a hub in the assembly of nuclear poly(A) domains that are essential for mouse oocyte development. *Sci Adv*, **8**, eabn9016.

46. Kim,J. and Lee,G. (2021) Metabolic Control of m6A RNA Modification. *Metabolites*, **11**, 80.

47. Shatsky,I.N., Dmitriev,S.E., Andreev,D.E. and Terenin,I.M. (2014) Transcriptome-wide studies uncover the diversity of modes of mRNA recruitment to eukaryotic ribosomes. *Crit Rev Biochem Mol Biol*, **49**, 164–177.

48. Yao,H., Gao,C.-C., Zhang,D., Xu,J., Song,G., Fan,X., Liang,D.-B., Chen,Y.-S., Li,Q., Guo,Y., *et al.* (2023) scm6A-seq reveals single-cell landscapes of the dynamic m6A during oocyte maturation and early embryonic development. *Nat Commun*, **14**, 315.

49. Zhao,B.S., Roundtree,I.A. and He,C. (2017) Post-transcriptional gene regulation by mRNA modifications. *Nat Rev Mol Cell Biol*, **18**, 31–42.

FIGURE LEGENDS

Figure 1. Global translation is decreased in the M-phase of meiosis and the two subsequent mitoses.

A. Immunocytochemical analysis of oocytes and early embryos in the interphase (LMN A/C, blue) and M-phase (H3-Ser10, red), DNA labelled with DAPI (gray), Actin (green, cortex). Scale bar, 15 µm. The lower row shows the zoomed nuclei/chromosomal area.

B. ^{35}S-methionine labelling of oocytes and embryos to visualize global translation of the specific stage of the developing oocyte and early embryo. GAPDH was used as a loading control, n≥3.

C. Normalized densitometric values of ^{35}S-methionine from stages in the Fig.1B. Data are represented as the mean ± s.d.; $^{**}p<0.01$ according to Student's t-test, n≥3.

D. Proximity ligation assay detecting *in situ* ribosome assembly using RPL24 and RPS6 markers (L24 + S6, green and grey dots). The white and black dashed line indicates cellular cortex; representative images from three independent experiments shown. Scale bar, 20 µm.

E. Quantification of ribosome assembly in the specific developmental stages. Data are represented as the mean ± s.d.; **P<0.01 and ***P<0.001 according to Student's t-test; from three independent experiments, n≥70. For additional analysis see **Supplementary Figure 1.**

Figure 2. Dynamics of polysome bound mRNAs coding for components of specific biological processes in the oocyte and early embryo development.

A. 12 different clusters demonstrate temporal patterns of polysome bound RNAs in the developing oocyte and early embryo. Connected to Supplementary File S1 and Supplementary File 2.
B. Gene Ontology categories that relate to distinct clusters (Fig. 2A) are plotted from over representation analysis (WebGestalt). Connected to **Supplementary File 3**.

Figure 3. Polysome occupancy is higher in the oocyte interphase compared to embryo interphase.
A. Scheme of comparison of meiotic oocyte interphase with embryonic interphase.
B. Differential mRNA translation analysis of GV vs. 1 and 2cell embryo stages. Volcano plots displaying candidate transcripts differentially enriched in polysomal fractions of oocytes and embryos from meiotic interphase and first mitotic interphases, highlighting those with FC > 2 (red) and FC < 2 (blue), adjusted $p<0.05$. Dashed lines indicate candidate mRNAs translated in interphases compared. Connected to **Supplementary File 4**.
C. Heatmaps of Subset of mRNAs down and up regulated in oocyte interphase compared to embryo interphase. **Connected to Supplementary File 4.**
D. Venn diagram showing the number downregulated genes in oocyte interphase compared to embryo interphases. Connected to **Supplementary File 4**.
E. Venn diagram showing the number of upregulated genes in oocyte interphase compared to embryo interphases. Connected to **Supplementary File 4**.
F. Dot plot of top differentially translated gene transcripts and gene ontology (GO) analysis from B. by WebGestalt for each cluster according to the top ranked genes for each cluster. The sizes and colours of the dots represent the number of genes and -log10-transformed *p*-values respectively. Connected to **Supplementary File 5**.

Figure 4. Meiotic M-phase has significantly higher translational activity than mitotic M-phases.
A. Scheme of comparison of meiotic M-phase with embryonic mitoses.
B. Differential mRNA translation analysis of meiotic M-phase vs. 1st and 2nd mitotic M-phases. Volcano plots displaying candidate transcripts differentially enriched in polysomal fractions of oocytes and embryos from interphase and M-phase comparisons, highlighting those with FC > 2 (red) and FC < 2 (blue), adjusted $p<0.05$. Dashed lines indicate candidate mRNAs translated in M-phases compared. **Connected to Supplementary File 6.**
C. Candidate mRNAs commonly downregulated and upregulated in M-phases. **Connected to Supplementary File 6.**
D. Venn diagram showing the number of downregulated genes in MII phase compared to 1st mitotic M-phase. **Connected to Supplementary File 6.**
E. Venn diagram showing the number upregulated genes in MII phase compared to 2nd mitotic M-phase. **Connected to Supplementary File 6.**
F. Dot plot of top differentially translated gene transcripts and gene ontology (GO) analysis from B. by WebGestalt for each cluster according to the top ranked genes for each cluster. The sizes and colours of the dots represent the number of genes and -log10-transformed P-values, respectively. **Connected to Supplementary File 7.**

Figure 5. Translational regulation is significantly enriched in meiosis and 2nd embryonic mitosis.
A. Scheme of interphases and M-phases comparisons.
B. Differential gene expression analysis of M-phase vs. interphase of oocytes and embryos. Volcano plots displaying candidate transcripts differentially enriched in polysomal fractions of oocytes and embryos from interphase and M-phase comparisons, highlighting those with FC > 2 (red) and FC < 2 (blue), adjusted $p<0.05$. Dashed lines indicate candidate mRNAs translated in M-phases compared. See also **Supplementary Fig. 4** for candidate mRNA validation. **Connected to Supplementary File 8.**
C. Venn diagram showing the number of downregulated genes in M-phase compared to interphase. **Connected to Supplementary File 8.**
D. Venn diagram showing the number upregulated genes in M-phase compared to interphase. **Connected to Supplementary File 8.**

E. Candidate mRNAs commonly downregulated and upregulated in M-phases. **Connected to Supplementary File 8.**
F. Dot plot of top differentially translated gene transcripts and gene ontology (GO) analysis from B. by WebGestalt for each group according to the top ranked genes for each cluster. The sizes and colours of the dots represent the number of genes and -log10-transformed P-values, respectively. **Connected to Supplementary File S9.**
G. Line graph derived from the dot plot (Fig.3F) highlighting the translation of cell cycle and translational gene in each group. **Connected to Supplementary File 5**.

Figure 6. Increased activity of eEF2, 4E-BP1 and mTOR translational pathways during M-phase.
A. Immunoblot analyses of the key protein for cap-dependent translation show activity in M-phase. Arrow denotes phosphorylated and arrowhead for total form of protein.
B. Normalized densitometric values from components from A. Data are represented as the mean ± s.d.; values obtained for relevant. stage with highest intensity was set as 100%. Data are represented as mean ± s.d.; **p*<0.05; ***p*<0.01; ****p*<0.001 according to Student's *t*-test; from three biological replicates.
C. Scheme representing the active translation derived from the A and B.
D. Western blot analysis of the key proteins for mTOR-related pathways.
E. Normalised densitometric values of immunoblot of D. Data are represented as mean ± s.d.; MII set as 100%; **p*<0.05; ***p*<0.01; ****p*<0.001 according to Student's *t*-test; from three biological replicates.
F. Scheme representing the mTOR activity derived from the D and E.

Figure 7. Modulation of eEF2K/ eEF2 axis negatively influences embryo development.
A. Scheme for inhibitor treatment of oocytes and impact on meiotic maturation. Representative images of meiotic progression of oocytes treated by 5μM p70KI inhibitor during meiotic maturation. For effect of inhibitor on the eEF2 phosphorylation see **Supplementary Figure 6A, B**.
B. Quantification of oocyte progression from GV to MII stage after inhibitor treatment. Data represented as mean ± s.d.; Student's t-test: *ns*, nonsignificant; from three biological replicates with presented n.
C. Scheme of inhibitor treatment in oocytes and followed by IVF. Representative image of embryo development after inhibitor treatment (p70KI) and IVF; n≥3.
D. Quantification of blastocyst formation after inhibition of eEF2 during oocyte progression followed by IVF. Data are represented as mean ± s.d.; ***p*<0.01 according to Student's *t*-test; from three biological replicates with presented n. For evaluation of fertilization see **Supplementary Figure 6C**.
E. Scheme for inhibitor treatment in embryos. Representative image of embryo development after 5μM inhibitor treatment (p70KI); n≥3.
F. Quantification of blastocyst formation after inhibition of eEF2 at zygote. Data are represented as mean ± s.d.; ***p*<0.01 according to Student's *t*-test; from three biological replicates with presented n. For evaluation of 2cell development see **Supplementary Figure 6D**. For additional inhibitor treatment see **Supplementary Figure 7.**

Graphical abstract
A. Line graph representing the activity of the eIF4F/eEF2 axis and mTOR1 and translational activity during oocyte and early embryo development.
B. Schematic illustration of translation initiation and elongation in the meiotic and mitotic progression of oocytes and early embryos. Green, active and red, inactive.

Figure 1

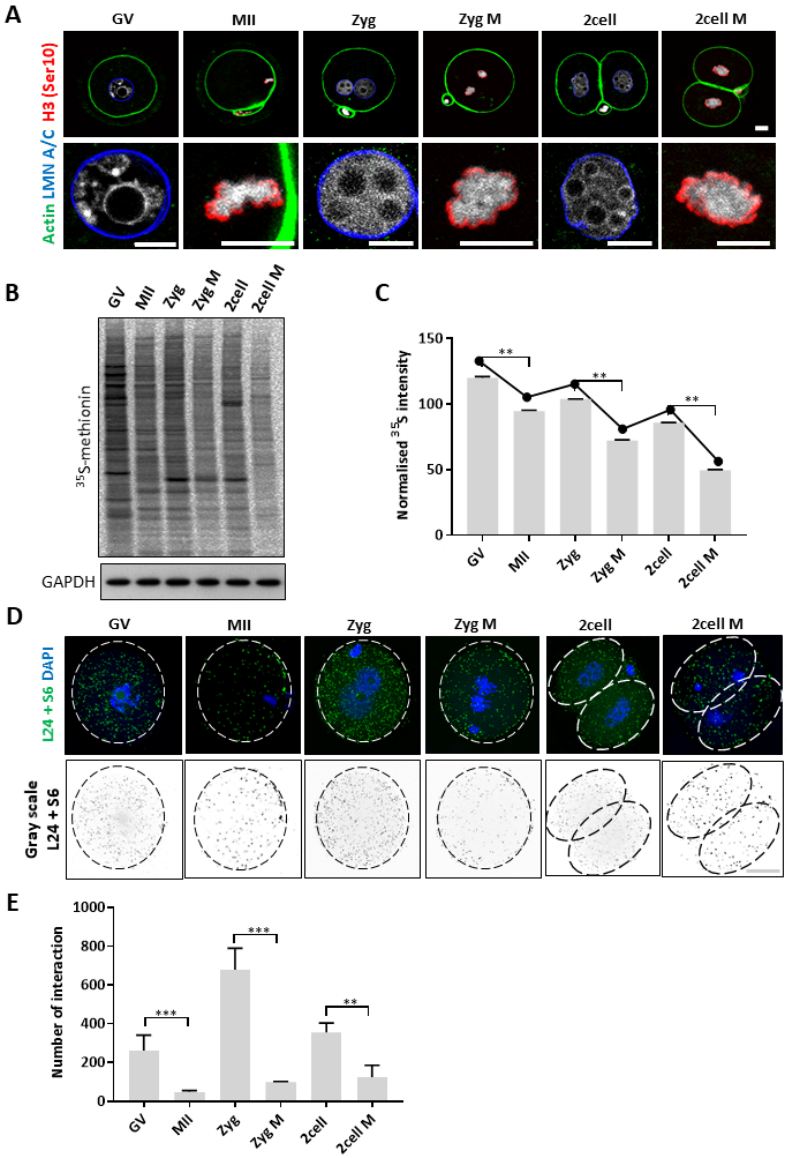

Figure 1

481x695mm (38 x 38 DPI)

Figure 2

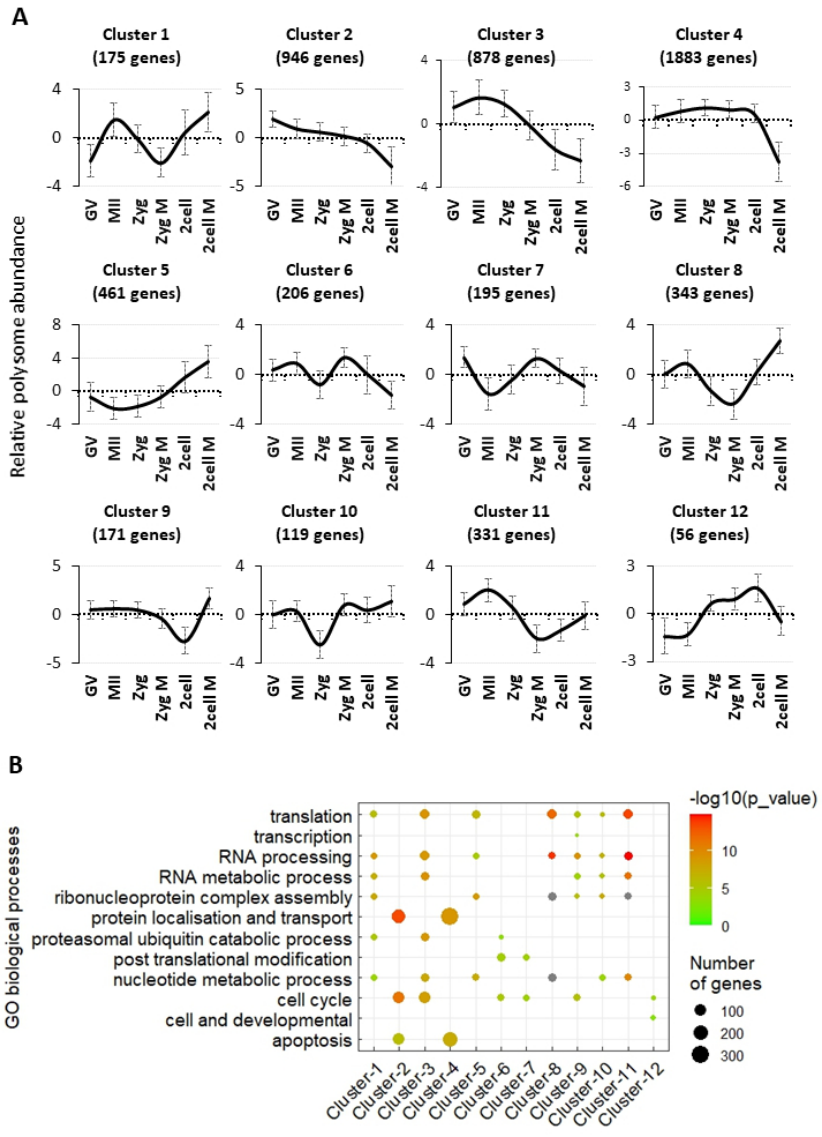

Figure 2

481x695mm (38 x 38 DPI)

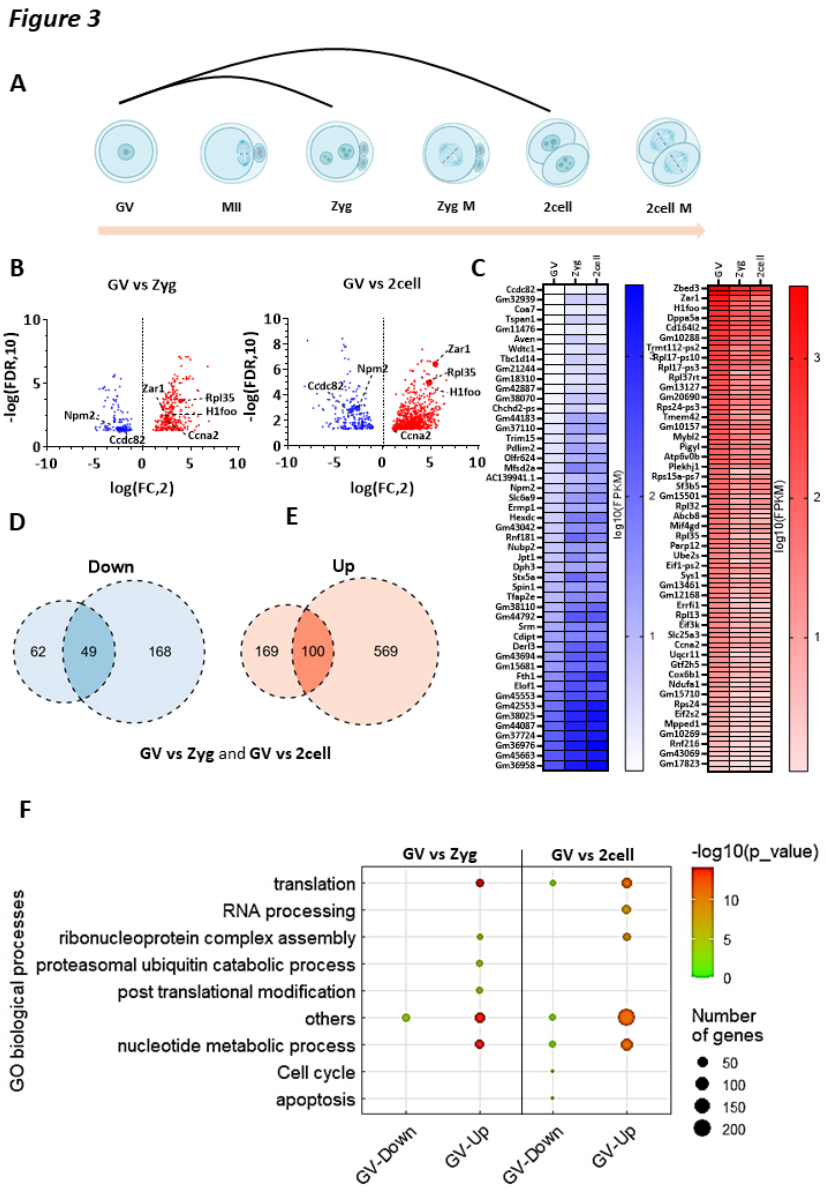

Figure 3

481x695mm (38 x 38 DPI)

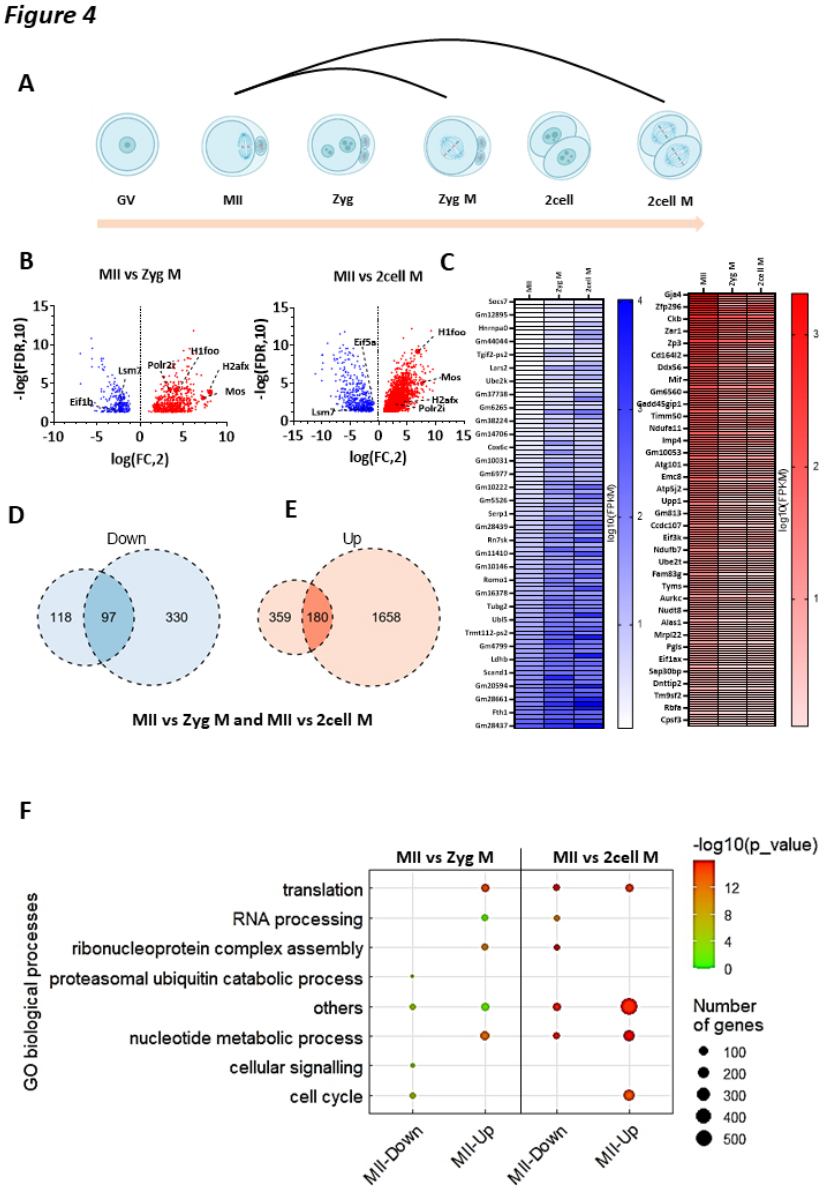

Figure 4

481x695mm (38 x 38 DPI)

Figure 5

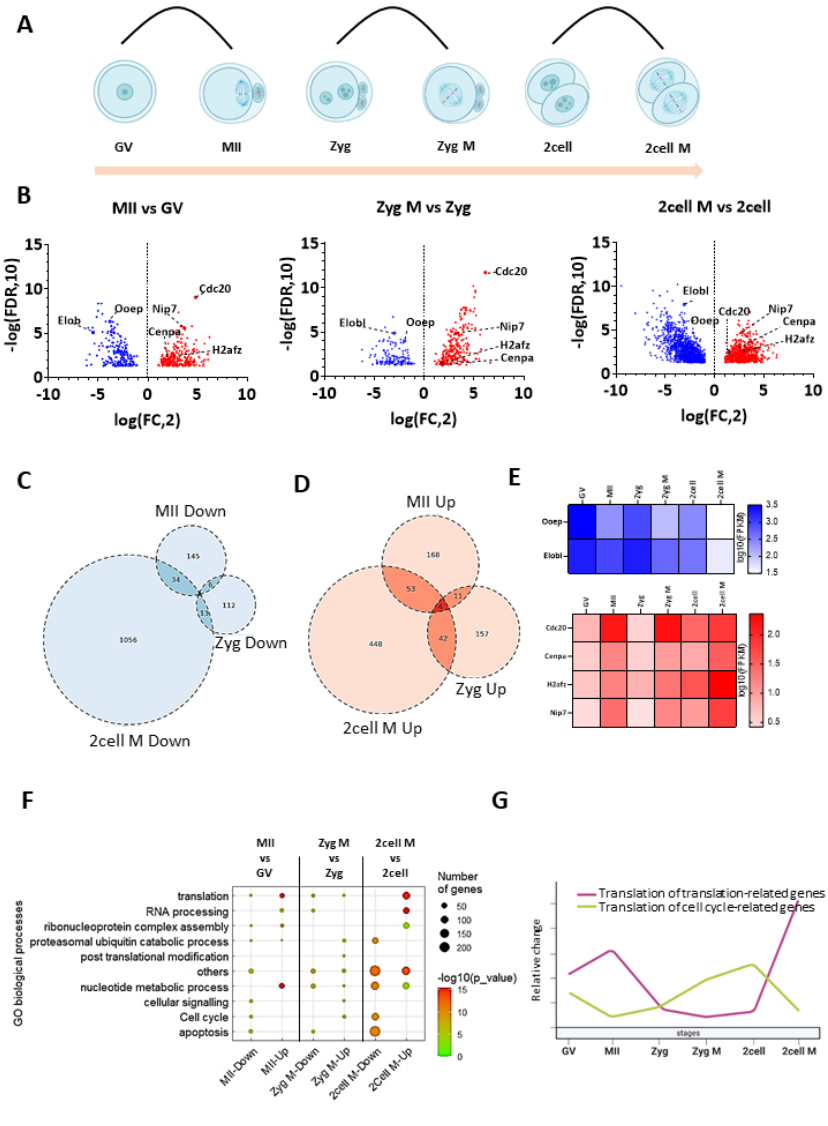

Figure 5

481x695mm (38 x 38 DPI)

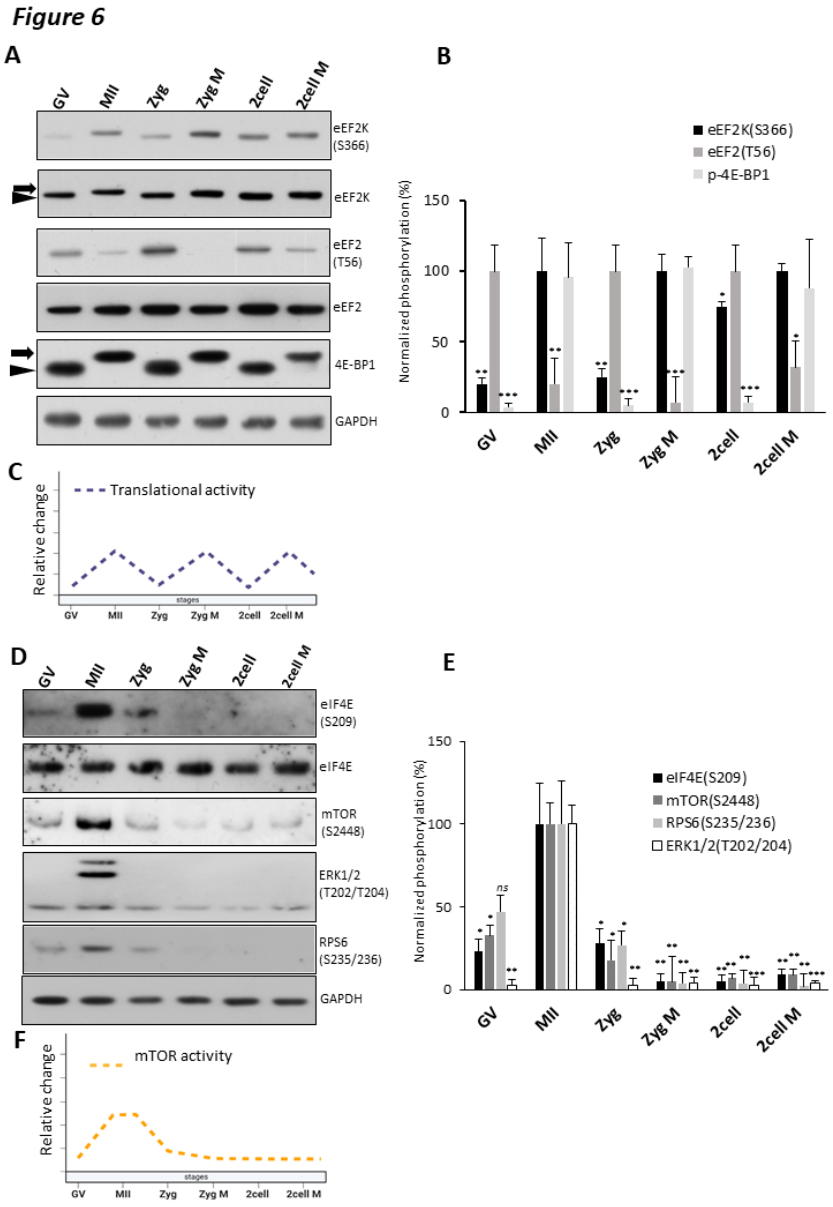

Figure 6

481x695mm (38 x 38 DPI)

Figure 7

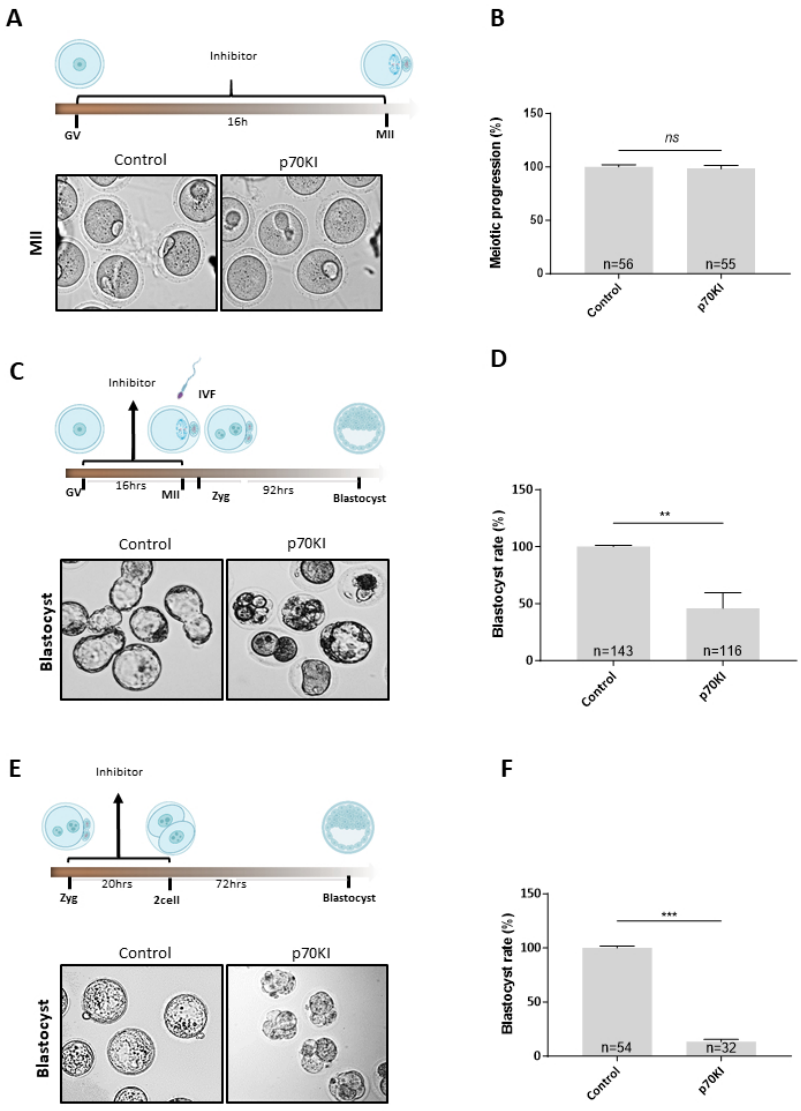

Figure 7

481x695mm (38 x 38 DPI)

Graphical abstract

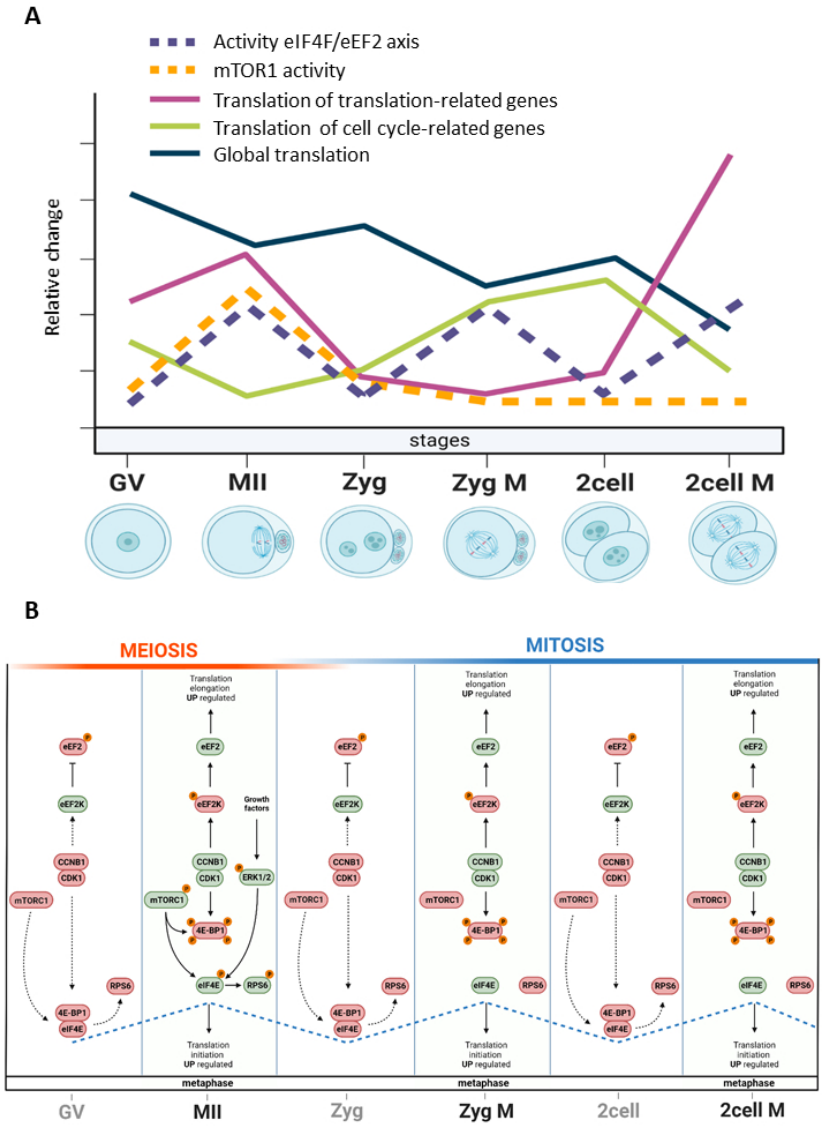

Graphical abstract

481x695mm (38 x 38 DPI)

SUPPLEMENTARY FIGURES LEGENDS

Supplementary Figure 1. Analysis of translational stress in the oocytes and early embryos used in the study.
A. DAPI stained oocytes and early embryos in the interphase and M-phase. Scale bar, 15 µm. The dashed lines represent cell cortex. The lower row shows the zoomed nuclei/chromosomal area.
B. Analysis of activity of the translational stress marker eIF2a (S51) by immunoblotting. GAPDH was used as a loading control. Representative image from three biological replicates.
C. Ratio of the eIF2a activity in the oocyte and early embryo development. Data are represented as the mean ± s.d.; ***p*<0.01; *ns*, nonsignificant; Student's *t*-tests; n≥5.
D. A comparative analysis of the impact of Nocodazole (Noco) on the activity of 4E-BP1, eIF2a, and eEF2K in naturally progressing oocytes. GAPDH was used as a loading control. Representative image from three biological replicates.
E. Immunoblotting analysis of effect of stressor $NaAsO_2$ on the phosphorylation of eIF2a, eEF2 and 4E-BP1 in the embryonic M-phases. GAPDH was used as a loading control. Representative image from three biological replicates.

Supplementary Figure 2. Validation of ribosomal fractionation for presence of 18S and 28S rRNA.
A. qRT-PCR analysis of distribution of 18S rRNA in non-polysomal and polysomal fractions in different developmental stages of oocytes and embryos. Data are represented as the mean ± s.d.
B. qRT-PCR analysis of distribution of 28S rRNA in non-polysomal and polysomal fractions in different developmental stages of oocytes and embryos. Data are represented as the mean ± s.d.

Supplementary Figure 3. RNAseq analysis of ribosomal fractionation from oocytes and early embryos.
A. Principal component analysis of polysomal and non-polysomal RNA in different stages of oocyte and early embryo development.
B. Total number of polysome occupied RNAs >0.1 FPKM in the oocytes and early embryos. No significant change in the total number of gene expressed in each stage. However, genes are differentially expressed based on the cell cycle stages.
C. Heat map showing the differential gene expression of GV and MII stage.
D. Heat map showing the differential gene expression of Zygote and Zygote M stage.
E. Heat map showing the differential gene expression of 2cell and 2cell M stage.

Supplementary Figure 4. Validation of datasets from RNA-seq polysomal fractions.
Analysis of *Cdc20, Ooep, Rpl35, Mos and Polr2i mRNA* expression in whole transcriptome in the different stages. Data are represented as mean ± s.d.; ns-nonsignificant; *p<0.05 according to Student's *t*-test; from three biological replicates. Polysome bound *Ccdc20, Ooep, Rpl35, Mos and Polr2i mRNA* detected by RNA-sequencing. Data are represented as mean ± s.d.; ***p<0.001 according to Student's *t*-test; from four biological replicates. qRT-RT analysis of *Cdc20, Ooep, Rpl35, Mos and Polr2i* mRNA presence in the polysomal fractions. Data are represented as mean ± s.d.; ****p*<0.001 according to Student's *t*-test; from three biological replicates. Immunoblot analysis of CDC20, RPL35, MOS, and POLR2I protein expression in the different developmental stages. Representative image from at least two independent replicates.

Supplementary figure 5. The mTOR1 translational pathway is abundant in the oocyte and decreases in early embryonic development.
A. Polysomal occupation of mRNAs coding for canonical mTOR1 translational pathway. Data are represented as the mean ± s.d.
B. Polysomal occupation of mRNAs coding for eukaryotic initiation factors. Data are represented as the mean ± s.d.

Supplementary Figure 6. Validation of the eEF2 activity with p70KI.
A. Immunoblot analysis of phosphorylation status of eEF2 on Thr56 in the oocytes treated with vehicle (control) and p70KI in different concentration. Representative images from three biological replicates.
B. Normalized densitometric values of eEF2(T51) from components from A. Data are represented as the mean ± s.d.; values obtained for relevant. stage with lowest intensity was set as 100%. Data are represented as mean ± s.d.; *ns*, non-significant; ***p*<0.01 according to Student's *t*-test; from three biological replicates.

C. Quantification of fertilization rate after inhibition of eEF2 using 5 µM p70KI inhibitor during oocyte maturation followed by IVF.
Data are represented as mean ± s.d.; *ns*, nonsignificant according to Student's *t*-test; from three biological replicates with presented n.
D. Quantification of 2cell development after inhibition of eEF2 post fertilization. Data are represented as mean ± s.d.; *ns*, nonsignificant according to Student's *t*-test; from three biological replicates with presented n.

Supplementary Figure 7. Validation of the eEF2 activity with Exotoxin A (ETA).
A. Immunoblot analysis of phosphorylation status of eEF2 on Thr56 in the oocytes treated with vehicle (control) and ETA in different concentration, from three biological replicates.
B. Normalized densitometric values of eEF2(T56) from components from **A**. Data are represented as the mean ± s.d.; values obtained for relevant. stage with lowest intensity was set as 100%. Data are represented as mean ± s.d.; *p<0.05 according to Student's *t*-test; from three biological replicates.
C. Scheme of the experiment and representative images of MII stage oocytes after 16h of 72 nM inhibitor treatment.
D. Quantification of meiotic progression after inhibition of eEF2 during oocyte maturation. Data are represented as mean ± s.d.; *ns*, nonsignificant according to Student's *t*-test; from three biological replicates with presented n.
E. Scheme of the experiment and representative images of the blastocysts from 72 nM ETA treated oocytes.
F. Quantification of fertilization rate after inhibition of eEF2 during oocyte maturation followed by IVF. Data are represented as mean ± s.d.; *ns*, nonsignificant according to Student's *t*-test; from three biological replicates with presented n.
G. Quantification of blastocyst development after inhibition of eEF2 during oocyte maturation followed by IVF and then assessed further development. Data are represented as mean ± s.d.; *ns*, nonsignificant according to Student's *t*-test; from three biological replicates with presented n.

Supplementary Table 1: Supplementary tables of primers used for qPCR (**A**) and primary antibodies used in Immunoblotting, immunocytochemistry and PLA (**B**).

SUPPLEMENTARY FILE LEGENDS

Supplementary File 1. Mouse Polysome_normalized FPKM. A complete list of genes after normalization from RNAseq data are listed in this file. F1: Non polysome, F6: Polysome (highlighted as green). A, B and C represents the first, second and third replicates.

Supplementary File 2. (Fig. 2A) Clusters. Total genes and its average values used for the cluster classification.

Supplementary File 3. (Fig. 2B) GO Dot plot Cluster major. GO analysis and the combined group of GO terms along with "*p*" values of each cluster.

Supplementary File 4. (Fig. 3B, D, E) DE genes interphase vs interphase. List of up and down regulated genes, fold change, and "*p*" values compared to GV *vs*. zygote and GV vs 2cell stage.

Supplementary File 5. (Fig. 3 F) GO Dot plot Oocyte interphase *vs* Embryo interphase. GO analysis and the combined group of GO terms along with "*p*" values of up and down regulated genes compared to GV *vs*. zygote and GV *vs.* 2cell stage.

Supplementary File 6. (Fig. 4B C, D, E) DE genes meiosis *vs* mitosis. List of up and down regulated genes, fold change, and "*p*" values compared to MII vs zygote M and MII *vs*. 2cell M stage.

Supplementary File 7. (Fig. 4F) GO Dot plot Oocyte meiosis *vs* Embryo Mitosis. GO analysis and the combined group of GO terms along with "*p*" values of up and down regulated genes compared to MII *vs*. zygote M and MII *vs*. 2cell M stage.

Supplementary File 8. (Fig. 5B, C, D, E) DE genes M-phase *vs* Interphase. List of up and down regulated genes, fold change, and "*p*" values compared to MII vs GV, zygote M *vs*. Zygote and 2cell M *vs*. 2cell stage.

Supplementary File 9. File (Fig. 5F) GO Dot plot M-phase *vs* Interphase. GO analysis and the combined group of GO terms along with "*p*" values of up and down regulated genes compared to MII vs GV, zygote M vs. Zygote and 2cell M *vs*. 2cell stage.

Supplementary Figure 1

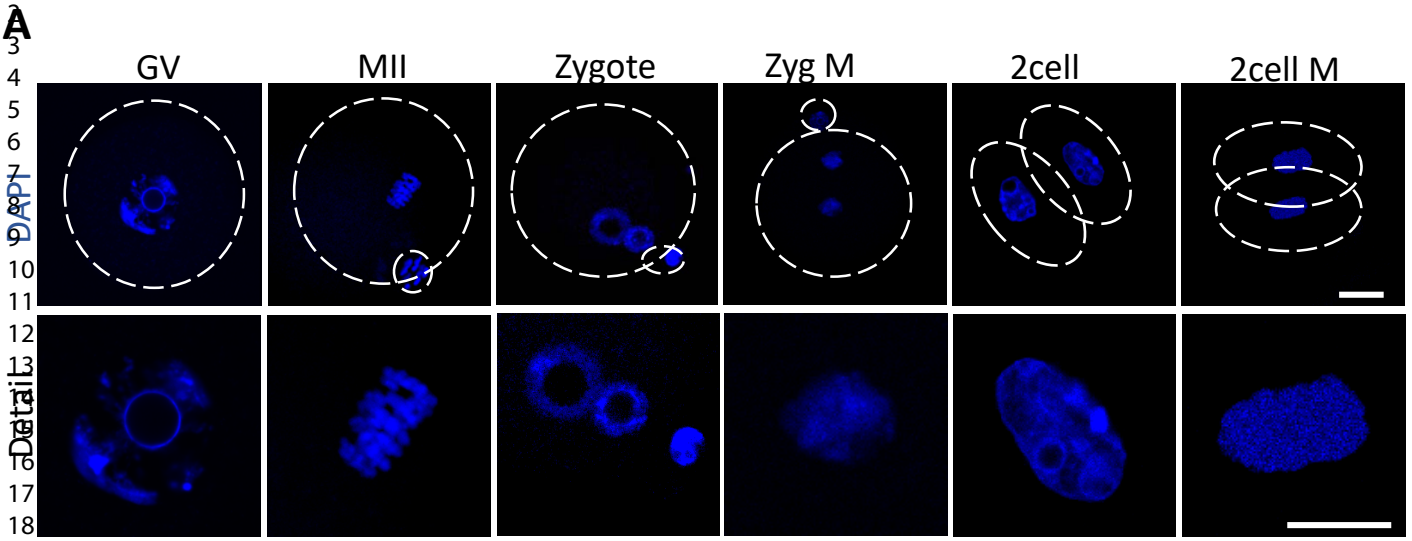

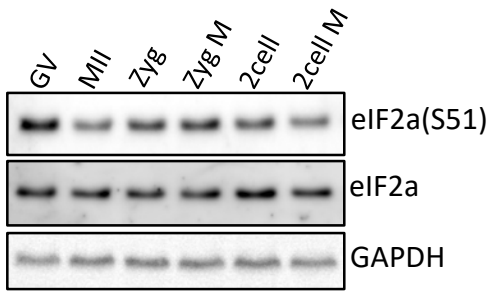

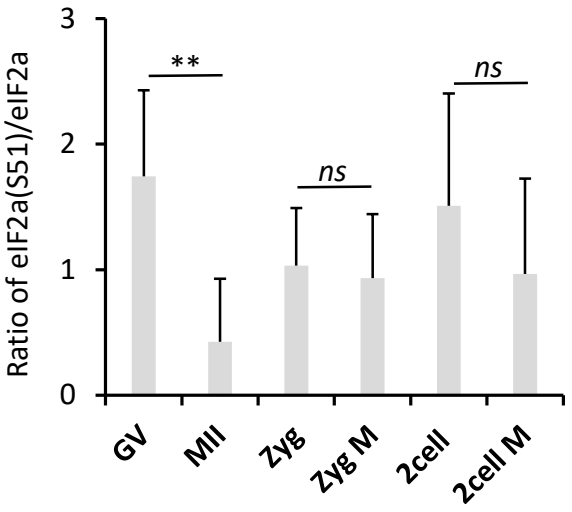

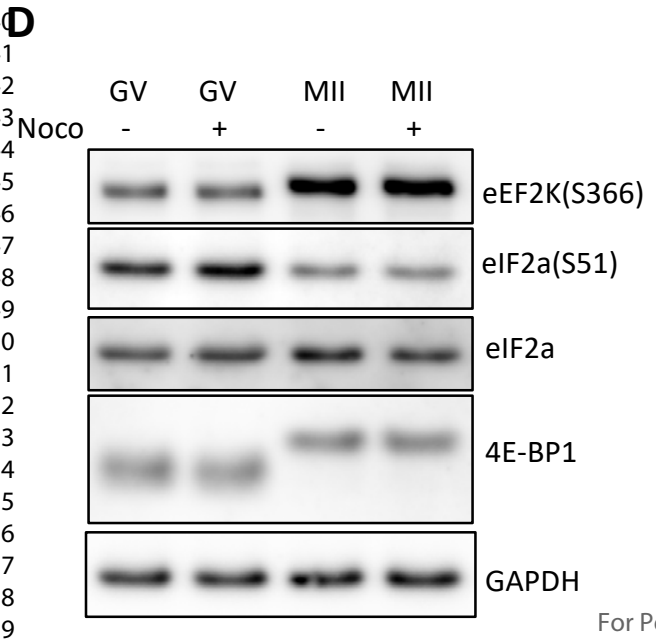

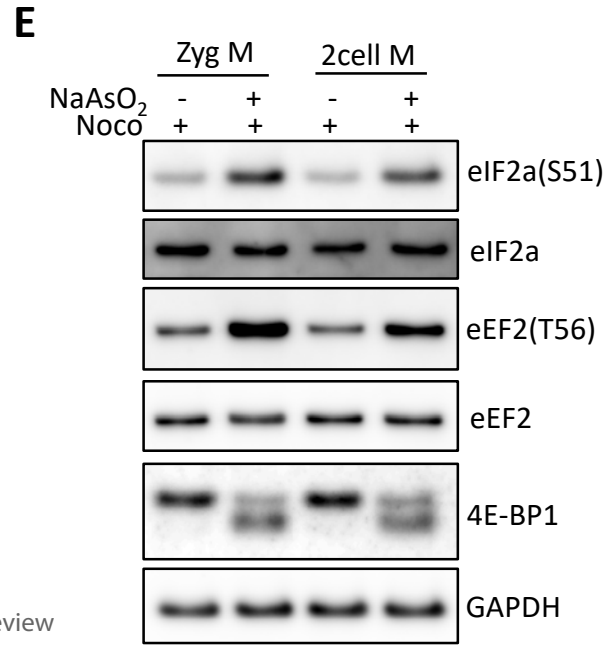

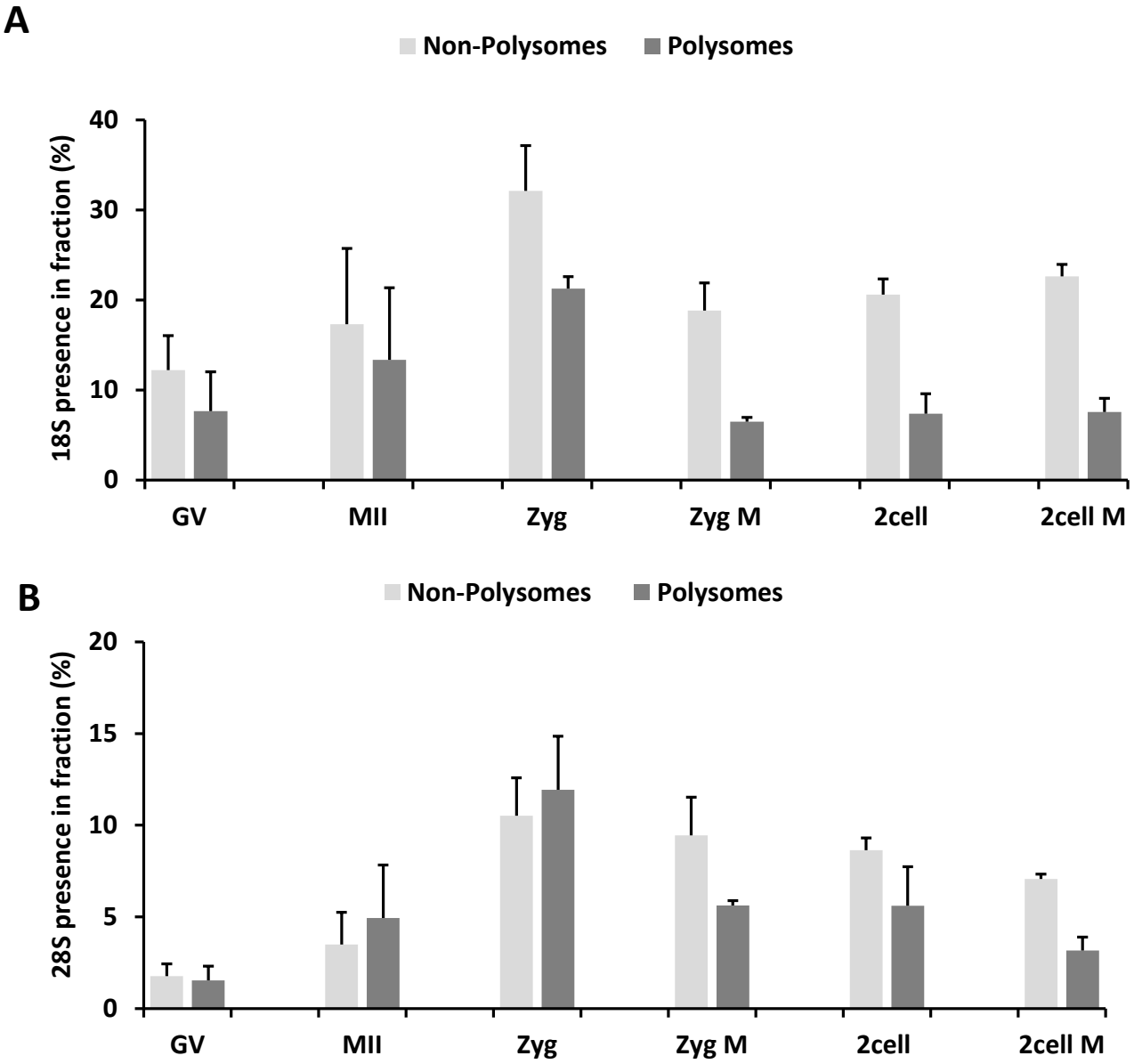
A
Non-Polysomes
Polysomes
18S presence in fraction (%)
40
30
20
10
0
GV
MII
Zyg
Zyg M
2cell
2cell M
B
Non-Polysomes
Polysomes
28S presence in fraction (%)
20
15
10
5
0
GV
MII
Zyg
Zyg M
2cell
2cell M

Supplementary Figure 3

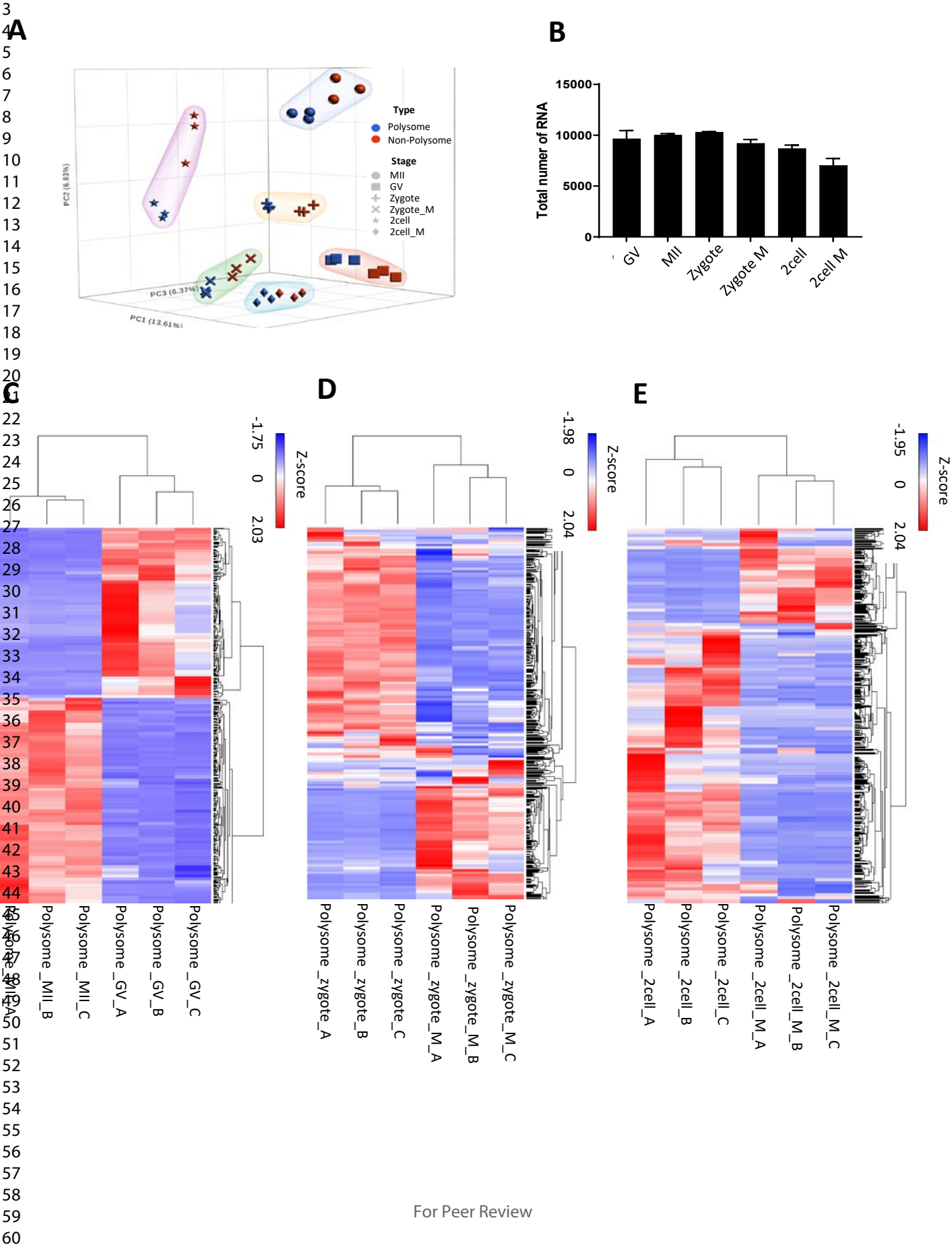

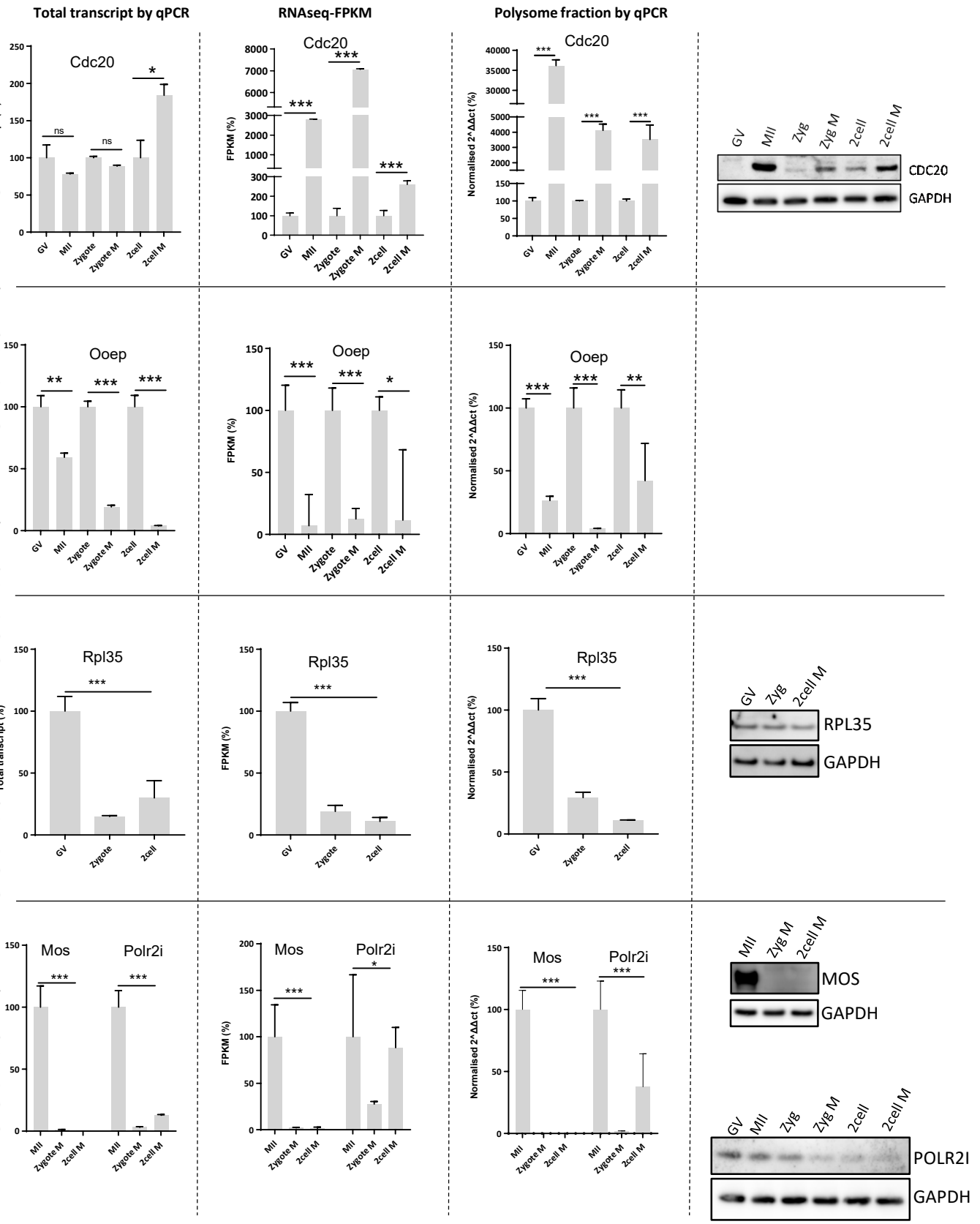
Total transcript by qPCR
RNAseq-FPKM
Polysome fraction by qPCR
Cdc20
Ooep
Rpl35
Mos
Polr2i
Total transcript (%)
FPKM (%)
Normalised 2^ΔΔct (%)
GV
MII
Zygote
Zygote M
2cell
2cell M
Zyg
Zyg M
CDC20
GAPDH
RPL35
MOS
POLR2I

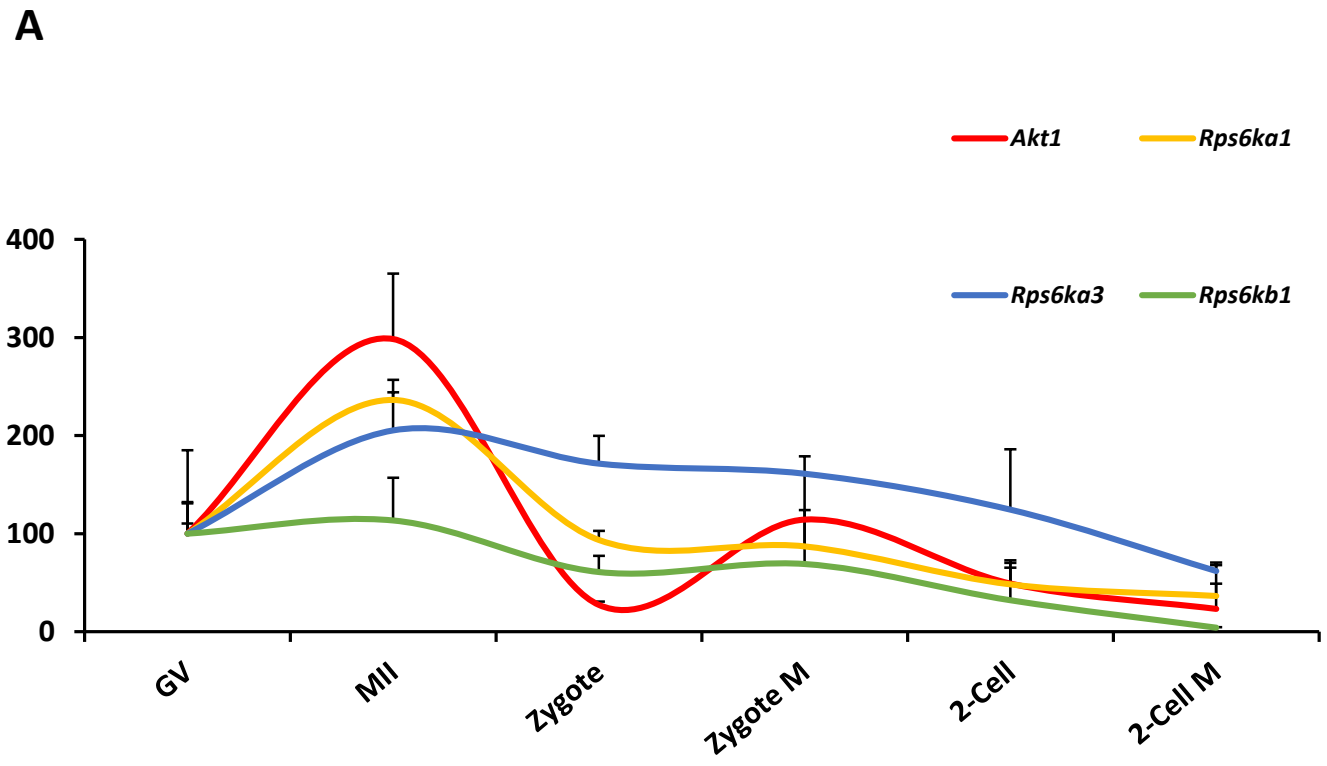
A
Akt1
Rps6ka1
Rps6ka3
Rps6kb1
FPKM (+1)
400
300
200
100
0
GV
MII
Zygote
Zygote M
2-Cell
2-Cell M

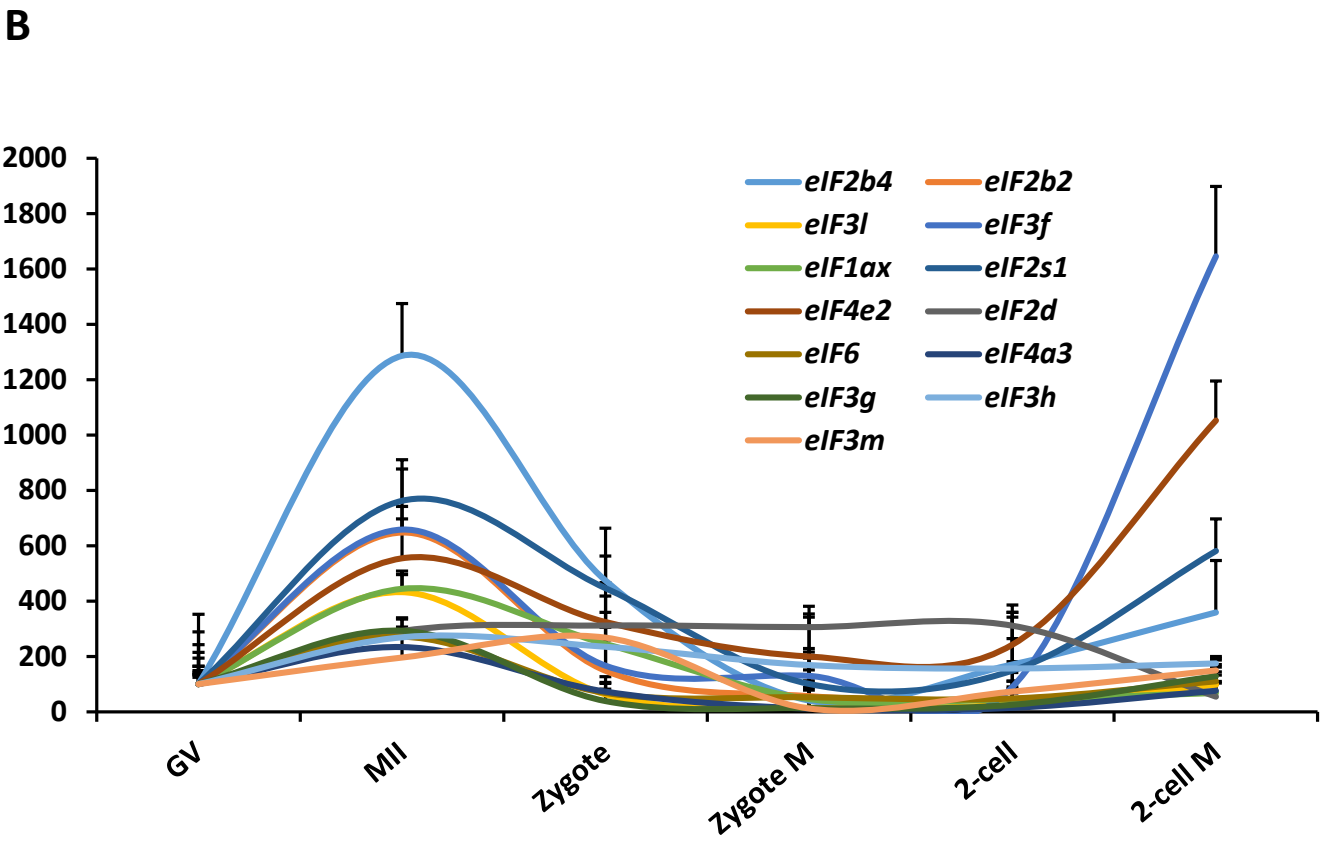
B
eIF2b4
eIF2b2
eIF3l
eIF3f
eIF1ax
eIF2s1
eIF4e2
eIF2d
eIF6
eIF4a3
eIF3g
eIF3h
eIF3m
FPKM (+1)
2000
1800
1600
1400
1200
1000
800
600
400
200
0
GV
MII
Zygote
Zygote M
2-cell
2-cell M

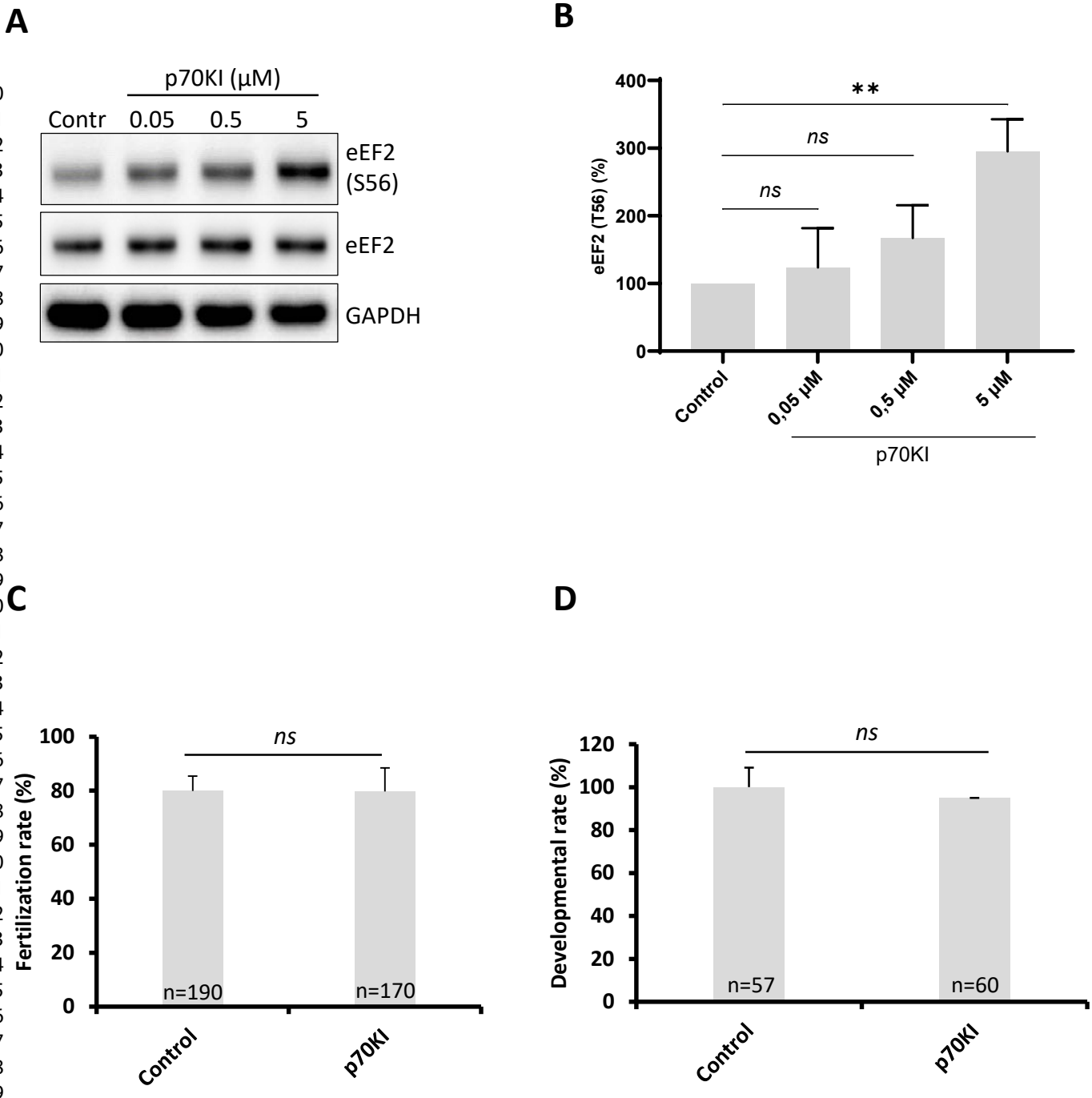
A
p70KI (μM)
Contr
0.05
0.5
5
eEF2 (S56)
eEF2
GAPDH
B
eEF2 (T56) (%)
400
300
200
100
0
**
ns
ns
Control
0,05 μM
0,5 μM
5 μM
p70KI
C
Fertilization rate (%)
100
80
60
40
20
0
ns
n=190
n=170
Control
p70KI
D
Developmental rate (%)
120
100
80
60
40
20
0
ns
n=57
n=60
Control
p70KI

Supplementary Figure 7

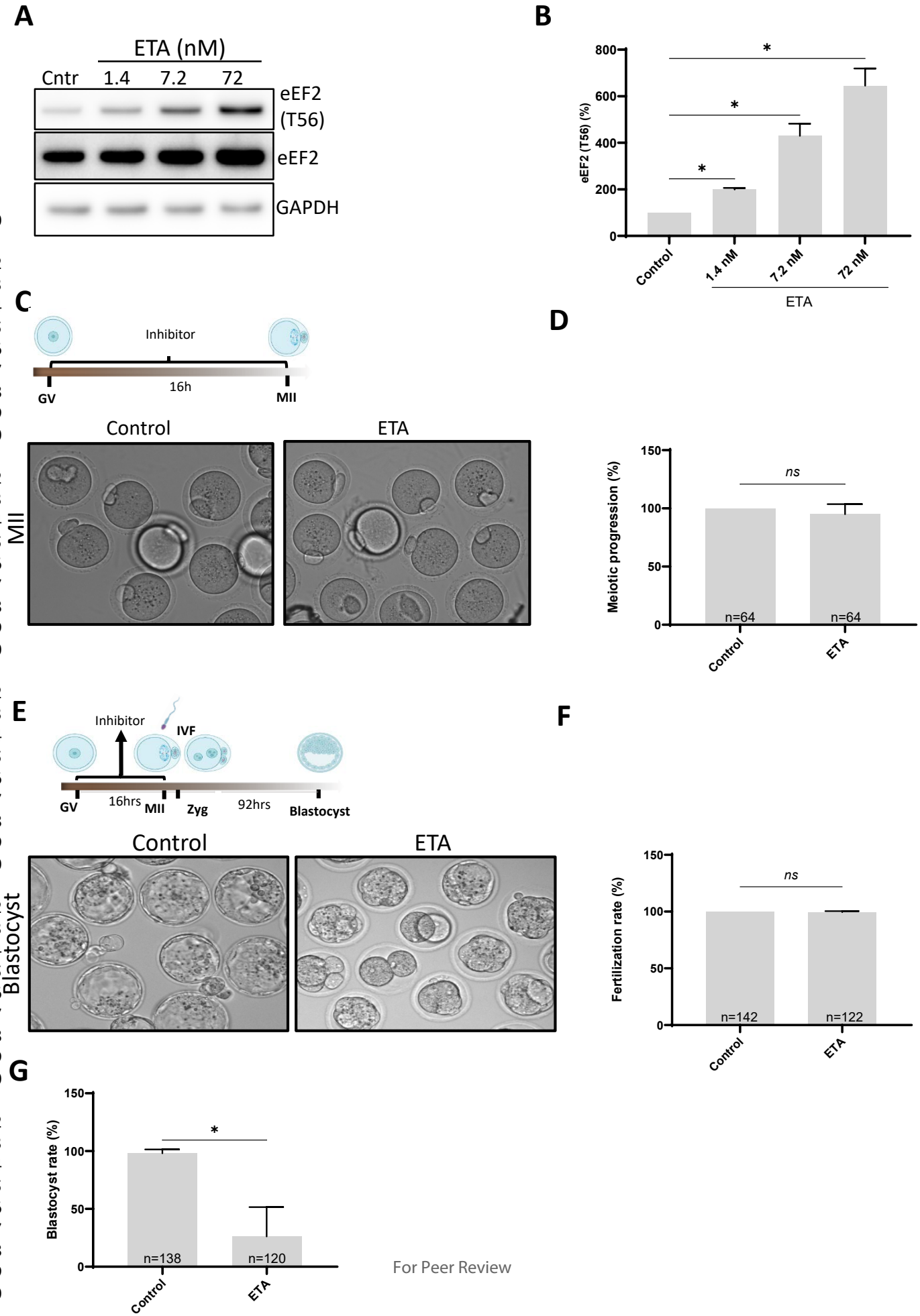

Supplementary Table 1

A

Official symbol (Gene)	Foward 5´-3´	Reverse 5´-3´	product size (bp)
Cdc20	GATCCTTGATGCCCCCGAAA	TGCAGGATGTCACCAGAACC	132
18S	CGCTCCACCAACTAAGAACG	CTCAACACGGGAAACCTCAC	110
28S	CTAAATACCGGCACGAGACC	TTCACGCCCTCTTGAACTCT	88
RPL35	GCCAAGATTAAGGCTCGGGA	GCGAACGACTCGTATCTTGGA	150
Mos	GTATAAAGCCACTTACCACGG	CAATGTTCAGTTCAGCCCA	107
Polr2i	CAGCCCAGTCGCTATGGAAC	CTGGGTCAGCTCGTCCACTT	214
Ooep	CTGTGTCCCTGAGACTTCGC	TGGTCTGTGCCTATGACCCT	115

B

Official symbol (Protein)	Cat. №	Manufacturer
eEF2K	3692	Cell Signalling
eEF2K(S366)	3691	Cell Signalling
eEF2	2332	Cell Signalling
eEF2(T56)	2331	Cell Signalling
4E-BP1	9644	Cell Signalling
eIF2a	9722	Cell Signalling
eIF2a(S51)	3398	Cell Signalling
mTOR (S2448)	5536	Cell Signalling
ERK (T202/T204)	9101	Cell Signalling
LMN A/C	SAB4200236	Sigma Aldrich
Histone H3 (Ser10)	9701	Cell Signalling
RPL24	PA562450	Thermo Fisher
RPS6	74459	Santa Cruz
RPS6 (S235/236)	4858	Cell Signalling
GAPDH	G9545	Sigma Aldrich
RPL35	SAB4500233	Sigma Aldrich
Mos	PA5-101081	Invitrogen
POLR2I	398049	Santa Cruz

biomedicines

MDPI

Review

An Interplay between Epigenetics and Translation in Oocyte Maturation and Embryo Development: Assisted Reproduction Perspective

Michal Dvoran, Lucie Nemcova and Jaroslav Kalous *

Institute of Animal Physiology and Genetics, Czech Academy of Sciences, 277 21 Libechov, Czech Republic; dvoran@iapg.cas.cz (M.D.); nemcova@iapg.cas.cz (L.N.)
* Correspondence: kalous@iapg.cas.cz

Abstract: Germ cell quality is a key prerequisite for successful fertilization and early embryo development. The quality is determined by the fine regulation of transcriptomic and proteomic profiles, which are prone to alteration by assisted reproduction technology (ART)-introduced in vitro methods. Gaining evidence shows the ART can influence preset epigenetic modifications within cultured oocytes or early embryos and affect their developmental competency. The aim of this review is to describe ART-determined epigenetic changes related to the oogenesis, early embryogenesis, and further in utero development. We confront the latest epigenetic, related epitranscriptomic, and translational regulation findings with the processes of meiotic maturation, fertilization, and early embryogenesis that impact the developmental competency and embryo quality. Post-ART embryo transfer, in utero implantation, and development (placentation, fetal development) are influenced by environmental and lifestyle factors. The review is emphasizing their epigenetic and ART contribution to fetal development. An epigenetic parallel among mouse, porcine, and bovine animal models and human ART is drawn to illustrate possible future mechanisms of infertility management as well as increase the awareness of the underlying mechanisms governing oocyte and embryo developmental complexity under ART conditions.

Keywords: epigenetics; protein translation; oocyte maturation; embryo development

Citation: Dvoran, M.; Nemcova, L.; Kalous, J. An Interplay between Epigenetics and Translation in Oocyte Maturation and Embryo Development: Assisted Reproduction Perspective. *Biomedicines* **2022**, *10*, 1689. https://doi.org/10.3390/biomedicines10071689

Academic Editors: Ning Qu and Tomohiko Wakayama

Received: 27 May 2022
Accepted: 28 June 2022
Published: 13 July 2022

1. Introduction

The purpose of living organisms' reproduction is to give rise to a new generation. According to the World Fertility Report from 2015, human fertility has halved in the past 65 years. In the 1950s, the norm was for one woman to give birth to 5 children, whereas in 2015 the average was only 2.5. If this pattern, along with demographic changes, continues, we would gradually face the need to support human fertility clinically by preserving the quality of germ cells, particularly oocytes.

Female fertility is influenced by genetic background, environmental factors, lifestyle, nutrition, psychosocial setting, and many other factors. The proper understanding of the molecular mechanisms underlying oocyte development is crucial for advancement in assisted reproduction technology. This review is focused on how oocyte and embryo development is affected by epigenetic changes, initially those originating from the in vitro methods of assisted reproduction technology (ART) followed by in utero changes caused by maternal diet, lifestyle, and environment. The epigenome is a complex of chemical compounds that modify or mark a genome but are not part of the DNA itself (Figure 1).

Epigenetic changes may cause temporary or heritable alterations of gene expression. Modifications to the epigenome are reversible and alter gene expression in different ways but do not interfere directly with the DNA genetic code. Epigenetic changes are categorized into DNA, RNA, histone modifications, and changes controlled by non-coding RNAs.

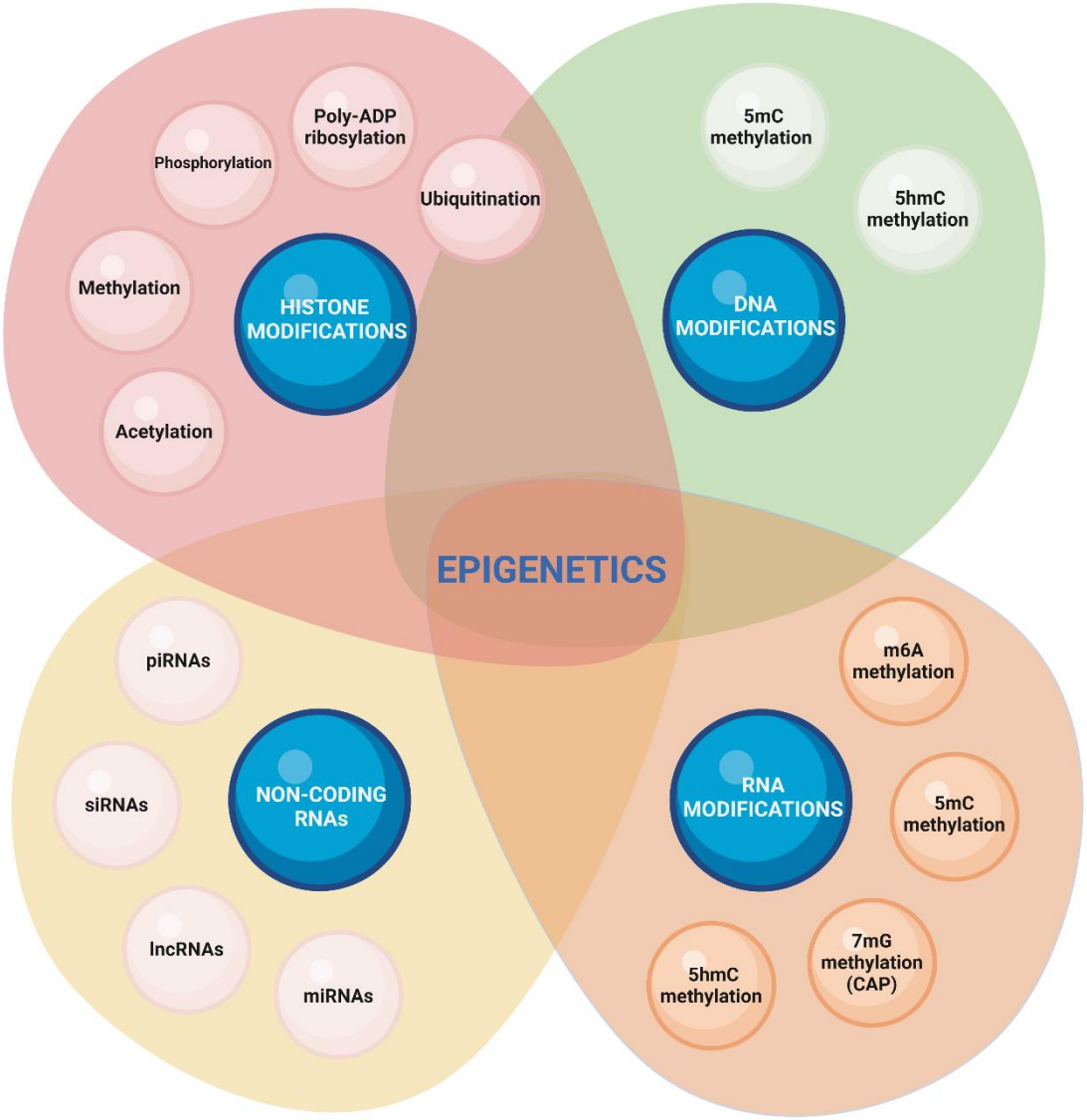

Figure 1. Epigenetic modifications: This diagram shows the complexity of epigenetic processes, which are divided into the following subgroups: DNA modifications—5-methylcytosine (5mC) DNA methylation; 5-hydroxymethylcytosine (5hmC) DNA methylation; Histone modifications—Acetylation, Methylation, Phosphorylation, Poly-ADP-ribosylation, Ubiquitination; Non-coding RNA interactions—piwi-RNA (piRNA), small interfering RNA (siRNA), long non-coding RNA (lncRNA), micro RNA (miRNA); RNA modifications—6-methyladenosine (6mA) RNA methylation, 5-methylcytosine (5mC) RNA methylation, 7-methylguanosine (7mG) RNA methylation, mRNA CAP, 5-hydroxymethylcytosine (5hmC) RNA methylation. The image was created with BioRender.com.

DNA methylation is the most studied epigenetic mechanism and plays a key role in transcriptional repression/activation (Figures 1 and 2).

Epigenetic changes may cause temporary or heritable alterations of gene expression. Modifications to the epigenome are reversible and alter gene expression in different ways but do not interfere directly with the DNA genetic code. Epigenetic changes are categorized into DNA, RNA, histone modifications, and changes controlled by non-coding RNAs.

DNA methylation is the most studied epigenetic mechanism and plays a key role in transcriptional repression/activation (Figures 1 and 2).

In vertebrates, DNA cytosine methylation is realized by the addition of a methyl group onto the fifth carbon of cytosine residue within cytosine-phosphate-guanin (CpG) sites, where a cytosine is followed by a guanine in the 5′ → 3′ direction of the DNA linear sequence. DNA methylation is functionally associated with gene silencing and is for the most part limited to CpG islands, i.e., areas rich in CpG dinucleotides that are typically located within and nearby sites of about 40% of mammalian gene promoters [4,5]. As the CpG dinucleotides are methylated symmetrically on both DNA strands, their methylation can be heritable during cell division [4].

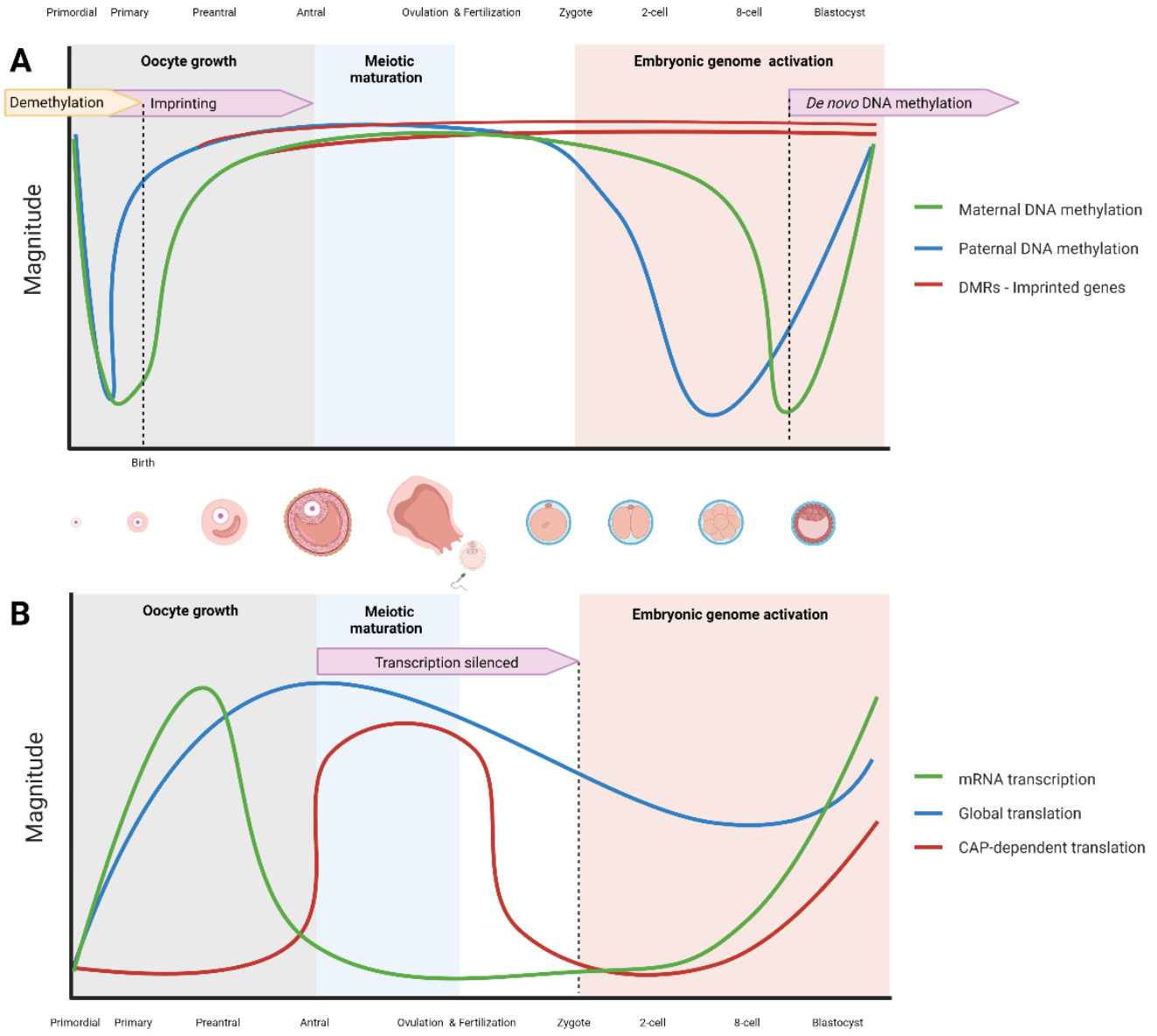

Figure 2. Dynamic DNA methylation and protein translation changes in human oogenesis and early embryogenesis: (**A**) Prenatal DNA demethylation in primordial germ cells (PGC) is followed by de novo DNA methylation, which occurs earlier in males than females. Genomic imprinting loci consisting of DMR (differentially methylated regions) maintain their methylation status despite the important genome-wide DNA demethylation in pre-implantation embryos [1]. (**B**) Oocytes are transcriptionally active during oocyte growth with rapid decline and silencing throughout meiotic maturation [2]. According to the new evidence human embryonic genome activation is initiated at the zygotic stage, but the transcriptional activity remains low until the 8-cell stage [3]. Correct regulation of CAP-dependent translation is a key process in meiotic maturation despite continuous decrease in global translational activity from oocytes to zygotes. The image was created with BioRender.com.

In vertebrates, DNA cytosine methylation is realized by the addition of a methyl group onto the fifth carbon of cytosine residue within cytosine phosphate-guanin (CpG) sites, where a cytosine is followed by a guanine in the 5′ → 3′ direction of the DNA linear sequence. DNA methylation is functionally associated with gene silencing and is for the most part limited to CpG islands, i.e., areas rich in CpG dinucleotides that are typically located within and nearby sites of about 40% of mammalian gene promoters [4,5]. As the CpG dinucleotides are methylated symmetrically on both DNA strands, their methylation

lated DNA strand [8]. In contrast, de novo methylation of un-methylated double stranded DNA is ensured by DNMT3A and DNMT3B along with their coactivator DNMT3L [9,10].

DNA cytosine methylation can affect DNA activity and when it occurs in a gene promoter, increased DNA methylation leads to a decrease in chromatin accessibility. Subsequently, gene transcription is repressed by recruiting gene-silencing repressive proteins to the methylated region, such as methyl-CpG-binding protein 2 (MeCP2) and methyl-binding-domain (MBD) proteins [11,12]. Methylated DNA also presents a spatial obstacle preventing binding of transcription factors and proteins to gene promoters [13,14]. However, methylation of CpGs over gene bodies is related to both active and repressed transcription according to the tissue in which it occurs [15,16]. Evidently, DNA methylation has dual roles, both inhibitory and permissive, depending on the genomic region.

Epigenetic modifications to RNA, the field of epitranscriptomics, have changed our perception on how epigenetics can directly modulate the translation and stability of mRNAs within oocytes and embryos. There are over 150 post-transcriptional mRNA transcript modifications in eukaryotes, but the most prevalent is the N^6-methyladenosine (m^6A) methylation (Figure 1) [17]. Generally, m^6A transcript methylation is present ubiquitously in every cell and across multiple species. Translation-related m^6A modification occurs within the 3′ UTR of mRNA. The interaction between the m^6A reader and translation initiation factors is needed for cap-dependent translation [18]. m^6A were also found to be capable of governing translation in a cap-independent manner by modifications within internal ribosome entry sites (IRES) [19] or 5′ UTR sequences [20]. A direct link between greater polysome occupancy and the presence of m^6A methylation on mRNAs was demonstrated in yeast [21] and HeLa cells [18].

Epigenetic regulation by non-coding RNAs (ncRNAs) recently gained more attention in developmental biology literature. ncRNAs represent RNA molecules that do not code for proteins but have a regulatory role at pre- and post-transcriptional levels [22]. Generally, both short and long ncRNAs do exist. Among the smaller ones are small-interfering RNA (siRNA), microRNA (miRNA), piwi-interacting RNA (piRNA), followed by long ncRNA (lncRNA) (Figure 1). As ncRNAs are also implicated in histone modification and DNA methylation, it has been suggested that gene silencing and upregulation by ncRNAs is a part of the epigenetic mechanism [23,24]. The importance of ncRNAs in regulating primordial germ cell specification, spermatogenesis, and oogenesis has been highlighted (reviewed in [25,26]). ncRNAs are intensely expressed in the early human embryo and their role in early human development remains to be fully investigated. It has been suggested that future studies of the ncRNAs role could expand to the field of ART optimization [27,28].

2. Epigenetics of Germ Cells Development

2.1. Epigenetic Reprogramming

Two different waves of epigenetic reprogramming occur in gametes and the early embryo, the first one during gametogenesis and the second in the preimplantation embryos (Figure 2) [29,30]. During mammalian gametogenesis, pre-existing epigenetic marks are globally deleted in the primordial germ cells. During sex determination in the developing fetus, the global DNA methylation remains at very low levels in both male and female primordial germ cells [31]. However, de novo methylation establishment proceeds in different manners in male and female germlines. In the male gonocytes, a rapid increase of methylation is initiated during embryo development, and the methylome of male germ cells is fully established before the birth [32,33]. In female germ cells, DNA methylation is re-established during the postnatal oocyte growth phase and is dependent on the functional interaction of the DNA methyltransferase Dnmt3a and the Dnmt3-like protein (Dnmt3L) [34,35]. DNA de novo methylation is completed when oocytes reach the germinal vesicle stage [1,36]. After a period of intense activity during oocyte growth, transcription is ceased when the oocyte becomes arrested at the prophase of meiosis I, and this arrest is released after a preovulatory hormonal surge of gonadotropins [37]. It has been proposed that the phenomenon of meiotic arrest possibly protects oocytes from oxidative stress and

DNA damage [38]. During oogenesis, the oocyte development and competence is not dependent on DNA methylation as oocytes with genetically ablated DNA methylation were successfully fertilized, and subsequent embryonic development progressed until the mid-gestation stage [39,40]. It has been suggested that methylation of CpG islands in gametes is not fully related to genomic imprinting but is an important factor in the regulation of gene expression in preimplantation embryos [34].

2.2. Histone Deacetylation in Oocyte Maturation and Energy Metabolism

Histones are positively charged proteins, which form the integral part of the chromatin core. The octamer core is composed of four histone variants—H2A, H2B, H3, and H4—with connecting histone H1 [41]. They are essential for packaging the DNA into superstructures, making it inaccessible for DNA-binding proteins to bind it and recruit further transcription or regulation machinery. Important modification regulating histone interactions are classified into methylations, acetylations, phosphorylations, ubiquitinations, and PolyADP ribosylations (Figure 1) [41]. Particularly, the regulation of histone acetylations is relevant for the final moments of oocyte maturation.

Histone deacetylases (HDACs) are enzymes that regulate a wide range of biological processes by removing acetyl groups from lysine ϵ-amino groups, not only on histones but also on many other proteins [42]. In particular, meiotic progression was discovered to be dependent on HDACs activity progression in mice. Histone acetylation of lysine residues was substantially reduced upon meiotic resumption in mouse oocytes [43]. Maintenance of genome integrity and chromatin structure is controlled by HDAC3. In meiosis, HDAC3 is located on the spindle. HDAC3 knockdown experiments on mice revealed defects in chromosome alignment, spindle structure, and microtubule-kinetochore attachment (MT-K) [44]. Suppression of HDAC3 activity in porcine oocytes led to similar phenotypes as in mice, spindle defects, chromosomal congression failure, and meiosis inhibition [45]. Disruption of oocyte maturation by the selective HDAC6 inhibitor tubastatin-A induced asymmetric division in maturing oocytes, failure to extrude the first polar body [46], increased α-tubulin acetylation, and incorrect MT-K attachment as seen in HDAC3 [47]. Recently, primordial follicle activation by mTOR signalling was associated with decreased HDAC6 activity. This finding may be of importance for the management of premature ovarian failure (POF) as an alternative approach to primordial follicle in vitro activation (IVA) [48]. HDAC8 has a similarly indispensable role as HDAC6 and is located on spindle poles. Its absence led to the defective recruitment of γ-tubulin and consequently caused aberrant spindle morphology and chromosome misalignment in mice [49] and pigs [50]. The activity of HDAC1/2 in embryos is required for proper DNA methylation, cell lineage development, and transformation from morula to blastocyst [51]. HDAC3 is closely connected with HDAC 11. Its inhibition increased the acetylation level of α-tubulin [45,52], significantly impaired the course of meiosis in mouse oocytes, and disrupted kinetochore–microtubule attachment and spindle assembly checkpoint [52], which resulted in abnormal spindle organization and chromosome misalignment.

The regulation of histone acetylation in oocyte meiosis is also reliant upon specific NAD^+-dependent HDACs, silent information regulator 2 (Sir2) proteins ("sirtuins") that belong to a seven-member family of deacetylases involved in the deacetylation of histones as well as nonhistone proteins. Moreover, sirtuins are employed in the regulation of metabolism, inflammation, and oxidative stress. [53]. SIRT1 plays a role in the activation of primordial follicles in a deacetylase-independent manner [54] and was reported to slow down the aging-related decrease of oocyte quality, which may under in vitro laboratory conditions impact oocyte maturation [55]. SIRT1 overexpression decreased H3 histone methylation and acetylation in post-ovulatory aged mouse oocytes as well as decreased aging related reactive oxygen species (ROS), spindle abnormalities, and mitochondrial dysfunction [56].

The SIRT2 impaired gap junctional communication during in vitro maturation of bovine oocytes by phosphorylation of connexin-43 [57] is another sirtuin activity. In human

serum samples from IVF patients, a basal SIRT2 level was proposed as a pregnancy outcome predictor in combination with age, anti-Mullerian hormone (AMH), and antral follicle count (AFC) [58].

At the GV stage of mouse oocytes, SIRT7 is located within the nucleus, then upon meiotic resumption it is dispersed in the cytoplasm, with the highest SIRT7 concentration occurring around the chromosomes. SIRT7 knockdown compromised mitochondria function, significantly decreased ATP levels, and increased ROS [59]. SIRT4 exhibited similar phenotype to SIRT7 [60]. On the other hand, SIRT6 interacts with chromatin proteins and is employed in DNA double-strand break (DSB) repair mechanisms. Its knockdown in early mouse embryos shortened telomeres and caused an increase in DNA damage [61].

Sirtuins are also implicated in the regulation of energy metabolism and stress resistance; particularly, SIRT3, SIRT4, and SIRT5 mainly localize in mitochondria [62]. SIRT1 and SIRT3 have been revealed to play a crucial role in ensuring protection against oxidative stress in oocytes, granulosa cells, and early embryos [63]. It has been reported that the SIRT1 anti-oxidative stress effect in mouse oocytes is attenuated during aging [64]. Recently, a decrease of ovarian reserve in mice was linked to SIRT1-related changes in mitochondrial oxidative phosphorylation [65]. Additionally, a protective role of SIRT3 against oxidative stress was revealed in preimplantation mouse embryos [66]. A correlation between the decreased expression of SIRT3 and lower embryonic developmental competence was found in human in vitro cultured embryos [67].

2.3. Fertilization & Mitochondria

Mitochondria play a major role in providing each cell with energy by generating adenosine triphosphate (ATP) through electron transport-linked oxidative phosphorylation (OXPHOS) [68]. Since the aerobic respiratory pathway in eukaryotic cells is the only system that fully relies on mitochondria function [69], any mutations in mtDNA or nuclear-encoded mitochondrial genes can result in mitochondrial dysfunction that induces a variety of pathologies and contributes to an abnormal aging process [70,71]. Mitochondria are the prominent source energy for successful oocyte and sperm biogenesis and function. This dependence is due to the high energy demand for the support of proper chromosome segregation and the fertilization process [72,73]. In mammalian oocytes, a sufficient mtDNA copy number is essential to promote fertilization and early embryo development. Human oocytes with fewer than 100,000 copies of mtDNA evince a significantly lower fertilization rate than oocytes with more than 150,000 copies [74,75]. In vertebrates, inheritance of mitochondria is maternal as the paternal mitochondria of sperm origin are eliminated during early embryo development [76,77].

Mitochondrial activity is an indicator of oocyte developmental competence [78]. Oocyte maturation and early embryo development depend on ATP derived mainly from mitochondrial oxidative phosphorylation [79,80]. Events such as the formation and maintenance of the meiotic spindle are also dependent on mitochondrial function [81]. Deficiency of ATP and low mtDNA copy number are associated with poor oocyte quality, retarded embryo development, aneuploidy, and decreased implantation and placentation rates [82,83]. mtDNA has a considerably higher mutation rate than the nuclear genome, and it is assumed that mtDNA is prone to oxidative damage induced by reactive oxygen species [84]. Mitochondrial dysfunction and deficiency of mitochondria-derived ATP provoked by oxidative stress induces spindle disruption in MII mouse oocytes [85]. Mutations of mtDNA can cause a set of physical and cognitive disabilities, including pathologies of the nervous and muscular systems. However, progress has been made recently in the field of inherited mitochondrial disease and therapeutic approaches, such as the development of pre-implantation genetic screening and mitochondrial replacement therapy [86,87].

A decrease of mitochondrial number, function, and mtDNA quantity affect the viability of oocytes and female fertility [88,89]. Advanced maternal age is associated with a reduction of ATP production that leads to decreased metabolic activity and can negatively affect cell cycle regulation, meiotic spindle formation, chromosome segregation,

fertilization, embryo development, and implantation [72,90,91]. An increased expression of the mitochondrial unfolded protein response gene *Hspd1* in GV oocytes of PMSG-treated aged mice reflects the mitochondrial stress caused by advanced age [88]. In ovaries of aged mice, a decreased mRNA expression of mitochondrial antioxidants *Prdx3* and *Txn2* was reported [92]. An increased expression of the mitochondrial antioxidant *TXN2* gene and mitochondrial transcription factor *TFAM* gene in cumulus cells of unstimulated aged cattle was detected [93]. To enhance the fertilization rate of aged oocytes, the technique of mitochondrial supplementation can be applied. For this purpose, it is possible to use the method of either partial or total cytoplasm transfer from donor to recipient oocyte [94,95].

2.4. Genomic Imprinting in Early Embryo

Genomic imprinting is defined as a monoallelic parent-of-origin-dependent gene expression in offspring and consists in differential methylation inherited from the gametes when one parental copy of the gene is silenced while the other parental allele is expressed [96]. DNA methylation is one of the epigenetic changes regulating the expression of imprinted genes during early development. It is an epigenetic process that involves DNA methylation and histone methylation without altering the genetic sequence. These epigenetic marks are established ("imprinted") in the germline (sperm or egg cells) of the parents and are maintained through mitotic cell divisions in the somatic cells of an organism [14]. Although extensive nuclear reprogramming occurs in preimplantation embryos, the methylation of imprints acquired through gametogenesis escapes from this global epigenetic reprogramming and persists in preimplantation embryos (Figure 2) [9,97]. The methylation of the imprinted genes is thus preserved and then transmitted to the offspring. As of 2019, around 260 imprinted genes have been identified in mice and 230 in humans [98]. Imprinted genes are involved in the regulation of embryonic growth, placental function, postnatal growth, and neurobehavioral processes [99,100]. In humans, abnormal expression of some imprinted genes has been related to numerous diseases, developmental abnormalities, and malignant tumours [101–103]. Although DNA methylation is a key player in genomic imprinting through the establishment of imprinted marks on either paternal or maternal alleles (Figure 2), the genomic imprinting process is significantly influenced also by histone modifications and non-coding RNA [104–106].

2.5. Embryonic Genome Activation

During early embryogenesis between fertilization and implantation, parental DNA is subjected to rapid and extensive demethylation, and consequently epigenetic information inherited from the gametes is vastly reset in the preimplantation embryos [9,107]. In human embryos, a sharp decrease of paternal DNA methylation occurs between fertilization and the two-cell stage; however, the decrease of maternal DNA methylation is milder (Figure 2) [108]. The DNA methylation level is also decreased during zygotic activation in mice, bovine, and goat preimplantation embryos [109–111]. In mice, the most intense demethylation occurs in the zygotes, and gradual demethylation continues until the blastocyst stage [112]. The newly activated DNA demethylation that occurs during the early pronuclear stage precedes the increase of DNA replication indicating that DNA demethylation in the early zygote is independent of DNA replication [113].

The early human embryo consists of a large number of transposable elements (TE) that could be a potential cause of gene rearrangements, mutations, deletions, or duplications. Therefore, as a precaution, silencing of these evolutionary younger TE is ensured by DNA methylation or histone modifications [108].

Nearly all methyl groups are removed from the paternal-origin DNA immediately after fertilization [97]. Methylation of maternal-origin DNA is diluted with each round of replication and results in a substantial decrease of DNA methylation during the morula stage [114]. Global epigenetic reprogramming occurs in the early embryo when DNA demethylation is at the highest levels in the early blastocyst stage [115]. The genome-wide

erasure of CpG methylation is more profound in early embryos from superovulated mice when compared to embryos from naturally mating control mice [116].

2.6. Intrauterine Epigenetic Inputs

Subsequent reinitiation of DNA methylation occurs in the blastocyst stage in the cells of the inner cell mass and establishment of new methylation marks continues during fetal development [97]. During post-implantation development the activity of DNMT3A and DNMT3B together with their coactivator DNMT3L are essential to establish the characteristic methylation profile in the developing embryo [117]. DNA methylation provides an epigenetic regulatory mechanism protecting the differentiating cells from regression to the undifferentiated state [115]. In post-implantation embryos, DNA methylation is an integral of epigenetic marks in the majority of embryonic tissues and persists in somatic tissues during the lifespan of adults [118]. Mice embryos with insufficient DNA methylation activity die at mid-gestation as a consequence of genome-wide demethylation [119].

3. Epigenetics within Translational Regulation: The Oocyte to Embryo Story

3.1. Active Transcription Fuels Maturing Oocyte

Primordial germ cells (PGCs) that are produced from female germ cells undergo mitosis, forming oogonia and during subsequent oogenesis, the oogonia become primary oocytes. Every oocyte originates from primordial germ cells (PGCs). PGCs migrate in utero into a future ovary and go through repeated mitotic cycles to form nests of germ cell syncytia [120]. All female mouse primordial germ cells are connected by intercellular bridges in the ovaries at embryonic day 11.5 to 17.5 and form synchronously dividing interconnected cysts or syncytia of up to 30 germ cells [121,122]. Following the homologous recombination and formation of cytoplasmic bridges, oocyte nuclei are arrested at the diplotene stage of meiotic prophase I. Following birth, germ cell nests are dispersed along with the invasion of pre-granulosa cells [121]. Individual primordial follicles made of primary oocytes enclosed by a basal layer of flattened granulosa cells are formed. However, a substantial amount of primordial follicles undergo atresia, and one of the proposed functions for follicular atresia is the selection of follicles containing oocytes of the highest developmental potential [123,124]. Activation of the primordial follicle that starts at prepubertal stage and extends throughout the reproductive life is cross-regulated by key transcriptional factors (FIGLA, LHX8, and SOHLH1) that cooperate on common downstream pathways in folliculogenesis [125]. If a primordial follicle is activated, it does so via the binding of Kit Ligand from granulosa cells (KL) onto a Kit receptor present on the oocyte and theca cells [126]. This Kit-KL system is connected downstream by a PI3K/Akt pathway [127]. A feedback loop is further secured by oocyte-secreted factors (OSFs) such as BMP-15 or GDF-9 [128,129]. As the oocyte grows further, macromolecules, proteins, and transcripts are rapidly accumulating within. Experiments on bovine oocytes have shown that a substantial amount of mRNA transcripts are capable of transport from granulosa cells into the oocyte via gap-junctions. These connections between the oocyte and cumulus cells were subsequently named as transzonal projections (TZPs) [130,131]. Once the oocyte reaches the fully grown germinal vesicle stage (GV), the transcription in the GV nucleus is ceased. Accumulated mRNAs are more stable than those present in somatic cells [132]. Further, during the MI/MII transition, the oocyte is dependent on the effective utilization of stored transcripts and proteins [133,134], which needs to be tightly regulated based on the metabolic requirement, nutrient availability, and presence of environmental stress. Fine tuning of oocyte meiosis and early embryo development is ensured by translational regulation.

3.2. Translational Regulation, the Key for Oocyte Success

The regulation of translation is orchestrated by many mechanisms, ranging from modulating polyA tail length, modifying mRNA post-transcriptionally, regulating interactions between proteins, degrading stored RNAs, clustering RNAs into ribonucleoproteins

(RNPs), up to the 5′-terminal oligopyrimidine (TOP) motif mRNA regulation under stress from nutrient or oxygen deprivation [135]. The best known regulation mechanism of selective mRNA translation is the 3′ UTR polyadenylation, which works for about 70% of the oocyte's mRNAs [136]. PolyA tail length positively correlates with ribosome occupancy. The ribosome loading itself is regulated by the CPE binding protein 1 (CPEB1) and deleted-in azoospermia such as (DAZL) binding to the cytoplasmic polyadenylation element (CPE) on the 3′ UTR of mRNA. Their absence compromises mouse oocyte meiotic maturation and MII oocyte development by dysregulating effector proteins, polyA binding protein 1 (PABP1), and polyA specific ribonuclease (PARN) responsible for mRNA polyadenylation and deadenylation respectively [137].

As oocyte meiosis is progressing, global translation decreases (Figure 2). However, translation of m7G capped mRNAs is mainly regulated by the mTOR/S6K1/4E-BP1 signalling (mTORC1 pathway) [2,138]. The main player here, the mammalian target of rapamycin (mTOR), a serine/threonine protein kinase, regulates diverse cellular functions (reviewed in [139]). It has been documented that mTOR activation and the protein synthesis initiation is influenced by the activity of cyclin-dependent kinase 1 [140]. mTOR is responsible for translational regulation of capped mRNAs containing a TOP motif by recruiting an eukaryotic initiation factor 4F (eIF4F) [2] and RNA-binding protein LARP1 [135]. Oocyte-specific conditional knockout of mTOR severely affected folliculogenesis. Deleting mTOR in meiotic maturation changed the oocyte's proteome composition, caused spindle instability, aneuploidy, and failure to form a methaphase II equatorial plane [141].

Translatability of mRNAs is also indirectly regulated by the formation of superstructures with proteins into RNP cytosolic granules. In such a way, translation, degradation, and storage of transcripts can be controlled simply by regulating their physical availability to the translational or degradational machinery. RNP granules commonly found in oocytes and embryos are stress granules or p-bodies. Stress granules are formed upon nutritional deprivation, heat, or oxidative stress by liquid-liquid phase separation [142]. P- bodies, on the other hand, are engaged in the storage of mRNAs with regulatory functions, previously thought to play a role in RNA decay [143]. Continuous degradation of stored RNA expressed during early stages of oogenesis occurring in meiosis and during early embryo development is preventing them from being inherited by simple eradication of redundant RNAs [144].

3.3. Epitranscriptomics—Translational Regulation by mRNA Methylation

Not only oocyte translational regulation is key for meiotic maturation, but also the recently discovered regulation by the epitranscriptomic m^6A mRNA methylation [145,146]. Earlier studies in Xenopus oocytes found m^6A methylation to inhibit mRNA recruitment for translation. Key cell cycle and translation-related transcripts in Xenopus were demethylated in order to become translated [145]. However, a study on porcine oocytes showed rapid accumulation of m^6A methylated transcripts inside the ooplasm as meiotic maturation progressed. Inhibition of m^6A methylation by cycloleucine, a specific inhibitor of adenosyl-transferase, impaired oocyte maturation and further development [147]. A role of m^6A mRNA methylation during meiotic maturation and maternal to zygotic transition has been confirmed in the mouse model [146], and proper regulation of m^6A mRNA methylation was shown to be crucial for both preimplantation [148] as well as in utero [149] embryo development.

Recent evidence stressed the importance of m^6A mRNA methylation in the development of fully matured and developmentally competent oocytes and early embryos. Epitranscriptomic m^6A RNA methylation is an ubiquitous and reversible process orchestrated by methyltransferases ("writers"), binding proteins ("readers") and demethylases ("erasers") [150,151].

Three major epitranscriptomic writers exist: METTL3, METTL14, and METTL3 adapter—WTAP [51,152]. The methyltransferase complex METTL3 was studied in detail on mouse oocytes. Transient knockdown of METTL3 by RNAi led to a substantial decrease

of mRNA translation efficiency, low oocyte maturation rate, problems with maternal to zygotic transition [146], and inability to form blastocysts [148]. METTL3 was found to play a role in folliculogenesis, ovulation, maintenance of DNA integrity, and preimplantation development [153]. The same enzyme is engaged in the angiogenesis of atherosclerotic mouse model embryos by upregulating vascular-endothelial growth factor (VEGF) [154] through m^6A [155]. In zebrafish embryos, METTL3 regulated PHLPP2/mTOR-AKT signalling [156]. The recently published data have shown METTL3 direct interaction with the known p53 transcription factor that enhanced p53 stability and together cooperatively modified p53 targeted RNAs by m^6A upon DNA damage [154]; METTL14 was found to be needed for embryonic post-implantation epiblast formation [149]. Further, data have shown the importance of methyltransferase KIAA1429 for folliculogenesis and oocyte development, as the KIAA1429 conditional knockout mice produced severe defects in oocyte growth, alterations in OSFs expression, and an inability to undergo nuclear envelope breakdown (NEBD) [157].

Many proteins can act as m^6A readers. The most known are YTH domain containing family proteins (YTHDF1,2,3) [158] and IGF2BP1 protein regulating JAK2/STAT3 signalling [159], as well as many others. YTHDF1 promotes active translation in HeLa cells by interconnecting m^6A mRNA transcripts with translation initiation factors, ribosomes, or stress granules [18]. YTHDF3 was shown in HeLa cells to enhance YTHDF1 upregulation of translation as well as the promotion of RNA decay via YTHDF2 [160]. The YTHDF2 reader in mice is responsible for the maintenance of correct gene dosage by utilizing RNA degradation machinery. This is coupled with the activation of CNOT7 deadenylase and DCP1A, DCP2 decapping enzymes. However, the most recent study on HeLa concluded that all YTHDF1,2,3 readers have common core sites and act together on selective m^6A mRNA degradation via CCR4-NOT deadenylation complex [158]. Female YTHDF2 double knockout mice are infertile and show cytokinesis defects in early zygotic development. Nevertheless, YTHDF2 double knockout oocytes are capable of ovulation and fertilization [161]. Additional enzymes do exist that relay m^6A regulation onto common physiologically important pathways. For example, recently discovered m^6A reader activity in Fragile-X mental retardation protein (FMRP) is important for the maternal RNA decay in Drosophilla embryos. FMRP used m^6A tagged mRNA transcripts for their sequestering into FMRP granules. [162]. FMRP was also shown to create granules at the onset of meiosis in human fetal ovaries, suggesting its importance in the translational regulation of oocyte maturation [163]. This was supported by the detection of FMRP in all stages of mouse oocyte meiotic maturation and its rapid decline in two cell embryos [26]. Therefore, m^6A methylation could both directly and indirectly regulate the translation of certain mRNAs.

The removal of m^6A methylation marks from transcripts is done by two main demethylases ("erasers"), fat mass- and obesity-associated (FTO), and α-ketoglutarate-dependent dioxygenase alkB homolog 5 (ALKBH5) [164]. A decrease of FTO expression with age was shown to increase m^6A methylation in aged mouse ovaries and human granulosa cells of elderly patients [162]. The same decrease of FTO expression followed by an increase in m^6A methylation was observed in ovarian tissues from premature ovarian failure (POF) patients and POF model mice [165]. Therefore, proper regulation of m^6A methylation is one of the factors to ensure follicular developmental competence. Decreased m^6A methylation in placental tissues of patients suffering from recurrent miscarriage caused by the upregulation of the second eraser, ALKB5H demethylase, revealed that in such endometrium the trophoblast is unable to nidate [166].

4. Translation of Epigenetics into ART

Assisted reproduction techniques (ARTs) are widely applied in the field of human reproduction (Figure 3) and animal breeding. Exposure to ART results in a decreased developmental competence of fertilized mouse oocytes, partially due to the induction of epigenetic changes [167] (Table 1).

4. Translation of Epigenetics into ART

Assisted reproduction techniques (ARTs) are widely applied in the field of huma reproduction (Figure 3) and animal breeding. Exposure to ART results in a decreased de velopmental competence of fertilized mouse oocytes, partially due to the induction of ep igenetic changes [167] (Table 1).

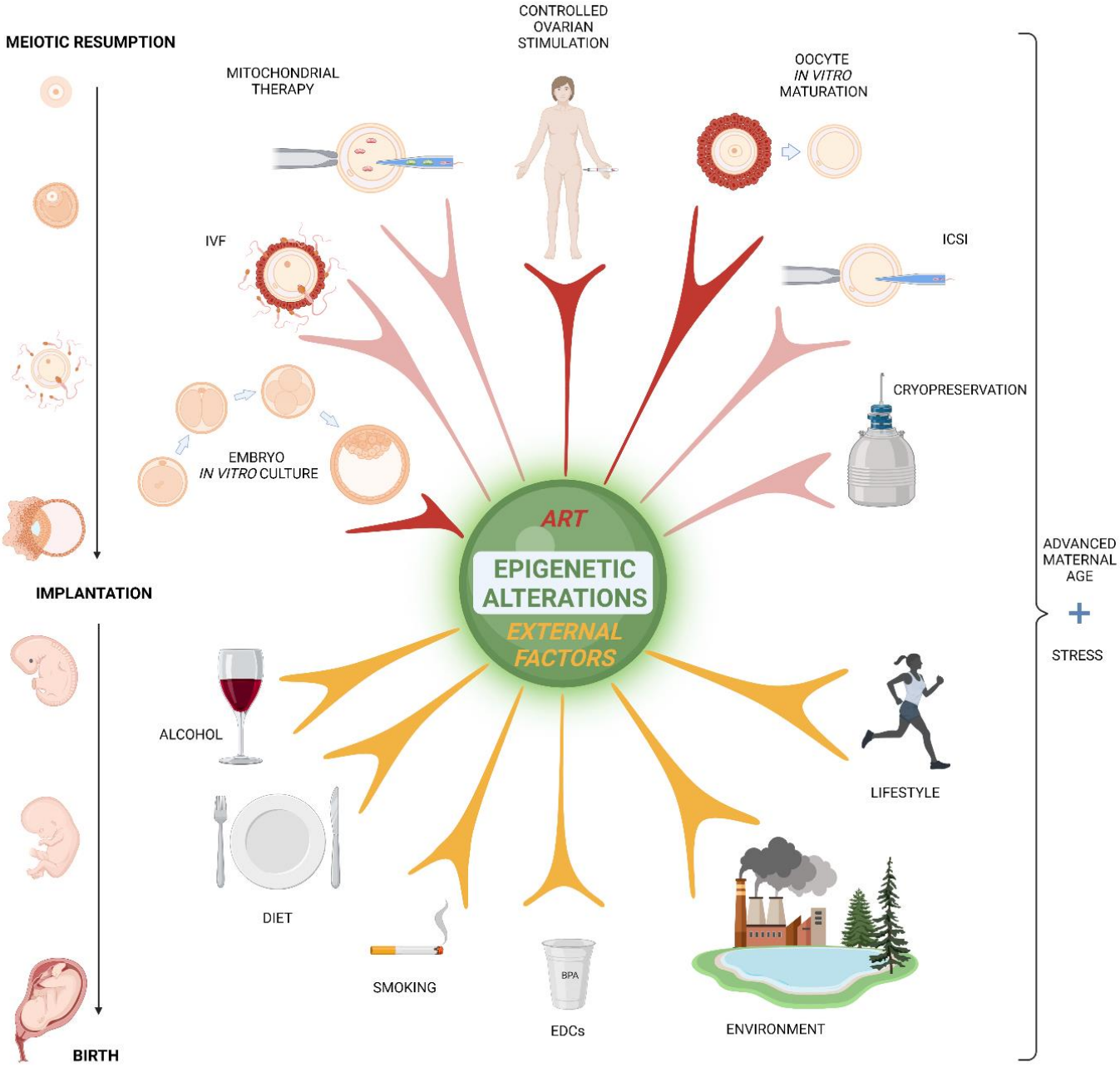

Figure 3. Assisted reproduction technology (ART) and external factors involved in epigenetic alterations: visualization of ART procedures employed in the process of oocyte meiotic maturation and early embryo development with proven (red arrows) or insignificant (pale red arrows) impact on the epigenome. External factors influencing epigenetics of post-implantation in utero embryo and fetal development (yellow arrows) are divided among nutritional (alcohol, diet) and lifestyle factors (advanced age, smoking, living environment, endocrine-disrupting chemicals (EDCs)). The image was created with BioRender.com.

Figure 3. Assisted reproduction technology (ART) and external factors involved in epigenetic alterations: visualization of ART procedures employed in the process of oocyte meiotic maturation and early embryo development with proven (red arrows) or insignificant (pale red arrows) impact on the epigenome. External factors influencing epigenetics of post-implantation in utero embryo and fetal development (yellow arrows) are divided among nutritional (alcohol, diet) and lifestyle factors (advanced age, smoking, living environment, endocrine-disrupting chemicals (EDCs)). The image was created with BioRender.com.

Table 1. Summary of effects induced by ART on DNA methylation in oocytes, early embryos an their influence on offspring. "NE" indicates specific gene effects were not evaluated.

Stressor	Species	Genes Affected	Main Findings	Reference
Ovarian Stimulation				

Table 1. Summary of effects induced by ART on epigenetic changes in oocytes, early embryos and their influence on offspring. "NE" indicates specific gene effects were not evaluated.

Stressor	Species	Genes Affected	Main Findings	Reference
		Ovarian Stimulation		
Controlled ovarian stimulation	human	NE	Chromosomal aneuploidy	[168]
Superovulation	mouse	*Dnmt1, Dnmt3A, Dnmt3B*	Affected expressin of methyltransferases in GV, MII oocytes, in one-cell and two-cell embryos	[169]
Superovulation	mouse	*Epab, Pabc1*	Altered expression of translational regulators *mRNA* in mouse GV and MII oocytes and in zygots	[170]
Superovulation	mouse	*Snrpn, Peg3, Kcnq1ot1, H19*	Disrupted methylation of imprinted genes in blastocysts	[171]
Superovulation	mouse	*Gfod2, Foxi3, Celf4, Syf2*	In oocytes, altered methylation of genes involved in glucose metabolism, nervous system development, cell cycle, cell proliferation, and mRNA processing	[172]
Superovulation	mouse	*H19*	Altered *H19* methylation in mouse blastocysts after in vivo fertilization	[173]
Superovulation	mouse	*Fasn, Dgat1, Dgat2*	Decreased fatty acid content in mice 2-cell embryos by reducing the *Fasn* and increasing the *Dgat1* and *Dgat2 expression*.	[174]
Repeated superovulation	mouse	*Cox1, Cytb, Nd2, Nd4*	Altered expression of mitochondrial genes in mouse cumulus cells	[175]
Repeated superovulation	mouse	NE	Abnormalities in mitochondrial structure and distribution in mouse oocytes	[176]
Superovulation	mouse	NE	Decrease of mitochondrial activity and ATP production in mouse oocytes	[177]
Superovulation	bovine	*TXN2, PDX3*	Decline of mtDNA copy number in bovine oocytes., decreased expression of antioxidant genes in bovine cumulus cells	[93]
		Oxidative stress		
Presence of reactive oxygen species	human	NE	Sperm originated changes to epigenetic regulation of human embryo development	[178]
Culture under 20% of oxygen	bovine	*CAT, GLRX2, HSP90AA1. KEAP1, NFR2, PRDX1, PRDX3, SOD1, TXN, TXNRD1, H2AFZ, H3F3B*	Increase of transcript of genes associated with epigenetic remodelling, oxidative stress and cellular stress response in blastocysts	[179]
Culture under 20% of oxygen	bovine	*DNMT3A*	Elevated DNMT3A expresiion and increase of global DNA methylation in 4-cell embryos and blastocysts	[180]
Oxidative stress (palmitic acid)	bovine	*PRDX3, HADHB, UQCRB, CYCS*	Upregulation of PRDX3 protein. Elevation of the mitochondrial HADHB, UQCRB and CYCS proteins in oocytes	[181]
Oxidative stress (H_2O_2)	mouse	NE	Decrease in mitochondria-derived ATP and disassembly of spindles in in vitro cultured MII oocytes	[85]
		In vitro techniques		
Oocyte in vitro maturation	human	*HDAC1*	Compromised deacetylation in oocytes. Residual acetylation linked to aneuploidy	[182]
Oocyte in vitro maturation	bovine	*SIRT2*	Faulty mitochondria	[183]

Table 1. *Cont.*

Stressor	Species	Genes Affected	Main Findings	Reference
Cytoplasmic transfer	human	Not tested yet	10–15% cytoplasm transfer into aged oocytes prroduced healthy offspring	[95]
Suboptimal culture media	rabbit	NE	Alteration of DNA methylation reprogramming in paternal pronuclei of zygotes	[184]
In vitro fertilization & ICSI	human	H19	ART caused demethylation resulted in the changes of genomic imprinting	[185]
Embryo in vitro culture	human	NE	miRNAS detected in spent culture medium downregulate embryonic mRNAs	[186]
Cryopreservation	human	*LINE1*	Differently methylated placental DNA between fresh and frozen embryotransfers	[187]
Suboptimal culture media	mouse	NE	Higher methylation disturbances in embryos from superovulated females and IVF	[188]
Intracytoplasmic sperm injection	mouse	*H19, Snrpn, Peg3, Igf2*	Imprinting defects in somatic tissues	[189]

In humans, no significant epigenetic changes were found between regular pregnancy and ART pregnancy in newborns, however only a few key imprinted genes were analyzed in a small cohort of patients [190]. Recently, epigenetic imprinting-related disorders were demonstrated on mouse models and also observed in ART newborns like Prader–Willi syndrome (PWS), Silver–Russell syndrome (SRS), Beckwith–Wiedemann syndrome (BWS), and Angelman syndrome (AS) [191]. The long-term epigenetic effects of ART still await evaluation. Needless to say, more extensive follow-up of children born from ART embryos should be carried out. Moreover, further investigations into the epigenetic impact of ART methodology on cultured oocytes and embryos should be done.

4.1. Hormonal Stimulation

Superovulation or the clinical term controlled ovarian stimulation (COS) is applied to statistically increase the chances of acquiring blastocyst stage embryos compared to normal ovulation and increase the likelihood of a successful pregnancy. The basis of COS is the stimulation by a recombinant follicle stimulating hormone (rFSH) and the ovulation trigger, human chorionic gonadotropin (hCG). A co-administration with gonadotropin-releasing hormone (GnRH) agonist or antagonist is needed to avoid premature ovulation.

Increased incidence of chromosomal aneuploidy in human COS oocytes was associated with changes in DNA methylation [168]. COS was also linked to embryo development retardation [192] and negative effects on child health [193–195] A loss of genomic imprinting, particularly associated with the overgrowth Beckwith–Wiedemann (BWS) syndrome was reported in bovine fetal tissues. Demethylation of imprinted genes was observed in other bovine genome loci [196].

Additionally, protein translation was affected using the mechanisms triggered by superovulation. The mRNA expression of two critical players in translational regulation of stored maternal mRNAs, the embryonic poly(A)-binding protein (ePAB), and the poly(A)-binding protein cytoplasmic 1 (PABPC1), was modified in oocytes and two-cell embryos [170]. After IVM oocyte culture in the presence of rFSH, a decreased global translation was observed in mouse, bovine, and porcine models including humans [197]. rFSH may compromise regulation of specific translatome essential for oocyte maturation and early embryo development. Therefore, the use and dosage of recombinant hormones in the conventional IVM should be thoroughly evaluated.

Superovulation in mouse oocytes and early embryos alters DNA methylation [198] and expression of methyltransferases [169] and impairs methylation of genes involved in glucose metabolism, nervous system development, cell cycle, cell proliferation, and mRNA

processing [172]. Disrupted DNA methylation of imprinted loci in mouse blastocysts affected, for example, a body-weight-limiting H19 gene [173], and was more frequent at higher hormonal superovulation dosages [171]. Superovulation caused imprinting defects leading to embryonic abnormalities and higher mortality [174,199]. Detected epigenetic differences in DNA methylation between superovulated and naturally ovulated oocytes suggested that superovulation also recruits growing oocytes with incomplete epigenetic maturation [172]

4.2. Oocyte In Vitro Maturation

When hormonal stimulation does not produce a satisfactory number of matured MII oocytes, in vitro maturation (IVM) is considered. IVM is based on the retrieval of fully grown cumulus enclosed GV oocyte complexes (COC) from ovarian follicles. COCs are meiotically matured by the IVM in the presence of rFSH and LH (rLH) to produce MII oocytes. The conventional IVM technology is understandably inferior to standard COS with maturation in vivo.

As just mentioned, rFSH promoted a decrease of global proteosynthesis marker, the radioactively labelled 35S methionine, in mouse, bovine, porcine, and human IVM oocytes [197]. The use of recombinant hormones in the IVM media is one of the factors affecting proper translational regulation and proteosynthesis during maturation.

A hypothesis was proposed that the resumption of meiosis upon COC ovarian puncture (OPU) is premature and could also have a negative impact on IVM quality. In response to that, an alternative approach called capacitation IVM (CAPA-IVM) was devised [200]. This experimental ART maintains high cAMP concentration within the in vitro cultured human COC by stimulating cumulus cells with rFSH, insulin, estradiol, and C-natriuretic peptide, thus indirectly inhibiting the NEBD in oocytes for about 24 h. The recent clinical study resulted in a live birth rate after the first embryo transfer of 35.2% for CAPA-IVM compared to 43.2% for standard IVF control [200]. It can be hypothesized that CAPA-IVM has a direct downstream impact on translational regulation as it gives the oocytes more time to equilibrate before meiotic maturation. These promising results from CAPA-IVM deserve further investigation, particularly the clarification of underlying molecular mechanisms and epigenetic regulation.

IVM quality is indeed determined by epigenetic m^6A transcript methylation or histone deacetylations. Numerous histone modifications are employed in oocyte meiotic maturation, ranging from most profound deacetylation to methylation, phosphorylation, ubiquitination, and SUMOylation as reviewed by He et al., 2021 [41]. General histone deacetylation was compromised throughout meiosis in aged human oocytes. The residual acetylation correlated with chromosome misalignment linked to aneuploidy [181]. Moreover, human IVM oocytes with reduced HDAC1 expression also exhibited MII spindle abnormalities. Comparatively, more HDAC1 transcripts were present in in vivo (IVO) matured oocytes than IVM [201].

Improved IVM technology could also utilize the discussed sirtuin deacetylase family as recently reviewed [53]. Authors of the review detected sirtuins application for the management of aging and stress related syndromes, PCOS, diabetes, or endometriosis, and concluded the beneficial improvement of the energy balance and ROS protection. Decreased SIRT3 expression for example, correlated with lower developmental competence in human in vitro cultured embryos, which was attributed to defective mitochondrial biogenesis [67]. Recently, basal human serum SIRT2 level was suggested as a novel biomarker of ART outcome [202]. This kind of IVM therapy is promising, however further investigation is needed to determine their best delivery, dosage, combination, and mode of action.

The IVM approach is most applied for the management of polycystic ovarian syndrome (PCOS) which is the most common endocrine disorder in 6–20% of women of reproductive age accompanied by oligoovulation and/or anovulation. PCOS is a multifactorial syndrome with strong epigenetic inheritance, where external environmental, lifestyle, and dietary factors play a significant role [203].

whether PCOS is trans-generationally inherited through offspring, who would again become clients of IVF clinics (Figure 4). Instead, could PCOS be cured by managing mentioned external epigenetic factors rather than just relayed onto the next generation by IVF?

PCOS infertility is managed through IVF centres. Recent evidence suggests intergenerational epigenetic inheritance of this syndrome [204]. The puzzling question arises whether PCOS is trans-generationally inherited through offspring, who would again become clients

ernal

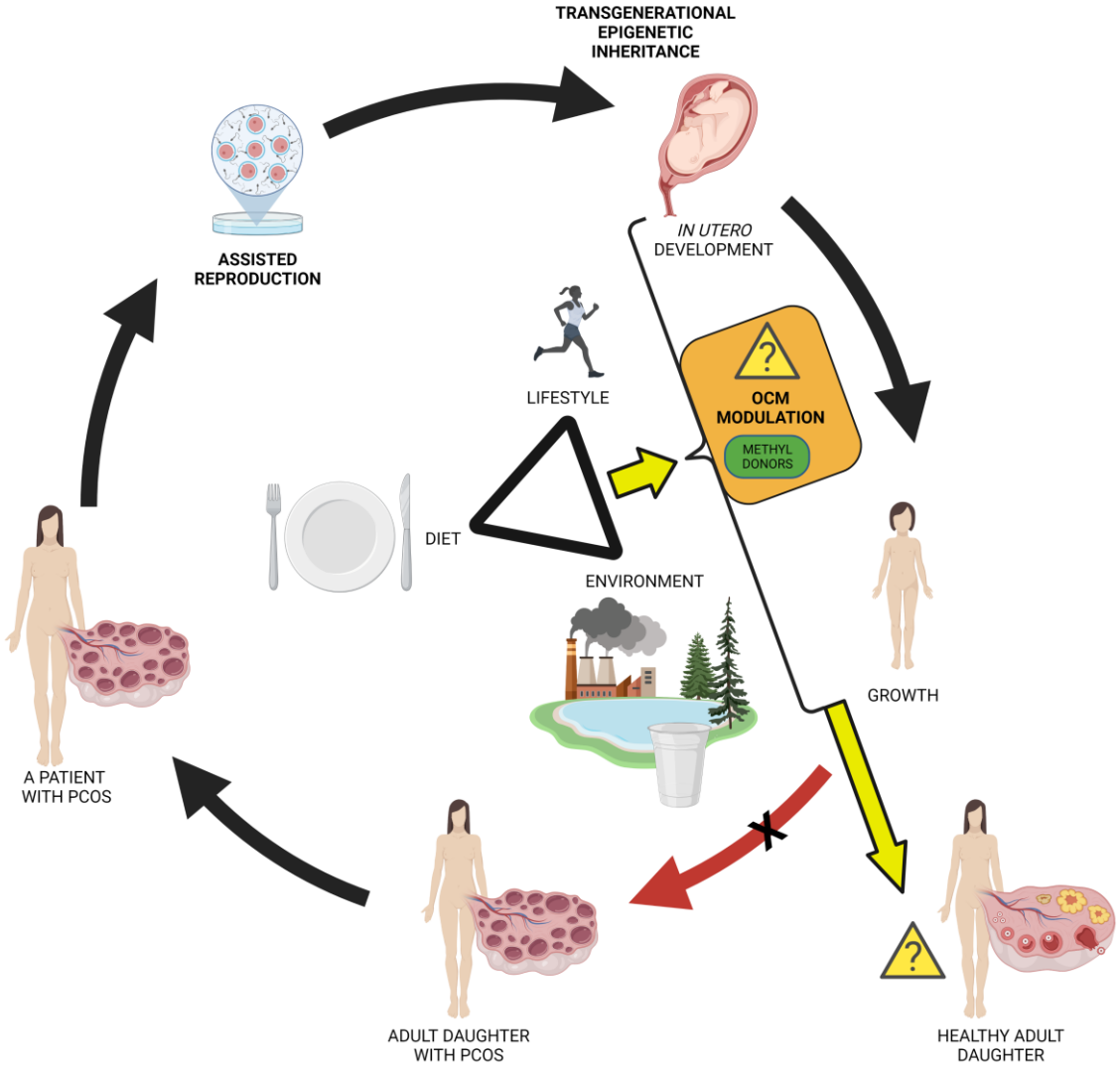

Figure 4. Transgenerational epigenetic inheritance and the therapy (the polycystic ovary syndrome (PCOS) case: Recent evidence showed that acquired epigenetic changes can be inherited between generations. One such example is the PCOS, which presents the main cause of infertility in humans. PCOS patients are usually managed by assisted reproduction techniques (ART), but there is high probability of transmission from mother to daughter. DNA hypomethylation in PCOS is also influenced by external factors such as nutrition, living environment, or lifestyle [205]. The nutritional supplementation with one carbon metabolism (OCM) compound, the methyl donor S-adenosylmethionine (SAM) could possibly have a therapeutic potential to mitigate or alleviate PCOS in humans [206]. The image was created with BioRender.com.

Figure 4. Transgenerational epigenetic inheritance and the therapy (the polycystic ovary syndrome (PCOS) case: Recent evidence showed that acquired epigenetic changes can be inherited between generations. One such example is the PCOS, which presents the main cause of infertility in humans. PCOS patients are usually managed by assisted reproduction techniques (ART), but there is high probability of transmission from mother to daughter. DNA hypomethylation in PCOS is also influenced by external factors such as nutrition, living environment, or lifestyle [205]. The nutritional supplementation with one carbon metabolism (OCM) compound, the methyl donor S-adenosylmethionine (SAM) could possibly have a therapeutic potential to mitigate or alleviate PCOS in humans [206]. The image was created with BioRender.com.

3.3. Mitochondrial Therapy

Oocyte developmental competence is tightly connected with energy availability. Meiotic maturation, fertilization, and embryonic genome activation are all energetically demanding processes depending on essential mitochondrial ATP production through OXPHOS. Metabolic disorders and aging are coupled with oocytes of inferior quality, which is largely attributable to energy production in the form of ATP by mitochondria as reviewed

by [207]. mtDNA copy number in human oocytes range from 20,000–600,000 [79,208] and was found to decline with increasing maternal age [209]. The ART solution to this trend in our population is to apply cutting-edge mitochondrial therapies and take advantage of enucleated donor oocytes in techniques such as Cytoplasmic Transfer (CT), Maternal Spindle Transfer (MST), first Polar Body Transfer (PB1T), or in case of zygotes, Pronuclear Transfer (PNT). Nuclear transfer in GVs has been described, but due to complete zygote arrest of such maturated and fertilized mouse model oocytes, is not further considered for clinical applications (reviewed by [210]).

CT of about 10–15% of donor oocyte cytoplasm into one of the two sibling oocytes of an aged patient increased their developmental competence. Newborns from such treated oocytes were considered being healthy [95].

The MST method is based on the removal of the MII spindle from a healthy donor oocyte. In the same way, MII spindle is transferred from the patient's affected oocyte into a healthy enucleated donor oocyte [211,212]. The first MST in human oocytes had low zygote survival ability, but with comparable blastocyst rates [211]. In 2017, MST was used for the first time therapeutically in the management of Leigh syndrome, which affects mtDNA and mitochondria [213]. Following a live birth, the load of mutated mtDNA was estimated to be below 10%. Concerns about MST introducing new epigenetic changes in donor oocytes were negligible as revealed by analysis of gene expression, which found no significant differences [214].

Whole genome RNA-sequencing of PNT derived blastocysts also found no major epigenetic differences [215]. An inferior method to MST, the PB1T method successfully reconstituted spindle in about 67% of enucleated donor oocytes but following fertilization only about half of the produced viable zygotes were capable of blastocyst development [216,217]. First polar bodies (PB1) were shown to mirror the methylomes of the oocytes they originated from, and therefore PB1s could have more of a diagnostic, rather than therapeutic, role [218].

Another non-invasive strategy to enhance oocyte and early embryo competence is to support mitochondrial functions in in vitro cultured oocytes by supplementing the culture media with compounds upregulating the functions of histone deacetylases sirtuins. SIRT1 for instance stimulates mitochondrial activity, enhances its biosynthesis and regulates degradation of mitochondria [219].

4.4. IVF & ICSI

New evidence from genome-wide sequencing of neonatal cord blood has shown that epigenomes of ART newborns exhibit the loss of CpG methylation compared to those of natural conception (NC). A total of 176 genes were differentially methylated including genes employed in growth and neurodevelopment [195]. Similar findings were obtained from 7–9 week old fetal human tissue after elective termination of pregnancy. A total of 164 differentially methylated genes were detected and associated with the development of the skeletal system, body size, lipid, and steroid synthesis [220]. Moreover, a study on histone modifications between IVF and ICSI found significant differences in global H3K4me3. ICSI placentas had lower H3K4me3 levels than IVF placentas in line with its lower transcription activity [221]. It is important to bear in mind that ART vs NC comparison will always accompany epigenetic changes acquired during the in vitro embryo culture so no clear epigenetic input of IVF and ICSI can be drawn.

4.5. Embryo In Vitro Culture

In the female reproductive tract, particularly the oviducts, developing early embryos are under the influence of hormones, nutrients, growth factors, and cytokines [222]. The epigenome of in vitro cultured mammalian embryos is vulnerable to exposed culture conditions as aberrant DNA demethylation kinetics was detected in in vitro grown embryos compared to embryos of in vivo origin [183].

During in vitro culture, early embryos are exposed to limited nutrient availability and furthermore, they are influenced by the end products of their metabolism [223]. A stress response can be induced through the manipulation of embryos by pipetting, exposure to thermal stress, and/or detrimental change in pH [224,225]. It is evident that embryo in vitro culture conditions contribute to its epigenetic status. Embryo exposure to suboptimal culture conditions or toxic substances in the medium can result in altered DNA methylation, genetic reprogramming, developmental disruption, and consequently early embryo loss as demonstrated in the mouse, rat, and rabbit [183,226].

In vivo early embryonic development takes place in the oviducts, but in vitro embryo culture conditions are far from the oviductal environment, respective to nutrients, oxygen concentration, or epigenetic messengers. One example for both, oviductal extracellular vesicles (oEV) were shown to harbour miRNA that can downregulate specific mRNAs or modify gene expression is other ways [185]. These oviduct–embryo interactions are missing in vitro and would most likely play much more important roles in the regulation of the embryonic epigenome that await their discovery [227–230].

Adequate oxygen supply is another crucial condition for the success of in vitro culture. Concentrations of 5% oxygen and 20% oxygen are commonly used during in vitro culture of oocytes and early embryos. DNA methylation and gene transcription of mouse oocytes grown in in vitro conditions under 20% oxygen correlated more with the reality of in vivo conditions, indicating that higher oxygen concentration is beneficial for mouse oocytes matured in vitro [231]. In contrast, exposure of in vitro cultured bovine preimplantation embryos to 20% oxygen was associated with an increase in global DNA methylation indicating that in this case oxidative stress can alter the embryonic epigenome [178,179]. These findings suggest variations in the optimal oxygen concentration among different species. In order to optimize the oxygen in in vitro culture of mammalian embryos, it was suggested to reduce the concentration up to the physiological oxygen tension as the median oxygen rate in the mammalian oviduct is around 8% [232,233]. The importance of oxygen tension reduction during in vitro embryo culture was confirmed by systematic review and meta-analysis of published human ART studies, revealing an increase in pregnancy and live birth rates of embryos cultured at 5% oxygen concentration [234].

At 20% oxygen concentration in bovine embryo blastocyst culture, elevated ROS were detected [178]. Although the ROS are important signalling molecules in certain biological processes and are normal products of oocyte metabolism, they can interact with biological molecules such as lipids, proteins, and nucleic acids, cause oxidative stress and cellular damage leading to the impairment of oocyte quality [235]. Oxidative stress can also increase the risk of aberrant DNA methylation in in vitro cultured preimplantation embryos [236,237].

In order to compensate for the adverse conditions of in vitro culture and maintain DNA methylation, a supply of methyl donors is needed, e.g., folates, which are often absent in culture media [237]. Methionine, an important intermediate metabolite of the one-carbon metabolism pathway (OCM) (Figure 5), contributes to epigenetic regulation by providing methyl groups for DNA methylation via S-adenosyl methionine (SAM) [238]. The methionine level is an important factor influencing the quality of the early embryo epigenome. Elevated concentrations of the methionine product homocysteine in the oocyte and embryo environment is, however, harmful due to its toxicity and has to be converted back to methionine. Limited remethylation of homocysteine to methionine leads to a decrease of SAM causing DNA hypomethylation [238].

A high level of homocysteine was also detected in the serum of PCOS patients and in the follicular fluid of polycystic ovaries and was linked with poor oocyte quality [242,243]. The aging process may be an indirect factor contributing to the decrease of embryo quality and oocyte maturation through increasing homocysteine levels in follicular fluid; hence, a decrease of homocysteine level in follicular fluid can significantly improve the oocyte maturation rate and embryo quality [244]. Elevated homocysteine levels in follicular fluid is also associated with hypermethylation of mitochondrial DNA accompanied with a mito-

chondrial malfunction in oocytes retrieved from porcine polycystic ovaries [245]. In porcine
al rate,
nibitor
ed the

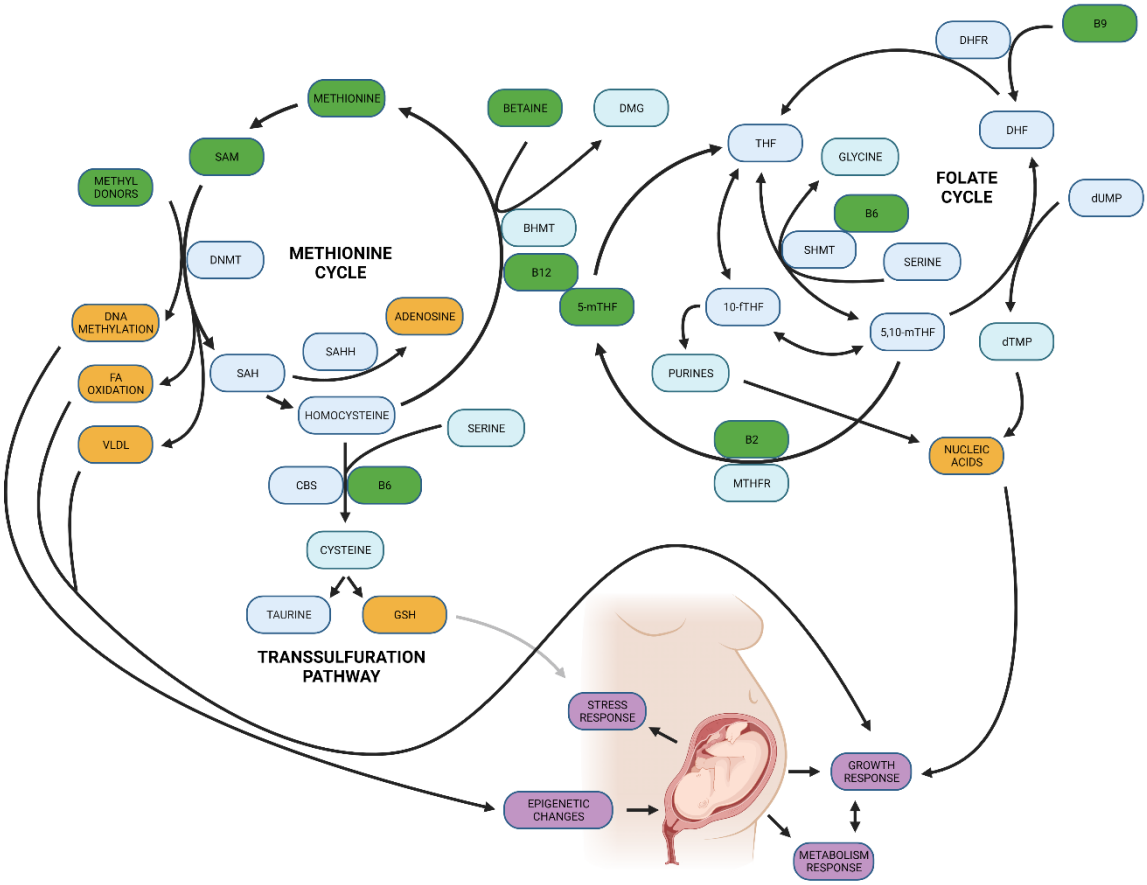

Figure 5. One-carbon metabolism (OCM)-associated pathways in nutrition and epigenetics: Many OCM compounds are nutritional supplements (green) such as B vitamins; Riboflavin (B2), Pyridoxine (B6), Folate (B9), or Cobalamin (B12). 5-methyl-tetrahydrofolate (5-mTHF) or methionine and betaine are another currently introduced nutritional supplements. OCM pathways produce molecules for epigenetic modifications [239], antioxidant production [240], and building compounds of nucleic acids, amino acids, or phospholipids (orange) [241], which are all together influencing in utero fetal development (purple). Abbreviations: 5,10-mTHF, 5,10-methenyl-tetrahydrofolate; 10-fTHF, 10-formyl-tetrahydrofolate; BHMT, betaine-homocysteine S-methyltransferase; CBS, cystathionine β-synthase; DHF, dihydrofolate; DHFR, dihydrofolate reductase; DMG, dimethylglycine; DNMTs, de novo and maintenance DNA methyltransferases; dTMP, deoxythymidine monophosphate; dUMP, deoxyuridine monophosphate; FA, fatty acids; GSH, reduced glutathione; MTHFR, 5,10-methylenetetrahydrofolate reductase; SAH, S-adenosylhomocysteine; SAHH, S-adenosylhomocysteine hydrolase; SAM, S-adenosylmethionine; SHMT, serine hydroxymethyltransferase; THF, tetrahydrofolate; VLDL, very-low density lipoprotein. The image was created with BioRender.com.

In vitro oxidative stress can also affect mitochondrial function. Treatment of in vitro cultured bovine oocytes with palmitic acid induced upregulation of peroxiredoxin 3, which is a mitochondrion-specific H_2O_2-scavenging enzyme, and elevation of the mitochondrial HADHB, UQCRB, and cytochrome C proteins suggesting that oxidative stress increased electron transport in bovine oocytes [180]. Exposure of MII mouse oocytes to $CoCl_2$ led to a decrease in mitochondria-derived ATP and disassembly of meiotic spindles [85].

A high level of homocysteine was also detected in the serum of PCOS patients and in the follicular fluid of polycystic ovaries and was linked with poor oocyte quality

4.6. Cryopreservation

Two main methods of germ cell cryopreservation exist: slow freezing and vitrification, both with the goal to eliminate ice crystal formation inside the cells. The slow freezing method is based on the continuous and steady decrease of temperature by 1–2 °C/min in the presence of cryoprotective agents and is conventionally applied for the preservation of human fertilized zygotes [246]. The second approach, called vitrification, is now the most widely used method for cryopreservation. It combines a rapid increase in media viscosity and solute concentration with snap freezing in liquid nitrogen. Vitrification has outperformed slow freezing in conventional ART human embryo cryopreservation by both higher clinical pregnancy and live births [247].

However, from the epigenetics perspective cryopreservation is still questionable [186]. Vitrifcation significantly reduced the ATP content in oocytes of various mammalian species, including humans [248,249]. Particularly changes in global DNA methylation, histone modifications and genetic imprinting are to be scrutinized. Research performed on vitrified mouse embryos found a common pattern of decreased global [250] and imprinted DNA [251] methylation. Vitrification of bovine oocytes was associated with a significant reduction in the expression profile of three epigenetic-related genes DNMT1, DNMT3B, and HDAC1 [252]. In vitrified porcine embryos, a greatly reduced expression of epigenetically associated key genes SMYD3, TET2, and HDAC8 led to altered epigenetic reprogramming and decreased blastocyst rates [253]. The cryoprotective agents present in IVF vitrification media might negatively affect the epigenetic profile in embryos, as dimethylsulfoxide (DMSO) was found to be responsible for the disruption of global DNA methylation and significant decrease of ATP content in vitrified human cardiac tissue [254]. A detailed analysis of molecular changes occurring in cryopreserved germ cells and embryos is necessary to distinguish possible molecular targets that could contribute to improve the cryopreservation procedures.

5. In Utero Epigenetics, beyond ART?

Exposure to unfavorable conditions before pregnancy and during intrauterine development lead inevitably to epigenetic alterations of a newborn and can evolve into pathogenesis of metabolic, cardiovascular, endocrine, and malignant disorders in adulthood [255]. As every ART-produced embryo has to be eventually planted into a mother's womb, these in vivo epigenetic factors deserve a closer look in order to understand the full story.

5.1. Endometrial Receptivity & Placentation

Following ART embryo transfer, each embryo faces the selective process of nidation and implantation into the endometrial tissue of the uterine wall. This in utero process itself is highly complex and involves the cooperation of many signalling pathways. Many epigenetical mechanisms are involved as well, such as DNA methylation [256], m^6A methylation [166], or interaction with ncRNAs secreted from exosomes [257]. It has even been suggested that DNA methylation profiles of cervical secretion could serve in the future as an alternative way for diagnosing endometrial receptivity [258]. Decidualization, the process of endometrial preparation for blastocyst implantation, is suppressed in human endometrial stromal cells by an ncRNA, the miR-542-3p. Overexpression of this miRNA also downregulates VEGF, cyclooxygenase-2 (COX-2), and matrix metalloproteinase (MMP-9), all linked with angiogenesis [259]. Most ncRNAs are able to exert their effects by transportation as cargos in lipophilic exosomes. In this way, ncRNAs influence the embryonic development in the oviduct and uterus [257]. So far, little is known about the scope of the influence of these ncRNAs on the epigenome of a developing individual.

Following successful implantation, the embryo turns to cardiac and neural development. These processes are energy-dependent and highly susceptible to proper dietary intake and environmental conditions. Defective placentation is associated with impaired mitochondrial function and associated low ATP production [82,83]. Incorrect DNA methy-

lation on imprinted genomic regions dysregulates placental function [99,100]. Nutritional and environmental status can influence the uterine and fetal epigenome to a large extent, and therefore their effects have to be taken seriously into account.

5.2. Nutritional Epigenetics

Numerous studies describe the effects of nutrition on the epigenome during embryonic development (reviewed in [238,260,261]). Particularly, the nutritional source of dietary methyl donors in early development can influence the DNA methylation process [239]. Methyl groups or so called one-carbon groups are produced through OCM, which integrates folate and methionine cycles and is a source for epigenetic DNA methylations, biosynthesis of DNA, proteins, and lipids. Amino acids such as methionine, glycine, and serine and appropriate levels of especially B class vitamins (B2, B6, B12) and folic acid (B9) are integral inputs for the successful functioning of one-carbon metabolism (Figure 4). Epigenetic changes in humans associated with OCM modifications affect pathways related to growth, metabolic functions, neural development, and stress response [239].

The modulation of epigenetic modifications, including DNA methylation, is done by the mTOR signalling through the OCM [262]. mTOR signalling is able to affect OCM by increasing the de novo synthesis of serine, one of the major single carbon donors [263]. Elevation of placental mTOR observed in obese women increased birth weight [264]. As one of the main functions of OCM is to produce S-adenosylmethionine (SAM) to ensure methyl-group transfer reactions, mTOR signalling, by influencing the OCM, is able to influence epigenetic modifications, including DNA methylation [262]. The epigenetic regulator methyltransferase DNMT1 is one of the downstream targets of the mTOR pathway [265]. The experimental inhibition of mTOR induced the suppression of DNA methyltransferase DNMT1 [260].

Microelements in the diet, e.g., Cu, Mn, Se, and Zn are often required for proper enzymatic function, neutralizing ROS, and are also involved in epigenetic regulation. For example, zinc is implicated in the correct functioning of methyltransferases and methyl-binding proteins and its deficiency has been suggested to affect the activities of zinc-dependent epigenetic enzymes, which are essential for DNA methylation [261]. Prolonged dietary Se supplementation in rats affected global and specific DNA methylation in liver and colon tissue [266]. Mn tends to accumulate in the placenta, and its supplementation experiments in chick embryos counteracted hyperthermic stress effects by modulating DNA methylation and histone acetylation [267]. A recent US study found a similar mode of action in Cu metabolism, which may be employed in DNA methylation and the regulation of human placentation [268].

Malnutrition can epigenetically induce in utero obesity in offspring, which usually manifests in adulthood. Blood analysis of human adults revealed that periconceptional exposure to famine altered the DNA methylation of genes implicated in growth and metabolic regulation. Prenatal famine exposure resulted in changes of DNA methylation patterns in genes associated with cell growth, metabolic health, mitochondrial function, adipogenesis, and its deposition [269,270]. A preovulatory protein restriction diet in rats induced abnormal mitochondrial ultrastructure in oocytes and negatively affected gene expression related to mitochondrial biogenesis [271].

This demonstrates epigenome vulnerability by famine in the early stages of development. There is strong evidence that maternal nutrition influences the development and future health of offspring. Studies done on mice [272] and cattle [273] confirmed maternal diet effects on oocyte DNA methylation. Postpartum cows exposed to negative energy balance and metabolic stress had a number of maternally imprinted genes in their oocytes hypomethylated [274].

Maternal obesity is another risk factor affecting offspring health epigenetically and has been shown when together with excessive nutrition intake to have a positive correlation with offspring obesity [275]. Causes of fetal overgrowth have been explored on the mouse model. It was documented that obesity in pregnancy is linked to stimulation of placental

insulin/IGF-1/mTOR and leptin signalling pathways [163]. The obesity mouse model resembles the changes in placental mTOR signalling and amino acid transporters activity observed in obese women giving birth to large babies [276]. DNA hypermethylation in the placentas of obese pregnant women was associated with reduced expression of the ten-eleven translocation (TET) methylcytosine dioxygenases, enzymes involved in DNA demethylation [58]. Increased gestational weight in early pregnancy is related to the enhanced CpG methylation of *MMP7, KCNK4, TRPM5*, and *NFKB1* genes in offspring cord blood DNA [277].

Maternal obesity and overnutrition affect mitochondria function and induce epigenetic changes of mtDNA. The mtDNA copy number, elevated expression of nuclear genes encoding mtDNA transcription factors *Tfam and Nrf1* were detected in oocytes of obese mice [278]. A maternal obesogenic diet (high fat/high sugar) was associated with elevated mtDNA content and increased expression of mtDNA biogenesis regulators *Tfam* and *Pgc-1α*, enhanced mitochondrial antioxidant defence, increased lipoxygenase expression, enhanced expression of transcriptional regulator NF-κB, and depletion of ovarian follicular reserve in young adult female mouse offspring [279]. The analysis of the newborn umbilical cord indicated that promoter methylation of the mitochondrial biogenesis regulator *PPARGC1A* in babies was positively correlated with maternal BMI [280]. It is evident that maternal obesity may affect the offspring metabolism through epigenetic regulation of specific genes.

It is common knowledge that consuming alcohol in pregnancy affects embryo development and can induce a variety of birth defects and neuronal disorders in offspring [281]. Alcohol intake interferes with normal folate metabolism (Figure 5) and decreases folate bioavailability for methyl donors by inhibiting methionine synthase and methionine adenosyl transferase [282].

It has been shown that alcohol metabolites, such as acetaldehyde, modify DNA methylation by inhibiting DNA methyltransferases [283].

The effect of alcohol abuse on the methylation of specific genes resulted in alterations of gene expression and neural development as reported in numerous studies (reviewed in [284]). In in vitro cultured fetal mouse neurons, the alcohol exposure induced a decrease of DNA methylation detected in the vicinity of the NMDA receptor subunit NR2B gene, which plays an important role in neural development and in learning and memory [285,286].

In human oocytes, alcohol-associated epigenetic changes were detected already in the growth phase when genomic imprints are established and could possibly affect the health of the child [287].The in vivo exposure of mice embryos to ethanol resulted in retardation of embryo development and was accompanied by epigenetic alteration of the *H19/Igf2* methylation in the placenta; the paternal allele of *H19/Igf2* was less methylated while the methylation of the maternal allele was elevated [288]. In mouse embryos exposed to alcohol, in vitro changes in methylation on chromosomes 7, 10, and X related to neural tube defects were detected [289].

6. Fetal Epigenetics Dependence on Maternal Lifestyle and Environment

In the present day, people live in a highly stressful world in compromised living environments. As we have already mentioned, both undernutrition and overnutrition can impact one's epigenome irrespective to ART. Here, we emphasize that postponing parenthood or living in physically and psychologically toxic environments can induce changes to the new generation's epigenome (Table 2).

Table 2. Summary of lifestyle, diet, and environment effect on epigenetic changes in oocytes, early embryos, and their impact on offspring. "NE" indicates specific gene effects were not evaluated.

Stressor	Species	Genes Affected	Main Findings	Reference
	Undernutrition			
Periconceptional exposure to famine	human	*IGF2*	*IGF2* hypomethylation in adults 60 years later	[290]

Table 2. *Cont.*

Stressor	Species	Genes Affected	Main Findings	Reference
Periconceptional exposure to famine	human	*IL10, INSIGF, LEP, MEG3, ABCA1, GNASAS*	Altered DNA methylation of genes implicated in growth and metabolic regulation	[270]
Prenatal exposure to famine	human	*ABCG1, PFKFB3, METTL8*	Altered DNA methylation of genes associated with lipid metabolism, glycolysis, and adipogenesis in adults	[269]
Low levels of dietary methyl donors during embryonic development	human	NE	Affected DNA methylation process and impact on postnatal long-term health	[291]
Protein restriction during pregnancy	mouse	*Lep*	Increased *Lep* promoter methylation and decreased leptin expression in offspring	[292]
Preovulatory protein restriction	rat	*Drp1, Opa1, Mfn1/2, Parl, Ndufb6, Hk2*	Altered expression of genes involved in mitochondrial biogenesis in superovulated oocytes	[271]
Negative energy balance and metabolic stress	bovine	NE	Hypomethylation of maternally inherited imprinted genes in oocytes of postpartum cows	[274]
	Obesity			
Obesity in pregnancy	human	*TET1, TET2. TET3*	DNA hypermethylation and reduced expression of methylcytosine dioxygenases in placenta	[58]
Gestational weight gain	human	*MMP7,KCNK4,TRPM5* and *NFKB1*	Increased DNA methylation in offspring.	[277]
Obesity in pregnancy	mouse	*IGF-1, mTOR, LEP*	Stimulation of placental insulin/IGF-1/mTOR and leptin signalling pathways	[163]
	Alcohol, smoking			
Alcohol	mouse, human	NE	Birth defects and neuronal disorders in offspring	[281,284]
Alcohol	mouse	*Cyp4f13, Nlgn3, Elavl2, Sox21, Sim1, Igf2r, Hist1h3d*	Decreased methylation of genes associated with development, imprinting and chromatin in embryos exposed to ethanol in vitro	[289]
Alcohol	mouse	*H19/Igf2*	Retardation of embryo development in vivo and alteration of the *H19/Igf2* methylation in placenta	[288]
Maternal smoking	human	*BMP4, BMHT2, DLGAP2, PRDM8, NRP2, ESR1, IL32, HOXB2*	In newborns, changes in CpGs methylation of genes involved in tooth and neuronal development and in cancer induction	[293]
	Maternal age			
Advanced maternal age (more than 40 years)	human	*BUB1B, BUB3, MAD3, BUB1, REC8, ATR, CHEK1, NBS1, RAD17, EIF4ENIF1*	In oocytes, reduced expression of spindle checkpoint and DNA damage checkpoint-related genes, lowered mRNA expression of the nuclear import mediator of eIF4E	[294]
Advanced maternal age (more than 40 years)	human	*REC8, SMC1B*	Decreased expression of the meiosis-specific cohesins components, REC8 proteins, and SMC1B in oocytes	[295]

Table 2. *Cont.*

Stressor	Species	Genes Affected	Main Findings	Reference
Advanced maternal age (41–44 years)	human	*PRDX1, PRDX2, PRDX4, PRDX6 COX5A, COX7B, COX8A, COX8C, COX11, COX14, COX17*	Down-regulation of the peroxiredoxin gene family members and attenuated expression of the cytochrome c oxidases in oocytes	[296]
Advanced age	mouse	*Dnmt3a, Dnmt3b, Tfam*	Downregulation of maintenance DNA methyltransferases and mitochondrial transcription factor in oocytes	[297]
Advanced age	mouse	*Hook1, Tuba1, Tubd1, Dncic2, Kif3, Rnf19/Dorfin, Pcnt2, Nin, Smc4l1, Dnmt1o, Dmap1, Dnmt3L*	Decrease of transcripts related to microtubule cytoskeleton and chromosome segregation, downregulation of methyltransferases in oocytes	[298]
Other causes				
Maternal stress during pregnancy	human	*HSD11B2, NR3C1, FKBP5*	Increased methylation and expression of glucocorticoid pathway-related genes in placenta and children blood.	[299,300]
Maternal gestational diabetes	human	*PDE6A, PRKCZ, PVT1, GALNT2, MS4A3, IL1RN, BTD*	In children, differentially methylated genes associated with type 2 diabetes, obesity, diabetic nephropathy, and coronary heart disease.	[301]
Eleveted homocysteine level	porcine	*mtDNA (12S, 16S rRNA and ND4) ND1, ND4L, ND5, COX1, CYTB mRNA*	Hypermethylation of mtDNA in oocytes from PCOS ovaries	[302]
Pollutants				
Bisphenol A	human	*MEST*	Hypomethylation of the obesity-associated mesoderm-specific-transcript (*MEST*) gene promoter and enhanced *MEST* expression in children	[303]
Bisphenol A	mouse	*Snrpn, Ube3a, Igf2, Kcnq1ot1, Cdkn1c, Ascl2*	Disruption of imprinted gene expression in embryos and placentas.	[304]
Polystyrene	mouse	NE	Negative effect on oocyte spindle assembly and chromosome alignment, increased oxidative stress, and mitochondrial agregation	[305]

6.1. Lifestyle

Advanced maternal age negatively influences oocyte maturation, meiotic divisions, and embryonic development [306,307]. Increasing maternal age raises the chances of miscarriage and adverse health issues in offspring, mainly due to chromosomal aneuploidies such as Down's syndrome [308]. Age-related decrease of ooplasm quality, mitochondrial defects, and abnormalities in meiotic maturation mechanisms are possible causes of the advanced maternal age-related decline of oocyte competence [168,309,310] A higher incidence of chromosomal abnormalities was reported in mammalian oocytes acquired from aged females (reviewed in [311]), and an elevated occurrence of aneuploidy related diseases was observed in babies born to mothers over 35 years of age [309]. The meiosis-specific cohesin subunits, REC8 and SMC1B, were found to be decreased in oocytes of women aged 40 and over, suggesting that age-related decrease of meiotic cohesin subunits impair sister chromatid cohesion and results in increased segregation errors [295]. The effect of maternal

age on oocyte quality and associated epigenetic changes have been well-documented and extensively reviewed in humans [310].

Oocytes of older women (41–44 years old) were more prone to oxidative damage by the attenuated expression of cytochrome c oxidases (COX gene family) involved in oxidative phosphorylation and energy production and down-regulation of members of the peroxiredoxin gene family [296]. Similarly, gene expression analysis of ovaries in aged mice revealed a decrease in mRNA expression of mitochondrial antioxidant genes, peroxiredoxin 3 (Prdx3), and thioredoxin 2 (Txn2) [92]. Gene transcriptome analysis of human oocytes retrieved from patients older than 40 years revealed a decreased expression of spindle checkpoint genes, DNA damage checkpoint-related genes, ADP ribosylation factors involved in protein trafficking, and mRNA coding for the EIF4ENIF1 protein, which mediates the nuclear import of eIF4E [294]. Closer analysis of MII aged mouse oocytes gene expression (42–45 weeks old) revealed a downregulation of genes involved in mitochondrial functions, antiapoptotic mechanisms, and those involved in the ubiquitin-proteasome degradation pathway. Moreover, expression was reduced in transcripts related to microtubule cytoskeleton, chromosome segregation, and maintenance of the DNA methyltransferases *Dnmt1o* and *Dnmt1s* [298]. Hence, reduced DNA methylation in MII oocytes and early embryos of aged mice together with a low abundance of DNA methyltransferases clearly points to a lower reproductive potential [297,312]. More recently, it was suggested that decreased DNA methylation related to advanced maternal age may partially induce significant changes to gene expression and alter developmental fitness (reviewed in [167,313]).

Maternal smoking in pregnancy remains a serious issue that gravely affects child health. Fetal exposure to maternal smoking during pregnancy induces changes in DNA methylation of different tissues. The impact of prenatal exposure to tobacco smoke on DNA methylation was mostly analyzed in the cord blood and placenta of newborns—reviewed in [314]. It was found that DNA methylation patterns associated with smoking are relayed to a low birthweight [315] and schizophrenia induction in adulthood [316]. Moreover, the meta-analysis mapping association between maternal smoking in pregnancy and newborn blood DNA methylation revealed that smoking whilst pregnant causes changes in the CpGs methylation of numerous genes including those involved in teeth and neurologic development as well as cancer induction [293]. *AHRR* and *CYP1A1*, genes of aryl hydrocarbon receptor signalling, which is engaged in detoxification, were also found to be differentially methylated in the cord blood of newborns exposed to maternal smoking [317].

Lifestyle can also be a factor determining the occurrence of gestational diabetes mellitus (GDM) in women. GDM is associated with an increased risk of cardiometabolic diseases and diabetes in the offspring [301]. DNA collected from venous blood of GDM women offspring detected differentially methylated CpGs in genes associated with type 2 diabetes, diabetic nephropathy, obesity, and coronary heart disease [301]. It has been shown that pregestational hyperglycemia renders the offspring more vulnerable to glucose intolerance. The expression of TET3 dioxygenase, responsible for 5-methylcytosine oxidation and DNA demethylation in the zygote, is decreased in oocytes from a mouse model of hyperglycaemia (HG mice) and in people with diabetes [318].

6.2. Environment

Endocrine Disrupting Chemicals (EDCs) cause serious defects in human health. EDCs are chemicals of natural or man-made origin that interfere with the endocrine system. Humans are exposed to EDCs from many sources, including diet, thermal receipt papers, cosmetics, cleaning products, pesticides etc. [319]. Exposure to EDCs during development can induce permanent alterations of physiology and increase predisposition to health issues such as obesity, asthma, and cancer [320].

Bisphenol A (BPA) is a ubiquitous plasticizer, EDC with probable estrogen-like activity. Newborn cord blood DNA studies revealed that prenatal exposure to BPA (but not bisphenol F and bisphenol S) induces hypomethylation of gene promoters related to

adipogenesis, growth and metabolism [321]. Hypomethylation of the obesity-associated mesoderm-specific-transcript (*MEST*) gene promoter enhanced *MEST* expression, which resulted in a significant increase of body mass index (BMI) in children [303]. Exposure to BPA during the late stages of oocyte development and the early stages of embryonic development disrupted the expression of imprinted genes in mouse embryos and placentas [304]. Mouse BPA exposure at 9–16 day of pregnancy led to decreased methylation and enhanced expression of the homeobox gene *Hoxa10* in offspring, a key regulator of in utero organ development [322]. Additionally, polystyrene nanoparticles inhibit meiotic maturation by negatively affecting spindle assembly and chromosome alignment in mice oocytes; moreover, exposure to polystyrene nanoparticles increased oxidative stress and mitochondrial aggregation during meiotic maturation [305]

Stress is a widespread environmental factor affecting human reproduction. Preconception and pregnancy time exposed to stress is associated with developmental problems and new-born physical and psychological health. Maternal stress has been linked to infant mortality, premature weight and low birth weight [323]. Increased DNA methylation of the glucocorticoid receptor NR3C1 gene promoter, which is related to maternal stress via controlling hypothalamic-pituitary-adrenal axis (HPA) has been reported in human cord and new-born blood [324]. Chronic maternal distress in pregnancy was accompanied by altered CpG methylation on glucocorticoid pathway genes in human placentas, which suggests that the placenta can be the main mediator between maternal and fetal stress. [299]. Similarly, differential DNA methylation of the HPA axis genes *CRH* and *NR3C1* was detected in cord blood of new-borns and *CRH, CRHBP, NR3C1*, and *FKBP5* in their placentas [325].

7. Conclusions

Over the past years, an increasing research interest has been focussed on understanding the regulation of the animal and human epigenomes. Many publications have demonstrated that DNA and RNA methylation, histone modifications, and non-coding RNA regulation are integral to the normal embryo development and future health of a newborn. However, our current understanding of these mechanisms is unsatisfactory. Here, we endeavoured to emphasize the connection between assisted reproduction technology and its epigenetic implications for oocyte and embryo development. We did not want to overlook the fact that following an embryo transfer, the in utero development is epigenetically affected by the actual fitness and age of the reproductive system as well as by external stimuli such as diet or nutrition. We want to show a complex picture of what is behind ART live-birth rates and the resulting health implications from the epigenetic point of view.

ART is of enormous importance to infertile couples and our society in general. Therefore, it is much needed to focus on improving ART and minimizing unnecessary negative impacts by discussing and bringing in the latest knowledge of epigenetic mechanisms involved in clinical infertility treatments. Many of the questions regarding epigenetics influencing in vitro oocyte and embryo culture protocols remain unanswered. Future studies should search for epigenetic key points in the concerned developmental pathways and investigate their clinical relevance as biomarkers or new treatments.

Author Contributions: Writing—original draft preparation, M.D.; writing and editing, L.N.; conceptualization, writing—review and editing, J.K. All authors have read and agreed to the published version of the manuscript.

Funding: This work was supported by the grant CZ.02.1.01/0.0/0.0/15_003/0000460 from the Operational Programme Research, Development and Education, by Institutional Research Concept RVO67985904, by GACR (22-27301S) and by GAUK 373621 for M.D.

Institutional Review Board Statement: Not applicable.

Informed Consent Statement: Not applicable.

Data Availability Statement: Not Applicable.

Conflicts of Interest: The authors declare no conflict of interest.

References

1. Ivanova, E.; Canovas, S.; Garcia-Martínez, S.; Romar, R.; Lopes, J.S.; Rizos, D.; Sanchez-Calabuig, M.J.; Krueger, F.; Andrews, S.; Perez-Sanz, F.; et al. DNA methylation changes during preimplantation development reveal inter-species differences and reprogramming events at imprinted genes. *Clin. Epigenet.* **2020**, *12*, 64. [CrossRef] [PubMed]
2. Susor, A.; Jansova, D.; Cerna, R.; Danylevska, A.; Anger, M.; Toralova, T.; Malik, R.; Supolikova, J.; Cook, M.S.; Oh, J.S.; et al. Temporal and spatial regulation of translation in the mammalian oocyte via the mTOR–eIF4F pathway. *Nat. Commun.* **2015**, *6*, 6078. [CrossRef] [PubMed]
3. Asami, M.; Lam, B.Y.H.; Ma, M.K.; Rainbow, K.; Braun, S.; VerMilyea, M.D.; Yeo, G.S.H.; Perry, A.C.F. Human embryonic genome activation initiates at the one-cell stage. *Cell Stem Cell* **2022**, *29*, 209–216. [CrossRef] [PubMed]
4. Bird, A.; Taggart, M.; Frommer, M.; Miller, O.J.; Macleod, D. A fraction of the mouse genome that is derived from islands of nonmethylated, CpG-rich DNA. *Cell* **1985**, *40*, 91–99. [CrossRef]
5. Illingworth, R.S.; Gruenewald-Schneider, U.; Webb, S.; Kerr, A.R.W.; James, K.D.; Turner, D.J.; Smith, C.; Harrison, D.J.; Andrews, R.; Bird, A.P. Orphan CpG Islands Identify numerous conserved promoters in the mammalian genome. *PLoS Genet.* **2010**, *6*, e1001134. [CrossRef]
6. Ehrlich, M.; Wang, R.Y.H. 5-Methylcytosine in eukaryotic DNA. *Science* **1981**, *212*, 1350–1357. [CrossRef]
7. Friso, S.; Choi, S.-W.; Girelli, D.; Mason, J.B.; Dolnikowski, G.G.; Bagley, P.J.; Olivieri, O.; Jacques, P.F.; Rosenberg, I.H.; Corrocher, R.; et al. A common mutation in the 5,10-methylenetetrahydrofolate reductase gene affects genomic DNA methylation through an interaction with folate status. *Proc. Natl. Acad. Sci. USA* **2002**, *99*, 5606–5611. [CrossRef]
8. Hermann, A.; Goyal, R.; Jeltsch, A. The Dnmt1 DNA-(cytosine-C5)-methyltransferase methylates DNA processively with high preference for hemimethylated target sites. *J. Biol. Chem.* **2004**, *279*, 48350–48359. [CrossRef]
9. Kaneda, M.; Okano, M.; Hata, K.; Sado, T.; Tsujimoto, N.; Li, E.; Sasaki, H. Essential role for de novo DNA methyltransferase Dnmt3a in paternal and maternal imprinting. *Nature* **2004**, *429*, 900–903. [CrossRef]
10. Okano, M.; Bell, D.W.; Haber, D.A.; Li, E. DNA methyltransferases Dnmt3a and Dnmt3b are essential for de novo methylation and mammalian development. *Cell* **1999**, *99*, 247–257. [CrossRef]
11. Cedar, H.; Bergman, Y. Linking DNA methylation and histone modification: Patterns and paradigms. *Nat. Rev. Genet.* **2009**, *10*, 295–304. [CrossRef] [PubMed]
12. Hackett, J.A.; Sengupta, R.; Zylicz, J.J.; Murakami, K.; Lee, C.; Down, T.A.; Surani, M.A. Germline DNA Demethylation Dynamics and Imprint Erasure Through 5-Hydroxymethylcytosine. *Science* **2013**, *339*, 448–452. [CrossRef] [PubMed]
13. Boyes, J.; Bird, A. DNA methylation inhibits transcription indirectly via a methyl-CpG binding protein. *Cell* **1991**, *64*, 1123–1134. [CrossRef]
14. Hark, A.T.; Schoenherr, C.J.; Katz, D.J.; Ingram, R.S.; Levorse, J.M.; Tilghman, S.M. CTCF mediates methylation-sensitive enhancer-blocking activity at the H19/Igf2 locus. *Nature* **2000**, *405*, 486–489. [CrossRef]
15. Arechederra, M.; Daian, F.; Yim, A.; Bazai, S.K.; Richelme, S.; Dono, R.; Saurin, A.J.; Habermann, B.H.; Maina, F. Hypermethylation of gene body CpG islands predicts high dosage of functional oncogenes in liver cancer. *Nat. Commun.* **2018**, *9*, 3164. [CrossRef]
16. Christopher, M.A.; Kyle, S.M.; Katz, D.J. Neuroepigenetic mechanisms in disease. *Epigenet. Chromatin* **2017**, *10*, 47. [CrossRef]
17. Rottman, F.; Shatkin, A.J.; Perry, R.P. Sequences containing methylated nucleotides at the 5′ termini of messenger RNAs: Possible implications for processing. *Cell* **1974**, *3*, 197–199. [CrossRef]
18. Wang, X.; Zhao, B.S.; Roundtree, I.A.; Lu, Z.; Han, D.; Ma, H.; Weng, X.; Chen, K.; Shi, H.; He, C. N6-methyladenosine Modulates Messenger RNA Translation Efficiency. *Cell* **2015**, *161*, 1388–1399. [CrossRef]
19. Dominissini, D.; Moshitch-Moshkovitz, S.; Schwartz, S.; Salmon-Divon, M.; Ungar, L.; Osenberg, S.; Cesarkas, K.; Jacob-Hirsch, J.; Amariglio, N.; Kupiec, M.; et al. Topology of the human and mouse m6A RNA methylomes revealed by m6A-seq. *Nature* **2012**, *485*, 201–206. [CrossRef]
20. Meyer, K.D.; Patil, D.P.; Zhou, J.; Zinoviev, A.; Skabkin, M.A.; Elemento, O.; Pestova, T.V.; Qian, S.-B.; Jaffrey, S.R. 5′ UTR m6A Promotes Cap-Independent Translation. *Cell* **2015**, *163*, 999–1010. [CrossRef]
21. Bodi, Z.; Bottley, A.; Archer, N.; May, S.T.; Fray, R.G. Yeast m6A Methylated mRNAs Are Enriched on Translating Ribosomes during Meiosis, and under Rapamycin Treatment. *PLoS ONE* **2015**, *10*, e0132090. [CrossRef]
22. Esteller, M. Non-coding RNAs in human disease. *Nat. Rev. Genet.* **2011**, *12*, 861–874. [CrossRef] [PubMed]
23. Wei, J.-W.; Huang, K.; Yang, C.; Kang, C.-S. Non-coding RNAs as regulators in epigenetics. *Oncol. Rep.* **2017**, *37*, 3–9. [CrossRef] [PubMed]
24. Peschansky, V.J.; Wahlestedt, C. Non-coding RNAs as direct and indirect modulators of epigenetic regulation. *Epigenetics* **2014**, *9*, 3–12. [CrossRef]
25. Robles, V.; Valcarce, D.G.; Riesco, M.F. Non-coding RNA regulation in reproduction: Their potential use as biomarkers. *Non-coding RNA Res.* **2019**, *4*, 54–62. [CrossRef]
26. Aleshkina, D.; Iyyappan, R.; Lin, C.J.; Masek, T.; Pospisek, M.; Susor, A. ncRNA BC1 influences translation in the oocyte. *RNA Biol.* **2021**, *18*, 1893–1904. [CrossRef]
27. Kalish, J.M.; Jiang, C.; Bartolomei, M.S. Epigenetics and imprinting in human disease. *Int. J. Dev. Biol.* **2014**, *58*, 291–298. [CrossRef]

28. Bouckenheimer, J.; Assou, S.; Riquier, S.; Hou, C.; Philippe, N.; Sansac, C.; Lavabre-Bertrand, T.; Commes, T.; Lemaître, J.-M.; Boureux, A.; et al. Long non-coding RNAs in human early embryonic development and their potential in ART. *Hum. Reprod. Update* **2016**, *23*, 19–40. [CrossRef]
29. Seisenberger, S.; Andrews, S.; Krueger, F.; Arand, J.; Walter, J.; Santos, F.; Popp, C.; Thienpont, B.; Dean, W.; Reik, W. The dynamics of genome-wide DNA methylation reprogramming in mouse primordial germ cells. *Mol. Cell* **2012**, *48*, 849–862. [CrossRef]
30. Saadeh, H.; Schulz, R. Protection of CpG islands against de novo DNA methylation during oogenesis is associated with the recognition site of E2f1 and E2f2. *Epigenet. Chromatin* **2014**, *7*, 26. [CrossRef]
31. Tomizawa, S.-I.I.; Nowacka-Woszuk, J.; Kelsey, G. DNA methylation establishment during oocyte growth: Mechanisms and significance. *Int. J. Dev. Biol.* **2012**, *56*, 867–875. [CrossRef] [PubMed]
32. Zamudio, N.M.; Chong, S.; O'Bryan, M.K. Epigenetic regulation in male germ cells. *Reproduction* **2008**, *136*, 131–146. [CrossRef]
33. Langenstroth-Röwer, D.; Gromoll, J.; Wistuba, J.; Tröndle, I.; Laurentino, S.; Schlatt, S.; Neuhaus, N. De novo methylation in male germ cells of the common marmoset monkey occurs during postnatal development and is maintained in vitro. *Epigenetics* **2017**, *12*, 527–539. [CrossRef] [PubMed]
34. Smallwood, S.A.; Kelsey, G. De novo DNA methylation: A germ cell perspective. *Trends Genet.* **2012**, *28*, 33–42. [CrossRef] [PubMed]
35. von Meyenn, F.; Berrens, R.V.; Andrews, S.; Santos, F.; Collier, A.J.; Krueger, F.; Osorno, R.; Dean, W.; Rugg-Gunn, P.J.; Reik, W. Comparative Principles of DNA Methylation Reprogramming during Human and Mouse In Vitro Primordial Germ Cell Specification. *Dev. Cell* **2016**, *39*, 104–115. [CrossRef] [PubMed]
36. Stewart, K.R.; Veselovska, L.; Kelsey, G. Establishment and functions of DNA methylation in the germline. *Epigenomics* **2016**, *8*, 1399–1413. [CrossRef]
37. De La Fuente, R.; Eppig, J.J. Transcriptional Activity of the Mouse Oocyte Genome: Companion Granulosa Cells Modulate Transcription and Chromatin Remodeling. *Dev. Biol.* **2001**, *229*, 224–236. [CrossRef]
38. Mira, A. Why is Meiosis Arrested? *J. Theor. Biol.* **1998**, *194*, 275–287. [CrossRef]
39. Kaneda, M.; Hirasawa, R.; Chiba, H.; Okano, M.; Li, E.; Sasaki, H. Genetic evidence for Dnmt3a-dependent imprinting during oocyte growth obtained by conditional knockout with Zp3-Cre and complete exclusion of Dnmt3b by chimera formation. *Genes Cells* **2010**, *15*, 169–179. [CrossRef]
40. Branco, M.R.; King, M.; Perez-Garcia, V.; Bogutz, A.B.; Caley, M.; Fineberg, E.; Lefebvre, L.; Cook, S.J.; Dean, W.; Hemberger, M.; et al. Maternal DNA Methylation Regulates Early Trophoblast Development. *Dev. Cell* **2016**, *36*, 152–163. [CrossRef]
41. He, M.; Zhang, T.; Yang, Y.; Wang, C. Mechanisms of Oocyte Maturation and Related Epigenetic Regulation. *Front. Cell Dev. Biol.* **2021**, *9*, 654028. [CrossRef] [PubMed]
42. Haberland, M.; Montgomery, R.L.; Olson, E.N. The many roles of histone deacetylases in development and physiology: Implications for disease and therapy. *Nat. Rev. Genet.* **2009**, *10*, 32–42. [CrossRef] [PubMed]
43. Kim, J.M.; Liu, H.; Tazaki, M.; Nagata, M.; Aoki, F. Changes in histone acetylation during mouse oocyte meiosis. *J. Cell Biol.* **2003**, *162*, 37–46. [CrossRef] [PubMed]
44. Li, X.; Liu, X.; Gao, M.; Han, L.; Qiu, D.; Wang, H.; Xiong, B.; Sun, S.C.; Liu, H.; Gu, L. HDAC3 promotes meiotic apparatus assembly in mouse oocytes by modulating tubulin acetylation. *Development* **2017**, *144*, 3789–3797. [CrossRef]
45. Gu, L.; Li, X.; Liu, X.; Gao, M.; He, Y.; Xiong, B.; Liu, H. HDAC3 inhibition disrupts the assembly of meiotic apparatus during porcine oocyte maturation. *J. Cell. Physiol.* **2019**, *234*, 10178–10183. [CrossRef]
46. Zhou, D.; Choi, Y.J.; Kim, J.H. Histone deacetylase 6 (HDAC6) is an essential factor for oocyte maturation and asymmetric division in mice. *Sci. Rep.* **2017**, *7*, 8131. [CrossRef]
47. Ling, L.; Hu, F.; Ying, X.; Ge, J.; Wang, Q. HDAC6 inhibition disrupts maturational progression and meiotic apparatus assembly in mouse oocytes. *Cell Cycle* **2018**, *17*, 550–556. [CrossRef]
48. Zhang, T.; He, M.; Zhao, L.; Qin, S.; Zhu, Z.; Du, X.; Zhou, B.; Yang, Y.; Liu, X.; Xia, G.; et al. HDAC6 regulates primordial follicle activation through mTOR signaling pathway. *Cell Death Dis.* **2021**, *12*, 559. [CrossRef]
49. Zhang, K.; Lu, Y.; Jiang, C.; Liu, W.; Shu, J.; Chen, X.; Shi, Y.; Wang, E.; Wang, L.; Hu, Q.; et al. HDAC8 functions in spindle assembly during mouse oocyte meiosis. *Oncotarget* **2017**, *8*, 20092–20102. [CrossRef]
50. Chen, Y.; Pan, C.; Lu, Y.; Miao, Y.; Xiong, B. HDAC8 drives spindle organization during meiotic maturation of porcine oocytes. *Cell Prolif.* **2021**, *54*, e13119. [CrossRef]
51. Zhao, P.; Wang, H.; Wang, H.; Dang, Y.; Luo, L.; Li, S.; Shi, Y.; Wang, L.; Wang, S.; Mager, J.; et al. Essential roles of HDAC1 and 2 in lineage development and genome-wide DNA methylation during mouse preimplantation development. *Epigenetics* **2020**, *15*, 369–385. [CrossRef] [PubMed]
52. Sui, L.; Zhang, S.; Huang, R.; Li, Z. HDAC11 promotes meiotic apparatus assembly during mouse oocyte maturation via decreasing H4K16 and α-tubulin acetylation. *Cell Cycle* **2020**, *19*, 354–362. [CrossRef] [PubMed]
53. Tatone, C.; di Emidio, G.; Barbonetti, A.; Carta, G.; Luciano, A.M.; Falone, S.; Amicarelli, F. Sirtuins in gamete biology and reproductive physiology: Emerging roles and therapeutic potential in female and male infertility. *Hum. Reprod. Update* **2018**, *24*, 267–289. [CrossRef] [PubMed]
54. Zhang, T.; Du, X.; Zhao, L.; He, M.; Lin, L.; Guo, C.; Zhang, X.; Han, J.; Yan, H.; Huang, K.; et al. SIRT1 facilitates primordial follicle recruitment independent of deacetylase activity through directly modulating Akt1 and mTOR transcription. *FASEB J.* **2019**, *33*, 14703–14716. [CrossRef] [PubMed]

55. Iljas, J.D.; Wei, Z.; Homer, H.A. Sirt1 sustains female fertility by slowing age-related decline in oocyte quality required for post-fertilization embryo development. *Aging Cell* **2020**, *19*, e13204. [CrossRef]
56. Xing, X.; Zhang, J.; Wu, T.; Zhang, J.; Wang, Y.; Su, J.; Zhang, Y. SIRT1 reduces epigenetic and non-epigenetic changes to maintain the quality of postovulatory aged oocytes in mice. *Exp. Cell Res.* **2021**, *399*, 112421. [CrossRef]
57. Xu, D.; He, H.; Liu, D.; Geng, G.; Li, Q. A novel role of SIRT2 in regulating gap junction communications via connexin-43 in bovine cumulus-oocyte complexes. *J. Cell. Physiol.* **2020**, *235*, 7332–7343. [CrossRef]
58. Shen, W.-B.; Ni, J.; Yao, R.; Goetzinger, K.R.; Harman, C.; Reece, E.A.; Wang, B.; Yang, P. Maternal obesity increases DNA methylation and decreases RNA methylation in the human placenta. *Reprod. Toxicol.* **2022**, *107*, 90–96. [CrossRef]
59. Gao, M.; Li, X.; He, Y.; Han, L.; Qiu, D.; Ling, L.; Liu, H.; Liu, J.; Gu, L. SIRT7 functions in redox homeostasis and cytoskeletal organization during oocyte maturation. *FASEB J.* **2018**, *32*, 6228–6238. [CrossRef]
60. Zeng, J.; Jiang, M.; Wu, X.; Diao, F.; Qiu, D.; Hou, X.; Wang, H.; Li, L.; Li, C.; Ge, J.; et al. SIRT4 is essential for metabolic control and meiotic structure during mouse oocyte maturation. *Aging Cell* **2018**, *17*, e12789. [CrossRef]
61. Ge, J.; Li, C.; Li, C.; Huang, Z.; Zeng, J.; Han, L.; Wang, Q. SIRT6 participates in the quality control of aged oocytes via modulating telomere function. *Aging* **2019**, *11*, 1965–1976. [CrossRef] [PubMed]
62. Kumar, S.; Lombard, D.B. Mitochondrial Sirtuins and Their Relationships with Metabolic Disease and Cancer. *Antioxid. Redox Signal.* **2015**, *22*, 1060–1077. [CrossRef] [PubMed]
63. Tatone, C.; Di Emidio, G.; Vitti, M.; Di Carlo, M.; Santini, S.; D'Alessandro, A.M.; Falone, S.; Amicarelli, F. Sirtuin Functions in Female Fertility: Possible Role in Oxidative Stress and Aging. *Oxid. Med. Cell. Longev.* **2015**, *2015*, 659687. [CrossRef] [PubMed]
64. Di Emidio, G.; Falone, S.; Vitti, M.; D'Alessandro, A.M.; Vento, M.; Di Pietro, C.; Amicarelli, F.; Tatone, C. SIRT1 signalling protects mouse oocytes against oxidative stress and is deregulated during aging. *Hum. Reprod.* **2014**, *29*, 2006–2017. [CrossRef]
65. Guo, L.; Liu, X.; Chen, H.; Wang, W.; Gu, C.; Li, B. Decrease in ovarian reserve through the inhibition of SIRT1-mediated oxidative phosphorylation. *Aging* **2022**, *14*, 2335–2347. [CrossRef]
66. Kawamura, Y.; Uchijima, Y.; Horike, N.; Tonami, K.; Nishiyama, K.; Amano, T.; Asano, T.; Kurihara, Y.; Kurihara, H. Sirt3 protects in vitro–fertilized mouse preimplantation embryos against oxidative stress–induced p53-mediated developmental arrest. *J. Clin. Investig.* **2010**, *120*, 2817–2828. [CrossRef]
67. Zhao, H.-C.; Ding, T.; Ren, Y.; Li, T.-J.; Li, R.; Fan, Y.; Yan, J.; Zhao, Y.; Li, M.; Yu, Y.; et al. Role of Sirt3 in mitochondrial biogenesis and developmental competence of human in vitro matured oocytes. *Hum. Reprod.* **2016**, *31*, 607–622. [CrossRef]
68. Hatefi, Y. The mitochondrial electron transport and oxidative phosphorylation system. *Annu. Rev. Biochem.* **1985**, *54*, 1015–1069. [CrossRef]
69. McBride, H.M.; Neuspiel, M.; Wasiak, S. Mitochondria: More Than Just a Powerhouse. *Curr. Biol.* **2006**, *16*, R551–R560. [CrossRef]
70. Shutt, T.E.; Shadel, G.S. A compendium of human mitochondrial gene expression machinery with links to disease. *Environ. Mol. Mutagen.* **2010**, *51*, 360–379. [CrossRef]
71. Wallace, D.C. A Mitochondrial Paradigm of Metabolic and Degenerative Diseases, Aging, and Cancer: A Dawn for Evolutionary Medicine. *Annu. Rev. Genet.* **2005**, *39*, 359–407. [CrossRef] [PubMed]
72. Van Blerkom, J. Mitochondrial function in the human oocyte and embryo and their role in developmental competence. *Mitochondrion* **2011**, *11*, 797–813. [CrossRef] [PubMed]
73. Chappel, S. The Role of Mitochondria from Mature Oocyte to Viable Blastocyst. *Obstet. Gynecol. Int.* **2013**, *2013*, 183024. [CrossRef] [PubMed]
74. Reynier, P.; May-Panloup, P.; Chretien, M.-F.; Morgan, C.J.; Jean, M.; Savagner, F.; Barriere, P.; Malthiery, Y. Mitochondrial DNA content affects the fertilizability of human oocytes. *Mol. Hum. Reprod.* **2001**, *7*, 425–429. [CrossRef]
75. Santos, T.A.; El Shourbagy, S.; John, J.C.S. Mitochondrial content reflects oocyte variability and fertilization outcome. *Fertil. Steril.* **2006**, *85*, 584–591. [CrossRef]
76. Al Rawi, S.; Louvet-Vallée, S.; Djeddi, A.; Sachse, M.; Culetto, E.; Hajjar, C.; Boyd, L.; Legouis, R.; Galy, V. Postfertilization Autophagy of Sperm Organelles Prevents Paternal Mitochondrial DNA Transmission. *Science* **2011**, *334*, 1144–1147. [CrossRef]
77. Cummins, J.M.; Wakayama, T.; Yanagimachi, R. Fate of microinjected sperm components in the mouse oocyte and embryo. *Zygote* **1997**, *5*, 301–308. [CrossRef]
78. Perry, J.R.B.; Murray, A.; Day, F.R.; Ong, K.K. Molecular insights into the aetiology of female reproductive ageing. *Nat. Rev. Endocrinol.* **2015**, *11*, 725–734. [CrossRef]
79. Ben-Meir, A.; Burstein, E.; Borrego-Alvarez, A.; Chong, J.; Wong, E.; Yavorska, T.; Naranian, T.; Chi, M.; Wang, Y.; Bentov, Y.; et al. Coenzyme Q10 restores oocyte mitochondrial function and fertility during reproductive aging. *Aging Cell* **2015**, *14*, 887–895. [CrossRef]
80. Harris, S.E.; Adriaens, I.; Leese, H.J.; Gosden, R.G.; Picton, H.M. Carbohydrate metabolism by murine ovarian follicles and oocytes grown in vitro. *Reproduction* **2007**, *134*, 415–424. [CrossRef]
81. Benkhalifa, M.; Ferreira, Y.J.; Chahine, H.; Louanjli, N.; Miron, P.; Merviel, P.; Copin, H. Mitochondria: Participation to infertility as source of energy and cause of senescence. *Int. J. Biochem. Cell Biol.* **2014**, *55*, 60–64. [CrossRef] [PubMed]
82. Wakefield, S.L.; Lane, M.; Mitchell, M. Impaired Mitochondrial Function in the Preimplantation Embryo Perturbs Fetal and Placental Development in the Mouse1. *Biol. Reprod.* **2011**, *84*, 572–580. [CrossRef] [PubMed]
83. Wai, T.; Ao, A.; Zhang, X.; Cyr, D.; Dufort, D.; Shoubridge, E.A. The Role of Mitochondrial DNA Copy Number in Mammalian Fertility1. *Biol. Reprod.* **2010**, *83*, 52–62. [CrossRef]

84. Guillaumet-Adkins, A.; Yañez, Y.; Peris-Diaz, M.D.; Calabria, I.; Palanca-Ballester, C.; Sandoval, J. Epigenetics and Oxidative Stress in Aging. *Oxid. Med. Cell. Longev.* **2017**, *2017*, 9175806. [CrossRef] [PubMed]
85. Zhang, X.; Wu, X.Q.; Lu, S.; Guo, Y.L.; Ma, X. Deficit of mitochondria-derived ATP during oxidative stress impairs mouse MII oocyte spindles. *Cell Res.* **2006**, *16*, 841–850. [CrossRef]
86. Smeets, H.J.M.; Sallevelt, S.C.E.H.; Dreesen, J.C.F.M.; de Die-Smulders, C.E.M.; de Coo, I.F.M. Preventing the transmission of mitochondrial DNA disorders using prenatal or preimplantation genetic diagnosis. *Ann. N. Y. Acad. Sci.* **2015**, *1350*, 29–36. [CrossRef]
87. Wolf, D.P.; Mitalipov, N.; Mitalipov, S. Mitochondrial replacement therapy in reproductive medicine. *Trends Mol. Med.* **2015**, *21*, 68–76. [CrossRef]
88. Babayev, E.; Wang, T.; Szigeti-Buck, K.; Lowther, K.; Taylor, H.S.; Horvath, T.; Seli, E. Reproductive aging is associated with changes in oocyte mitochondrial dynamics, function, and mtDNA quantity. *Maturitas* **2016**, *93*, 121–130. [CrossRef]
89. Spikings, E.C.; Alderson, J.; John, J.C.S. Regulated Mitochondrial DNA Replication During Oocyte Maturation Is Essential for Successful Porcine Embryonic Development. *Biol. Reprod.* **2007**, *76*, 327–335. [CrossRef]
90. Rambags, B.P.B.; van Boxtel, D.C.J.; Tharasanit, T.; Lenstra, J.A.; Colenbrander, B.; Stout, T.A.E. Advancing maternal age predisposes to mitochondrial damage and loss during maturation of equine oocytes in vitro. *Theriogenology* **2014**, *81*, 959–965. [CrossRef]
91. Igarashi, H.; Takahashi, T.; Takahashi, E.; Tezuka, N.; Nakahara, K.; Takahashi, K.; Kurachi, H. Aged Mouse Oocytes Fail to Readjust Intracellular Adenosine Triphosphates at Fertilization1. *Biol. Reprod.* **2005**, *72*, 1256–1261. [CrossRef] [PubMed]
92. Lim, J.; Luderer, U. Oxidative Damage Increases and Antioxidant Gene Expression Decreases with Aging in the Mouse Ovary. *Biol. Reprod.* **2011**, *84*, 775–782. [CrossRef] [PubMed]
93. Cree, L.M.; Hammond, E.R.; Shelling, A.N.; Berg, M.C.; Peek, J.C.; Green, M.P. Maternal age and ovarian stimulation independently affect oocyte mtDNA copy number and cumulus cell gene expression in bovine clones. *Hum. Reprod.* **2015**, *30*, 1410–1420. [CrossRef]
94. Ferreira, A.F.; Soares, M.; Almeida Reis, S.; Ramalho-Santos, J.; Sousa, A.P.; Almeida-Santos, T. Does supplementation with mitochondria improve oocyte competence? A systematic review. *Reproduction* **2021**, *161*, 269–287. [CrossRef]
95. Sobek, A.; Tkadlec, E.; Klaskova, E.; Prochazka, M. Cytoplasmic Transfer Improves Human Egg Fertilization and Embryo Quality: An Evaluation of Sibling Oocytes in Women with Low Oocyte Quality. *Reprod. Sci.* **2021**, *28*, 1362–1369. [CrossRef]
96. Ferguson-Smith, A.C. Genomic imprinting: The emergence of an epigenetic paradigm. *Nat. Rev. Genet.* **2011**, *12*, 565–575. [CrossRef] [PubMed]
97. Santos, F.; Hendrich, B.; Reik, W.; Dean, W. Dynamic Reprogramming of DNA Methylation in the Early Mouse Embryo. *Dev. Biol.* **2002**, *241*, 172–182. [CrossRef]
98. Tucci, V.; Isles, A.R.; Kelsey, G.; Ferguson-Smith, A.C.; Tucci, V.; Bartolomei, M.S.; Benvenisty, N.; Bourc'his, D.; Charalambous, M.; Dulac, C.; et al. Genomic Imprinting and Physiological Processes in Mammals. *Cell* **2019**, *176*, 952–965. [CrossRef]
99. McGrath, J.; Solter, D. Completion of mouse embryogenesis requires both the maternal and paternal genomes. *Cell* **1984**, *37*, 179–183. [CrossRef]
100. Surani, M.A. Imprinting and the Initiation of Gene Silencing in the Germ Line. *Cell* **1998**, *93*, 309–312. [CrossRef]
101. Goovaerts, T.; Steyaert, S.; Vandenbussche, C.A.; Galle, J.; Thas, O.; Van Criekinge, W.; De Meyer, T. A comprehensive overview of genomic imprinting in breast and its deregulation in cancer. *Nat. Commun.* **2018**, *9*, 4120. [CrossRef] [PubMed]
102. Kato, N.; Kamataki, A.; Kurotaki, H. Methylation profile of imprinted genes provides evidence for teratomatous origin of a subset of mucinous ovarian tumours. *J. Pathol.* **2021**, *254*, 567–574. [CrossRef] [PubMed]
103. Paulsen, M.; Ferguson-Smith, A.C. DNA methylation in genomic imprinting, development, and disease. *J. Pathol.* **2001**, *195*, 97–110. [CrossRef] [PubMed]
104. Elhamamsy, A.R. Role of DNA methylation in imprinting disorders: An updated review. *J. Assist. Reprod. Genet.* **2017**, *34*, 549–562. [CrossRef] [PubMed]
105. Kobayashi, H.; Sakurai, T.; Imai, M.; Takahashi, N.; Fukuda, A.; Yayoi, O.; Sato, S.; Nakabayashi, K.; Hata, K.; Sotomaru, Y.; et al. Contribution of Intragenic DNA Methylation in Mouse Gametic DNA Methylomes to Establish Oocyte-Specific Heritable Marks. *PLoS Genet.* **2012**, *8*, e1002440. [CrossRef] [PubMed]
106. Paczkowski, M.; Schoolcraft, W.B.; Krisher, R.L. Dysregulation of methylation and expression of imprinted genes in oocytes and reproductive tissues in mice of advanced maternal age. *J. Assist. Reprod. Genet.* **2015**, *32*, 713–723. [CrossRef]
107. Duranthon, V.; Watson, A.J.; Lonergan, P. Preimplantation embryo programming: Transcription, epigenetics, and culture environment. *Reproduction* **2008**, *135*, 141–150. [CrossRef]
108. Guo, H.; Zhu, P.; Yan, L.; Li, R.; Hu, B.; Lian, Y.; Yan, J.; Ren, X.; Lin, S.; Li, J.; et al. The DNA methylation landscape of human early embryos. *Nature* **2014**, *511*, 606–610. [CrossRef]
109. Smith, Z.D.; Chan, M.M.; Mikkelsen, T.S.; Gu, H.; Gnirke, A.; Regev, A.; Meissner, A. A unique regulatory phase of DNA methylation in the early mammalian embryo. *Nature* **2012**, *484*, 339–344. [CrossRef]
110. Duan, J.E.; Jiang, Z.C.; Alqahtani, F.; Mandoiu, I.; Dong, H.; Zheng, X.; Marjani, S.L.; Chen, J.; Tian, X.C. Methylome Dynamics of Bovine Gametes and in vivo Early Embryos. *Front. Genet.* **2019**, *10*, 512. [CrossRef]
111. Deng, M.; Zhang, G.; Cai, Y.; Liu, Z.; Zhang, Y.; Meng, F.; Wang, F.; Wan, Y. DNA methylation dynamics during zygotic genome activation in goat. *Theriogenology* **2020**, *156*, 144–154. [CrossRef] [PubMed]

112. Hanna, C.W.; Demond, H.; Kelsey, G. Epigenetic regulation in development: Is the mouse a good model for the human? *Hum. Reprod. Update* **2018**, *24*, 556–576. [CrossRef] [PubMed]
113. Amouroux, R.; Nashun, B.; Shirane, K.; Nakagawa, S.; Hill, P.W.S.; D'Souza, Z.; Nakayama, M.; Matsuda, M.; Turp, A.; Ndjetehe, E.; et al. De novo DNA methylation drives 5hmC accumulation in mouse zygotes. *Nat. Cell Biol.* **2016**, *18*, 225–233. [CrossRef] [PubMed]
114. Haaf, T. The battle of the sexes after fertilization: Behaviour of paternal and maternal chromosomes in the early mammalian embryo. *Chromosome Res.* **2001**, *9*, 263–271. [CrossRef]
115. Messerschmidt, D.M.; Knowles, B.B.; Solter, D. DNA methylation dynamics during epigenetic reprogramming in the germline and preimplantation embryos. *Genes Dev.* **2014**, *28*, 812–828. [CrossRef]
116. Yu, B.; Jayavelu, N.D.; Battle, S.L.; Mar, J.C.; Schimmel, T.; Cohen, J.; Hawkins, R.D. Single-cell analysis of transcriptome and DNA methylome in human oocyte maturation. *PLoS ONE* **2020**, *15*, e0241698. [CrossRef]
117. Zeng, Y.; Ren, R.; Kaur, G.; Hardikar, S.; Ying, Z.; Babcock, L.; Gupta, E.; Zhang, X.; Chen, T.; Cheng, X. The inactive Dnmt3b3 isoform preferentially enhances Dnmt3b-mediated DNA methylation. *Genes Dev.* **2020**, *34*, 1546–1558. [CrossRef]
118. Sabag, O.; Zamir, A.; Keshet, I.; Hecht, M.; Ludwig, G.; Tabib, A.; Moss, J.; Cedar, H. Establishment of methylation patterns in ES cells. *Nat. Struct. Mol. Biol.* **2014**, *21*, 110–112. [CrossRef]
119. Li, E.; Bestor, T.H.; Jaenisch, R. Targeted mutation of the DNA methyltransferase gene results in embryonic lethality. *Cell* **1992**, *69*, 915–926. [CrossRef]
120. Ginsburg, M.; Snow, M.H.L.; McLaren, A. Primordial germ cells in the mouse embryo during gastrulation. *Development* **1990**, *110*, 521–528. [CrossRef]
121. Pepling, M.E.; Spradling, A.C. Mouse Ovarian Germ Cell Cysts Undergo Programmed Breakdown to Form Primordial Follicles. *Dev. Biol.* **2001**, *234*, 339–351. [CrossRef] [PubMed]
122. Pepling, M.E.; Spradling, A.C. Female mouse germ cells form synchronously dividing cysts. *Development* **1998**, *125*, 3323–3328. [CrossRef] [PubMed]
123. Skinner, M.K. Regulation of primordial follicle assembly and development. *Hum. Reprod. Update* **2005**, *11*, 461–471. [CrossRef] [PubMed]
124. HSUEH, A.J.W.; BILLIG, H.; TSAFRIRI, A. Ovarian Follicle Atresia: A Hormonally Controlled Apoptotic Process*. *Endocr. Rev.* **1994**, *15*, 707–724. [CrossRef]
125. Wang, Z.; Liu, C.Y.; Zhao, Y.; Dean, J. FIGLA, LHX8 and SOHLH1 transcription factor networks regulate mouse oocyte growth and differentiation. *Nucleic Acids Res.* **2020**, *48*, 3525–3541. [CrossRef]
126. Driancourt, M.A.; Reynaud, K.; Cortvrindt, R.; Smitz, J. Roles of KIT and KIT LIGAND in ovarian function. *Rev. Reprod.* **2000**, *5*, 143–152. [CrossRef]
127. Jin, X.; Han, C.S.; Yu, F.Q.; Wei, P.; Hu, Z.Y.; Liu, Y.X. Anti-apoptotic action of stem cell factor on oocytes in primordial follicles and its signal transduction. *Mol. Reprod. Dev.* **2005**, *70*, 82–90. [CrossRef]
128. Eppig, J.J. Oocyte control of ovarian follicular development and function in mammals. *Reproduction* **2001**, *122*, 829–838. [CrossRef]
129. Gilchrist, R.B.; Ritter, L.J.; Myllymaa, S.; Kaivo-Oja, N.; Dragovic, R.A.; Hickey, T.E.; Ritvos, O.; Mottershead, D.G. Molecular basis of oocyte-paracrine signalling that promotes granulosa cell proliferation. *J. Cell Sci.* **2006**, *119*, 3811–3821. [CrossRef]
130. Macaulay, A.D.; Gilbert, I.; Caballero, J.; Barreto, R.; Fournier, E.; Tossou, P.; Sirard, M.A.; Clarke, H.J.; Khandjian, É.W.; Richard, F.J.; et al. The gametic synapse: RNA transfer to the bovine oocyte. *Biol. Reprod.* **2014**, *91*, 1–12. [CrossRef]
131. Macaulay, A.D.; Gilbert, I.; Scantland, S.; Fournier, E.; Ashkar, F.; Bastien, A.; Shojaei Saadi, H.A.; Gagné, D.; Sirard, M.A.; Khandjian, É.W.; et al. Cumulus cell transcripts transit to the bovine oocyte in preparation for maturation. *Biol. Reprod.* **2016**, *94*, 16–17. [CrossRef] [PubMed]
132. Sternlicht, A.L.; Schultz, R.M. Biochemical studies of mammalian oogenesis: Kinetics of accumulation of total and poly(A)-containing RNA during growth of the mouse oocyte. *J. Exp. Zool.* **1981**, *215*, 191–200. [CrossRef] [PubMed]
133. Sánchez, F.; Smitz, J. Molecular control of oogenesis. *Biochim. Biophys. Acta Mol. Basis Dis.* **2012**, *1822*, 1896–1912. [CrossRef] [PubMed]
134. Fernández-Gonzalez, R.; Moreira, P.N.; Pérez-Crespo, M.; Sánchez-Martín, M.; Ramirez, M.A.; Pericuesta, E.; Bilbao, A.; Bermejo-Alvarez, P.; Hourcade, J.D.; Fonseca, F.R.; et al. Long-Term Effects of Mouse Intracytoplasmic Sperm Injection with DNA-Fragmented Sperm on Health and Behavior of Adult Offspring1. *Biol. Reprod.* **2008**, *78*, 761–772. [CrossRef]
135. Jia, J.-J.; Lahr, R.M.; Solgaard, M.T.; Moraes, B.J.; Pointet, R.; Yang, A.-D.; Celucci, G.; Graber, T.E.; Hoang, H.-D.; Niklaus, M.R.; et al. mTORC1 promotes TOP mRNA translation through site-specific phosphorylation of LARP1. *Nucleic Acids Res.* **2021**, *49*, 3461–3489. [CrossRef] [PubMed]
136. Clegg, K.B.; Pikó, L. Quantitative aspects of RNA synthesis and polyadenylation in 1-cell and 2-cell mouse embryos. *J. Embryol. Exp. Morphol.* **1983**, *74*, 169–182. [CrossRef]
137. Martins, J.P.S.; Liu, X.; Oke, A.; Arora, R.; Franciosi, F.; Viville, S.; Laird, D.J.; Fung, J.C.; Conti, M. DAZL and CPEB1 regulate mRNA translation synergistically during oocyte maturation. *J. Cell Sci.* **2016**, *129*, 1271–1282. [CrossRef]
138. Jansova, D.; Koncicka, M.; Tetkova, A.; Cerna, R.; Malik, R.; del Llano, E.; Kubelka, M.; Susor, A. Regulation of 4E-BP1 activity in the mammalian oocyte. *Cell Cycle* **2017**, *16*, 927–939. [CrossRef]
139. Kim, J.; Guan, K.-L.L. mTOR as a central hub of nutrient signalling and cell growth. *Nat. Cell Biol.* **2019**, *21*, 63–71. [CrossRef]

140. Kalous, J.; Jansová, D.; Šušor, A. Role of Cyclin-Dependent Kinase 1 in Translational Regulation in the M-Phase. *Cells* **2020**, *9*, 1568. [CrossRef]
141. Guo, J.; Zhang, T.; Guo, Y.; Sun, T.; Li, H.; Zhang, X.; Yin, H.; Cao, G.; Yin, Y.; Wang, H.; et al. Oocyte stage-specific effects of MTOR determine granulosa cell fate and oocyte quality in mice. *Proc. Natl. Acad. Sci. USA* **2018**, *115*, E5326–E5333. [CrossRef] [PubMed]
142. Schisa, J.A. Germ Cell Responses to Stress: The Role of RNP Granules. *Front. Cell Dev. Biol.* **2019**, *7*, 220. [CrossRef] [PubMed]
143. Standart, N.; Weil, D. P-Bodies: Cytosolic Droplets for Coordinated mRNA Storage. *Trends Genet.* **2018**, *34*, 612–626. [CrossRef] [PubMed]
144. Blatt, P.; Wong-Deyrup, S.W.; McCarthy, A.; Breznak, S.; Hurton, M.D.; Upadhyay, M.; Bennink, B.; Camacho, J.; Lee, M.T.; Rangan, P. RNA degradation is required for the germ-cell to maternal transition in Drosophila. *Curr. Biol.* **2021**, *31*, 2984–2994. [CrossRef]
145. Qi, S.T.; Ma, J.Y.; Wang, Z.B.; Guo, L.; Hou, Y.; Sun, Q.Y. N6-Methyladenosine Sequencing Highlights the Involvement of mRNA Methylation in Oocyte Meiotic Maturation and Embryo Development by Regulating Translation in Xenopus laevis. *J. Biol. Chem.* **2016**, *291*, 23020–23026. [CrossRef]
146. Sui, X.; Hu, Y.; Ren, C.; Cao, Q.; Zhou, S.; Cao, Y.; Li, M.; Shu, W.; Huo, R. METTL3-mediated m6A is required for murine oocyte maturation and maternal-to-zygotic transition. *Cell Cycle* **2020**, *19*, 391–404. [CrossRef]
147. Zhang, M.; Zhang, S.; Zhai, Y.; Han, Y.; Huang, R.; An, X.; Dai, X.; Li, Z. Cycloleucine negatively regulates porcine oocyte maturation and embryo development by modulating N6-methyladenosine and histone modifications. *Theriogenology* **2022**, *179*, 128–140. [CrossRef]
148. Kwon, J.; Jo, Y.J.; Namgoong, S.; Kim, N.H. Functional roles of hnRNPA2/B1 regulated by METTL3 in mammalian embryonic development. *Sci. Rep.* **2019**, *9*, 8640. [CrossRef]
149. Meng, T.G.; Lu, X.; Guo, L.; Hou, G.M.; Ma, X.S.; Li, Q.N.; Huang, L.; Fan, L.H.; Zhao, Z.H.; Ou, X.H.; et al. Mettl14 is required for mouse postimplantation development by facilitating epiblast maturation. *FASEB J.* **2019**, *33*, 1179–1187. [CrossRef]
150. Shi, H.; Zhang, X.; Weng, Y.-L.; Lu, Z.; Liu, Y.; Lu, Z.; Li, J.; Hao, P.; Zhang, Y.; Zhang, F.; et al. m6A facilitates hippocampus-dependent learning and memory through YTHDF1. *Nature* **2018**, *563*, 249–253. [CrossRef]
151. Yang, Y.; Hsu, P.J.; Chen, Y.-S.; Yang, Y.-G. Dynamic transcriptomic m6A decoration: Writers, erasers, readers and functions in RNA metabolism. *Cell Res.* **2018**, *28*, 616–624. [CrossRef]
152. Ping, X.-L.; Sun, B.-F.; Wang, L.; Xiao, W.; Yang, X.; Wang, W.-J.; Adhikari, S.; Shi, Y.; Lv, Y.; Chen, Y.-S.; et al. Mammalian WTAP is a regulatory subunit of the RNA N6-methyladenosine methyltransferase. *Cell Res.* **2014**, *24*, 177–189. [CrossRef] [PubMed]
153. Mu, H.; Zhang, T.; Yang, Y.; Zhang, D.; Gao, J.; Li, J.; Yue, L.; Gao, D.; Shi, B.; Han, Y.; et al. METTL3-mediated mRNA N6-methyladenosine is required for oocyte and follicle development in mice. *Cell Death Dis.* **2021**, *12*, 989. [CrossRef] [PubMed]
154. Raj, N.; Wang, M.; Seoane, J.A.; Zhao, R.L.; Kaiser, A.M.; Moonie, N.A.; Demeter, J.; Boutelle, A.M.; Kerr, C.H.; Mulligan, A.S.; et al. The Mettl3 epitranscriptomic writer amplifies p53 stress responses. *Mol. Cell* **2022**, *in press*. [CrossRef] [PubMed]
155. Dong, S.; Wu, Y.; Liu, Y.; Weng, H.; Huang, H. N 6 -methyladenosine Steers RNA Metabolism and Regulation in Cancer. *Cancer Commun.* **2021**, *41*, 538–559. [CrossRef]
156. Parial, R.; Li, H.; Li, J.; Archacki, S.; Yang, Z.; Wang, I.Z.; Chen, Q.; Xu, C.; Wang, Q.K. Role of epigenetic m 6 A RNA methylation in vascular development: Mettl3 regulates vascular development through PHLPP2/mTOR-AKT. signaling. *FASEB J.* **2021**, *35*, e21465. [CrossRef]
157. Fan, L.H.; Wang, Z.B.; Li, Q.N.; Meng, T.G.; Dong, M.Z.; Hou, Y.; Ouyang, Y.C.; Schatten, H.; Sun, Q.Y. Absence of mitochondrial DNA methylation in mouse oocyte maturation, aging and early embryo development. *Biochem. Biophys. Res. Commun.* **2019**, *513*, 912–918. [CrossRef]
158. Zaccara, S.; Jaffrey, S.R. A Unified Model for the Function of YTHDF Proteins in Regulating m6A-Modified mRNA. *Cell* **2020**, *181*, 1582–1595. [CrossRef]
159. Dong, G.; Yu, J.; Shan, G.; Su, L.; Yu, N.; Yang, S. N6-Methyladenosine Methyltransferase METTL3 Promotes Angiogenesis and Atherosclerosis by Upregulating the JAK2/STAT3 Pathway via m6A Reader IGF2BP1. *Front. Cell Dev. Biol.* **2021**, *9*, 731810. [CrossRef]
160. Shi, H.; Wang, X.; Lu, Z.; Zhao, B.S.; Ma, H.; Hsu, P.J.; Liu, C.; He, C. YTHDF3 facilitates translation and decay of N6-methyladenosine-modified RNA. *Cell Res.* **2017**, *27*, 315–328. [CrossRef]
161. Ivanova, I.; Much, C.; Di Giacomo, M.; Azzi, C.; Morgan, M.; Moreira, P.N.; Monahan, J.; Carrieri, C.; Enright, A.J.; O'Carroll, D. The RNA m 6 A Reader YTHDF2 Is Essential for the Post-transcriptional Regulation of the Maternal Transcriptome and Oocyte Competence. *Mol. Cell* **2017**, *67*, 1059–1067. [CrossRef] [PubMed]
162. Guo, Y.; Sun, J.; Bu, S.; Li, B.; Zhang, Q.; Wang, Q.; Lai, D. Melatonin protects against chronic stress-induced oxidative meiotic defects in mice MII oocytes by regulating SIRT1. *Cell Cycle* **2020**, *19*, 1677–1695. [CrossRef]
163. Rosario, F.J.; Powell, T.L.; Jansson, T. Activation of placental insulin and mTOR signaling in a mouse model of maternal obesity associated with fetal overgrowth. *Am. J. Physiol. Integr. Comp. Physiol.* **2016**, *310*, R87–R93. [CrossRef] [PubMed]
164. Shi, H.; Wei, J.; He, C. Where, When, and How: Context-Dependent Functions of RNA Methylation Writers, Readers, and Erasers. *Mol. Cell* **2019**, *74*, 640–650. [CrossRef] [PubMed]

165. Ding, L.; Yan, G.; Wang, B.; Xu, L.; Gu, Y.; Ru, T.; Cui, X.; Lei, L.; Liu, J.; Sheng, X.; et al. Transplantation of UC-MSCs on collagen scaffold activates follicles in dormant ovaries of POF patients with long history of infertility. *Sci. China Life Sci.* **2018**, *61*, 1554–1565. [CrossRef] [PubMed]
166. He, J.; Li, X.; Lü, M.; Wang, J.; Tang, J.; Luo, S.; Qian, Y. ALKBH5 suppresses migration and invasion of human trophoblast cells by inhibiting epithelial-mesenchymal transition. *Nan Fang Yi Ke Da Xue Xue Bao* **2020**, *40*, 1720–1725. [CrossRef] [PubMed]
167. Marshall, K.L.; Rivera, R.M. The effects of superovulation and reproductive aging on the epigenome of the oocyte and embryo. *Mol. Reprod. Dev.* **2018**, *85*, 90–105. [CrossRef]
168. Xu, Y.-W.; Peng, Y.-T.; Wang, B.; Zeng, Y.-H.; Zhuang, G.-L.; Zhou, C.-Q. High follicle-stimulating hormone increases aneuploidy in human oocytes matured in vitro. *Fertil. Steril.* **2011**, *95*, 99–104. [CrossRef]
169. Uysal, F.; Ozturk, S.; Akkoyunlu, G. Superovulation alters DNA methyltransferase protein expression in mouse oocytes and early embryos. *J. Assist. Reprod. Genet.* **2018**, *35*, 503–513. [CrossRef]
170. Ozturk, S.; Yaba-Ucar, A.; Sozen, B.; Mutlu, D.; Demir, N. Superovulation alters embryonic poly(A)-binding protein (Epab) and poly(A)-binding protein, cytoplasmic 1 (Pabpc1) gene expression in mouse oocytes and early embryos. *Reprod. Fertil. Dev.* **2016**, *28*, 375. [CrossRef]
171. Market-Velker, B.A.; Zhang, L.; Magri, L.S.; Bonvissuto, A.C.; Mann, M.R.W. Dual effects of superovulation: Loss of maternal and paternal imprinted methylation in a dose-dependent manner. *Hum. Mol. Genet.* **2010**, *19*, 36–51. [CrossRef] [PubMed]
172. Huo, Y.; Yan, Z.Q.; Yuan, P.; Qin, M.; Kuo, Y.; Li, R.; Yan, L.Y.; Feng, H.L.; Qiao, J. Single-cell DNA methylation sequencing reveals epigenetic alterations in mouse oocytes superovulated with different dosages of gonadotropins. *Clin. Epigenet.* **2020**, *12*, 75. [CrossRef] [PubMed]
173. Fauque, P.; Jouannet, P.; Lesaffre, C.; Ripoche, M.-A.; Dandolo, L.; Vaiman, D.; Jammes, H. Assisted Reproductive Technology affects developmental kinetics, H19 Imprinting Control Region methylation and H19 gene expression in individual mouse embryos. *BMC Dev. Biol.* **2007**, *7*, 116. [CrossRef]
174. Wang, L.-Y.; Wang, N.; Le, F.; Li, L.; Lou, H.-Y.; Liu, X.-Z.; Zheng, Y.-M.; Qian, Y.-Q.; Chen, Y.-L.; Jiang, X.-H.; et al. Superovulation Induced Changes of Lipid Metabolism in Ovaries and Embryos and Its Probable Mechanism. *PLoS ONE* **2015**, *10*, e0132638. [CrossRef] [PubMed]
175. Xie, J.-K.; Wang, Q.; Zhang, T.-T.; Yin, S.; Zhang, C.-L.; Ge, Z.-J. Repeated superovulation may affect mitochondrial functions of cumulus cells in mice. *Sci. Rep.* **2016**, *6*, 31368. [CrossRef] [PubMed]
176. Kalthur, G.; Salian, S.R.; Nair, R.; Mathew, J.; Adiga, S.K.; Kalthur, S.G.; Zeegers, D.; Hande, M.P. Distribution pattern of cytoplasmic organelles, spindle integrity, oxidative stress, octamer-binding transcription factor 4 (Oct4) expression and developmental potential of oocytes following multiple superovulation. *Reprod. Fertil. Dev.* **2016**, *28*, 2027. [CrossRef]
177. Lee, M.; Ahn, J.I.; Lee, A.R.; Ko, D.W.; Yang, W.S.; Lee, G.; Ahn, J.Y.; Lim, J.M. Adverse Effect of Superovulation Treatment on Maturation, Function and Ultrastructural Integrity of Murine Oocytes. *Mol. Cells* **2017**, *40*, 558–566. [CrossRef]
178. Bui, A.D.; Sharma, R.; Henkel, R.; Agarwal, A. Reactive oxygen species impact on sperm DNA and its role in male infertility. *Andrologia* **2018**, *50*, e13012. [CrossRef]
179. Bomfim, M.M.; Andrade, G.M.; del Collado, M.; Sangalli, J.R.; Fontes, P.K.; Nogueira, M.F.G.; Meirelles, F.V.; da Silveira, J.C.; Perecin, F. Antioxidant responses and deregulation of epigenetic writers and erasers link oxidative stress and DNA methylation in bovine blastocysts. *Mol. Reprod. Dev.* **2017**, *84*, 1296–1305. [CrossRef]
180. Li, W.; Goossens, K.; Van Poucke, M.; Forier, K.; Braeckmans, K.; Van Soom, A.; Peelman, L.J. High oxygen tension increases global methylation in bovine 4-cell embryos and blastocysts but does not affect general retrotransposon expression. *Reprod. Fertil. Dev.* **2016**, *28*, 948. [CrossRef]
181. Marei, W.F.A.; Van den Bosch, L.; Pintelon, I.; Mohey-Elsaeed, O.; Bols, P.E.J.; Leroy, J.L.M.R. Mitochondria-targeted therapy rescues development and quality of embryos derived from oocytes matured under oxidative stress conditions: A bovine in vitro model. *Hum. Reprod.* **2019**, *34*, 1984–1998. [CrossRef]
182. van den Berg, M.M.J.; van Maarle, M.C.; van Wely, M.; Goddijn, M. Genetics of early miscarriage. *Biochim. Biophys. Acta. Mol. Basis Dis.* **2012**, *1822*, 1951–1959. [CrossRef]
183. Xu, D.; Wu, L.; Jiang, X.; Yang, L.; Cheng, J.; Chen, H.; Hua, R.; Geng, G.; Yang, L.; Li, Q. SIRT2 Inhibition Results in Meiotic Arrest, Mitochondrial Dysfunction, and Disturbance of Redox Homeostasis during Bovine Oocyte Maturation. *Int. J. Mol. Sci.* **2019**, *20*, 1365. [CrossRef]
184. Reis e Silva, A.R.; Bruno, C.; Fleurot, R.; Daniel, N.; Archilla, C.; Peynot, N.; Lucci, C.M.; Beaujean, N.; Duranthon, V. Alteration of DNA demethylation dynamics by in vitro culture conditions in rabbit pre-implantation embryos. *Epigenetics* **2012**, *7*, 440–446. [CrossRef]
185. Estill, M.S.; Bolnick, J.M.; Waterland, R.A.; Bolnick, A.D.; Diamond, M.P.; Krawetz, S.A. Assisted reproductive technology alters deoxyribonucleic acid methylation profiles in bloodspots of newborn infants. *Fertil. Steril.* **2016**, *106*, 629–639. [CrossRef]
186. Bauersachs, S.; Mermillod, P.; Almiñana, C. The Oviductal Extracellular Vesicles' RNA Cargo Regulates the Bovine Embryonic Transcriptome. *Int. J. Mol. Sci.* **2020**, *21*, 1303. [CrossRef]
187. Ghosh, J.; Coutifaris, C.; Sapienza, C.; Mainigi, M. Global DNA methylation levels are altered by modifiable clinical manipulations in assisted reproductive technologies. *Clin. Epigenet.* **2017**, *9*, 14. [CrossRef]
188. El Hajj, N.; Haaf, T. Epigenetic disturbances in in vitro cultured gametes and embryos: Implications for human assisted reproduction. *Fertil. Steril.* **2013**, *99*, 632–641. [CrossRef]

189. de Waal, E.; Vrooman, L.A.; Fischer, E.; Ord, T.; Mainigi, M.A.; Coutifaris, C.; Schultz, R.M.; Bartolomei, M.S. The cumulative effect of assisted reproduction procedures on placental development and epigenetic perturbations in a mouse model. *Hum. Mol. Genet.* **2015**, *24*, 6975–6985. [CrossRef]
190. Pliushch, G.; Schneider, E.; Schneider, T.; El Hajj, N.; Rösner, S.; Strowitzki, T.; Haaf, T. In vitro maturation of oocytes is not associated with altered deoxyribonucleic acid methylation patterns in children from in vitro fertilization or intracytoplasmic sperm injection. *Fertil. Steril.* **2015**, *103*, 720–727. [CrossRef]
191. Horánszky, A.; Becker, J.L.; Zana, M.; Ferguson-Smith, A.C.; Dinnyés, A. Epigenetic Mechanisms of ART-Related Imprinting Disorders: Lessons From iPSC and Mouse Models. *Genes* **2021**, *12*, 1704. [CrossRef] [PubMed]
192. Jiang, Z.; Wang, Y.; Lin, J.; Xu, J.; Ding, G.; Huang, H. Genetic and epigenetic risks of assisted reproduction. *Best Pract. Res. Clin. Obstet. Gynaecol.* **2017**, *44*, 90–104. [CrossRef] [PubMed]
193. La Bastide-Van Gemert, S.; Seggers, J.; Haadsma, M.L.; Heineman, M.J.; Middelburg, K.J.; Roseboom, T.J.; Schendelaar, P.; Hadders-Algra, M.; Van den Heuvel, E.R. Is ovarian hyperstimulation associated with higher blood pressure in 4-year-old IVF offspring? Part II: An explorative causal inference approach. *Hum. Reprod.* **2014**, *29*, 510–517. [CrossRef] [PubMed]
194. Ceelen, M.; van Weissenbruch, M.M.; Vermeiden, J.P.W.; van Leeuwen, F.E.; Delemarre-van de Waal, H.A. Growth and development of children born after in vitro fertilization. *Fertil. Steril.* **2008**, *90*, 1662–1673. [CrossRef] [PubMed]
195. Håberg, S.E.; Page, C.M.; Lee, Y.; Nustad, H.E.; Magnus, M.C.; Haftorn, K.L.; Carlsen, E.Ø.; Denault, W.R.P.; Bohlin, J.; Jugessur, A.; et al. DNA methylation in newborns conceived by assisted reproductive technology. *Nat. Commun.* **2022**, *13*, 1896. [CrossRef] [PubMed]
196. Chen, Z.; Hagen, D.E.; Elsik, C.G.; Ji, T.; Morris, C.J.; Moon, L.E.; Rivera, R.M. Characterization of global loss of imprinting in fetal overgrowth syndrome induced by assisted reproduction. *Proc. Natl. Acad. Sci. USA* **2015**, *112*, 4618–4623. [CrossRef]
197. Tetkova, A.; Susor, A.; Kubelka, M.; Nemcova, L.; Jansova, D.; Dvoran, M.; Del Llano, E.; Holubcova, Z.; Kalous, J. Follicle-stimulating hormone administration affects amino acid metabolism in mammalian oocytes. *Biol. Reprod.* **2019**, *101*, 719–732. [CrossRef]
198. Saenz-De-Juano, M.D.; Ivanova, E.; Romero, S.; Lolicato, F.; Sánchez, F.; Van Ranst, H.; Krueger, F.; Segonds-Pichon, A.; De Vos, M.; Andrews, S.; et al. DNA methylation and mRNA expression of imprinted genes in blastocysts derived from an improved in vitro maturation method for oocytes from small antral follicles in polycystic ovary syndrome patients. *Hum. Reprod.* **2019**, *34*, 1640–1649. [CrossRef]
199. Fortier, A.L.; Lopes, F.L.; Darricarrère, N.; Martel, J.; Trasler, J.M. Superovulation alters the expression of imprinted genes in the midgestation mouse placenta. *Hum. Mol. Genet.* **2008**, *17*, 1653–1665. [CrossRef]
200. Vuong, L.N.; Le, A.H.; Ho, V.N.A.; Pham, T.D.; Sanchez, F.; Romero, S.; De Vos, M.; Ho, T.M.; Gilchrist, R.B.; Smitz, J. Live births after oocyte in vitro maturation with a prematuration step in women with polycystic ovary syndrome. *J. Assist. Reprod. Genet.* **2020**, *37*, 347–357. [CrossRef]
201. Huang, J.; Li, T.; Ding, C.-H.; Brosens, J.; Zhou, C.-Q.; Wang, H.-H.; Xu, Y.-W. Insufficient histone-3 lysine-9 deacetylation in human oocytes matured in vitro is associated with aberrant meiosis. *Fertil. Steril.* **2012**, *97*, 178–184. [CrossRef] [PubMed]
202. Yao, L.-N.; Zhang, T.-F.; Lin, W.-Q.; Jiang, N.; Cao, H.-F.; Li, H.; Qian, J.-H. Value of serum and follicular fluid sirtuin (SIRT)1 and SIRT2 protein levels in predicting the outcome of assisted reproduction. *Ann. Transl. Med.* **2021**, *9*, 343. [CrossRef] [PubMed]
203. Escobar-Morreale, H.F. Polycystic ovary syndrome: Definition, aetiology, diagnosis and treatment. *Nat. Rev. Endocrinol.* **2018**, *14*, 270–284. [CrossRef] [PubMed]
204. Stener-Victorin, E.; Deng, Q. Epigenetic inheritance of polycystic ovary syndrome—challenges and opportunities for treatment. *Nat. Rev. Endocrinol.* **2021**, *17*, 521–533. [CrossRef] [PubMed]
205. Bruni, V.; Capozzi, A.; Lello, S. The Role of Genetics, Epigenetics and Lifestyle in Polycystic Ovary Syndrome Development: The State of the Art. *Reprod. Sci.* **2022**, *29*, 668–679. [CrossRef]
206. Mimouni, N.E.H.; Paiva, I.; Barbotin, A.-L.; Timzoura, F.E.; Plassard, D.; Le Gras, S.; Ternier, G.; Pigny, P.; Catteau-Jonard, S.; Simon, V.; et al. Polycystic ovary syndrome is transmitted via a transgenerational epigenetic process. *Cell Metab.* **2021**, *33*, 513–530. [CrossRef]
207. Schatten, H.; Sun, Q.-Y.; Prather, R. The impact of mitochondrial function/dysfunction on IVF and new treatment possibilities for infertility. *Reprod. Biol. Endocrinol.* **2014**, *12*, 111. [CrossRef]
208. Wang, Q.; Moley, K.H. Maternal diabetes and oocyte quality. *Mitochondrion* **2010**, *10*, 403–410. [CrossRef]
209. May-Panloup, P.; Boucret, L.; Chao de la Barca, J.-M.; Desquiret-Dumas, V.; Ferré-L'Hotellier, V.; Morinière, C.; Descamps, P.; Procaccio, V.; Reynier, P. Ovarian ageing: The role of mitochondria in oocytes and follicles. *Hum. Reprod. Update* **2016**, *22*, 725–743. [CrossRef]
210. Craven, L.; Tang, M.-X.; Gorman, G.S.; De Sutter, P.; Heindryckx, B. Novel reproductive technologies to prevent mitochondrial disease. *Hum. Reprod. Update* **2017**, *23*, 501–519. [CrossRef]
211. Tachibana, M.; Amato, P.; Sparman, M.; Woodward, J.; Sanchis, D.M.; Ma, H.; Gutierrez, N.M.; Tippner-Hedges, R.; Kang, E.; Lee, H.-S.; et al. Towards germline gene therapy of inherited mitochondrial diseases. *Nature* **2013**, *493*, 627–631. [CrossRef] [PubMed]
212. Kang, E.; Wu, J.; Gutierrez, N.M.; Koski, A.; Tippner-Hedges, R.; Agaronyan, K.; Platero-Luengo, A.; Martinez-Redondo, P.; Ma, H.; Lee, Y.; et al. Mitochondrial replacement in human oocytes carrying pathogenic mitochondrial DNA mutations. *Nature* **2016**, *540*, 270–275. [CrossRef]

213. Zhang, J.; Liu, H.; Luo, S.; Lu, Z.; Chávez-Badiola, A.; Liu, Z.; Yang, M.; Merhi, Z.; Silber, S.J.; Munné, S.; et al. Live birth derived from oocyte spindle transfer to prevent mitochondrial disease. *Reprod. Biomed. Online* **2017**, *34*, 361–368. [CrossRef] [PubMed]
214. de Paula, W.B.M.; Lucas, C.H.; Agip, A.-N.A.; Vizcay-Barrena, G.; Allen, J.F. Energy, ageing, fidelity and sex: Oocyte mitochondrial DNA as a protected genetic template. *Philos. Trans. R. Soc. B Biol. Sci.* **2013**, *368*, 20120263. [CrossRef] [PubMed]
215. Hyslop, L.A.; Blakeley, P.; Craven, L.; Richardson, J.; Fogarty, N.M.E.; Fragouli, E.; Lamb, M.; Wamaitha, S.E.; Prathalingam, N.; Zhang, Q.; et al. Towards clinical application of pronuclear transfer to prevent mitochondrial DNA disease. *Nature* **2016**, *534*, 383–386. [CrossRef]
216. Ma, H.; O'Neil, R.C.; Marti Gutierrez, N.; Hariharan, M.; Zhang, Z.Z.; He, Y.; Cinnioglu, C.; Kayali, R.; Kang, E.; Lee, Y.; et al. Functional Human Oocytes Generated by Transfer of Polar Body Genomes. *Cell Stem Cell* **2017**, *20*, 112–119. [CrossRef]
217. Zhang, S.-P.; Lu, C.-F.; Gong, F.; Xie, P.-Y.; Hu, L.; Zhang, S.-J.; Lu, G.-X.; Lin, G. Polar body transfer restores the developmental potential of oocytes to blastocyst stage in a case of repeated embryo fragmentation. *J. Assist. Reprod. Genet.* **2017**, *34*, 563–571. [CrossRef]
218. Yuan, P.; Guo, Q.; Guo, H.; Lian, Y.; Zhai, F.; Yan, Z.; Long, C.; Zhu, P.; Tang, F.; Qiao, J.; et al. The methylome of a human polar body reflects that of its sibling oocyte and its aberrance may indicate poor embryo development. *Hum. Reprod.* **2021**, *36*, 318–330. [CrossRef]
219. Takeo, S.; Sato, D.; Kimura, K.; Monji, Y.; Kuwayama, T.; Kawahara-miki, R.; Iwata, H. Resveratrol Improves the Mitochondrial Function and Fertilization Outcome of Bovine Oocytes. *J. Reprod. Dev.* **2014**, *60*, 92–99. [CrossRef]
220. Liu, Y.; Li, X.; Chen, S.; Wang, L.; Tan, Y.; Li, X.; Tang, L.; Zhang, J.; Wu, D.; Wu, Y.; et al. Comparison of Genome-Wide DNA Methylation Profiles of Human Fetal Tissues Conceived by in vitro Fertilization and Natural Conception. *Front. Cell Dev. Biol.* **2021**, *9*, 694769. [CrossRef]
221. Yang, H.; Ma, Z.; Peng, L.; Kuhn, C.; Rahmeh, M.; Mahner, S.; Jeschke, U.; von Schönfeldt, V. Comparison of Histone H3K4me3 between IVF and ICSI Technologies and between Boy and Girl Offspring. *Int. J. Mol. Sci.* **2021**, *22*, 8574. [CrossRef] [PubMed]
222. Gardner, D.K.; Lane, M.; Stevens, J.; Schoolcraft, W.B. Noninvasive assessment of human embryo nutrient consumption as a measure of developmental potential. *Fertil. Steril.* **2001**, *76*, 1175–1180. [CrossRef]
223. Bolton, V.N.; Cutting, R.; Clarke, H.; Brison, D.R. ACE consensus meeting report: Culture systems. *Hum. Fertil.* **2014**, *17*, 239–251. [CrossRef] [PubMed]
224. Pöhland, R.; Souza-Cácares, M.B.; Datta, T.K.; Vanselow, J.; Martins, M.I.M.; da Silva, W.A.L.; Cardoso, C.J.T.; de Andrade Melo-Sterza, A. Influence of long-term thermal stress on the in vitro maturation on embryo development and Heat Shock Protein abundance in zebu cattle. *Anim. Reprod.* **2020**, *17*, e20190085. [CrossRef] [PubMed]
225. Swain, J.E. Is there an optimal pH for culture media used in clinical IVF? *Hum. Reprod. Update* **2012**, *18*, 333–339. [CrossRef] [PubMed]
226. Shi, W.; Haaf, T. Aberrant methylation patterns at the two-cell stage as an indicator of early developmental failure. *Mol. Reprod. Dev.* **2002**, *63*, 329–334. [CrossRef]
227. Takamura, M.; Zhou, W.; Rombauts, L.; Dimitriadis, E. The long noncoding RNA PTENP1 regulates human endometrial epithelial adhesive capacity in vitro: Implications in infertility. *Biol. Reprod.* **2020**, *102*, 53–62. [CrossRef]
228. Ibrahim, S.; Salilew-Wondim, D.; Rings, F.; Hoelker, M.; Neuhoff, C.; Tholen, E.; Looft, C.; Schellander, K.; Tesfaye, D. Expression Pattern of Inflammatory Response Genes and Their Regulatory MicroRNAs in Bovine Oviductal Cells in Response to Lipopolysaccharide: Implication for Early Embryonic Development. *PLoS ONE* **2015**, *10*, e0119388. [CrossRef]
229. Barrera, A.D.; García, E.V.; Hamdi, M.; Sánchez-Calabuig, M.J.; López-Cardona, Á.P.; Balvís, N.F.; Rizos, D.; Gutiérrez-Adán, A. Embryo culture in presence of oviductal fluid induces DNA methylation changes in bovine blastocysts. *Reproduction* **2017**, *154*, 1–12. [CrossRef]
230. Capalbo, A.; Ubaldi, F.M.; Cimadomo, D.; Noli, L.; Khalaf, Y.; Farcomeni, A.; Ilic, D.; Rienzi, L. MicroRNAs in spent blastocyst culture medium are derived from trophectoderm cells and can be explored for human embryo reproductive competence assessment. *Fertil. Steril.* **2016**, *105*, 225–235. [CrossRef]
231. Naillat, F.; Saadeh, H.; Nowacka-Woszuk, J.; Gahurova, L.; Santos, F.; Tomizawa, S.; Kelsey, G. Oxygen concentration affects de novo DNA methylation and transcription in in vitro cultured oocytes. *Clin. Epigenet.* **2021**, *13*, 132. [CrossRef] [PubMed]
232. Fischer, B.; Bavister, B.D. Oxygen tension in the oviduct and uterus of rhesus monkeys, hamsters and rabbits. *Reproduction* **1993**, *99*, 673–679. [CrossRef] [PubMed]
233. Kasterstein, E.; Strassburger, D.; Komarovsky, D.; Bern, O.; Komsky, A.; Raziel, A.; Friedler, S.; Ron-El, R. The effect of two distinct levels of oxygen concentration on embryo development in a sibling oocyte study. *J. Assist. Reprod. Genet.* **2013**, *30*, 1073–1079. [CrossRef] [PubMed]
234. Nastri, C.O.; Nóbrega, B.N.; Teixeira, D.M.; Amorim, J.; Diniz, L.M.M.; Barbosa, M.W.P.; Giorgi, V.S.I.; Pileggi, V.N.; Martins, W.P. Low versus atmospheric oxygen tension for embryo culture in assisted reproduction: A systematic review and meta-analysis. *Fertil. Steril.* **2016**, *106*, 95–104. [CrossRef]
235. Rodríguez-Varela, C.; Labarta, E. Clinical Application of Antioxidants to Improve Human Oocyte Mitochondrial Function: A Review. *Antioxidants* **2020**, *9*, 1197. [CrossRef] [PubMed]
236. Martín-Romero, F.J.; Miguel-Lasobras, E.M.; Domínguez-Arroyo, J.A.; González-Carrera, E.; Álvarez, I.S. Contribution of culture media to oxidative stress and its effect on human oocytes. *Reprod. Biomed. Online* **2008**, *17*, 652–661. [CrossRef]

237. Menezo, Y.; Clément, P.; Dale, B. DNA methylation patterns in the early human embryo and the epigenetic/imprinting problems: A plea for a more careful approach to human assisted reproductive technology (ART). *Int. J. Mol. Sci.* **2019**, *20*, 1342. [CrossRef]
238. Menezo, Y.; Clement, P.; Dale, B.; Elder, K. Modulating oxidative stress and epigenetic homeostasis in preimplantation IVF embryos. *Zygote* **2022**, *30*, 149–158. [CrossRef]
239. Korsmo, H.W.; Jiang, X. One carbon metabolism and early development: A diet-dependent destiny. *Trends Endocrinol. Metab.* **2021**, *32*, 579–593. [CrossRef]
240. Burgess, K.; Bennett, C.; Mosnier, H.; Kwatra, N.; Bethel, F.; Jadavji, N.M. The Antioxidant Role of One-Carbon Metabolism on Stroke. *Antioxidants* **2020**, *9*, 1141. [CrossRef]
241. Clare, C.E.; Brassington, A.H.; Kwong, W.Y.; Sinclair, K.D. One-Carbon Metabolism: Linking Nutritional Biochemistry to Epigenetic Programming of Long-Term Development. *Annu. Rev. Anim. Biosci.* **2019**, *7*, 263–287. [CrossRef] [PubMed]
242. Schachter, M. Insulin resistance in patients with polycystic ovary syndrome is associated with elevated plasma homocysteine. *Hum. Reprod.* **2003**, *18*, 721–727. [CrossRef] [PubMed]
243. Berker, B.; Kaya, C.; Aytac, R.; Satiroglu, H. Homocysteine concentrations in follicular fluid are associated with poor oocyte and embryo qualities in polycystic ovary syndrome patients undergoing assisted reproduction. *Hum. Reprod.* **2009**, *24*, 2293–2302. [CrossRef]
244. Razi, Y.; Eftekhar, M.; Fesahat, F.; Dehghani Firouzabadi, R.; Razi, N.; Sabour, M.; Razi, M.H. Concentrations of homocysteine in follicular fluid and embryo quality and oocyte maturity in infertile women: A prospective cohort. *J. Obstet. Gynaecol.* **2021**, *41*, 588–593. [CrossRef] [PubMed]
245. Jia, L.; Zeng, Y.; Hu, Y.; Liu, J.; Yin, C.; Niu, Y.; Wang, C.; Li, J.; Jia, Y.; Hong, J.; et al. Homocysteine impairs porcine oocyte quality via deregulation of one-carbon metabolism and hypermethylation of mitochondrial DNA. *Biol. Reprod.* **2019**, *100*, 907–916. [CrossRef]
246. Li, Z.; Wang, Y.A.; Ledger, W.; Edgar, D.H.; Sullivan, E.A. Clinical outcomes following cryopreservation of blastocysts by vitrification or slow freezing: A population-based cohort study. *Hum. Reprod.* **2014**, *29*, 2794–2801. [CrossRef]
247. Fasano, G.; Fontenelle, N.; Vannin, A.-S.; Biramane, J.; Devreker, F.; Englert, Y.; Delbaere, A. A randomized controlled trial comparing two vitrification methods versus slow-freezing for cryopreservation of human cleavage stage embryos. *J. Assist. Reprod. Genet.* **2014**, *31*, 241–247. [CrossRef]
248. Zhao, X.-M.; Du, W.-H.; Wang, D.; Hao, H.-S.; Liu, Y.; Qin, T.; Zhu, H.-B. Effect of cyclosporine pretreatment on mitochondrial function in vitrified bovine mature oocytes. *Fertil. Steril.* **2011**, *95*, 2786–2788. [CrossRef]
249. Wang, N.; Hao, H.-S.; Li, C.-Y.; Zhao, Y.-H.; Wang, H.-Y.; Yan, C.-L.; Du, W.-H.; Wang, D.; Liu, Y.; Pang, Y.-W.; et al. Calcium ion regulation by BAPTA-AM and ruthenium red improved the fertilisation capacity and developmental ability of vitrified bovine oocytes. *Sci. Rep.* **2017**, *7*, 10652. [CrossRef]
250. Yao, J.; Geng, L.; Huang, R.; Peng, W.; Chen, X.; Jiang, X.; Yu, M.; Li, M.; Huang, Y.; Yang, X. Effect of vitrification on in vitro development and imprinted gene Grb10 in mouse embryos. *Reproduction* **2017**, *154*, 197–205. [CrossRef]
251. Saenz-de-Juano, M.D.; Billooye, K.; Smitz, J.; Anckaert, E. The loss of imprinted DNA methylation in mouse blastocysts is inflicted to a similar extent by in vitro follicle culture and ovulation induction. *Mol. Hum. Reprod.* **2016**, *22*, 427–441. [CrossRef] [PubMed]
252. Shirazi, A.; Naderi, M.M.; Hassanpour, H.; Heidari, M.; Borjian, S.; Sarvari, A.; Akhondi, M.M. The effect of ovine oocyte vitrification on expression of subset of genes involved in epigenetic modifications during oocyte maturation and early embryo development. *Theriogenology* **2016**, *86*, 2136–2146. [CrossRef] [PubMed]
253. Xu, T.; Liu, C.; Zhang, M.; Wang, X.; Yan, Y.; Liu, Q.; Ma, Y.; Yu, T.; Sathanawongs, A.; Jiao, J.; et al. Vitrification of Pronuclear Zygotes Perturbs Porcine Zygotic Genome Activation. *Animals* **2022**, *12*, 610. [CrossRef] [PubMed]
254. Verheijen, M.; Lienhard, M.; Schrooders, Y.; Clayton, O.; Nudischer, R.; Boerno, S.; Timmermann, B.; Selevsek, N.; Schlapbach, R.; Gmuender, H.; et al. DMSO induces drastic changes in human cellular processes and epigenetic landscape in vitro. *Sci. Rep.* **2019**, *9*, 4641. [CrossRef]
255. Sales, V.M.; Ferguson-Smith, A.C.; Patti, M.-E. Epigenetic Mechanisms of Transmission of Metabolic Disease across Generations. *Cell Metab.* **2017**, *25*, 559–571. [CrossRef] [PubMed]
256. Pathare, A.D.S.; Hinduja, I. Aberrant DNA methylation profiling affecting the endometrial receptivity in recurrent implantation failure patients undergoing in vitro fertilization. *Am. J. Reprod. Immunol.* **2020**, *83*, e13196. [CrossRef]
257. Jiang, N.-X.; Li, X.-L. The Complicated Effects of Extracellular Vesicles and Their Cargos on Embryo Implantation. *Front. Endocrinol.* **2021**, *12*, 681266. [CrossRef]
258. Chen, C.-W.; Huang, R.-L.; Do, A.Q.; Wang, H.-C.; Lee, Y.-X.; Wang, C.-W.; Hsieh, C.-C.; Tzeng, C.-R.; Hu, Y.-M.; Chen, C.-H.; et al. Genome-wide analysis of cervical secretions obtained during embryo transfer reveals the association between deoxyribonucleic acid methylation and pregnancy outcomes. *F&S Sci.* **2022**, *3*, 74–83. [CrossRef]
259. Qu, X.; Fang, Y.; Zhuang, S.; Zhang, Y. Micro-RNA miR-542-3p suppresses decidualization by targeting ILK pathways in human endometrial stromal cells. *Sci. Rep.* **2021**, *11*, 7186. [CrossRef]
260. Zhang, Y.-P.; Huang, Y.-T.; Huang, T.-S.; Pang, W.; Zhu, J.-J.; Liu, Y.-F.; Tang, R.-Z.; Zhao, C.-R.; Yao, W.-J.; Li, Y.-S.; et al. The Mammalian Target of Rapamycin and DNA methyltransferase 1 axis mediates vascular endothelial dysfunction in response to disturbed flow. *Sci. Rep.* **2017**, *7*, 14996. [CrossRef]
261. Jing, M.; Rech, L.; Wu, Y.; Goltz, D.; Taylor, C.G.; House, J.D. Effects of zinc deficiency and zinc supplementation on homocysteine levels and related enzyme expression in rats. *J. Trace Elem. Med. Biol.* **2015**, *30*, 77–82. [CrossRef] [PubMed]

262. Friso, S.; Udali, S.; De Santis, D.; Choi, S.-W. One-carbon metabolism and epigenetics. *Mol. Aspects Med.* **2017**, *54*, 28–36. [CrossRef] [PubMed]
263. Ben-Sahra, I.; Hoxhaj, G.; Ricoult, S.J.H.; Asara, J.M.; Manning, B.D. mTORC1 induces purine synthesis through control of the mitochondrial tetrahydrofolate cycle. *Science* **2016**, *351*, 728–733. [CrossRef] [PubMed]
264. Jansson, N.; Rosario, F.J.; Gaccioli, F.; Lager, S.; Jones, H.N.; Roos, S.; Jansson, T.; Powell, T.L. Activation of Placental mTOR Signaling and Amino Acid Transporters in Obese Women Giving Birth to Large Babies. *J. Clin. Endocrinol. Metab.* **2013**, *98*, 105–113. [CrossRef]
265. Cheng, M.; Lv, X.; Zhang, C.; Du, W.; Liu, Y.; Zhu, L.; Hao, J. DNMT1, a Novel Regulator Mediating mTORC1/mTORC2 Pathway-Induced NGF Expression in Schwann Cells. *Neurochem. Res.* **2018**, *43*, 2141–2154. [CrossRef]
266. Zeng, H.; Yan, L.; Cheng, W.-H.; Uthus, E.O. Dietary Selenomethionine Increases Exon-Specific DNA Methylation of the p53 Gene in Rat Liver and Colon Mucosa. *J. Nutr.* **2011**, *141*, 1464–1468. [CrossRef]
267. Zhu, Y.; Lu, L.; Liao, X.; Li, W.; Zhang, L.; Ji, C.; Lin, X.; Liu, H.-C.; Odle, J.; Luo, X. Maternal dietary manganese protects chick embryos against maternal heat stress via epigenetic-activated antioxidant and anti-apoptotic abilities. *Oncotarget* **2017**, *8*, 89665–89680. [CrossRef]
268. Kennedy, E.; Everson, T.M.; Punshon, T.; Jackson, B.P.; Hao, K.; Lambertini, L.; Chen, J.; Karagas, M.R.; Marsit, C.J. Copper associates with differential methylation in placentae from two US birth cohorts. *Epigenetics* **2020**, *15*, 215–230. [CrossRef]
269. Tobi, E.W.; Slieker, R.C.; Luijk, R.; Dekkers, K.F.; Stein, A.D.; Xu, K.M.; Slagboom, P.E.; van Zwet, E.W.; Lumey, L.H.; Heijmans, B.T. DNA methylation as a mediator of the association between prenatal adversity and risk factors for metabolic disease in adulthood. *Sci. Adv.* **2018**, *4*, eaao4364. [CrossRef]
270. Tobi, E.W.; Lumey, L.H.; Talens, R.P.; Kremer, D.; Putter, H.; Stein, A.D.; Slagboom, P.E.; Heijmans, B.T. DNA methylation differences after exposure to prenatal famine are common and timing- and sex-specific. *Hum. Mol. Genet.* **2009**, *18*, 4046–4053. [CrossRef]
271. Schutt, A.K.; Blesson, C.S.; Hsu, J.W.; Valdes, C.T.; Gibbons, W.E.; Jahoor, F.; Yallampalli, C. Preovulatory exposure to a protein-restricted diet disrupts amino acid kinetics and alters mitochondrial structure and function in the rat oocyte and is partially rescued by folic acid. *Reprod. Biol. Endocrinol.* **2019**, *17*, 12. [CrossRef]
272. Dahlhoff, M.; Pfister, S.; Blutke, A.; Rozman, J.; Klingenspor, M.; Deutsch, M.J.; Rathkolb, B.; Fink, B.; Gimpfl, M.; Hrabě de Angelis, M.; et al. Peri-conceptional obesogenic exposure induces sex-specific programming of disease susceptibilities in adult mouse offspring. *Biochim. Biophys. Acta Mol. Basis Dis.* **2014**, *1842*, 304–317. [CrossRef] [PubMed]
273. O'Doherty, A.M.; O'Gorman, A.; al Naib, A.; Brennan, L.; Daly, E.; Duffy, P.; Fair, T. Negative energy balance affects imprint stability in oocytes recovered from postpartum dairy cows. *Genomics* **2014**, *104*, 177–185. [CrossRef] [PubMed]
274. Fair, T. DNA methylation dynamics during oocyte and embryo development and its association with environmental induced alterations. *Anim. Reprod.* **2016**, *13*, 250–256. [CrossRef]
275. Desai, M.; Jellyman, J.K.; Han, G.; Beall, M.; Lane, R.H.; Ross, M.G. Maternal obesity and high-fat diet program offspring metabolic syndrome. *Am. J. Obstet. Gynecol.* **2014**, *211*, 237. [CrossRef] [PubMed]
276. Jansson, N.; Nilsfelt, A.; Gellerstedt, M.; Wennergren, M.; Rossander-Hultheén, L.; Powell, T.L.; Jansson, T. Maternal hormones linking maternal body mass index and dietary intake to birth weight. *Am. J. Clin. Nutr.* **2008**, *87*, 1743–1749. [CrossRef] [PubMed]
277. Morales, E.; Groom, A.; Lawlor, D.A.; Relton, C.L. DNA methylation signatures in cord blood associated with maternal gestational weight gain: Results from the ALSPAC cohort. *BMC Res. Notes* **2014**, *7*, 278. [CrossRef]
278. Igosheva, N.; Abramov, A.Y.; Poston, L.; Eckert, J.J.; Fleming, T.P.; Duchen, M.R.; McConnell, J. Maternal Diet-Induced Obesity Alters Mitochondrial Activity and Redox Status in Mouse Oocytes and Zygotes. *PLoS ONE* **2010**, *5*, e10074. [CrossRef]
279. Aiken, C.E.; Tarry-Adkins, J.L.; Penfold, N.C.; Dearden, L.; Ozanne, S.E. Decreased ovarian reserve, dysregulation of mitochondrial biogenesis, and increased lipid peroxidation in female mouse offspring exposed to an obesogenic maternal diet. *FASEB J.* **2016**, *30*, 1548–1556. [CrossRef]
280. Gemma, C.; Sookoian, S.; Alvariñas, J.; García, S.I.; Quintana, L.; Kanevsky, D.; González, C.D.; Pirola, C.J. Maternal Pregestational BMI Is Associated With Methylation of the PPARGC1A Promoter in Newborns. *Obesity* **2009**, *17*, 1032–1039. [CrossRef]
281. Hoyme, H.E.; May, P.A.; Kalberg, W.O.; Kodituwakku, P.; Gossage, J.P.; Trujillo, P.M.; Buckley, D.G.; Miller, J.H.; Aragon, A.S.; Khaole, N.; et al. A Practical Clinical Approach to Diagnosis of Fetal Alcohol Spectrum Disorders: Clarification of the 1996 Institute of Medicine Criteria. *Pediatrics* **2005**, *115*, 39–47. [CrossRef] [PubMed]
282. Halsted, C.H.; Medici, V. Aberrant Hepatic Methionine Metabolism and Gene Methylation in the Pathogenesis and Treatment of Alcoholic Steatohepatitis. *Int. J. Hepatol.* **2012**, *2012*, 959746. [CrossRef] [PubMed]
283. Chen, C.-H.; Pan, C.-H.; Chen, C.-C.; Huang, M.-C. Increased Oxidative DNA Damage in Patients With Alcohol Dependence and Its Correlation With Alcohol Withdrawal Severity. *Alcohol. Clin. Exp. Res.* **2011**, *35*, 338–344. [CrossRef]
284. Ungerer, M.; Knezovich, J.; Ramsay, M. In utero alcohol exposure, epigenetic changes, and their consequences. *Alcohol Res.* **2013**, *35*, 37–46. [PubMed]
285. Wang, D.; Jacobs, S.A.; Tsien, J.Z. Targeting the NMDA receptor subunit NR2B for treating or preventing age-related memory decline. *Expert Opin. Ther. Targets* **2014**, *18*, 1121–1130. [CrossRef]
286. Qiang, M.; Denny, A.; Chen, J.; Ticku, M.K.; Yan, B.; Henderson, G. The site specific demethylation in the 5′-regulatory area of NMDA receptor 2B subunit gene associated with CIE-induced up-regulation of transcription. *PLoS ONE* **2010**, *5*, e8798. [CrossRef]

287. Carpenter, B.L.; Remba, T.K.; Thomas, S.L.; Madaj, Z.; Brink, L.; Tiedemann, R.L.; Odendaal, H.J.; Jones, P.A. Oocyte age and preconceptual alcohol use are highly correlated with epigenetic imprinting of a noncoding RNA (nc886). *Proc. Natl. Acad. Sci. USA* **2021**, *118*, e2026580118. [CrossRef]
288. Haycock, P.C.; Ramsay, M. Exposure of Mouse Embryos to Ethanol During Preimplantation Development: Effect on DNA Methylation in the H19 Imprinting Control Region1. *Biol. Reprod.* **2009**, *81*, 618–627. [CrossRef]
289. Liu, Y.; Balaraman, Y.; Wang, G.; Nephew, K.P.; Zhou, F.C. Alcohol exposure alters DNA methylation profiles in mouse embryos at early neurulation. *Epigenetics* **2009**, *4*, 500–511. [CrossRef]
290. Heijmans, B.T.; Tobi, E.W.; Stein, A.D.; Putter, H.; Blauw, G.J.; Susser, E.S.; Slagboom, P.E.; Lumey, L.H. Persistent epigenetic differences associated with prenatal exposure to famine in humans. *Proc. Natl. Acad. Sci. USA* **2008**, *105*, 17046–17049. [CrossRef]
291. Geraghty, A.A.; Lindsay, K.L.; Alberdi, G.; McAuliffe, F.M.; Gibney, E.R. Nutrition during Pregnancy Impacts Offspring's Epigenetic Status—Evidence from Human and Animal Studies. *Nutr. Metab. Insights* **2015**, *8*, S29527. [CrossRef] [PubMed]
292. Jousse, C.; Parry, L.; Lambert-Langlais, S.; Maurin, A.; Averous, J.; Bruhat, A.; Carraro, V.; Tost, J.; Letteron, P.; Chen, P.; et al. Perinatal undernutrition affects the methylation and expression of the leptin gene in adults: Implication for the understanding of metabolic syndrome. *FASEB J.* **2011**, *25*, 3271–3278. [CrossRef] [PubMed]
293. Joubert, B.R.; Felix, J.F.; Yousefi, P.; Bakulski, K.M.; Just, A.C.; Breton, C.; Reese, S.E.; Markunas, C.A.; Richmond, R.C.; Xu, C.-J.; et al. DNA Methylation in Newborns and Maternal Smoking in Pregnancy: Genome-wide Consortium Meta-analysis. *Am. J. Hum. Genet.* **2016**, *98*, 680–696. [CrossRef] [PubMed]
294. Steuerwald, N.M.; Bermúdez, M.G.; Wells, D.; Munné, S.; Cohen, J. Maternal age-related differential global expression profiles observed in human oocytes. *Reprod. Biomed. Online* **2007**, *14*, 700–708. [CrossRef]
295. Tsutsumi, M.; Fujiwara, R.; Nishizawa, H.; Ito, M.; Kogo, H.; Inagaki, H.; Ohye, T.; Kato, T.; Fujii, T.; Kurahashi, H. Age-Related Decrease of Meiotic Cohesins in Human Oocytes. *PLoS ONE* **2014**, *9*, e96710. [CrossRef]
296. Ntostis, P.; Iles, D.; Kokkali, G.; Vaxevanoglou, T.; Kanavakis, E.; Pantou, A.; Huntriss, J.; Pantos, K.; Picton, H.M. The impact of maternal age on gene expression during the GV to MII transition in euploid human oocytes. *Hum. Reprod.* **2021**, *37*, 80–92. [CrossRef]
297. Battaglia, R.; Vento, M.E.; Ragusa, M.; Barbagallo, D.; La Ferlita, A.; Di Emidio, G.; Borzi, P.; Artini, P.G.; Scollo, P.; Tatone, C.; et al. MicroRNAs Are Stored in Human MII Oocyte and Their Expression Profile Changes in Reproductive Aging. *Biol. Reprod.* **2016**, *95*, 131. [CrossRef]
298. Hamatani, T.; Falco, G.; Carter, M.G.; Akutsu, H.; Stagg, C.A.; Sharov, A.A.; Dudekula, D.B.; VanBuren, V.; Ko, M.S.H. Age-associated alteration of gene expression patterns in mouse oocytes. *Hum. Mol. Genet.* **2004**, *13*, 2263–2278. [CrossRef]
299. Monk, C.; Feng, T.; Lee, S.; Krupska, I.; Champagne, F.A.; Tycko, B. Distress During Pregnancy: Epigenetic Regulation of Placenta Glucocorticoid-Related Genes and Fetal Neurobehavior. *Am. J. Psychiatry* **2016**, *173*, 705–713. [CrossRef]
300. Mulligan, C.; D'Errico, N.; Stees, J.; Hughes, D. Methylation changes at NR3C1 in newborns associate with maternal prenatal stress exposure and newborn birth weight. *Epigenetics* **2012**, *7*, 853–857. [CrossRef]
301. Hjort, L.; Martino, D.; Grunnet, L.G.; Naeem, H.; Maksimovic, J.; Olsson, A.H.; Zhang, C.; Ling, C.; Olsen, S.F.; Saffery, R.; et al. Gestational diabetes and maternal obesity are associated with epigenome-wide methylation changes in children. *JCI Insight* **2018**, *3*, e122572. [CrossRef] [PubMed]
302. Jia, L.; Li, J.; He, B.; Jia, Y.; Niu, Y.; Wang, C.; Zhao, R. Abnormally activated one-carbon metabolic pathway is associated with mtDNA hypermethylation and mitochondrial malfunction in the oocytes of polycystic gilt ovaries. *Sci. Rep.* **2016**, *6*, 19436. [CrossRef] [PubMed]
303. Junge, K.M.; Leppert, B.; Jahreis, S.; Wissenbach, D.K.; Feltens, R.; Grützmann, K.; Thürmann, L.; Bauer, T.; Ishaque, N.; Schick, M.; et al. MEST mediates the impact of prenatal bisphenol A exposure on long-term body weight development. *Clin. Epigenet.* **2018**, *10*, 58. [CrossRef] [PubMed]
304. Susiarjo, M.; Sasson, I.; Mesaros, C.; Bartolomei, M.S. Bisphenol A Exposure Disrupts Genomic Imprinting in the Mouse. *PLoS Genet.* **2013**, *9*, e1003401. [CrossRef]
305. Park, S.; Jeon, H.-J.; Choi, D.Y.; Oh, J.S. Polystyrene nanoparticles incorporate into the endoplasmic reticulum and disturb translation during meiotic maturation in mouse oocytes. *Toxicol. In Vitro* **2022**, *82*, 105380. [CrossRef] [PubMed]
306. Llonch, S.; Barragán, M.; Nieto, P.; Mallol, A.; Elosua-Bayes, M.; Lorden, P.; Ruiz, S.; Zambelli, F.; Heyn, H.; Vassena, R.; et al. Single human oocyte transcriptome analysis reveals distinct maturation stage-dependent pathways impacted by age. *Aging Cell* **2021**, *20*, e13360. [CrossRef] [PubMed]
307. Lebovitz, O.; Michaeli, M.; Aslih, N.; Poltov, D.; Estrada, D.; Atzmon, Y.; Shalom-Paz, E. Embryonic Development in Relation to Maternal Age and Conception Probability. *Reprod. Sci.* **2021**, *28*, 2292–2300. [CrossRef]
308. Hassold, T.; Hunt, P. Maternal age and chromosomally abnormal pregnancies: What we know and what we wish we knew. *Curr. Opin. Pediatr.* **2009**, *21*, 703–708. [CrossRef]
309. Sanders, K.D.; Silvestri, G.; Gordon, T.; Griffin, D.K. Analysis of IVF live birth outcomes with and without preimplantation genetic testing for aneuploidy (PGT-A): UK Human Fertilisation and Embryology Authority data collection 2016–2018. *J. Assist. Reprod. Genet.* **2021**, *38*, 3277–3285. [CrossRef]
310. Ge, Z.-J.J.; Schatten, H.; Zhang, C.-L.L.; Sun, Q.-Y.Y. Oocyte ageing and epigenetics. *Reproduction* **2015**, *149*, R103–R114. [CrossRef]
311. Ma, J.-Y.; Li, S.; Chen, L.-N.; Schatten, H.; Ou, X.-H.; Sun, Q.-Y. Why is oocyte aneuploidy increased with maternal aging? *J. Genet. Genom.* **2020**, *47*, 659–671. [CrossRef]

312. Yue, M.X.; Fu, X.W.; Zhou, G.B.; Hou, Y.P.; Du, M.; Wang, L.; Zhu, S.E. Abnormal DNA methylation in oocytes could be associated with a decrease in reproductive potential in old mice. *J. Assist. Reprod. Genet.* **2012**, *29*, 643–650. [CrossRef] [PubMed]
313. Cimadomo, D.; Fabozzi, G.; Vaiarelli, A.; Ubaldi, N.; Ubaldi, F.M.; Rienzi, L. Impact of Maternal Age on Oocyte and Embryo Competence. *Front. Endocrinol.* **2018**, *9*, 327. [CrossRef] [PubMed]
314. Nakamura, A.; François, O.; Lepeule, J. Epigenetic Alterations of Maternal Tobacco Smoking during Pregnancy: A Narrative Review. *Int. J. Environ. Res. Public Health* **2021**, *18*, 5083. [CrossRef] [PubMed]
315. Murphy, S.K.; Adigun, A.; Huang, Z.; Overcash, F.; Wang, F.; Jirtle, R.L.; Schildkraut, J.M.; Murtha, A.P.; Iversen, E.S.; Hoyo, C. Gender-specific methylation differences in relation to prenatal exposure to cigarette smoke. *Gene* **2012**, *494*, 36–43. [CrossRef]
316. Wiklund, P.; Karhunen, V.; Richmond, R.C.; Parmar, P.; Rodriguez, A.; De Silva, M.; Wielscher, M.; Rezwan, F.I.; Richardson, T.G.; Veijola, J.; et al. DNA methylation links prenatal smoking exposure to later life health outcomes in offspring. *Clin. Epigenet.* **2019**, *11*, 97. [CrossRef]
317. Joubert, B.R.; Håberg, S.E.; Nilsen, R.M.; Wang, X.; Vollset, S.E.; Murphy, S.K.; Huang, Z.; Hoyo, C.; Midttun, Ø.; Cupul-Uicab, L.A.; et al. 450K Epigenome-Wide Scan Identifies Differential DNA Methylation in Newborns Related to Maternal Smoking during Pregnancy. *Environ. Health Perspect.* **2012**, *120*, 1425–1431. [CrossRef]
318. Chen, B.; Du, Y.-R.; Zhu, H.; Sun, M.-L.; Wang, C.; Cheng, Y.; Pang, H.; Ding, G.; Gao, J.; Tan, Y.; et al. Maternal inheritance of glucose intolerance via oocyte TET3 insufficiency. *Nature* **2022**, *605*, 761–766. [CrossRef]
319. Gore, A.C. Endocrine-Disrupting Chemicals. *JAMA Intern. Med.* **2016**, *176*, 1705. [CrossRef]
320. Prusinski, L.; Al-Hendy, A.; Yang, Q. Developmental Exposure to Endocrine Disrupting Chemicals Alters the Epigenome: Identification of Reprogrammed Targets. *Gynecol. Obstet. Res. Open J.* **2016**, *3*, 1–6. [CrossRef]
321. McCabe, C.F.; Padmanabhan, V.; Dolinoy, D.C.; Domino, S.E.; Jones, T.R.; Bakulski, K.M.; Goodrich, J.M. Maternal environmental exposure to bisphenols and epigenome-wide DNA methylation in infant cord blood. *Environ. Epigenet.* **2020**, *6*, dvaa021. [CrossRef]
322. Bromer, J.G.; Zhou, Y.; Taylor, M.B.; Doherty, L.; Taylor, H.S. Bisphenol-A exposure in utero leads to epigenetic alterations in the developmental programming of uterine estrogen response. *FASEB J.* **2010**, *24*, 2273–2280. [CrossRef] [PubMed]
323. Hobel, C.J.; Goldstein, A.; Barrett, E.S. Psychosocial Stress and Pregnancy Outcome. *Clin. Obstet. Gynecol.* **2008**, *51*, 333–348. [CrossRef] [PubMed]
324. Hompes, T.; Izzi, B.; Gellens, E.; Morreels, M.; Fieuws, S.; Pexsters, A.; Schops, G.; Dom, M.; Van Bree, R.; Freson, K.; et al. Investigating the influence of maternal cortisol and emotional state during pregnancy on the DNA methylation status of the glucocorticoid receptor gene (NR3C1) promoter region in cord blood. *J. Psychiatr. Res.* **2013**, *47*, 880–891. [CrossRef] [PubMed]
325. Kertes, D.A.; Kamin, H.S.; Hughes, D.A.; Rodney, N.C.; Bhatt, S.; Mulligan, C.J. Prenatal Maternal Stress Predicts Methylation of Genes Regulating the Hypothalamic–Pituitary–Adrenocortical System in Mothers and Newborns in the Democratic Republic of Congo. *Child. Dev.* **2016**, *87*, 61–72. [CrossRef] [PubMed]

© 2022. Published by The Company of Biologists Ltd | Development (2022) 149, dev200819. doi:10.1242/dev.200819

RESEARCH ARTICLE

High-resolution ribosome profiling reveals translational selectivity for transcripts in bovine preimplantation embryo development

Linkai Zhu[1,‡], Tong Zhou[2,‡], Rajan Iyyappan[3], Hao Ming[1], Michal Dvoran[3], Yinjuan Wang[1], Qi Chen[4], R. Michael Roberts[5], Andrej Susor[3] and Zongliang Jiang[1,*,§]

ABSTRACT

High-resolution ribosome fractionation and low-input ribosome profiling of bovine oocytes and preimplantation embryos has enabled us to define the translational landscapes of early embryo development at an unprecedented level. We analyzed the transcriptome and the polysome- and non-polysome-bound RNA profiles of bovine oocytes (germinal vesicle and metaphase II stages) and early embryos at the two-cell, eight-cell, morula and blastocyst stages, and revealed four modes of translational selectivity: (1) selective translation of non-abundant mRNAs; (2) active, but modest translation of a selection of highly expressed mRNAs; (3) translationally suppressed abundant to moderately abundant mRNAs; and (4) mRNAs associated specifically with monosomes. A strong translational selection of low-abundance transcripts involved in metabolic pathways and lysosomes was found throughout bovine embryonic development. Notably, genes involved in mitochondrial function were prioritized for translation. We found that translation largely reflected transcription in oocytes and two-cell embryos, but observed a marked shift in the translational control in eight-cell embryos that was associated with the main phase of embryonic genome activation. Subsequently, transcription and translation become more synchronized in morulae and blastocysts. Taken together, these data reveal a unique spatiotemporal translational regulation that accompanies bovine preimplantation development.

KEY WORDS: Ribosome profiling, Translational selectivity, Translation, Transcription, Preimplantation embryo development, Bovine

INTRODUCTION

Preimplantation embryo development is a complex and precisely regulated process orchestrated by both maternal stored mRNAs and newly synthesized transcripts that appear following embryonic genome activation (EGA). In the last decade, transcriptome analyses of early mammalian embryos from multiple species have been comprehensively conducted and have established precise gene transcription programs during preimplantation development. However, the levels of mRNA and the amount of its protein product often do not directly correlate (Becker et al., 2018), suggesting that the mRNAs detected from global transcriptomic profile do not necessarily represent their functional status in early embryo development. Although the protein expression landscape of oocytes and preimplantation embryos has been characterized in mouse (Gao et al., 2017; Wang et al., 2010) and bovine (Banliat et al., 2021, 2022; Demant et al., 2015; Deutsch et al., 2014; Marei et al., 2019), the proteomic analysis offers limited coverage and information due to scarcity of the sample material available and has not been explored in other mammalian species. More importantly, a central gap in our understanding of post-transcriptional regulation exists, namely, how mRNAs are selected for spatial and temporal regulation during cell-fate specification and in processes such as oocyte maturation, fertilization, EGA and early differentiation. Thus, the understanding of mRNA translational dynamics may provide new insights into gene regulation during embryogenesis.

Accordingly, in some systems, ribosome profiling coupled to RNA sequencing (Ribo-seq) has been developed to quantify ribosome occupancy and to analyze selective genome-wide mRNA translation (Chassé et al., 2017; Ingolia et al., 2009). However, the broad application of Ribo-seq has been slowed by its complexity and the difficulty of adapting it to low amounts of input material. Recently, two powerful single-cell Ribo-seq (scRibo-seq) protocols have been developed. The first, Ribo-STAMP (Surveying Targets by APOBEC-Mediated Profiling), utilizes a cytosine deaminase (APOBEC) that catalyzes RNA cytosine-to-uracil conversion to edit transcripts associated with ribosomes (Brannan et al., 2021). The second scRibo-seq protocol utilizes the micrococcal nuclease MNase to digest RNA not bound to ribosomes in lysates of single cells and allows the capture of the ribosome-protected footprints (VanInsberghe et al., 2021). Both approaches require complex quality control and analysis due to the high 'noise' observed with single-cell data. In addition, it has been shown that mRNAs engaged in translation are bound by ribosomes, whereas dormant or stored transcripts are accumulated in diverse forms of ribonucleoprotein complexes and particles (Anderson and Kedersha, 2006; Eulalio et al., 2007; Parker and Sheth, 2007). It is also well known that actively translated mRNAs are bound by multiple ribosomes, or polysomes. The above-mentioned approaches limit analysis of the variation encountered in the different numbers of ribosome-bound mRNAs as a whole, while ignoring how the specific mRNAs are preferentially selected for translation. It should be noted that two recent studies have also optimized a low-input ribosome profiling (LiRibo-seq) approach and provided for the

[1]School of Animal Sciences, AgCenter, Louisiana State University, Baton Rouge, LA 70803, USA. [2]Department of Physiology and Cell Biology, University of Nevada, Reno School of Medicine, Reno, NV 89557-0352, USA. [3]Laboratory of Biochemistry and Molecular Biology of Germ Cells, Institute of Animal Physiology and Genetics, CAS, 277 21 Liběchov, Czech Republic. [4]Division of Biomedical Sciences, School of Medicine, University of California, Riverside, CA 92521, USA. [5]Department of Animal Sciences, Bond Life Sciences Center, University of Missouri, Columbia, MO 65211-7310, USA.
*Present address: Department of Animal Sciences, University of Florida, Gainesville, FL 32611-0910, USA.
‡These authors contributed equally to this work

§Author for correspondence (z.jiang1@ufl.edu)

R.I., 0000-0002-6356-7093; Q.C., 0000-0001-6353-9589; Z.J., 0000-0002-3040-7771

Handling Editor: Samantha Morris
Received 5 April 2022; Accepted 26 September 2022

Development (2022) 149, dev200819. doi:10.1242/dev.200819

first time the translational dynamics of mouse oocytes and preimplantation embryos (Xiong et al., 2022; Zhang et al., 2022), but again, these two studies were confined to an analysis of ribosome-bound mRNAs as a whole. In contrast, an imaging-based approach performed on living *Drosophila* embryos has allowed the direct exploration of the location and dynamics of translation of individual mRNAs (Dufourt et al., 2021), and has opened up new avenues for understanding gene regulation during development; however, this technology is still in its infancy.

In our study, we have improved a recent advance of scarce sample polysome profiling (SSP-profiling) (Masek et al., 2020) based on physical polysome fractionation (Chassé et al., 2017; Scantland et al., 2011). We substantially increased the resolution of the procedure to enable the sequencing of transcripts associated with monosomes and different sizes of polysomes extracted from bovine oocytes and preimplantation embryos. The data obtained have allowed us to study both genome-wide translational dynamics and translational selectivity mechanisms that accompany bovine early embryo development.

RESULTS

mRNA translational landscapes in bovine oocytes and preimplantation embryos

Polysome profiling has traditionally required a large amount of input material in order to fractionate polysome-bound RNA, making the procedure challenging to apply to mammalian oocytes and embryos. SSP-profiling (fractionation of mRNAs based on the number of translating ribosomes by using sucrose-density gradients) overcomes some of the obstacles posed by low sample size (Masek et al., 2020). The improved SSP-profiling when followed by RNA sequencing (RNA-seq) allowed us to analyze mRNA translational profiles of bovine oocytes at the germinal vesicle (GV) and metaphase II (MII) stages, as well as of preimplantation embryos at the two-cell, eight-cell, morula and blastocyst stages (Fig. 1A). For each sample, 100 oocytes or embryos were used, and the experiment was performed twice. We split each developmental stage by ultracentrifugation on sucrose gradients into ten equal volumes of fractions to provide a high resolution translatomic profile (transcripts associated with ribosomes from all fractionations) (Fig. 1A). We conducted two analyses to validate the translatomic data. First, we assessed the RNA isolated from each of the ten fractions by quantitative reverse transcription PCR (qRT-PCR)-based quantification of 18S and 28S ribosomal RNA (rRNA) (Fig. S1), which allowed us to confirm the successful separation of free RNAs, 40S small ribosomal subunits, 60S large ribosomal subunits, monosomes (80S) and polysomes (see Materials and Methods). The amount of 18S and 28S RNA provided an assessment of the reproducibility of fraction collection (Fig. S1). Additionally, principal component (PC) analysis (PCA) and Pearson correlation analysis of translatomic data indicated consistent values between biological replicates in each fraction and across developmental stage (Fig. 1B, Fig. 2). Based on these analyses, we classified the ten fractionations into free RNA (F1-F2), monosome-bound mRNA (F3-F5, with F6-F7 as an intermediate stage) and polysome-bound mRNA (F8-10, regarded as polysomes hereafter) profiles. In addition to ribosome-profiling analysis, global transcriptome analysis was performed on 20 oocytes (GV and MII stages) (n=3) and 20 embryos (n=3) at each developmental stage collected from the same batches used for ribosome fractionation and RNA-seq profiling. The transcriptomic data (triangles in Fig. 1C), especially in the PC1 dimension, appeared to organize roughly as two, seemingly distinct groupings, namely, the stages representing oocytes and two-cell-stage embryos and the stages from eight-cell to blastocyst (Fig. 1C), which is consistent with the notion that bovine major EGA occurs at the eight-cell stage (Graf et al., 2014; Jiang et al., 2014).

Overall, the translatome profile contrasted markedly with the transcriptome profile across different development stages (Fig. 1C), suggesting discordance between the global transcriptome and actively translated mRNAs. Again, there was a separation of the translatome data by stage. In particular, the morula and blastocyst values were clustered together at the far right of the PC1 plot and well distanced from early-stage data, which were clustered mainly towards the left of the PC1 plot and further separated from the rest of the developmental stages. Values for the eight-cell embryos fell somewhere in between (Fig. 1B,C). Our data also indicated that the changes in the translatome appeared to be gradual across the fractions from F1 to F10 (Fig. 1B,C), reflecting the continuous physical fractionation of mRNAs based on the number of translating ribosomes. Although considerable differences existed between the transcripts that were transcribed and those that were translated, the various PCAs confirmed the largely similar trajectories of translatome and transcriptome dynamics during the development transition from oocytes to blastocysts, with a major shift occurring at the crucial eight-cell stage (Fig. 1C).

Diverse modes of translational selectivity during bovine oocyte and preimplantation development

To delineate the relationship between translation and transcription during bovine oocyte and preimplantation development, we assessed the correlation of all the detected genes between the translatome and the transcriptome that had been generated from each of the six developmental stages. The F1-F2 fractions were excluded in order to allow us to focus on the translatome analysis (see Materials and Methods). Overall, we found considerable differences between polysome-occupied (F8-10) and monosome-occupied (F3-F5) mRNAs over the course of development (Fig. 2). We identified four modes of translational selectivity in each developmental stage: mode 1, selective translation of non-abundant mRNAs (Fig. 2, gold bar); mode 2, active, but modest translation of a selection of highly expressed mRNAs (Fig. 2, brown bar); mode 3, translationally suppressed abundant to moderately abundant mRNAs (Fig. 2, purple bar); and mode 4, mRNAs associated specifically with monosomes (Fig. 2, cyan bar). A complete list of genes (Fig. 2) from the four identified modes across bovine oocyte and preimplantation development are presented in Table S1, which should provide a valuable resource for others interested in translational regulation during bovine early embryo development.

Analysis of the functions of genes in mode 2 (active, but modest translation of a selection of highly expressed mRNAs) revealed a sequential progression of stage-specific gene networks. Gene enrichments shifted from ‘cell division’, ‘chromosome organization’ and ‘mitotic nuclear division’ in oocytes (GV and MII stages), to ‘embryonic cleavage’ and ‘regulation of DNA replication’ in two-cell embryos, to ‘translation’ in eight-cell embryos, and finally to ‘cell-cell adhesion’ and ‘protein folding’ in the morula and blastocyst stages, when junctional complexes between cells become evident (Table 1).

Besides the gene groups that were highly expressed and actively translated, we identified a second class of genes, sometimes relatively large in number, which had a low abundance of transcripts; however, these transcripts appeared to be actively translated as they were occupied by polysomes (mode 1, selective translation of non-abundant mRNAs; Fig. 2). The common dominant biological processes represented in this mode

Development (2022) 149, dev200819. doi:10.1242/dev.200819

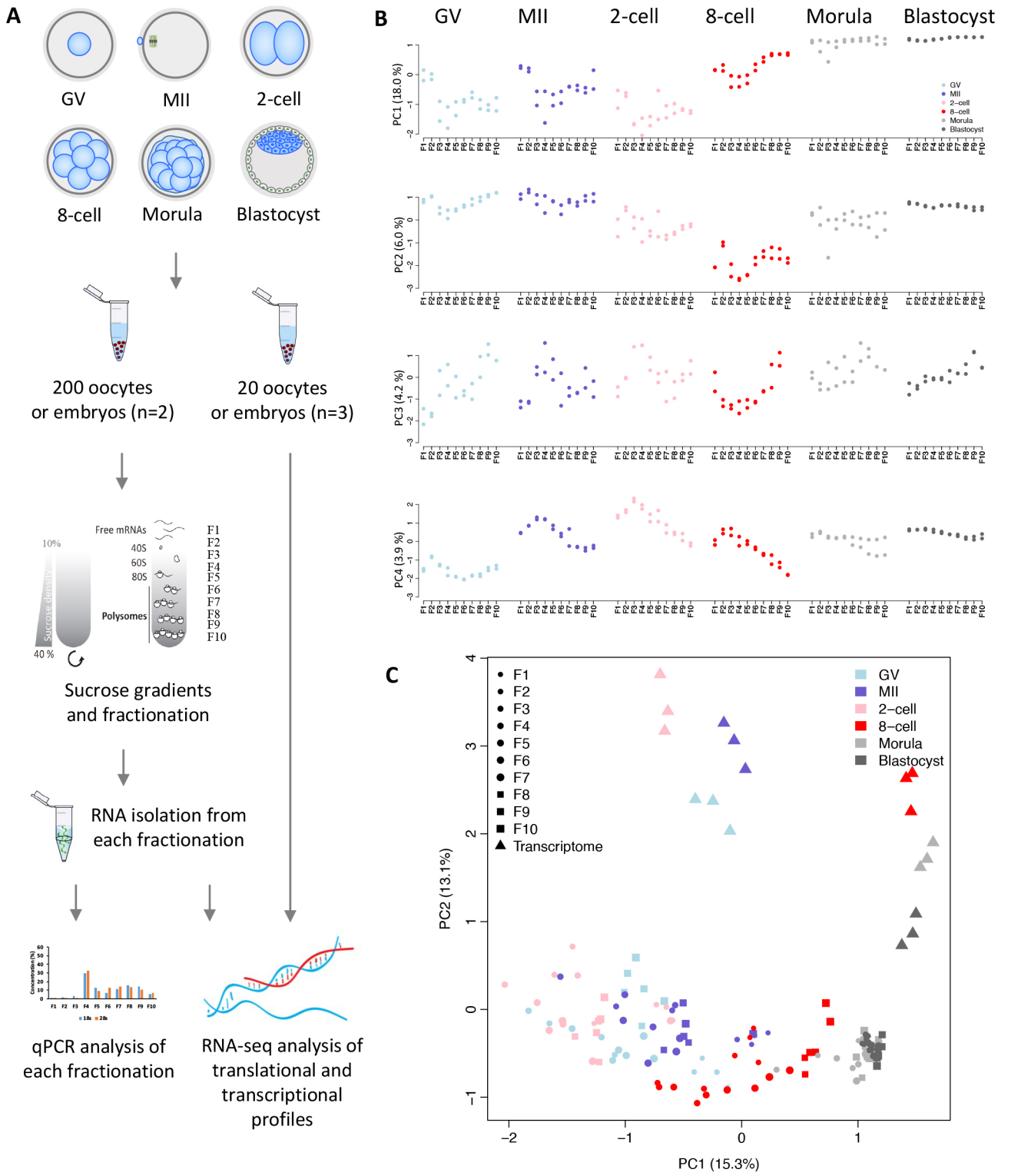

Fig. 1. Genome-wide high-resolution ribosome profiling of bovine oocytes and early embryos. (A) Scheme of genome-wide high-resolution polysome profiling in bovine oocytes and preimplantation embryos. (B) Principal component analysis (PCA) of polysome- and nonpolysome-bound mRNA profiles in ten fractions of bovine oocytes and early embryos. (C) PCA analysis of translatomes (F1-F10) (*n*=2) and transcriptomes (*n*=3) of bovine oocytes and early embryos.

included ‘translation’, ‘oxidation-reduction process’ and ‘mitochondrial translation’; these functions were evident across all developmental stages (Table 1). Stage-specific programs included ‘hydrogen ion transmembrane transport’ and ‘apoptotic signaling’ from the oocyte to the eight-cell stage, and ‘cell-cell adhesion’ and ‘cell redox homeostasis’ at the morula and blastocyst stages (Table 1).

The highly expressed but poorly translated transcripts (mode 3, translationally suppressed abundant to moderately abundant mRNAs; Fig. 2) were primarily involved in ‘transcription,

Development (2022) 149, dev200819. doi:10.1242/dev.200819

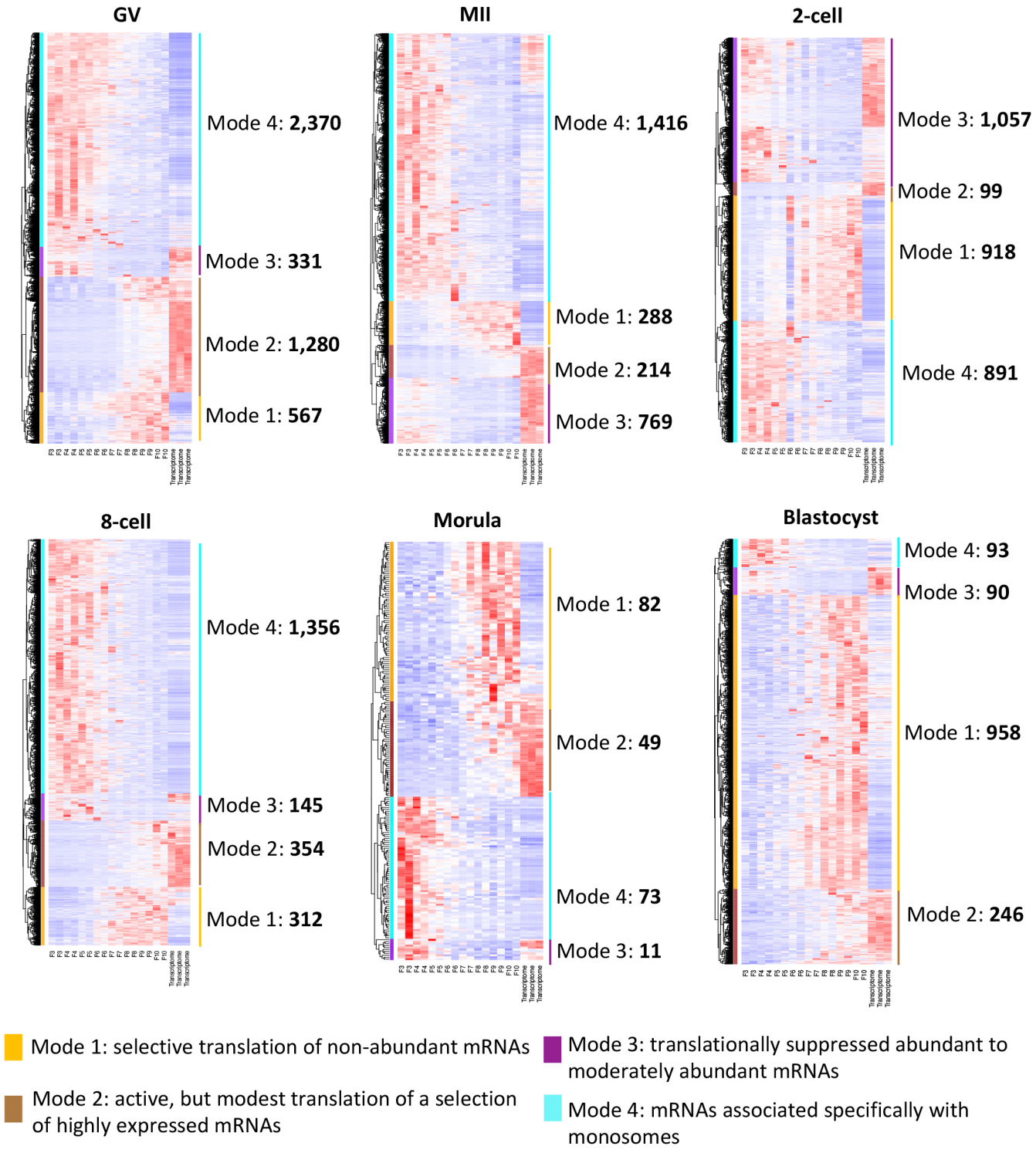

Fig. 2. Diverse modes of translational selectivity during bovine oocyte and preimplantation development. Heatmaps showing four modes of translational selectivity in bovine oocyte and preimplantation development. The color spectrum, ranging from red to white to blue, indicates high to low levels of gene expression. Mode 1, selective translation of non-abundant mRNAs (gold bar); mode 2, active, but modest translation of a selection of highly expressed mRNAs (brown bar); mode 3, translationally suppressed abundant to moderately abundant mRNAs (purple bar); and mode 4, mRNAs associated specifically with monosomes (cyan bar). The numbers of genes identified in individual modes of in each development stage are indicated.

DNA-templated' and 'RNA regulation' in oocytes, 'protein transport' and 'cell division' at the two-cell stage, 'viral process' and 'Ras protein signal transduction' at the eight-cell stage, and 'negative regulation of autophagy' and 'negative regulation of cell proliferation' at the morula and blastocyst stages (Table 1).

We also identified mRNAs occupying monosomes (mode 4) from each developmental stage (Fig. 2). Gene Ontology (GO) analysis indicated significant gene enrichments related to 'transcription, DNA-templated' and 'protein phosphorylation' at the GV stage, 'transcription, DNA-templated' and 'telomerase

Development (2022) 149, dev200819. doi:10.1242/dev.200819

Table 1. Top enriched GO terms associated with the genes from the identified four modes of translational selectivity in each stage of bovine oocyte and preimplantation development

	Mode 1	Mode 2	Mode 3	Mode 4
GV	Translation Oxidation-reduction process Mitochondrial translation Mitochondrial electron transport Hydrogen ion transmembrane transport	Cell division Chromosome segregation Mitotic nuclear division Protein folding Translation	Transcription, DNA-templated Regulation of RNA polymerase II Ribosomal large subunit biogenesis Ubiquitin-dependent protein catabolic Cell cycle	Transcription, DNA-templated Protein phosphorylation Respiratory system process *In utero* embryonic development Covalent chromatin modification
MII	Translation Oxidation-reduction process Mitochondrial translation Extrinsic apoptotic signaling Aerobic respiration	Cell division Translation Cytokinesis Chromosome organization Mitotic nuclear division	Transcription, DNA-templated Alternative mRNA splicing DNA methylation Chromatin remodeling Protein transport	Transcription, DNA-templated Telomere maintenance Protein localization to Cajal body Protein localization to telomere Telomerase RNA localization
Two-cell stage	Translation Oxidation-reduction process Mitochondrial translational, initiation and elongation Mitochondrial translation Hydrogen ion transmembrane transport	DNA replication Embryonic cleavage Cytokinesis ATP synthesis coupled electron transport Hydrogen ion transmembrane transport	Protein transport Cell division Mitotic nuclear division mRNA processing Transcription, DNA-templated	Oxidation-reduction process Regulation of gene expression Mitotic cell cycle checkpoint Circadian regulation of gene expression Neuron projection development
Eight-cell stage	Translation Oxidation-reduction process Mitochondrial translational, initiation and elongation Hydrogen ion transmembrane transport Ribosomal small subunit assembly	Translation Cell proliferation Cell-cell adhesion Protein folding Ribosomal large subunit biogenesis	Viral process Ras protein signal – negative DNA recombination NFκB signaling – positive Steroid metabolic process	Small GTPase-mediated signal transduction Glucose homeostasis RNA polymerase II promoter – negative Transcription, DNA-templated Histone H3 acetylation
Morula	Translation Oxidation-reduction process Metabolic process Cell-cell adhesion Cell redox homeostasis	Cell-cell adhesion Protein folding Translation Ribosomal large subunit biogenesis Ubiquitin-dependent protein catabolic	Negative regulation of autophagy Negative regulation of cell proliferation Endothelial cell differentiation Response to interferon-γ Regulation of RNA polymerase II	Regulation of cell death RNA polymerase II promoter – negative Regulation of cell differentiation Insulin receptor signaling pathway JAK-STAT cascade
Blastocyst	Translation Oxidation-reduction process Mitochondrial translation, initiation and elongation Cell-cell adhesion Cell redox homeostasis	Protein folding Protein transport Translation Cell redox homeostasis Ribosomal large subunit biogenesis	Negative regulation of cell proliferation ATP synthesis coupled electron transport Hydrogen ion transmembrane transport	Intracellular sequestering of iron ion Regulation of cell death

protein localization' at MII, 'oxidation-reduction process' and 'regulation of gene expression' at the two-cell stage, 'small GTP signal transduction' and 'glucose homeostasis' at the eight-cell stage, 'regulation of cell death' and 'cell differentiation' at the morula stage, and 'intracellular sequestering of iron ion' and 'regulation of cell death' at the blastocyst stage (Table 1).

We then sought to understand how such modes of translational selectivity are established. First, we performed a genome-wide correlation between the transcripts that constituted the four different modes and certain characteristic mRNA features. These features included the presence of cytoplasmic polyadenylation elements (CPEs), known to be important for translational regulation (Piqué et al., 2008), and 3′ untranslated regions (UTR) and 5′ UTR lengths. We observed that the transcripts in mode 1 [highest translational efficiency (TE) of polysome/mRNA] had the lowest CPE number and density, whereas transcripts in mode 2 (moderate TE) and mode 3 (lowest TE) demonstrated a higher CPE number and density than those of mode 1 both before (Fig. S2A) and after the EGA stage (Fig. S2B). When the TE was compared with CPE number and density on all detected transcripts, we confirmed that these values were negatively correlated (Fig. S2C,D).

The decrease in TE in the progression from mode 1 to mode 4 was also accompanied by increased lengths of 3′ UTRs, but not of 5′ UTRs of the transcripts (Fig. S3A,B) across all stages, and, for all transcripts identified, TE was in general negatively correlated with 3′ UTR length and positively correlated with 5′ UTR length. It should be noted, however, that these correlations were quite weak (Fig. S2C,D). Taken together, these data reveal a role of CPEs, and possibly the lengths of the 3′ UTRs and 5′ UTRs for translational regulation in bovine early embryonic development.

Finally, we calculated the proportion of maternal or embryonic transcripts in each of the four modes across developmental stages. The proportion of maternal transcripts was high and that of embryonic transcripts low in all four modes in the early stages (GV through two-cell stage) of development (Fig. S4A,B). At the eight-cell stage and thereafter, when transcription from the embryonic genome became much more active, the proportion of embryonic transcripts, as expected, rose markedly, especially in modes 1 and 2 at the eight-cell stage (Fig. S4B). The eight-cell stage was also distinguished by a high proportion of remaining maternal transcripts occupying monosomes (Fig. S4A). By the morula stage, maternal transcripts associated with ribosomes were rare; however, we observed a high

Development (2022) 149, dev200819. doi:10.1242/dev.200819

proportion of monosome-bound maternal transcripts that persisted to the blastocyst stage (Fig. S4A).

Collectively, our analysis captured four modes of translational selectivity for transcripts during bovine oocyte and preimplantation development. In particular, the analysis revealed gene activities (modes 1 and 3) that could not be readily inferred from transcriptomic data alone.

Translational control in bovine oocyte and preimplantation development

To gain insight into the broad translational regulation landscape across bovine oocyte and preimplantation development, we integrated the translatomes, i.e. transcripts associated with polysomes, with transcriptomes. The correlation between the translatome and the transcriptome was reasonably robust in GV and MII oocytes and in two-cell embryos, but appeared strongest in GV oocytes (Fig. 3A), in which transcription is silenced, with the oocytes relying largely on abundant maternally stored RNAs, which are translated for oocyte growth and for the oocyte maturation process (Schultz et al., 2018). Translatomic data correlated less well with the transcriptome in MII oocytes than in GV oocytes, in which there remains a reliance on maternal transcripts but with more selective translation from the embryonic genome, possibly in preparation for fertilization (Schultz et al., 2018). In contrast to the earlier stages, marked translational control was observed in eight-cell embryos (Fig. 3A). In other words, polysome occupancy poorly reflects the transcriptome, most likely because the eight-cell stage is when large-scale transcription of the embryonic genome is being initiated, but the newly synthesized mRNAs may not yet fully occupy the ribosomal machinery. Of note, partial polysome-occupied mRNAs were selected to be translated immediately in the eight-cell embryo (Fig. 3A), suggesting that these genes are essential for the major EGA. Subsequent to the eight-cell stage, translation and transcription appear to gradually become more synchronized in morulae and particularly in blastocysts (Fig. 3A), suggesting that this burst of protein production and cell proliferation is necessary to prepare the blastocyst for impending events, such as divergence of the hypoblast and epiblast.

To explore previously undefined translational dynamics in bovine oocyte and preimplantation development, we examined the pathways inferred from upregulated and downregulated, polysome-associated transcripts compared with the transcriptome at each developmental stage using a stringent cutoff with false discovery rate (FDR)<0.05 and fold change (FC)>8 (Fig. 3B). Transcripts associated with the broad term ‘metabolic pathways’ and the narrower term ‘lysosome’ were upregulated and, therefore, these mRNAs appeared to be preferentially translated throughout bovine preimplantation development (Fig. 3B). ‘RNA transport’, ‘spliceosome’ and ‘oocyte meiosis’ were pathways that were generally downregulated before the major EGA stages (GV, MII and two-cell stage), whereas commonly downregulated pathways at or after the major EGA stages (eight-cell stage, morula and blastocyst) included various ligand-receptor interactions and extracellular matrix (ECM)-receptor interactions (Fig. 3B). Additionally, classical pathways, including those for mTOR and MAPK signaling, were the most dynamic pathways translationally controlled throughout early development (Fig. 3B).

The data also revealed that the same polysome-occupied mRNAs in GV oocytes were largely retained in MII oocytes and only lost their translational selectivity at the eight-cell stage and beyond (Fig. 3C), whereas the translationally suppressed mRNAs in GV oocytes were also essentially the same as the ones identified in MII oocytes and eight-cell stage embryos (Fig. 3C).

A translational switch occurs during bovine major EGA

To identify the genes with distinct translational trends as development progressed, we attempted to correlate the polysome-occupied mRNAs with stage. This analysis confirmed the dramatic translatome shift associated with the major EGA stage in the eight-cell embryo (Fig. 4A, top panel). Until then, the upregulated polysome-occupied transcripts detected in the later developmental stages, i.e. the eight-cell, morula and blastocyst stages, were significantly enriched for processes associated with ‘translation’, ‘hydrogen ion transmembrane transport’, ‘cytoplasmic translation’, ‘ribosomal subunit assembly’ and ‘cell-cell adhesion’ (Fig. 4A, bottom panel), whereas pathway analysis revealed a significant enrichment for ‘ribosome assembly’ and ‘oxidative phosphorylation’ (Fig. 4A, bottom panel). The pathway analyses were also in agreement with these activities, especially in relation to energy metabolism. By contrast, the downregulated polysome-occupied transcripts from the later stages, i.e. those upregulated in oocytes and two-cell embryos, were associated with ‘cell division’, ‘mitotic nuclear division’ and ‘DNA repair’ (Fig. 4A, bottom panel), consistent with roles in oocyte maturation and the early cleavage stages. The pathway analyses were also in agreement with these activities including ‘cell cycle’, ‘RNA transport’ and ‘oocyte meiosis’, especially in relation to oocyte maturation (Fig. 4A, bottom panel).

We then identified 90 genes that have the most dynamic translational selectivity across development (Fig. 4B), of which most are actively translated in the oocyte to the two-cell stage and downregulated thereafter. Among the top ranked downregulated, polysome-occupied transcripts across developmental stages were *LRWD1*, *KAT2A*, *SUV39H1*, *TAB1*, *XAB2* and *MCM4* (Fig. 4C), all of which have functions linked to chromatin state. For example, *LRWD1* is a subunit of the origin recognition complex and plays a role in heterochromatin organization and cell cycle control (Bartke et al., 2010; Hsu et al., 2020; Wang et al., 2018a, 2017). *KAT2A* (also known as *GCN5*) is a histone acetyltransferase, whereas *SUV39H1* is a histone methyltransferase that trimethylates lysine 9 of histone H3 and plays pivotal roles in sculpting the epigenetic landscape through chromatin modification (Haque et al., 2021; Morgan and Shilatifard, 2020). Given that a hallmark feature of a competent oocyte is chromatin condensation, the surprisingly highly selective translation of these genes in oocytes (both GV and MII) and the likely role of the translated proteins in maintaining the repressive heterochromatic state suggest that, in combination, these genes may have important functions in the epigenetic control of bovine oocyte competence. *SUV39H1* and *TAB1* (Fig. 4C) have previously been shown to have essential roles in the maternal to zygotic transition (Yang et al., 2017; Zhou et al., 2021) and bovine preimplantation development (Jafarpour et al., 2020; Zhang et al., 2016, 2018), respectively. In contrast, the top-ranked upregulated polysome-occupied transcripts across developmental stages are those of *RAB17* (Fig. 4C). RAB17 belongs to a subfamily of small GTPases and plays an important role in the regulation of membrane trafficking (Lütcke et al., 1993). The translation of *RAB17*, which begins after the major EGA, is especially high at the blastocyst stage when the trophectoderm lineage emerges and the blastocoel cavity forms. Two other transcripts with similar dynamics to those of *RAB17* are *SMIM7* and *POLD4* (Fig. 4B), which encode a small integral membrane protein and a DNA polymerase subunit, respectively. However, neither appears to have anything in

Development (2022) 149, dev200819. doi:10.1242/dev.200819

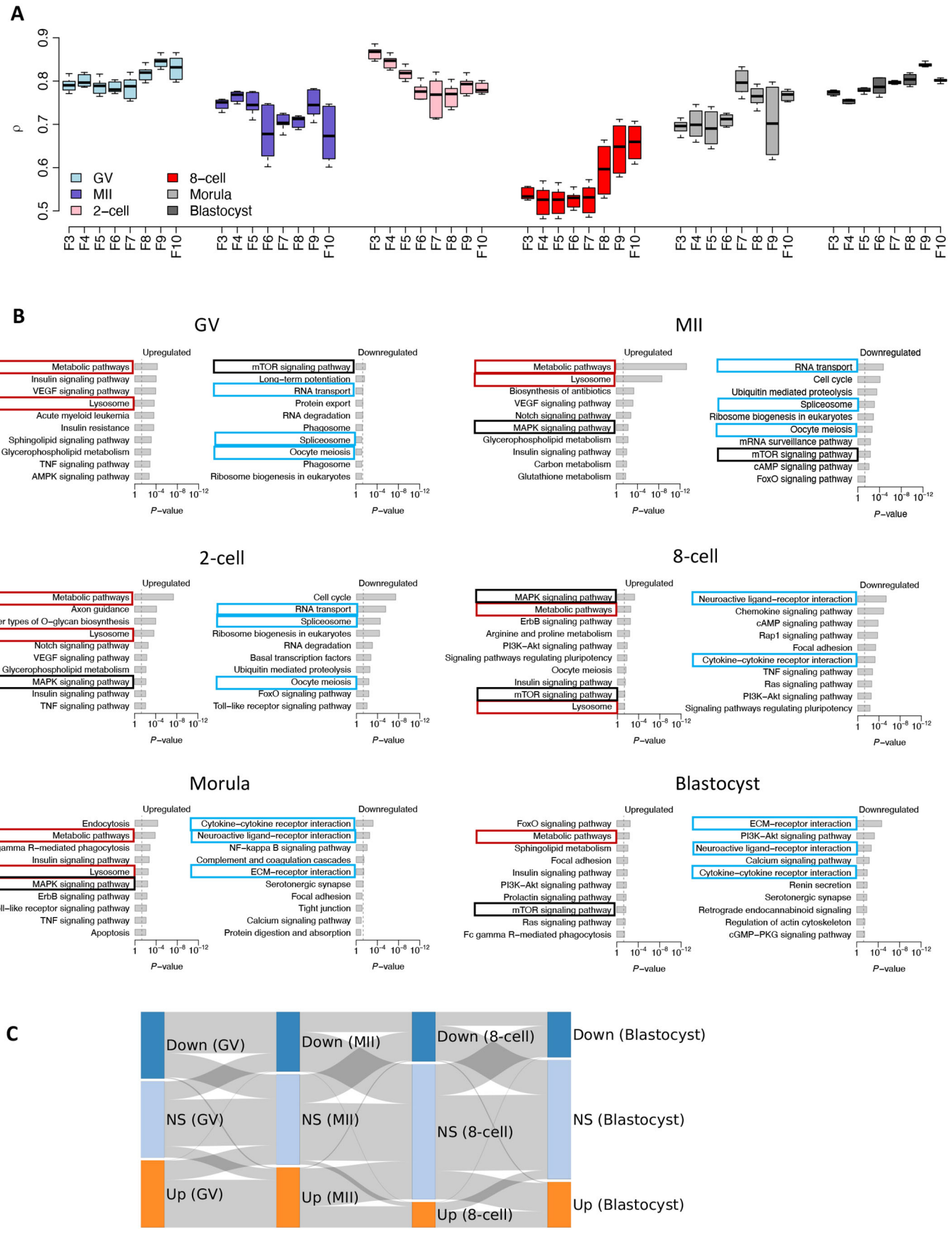

Fig. 3. See next page for legend.

Development (2022) 149, dev200819. doi:10.1242/dev.200819

Fig. 3. Translational control in bovine oocyte and preimplantation embryo development. (A) Translational control is summarized by the correlation analysis of the translatome (F3-F10) and the transcriptome at each developmental stage. Data show the mean±s.e.m. *n*=2. (B) KEGG pathway analysis of the differentially expressed genes between polysome-occupied mRNAs (F8-F10) and the transcriptome in bovine oocyte and preimplantation development. Red boxes highlight commonly upregulated pathways that are preferentially translated throughout bovine oocyte and preimplantation development. Cyan boxes highlight commonly downregulated pathways that are inactive or translated before (GV, MII and two-cell stage) or after (eight-cell, morula and blastocyst stage) major EGA stages. Black boxes highlight the most dynamic pathways that are translationally controlled throughout early development. Upregulated or downregulated pathways: FDR<0.05, FC>8; KEGG disease pathways are excluded. (C) Sankey diagram showing the upregulated and downregulated genes (FDR<0.05) between polysome-occupied mRNAs (F8-F10) and the transcriptome in each developmental stage. Down, downregulated; Up, upregulated; NS: not significantly regulated.

common with each other or with *RAB17*. Their specific functions in bovine preimplantation development are unknown.

Genes showing discordance between transcription and translation

We next analyzed the genes that showed contrasting trends in transcription versus translation (FDR<0.05 and FC>2) between stages during development from the oocyte to blastocyst (Fig. 5A). Genes that had decreased transcription but an upregulation of translation are represented by gold dots, whereas genes with increased transcription but decreased translation are in blue (Fig. 5A). A total of 103 genes showed a decrease in transcript number and at the same time had increased expression in the transition from GV oocyte to the MII stage (Table S2). Annotation of these genes revealed significant enrichment of 'mitochondrial translational initiation' and 'translational elongation' (Fig. 5B). These findings suggest that oocyte maturation requires a surge in the biosynthesis of mitochondrial components, which is consistent with the reported rise in aerobic metabolism accompanying oocyte maturation and gain of oocyte competence (Wang et al., 2018b; Zhang et al., 2019a,b). By contrast, 65 genes had increased transcription but decreased translation (blue dots) during the two-cell stage and eight-cell stage transition (Table S3). However, conventional annotation analysis of these genes was not particularly informative (Fig. 5B), although it must be assumed that some of these gene products play key roles in preparation for the major EGA occurring at the culmination of this transition.

We also identified several genes that are highly translated and transcribed at one particular stage of development but have low expression at other stages (Fig. 5C), suggesting that they likely have a specific regulatory function associated with that particular transition. We used the bovine embryo proteome data that had been acquired by nanoliquid chromatography coupled with tandem mass spectrometry (Banliat et al., 2022). Transcripts for five genes (*ORM1*, *PLAT*, *SERPINH1*, *TAGLN* and *TUT7*) encoding proteins found to be abundant in eight-cell embryos were also highly expressed at this stage of development (Fig. S5). Several other genes with stage-specific expression as assessed by the number of polysome-bound transcripts (*CARS2*, *CST6*, *DAG1*, *MMAB*, *SUN1*, *TUBG1*, *UHRF1*, *WFS1* and *ZP3*) were also validated by their protein expression (Fig. S5). Finally, the well-known pluripotency genes *NANOG*, *KLF17* and *MYC* and the interferon-response gene *ISG15* were highly translated and transcribed at the eight-cell stage but much less so elsewhere. Again, the major EGA stage appears to be one that is particularly dynamic with regard to changes in gene expression.

DISCUSSION

Early embryonic loss greatly affects fertility of both humans and agriculturally important animals such as cattle, yet the underlying causes are for the most part unknown. A characterization of the molecular events accompanying the maturation of the oocyte, fertilization and the early cleavage stages of embryonic development may provide some insight into what can potentially go wrong in the pregnancies that fail in these early stages. Omics technologies have enabled in-depth analysis of molecular mechanisms of bovine preimplantation development including a catalog of the transcripts (Graf et al., 2014; Jiang et al., 2014; Kues et al., 2008; Misirlioglu et al., 2006; Xie et al., 2010) and proteins (Banliat et al., 2021, 2022; Demant et al., 2015; Deutsch et al., 2014; Marei et al., 2019) present; the state of the epigenome, for example, DNA methylation status (Duan et al., 2019; Jiang et al., 2018); chromatin dynamics (Halstead et al., 2020; Ming et al., 2021); histone modifications (Lu et al., 2021); and the expression of small RNAs (Cuthbert et al., 2021; Cuthbert et al., 2019). However, the mRNA translation landscape and particularly the translational controls operating on specific mRNAs in oocytes and embryos remain largely unstudied. Here, we have developed a low-input, high-resolution, ribosome-profiling approach and provided a genome-wide characterization of the important but often overlooked translational regulation process. The datasets, particularly when mined in further detail and integrated with epigenome information, are expected to greatly expand our understanding of the gene regulation mechanisms governing bovine embryonic development. Perhaps most importantly, significant discordance was frequently observed to exist between the linked processes of translation and transcription at each developmental stage of bovine early development, highlighting the importance of evaluating the translatome in addition to the more accessible transcriptome. Our study represents the first insights into mRNA translational dynamics and a comparison of the transcriptome with polysome- and non-polysome-bound mRNA profiles during mammalian oocyte and preimplantation development. In this regard, the bovine is recognized as a highly informative model for human embryo development (Daigneault et al., 2018; Halstead et al., 2020; Jiang et al., 2014; Rossant, 2011), on which such experiments are profoundly more difficult to conduct.

Our study was able to capture four diverse, although somewhat empirical, modes of translational selectivity for transcripts. In particular, mode 1 (selective translation of non-abundant mRNAs) and mode 3 (translational suppression of abundant to moderately abundant mRNAs) provide information that could not be inferred by transcriptome analysis alone. The mRNAs in mode 1 provide a database for transcripts that are prioritized for translation relative to more abundant transcripts at each of the six stages of bovine preimplantation development examined. The identification of so many translationally suppressed, abundant to moderately abundant, transcribed genes, i.e. mode 3 genes, was somewhat surprising. The transcripts of these genes were largely absent from the polysome fractions, were most abundant in the oocyte and two-cell stages, and diminished in number thereafter. A more detailed informatics analysis of these transcripts and an even more comprehensive time-course analysis seems warranted. One possibility is that the proteins encoded by these transcripts may be extremely stable or particularly efficient in their roles, so that low amounts of protein relative to mRNA are required for early development. Clearly, any interpretation of the roles of the genes within either of these groups based solely on the levels of their transcripts is bound to be incomplete. In conclusion, our study reveals unanticipated translational selectivity mechanisms operating

Development (2022) 149, dev200819. doi:10.1242/dev.200819

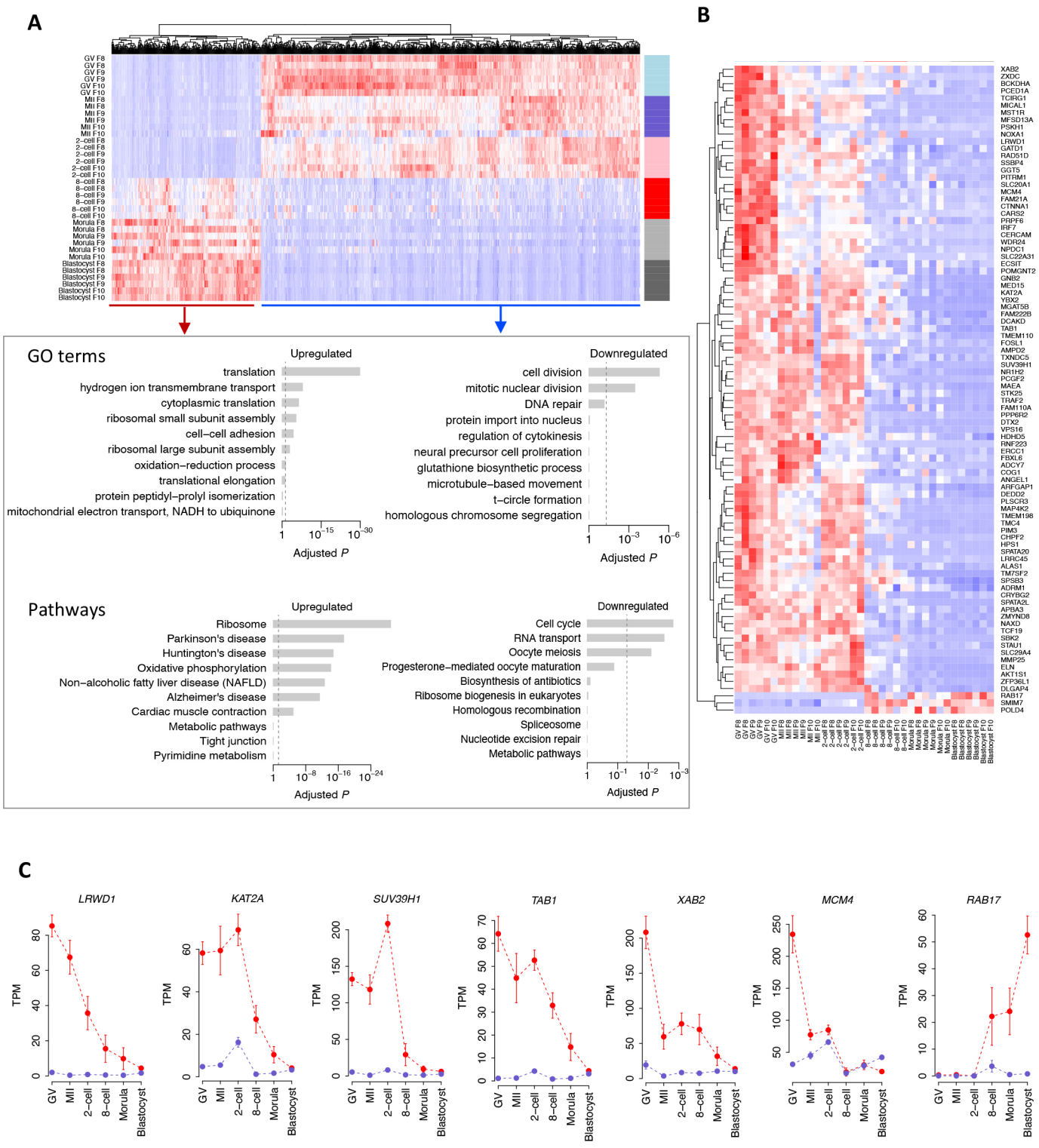

Fig. 4. A translational switch occurs during bovine major EGA. (A) Heatmap (top panel) showing that the polysome-occupied mRNAs (F8-F10) are correlated with developmental progression. The color spectrum, ranging from red to white to blue, represents high to low levels of gene expression. Top enriched GO terms and KEGG pathways (bottom panel) associated with upregulated (i.e. upregulation in eight-cell, morula and blastocyst stages) or downregulated (i.e. upregulation in oocytes and two-cell embryos) polysome-occupied genes towards the developmental progression are presented. (B) Heatmap of 90 prioritized genes with the most dynamic translational selectivity across bovine oocyte and preimplantation development. The color spectrum, ranging from red to white to blue, represents high to low levels of gene expression. (C) Exemplary genes with distinct patterns between translation (red) and transcription (blue) in bovine oocyte and preimplantation development. Data show the mean±s.e.m. *n*=2 (translation), *n*=3 (transcription).

on numerous genes across the genome. It identifies potentially important candidate regulators in embryonic programming that most likely have been overlooked in prior studies.

The analysis of genes in mode 2 (active, but modest translation of a selection of highly expressed mRNAs), i.e. those that would likely predominate in a bulk transcriptomic analysis, revealed a sequential

Development (2022) 149, dev200819. doi:10.1242/dev.200819

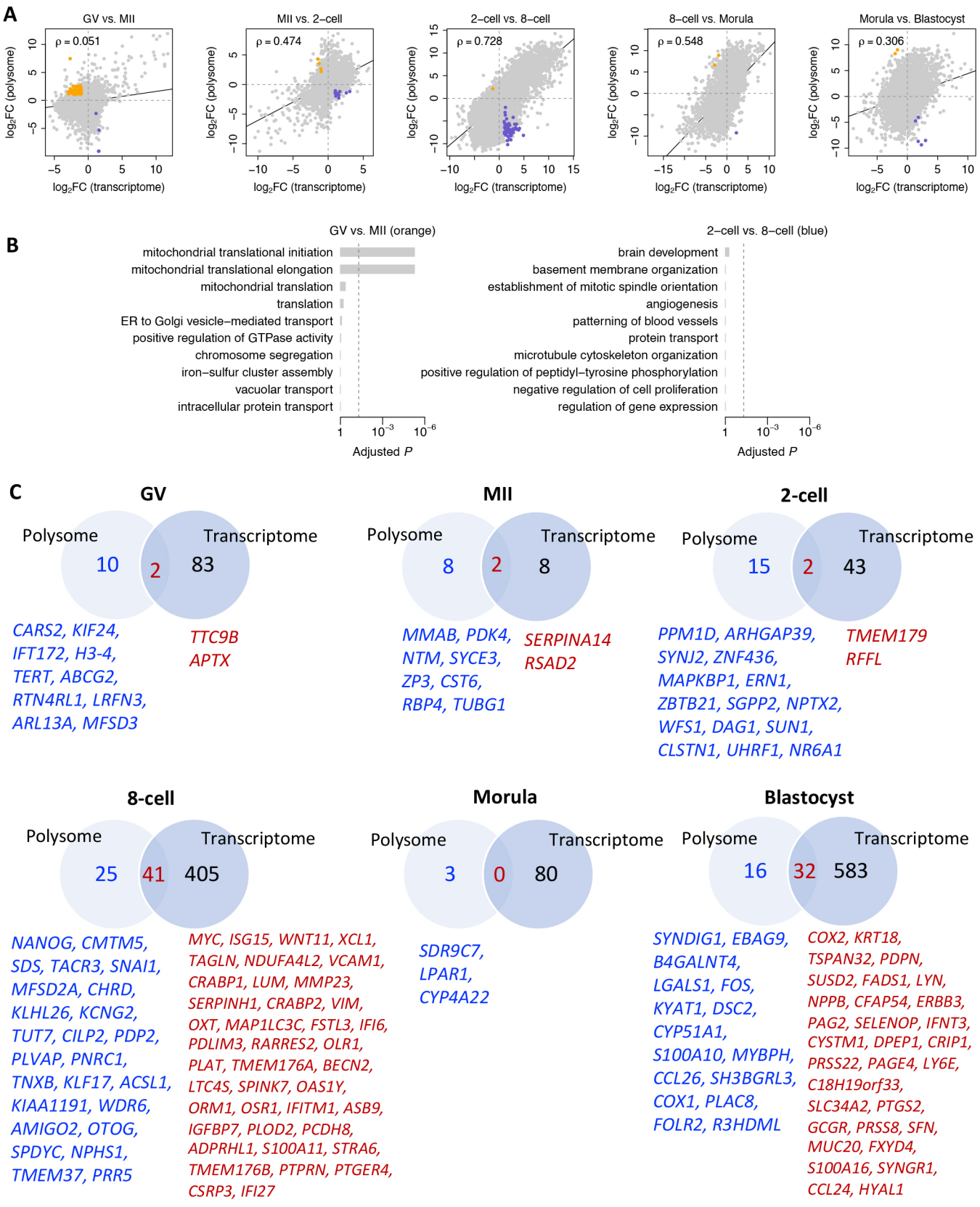

Fig. 5. See next page for legend.

progression of stage-specific gene networks accompanying development. The data are largely consistent with the sequential changes revealed in our previous analysis of co-expressed genes in bovine oocyte and preimplantation embryo transcriptomes (Jiang et al., 2014), but again reveal how transcriptomic data alone can be misleading and might overestimate the contribution of specific gene

Development (2022) 149, dev200819. doi:10.1242/dev.200819

Fig. 5. Genes showing discordance between transcription and translation. (A) Differential gene expression analysis between polysome-occupied mRNAs and the transcriptome in each developmental transition during bovine oocyte and preimplantation development. Gold dots represent genes that have decreased transcription but upregulation of translation in each developmental transition (FDR<0.05 and FC>2). Blue dots represent genes that have increased transcription but decreased translation in each developmental transition (FDR<0.05 and FC>2). ρ indicates Spearman correlation coefficient and the black line indicates regression. (B) The GO terms associated with the genes with decreased expression and upregulated translation in MII compared with those of genes in GV oocytes (left), and the GO terms associated with the genes with increased transcription and decreased translation during the two-cell stage and eight-cell stage transition. (C) Venn diagram showing the genes that are specifically and highly translated or transcribed in one particular stage across bovine oocyte and preimplantation development. The highly translated genes (blue) and the highly translated and most abundant genes (red) specific to each development stage are listed.

products to development. The transcripts that comprise mode 4 contribute weakly to the transcriptome except at the MII oocyte stage (Fig. 2), but appear to associate largely with monosomes and not be actively translated at the stages examined. Perhaps this association provides a mechanism wherein excess transcripts are not always translated but remain poised for future active translation. In other words, mode 4 mRNAs associated specifically with monosomes may constitute a novel but temporary storage state for transcripts.

Our analysis attempted to find whether there were genome-wide correlations between translational efficiency, which, for example, appears to be high in mode 1 genes and low in mode 3 and 4 genes, and certain transcript features. Consistent with the findings in mouse oocytes and embryos (Luong et al., 2020; Xiong et al., 2022), a high CPE density and length of 3′ UTR correlated with low TE. A complete annotation of the bovine functional genome will likely provide more insights into how such modes of translational selectivity are established.

The data also show that there are consistent translational similarities between the GV oocyte, the MII oocyte and the two-cell stage (Fig. 3A,C), but that there is a major translational perturbance evident at the eight-cell stage (Fig. 1B, Fig. 3A, Fig. 4A; Fig. S4), when the embryonic genome begins to contribute in a major way to the transcriptome. The transcripts identified in these early stages, i.e. GV oocyte to two-cell embryo were, as expected, mainly of maternal origin (Fig. S4A,B), but still fell within the four modes with different levels of TE. Prior to the eight-cell stage and also subsequently at the morula and blastocyst stages, translational dynamics were broadly correlated with the transcriptome. There was, however, a minor amount of transcriptional activity involving the embryonic genome at the two-cell stage that was reported (Graf et al., 2014; Jiang et al., 2014), and this appeared to correlate with high monosome occupancy by mRNA (Fig. 1C, Fig. 3A). The implications of this observation are unclear.

Transcripts encoding proteins involved in mitochondrial function, including ‘oxidation-reduction’, ‘electron transport chain’ and ‘mitochondrial translational initiation and elongation’, although not necessarily abundant, are efficiently selected for translation at all stages of development (Table 1), reflecting the essential role of mitochondria in generating energy to support oocyte and embryo development (Fragouli and Wells, 2015). Transcripts encoding enzymes involved in a wide array of metabolic pathways are also preferentially translated at all stages, again not an unsurprising observation (Botros et al., 2008; Bracewell-Milnes et al., 2017; Krisher and Prather, 2012; Nel-Themaat and Nagy, 2011; Redel et al., 2012; Singh and Sinclair, 2007; Vander Heiden et al., 2009). Why these mRNAs are so efficiently handled by the protein synthesis machinery remains unclear. However, a deeper understanding of the metabolic networks operating during these stages might facilitate the improvement of medium formulations for *in vitro* oocyte maturation and embryo culture, and allow the development of biomarker assays for assessing oocyte and embryo competence.

It should be recognized that the oocytes and embryos used in this study are products of *in vitro* protocols. Neither oocyte maturation nor embryo development occur as efficiently under these conditions as they do *in vivo*, although new formulations are constantly being tested to improve the procedures. There is concern, therefore, that *in vitro* procedures not only contribute to some degree of developmental failure (Zhu et al., 2021), but also cause alterations in the transcriptome (Gad et al., 2012; Kepkova et al., 2011; Rabaglino et al., 2021) and the translatome. Thus, the translational dynamic trajectory observed here *in vitro* might be somewhat different from that occurring *in vivo*. Nonetheless, *in vitro* fertilization and embryo *in vitro* culture are widely used in livestock species and in human *in vitro* fertilization programs. In particular, transfer of *in vitro*-produced bovine embryos is a successful commercial practice in the cattle industry and has already surpassed the numbers of pregnancies achieved from *in vivo*-derived embryo transfers (www.iets.org). Therefore, the data obtained from the standard *in vitro* system used in the present paper has direct relevance to current practice in the clinic and on the farm. Although not currently feasible because of cost considerations relating to the numbers of oocytes and embryos required, a comprehensive comparison of translational dynamics of *in vitro* embryos with their *in vivo* counterparts might be of considerable interest.

Several new methods, including Ribo-STAMP (Brannan et al., 2021), LiRibo-seq (Zhang et al., 2022), scRibo-seq (VanInsberghe et al., 2021), imaging-based SunTag (Dufourt et al., 2021) and RNA-fluorescence *in situ* hybridization and the puromycilation proximity ligation assay (RNA-puro-PLA) (Jansova et al., 2021), have recently opened avenues for understanding translational regulation with unprecedented cellular resolution. The main advantage of SunTag and RNA-puro-PLA, in particular, is to permit the localization and dynamics of mRNA translation to be observed at a single-molecule resolution. The development of the optimized SSP-profiling protocol described in the present study has enabled the characterization of the translational status of mRNAs bound to different kinds of ribosomes (free subunits, monosomes and polysomes) to be studied and has provided a more comprehensive picture of translational control during bovine early development than ever achieved previously. Combined with highly sensitive, high-throughput mass spectrometry to permit full proteomics analyses (Budnik et al., 2018; Gao et al., 2017), our technology should be capable of providing detailed insights into the relative contributions of transcription, translation and protein stability to the amounts of individual proteins in the developing embryo, as well as into detailed regulatory mechanisms at play.

In summary, our study has revealed a previously unappreciated level of complexity in genome-wide translational selectivity mechanisms associated with oocyte maturation and embryo development. In particular, the selective translation of non-abundant mRNAs for vital metabolic purposes throughout development, the stage-specific translational suppression of abundant to moderately abundant mRNAs, and the range of mRNAs associated with monosomes were particularly striking

Development (2022) 149, dev200819. doi:10.1242/dev.200819

observations. Our work has filled a significant knowledge gap in the study of translational regulation over a period of rapid developmental change and provided an extensive database that can be mined for more detailed insights into bovine oocyte and preimplantation development.

MATERIALS AND METHODS

Bovine oocytes and *in vitro* embryo production

Germinal vesicle stage oocytes (GV oocytes) were collected as cumulus-oocyte complexes from follicles of 3-5 mm in diameter aspirated from slaughterhouse *Bos taurus* ovaries. BO-IVM medium (IVF Bioscience) was used for oocyte *in vitro* maturation. Maturation was conducted in four-well dishes for 22-23 h at 38.5°C with 6% CO_2 to collect MII oocytes. Cumulus cells were completely removed and maturation was confirmed by light microscopy examination. Cryopreserved semen from a Holstein bull with proven fertility was diluted with BO-SemenPrep medium (IVF Bioscience) and added to drops containing cumulus-oocyte complexes (COCs) with a final concentration of 2×10^6 spermatozoa/ml. Gametes were co-incubated in 6% CO_2 in air at 38.5°C for 18 h. Embryos were then washed and cultured in BO-IVC medium (IVF Bioscience) at 38.5°C with 6% CO_2. Different developmental stage embryos (two-cell, eight-cell, morula and blastocyst) were then evaluated under light microscopy and only Grade 1 embryos by the standards of the International Embryo Technology Society (https://www.iets.org) were selected for further study. Prior to oocyte and embryo collection, 100 µg/ml of cycloheximide (Sigma-Aldrich) was added into the culture for 10 min to stabilize and halt ribosomes on transcripts. Oocytes and embryos were then washed with D-PBS (Thermo Fisher Scientific) containing 1 mg/ml polyvinylpyrrolidone (Sigma-Aldrich) (PBS-PVP) and transferred into 50 µl droplets of 0.1% protease (QIAGEN) to remove the zona pellucida. Oocytes and embryos were rinsed three times in PBS-PVP and confirmed to be free of contaminating cells, and then snap frozen in minimal medium and stored at −80°C until polysome fractionation.

Isolation of ribosome-bound mRNA

Approximately 100 oocytes (GV or MII oocyte) or embryos at different developmental stages (two-cell, eight-cell, morula and blastocyst) were combined with lysis buffer containing 10 mM HEPES (pH 7.5), 5 mM KCl, 5 mM $MgCl_2$, 2 mM dithiothreitol, 1% Triton X-100, 100 µg/ml cycloheximide, complete EDTA-free protease inhibitor (Roche) and 40 U/ml RNase inhibitor (RNase-OUT, Invitrogen). Oocytes and embryos were disrupted by zirconium silica beads (Sigma-Aldrich) in the mixer mill apparatus MM301 (shake frequency 30, total time 45 s, Retsch). Lysates were cleaned by centrifugation in 10,000 ***g*** for 5 min at 4°C and the supernatants were loaded into 10-40% linear sucrose gradients containing 10 mM HEPES (pH 7.5), 100 mM KCl, 5 mM $MgCl_2$, 2 mM dithiothreitol, 100 µg/ml cycloheximide, complete EDTA-free protease inhibitor and 5 U/ml RNase inhibitor. Ultracentrifugation was carried out with a SW55Ti rotor and Optima L-90 ultracentrifuge (Beckman Coulter) at 45,000 RPM (246,078 ***g***). Ribosome profiles were recorded by ISCO UV absorbance reader (Teledyne, ISCO). The overall quality of ribosome fractionation experiments was monitored by parallel analysis of a HEK293 cell sample. Ten equal fractions were then recovered and subjected to RNA isolation by Trizol reagent (Sigma-Aldrich).

qRT-PCR analysis

The RNA profile from each fraction was tested by qRT-PCR analysis with 18S and 28S rRNA-specific primers to reconstruct a distribution of non-polysomal and polysomal RNA complexes in each profile (Masek et al., 2020). Briefly, 2 µl of RNA from each fraction were reverse-transcribed using 20 U of M-MuLV Reverse Transcriptase (Thermo Fisher Scientific) and 0.3 µg of random hexamer primers in a reaction volume of 20 µl. cDNA synthesis was performed at 25°C for 10 min and then in 37°C for 5 min, followed by incubation at 42°C for 1 h and subsequent inactivation at 70°C for 10 min. qRT-PCR experiments were performed using the LightCycler480 SYBR Green I Master mix (Roche) on a LightCycler480 (Roche). The 10 µl reactions were performed in triplicate. Each reaction contained 2 µl of cDNA and 500 nM gene-specific primers (the list of primers used are provided in Table S4). The amplification protocol was as follows: 95°C for 5 min; 44 cycles of 95°C for 10 s, 58°C for 15 s, 72°C for 15 s; followed by melting curve determination. For absolute qRT-PCR quantification, we created recombinant pCRTM4-Topo plasmids (Invitrogen) containing 18S and 28S ribosomal RNA PCR amplicons. The relative quantification mode was applied and the mean of 18S and 28S RNA levels was used for the normalization of each fractionation (Fig. S1).

As described above, the RNA was separated in a sucrose gradient solution based on the number of ribosomes bound to the RNA. The 18S and 28S ribosomal subunits are central components of the 40S and 60S ribosomal subunits, respectively. Fractions 1 and 2 contained primarily free RNA; as a result, the concentration of the 18S and 28S would be expected to be low in comparison with the other fractions. Then, based on density, we anticipated high 18S rRNA and low 28S rRNA in fractions with 40S small ribosomal subunits, and low 18S rRNA and high 28S rRNA in fractions with the 60S large subunits. Both would be present in the 80S monosomes and in polysomes, the sizes of which would be evident from their alternating increasing content of both rRNAs. Therefore, the quantification of the 18S and 28S rRNA provides direct information on the reliability of fraction collection (Masek et al., 2020).

Library preparation and RNA-seq

The RNA-seq libraries were generated from individual fractions by using the Smart-seq2 v4 kit (Clontech) with minor modifications from the manufacturer's instructions. Briefly, individual cells were lysed and mRNA was captured and amplified with the Smart-seq2 v4 kit. After AMPure XP beads (Beckman) purification, the amplified RNAs were quality checked by using the High Sensitivity D5000 kit (Agilent Technologies). High-quality amplified RNAs were subject to library preparation (Nextera XT DNA Library Preparation Kit; Illumina) and multiplexed by Nextera XT Indexes (Illumina). The concentration of sequencing libraries was determined by using the Qubit dsDNA HS Assay Kit (Life Technologies) and KAPA Library Quantification Kits (KAPA Biosystems). The size of sequencing libraries was determined by the High Sensitivity D5000 Assay in a TapeStation 4200 system (Agilent). Pooled indexed libraries were then sequenced on the Illumina HiSeq X platform with 150-bp paired-end reads.

A pool of 20 oocytes or preimplantation embryos (n=3) selected from the same batch in each developmental stage used for ribosome profiling was used to profile transcriptomes by RNA-seq following the Smart-seq2 protocol as above described. In total, we sequenced 138 RNA-seq libraries (120 ribosome-bound mRNA libraries and 18 whole transcriptomes) and we generated approximately 40 million 150 bp paired-end reads per sample.

RNA-seq data analysis

The Salmon tool (Patro et al., 2017) was applied to quantify the genome-wide gene expression profile from the raw sequencing data, by using the Ensembl bovine genome annotation (ARS-UCD1.2). Transcript per million reads (TPM) was used as the unit of mRNA level. The edgeR tool (Robinson et al., 2010) was applied to identify differentially expressed genes. The TMM algorithm implemented in the edgeR package was used to perform normalization of the read counts and estimation of the effective library sizes. Differential expression analysis was performed by the likelihood ratio test implemented in the edgeR package.

In this study, the fractions of free RNAs (F1 and F2) were excluded because of the discontinuity with the other fractions in the global expression pattern (Fig. 1B), and also because no ribosome-bound RNA was detected in these fractions by qRT-PCR analysis as described above. We anticipated that the largely free RNA (not attached to any ribosomes or proteins) in the F1 and F2 fractions might include microRNAs or non-coding RNAs, which play a significant function in early development based on recently studies (Ganesh et al., 2020; Hasuwa et al., 2021; Kataruka et al., 2020; Loubalova et al., 2021). The inadequate annotation of such RNAs in the bovine genome also limited the comprehensive characterizations in this study.

To understand the translational selectivity in each developmental stage, Spearman's rank correlation test was applied to compute the relationship between gene expression and consecutive ribosomal fractions (F3-F10). The

genes with significant gradual increase or decrease in expression were retained for further analysis.

We also performed genome-wide correlation analysis between the transcripts that constituted the four different modes and had certain characteristic mRNA features. The transcripts with 5′ UTR or 3′ UTR length ≤100 nt were excluded when investigating 5′ UTRs and 3′ UTRs. The CPEs within 3′ UTRs were identified based on the motif sequences 'TTTTAT', 'TTTTAAT', 'TTTTACT', 'TTTTCAT', 'TTTTAAAT' and 'TTTTAAGT' (Luong et al., 2020; Xiong et al., 2022). We only retained the exact motif matches for the CPE number and density analysis.

We further performed analysis to determine whether or how maternal or embryonic transcripts are associated with different translational efficiency (four different modes). The maternal genes were defined as the genes strongly upregulated in both the GV and MII stages compared with the eight-cell, morula and blastocyst stages (FDR<0.05 and FC>4). The embryonic genes were the genes that were strongly upregulated in the eight-cell, morula and blastocyst stages relative to the GV and MII stages (FDR<0.05 and FC>4). The proportion of maternal/embryonic genes within each mode was computed as the number of maternal/embryonic genes in one given mode divided by the total number of genes in that mode.

All the conventional statistical analyses were performed using the R platform. The 'cor.test' function was used to perform Spearman's rank correlation test. A linear model controlling for fractionation was applied to prioritize the polysome-occupied genes with a gradual increase or decrease in expression across the developmental stages using the 'lm' function. If multiple testing needed to be accounted for, the 'p.adjust' function was applied for *P*-value correction. Principal component analysis on the genome-wide gene expression profile was performed by using the 'dudi.pca' function within the package 'ade4'. All the heatmaps were plotted by the 'heatmap.2' function within the package 'gplots'. The Gene Ontology and pathway analyses were performed by the David tool (Huang et al., 2009).

Acknowledgements
We thank Dr Tomas Masek and Dr Martin Pospisek from Department of Genetics and Microbiology at the Charles University in Prague for providing the facility and assistance with polysome fractionation.

Competing interests
The authors declare no competing or financial interests.

Author contributions
Conceptualization: Z.J.; Methodology: L.Z., T.Z., R.I., H.M., M.D., Y.W., A.S.; Software: T.Z.; Validation: Z.J.; Formal analysis: L.Z., T.Z., Q.C., A.S.; Investigation: L.Z., R.I., H.M., M.D., Y.W.; Resources: Z.J.; Data curation: Z.J.; Writing - original draft: Z.J.; Writing - review & editing: T.Z., R.M.R., A.S., Z.J.; Visualization: Z.J.; Supervision: Z.J.; Project administration: Z.J.; Funding acquisition: Z.J.

Funding
This work was supported by the National Institutes of Health (NIH) Eunice Kennedy Shriver National Institute of Child Health and Human Development (R01HD102533) and the United States Department of Agriculture (USDA) National Institute of Food and Agriculture (2019-67016-29863). A.S. and M.D. are supported by the Grantová Agentura České Republiky (GACR) grant 22-27301S. Q.C. and T.Z. are in part supported by the National Institutes of Health (R01ES032024). Open Access funding provided by University of Florida. Deposited in PMC for immediate release.

Data availability
The raw FASTQ files and normalized read accounts per gene are available at the Gene Expression Omnibus under the accession number GSE196484.

Peer review history
The peer review history is available online at https://journals.biologists.com/dev/lookup/doi/10.1242/dev.200819.reviewer-comments.pdf.

References
Anderson, P. and Kedersha, N. (2006). RNA granules. *J. Cell Biol.* **172**, 803-808. doi:10.1083/jcb.200512082

Banliat, C., Labas, V., Tomas, D., Teixeira-Gomes, A.-P., Guyonnet, B., Mermillod, P. and Saint-Dizier, M. (2021). Use of MALDI-TOF mass spectrometry to explore the peptidome and proteome of *in-vitro* produced bovine embryos pre-exposed to oviduct fluid. *Reprod. Biol.* **21**, 100545. doi:10.1016/j.repbio.2021.100545

Banliat, C., Mahé, C., Lavigne, R., Com, E., Pineau, C., Labas, V., Guyonnet, B., Mermillod, P. and Saint-Dizier, M. (2022). Dynamic changes in the proteome of early bovine embryos developed in vivo. *Front. Cell Dev. Biol.* **10**, 863700. doi:10.3389/fcell.2022.863700

Bartke, T., Vermeulen, M., Xhemalce, B., Robson, S. C., Mann, M. and Kouzarides, T. (2010). Nucleosome-interacting proteins regulated by DNA and histone methylation. *Cell* **143**, 470-484. doi:10.1016/j.cell.2010.10.012

Becker, K., Bluhm, A., Casas-Vila, N., Dinges, N., Dejung, M., Sayols, S., Kreutz, C., Roignant, J.-Y., Butter, F. and Legewie, S. (2018). Quantifying post-transcriptional regulation in the development of Drosophila melanogaster. *Nat. Commun.* **9**, 4970. doi:10.1038/s41467-018-07455-9

Botros, L., Sakkas, D. and Seli, E. (2008). Metabolomics and its application for non-invasive embryo assessment in IVF. *Mol. Hum. Reprod.* **14**, 679-690. doi:10.1093/molehr/gan066

Bracewell-Milnes, T., Saso, S., Abdalla, H., Nikolau, D., Norman-Taylor, J., Johnson, M., Holmes, E. and Thum, M.-Y. (2017). Metabolomics as a tool to identify biomarkers to predict and improve outcomes in reproductive medicine: a systematic review. *Hum. Reprod. Update* **23**, 723-736. doi:10.1093/humupd/dmx023

Brannan, K. W., Chaim, I. A., Marina, R. J., Yee, B. A., Kofman, E. R., Lorenz, D. A., Jagannatha, P., Dong, K. D., Madrigal, A. A., Underwood, J. G. et al. (2021). Robust single-cell discovery of RNA targets of RNA-binding proteins and ribosomes. *Nat. Methods* **18**, 507-519. doi:10.1038/s41592-021-01128-0

Budnik, B., Levy, E., Harmange, G. and Slavov, N. (2018). SCoPE-MS: mass spectrometry of single mammalian cells quantifies proteome heterogeneity during cell differentiation. *Genome Biol.* **19**, 161. doi:10.1186/s13059-018-1547-5

Chassé, H., Boulben, S., Costache, V., Cormier, P. and Morales, J. (2017). Analysis of translation using polysome profiling. *Nucleic Acids Res.* **45**, e15. doi:10.1093/nar/gkw907

Cuthbert, J. M., Russell, S. J., White, K. L. and Benninghoff, A. D. (2019). The maternal-to-zygotic transition in bovine in vitro-fertilized embryos is associated with marked changes in small non-coding RNAs. *Biol. Reprod.* **100**, 331-350. doi:10.1093/biolre/ioy190

Cuthbert, J. M., Russell, S. J., Polejaeva, I. A., Meng, Q., White, K. L. and Benninghoff, A. D. (2021). Dynamics of small non-coding RNAs in bovine scNT embryos through the maternal-to-embryonic transition. *Biol. Reprod.* **105**, 918-933. doi:10.1093/biolre/ioab107

Daigneault, B. W., Rajput, S., Smith, G. W. and Ross, P. J. (2018). Embryonic POU5F1 is Required for Expanded Bovine Blastocyst Formation. *Sci. Rep.* **8**, 7753. doi:10.1038/s41598-018-25964-x

Demant, M., Deutsch, D. R., Fröhlich, T., Wolf, E. and Arnold, G. J. (2015). Proteome analysis of early lineage specification in bovine embryos. *Proteomics* **15**, 688-701. doi:10.1002/pmic.201400251

Deutsch, D. R., Fröhlich, T., Otte, K. A., Beck, A., Habermann, F. A., Wolf, E. and Arnold, G. J. (2014). Stage-specific proteome signatures in early bovine embryo development. *J. Proteome Res.* **13**, 4363-4376. doi:10.1021/pr500550t

Duan, J. E., Jiang, Z. C., Alqahtani, F., Mandoiu, I., Dong, H., Zheng, X., Marjani, S. L., Chen, J. and Tian, X. C. (2019). Methylome dynamics of bovine gametes and in vivo early embryos. *Front. Genet.* **10**, 512. doi:10.3389/fgene.2019.00512

Dufourt, J., Bellec, M., Trullo, A., Dejean, M., De Rossi, S., Favard, C. and Lagha, M. (2021). Imaging translation dynamics in live embryos reveals spatial heterogeneities. *Science* **372**, 840-844. doi:10.1126/science.abc3483

Eulalio, A., Behm-Ansmant, I. and Izaurralde, E. (2007). P bodies: at the crossroads of post-transcriptional pathways. *Nat. Rev. Mol. Cell Biol.* **8**, 9-22. doi:10.1038/nrm2080

Fragouli, E. and Wells, D. (2015). Mitochondrial DNA assessment to determine oocyte and embryo viability. *Semin. Reprod. Med.* **33**, 401-409. doi:10.1055/s-0035-1567821

Gad, A., Hoelker, M., Besenfelder, U., Havlicek, V., Cinar, U., Rings, F., Held, E., Dufort, I., Sirard, M.-A., Schellander, K. et al. (2012). Molecular mechanisms and pathways involved in bovine embryonic genome activation and their regulation by alternative in vivo and in vitro culture conditions. *Biol. Reprod.* **87**, 100. doi:10.1095/biolreprod.112.099697

Ganesh, S., Horvat, F., Drutovic, D., Efenberkova, M., Pinkas, D., Jindrova, A., Pasulka, J., Iyyappan, R., Malik, R., Susor, A. et al. (2020). The most abundant maternal lncRNA Sirena1 acts post-transcriptionally and impacts mitochondrial distribution. *Nucleic Acids Res.* **48**, 3211-3227. doi:10.1093/nar/gkz1239

Gao, Y., Liu, X., Tang, B., Li, C., Kou, Z., Li, L., Liu, W., Wu, Y., Kou, X., Li, J. et al. (2017). Protein expression landscape of mouse embryos during pre-implantation development. *Cell Rep.* **21**, 3957-3969. doi:10.1016/j.celrep.2017.11.111

Graf, A., Krebs, S., Zakhartchenko, V., Schwalb, B., Blum, H. and Wolf, E. (2014). Fine mapping of genome activation in bovine embryos by RNA sequencing. *Proc. Natl. Acad. Sci. USA* **111**, 4139-4144. doi:10.1073/pnas.1321569111

Halstead, M. M., Ma, X., Zhou, C., Schultz, R. M. and Ross, P. J. (2020). Chromatin remodeling in bovine embryos indicates species-specific regulation of genome activation. *Nat. Commun.* **11**, 4654. doi:10.1038/s41467-020-18508-3

Haque, M. E., Jakaria, M., Akther, M., Cho, D.-Y., Kim, I.-S. and Choi, D.-K. (2021). The GCN5: its biological functions and therapeutic potentials. *Clin. Sci. (Lond.)* **135**, 231-257. doi:10.1042/CS20200986

Hasuwa, H., Iwasaki, Y. W., Au Yeung, W. K., Ishino, K., Masuda, H., Sasaki, H. and Siomi, H. (2021). Production of functional oocytes requires maternally expressed PIWI genes and piRNAs in golden hamsters. *Nat. Cell Biol.* **23**, 1002-1012. doi:10.1038/s41556-021-00745-3

Hsu, R. Y. C., Lin, Y.-C., Redon, C., Sun, Q., Singh, D. K., Wang, Y., Aggarwal, V., Mitra, J., Matur, A., Moriarity, B. et al. (2020). ORCA/LRWD1 regulates homologous recombination at ALT-telomeres by Modulating Heterochromatin Organization. *iScience* **23**, 101038. doi:10.1016/j.isci.2020.101038

Huang, D. W., Sherman, B. T. and Lempicki, R. A. (2009). Bioinformatics enrichment tools: paths toward the comprehensive functional analysis of large gene lists. *Nucleic Acids Res.* **37**, 1-13. doi:10.1093/nar/gkn923

Ingolia, N. T., Ghaemmaghami, S., Newman, J. R. and Weissman, J. S. (2009). Genome-wide analysis in vivo of translation with nucleotide resolution using ribosome profiling. *Science* **324**, 218-223. doi:10.1126/science.1168978

Jafarpour, F., Ghazvini Zadegan, F., Ostadhosseini, S., Hajian, M., Kiani-Esfahani, A. and Nasr-Esfahani, M. H. (2020). siRNA inhibition and not chemical inhibition of Suv39h1/2 enhances pre-implantation embryonic development of bovine somatic cell nuclear transfer embryos. *PLoS ONE* **15**, e0233880. doi:10.1371/journal.pone.0233880

Jansova, D., Aleshkina, D., Jindrova, A., Iyyappan, R., An, Q., Fan, G. and Susor, A. (2021). Single molecule RNA localization and translation in the mammalian oocyte and embryo. *J. Mol. Biol.* **433**, 167166. doi:10.1016/j.jmb.2021.167166

Jiang, Z., Sun, J., Dong, H., Luo, O., Zheng, X., Obergfell, C., Tang, Y., Bi, J., O'Neill, R., Ruan, Y. et al. (2014). Transcriptional profiles of bovine in vivo pre-implantation development. *BMC Genomics* **15**, 756. doi:10.1186/1471-2164-15-756

Jiang, Z., Lin, J., Dong, H., Zheng, X., Marjani, S. L., Duan, J., Ouyang, Z., Chen, J. and Tian, X. C. (2018). DNA methylomes of bovine gametes and in vivo produced preimplantation embryos. *Biol. Reprod.* **99**, 949-959. doi:10.1093/biolre/ioy138

Kataruka, S., Modrak, M., Kinterova, V., Malik, R., Zeitler, D. M., Horvat, F., Kanka, J., Meister, G. and Svoboda, P. (2020). MicroRNA dilution during oocyte growth disables the microRNA pathway in mammalian oocytes. *Nucleic Acids Res.* **48**, 8050-8062. doi:10.1093/nar/gkaa543

Kepkova, K. V., Vodicka, P., Toralova, T., Lopatarova, M., Cech, S., Dolezel, R., Havlicek, V., Besenfelder, U., Kuzmany, A., Sirard, M.-A. et al. (2011). Transcriptomic analysis of in vivo and in vitro produced bovine embryos revealed a developmental change in cullin 1 expression during maternal-to-embryonic transition. *Theriogenology* **75**, 1582-1595. doi:10.1016/j.theriogenology.2010.12.019

Krisher, R. L. and Prather, R. S. (2012). A role for the Warburg effect in preimplantation embryo development: metabolic modification to support rapid cell proliferation. *Mol. Reprod. Dev.* **79**, 311-320. doi:10.1002/mrd.22037

Kues, W. A., Sudheer, S., Herrmann, D., Carnwath, J. W., Havlicek, V., Besenfelder, U., Lehrach, H., Adjaye, J. and Niemann, H. (2008). Genome-wide expression profiling reveals distinct clusters of transcriptional regulation during bovine preimplantation development in vivo. *Proc. Natl. Acad. Sci. USA* **105**, 19768-19773. doi:10.1073/pnas.0805616105

Loubalova, Z., Fulka, H., Horvat, F., Pasulka, J., Malik, R., Hirose, M., Ogura, A. and Svoboda, P. (2021). Formation of spermatogonia and fertile oocytes in golden hamsters requires piRNAs. *Nat. Cell Biol.* **23**, 992-1001. doi:10.1038/s41556-021-00746-2

Lu, X., Zhang, Y., Wang, L., Wang, L., Wang, H., Xu, Q., Xiang, Y., Chen, C., Kong, F., Xia, W. et al. (2021). Evolutionary epigenomic analyses in mammalian early embryos reveal species-specific innovations and conserved principles of imprinting. *Sci. Adv.* **7**, eabi6178. doi:10.1126/sciadv.abi6178

Luong, X. G., Daldello, E. M., Rajkovic, G., Yang, C.-R. and Conti, M. (2020). Genome-wide analysis reveals a switch in the translational program upon oocyte meiotic resumption. *Nucleic Acids Res.* **48**, 3257-3276. doi:10.1093/nar/gkaa010

Lütcke, A., Jansson, S., Parton, R. G., Chavrier, P., Valencia, A., Huber, L. A., Lehtonen, E. and Zerial, M. (1993). Rab17, a novel small GTPase, is specific for epithelial cells and is induced during cell polarization. *J. Cell Biol.* **121**, 553-564. doi:10.1083/jcb.121.3.553

Marei, W. F. A., Van Raemdonck, G., Baggerman, G., Bols, P. E. J. and Leroy, J. L. M. R. (2019). Proteomic changes in oocytes after in vitro maturation in lipotoxic conditions are different from those in cumulus cells. *Sci. Rep.* **9**, 3673. doi:10.1038/s41598-019-40122-7

Masek, T., del Llano, E., Gahurova, L., Kubelka, M., Susor, A., Roucova, K., Lin, C.-J., Bruce, A. W. and Pospisek, M. (2020). Identifying the translatome of mouse NEBD-stage oocytes via SSP-profiling; a novel polysome fractionation method. *Int. J. Mol. Sci.* **21**, 1254. doi:10.3390/ijms21041254

Ming, H., Sun, J., Pasquariello, R., Gatenby, L., Herrick, J. R., Yuan, Y., Pinto, C. R., Bondioli, K. R., Krisher, R. L. and Jiang, Z. (2021). The landscape of accessible chromatin in bovine oocytes and early embryos. *Epigenetics* **16**, 300-312. doi:10.1080/15592294.2020.1795602

Misirlioglu, M., Page, G. P., Sagirkaya, H., Kaya, A., Parrish, J. J., First, N. L. and Memili, E. (2006). Dynamics of global transcriptome in bovine matured oocytes and preimplantation embryos. *Proc. Natl. Acad. Sci. USA* **103**, 18905-18910. doi:10.1073/pnas.0608247103

Morgan, M. A. J. and Shilatifard, A. (2020). Reevaluating the roles of histone-modifying enzymes and their associated chromatin modifications in transcriptional regulation. *Nat. Genet.* **52**, 1271-1281. doi:10.1038/s41588-020-00736-4

Nel-Themaat, L. and Nagy, Z. P. (2011). A review of the promises and pitfalls of oocyte and embryo metabolomics. *Placenta* **32** Suppl. 3, S257-S263. doi:10.1016/j.placenta.2011.05.011

Parker, R. and Sheth, U. (2007). P bodies and the control of mRNA translation and degradation. *Mol. Cell* **25**, 635-646. doi:10.1016/j.molcel.2007.02.011

Patro, R., Duggal, G., Love, M. I., Irizarry, R. A. and Kingsford, C. (2017). Salmon provides fast and bias-aware quantification of transcript expression. *Nat. Methods* **14**, 417-419. doi:10.1038/nmeth.4197

Piqué, M., López, J. M., Foissac, S., Guigó, R. and Méndez, R. (2008). A combinatorial code for CPE-mediated translational control. *Cell* **132**, 434-448. doi:10.1016/j.cell.2007.12.038

Rabaglino, M. B., O'Doherty, A., Bojsen-Møller Secher, J., Lonergan, P., Hyttel, P., Fair, T. and Kadarmideen, H. N. (2021). Application of multi-omics data integration and machine learning approaches to identify epigenetic and transcriptomic differences between in vitro and in vivo produced bovine embryos. *PLoS ONE* **16**, e0252096. doi:10.1371/journal.pone.0252096

Redel, B. K., Brown, A. N., Spate, L. D., Whitworth, K. M., Green, J. A. and Prather, R. S. (2012). Glycolysis in preimplantation development is partially controlled by the Warburg Effect. *Mol. Reprod. Dev.* **79**, 262-271. doi:10.1002/mrd.22017

Robinson, M. D., McCarthy, D. J. and Smyth, G. K. (2010). edgeR: a Bioconductor package for differential expression analysis of digital gene expression data. *Bioinformatics* **26**, 139-140. doi:10.1093/bioinformatics/btp616

Rossant, J. (2011). Developmental biology: a mouse is not a cow. *Nature* **471**, 457-458. doi:10.1038/471457a

Scantland, S., Grenon, J.-P., Desrochers, M.-H., Sirard, M.-A., Khandjian, E. W. and Robert, C. (2011). Method to isolate polyribosomal mRNA from scarce samples such as mammalian oocytes and early embryos. *BMC Dev. Biol.* **11**, 8. doi:10.1186/1471-213X-11-8

Schultz, R. M., Stein, P. and Svoboda, P. (2018). The oocyte-to-embryo transition in mouse: past, present, and future. *Biol. Reprod.* **99**, 160-174. doi:10.1093/biolre/ioy013

Singh, R. and Sinclair, K. D. (2007). Metabolomics: approaches to assessing oocyte and embryo quality. *Theriogenology* **68** Suppl. 1, S56-S62. doi:10.1016/j.theriogenology.2007.04.007

Vander Heiden, M. G., Cantley, L. C. and Thompson, C. B. (2009). Understanding the Warburg effect: the metabolic requirements of cell proliferation. *Science* **324**, 1029-1033. doi:10.1126/science.1160809

VanInsberghe, M., van den Berg, J., Andersson-Rolf, A., Clevers, H. and van Oudenaarden, A. (2021). Single-cell Ribo-seq reveals cell cycle-dependent translational pausing. *Nature* **597**, 561-565. doi:10.1038/s41586-021-03887-4

Wang, S., Kou, Z., Jing, Z., Zhang, Y., Guo, X., Dong, M., Wilmut, I. and Gao, S. (2010). Proteome of mouse oocytes at different developmental stages. *Proc. Natl. Acad. Sci. USA* **107**, 17639-17644. doi:10.1073/pnas.1013185107

Wang, Y., Khan, A., Marks, A. B., Smith, O. K., Giri, S., Lin, Y.-C., Creager, R., MacAlpine, D. M., Prasanth, K. V., Aladjem, M. I. et al. (2017). Temporal association of ORCA/LRWD1 to late-firing origins during G1 dictates heterochromatin replication and organization. *Nucleic Acids Res.* **45**, 2490-2502. doi:10.1093/nar/gkw1211

Wang, C. Y., Hong, Y. H., Syu, J. S., Tsai, Y. C., Liu, X. Y., Chen, T. Y., Su, Y. M., Kuo, P. L., Lin, Y. M. and Teng, Y. N. (2018a). LRWD1 regulates microtubule nucleation and proper cell cycle progression in the human testicular embryonic carcinoma cells. *J. Cell. Biochem.* **119**, 314-326. doi:10.1002/jcb.26180

Wang, T., Babayev, E., Jiang, Z., Li, G., Zhang, M., Esencan, E., Horvath, T. and Seli, E. (2018b). Mitochondrial unfolded protein response gene Clpp is required to maintain ovarian follicular reserve during aging, for oocyte competence, and development of pre-implantation embryos. *Aging Cell* **17**, e12784. doi:10.1111/acel.12784

Xie, D., Chen, C.-C., Ptaszek, L. M., Xiao, S., Cao, X., Fang, F., Ng, H. H., Lewin, H. A., Cowan, C. and Zhong, S. (2010). Rewirable gene regulatory networks in the preimplantation embryonic development of three mammalian species. *Genome Res.* **20**, 804-815. doi:10.1101/gr.100594.109

Xiong, Z., Xu, K., Lin, Z., Kong, F., Wang, Q., Quan, Y., Sha, Q.-Q., Li, F., Zou, Z., Liu, L. et al. (2022). Ultrasensitive Ribo-seq reveals translational landscapes during mammalian oocyte-to-embryo transition and pre-implantation development. *Nat. Cell Biol.* **24**, 968-980. doi:10.1038/s41556-022-00928-6

Yang, Y., Zhou, C., Wang, Y., Liu, W., Liu, C., Wang, L., Liu, Y., Shang, Y., Li, M., Zhou, S. et al. (2017). The E3 ubiquitin ligase RNF114 and TAB1 degradation are required for maternal-to-zygotic transition. *EMBO Rep.* **18**, 205-216. doi:10.15252/embr.201642573

Zhang, S., Wang, F., Fan, C., Tang, B., Zhang, X. and Li, Z. (2016). Dynamic changes of histone H3 lysine 9 following trimethylation in bovine oocytes and pre-

implantation embryos. *Biotechnol. Lett.* **38**, 395-402. doi:10.1007/s10529-015-2001-3

Zhang, Y.-L., Zhao, L.-W., Zhang, J., Le, R., Ji, S.-Y., Chen, C., Gao, Y., Li, D., Gao, S. and Fan, H.-Y. (2018). DCAF13 promotes pluripotency by negatively regulating SUV39H1 stability during early embryonic development. *EMBO J.* **37**, e98981. doi:10.15252/embj.201898981

Zhang, M., Bener, M. B., Jiang, Z., Wang, T., Esencan, E., Scott, R., III, Horvath, T. and Seli, E. (2019a). Mitofusin 1 is required for female fertility and to maintain ovarian follicular reserve. *Cell Death Dis.* **10**, 560. doi:10.1038/s41419-019-1799-3

Zhang, M., Bener, M. B., Jiang, Z., Wang, T., Esencan, E., Scott, R., Horvath, T. and Seli, E. (2019b). Mitofusin 2 plays a role in oocyte and follicle development, and is required to maintain ovarian follicular reserve during reproductive aging. *Aging (Albany NY)* **11**, 3919-3938. doi:10.18632/aging.102024

Zhang, C., Wang, M., Li, Y. and Zhang, Y. (2022). Profiling and functional characterization of maternal mRNA translation during mouse maternal-to-zygotic transition. *Sci. Adv.* **8**, eabj3967. doi:10.1126/sciadv.abj3967

Zhou, S., Guo, Y., Sun, H., Liu, L., Yao, L., Liu, C., He, Y., Cao, S., Zhou, C., Li, M. et al. (2021). Maternal RNF114-mediated target substrate degradation regulates zygotic genome activation in mouse embryos. *Development* **148**, dev199426. doi:10.1242/dev.199426

Zhu, L., Marjani, S. L. and Jiang, Z. (2021). The epigenetics of gametes and early embryos and potential long-range consequences in livestock species-filling in the picture with epigenomic analyses. *Front. Genet.* **12**, 557934. doi:10.3389/fgene.2021.557934

European Journal of Cell Biology 101 (2022) 151210

Contents lists available at ScienceDirect

European Journal of Cell Biology

journal homepage: www.elsevier.com/locate/ejcb

SGK1 is essential for meiotic resumption in mammalian oocytes

Edgar del Llano [a,*], Rajan Iyyappan [a], Daria Aleshkina [a], Tomas Masek [c], Michal Dvoran [a], Zongliang Jiang [b], Martin Pospisek [c], Michal Kubelka [a], Andrej Susor [a,*]

[a] Laboratory of Biochemistry and Molecular Biology of Germ Cells, Institute of Animal Physiology and Genetics, CAS, Libechov, Czech Republic
[b] School of Animal Sciences, AgCenter, Louisiana State University, Baton Rouge, LA 70803, United States
[c] Laboratory of RNA Biochemistry, Department of Genetics and Microbiology, Faculty of Science, Charles University, Viničná 5, Prague 128 44, Czech Republic

ARTICLE INFO

Keywords:
Oocyte
MPF
CDK1
SGK1
Meiosis
Nuclear envelope breakdown

ABSTRACT

In mammalian females, oocytes are stored in the ovary and meiosis is arrested at the diplotene stage of prophase I. When females reach puberty oocytes are selectively recruited in cycles to grow, overcome the meiotic arrest, complete the first meiotic division and become mature (ready for fertilization). At a molecular level, the master regulator of prophase I arrest and meiotic resumption is the maturation-promoting factor (MPF) complex, formed by the active form of cyclin dependent kinase 1 (CDK1) and Cyclin B1. However, we still do not have complete information regarding the factors implicated in MPF activation.

In this study we document that out of three mammalian serum-glucocorticoid kinase proteins (SGK1, SGK2, SGK3), mouse oocytes express only SGK1 with a phosphorylated (active) form dominantly localized in the nucleoplasm. Further, suppression of SGK1 activity in oocytes results in decreased CDK1 activation via the phosphatase cell division cycle 25B (CDC25B), consequently delaying or inhibiting nuclear envelope breakdown. Expression of exogenous constitutively active CDK1 can rescue the phenotype induced by SGK1 inhibition. These findings bring new insights into the molecular pathways acting upstream of MPF and a better understanding of meiotic resumption control by presenting a new key player SGK1 in mammalian oocytes.

1. Introduction

In women, oocyte quality is an essential factor for a successful fertilization, pregnancy and embryo development. Consequently, poor oocyte quality is one of the most common hindrances to natural and assisted reproduction (Homer, 2020; Keefe et al., 2015; Krisher, 2004). Unlike somatic cells, oocytes undergo a meiotic cell division instead of mitosis. Therefore, in order to tackle poor oocyte quality, a better understanding of the mechanisms orchestrating the oocyte meiotic divisions is needed. In mammals, oocyte formation and entry into meiosis occur during the early stages of development, meaning that mammalian females are born with a determined pool of oocytes in their ovaries. Interestingly, the reserve of oocytes in the ovaries are arrested at the diplotene stage of prophase of the first meiotic cell division (prophase I) (van den Hurk and Zhao, 2005). At this stage, also referred to as the germinal vesicle (GV) stage, the chromatin is still not fully condensed and the nuclear envelope is intact and visible. This arrest continues until the female reaches puberty. From that point onwards, oocytes are selected in cycles to develop further and ovulate, resuming their meiotic cell divisions and becoming able to be fertilized (Edson et al., 2009).

The maturation-promoting factor (MPF) complex is the master regulator of this release from the prophase I arrest and subsequent meiotic resumption. It is a heterodimer composed of Cyclin Dependent Kinase 1 (CDK1) and Cyclin B1 (Gautier et al., 1990; Sharma et al., 2018; Pan and Li, 2019). Up to date several other proteins have been identified as regulators of MPF activity during meiosis, mainly related to the inhibitory phosphosites of CDK1 (Thr14 and Tyr15) and the amount of Cyclin B1 in the cell. In order to activate MPF, Cyclin B1 levels increase during M phase and the above-mentioned residues must be dephosphorylated. The prophase I arrest is maintained by protein kinase A (PKA), which activates the WEE1 kinase (which phosphorylates Thr14 and Tyr15) and inactivates CDC25 (responsible for dephosphorylating these inhibitory sites). At the time of ovulation, a drop in cGMP levels allows PDE3A to reduce cAMP in the oocyte. With low cAMP, PKA becomes inactive which ultimately results in the activation of MPF (Tripathi et al., 2010). Active MPF triggers meiotic resumption and the release of oocytes from the prophase I block characterized by nuclear envelope breakdown (NEBD), chromosome condensation and the

* Corresponding authors.
E-mail addresses: llano@iapg.cas.cz (E. del Llano), susor@iapg.cas.cz (A. Susor).

https://doi.org/10.1016/j.ejcb.2022.151210
Received 14 December 2021; Received in revised form 21 February 2022; Accepted 22 February 2022
Available online 25 February 2022

subsequent first meiotic division (MI) (Norris et al., 2009; Sharma et al., 2018).

The Phosphoinositide 3-kinase/ Protein Kinase B (PI3K/AKT) pathway is also involved in meiotic resumption. In mammals, PI3K/AKT has been reported to be involved in Cyclin B1 expression and CDK1 activation (Roberts et al., 2002). Specifically, when AKT activity is suppressed in mouse oocytes, their meiotic resumption potential is significantly diminished (Kalous et al., 2006). Interestingly, in starfish oocytes Hiraoka et al. (2016a) observed that the PI3K/AKT pathway alone may not be enough to activate CDK1 and therefore other pathways should be involved. Later, the same group discovered that serum-glucocorticoid-regulated kinase (SGK) was indispensable for CDC25 phosphorylation and Myt1 inactivation (Hiraoka et al., 2019).

Until now, studies on SGK function in oocytes have been performed only on starfish (Hiraoka et al., 2019; Hosoda et al., 2019) leaving the role of SGKs in mammalian oocytes largely unknown. As SGK proteins are evolutionary conserved in mammals it is highly possible that they also have functional roles in higher animal species. In this study using the mouse model, we have shown for the first time the role of SGKs for the resumption of meiosis in mammalian oocytes.

Our results show that only SGK1 isoform is expressed in fully grown oocytes. Moreover, we demonstrate that SGK1 inhibition delays NEBD via negative influence of CDK1 activation. Our findings strengthen the hypothesis that SGK (SGK1 in mammals) is essential for MPF activation and oocyte meiotic resumption.

2. Results

2.1. Of the SGK genes only SGK1 is expressed in the mouse oocyte and its inhibition hinders nuclear envelope breakdown

In mammals, there are three genes coding for different SGK proteins: SGK1, SGK2 and SGK3. Although all proteins have a very similar structure, they differ in specific regions and their expression are dynamic throughout various tissues (Bruhn et al., 2010; Kobayashi et al., 1999; Lang and Cohen, 2001). To determine which SGKs are expressed in the mammalian oocyte, we first performed RT-PCR to verify the presence or absence of their respective mRNAs. The results showed that mRNAs coding for all SGKs are present in the mouse kidney and brain while ovaries and oocytes contain only *Sgk1* and *Sgk3* (Fig. S1A, B). Furthermore, we performed Western Blot (WB) to detect SGK protein expression in mouse oocytes. As expected, all SGK proteins were expressed in the mouse kidney while ovaries expressed SGK1 and SGK3. Interestingly, despite the presence of both *Sgk1* and *Sgk3* mRNAs in oocytes, only the SGK1 protein was expressed at similar levels throughout all oocyte maturation stages (Fig. 1A). Furthermore, polysomal datasets showed that *Sgk1* mRNA has the highest translation in the GV oocyte (Fig. S1C) while mRNA coding for SGK3 is absent. However, SGK3 translation was significantly increased in the 2 cell embryo (Fig. S1C).

The detection of SGK1 indicated its potential role in the oocyte. To unveil this role, we treated GV oocytes with a specific SGK1 inhibitor

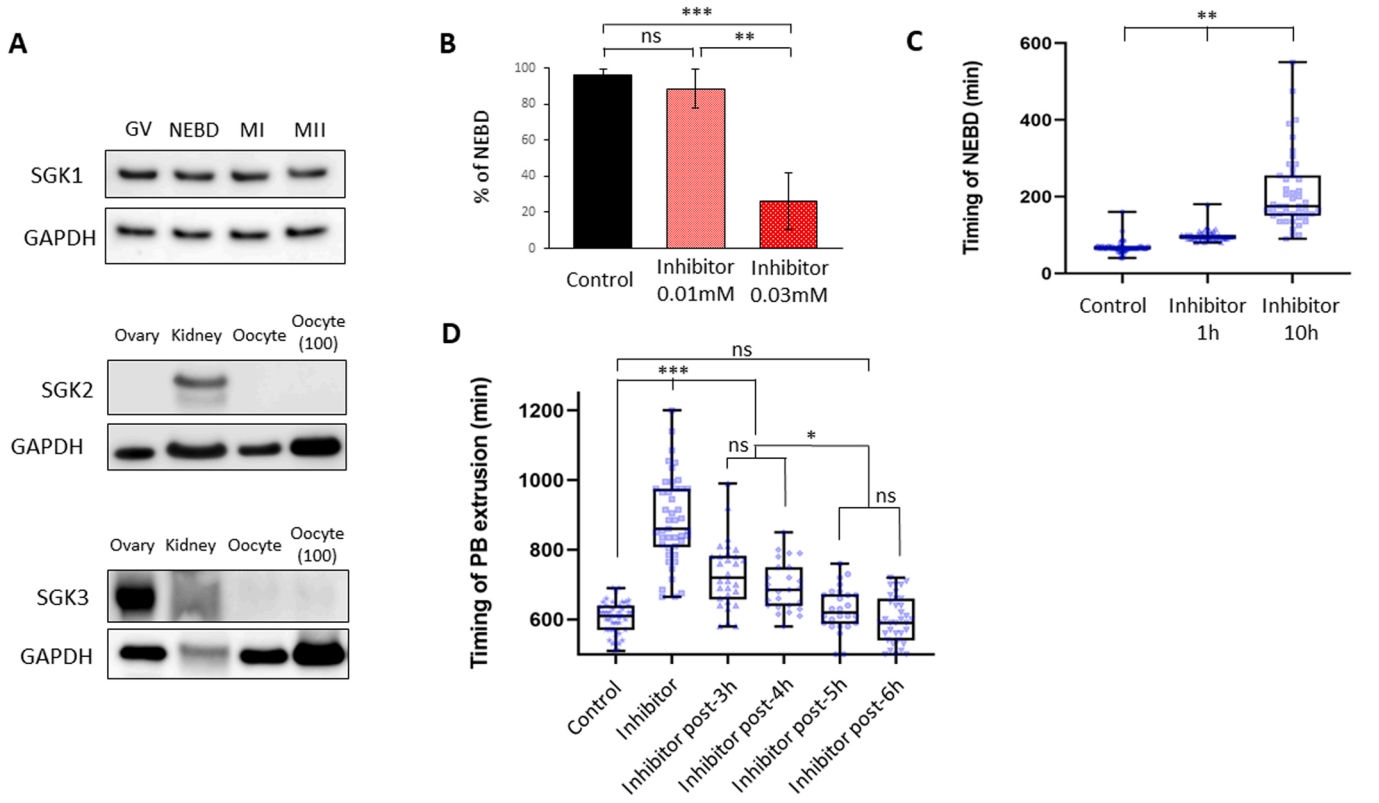

Fig. 1. Of the SGK genes only SGK1 is expressed in the mouse oocyte and its inhibition hinders nuclear envelope breakdown. A) WB analysis of the expression of the three SGK proteins in oocytes (30 or 100 per sample) and control tissue; GAPDH was used as loading control. The images are representative from at least three biological replicates. For mRNA expression see Fig. S1. B) Quantification of oocytes undergoing nuclear envelope breakdown (NEBD) in the control (0.06% vehicle, DMSO) and presence of SGK1 inhibitor (GSK-650394). Data are represented as the mean ± SEM of at least three independent experiments; n ≥ 44 oocytes; ns, not significant; *** $p < 0.001$; ** $p < 0.01$ according to One-way ANOVA after arcsine transformation. For inhibitor validation see Fig. S2. C) Timing of oocyte NEBD after IBMX wash in absence (Control, 0.06% vehicle DMSO) or presence of SGK1 inhibitor (0.01 mM) for 10 h and 1 h. Box plot displays mean, 25th and 75th percentile and ± SD of at least three independent experiments; n ≥ 45 oocytes; ns, not significant; ** $p < 0.01$ according One-way ANOVA. D) Timing of oocyte cytokinesis (polar body extrusion) in absence (control, 0.06% vehicle DMSO) or presence of SGK1 inhibitor (0.01 mM) added at different time points post-IBMX wash. Box plot displays mean, 25th and 75th percentile and ± SD of at least three independent experiments; n ≥ 26 oocytes; ns, not significant; * $p < 0.05$; *** $p < 0.001$; according One-way ANOVA.

(GSK-650394, Merck, Darmstadt, Germany; Sherk et al., 2008) which restricts SGK1 activity (and SGK2 with less affinity) and has been already used in several fields of research (Berdel et al., 2014; Bomberger et al., 2014; Xiao et al., 2019). We applied concentrations of 0.01 mM and 0.03 mM of SKG1 inhibitor based on previously published results to keep cells viable for 48 h (Alamares-Sapuay et al., 2013). Initially, we validated the effect of the SGK1 inhibitor on oocytes by checking the phosphorylation status of the known SGK1 substrate NDRG1 (Thr346) (Murray et al., 2004). The results confirmed that the inhibitor treatment suppressed SGK1 activity, as phosphorylation of NDRG was significantly reduced (Figure S2). When SGK1 was inhibited, 88% of oocytes treated with 0.01 mM concentration underwent nuclear envelope breakdown (NEBD), which was similar as the control group, however, when treated with the 0.03 mM concentration, only 26% of oocytes underwent NEBD (Fig. 1B). Nonetheless, although most of the oocytes from the 0.01 mM group underwent NEBD, there was a significant delay compared to the control oocytes (211 ± 98 min and 67 ± 15 min, respectively) (Fig. 1C). To analyse the reversibility of the SGK1 inhibitor, oocytes were cultured in the presence of the inhibitor (0.01 mM) for one hour and then released. Those oocytes were able to undergo NEBD in 97 ± 14 min, that is, 30 min later than the control.

Moreover, we noticed a significant delay in polar body extrusion (PBE) when SGK1 was inhibited (Fig. 1D). To determine if this effect is due to the reported NEBD delay itself or whether SGK1 inhibition affects further meiotic stages, we introduced the SGK1 inhibitor at different time points during meiosis. The results show that SGK1 inhibition has a delaying effect on PB extrusion when oocytes were treated with the inhibitor up to four hours after IBMX removal (Fig. 1D). However, the timing of PBE was not affected when SGK1 was inhibited later (Fig. 1D).

In conclusion, our results show that only one member of the SGKs family (SGK1) is expressed in mouse oocytes and also suggest a role in the regulation of NEBD and PBE up to the first 4 h after meiotic resumption.

2.2. *The active form of SGK1 is concentrated in the oocyte nucleus and its expression decreases along the first meiotic division*

SGK1 becomes active when phosphorylated at Thr256 (Kobayashi and Cohen, 1999; Chen et al., 2009). To better understand the role of SGK1 in the mammalian oocyte we further focused on the localization of its active form by immunocytochemistry (ICC) at different meiotic stages. We found that SGK1 (Thr256) is dominantly localized in the nucleus of the GV oocyte and at the subsequently newly forming spindle (Fig. 2A and B). Similarly, the highest SGK1 phosphorylation levels were detected in the GV oocyte with a continuous significant decrease during meiotic progression to minimum in the MII stage (Fig. 2A and B). These results are in accordance with the previous live cell experiments, which show that SGK1 inhibition has its strongest effect on meiotic GV-NEBD transition (Fig. 1C and D).

2.3. *Inhibition of SGK1 impairs CDK1 activation through CDC25B (Cell Division Cycle 25B) phosphatase in the oocyte prior to NEBD*

The delay of NEBD caused by SGK1 inhibition pointed towards a possible effect of SGK1 on the master regulator of meiosis, CDK1. To test this hypothesis, we performed WB experiments to detect the inactive

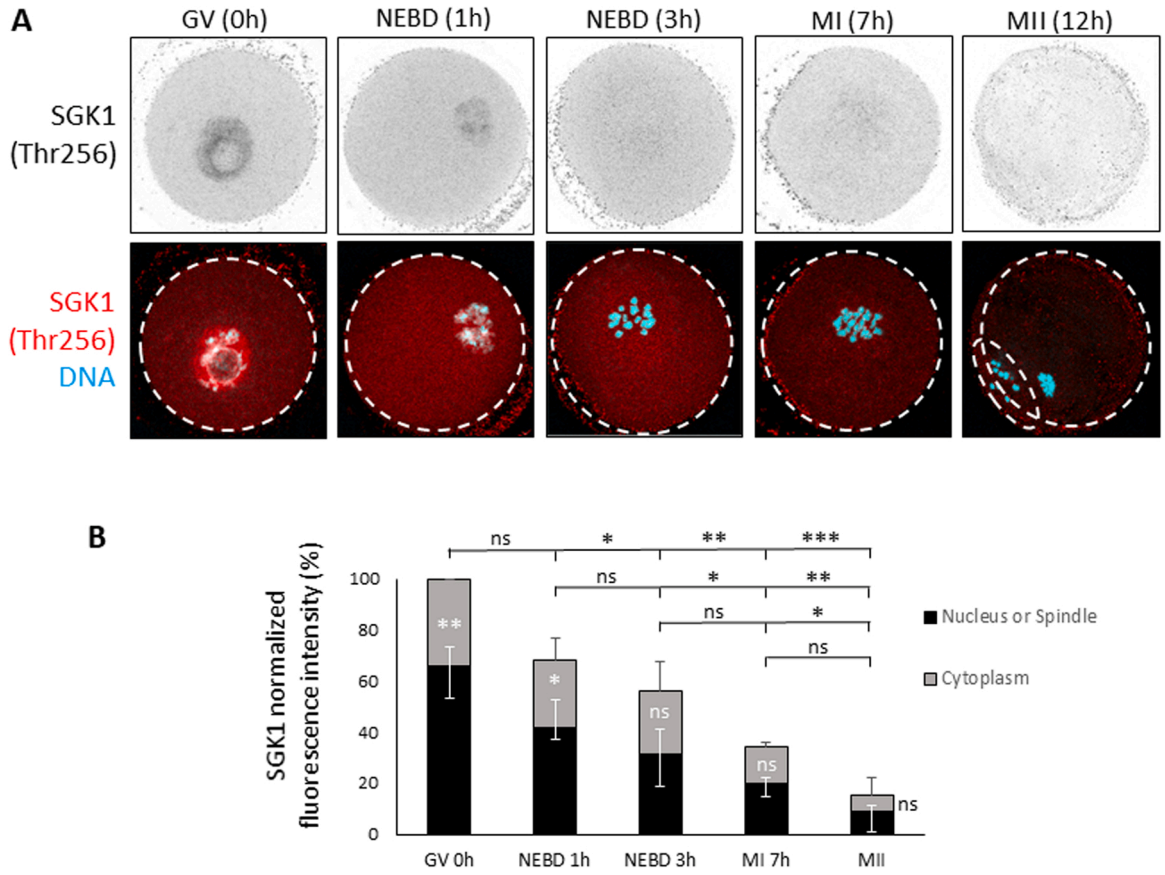

Fig. 2. Active SGK1 is concentrated in the oocyte nucleus and its expression decreases along the first meiotic division. A) Immunocytochemistry shows dominant localization of SGK1 phosphorylated at Thr256 in the oocyte nucleus (grey and red). DAPI (blue), scale bar 15 μm. B) Quantification of SGK1 (Thr256) fluorescence at different oocyte areas and stages of meiosis. Data are represented as the mean ± SEM of at least three independent experiments normalized to the group with highest intensity (GV) as 100% fluorescence; n ≥ 40 oocytes; ns, not significant; * $p < 0.05$; ** $p < 0.01$; *** $p < 0.001$ according to One-way ANOVA for comparing oocyte stages and Student's t test for comparing oocyte areas.

form of CDK1 (Tyr15) in oocytes in absence (control, DMSO 0.02%) or presence of SGK1 inhibitor (0.01 mM) at different time points after an IBMX wash (0, 30 and 60 min) (Fig. 3A and B). It is well known that the phosphorylation of CDK1 at Tyr15 must be removed to activate the kinase in order to resume meiosis (Coleman and Dunphy, 1994; Schmidt et al., 2017). The GV arrested oocyte group (0 min) was incubated for one hour in the presence of IBMX and treated with SGK1 inhibitor (or DMSO). Both groups showed maximal levels of CDK1 (Tyr15) as expected without any major differences. However, after 30 min post IBMX wash, inactive CDK1 levels (phosphorylated on Tyr 15) significantly decreased in non-treated oocytes while oocytes in SGK1 inhibitor continued to show high levels. After one hour, the differences were even more pronounced between the two groups, as non-treated oocytes were already at the NEBD stage and treated oocytes were still at the GV stage (Fig. 3A and B).

As SGK1 is a protein kinase and CDK1 activation occurs through dephosphorylation (of Thr14 and Tyr15), we hypothesised that it must act through other proteins. Based on the literatures (Cazales et al., 2005; Pirino et al., 2009; Hiraoka et al., 2016b) and our *in silico* prediction interaction (Supplementary Table 1) the phosphatase CDC25B (which is known to dephosphorylate CDK1 on Tyr 15) proved to be a potential candidate as an SGK1 substrate. Therefore, we conducted a similar WB analysis to detect the activation of CDC25B phosphatase. The obtained results were in positive correlation with the previously detected activity of CDK1 (Fig. 3A and B). Arrested GV oocytes (0 min) showed no difference between the control and SGK1 inhibition with regards to the level of total CDC25B nor to its phosphorylation state (represented by two shifted bands) (Fig. 3C and D). However, when the oocytes were released from the IBMX block, differences became apparent. After 30 min, the lower band of control oocytes was fainter in comparison with SGK1 inhibited oocytes, indicating the activation of CDC25B. This shift was even more profound at 45 min after meiotic resumption, when a new higher band (representing the hyperphosphorylated CDC25B) appeared in control oocytes, while the lowest (hypophosphorylated) band disappeared. On the other hand, the oocytes cultured in the presence of SGK1 inhibitor still showed the presence of the lower hypophosphorylated band without any apparent hyperphosphorylated band visible (Fig. 3C and D).

These results indicate that SGK1 plays a regulatory role in CDK1 activation and meiotic resumption upstream of CDC25B, and that CDC25B may in fact be its direct substrate.

2.4. The phenotype resulting from SGK1 inhibition can be reversed by activation of CDK1

Based on the above presented data which show that activation of CDK1 by SGK1 inhibition is negatively influenced (Fig. 3A and B) and that CDK1 activation is a key event for the timing and promoting of NEBD (Koncicka et al., 2018), we sought to confirm that the SGK1 effect in oocytes is upstream of CDK1 activation. To that end, we microinjected oocytes with mRNA coding for CDK1-AF, a constitutively active CDK1 which cannot be phosphorylated on Tyr15 or Thr14 and therefore, allows oocytes to overcome meiotic arrest even in the presence of IBMX (Fig. 4A) (Adhikari et al., 2016; Akaike and Chibazakura, 2020; Hagting et al., 1998). WB of injected oocytes confirmed that the CDK1 protein was overexpressed compared to non-injected controls (Figure S3). First we expressed CDK1-AF in oocytes by microinjecting RNA coding for CDK1-AF + H2B-GFP in the presence of a higher concentration of SGK1 inhibitor (0.03 mM) as seen in Fig. 1B. The meiotically arrested phenotype caused by SGK1 inhibition was successfully overcome after CDK1-AF overexpression as 83% (± 0.35) of these oocytes went through NEBD compared to only 27% (± 0.75) of control oocytes (microinjected with RNA coding for H2B-GFP) (Fig. 4A).

Next, we performed experiments with a smaller concentration of SGK1 inhibitor (0.01 mM), which caused oocyte meiotic resumption delay (Fig. 1C). For this experiment, one group of oocytes was microinjected with *H2b-gfp* RNA as a negative control and was cultivated in the presence of SGK1 inhibitor. The other two groups were microinjected with *Cdk1-AF* + *H2b-gfp* RNA; one group was cultivated in the presence of a solvent vehicle (0.02% DMSO) and another group in the presence of SGK1 inhibitor. All oocyte groups were arrested at the NEBD stage for 4 h in the presence of IBMX after microinjection. After IBMX

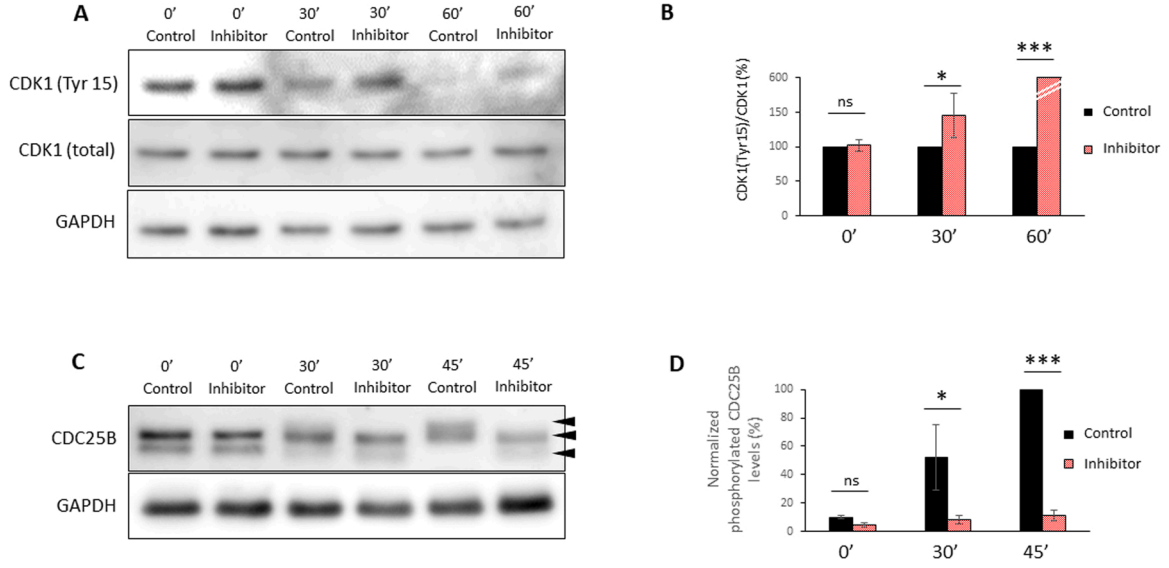

Fig. 3. Inhibition of SGK1 impairs CDK1 activation through CDC25B in the oocyte prior to NEBD. A) WB analysis of CDK1 (Tyr 15) at different timing of oocyte meiotic resumption in absence (control, 0.02% vehicle DMSO) and presence of SGK1 inhibitor (GSK-650394; 0.01 mM). GAPDH and CDK1 (total) were used as a loading control. The images are representative from at least three biological replicates of 30 oocytes per sample. B) WB quantification of CDK1 (Tyr15) normalized to CDK1 (total). Data are represented as the mean ± SEM from at least three independent experiments; n = 30 oocytes per sample; ns, not significant, * $p < 0.05$, *** $p < 0.001$ according to Student's t test. C) WB analysis of CDC25B at different timing of oocyte meiotic resumption in absence (control, 0.02% vehicle DMSO) and presence of SGK1 inhibitor (0.01 mM). GAPDH was used as a loading control. The images are representative from at least three biological replicates of 30 oocytes per sample. The arrowheads depict phosphorylated variants of CDC25B. D) WB quantification of CDC25B protein normalized to GAPDH. Data are represented as the mean ± SEM from at least three independent experiments; 30 oocytes per sample; ns = not significant, * $p < 0.05$, *** $p < 0.001$ according to Student's t test.

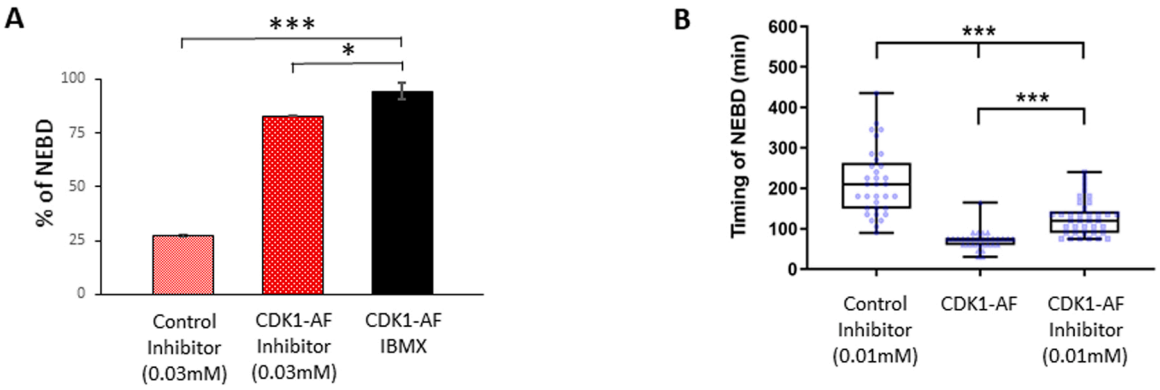

Fig. 4. The phenotype resulting from SGK1 inhibition can be reversed by activation of CDK1. A) Quantification of oocytes undergoing NEBD after microinjection with RNA coding for *H2b-gfp* RNA (control) in the presence of SGK1 inhibitor or microinjected with RNA coding for H2B-GFP + CDK1-AF RNA in the presence of SGK1 inhibitor or IBMX. Data are represented as mean ± SEM of at least three independent experiments; n = 39 oocytes per group; ns, not significant, * $p < 0.05$, *** $p < 0.001$ according to One-way ANOVA. B) Timing of NEBD after IBMX wash in oocytes microinjected with H2B-GFP RNA (control) in the presence of inhibitor or microinjected with H2B-GFP+CDK1-AF RNA in absence and presence of SGK1 inhibitor. Box plot displays mean, 25th and 75th percentile and ± SD of at least three independent experiments; n ≥ 30 oocytes per group; ns, not significant; *** $p < 0.001$ according to One-way ANOVA.

release, oocytes without expression of the constitutively active form of CDK1 showed a significant NEBD delay (214 ± 15 min) similarly as seen in Fig. 1C. On the other hand, oocytes expressing CDK1-AF underwent NEBD significantly faster (127 ± 8 min) even in the presence of SGK1 inhibition (Fig.4B). Altogether, these results suggest a role of SGK1 in the regulation of NEBD in mammalian oocytes by influencing the regulatory pathway involved in CDK1 activation.

3. Discussion

Oocyte meiotic arrest and timely resumption are fundamental steps in mammalian meiosis. After much research, MPF has been accepted as a master regulator of such events. However, so far only a few key elements have been identified and described in detail as being involved in the MPF pathway (Edson et al., 2009, 2019). Data of the present study suggest SGK1 as a new player in mammalian oocyte meiotic resumption which is of great importance for the better understanding of the regulation of meiosis.

Up to now, no SGK protein has ever been linked to the process of meiosis (Bruhn et al., 2010; Lien et al., 2017; Di Cristofano, 2017). Only the recent studies by Hiraoka et al. (2019) have demonstrated that SGK protein was needed to overcome prophase I arrest at the GV stage in starfish oocytes (*Asterina pectinifera*). According to their work, SGK phosphorylates and activates CDC25, which in turn leads to the activation of MPF (cyclinB-CDK1) so the oocyte can proceed through the G2/M phase and continue meiosis. However, there are no reports on the matter outside of the starfish and, despite its advantages to study early reproduction, it is evolutionary far from vertebrates including humans. Therefore, our study provides much-needed information by focusing on the SGK role in mammals using the mouse model (*Mus musculus*).

Compared to the starfish whose genome codes for a single SGK protein, the mouse genome contains three different genes coding for three known SGK isoforms (SGK1, SGK2 and SGK3). These proteins share a sequence identity of 80% in their catalytic domain but only SGK3 contains an N-terminal phosphoinositide-binding Phox homology (PX) domain (Bruhn et al., 2010; Kobayashi et al., 1999; Lang and Cohen, 2001). Interestingly, despite their high similarity, SGKs have different tissue expression: SGK1 and SGK3 seem to be found in all tissues but tightly regulated, whereas SGK2 expression is dominant in the liver, pancreas, brain and kidney (Kobayashi et al., 1999). Accordingly, our results document the presence of *Sgk1* and *Sgk3* mRNAs in both ovaries and oocytes. However, despite both SGK1 and SGK3 proteins being expressed in mouse ovaries, we detected only the SGK1 in mouse oocytes. These results correlate with previously published oocyte translatome data (del Llano et al., 2020; Masek et al., 2020). Importantly, *Sgk3* mRNA is absent from oocyte polysomes but it starts to have a stronger polysomal presence after fertilization (Masek et al., 2020; Potireddy et al., 2006) and Figure S1C concomitantly with its transcription (Zeng et al., 2004). This suggests SGK1 as the sole isoform present in mouse oocytes and functioning in meiosis regulation while SGK3 is become translated after fertilization.

Hiraoka et al. (2019) speculated that SGK3 could be involved in mammalian oocyte meiosis based on the fact that it is the isoform most related to starfish SGK as both contain the N-terminal PX domain. In their experiments SGK was knocked-down from starfish oocytes causing a perpetually arrested GV phenotype which was later successfully reversed by exogenously expressing human SGK3. However, our findings suggest that SGK1 and not SGK3 is present in mouse oocytes. This seeming contradiction might be explained by the fact that only the catalytic domain may have a role in oocyte meiosis from both starfish and mammals, whereas the N-terminal PX domain would be irrelevant. This indicates that both SGK1 and SGK3 with 80% similarity of the catalytic domain can phosphorylate similar targets (Kobayashi et al., 1999; Bruhn et al., 2010). Therefore, it would be interesting to repeat Hiraoka et al. (2019) rescue experiments expressing human SGK1 or SGK2 instead of SGK3 and analyse the effect on oocyte meiosis. This could prove the conclusion that the N-terminal PX domain is not necessary for oocyte meiotic resumption.

To investigate the potential role of SGK1 in the fully grown mammalian GV oocyte, we decided to perform several experiments using a selective SGK1 inhibitor (GSK-650394). The inhibitor concentrations of 0.01 mM and 0.03 mM were selected according to a previously published study reporting them as being able to keep cells viable for 48 h (Alamares-Sapuay et al., 2013). Surprisingly, our results after SGK1 inhibition at 0.03 mM were similar to those obtained by Hiraoka et al. (2019): meiotic resumption (G2/M transition) was suppressed and most oocytes did not continue through NEBD. In other words, selective SGK1 inhibition in mammalian oocytes had a similar effect as inhibition of SGK in starfish oocytes. Our results reinforce the essential role of SGK in meiotic resumption in both starfish and mouse oocytes. Moreover, smaller amounts of SGK1 inhibitor (0.01 mM) allowed oocytes to go through NEBD but at a much slower pace, pointing out that even small amounts of SGK1 can phosphorylate the necessary levels of G2/M transition key players if given enough time. The inhibitory effect was fully reversible for both concentrations as removing the inhibitor from the media allowed the oocytes to reach the MII stage. It is also noteworthy to mention that in our previous research we showed that these oocytes which underwent the first meiotic division in the presence of the

inhibitor at 0.01 mM suffered from significantly abnormal cytokinesis (del Llano et al., 2020). Whether these abnormalities are the result of SGK1 acting on the oocyte spindle itself or the result of a delayed meiotic resumption is not clear and needs further investigation, however, the new results presented here point towards the latter possibility.

Furthermore, we were able to uncover the time window of action of SGK1 in meiotic resumption thanks to the slower meiotic division caused by SGK1 inhibitor (0.01 mM). By adding inhibitor at different time points and following the timing of PB extrusion we concluded that SGK1 activity is necessary up to 4 h after meiotic resumption. Nonetheless, its role is most relevant at the beginning of the resumption of meiosis.

At the molecular level, we found that the cause of meiotic arrest (or delay) in GV oocytes treated with SGK1 inhibitor was caused by a failure in MPF activation, more specifically by impeding the removal of the inhibitory Tyr15 phosphorylation of CDK1. However, as a protein kinase, SGK1 cannot act directly to dephosphorylate CDK1. To that end, we further investigated and proved that SGK1 inhibition also had an effect on CDC25B activation, the upstream phosphatase of CDK1 at Tyr15 (Cazales et al., 2005; Pirino et al., 2009; Hiraoka et al., 2016b). This also positively correlated with the data on SGK in starfish oocytes, where it was proven that SGK inhibition blocked meiotic resumption by preventing the activation of CDC25 and therefore MPF remained inactive (Hiraoka et al., 2019). Surprisingly, we observed that fully-grown GV oocytes already displayed high levels of active SGK1 (phosphorylated at Thr256). At this stage, the activator phosphosites of CDC25B are not yet phosphorylated and it is not until oocytes are released from a high cAMP environment that they are ''allowed'' to be phosphorylated (Coleman and Dunphy, 1994; Norris et al., 2009). The fact that SGK1 is active already in the GV oocyte might seem contradictory at first glance as it could be able to keep CDC25B phosphorylated and active the whole time. However, we also noticed that at that stage SGK1 (Thr256) is strongly localized in the nucleus, while CDC25B is known to remain in the cytoplasm before meiotic resumption and it is not until PKA is inhibited (by low cAMP levels) that CDC25B is quickly translocated to the oocyte nucleus right before NEBD (Lincoln et al., 2002; Solc et al., 2008; Ferencova et al.,). Therefore, we hypothesize that SGK1 (Thr256) is active but restricted to the nucleus, which keeps it physically apart from CDC25B, which would further activate it. When cAMP levels decline CDC25B translocates to the nucleus, where SGK1 (Thr256) could phosphorylate and activate it, allowing the further dephosphorylation of CDK1 inhibitory sites. This makes MPF active and capable to induce meiosis resumption (Fig. 5). Our hypothesis can be further strengthened by the fact that SGK1 and CDC25B display a high degree of interaction potential according to the online software PSOPIA. However, it must be taken into account that the evidence presented here together with the published data on starfish oocytes, are indirect and need to be addressed more specifically to be fully proven. Otherwise, despite the clear relation between SGK1 and CDC25B in oocytes, it is not possible to exclude the possibility that they do not interact directly but that there is a longer pathway, which connects them both through other proteins.

Furthermore, it is important to note that research groups studying SGK1 in kidneys reported that mouse homozygous knockouts for SGK1 are subfertile (Fejes-Tóth et al., 2008; Faresse et al., 2012). On one hand, this highlights the potential importance of this protein in female reproductive cells, adding support to our data. On the other hand, however, it is not possible to exclude that the effect on litter size was due to SGK1 absence affecting other reproductive tissues (testes, ovary, uterus, etc.) as the mice were full KO.

In summary, we present evidence that SGK1 has an important and previously unknown role in mammalian meiosis, specifically for the process of meiotic resumption. We suggest SGK1 acts through the phosphorylation of CDC25B, which ultimately leads to MPF activation. This role might be extrapolated to other species as it seems to be evolutionary conserved between the mouse and starfish. This research contributes to further understanding of the pathways controlling MPF, the master regulator of oocyte meiotic resumption.

4. Material and methods

4.1. Oocyte collection and culture

ICR mice (bred in-house) were injected 46 h prior to oocyte collection to be primed with 5 IU pregnant mare serum gonadothropin (PMSG HOR 272, ProSpec, Rehovot, Israel). All oocytes were collected at the GV stage from the mice ovaries in the presence of transfer media

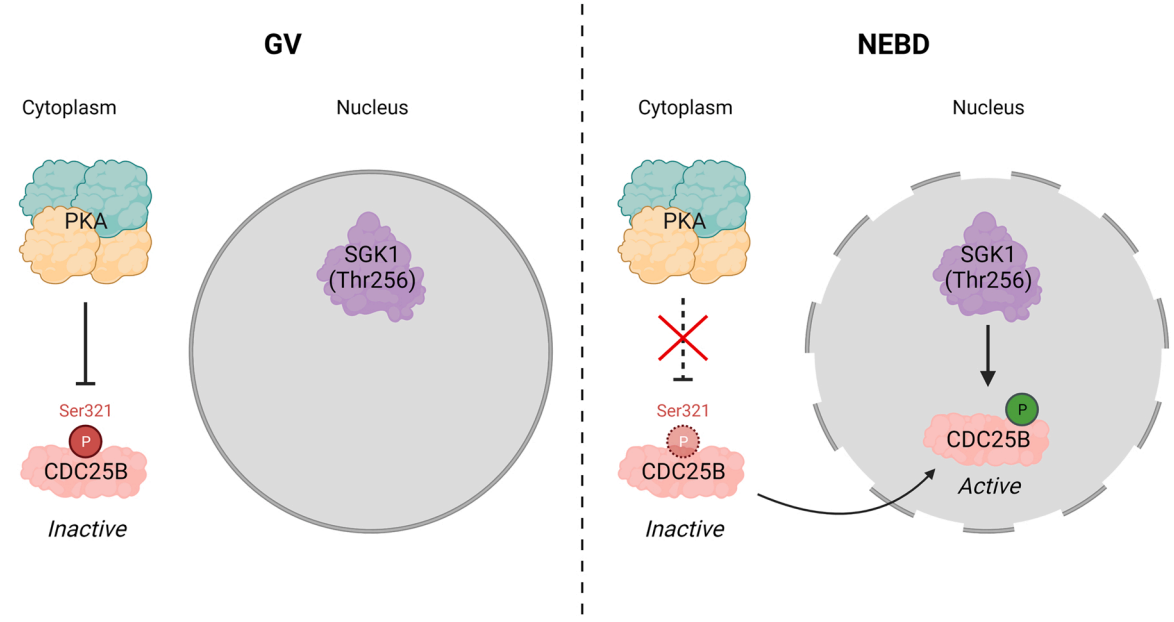

Fig. 5. Hypothesis of role of the SGK1 in the resumption of meiosis. At the GV stage, SGK1 (Thr256) is active enclosed in the oocyte nucleus without effect on meiotic resumption. PKA is active when cAMP levels are high, phosphorylating CDC25B (Ser321), inhibiting this phosphatase and keeping it in the cytoplasm. Prior to nuclear envelope breakdown (NEBD), cAMP levels decline, PKA becomes inactive and CDC25B is dephosphorylated. Consequently, CDC25B localize to the nucleus where active SGK1 (Thr256) phosphorylate the activation sites of CDC25B, and thus promote the NEBD process.

supplemented with 100 μM 3-isobutyl-1-methylxanthine (IBMX, Sigma-Aldrich, Darmstadt, Germany) to block meiotic resumption (as described in Tetkova and Hancova, 2016). From the GV collected oocytes, only the fully grown were selected, denuded by pipetting and transferred to M16 media (Sigma-Aldrich, Darmstadt, Germany) with IBMX at 37 °C, 5% CO2. For oocyte samples at further advanced meiotic stages than GV, the oocytes were placed in M16 media (Sigma-Aldrich, Darmstadt, Germany) at 37 °C, 5% CO2 without IBMX. For SGK1 inhibitor treatments, the oocytes were transferred in M16 media (without IBMX) supplemented with 0.02% or 0.06% Dimethyl Sulphoxide (DMSO) for solvent vehicle control or 0.01 mM or 0.03 mM GSK-650394 (Merck, Darmstadt, Germany) inhibitor.

All animal work was conducted according to Act No 246/1992 for the protection of animals against cruelty; from 25.09.2014 no. CZ02389, issued by Ministry of Agriculture.

4.2. Live cell imaging

Oocytes were transferred from M16 media to a 4-well culture chamber (Sarstedt, Prague, Czech Republic) in 15 μl of M16 covered with mineral oil (M8410; Sigma-Aldrich) so they could be cultivated further under an inverted microscope Leica DMI 6000B (Leica Microsystems, Wetzlar, Germany) under the same culture conditions (Tempcontroller 2000–2 Pecon, and a CO2 controller, Pecon, Erbach, Germany) and monitored live. The live cell time lapse images were taken using LAS X software (Leica microsystems, Wetzlar, Germany) every 5 and 15 min.

4.3. RNA isolation and RT-PCR

RNA was extracted from oocytes using RNeasy Plus Micro kit (74034, Qiagen, Hilden, Germany) which includes a step for genomic DNA depletion using gDNA Eliminator columns. Afterwards, RT-PCR was performed using a qPCRBIO cDNA synthesis kit (PCR BIOSYSTEMS, London, UK). For regular PCR the PPP Mastermix kit (Top-Bio, Vestec, Czech Republic) was used. Primer sequences are listed in Table S2A.

4.4. Immunoblotting

Oocyte samples were lysed using 10 ul 1x Reducing SDS Loading Buffer (lithium dodecyl sulphate sample buffer NP 0007 and reduction buffer NP 0004 [Thermo Fisher Scientific, Waltham, MA, USA]) and heated at 100 °C for 5 min. Separation of proteins was carried out in gradient precast 4–12% SDS–PAGE gels (NP 0323, Thermo Fisher Scientific) and transferred onto an Immobilon P membrane (IPVD 00010, Millipore, Merck group, Darmstadt, Germany) using a semidry blotting system (Biometra GmbH, Analytik Jena, Jena, Germany) for 25 min at 5 mA per cm^{-2}. Blocking was done using 5% skimmed milk dissolved in 0.05% Tween-Tris buffer saline (TTBS) with pH 7.4 for 1 h. The membranes were then briefly washed with TTBS and incubated with 1% milk/TTBS diluted primary antibodies (see Table S2B) at 4 °C O/N. Secondary antibodies, Peroxidase Anti-Rabbit Donkey and Peroxidase Anti-Mouse Donkey (711–035–152 and 715–035–151, Jackson ImmunoResearch, West Grove, PA, USA) were diluted 1:7500 in 1% milk/TTBS. Membranes were incubated with secondary antibodies for 1 h at room temperature. Proteins were visualised by chemiluminescence using ECL (Amersham) and imaged on Azure 600 Imager (Azure Biosystems) and acquired signals were quantified using ImageJ (http://rsbweb.nih.gov/ij/).

4.5. Immunocytochemistry

Oocytes were fixed in 4% paraformaldehyde (PFA, Alfa Aesar, Thermo Fisher Scientific, Waltham, MA, USA) in PBS/PVA and left for 15 min followed by permeabilization in 0.1% Triton (X-100, Sigma-Aldrich) PBS/PVA for 10 min. The oocytes were then washed in PBS/PVA and incubated with primary antibodies (see Table S2B) at 4 °C O/N. The next day, two washes in PBS/PVA were applied followed by incubation with the corresponding secondary antibody and conjugation with Alexa Fluor 488 or 647 (Invitrogen, Carlsbad, CA, USA) for 1 h at room temperature protected from light. Next, the oocytes were washed in PBS/PVA twice and mounted on glass slides using ProLong™ Gold antifade reagent with DAPI (Invitrogen, Carlsbad, CA, USA). Images of samples were taken with a Leica SP5 inverted confocal microscope (Leica Microsystems, Wetzlar, Germany). Images were assembled in software LAS X (Leica Microsystems) and signal intensity from the spindle area was quantified with ImageJ.

4.6. RNA synthesis and microinjection

Cdk1-AF and *H2b:gfp* RNAs were in vitro transcribed by using the correspondent plasmid templates (Cdk1-AF: pcDNA3-CDC2-AF (718) was a gift from Jonathon Pines (Addgene plasmid # 39872; http://n2t.net/addgene:39872; RRID: Addgene 39872); H2B-GFP: provided by Dr Martin Anger, Laboratory of Cell Division Control, IAPG CAS) and mMESSAGE mMACHINE™ Transcription Kit (Invitrogen, Carlsbad, CA, USA). In vitro transcribed RNA was then injected into GV oocytes at a final concentration of 50 ng/μl in the presence of transfer media and IBMX. Microinjection of GV oocytes was performed using FemtoJet (Eppendorf) and TransferMan NK2 (Eppendorf, Hamburg, Germany) using an inverted microscope Leica DMI 6000B (Leica Microsystems, Wetzlar, Germany). Afterwards, injected oocytes in IBMX were incubated at 37 °C, 5% CO2 for 6 h to give them enough time to translate the injected RNAs.

4.6.1. Polysome fractionation and RNA sequencing

Polysome fractionation followed by RNA isolation was carried out according to the Scarce Sample Polysome profiling (SSP-profiling) method from Masek et al. (2020). Then, polysomal fractions (P; fractions 6–10) were pooled and subjected to qRT-PCR (QuantStudio 3 cycler, Applied Biosystems). Sequencing libraries were prepared using SMART-seq v4 ultra low input RNA kit (Takara Bio). Sequencing was performed with HiSeq 2500 (Illumina) as 150-bp paired-ends. Reads were trimmed using Trim Galore v0.4.1 and mapped onto the mouse GRCm38 genome assembly using Hisat2 v2.0.5. Gene expression was quantified as fragments per kilobase per million (FPKM) values in Seqmonk v1.40.0.

4.7. Statistical Analysis

Data are mean ± standard error of mean (SEM) of (n) replicates. All percentage data are first subjected to arcsine squire-root transformation and then subjected to statistical analysis. Data were analyzed either by Student's t- test or One-way ANOVA using GraphPad Prism Software (San Diego, California, USA) with post-hoc analyses with a 95% confidence interval. * $p < 0.05$, ** $p < 0.01$, *** $p < 0.001$ considered as statistically significant.

Funding

This research was funded by MSMT (EXCELLENCECZ.02.1.01/0.0/0.0/15_003/0000460 OP RDE), GACR (19–1349S) and by Institutional Research Concept VO67985904. ZJ was supported by the NIH (R01HD102533) and USDA-AFRI-NIFA (2019–67016–29863). The funders had no role in study design, data collection and analysis, decision to publish or preparation of the manuscript.

Ethics statement

All animal work was conducted according to Act No 246/1992 for the protection of animals against cruelty; from 25.09.2014 no. CZ02389, issued by the Ministry of Agriculture.

CRediT authorship contribution statement

EDL and AS designed the experiments. EDL, AS and MK drafted and revised the manuscript. EDL was involved in all experiments and performed most of them. RY and DA performed oocyte microinjections. RY, MD, TM and MP prepared samples and polysomal fractions. ZJ sequences and analysed polysome bound RNA. AS and MK supervised the study.

Data Availability

No data was used for the research described in the article.

Acknowledgments

The authors acknowledge Marketa Hancova and Jaroslava Supolikova (Institute of Animal Physiology and Genetics, Libechov, Czech Republic) for their valuable help in collecting oocyte samples. Jaroslava Supolikova was also important in performing Western Blots. The plasmid containing Cdk1-AF (pcDNA3-cdc2-AF (718)) was a gift from Jonathon Pines (Addgene plasmid # 39872; http://n2t.net/addgene:39872; RRID: Addgene_39872) and H2b:gfp was provided by Dr. Martin Anger (Laboratory of Cell Division Control, IAPG CAS).

Appendix A. Supporting information

Supplementary data associated with this article can be found in the online version at doi:10.1016/j.ejcb.2022.151210.

References

Adhikari, D., Busayavalasa, K., Zhang, J., Hu, M., Risal, S., Bayazit, M.B., Singh, M., Diril, M.K., Kaldis, P., Liu, K., 2016. Inhibitory phosphorylation of Cdk1 mediates prolonged prophase I arrest in female germ cells and is essential for female reproductive lifespan. Cell Res. 26, 1212–1225.

Akaike, Y., Chibazakura, T., 2020. Aberrant activation of cyclin A-CDK induces G2/M-phase checkpoint in human cells. Cell Cycle 19, 84–96.

Alamares-Sapuay, J.G., Martinez-Gil, L., Stertz, S., Miller, M.S., Shaw, M.L., Palese, P., 2013. Serum- and glucocorticoid-regulated kinase 1 is required for nuclear export of the ribonucleoprotein of influenza A virus. J. Virol. 87, 6020–6026.

Berdel, H.O., Yin, H., Liu, J.Y., Grochowska, K., Middleton, C., Yanasak, N., Abdelsayed, R., Berdel, W.E., Mozaffari, M., Yu, J.C., Baban, B., 2014. Targeting serum glucocorticoid-regulated Kinase-1 in squamous cell Carcinoma of the head and neck: a novel modality of local control. PLOS ONE 9, e113795.

Bomberger, J.M., Coutermarsh, B.A., Barnaby, R.L., Sato, J.D., Chapline, M.C., Stanton, B.A., 2014. Serum and Glucocorticoid-inducible Kinase1 increases plasma membrane wt-CFTR in human airway Epithelial cells by inhibiting its Endocytic retrieval. PLOS ONE 9, e89599.

Bruhn, M.A., Pearson, R.B., Hannan, R.D., Sheppard, K.E., 2010. Second AKT: The rise of SGK in cancer signalling. Growth Factors 28, 394–408.

Cazales, M., Schmitt, E., Montembault, E., Dozier, C., Prigent, C., Ducommun, B., 2005. CDC25B Phosphorylation by Aurora A occurs at the G2/M transition and is inhibited by DNA damage. Cell Cycle 4, 1233–1238.

Chen, W., Chen, Y., Xu, B., Juang, Y.-C., Stippec, S., Zhao, Y., Cobb, M.H., 2009. Regulation of a third conserved Phosphorylation site in SGK1*. J. Biol. Chem. 284, 3453–3460.

Coleman, T.R., Dunphy, W.G., 1994. Cdc2 regulatory factors. Curr. Opin. Cell Biol. 6, 877–882.

van den Hurk, R., Zhao, J., 2005. Formation of mammalian oocytes and their growth, differentiation and maturation within ovarian follicles. Theriogenology 63, 1717–1751.

Di Cristofano, A., 2017. SGK1: the dark side of PI3K signaling. Curr. Top. Dev. Biol. 123, 49–71.

Edson, M.A., Nagaraja, A.K., Matzuk, M.M., 2009. The mammalian ovary from genesis to revelation. Endocr. Rev. 30, 624–712.

Faresse, N., Lagnaz, D., Debonneville, A., Ismailji, A., Maillard, M., Fejes-Toth, G., Náray-Fejes-Tóth, A., Staub, O., 2012. Inducible kidney-specific Sgk1 knockout mice show a salt-losing phenotype. American Journal of Physiology - Renal Physiology 302 (8), F977–85.

Fejes-Tóth, G., Frindt, G., Náray-Fejes-Tóth, A., Palmer, L.G., 2008. Epithelial Na^+ channel activation and processing in mice lacking SGK1. American Journal of Physiology - Renal Physiology 294 (6), F1298–305.

Ferencova, I., Vaskovicova, M., Drutovic, D., Knoblochova, L., Macurek, L., Schultz, R. M., and Solc, P.. (under revision). CDC25B is required for the metaphase I-metaphase II transition in mouse oocytes. Journal of Cell Science.

Gautier, J., Minshull, J., Lohka, M., Glotzer, M., Hunt, T., Maller, J.L., 1990. Cyclin is a component of maturation-promoting factor from Xenopus. Cell 60, 487–494.

Hagting, A., Karlsson, C., Clute, P., Jackman, M., Pines, J., 1998. MPF localization is controlled by nuclear export. EMBO J. 17, 4127–4138.

Hiraoka, D., Hosoda, E., Chiba, K., Kishimoto, T., 2019. SGK phosphorylates Cdc25 and Myt1 to trigger cyclin B–Cdk1 activation at the meiotic G2/M transition. J. Cell Biol. 218, 3597–3611.

Hiraoka, D., Aono, R., Hanada, S., Okumura, E., Kishimoto, T., 2016a. Two new competing pathways establish the threshold for cyclin-B–Cdk1 activation at the meiotic G2/M transition. J. Cell Sci. 129, 3153–3166.

Hiraoka, D., Aono, R., Hanada, S., Okumura, E., Kishimoto, T., 2016b. Two new competing pathways establish the threshold for cyclin-B–Cdk1 activation at the meiotic G2/M transition. J. Cell Sci. 129, 3153–3166.

Homer, H.A., 2020. The Role of Oocyte quality in explaining "unexplained" infertility. Semin Reprod. Med. 38, 21–28.

Hosoda, E., Hiraoka, D., Hirohashi, N., Omi, S., Kishimoto, T., Chiba, K., 2019. SGK regulates pH increase and cyclin B–Cdk1 activation to resume meiosis in starfish ovarian oocytes. J. Cell Biol. 218, 3612–3629.

Kalous, J., Solc, P., Baran, V., Kubelka, M., Schultz, R.M., Motlik, J., 2006. PKB/AKT is involved in resumption of meiosis in mouse oocytes. Biol. Cell 98, 111–123.

Keefe, D., Kumar, M., Kalmbach, K., 2015. Oocyte competency is the key to embryo potential. Fertil. Steril. 103, 317–322.

Kobayashi, T., Cohen, P., 1999. Activation of serum- and glucocorticoid-regulated protein kinase by agonists that activate phosphatidylinositide 3-kinase is mediated by 3-phosphoinositide-dependent protein kinase-1 (PDK1) and PDK2. Biochem. J. 339 (Pt 2), 319–328.

Kobayashi, T., Deak, M., Morrice, N., Cohen, P., 1999. Characterization of the structure and regulation of two novel isoforms of serum- and glucocorticoid-induced protein kinase. Biochem J. 344 (Pt 1), 189–197.

Koncicka, M., Tetkova, A., Jansova, D., Del Llano, E., Gahurova, L., Kracmarova, J., Prokesova, S., Masek, T., Pospisek, M., Bruce, A.W., Kubelka, M., Susor, A., 2018. Increased expression of maturation promoting factor components speeds up Meiosis in Oocytes from aged females. Int. J. Mol. Sci. 19, 2841.

Krisher, R.L., 2004. The effect of oocyte quality on development. J. Anim. Sci. 82, E14–E23.

Lang, F., Cohen, P., 2001. Regulation and physiological roles of serum- and Glucocorticoid-induced protein Kinase isoforms. Sci. STKE 2001, re17.

Lien, E.C., Dibble, C.C., Toker, A., 2017. PI3K signaling in cancer: beyond AKT. Curr. Opin. Cell Biol. 45, 62–71.

Lincoln, A.J., Wickramasinghe, D., Stein, P., Schultz, R.M., Palko, M.E., De Miguel, M.P. D., Tessarollo, L., Donovan, P.J., 2002. Cdc25b phosphatase is required for resumption of meiosis during oocyte maturation. Nat. Genet 30, 446–449.

del Llano, E., Masek, T., Gahurova, L., Pospisek, M., Koncicka, M., Jindrova, A., Jansova, D., Iyyappan, R., Roucova, K., Bruce, A.W., Kubelka, M., Susor, A., 2020. Age-related differences in the translational landscape of mammalian oocytes. Aging Cell 19, e13231.

Masek, T., Del Llano, E., Gahurova, L., Kubelka, M., Susor, A., Roucova, K., Lin, C.-J., Bruce, A.W., Pospisek, M., 2020. Identifying the translatome of mouse NEBD-stage oocytes via SSP-profiling; a novel Polysome fractionation method. Int J. Mol. Sci. 21, E1254.

Murray, J.T., Campbell, D.G., Morrice, N., Auld, G.C., Shpiro, N., Marquez, R., Peggie, M., Bain, J., Bloomberg, G.B., Grahammer, F., Lang, F., Wulff, P., Kuhl, D., Cohen, P., 2004. Exploitation of KESTREL to identify NDRG family members as physiological substrates for SGK1 and GSK3. Biochem. J. 384, 477–488.

Norris, R.P., Ratzan, W.J., Freudzon, M., Mehlmann, L.M., Krall, J., Movsesian, M.A., Wang, H., Ke, H., Nikolaev, V.O., Jaffe, L.A., 2009. Cyclic GMP from the surrounding somatic cells regulates cyclic AMP and meiosis in the mouse oocyte. Development 136, 1869–1878.

Pan, B., Li, J., 2019. The art of oocyte meiotic arrest regulation. Reprod. Biol. Endocrinol. 17, 8.

Pirino, G., Wescott, M.P., Donovan, P.J., 2009. Protein Kinase A regulates resumption of meiosis by phosphorylation of Cdc25B in mammalian oocytes. Cell Cycle 8, 665–670.

Potireddy, S., Vassena, R., Patel, B.G., Latham, K.E., 2006. Analysis of polysomal mRNA populations of mouse oocytes and zygotes: Dynamic changes in maternal mRNA utilization and function. Dev. Biol. 298, 155–166.

Roberts, E.C., Shapiro, P.S., Nahreini, T.S., Pages, G., Pouyssegur, J., Ahn, N.G., 2002. Distinct cell cycle timing requirements for extracellular signal-regulated Kinase and Phosphoinositide 3-Kinase signaling pathways in somatic cell Mitosis. Mol. Cell Biol. 22, 7226–7241.

Schmidt, M., Rohe, A., Platzer, C., Najjar, A., Erdmann, F., Sippl, W., 2017. Regulation of G2/M transition by inhibition of WEE1 and PKMYT1 Kinases. Molecules 22, 2045.

Sharma, A., Tiwari, M., Gupta, A., Pandey, A.N., Yadav, P.K., Chaube, S.K., 2018. Journey of oocyte from metaphase-I to metaphase-II stage in mammals. J. Cell. Physiol. 233, 5530–5536.

Sherk, A.B., Frigo, D.E., Schnackenberg, C.G., Bray, J.D., Laping, N.J., Trizna, W., Hammond, M., Patterson, J.R., Thompson, S.K., Kazmin, D., Norris, J.D., McDonnell, D.P., 2008. Development of a small-molecule serum- and glucocorticoid-regulated Kinase-1 antagonist and its evaluation as a prostate cancer therapeutic. Cancer Res. 68, 7475–7483.

Solc, P., Saskova, A., Baran, V., Kubelka, M., Schultz, R.M., Motlik, J., 2008. CDC25A phosphatase controls meiosis I progression in mouse oocytes. Dev. Biol. 317, 260–269.

Tetkova, A., Hancova, M., 2016. Mouse oocyte isolation. Cultiv. RNA Micro Bio-Protoc. 6, e1729.

Tripathi, A., Kumar, K.V.P., Chaube, S.K., 2010. Meiotic cell cycle arrest in mammalian oocytes. J. Cell. Physiol. 223, 592–600.
Xiao, L., Han, X., Wang, X., Li, Q., Shen, P., Liu, Z., Cui, Y., Chen, Y., 2019. Spinal serum- and glucocorticoid-regulated Kinase 1 (SGK1) signaling contributes to Morphine-induced Analgesic tolerance in rats. Neuroscience 413, 206–218.
Zeng, F., Baldwin, D.A., Schultz, R.M., 2004. Transcript profiling during preimplantation mouse development. Dev. Biol. 272, 483–496.

Biology of Reproduction, 2019, 101(4), 719–732
doi:10.1093/biolre/ioz117
Research Article
Advance Access Publication Date: 16 July 2019

Research Article

Follicle-stimulating hormone administration affects amino acid metabolism in mammalian oocytes†

Anna Tetkova[1,2], Andrej Susor[1,*], Michal Kubelka[1], Lucie Nemcova[1], Denisa Jansova[1], Michal Dvoran[1,2], Edgar Del Llano[1,2], Zuzana Holubcova[3,4] and Jaroslav Kalous[1,*]

[1]Institute of Animal Physiology and Genetics, Czech Academy of Science, Libechov, Czech Republic [2]Department of Cell Biology, Faculty of Science, Charles University in Prague, Prague 2, Czech Republic [3]Department of Histology and Embryology, Faculty of Medicine, Masaryk University, Brno, Czech Republic and [4]Reprofit International, Clinic of Reproductive Medicine, Brno, Czech Republic

***Correspondence:** Laboratory of Biochemistry and Molecular Biology of Germ Cells, Institute of Animal Physiology and Genetics, Czech Academy of Sciences, Rumburska 89, 27721 Libechov, Czech Republic. E-mail: susor@iapg.cas.cz; kalous@iapg.cas.cz

†**Grant Support:** This research was funded by MSMT (EXCELLENCECZ.02.1.01/0.0/0.0/15_003/0000460 OP RDE), GACR (18-19395S; 19-13491S) and Institutional Research Concept RVO67985904.
Conference Presentation: Presented in part at the Visegrad Group Society for Developmental Biology Inaugural meeting, 2018, Brno, Czech Republic.

Received 21 March 2019; Revised 18 June 2019; Accepted 4 July 2019

Abstract

Culture media used in assisted reproduction are commonly supplemented with gonadotropin hormones to support the nuclear and cytoplasmic maturation of in vitro matured oocytes. However, the effect of gonadotropins on protein synthesis in oocytes is yet to be fully understood. As published data have previously documented a positive in vitro effect of follicle-stimulating hormone (FSH) on cytoplasmic maturation, we exposed mouse denuded oocytes to FSH in order to evaluate the changes in global protein synthesis. We found that dose-dependent administration of FSH resulted in a decrease of methionine incorporation into de novo synthesized proteins in denuded mouse oocytes and oocytes cultured in cumulus-oocyte complexes. Similarly, FSH influenced methionine incorporation in additional mammalian species including human. Furthermore, we showed the expression of FSH-receptor protein in oocytes. We found that major translational regulators were not affected by FSH treatment; however, the amino acid uptake became impaired. We propose that the effect of FSH treatment on amino acid uptake is influenced by FSH receptor with the effect on oocyte metabolism and physiology.

Summary Sentence

FSH treatment decrease methionine incorporation into de novo synthesized proteins in mouse, porcine, and bovine oocytes, and FSHR protein is expressed in oocytes and 2cell embryo.

Key words: oocyte, oocyte maturation, FSH/FSH receptor, translation

Introduction

Conditions of in vitro maturation (IVM) influence the nuclear and cytoplasmic maturation of oocytes [1, 2]. In order to support the nuclear and cytoplasmic IVM of oocytes, culture media used in programs of assisted reproduction are commonly supplemented with gonadotropin hormones. Follicle-stimulating hormone (FSH), a pituitary gonadotropin glycoprotein hormone, regulates a number of transcriptional and metabolic events in the ovary that are essential for proliferation and differentiation during follicular growth and oocyte maturation [3, 4]. FSH acts through the FSH receptor (FSHR), a G protein coupled receptor. It is generally accepted that FSHR is expressed exclusively in the granulosa cells in ovarian follicles and in testicular Sertoli cells [5]. Activated FSHR stimulates many intracellular signaling pathways including events initiated by adenylyl cyclase activation, followed by the induction of cyclic adenosine monophosphate (cAMP), protein kinase A activation, and protein phosphorylation [6, 7]. The binding of FSH to its receptor is also implicated in intracellular calcium increase, mitogen-activated protein kinase (MAPK) activation, and inositol triphosphate stimulation [8].

During the growth phase of development, oocytes accumulate macromolecules in order to cease transcription at the completion of this stage. Gene expression in fully grown oocytes is then regulated based on the level of mRNA stabilization and translation [9]. Transcription remains suppressed during the meiotic progression of the oocyte, as well as during fertilization and early embryo development, until a species-specific time of embryonic genome activation [10, 11]. In particular, the process of protein translation in oocytes is controlled by the phosphorylation/dephosphorylation of eukaryotic initiation factors (eIFs) and their regulators [12–15]. Protein translation in germinal vesicle (GV)-stage oocytes is at low levels, while during germinal vesicle breakdown (GVBD), a three-fold increase of protein synthesis is preceded by the phosphorylation of eIF4E. In oocytes at the metaphase II (MII) stage, protein translation drops to low levels compared to the rate occurring at the GV-stage [15].

Protein synthesis in oocytes during meiotic maturation is crucial for the completion of meiosis [16] and pronuclear development in porcine fertilized oocytes [17, 18]. The results of [^{35}S]-methionine incorporation into ovine cumulus-oocyte complexes (COCs) suggested a more intense protein synthesis in oocytes exhibiting higher developmental competence [19]. It has been shown that protein translation of maternal mRNAs was enhanced in mouse oocytes and embryo development was improved when COCs were subjected to FSH in vitro (10 ng/ml) [20]. On the other hand, the negative effect of administration of gonadotropin in vivo on early embryo development has also been reported before [21–24] as well as in vitro treatment of oocytes with recombinant FSH (Gonal-F) inducing a lower developmental competence of early embryos in vitro [25, 26].

The expression of FSHR in the mammalian oocyte and in connection with the direct effect of FSH on oocyte physiology is controversial. Although IVM protocols use FSH, the effect of gonadotropins on oocytes is not well understood. We have found that FSHR is expressed in the mammalian oocytes and FSH shows effect on amino acid uptake in oocytes of various mammalian species including human.

Materials and methods

Ethics Statement

All animal work was conducted according to Act No. 246/1992 on the protection of animals against cruelty, issued by experimental project #215/2011, certificate #CZ02389. Bovine and porcine ovaries were obtained from local slaughterhouses where they are discarded without utilization (hence no ethics statement was required). Surplus human oocytes were provided for research only when written informed consent was obtained.

Oocyte isolation and IVM

Mice (CD1 strain) were stimulated with pregnant mare serum gonadotropin (PMSG, Folligon, Merck Animal Health) 46 h prior to oocyte isolation; 5 IU per mouse. Oocytes were isolated by disrupting the ovaries into transfer media [27] supplemented with 100 μM 3-isobutyl-1-methylxanthine (IBMX, Sigma Aldrich) to prevent spontaneous meiotic resumption. Isolated mouse COCs or oocytes deprived of cumulus oocytes (denuded oocytes, DOs) were cultured in the presence of IBMX for 2 h in M16 medium supplemented with either 10 ng/ml (0.136 IU/ml) or 100 ng/ml (1.36 IU/ml) of FSH (Gonal-F; Serono Laboratories; Puregon, N.V. Organon) diluted in M16 medium (Millipore). Culture was performed in M16 medium pre-equilibrated at 37.5 °C and 5% CO_2. For IVM, isolated DOs were washed with IBMX and cultured for 12 h to MII-stage in M16 medium.

Follicles with 5–9 mm (bovine) and 3–5 mm (porcine) in diameter were dissected and punctured to isolate the oocytes. Bovine and porcine COCs were evaluated and selected according to the morphology of the cumuli. COCs with at least three layers of compact cumulus cells (CCs) were used for the experiments. Earlier, the culture COCs were deprived of CCs using hand micropipette (bovine) or by vortexing for ~7 min (porcine). Bovine and porcine DOs (GV oocytes) were subsequently cultured in M-16 medium supplemented with 100 ng/ml FSH (Gonal-F) for 2 h. See also experimental schemes in Figure 1.

The collection of human oocytes was carried out in IVF center Reprofit International (Brno, Czech Republic). Ovarian stimulation and oocyte retrieval were performed as described earlier [28]. Donated immature oocytes were incubated overnight in continuous single culture (CSC) medium (#90165, Irvine Scientific, USA) at 37 °C in a humidified atmosphere of 5% O_2 and 6% CO_2. Next day, the developmental maturity of each oocyte was confirmed by the presence of a polar body and MII spindle (Octax polarAIDE, MTG, Germany). A total of 15 MII oocytes from 7 IVF patients and 6 egg donors (average age 30.15 years) were frozen using VT801 vitrification media and Cryotop—open system (Kitazato BioPharma, Japan) according to the manufacturer's instructions and stored in liquid nitrogen (LN2) until thawing. Frozen oocytes were thawed using VT802 warming media (Kitazato BioPharma, Japan) according to the manufacturer's instructions. After thawing, oocytes were incubated for 2 h in CSC medium at 37 °C in a humidified atmosphere of 5% CO_2. Next, oocytes were further processed for [^{35}S]-methionine labeling (Figure 1B). The use of spare human oocytes for research was approved by the Institutional Ethics Committee of Reprofit International (# 1/2015) and Faculty of Medicine, Masaryk University, Brno, Czech Republic (# 16/2016).

In vivo MII oocytes and 2cell embryos

To obtain embryos, mice were primed with 5 IU of human chorionic gonadotropin (hCG, Pregnyl, N.V. Organon) 46 h after PMSG administration and mated with males. Zygotes were collected from fallopian tubes 17 h after mating and cultured to the 2cell stage for 24 h in M16 medium at 37.5 °C under 5% CO_2. Subsequently, 2cell embryos were treated for 2 h with 100 ng/ml FSH (Serono Laboratories) diluted in M16 medium.

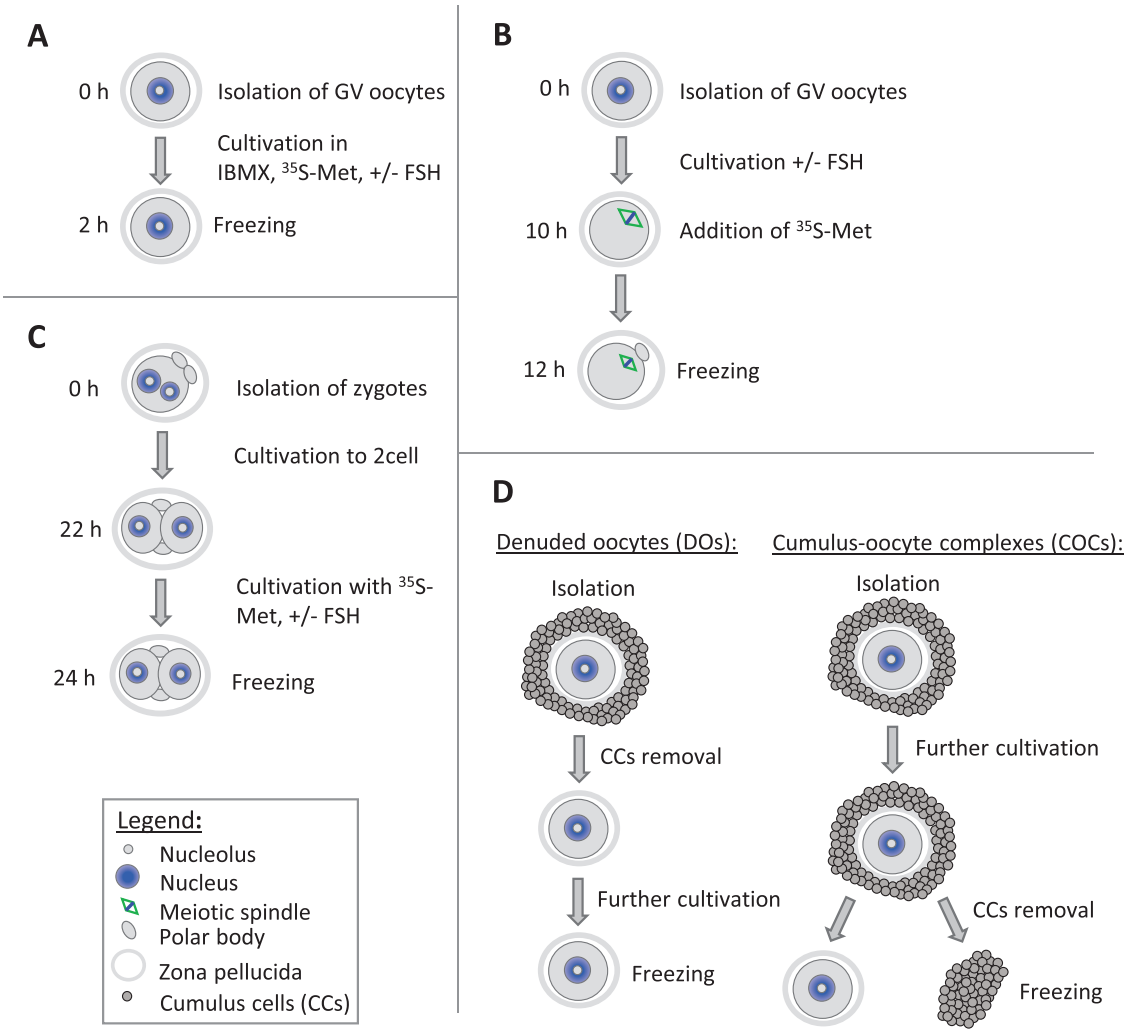

Figure 1. Experimental design schemes. (A) Labeling of GV oocytes with [^{35}S]-methionine in the presence (+) or absence (−) of FSH. (B) Labeling of MII oocytes with [^{35}S]-methionine. Isolated DOs were cultured with presence (+) or absence (−) of FSH and then labeled with [^{35}S]-methionine for 2 h. (C) Labeling of 2cell embryos with [^{35}S]-methionine. In vivo isolated zygotes were cultured for 22 h to 2cell stage. 2cell embryos were labeled with [^{35}S]-methionine for 2 h with presence (+) or absence (−) of FSH. (D) Scheme of culture of COCs and DOs. DOs were stripped from CCs prior culture. Cells from COCs were separated after culture. All cells types were frozen separately.

Natural stimulation of the mice

For natural stimulation, females that are previously not exposed to males were housed on bedding containing male urine and feces for three consecutive days prior to hCG administration. The bedding was changed daily in order to maintain the level of male pheromones. Mice were injected with 5 IU of hCG on the third day of natural stimulation.

Metaphase II oocytes from naturally stimulated mice were compared with in vivo maturated MIIs. Females were primed with 5 IU of PMSG and subsequently after 46 h with 5 IU of hCG. In both cases, MII oocytes were obtained by puncturing oviducts 17 h after hCG administration. Cumulus cells were removed by hyaluronidase (H-3506, Sigma Aldrich) treatment for 30 min and the immunocytochemistry (ICC) protocol was then applied to the DOs.

[^{35}S]-methionine labeling

To analyze de novo protein synthesis, oocytes and early embryos were cultured either in the absence or presence of FSH as well as of the protein synthesis markers [^{35}S]-methionine or homopropargylglycine (HPG) for 2 h. To measure de novo protein synthesis, oocytes and embryos were exposed to 25 µCi/ml of [^{35}S]-methionine (Hartmann analytics) for 2 h. Samples were then washed in polyvinyl alcohol (PVA)/phosphate buffer saline (PBS) and stored in −80 °C prior to usage. Lysed samples were subjected to SDS-polyacrylamide gel electrophoresis (PAGE) and transferred to Immobilon-P membrane using a semidry blotting system for 25 min at 5 mA/cm^2 (the same method as immunoblotting). The labeled proteins were visualized by autoradiography on FujiFilm membrane (exposed for at least 7 days at −80 °C), scanned using BAS-2500 Photo Scanner (FujiFilm Life Science) and quantified by ImageJ software (http://rsbweb.nih.gov/ij/). Western blotting with glyceraldehyde 3-phosphate dehydrogenase (GAPDH) antibody was used as a loading control.

In situ translation

For nascent protein synthesis, oocytes were cultured in M16 with 50 µM L-HPG (C10186; Thermo Fisher Scientific) for 2 h in the presence or absence of FSH. For detection of HPG influx, cells were treated with 100 µM CHX for 2 h in M16. Oocytes were fixed in

4% paraformaldehyde (PFA) in PVA/PBS for 15 min. Homopropargylglycine was detected using Click-iT Cell Reaction Kit (Thermo Fisher Scientific). 4',6-diamidin-2-fenylindol (DAPI) was used for chromosome staining (H-1500; Vector Laboratories). Samples were visualized using an inverted confocal microscope in 16-bit depth (TCS SP5; Leica). Images were assembled in Photoshop CS3 and quantified by Image J software.

Immunocytochemistry

For protein visualization, oocytes and embryos were fixed for 15 min in 4% PFA (Sigma Aldrich) in PBS. Fixed oocytes were permeabilized in 0.1% Triton X-100 for 10 min, washed in PBS supplemented with PVA (Sigma Aldrich) and then incubated with primary antibodies overnight at 4 °C. Primary antibodies are listed in Supplementary Table 1. Oocytes were then washed 2× 15 min in PVA/PBS and the detection of primary antibodies was performed using relevant Alexa Fluor 488, 594 conjugates (Invitrogen) diluted 1:250, 1 h at room temperature. Washed oocytes (2× 15 min in PVA/PBS) were then mounted in Vectashield Mounting Medium with DAPI (Vector Laboratories).

Mouse ovaries and thigh muscles were mounted in tissue freezing medium (#14020108926, Leica), frozen in liquid nitrogen, and subsequently cut in cryotome (Leica CM1850). Slices of tissues were stored at −20 °C and fixed for 15 min in 4% PFA prior staining. A similar protocol for immuno-staining as mentioned above was followed, with washes in PBS. Rabbit polyclonal anti-FSH-R antibody with secondary antibody Alexa Fluor 594 conjugate were used. Phalloidin Alexa 488 conjugate (Thermo Fisher) was added for 10 min to visualize actin filaments. Inverted confocal microscope (Leica SP5) was used for sample visualization. Image quantification and assembly were performed using ImageJ and Adobe Photoshop CS3.

Western blotting

Oocytes, embryos or tissues (ovaries and muscle) were lysed with 6 µl of Millipore H_2O and 2.5 µl of 4× lithium dodecyl sulfate, sample buffer NP 0007, and 1 µl reduction buffer NP 0004 (Novex, Thermo Fisher Scientific) at 100 °C for 5 min. Lysates were separated using a 4–12% gradient SDS-PAGE (NP323BOX, Life Technologies) and transferred to an Immobilon-P membrane (PVDF; Millipore) using semidry blotting system (Biometra GmbH). Membranes were blocked for 1 h, in 1–5% skimmed milk dissolved in Tween-Tris-buffer saline (TTBS, pH 7.4) according to the antibody (list of primary antibodies and dilutions is below). After 3× 10 min of washing in TTBS, membranes were incubated at 4 °C overnight in 1–5% skimmed milk/TTBS with primary antibodies listed in Supplementary Table 1. After 3× 10 min washing in TTBS, the membranes were incubated for 1 h with secondary antibody Peroxidase Anti-Rabbit Donkey (711-035-152, Jackson Immunoresearch) 1:7500 in 1% milk/TTBS 1 h at room temperature. Immunodetected proteins were visualizd by ECL (Amersham, GE Healthcare life science), films were scanned using a GS-800 calibrated densitometer (Bio-Rad) and quantified using Image J software.

Silver staining

The membranes were incubated in staining solution (1 g of sodium citrate, 0.4 g FeSO4, 0.1 g AgNO3, 50 ml Milli-Q water) for 10 min. The staining reaction was terminated by rinsing the membranes in Milli-Q water (5 times for 2 min) and membranes were subsequently dried.

Reverse transcriptase PCR and quantitative RT-PCR

The total RNA was from 20 mouse oocytes, 20 2cell embryos, 20 cumulus layers from 20 COCs, as well as pieces of the ovary and thigh muscle which were isolated using a RNeasy Plus micro kit (Qiagen) according to the manufacturer's instructions. Isolated RNA was stored at −80°C. Complementary DNA was synthetized by qPCRBIO cDNA synthesis kit (PCR Biosystems) using oligo (dT) (Thermo Scientific) and random hexamer primers (Thermo Scientific). The reaction was performed for 30 min at 42 °C (PTC200, Bio-Rad). For PCR, PPP Mix kit (Top-Bio) was used according to the manufacturer's instructions: 94 °C for 1 min followed by 40 cycles of 94 °C for 15 s, 58 °C for 15 s, 72 °C for 20 s, and 72 °C for 7 min. Products were verified by 1.5% agarose gel electrophoresis with ethidium bromide staining. Quantitative PCR was performed by CFX96 Realtime system (Biorad) using appropriate primers (primer names and sequences are listed in Supplementary Table 2) by TaqMan Gene Expression Master Mix XS (Applied Biosystems) according to manufacturer's instructions: 50 °C for 2 min and heated at 95 °C for 10 min followed by 40 cycles of 95 °C for15 s, 50 °C for 20 s, and 58 °C for 60 s. The data are from at least three biological replicates. Products were verified by melting analysis. The relative concentrations of templates in different samples were determined using method $2^{(-ddCT)}$. The results were normalized according to the relative internal standard glyceraldehyde 3-phosphate dehydrogenase *(Gapdh)*.

Statistics

All experiments were repeated at least three times. Western blot (WB) and radiography images were analyzed using ImageJ software (http://rsbweb.nih.gov/ij/), ICC and immunohistochemical (IHC) images were processed with LAS X (Leica) and ImageJ. Mean and standard deviation values were calculated using MS Excel, the statistical significance of the differences between groups were tested using Student's *t*-test or ANOVA and $p < 0.05$ was considered as statistically significant. P values were distinguished: $p < 0.05$; $p < 0.01$; and $p < 0.001$. Statistical results that were not significant are designated with "NS".

Results

FSH suppresses de novo methionine incorporation into oocytes and 2cell embryos

To elucidate the influence of FSH on methionine incorporation, we analyzed two different maturation stages of oocytes (GV and MII), 2cell embryos, and CCs; two different groups of oocytes were tested: either cultivated in the presence (COCs) or absence of CCs (DOs) (Figure 1). In FSH-treated cells, the incorporation of [^{35}S]-methionine protein synthesis marker was significantly ($p < 0.01$) reduced to 17% (± 3%) in cumulus-free GV-stage DOs, 15% (± 5%) in MII oocytes, and 19% (± 2%) in 2cell embryos, respectively (Figure 2A). The expression of the loading control GAPDH was the same in oocytes and 2cell embryos regardless of FSH treatment (Figure 2A). The effect of FSH on [^{35}S]-methionine incorporation into oocytes was dose dependent. The decrease of [^{35}S]-methionine incorporation was evident in oocytes treated with 10 ng/ml FSH (Supplementary Figure 1A and B). To avoid the possibility that the observed effect on [^{35}S]-methionine incorporation was specific to a particular commercial FSH, we compared the effect of Gonal with a different recombinant FSH, Puregon. Treatment of DOs with either FSH-Gonal or FSH-Puregon resulted in both cases in decreased [^{35}S]-methionine incorporation (Supplementary Figure 1C and D).

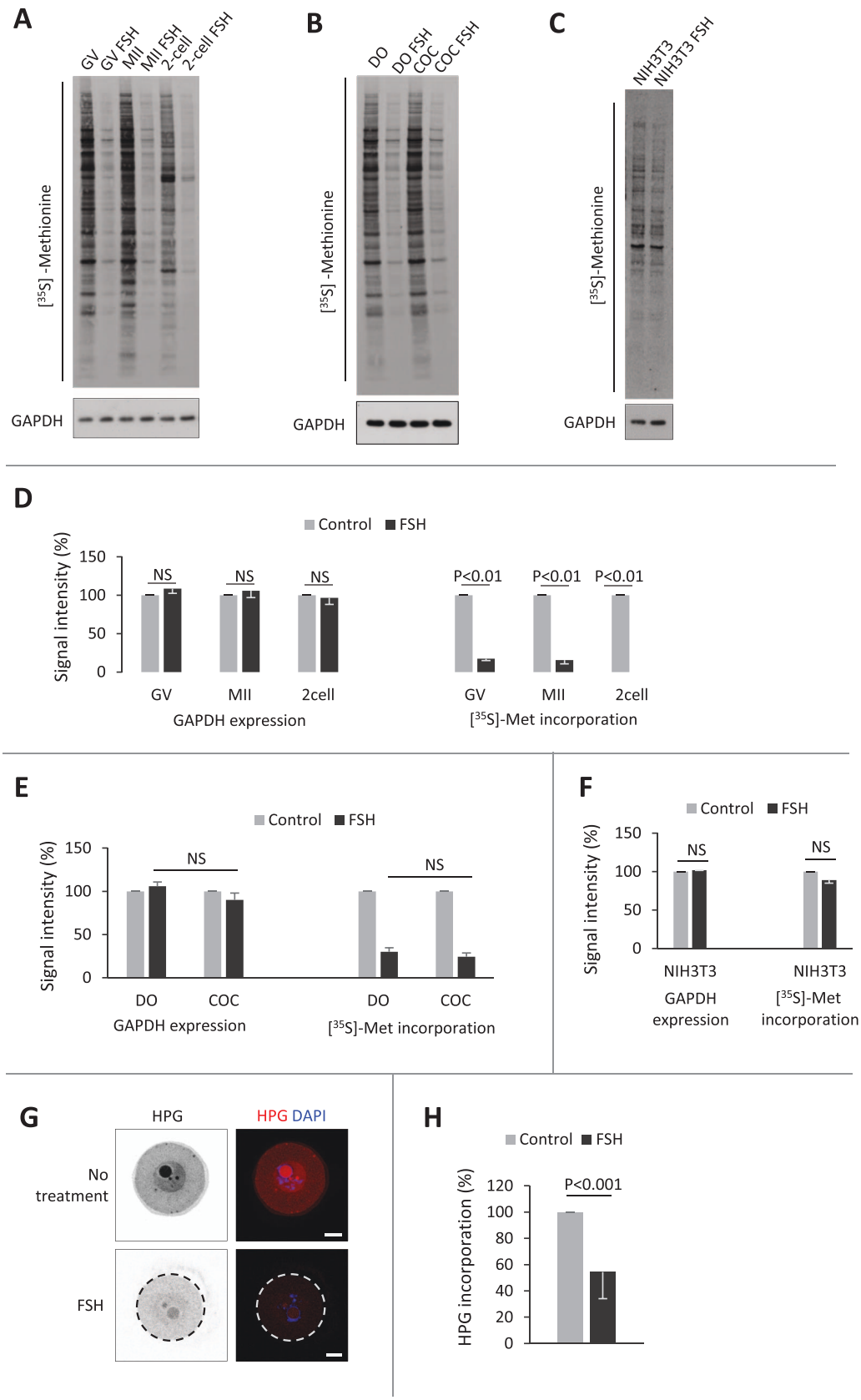

Figure 2. Effect of FSH on [^{35}S]-methionine incorporation to mouse oocytes and 2cell embryos. (A) A representative autoradiography image of [^{35}S]-methionine incorporation into de novo synthetized proteins during 2 h labeling of denuded GV and MII oocytes and 2cell embryos exposed to FSH (100 ng/ml). GAPDH protein levels were used as a loading control. (B) Incorporation of [^{35}S]-methionine to oocytes cultured with absence (DO) or presence (COC) of CCs treated

Next, we examined the difference in [^{35}S]-methionine incorporation into GV-stage DOs and COCs. COCs treated with FSH (100 ng/ml) for 2 h and stripped of cumulus (Figure 1D) after the treatment showed a similar decrease in [^{35}S]-methionine incorporation (22% ± 3%; $p < 0.05$) as was the case in DOs, without any significant difference ($p > 0.05$) (Figure 2B and E). In CCs originating from FSH-treated COCs (Figure 1D), a 48% reduction in [^{35}S]-methionine incorporation was induced (Supplementary Figure 1E and F). Importantly, treatment of fibroblasts (NIH3T3) with FSH (100 ng/ml) did not show any significant ($p > 0.05$) change in methionine incorporation (Figure 2C). Using an additional protein synthesis marker, the methionine analog HPG, showed significant ($p < 0.001$) reduction (54% ± 20%) of HPG incorporation into FSH-treated (100 ng/ml) GV-stage DOs occurred (Figure 2G and H).

We found that FSH had a biological effect on de novo protein synthesis measured as methionine incorporation into the oocytes and 2cell embryos. The FSH-treated GV and MII oocytes and 2cell embryos exhibited decreased [^{35}S]-methionine incorporation into proteins suggesting a direct effect of FSH on the amino acid metabolism in DOs and embryos.

FSH receptor expressed in mouse oocytes and 2cell embryos

As our results revealed the inhibitory effect of FSH on [^{35}S]-methionine incorporation into oocytes and 2cell embryos (Figure 2A), we further investigated the putative expression of FSHR in oocytes and embryos. Applying qRT-PCR, follicle stimulating hormone receptor *(Fshr)* mRNA was detected in GV and MII oocytes and in 2cell embryos (Figure 3A). We found that *Fshr* mRNA was present in oocytes during meiotic maturation and was significantly decreased in 2cell embryos (Figure 3A, Supplementary Figure 2A). To exclude possible contamination by mRNAs from transzonal projections of CCs, we analyzed the presence of *Fshr* transcripts in zona pellucida enclosed (ZP+) and zona pellucida free (ZP−) oocytes. ZP− oocytes exhibited a similar amount of *Fshr* mRNA as ZP+ samples (Supplementary Figure 2B). Sequence analysis of RT-PCR product confirmed that PCR product is *Fshr* specific.

Western blot analysis revealed that the FSHR protein was expressed in GV and MII mouse oocytes and in 2cell embryos (Figure 3B) with non-significant differences between the groups (Figure 3C). As expected, FSHR was expressed in the mouse ovary and it was not present in the negative control, muscle tissue (Figure 3B). We also analyzed the expression of FSHR in the separated CCs, where the presence of FSHR protein had previously been confirmed [29, 30]. Similarly as in the oocyte sample, we detected the high expression of FSHR in the CCs (Supplementary Figure 3). The presence of FSHR was not detected in mouse fibroblasts (NIH3T3 cells) (Figure 3D and E) and muscle tissue (Figure 3B and C; Supplementary Figure 3A and B). Additionally, ICC revealed the presence of FSHR protein in the oocytes, embryos, CCs, and ovary, but not in the muscle (Supplementary Figure 4). The signal was distributed evenly in the oocytes (Supplementary Figure 4A), however, without Triton X-100 permeabilization of cytoplasmic membrane FSHR showed abundant membrane localization (Supplementary Figure 4B).

Our results reveal that the FSHR protein is expressed in GV and MII oocytes and persists until at least the 2cell embryo stage.

FSH treatment does not affect the translational pathway in oocytes and 2cell embryos, despite the negative FSH effect on methionine incorporation

Our results demonstrate that FSH negatively affects the incorporation of the global protein translation marker [^{35}S]-methionine into oocytes and 2cell embryos, in which FSHR is expressed. We assumed that the key translational regulators are possibly affected by FSH. Active mTOR (Ser2448) and ERK1/2(Thr202/Thr204) kinases, translational repressor 4E-BP1, and elongation factor eEF2(Thr56) were analyzed, as well as initiation factor eIF2α and translational stress repressor marker. However, the expression and phosphorylation of tested key players of translational regulation were not changed in FSH-treated oocytes and embryos (Supplementary Figure 4A and B) and, moreover, phosphorylation of eIF2α (Ser51) was not affected (Supplementary Figure 4A and B). Furthermore, silver staining of the WB membrane did not reveal any FSH effect on the alteration of the global protein quantity (Supplementary Figure 5A and B).

These results suggest that FSH has no influence on the activity of translational activators (mTOR and ERK), repressors (4E-BP1, eIF2a), or elongation factor (eEF2), and except for the suppression of methionine incorporation FSH does not impose any stress on global protein translation in oocytes and 2cell embryos.

Similar to methionine, in situ translational marker HPG is negatively influenced by FSH (Figure 2G and H). To detect amino acid transport to the oocyte, we used HPG in combination with translational repressor CHX. In the presence of FSH detection of intracytoplasmic HPG, the fluorescence signal was significantly reduced to 48% (±3%; $p < 0.001$) (Figure 4C and D).

Our data show that despite the translational machinery not being influenced by the presence of FSH, the influx of exogenous amino acid is significantly reduced.

FSHR protein is expressed in oocytes from various mammalian species and treatment of FSH negatively influences methionine incorporation

We further investigated if FSHR was expressed in other mammalian species. Expression of similar levels of FSHR protein was observed

with absence or presence of FSH. GAPDH was used as a loading control. (C) Incorporation of [^{35}S]-methionine in FSH-treated NIH3T3 cells. GAPDH expression was used as a loading control. (D) Quantification of GAPDH and autoradiography of FSH-treated/non-treated oocytes and embryos shown in A. Non-treated controls were set as 100% (means ± SEM). Data from three independent experiments are presented with equal number of cells per experimental group. Statistical differences were tested using Student's *t*-test; NS—not significant. (E) Quantification of GAPDH and autoradiography shown in B. The value of GAPDH expression and [^{35}S]-methionine incorporation after FSH-treatment is compared to the values of non-treated COCs and DOs (means ± SEM, $n \geq 3$). ^{35}S-Met labeled COCs were stripped of CCs after culture. Student's *t*-test; NS—not significant. (F) Quantification of results shown in C. The value of GAPDH expression and [^{35}S]-methionine incorporation after FSH-treatment is compared to the values of non-treated NIH3T3 cells (means ± SEM); Student's *t*-test; NS—not significant. (G) Representative confocal images of methionine analog HPG incorporation into DOs treated with FSH (100 ng/ml) compared to non-treated ones. (H) Quantification of results shown in Figure 2G. The value of HPG incorporation was compared to the values of non-treated DOs (means ± SEM); data from three independent experiments. Student's *t*-test; NS—not significant. See also Figure 1 and Supplementary Figure 1.

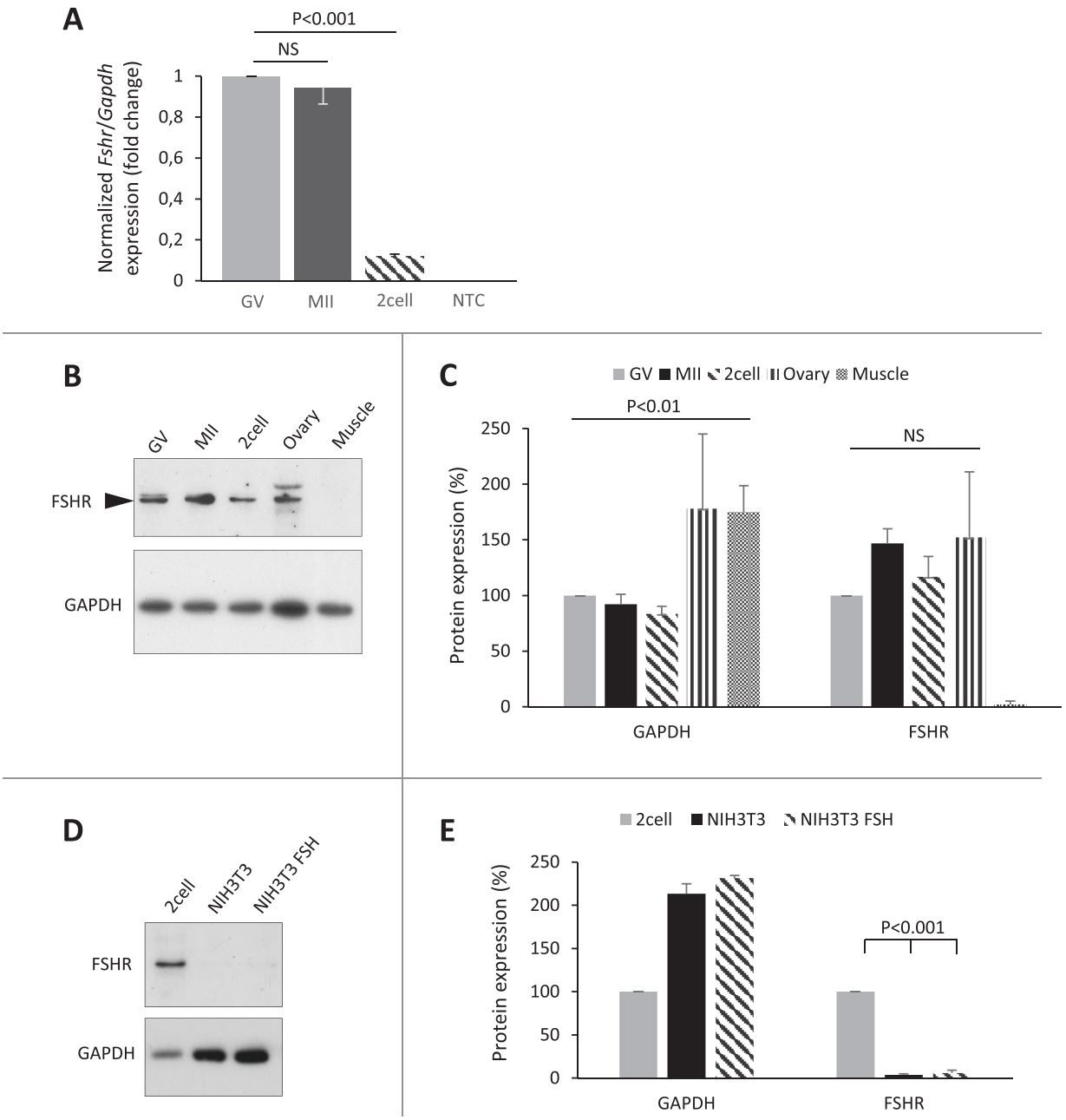

Figure 3. Expression of FSHR in mouse oocytes and 2cell embryos. (A) Quantification of *Fshr* mRNA expression of by real time PCR. The values of *Fshr* expression in MII DOs and 2cell embryos were compared to the values of GV-stage DOs. ANOVA, data from three independent experiments, $n = 30$ oocytes per group, NS—not significant. See also Supplementary Figure 2. (B) Representative WB image of FSHR protein expression in GV and MII DOs and 2cell embryos. See also Supplementary Figure 3. (C) Quantification of WB results shown in B. Follicle-stimulating hormone receptor and GAPDH expression levels are relative to the values in GV DOs (means ± SEM); ANOVA; NS—not significant. Data from at least three independent experiments. (D) Representative WB image of FSHR and GAPDH protein expression in FSH-treated and non-treated NIH3T3 cells. 2cell embryos were used as positive control. (E) Quantification of WB results shown in D. Data from three independent experiments; means ± SEM; Student's *t*-test.

in bovine, porcine, and human DOs (Figure 5A and B). Exposure of bovine, porcine, and human DOs to FSH exhibited a similar suppression of [^{35}S]-methionine incorporation as in mouse oocytes (Figure 5C and D).

Our data clearly show that FSHR is expressed in the oocytes of at least three mammalian species. Treatment with FSH significantly suppressed methionine incorporation into newly synthesized proteins in mouse, bovine, porcine, and human oocytes.

Exogenous gonadotropins influence MII-spindle morphology

We studied whether the oocyte morphology was also influenced by FSH treatment. Although the oocytes treated with FSH accomplished first meiotic division with polar body extrusion, the morphology of MII spindle was altered. We measured the MII spindle morphology at two axes (Figure 6A) and we found that the spindle length and width was significantly larger in in vitro FSH-treated oocytes (Figure 6B).

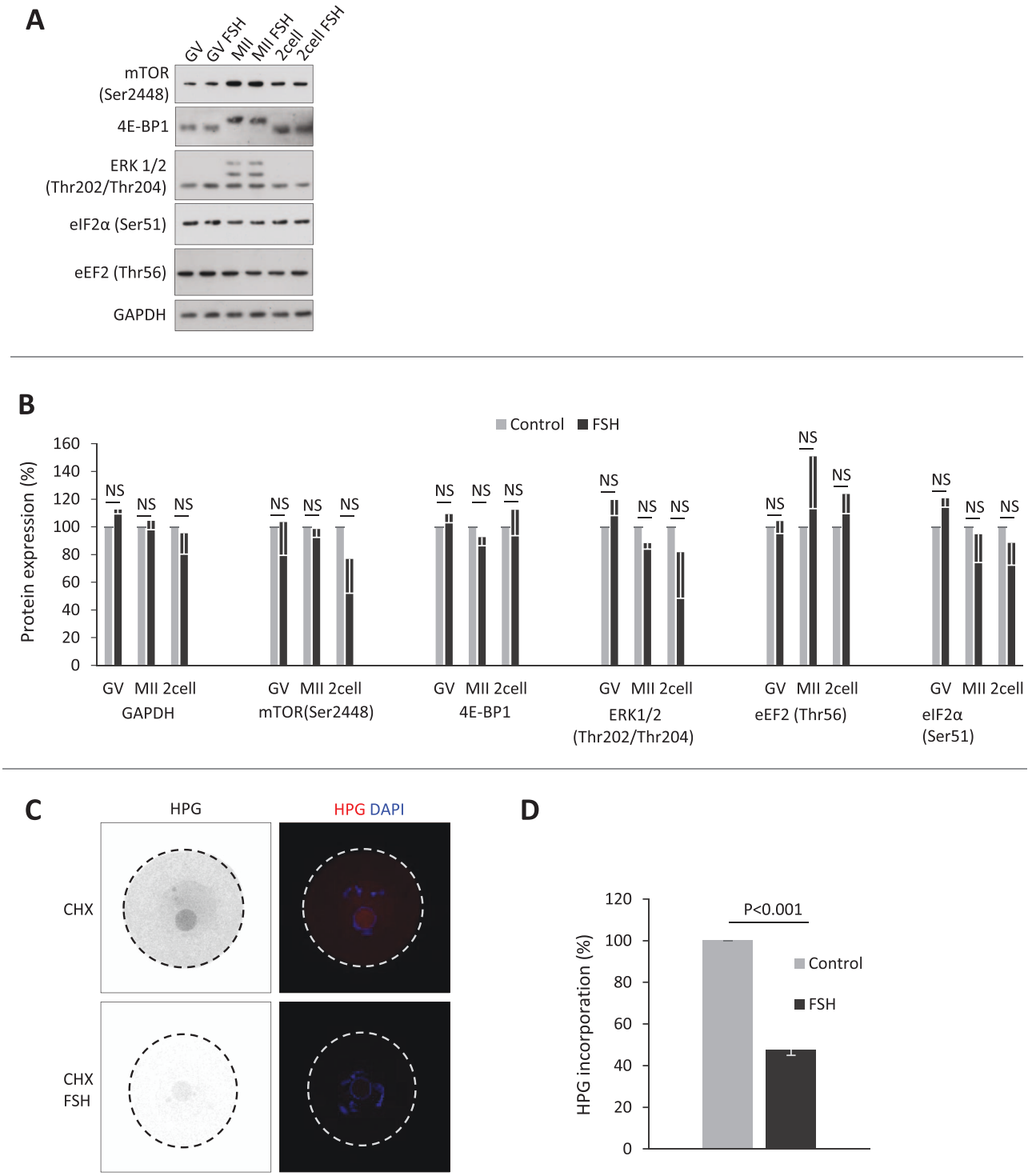

Figure 4. Effect of FSH on translational regulators. (A) A representative WB images of protein expression of selected markers involved in translation regulation in GV and MII oocytes and 2cell embryos treated and non-treated with FSH. (B) Quantification of WB results shown in A. The values are normalized to the non-treated controls; (means ± SEM); data from at least three independent experiments; Student's *t*-test; NS—not significant. (C) Representative confocal images of amino acid uptake (HPG) in GV oocytes with ceased translation. CHX was used for suppression of translational and methionine analog HPG staining serves as amino acid uptake marker. (D) Quantification of confocal images shown in C. Data from at least three independent experiments; $n \geq 10$; Student's *t*-test.

Moreover, MII oocytes obtained from naturally stimulated (Whitten effect; [31, 32]; see methods) and PMSG-primed mouse females showed similarly altered spindle morphology (Figure 6C).

Hence our data suggest that exogenous gonadotropins affect the spindle morphology of MII oocytes progressing through meiosis in both in vitro and in vivo conditions.

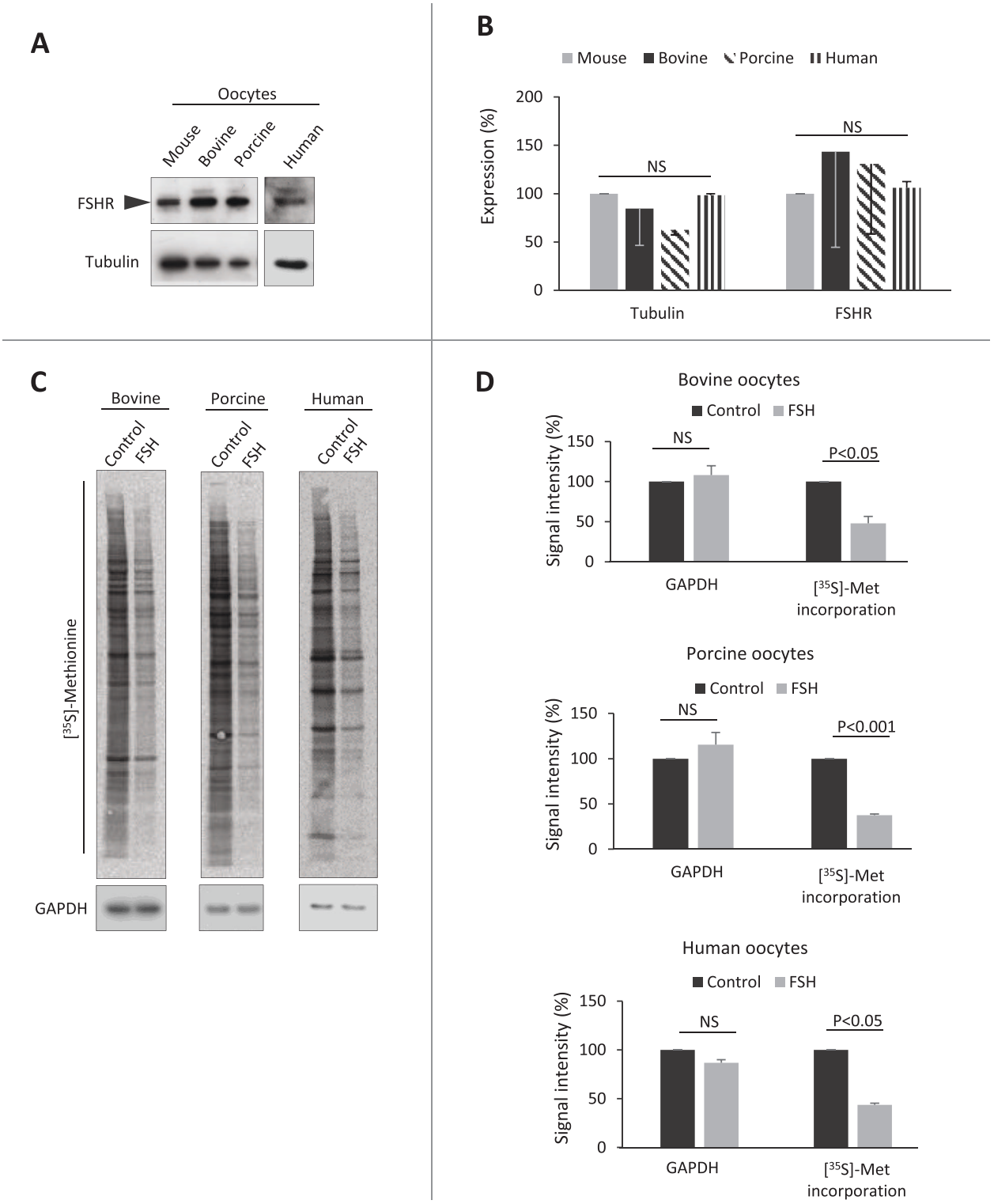

Figure 5. Expression of FSHR in bovine, porcine, and human DOs and effect of FSH treatment on the rate of methionine incorporation into bovine, porcine, and human DOs. (A) A representative image of FSHR protein detection by WB in mouse, bovine, porcine, and human oocytes. Tubulin and GAPDH were used as a loading control. (B) Quantification of WB results shown in A relative to the levels of FSHR and Tubulin in mouse, bovine, porcine, and human oocytes (means ± SEM, data from three independent experiments; ANOVA). (C) Incorporation of [^{35}S]-methionine into proteins during 2 h labeling of bovine, porcine, and human DOs. GAPDH was used as a loading control. (D) Quantification of autoradiography and GAPDH WB data shown in C relative to the levels in control bovine, porcine, and human DOs (means ± SEM, data from at least two independent experiments; Student's *t*-test).

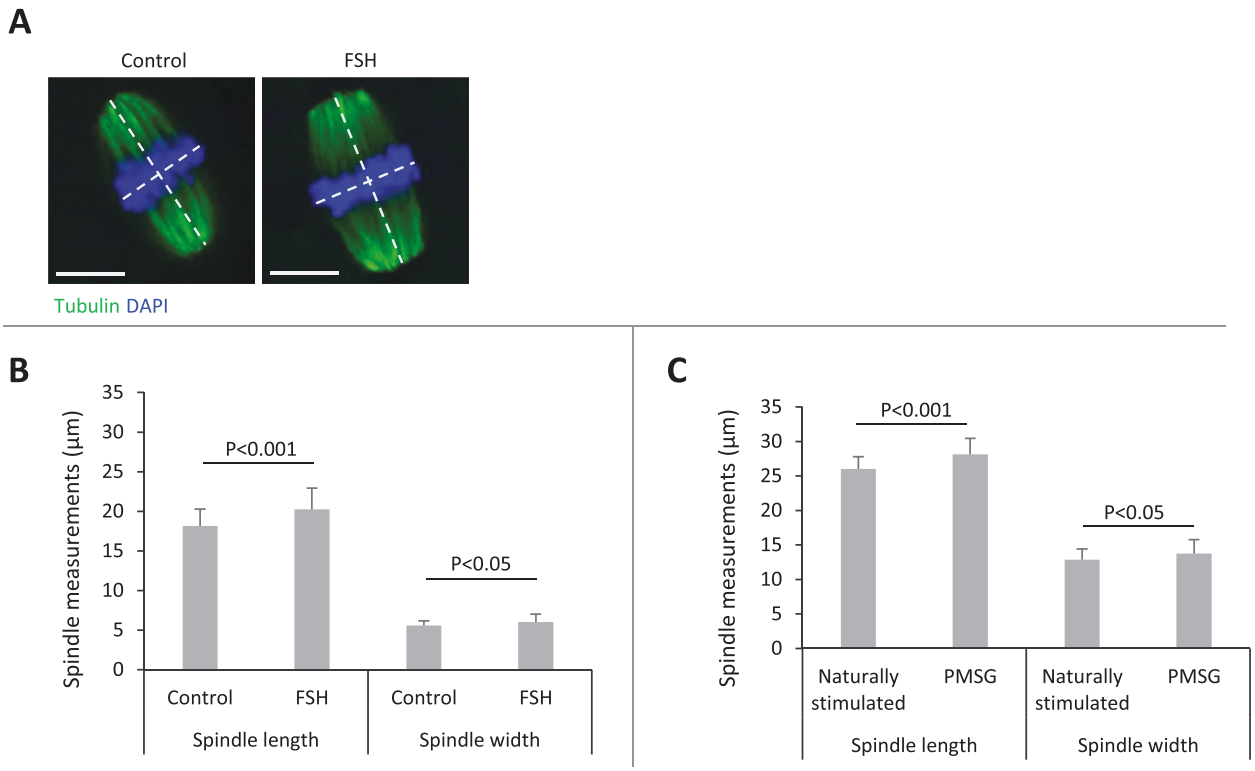

Figure 6. The effect of exogenous FSH on MII-spindle morphology. (A) Depiction of spindle axis measurements in control and FSH oocytes. Tubulin depicted in green, chromosomes in blue. Dashed lines represents measured spindle axes. Scale bars 20 µm. (B) Quantification of MII spindle axes in in vitro oocytes cultured with presence or absence of FSH. Data from threeindependent experiments, means ± SEM; $n \geq 15$; Student's *t*-test. (C) Quantification of MII spindle axes in in vivo MII oocytes form naturally and PMSG-primed females. Data from three independent experiments; means ± SEM; $n \geq 15$; Student's *t*-test.

Discussion

In fully grown mammalian oocytes, gene expression is regulated mainly at the level of protein synthesis, since the transcription is ceased during meiotic maturation [33]. Gene expression in oocytes is regulated almost exclusively at the level of mRNA translation and posttranslational modifications of proteins. It has been documented earlier that increased concentration of gonadotropins in culture medium results in an increase of the percentage of oocytes reaching MII, a normal configuration of the spindle and correct chromosomal alignment, cortical granule migration, and mitochondrial aggregation. Accumulation of oocyte proteins associated with improved oocyte quality is increased when COCs are incubated with FSH [20]. However, in our experiments, exposure to FSH results in a considerable decrease of [^{35}S]-methionine incorporation into the newly synthesized proteins in mouse COCs, DOs, 2cell embryos, as well as in CCs. Moreover, we detected the suppression of [^{35}S]-methionine incorporation in bovine, porcine, and human DOs. Furthermore, this study and Wetzels et al. [22] show a significant decrease of [^{35}S]-methionine uptake in mouse oocytes, 2cell embryos, and blastocysts after in vitro or in vivo gonadotropins administration. It has also been shown in starfish oocytes that when exposed to the maturation-inducing hormone 1-methyladenine [34], amino acid uptake is reduced. The authors conclude that the nearly immediate decrease in permeability for amino acids indicates that the site of action of 1-methyladenine is on the surface of oocytes.

The effect of FSH on oocytes and early embryos has been reported in the number of studies, however, the results of these studies are rather different. An in vitro stimulatory effect of FSH on protein synthesis in porcine CCs and bovine granulosa cells, as well as on the number of pig oocytes MII stage has been documented [35, 36]. On the other hand, a negative effect of FSH and PMSG treatment on oocyte and embryo development has been also shown. When bovine oocytes are subjected to IVM in the presence of purified pituitary FSH (pFSH), lower cleavage and decreased blastocyst rates were observed after fertilization, and when pFSH was replaced by recombinant FSH, the reduction of embryo development was more pronounced [25]. In bovine oocytes treated with high gonadotropin concentrations of genes implicated in spindle formation, cell cycle control and methylation was downregulated [21]. In vitro embryo development and in vivo blastocyst formation in super-ovulated mice was delayed [23] and a lower cell number with decreased mitosis index in in vitro gonadotropin-stimulated mouse embryos was observed [24]. In FSH-treated sheep oocytes, the passage of labeled choline was suppressed [37] and the decrease of uridine and choline uptake was also reported in porcine oocytes exposed to FSH [38]. The results of our experiments show suppression of both [^{35}S]-methionine and methionine analog HPG incorporation into oocytes and early embryos treated with recombinant FSH (Gonal-F). In Gonal-F-treated NIH3T3 cells, no changes in [^{35}S]-methionine incorporation rates have been observed. It has been previously reported that the FSHR is expressed in human endometrial cells [39] and that the proliferation of these cells treated with recombinant FSH (Gonal-F and Puregon) has been significantly inhibited [40]. These published data and our presented results suggest that in cells expressing FSHR, recombinant FSH negatively affects the proliferation (endometrial cells) and amino acid incorporation in oocytes and 2cell embryos.

FSH influences granulosa and Sertoli cells, in which a receptor for FSH (FSHR) is expressed naturally. In vitro FSH treatment caused a decrease of nuclear proteins synthesis in porcine Sertoli cells [41] and elicited morphological changes in rat Sertoli cells [42]. In FSH-treated human or rat granulosa cells, a reduction in the synthesis of the adherent junction proteins and a considerable suppression of the [^{35}S]-methionine incorporation to vinculin, α-actinin, and actin was detected, suggesting that FSH did not affect protein turnover, but rather induced changes in protein synthesis [43–45].

We and others [46–52] clearly show the presence of *Fshr* mRNA in oocytes and early embryos of various mammalian species including human. We have confirmed FSHR expression on the protein level in mouse, bovine, porcine, and human GV oocytes, in mouse MII oocytes and 2cell embryos employing WB and ICC. While our WB data reveal a single FSHR band of 75–77 kDa in mouse, bovine, and porcine DOs and 2cell mouse embryos, in control mouse ovarian extracts, additional FSHR bands are also apparent. It is possible to deduce that the additional FSHR bands are specific to FSHR expression in adult rodent ovary, similar to those reported earlier in the hamster [53]. The molecular weight of the FSHR protein and the specificity of our findings are confirmed by the previously published studies on human ovary and rat granulosa cells [54, 55]. Moreover, *Fshr* mRNA is present at the actively translating polyribosomal fractions [56] of mouse oocyte and zygote. Although no other WB data of FSHR detection in oocytes has been published, our findings of FSHR expression in oocytes and 2cell embryos are well supported by the results of IHC FSHR localization.

In sections of ovaries from mice, mare, porcine, and human, FSHR-staining has been observed [48, 57, 58]. Our data of ICC analysis reveal a diffuse distribution of FSHR and this finding corresponds to different non-membrane bound FSHR variants and the receptor precursors that accumulate in the cells [54, 59]. Additionally, we show uniform membrane localization of FSHR when membrane lipid structures are preserved which suggest that FSHR might be present at the cell membrane with detergent soluble structures. Although there are no other published data on FSHR detection by ICC in oocytes, a distinct localization of the [^{125}I]-labeled FSH suggests the presence of translated FSHR in human and porcine DOs [48]. We and others show that gonadotropins can affect the size of MII spindles. Pregnant mare serum gonadotropin used in mammalian superovulation treatment protocols exhibits FSH and luteinizing hormone activity [60]. The MII spindles in in vitro cultured oocytes from PMSG-primed mice are significantly larger than those from un-primed mice [61, 62]. Consistent with the published data, our results reveal different MII-spindle proportions in oocytes originating either from PMSG-stimulated or naturally stimulated mice. Follicle-stimulating hormone treatment can also affect meiotic spindle organization both in in vitro and in vivo conditions, as, for example, in matured mouse oocytes [63, 64] where spindle misalignments occur in oocytes stimulated in vivo with FSH [65]. Moreover, mouse oocytes treated with high doses of FSH (2 µg/ml) showed chromosome displacement of the meiotic spindle that has been observed [66, 67]. Moreover, it has also been shown that expression of genes that function in spindle formation, cell cycle control, and methylation was downregulated in bovine oocytes treated with FSH [21].

Here we show the occurrence of FSHR transcript and translated protein in oocytes of various mammalian species and we propose that FSH exerts its effect on oocytes and embryos through this receptor similar as in granulosa and CCs [4, 68]. Moreover, we have not detected any effect of FSH on [^{35}S]-methionine incorporation in mouse embryonic fibroblasts, which do not contain a FSHR. As the incorporation of [^{35}S]-methionine is a marker of translational levels, we have examined the state of key factors controlling protein translation in oocytes and embryos treated with FSH. Proteins with a known role in translational regulation were tested: mTOR [13, 69], 4E-BP1 [13, 14, 70, 71], eIF2α [72], eEF2 [73], and ERK1/2 [74, 75]. Interestingly, in FSH-treated oocytes and 2cell embryos, we did not detect any changes in the phosphorylation of the mentioned components of the protein translation pathway. This suggests that the decrease of methionine incorporation into newly translated proteins in FSH-treated cells was not caused by decreased activity of these proteins. Amino acid transport through the cytoplasmic membrane of the oocyte is affected, as we also observed lower incorporation of methionine analog HPG in FSH-treated oocytes in conditions when the translation was blocked by cycloheximide. Here, we showed that total protein level is not affected and assumed that oocyte/embryo is able to recycle internal proteins through proteasome system [76] and used its internal amino acids to maintain its physiological requirements. The mild phenotypic effect on the oocyte maturation might be due to sufficient usage of internal amino acids in this cell type which may explain why we do not detect any influence on amino acid-sensing pathway which we studied through analysis of mTOR and stress effector eIF2α.

Our data confirm that recombinant FSH of different sources (Gonal-F and Puregon) has a negative effect on methionine uptake in mouse oocytes, supported by results on human endometrial cells expressing FSHR, where Gonal-F and Puregon significantly inhibited cell proliferation [39, 40]. However, the possible different effect of other types of FSH cannot be excluded, since the accumulation of oocyte proteins associated with improved oocyte quality has been reported in mouse COCs incubated with ovine FSH [20].

In conclusion, we show that FSH treatment negatively affects methionine incorporation into mammalian oocytes and 2cell embryos, possibly through FSHR expressed in cumulus-free mouse, bovine, porcine, and human oocytes on mRNA and protein levels. As FSH is frequently used for the in vitro culture of oocytes and, moreover, PMSG treatment is applied for superovulation induction in females, these results may provide vital new insights into the physiology of female germ cells and should be taken into consideration by specialists in the field of assisted reproduction and animal breeding.

Supplementary data

Supplementary data are available at *BIOLRE* online.

Supplementary Figure 1. [^{35}S]-methionine incorporation into mouse oocytes and CCs. (A) Dose-dependent [^{35}S]-methionine incorporation. DOs were exposed to either 10 or 100 ng/ml of FSH for 2 h. GAPDH was used as a loading control. (B) Quantification of results shown in Supplementary Figure 1C. Data from three independent experiments; means ± SEM; Student's *t*-test; NS—not significant. (C) [^{35}S]-methionine incorporation significantly decreases using different sources. GV oocytes were cultured for 2 h in 100 ng/ml of FSH (Gonal or Puregon). GAPDH was used as a loading control. (D) Quantification of results shown in Supplementary Figure 1E. Data from three independent experiments; means ± SEM; Student's *t*-test; NS—not significant. (E) Autoradiography of mouse oocytes and CCs. COCs were exposed to [^{35}S]-methionine and 100 ng/ml of FSH for 2 h. Stripped oocytes and the separated CCs

were subjected to autoradiography GAPDH was used as a loading control. See also Figure 1. (F) Quantification of results shown in Supplementary Figure 1A. Autoradiography and GAPDH WB data were quantified relatively to the levels in no FSH treated COCs. Data from three independent experiments; means ± SEM; Student's *t*-test; NS—not significant.

Supplementary Figure 2. *Fshr* mRNA expression in mouse oocytes, embryos and ovary. (A) A representative image of *GAPDH* and *Fshr* expression in GV and MII mouse DOs, 2cell embryos and ovary. (B) *Fshr* mRNA expression in oocytes with ZP+ and ZP−. Ovary and CCs were used as a positive control; NTC; PCR reactions without cDNA template.

Supplementary Figure 3. FSHR protein is present in mouse DOs and in CCs. (A) Representative WB images of the FSHR and GAPDH in mouse GV oocytes, CCs and muscle. GAPDH was used as a loading control. (B) Quantification of FSHR and GAPDH expression levels shown in Supplementary Figure 3A. Protein expression in oocytes was set as 100%; means ± SEM; ANOVA, NS—not significant.

Supplementary Figure 4. ICC/IHC detection of FSHR in oocytes, embryos and ovaries. (A) Representative confocal images of FSHR (green) in mouse GV and MII oocytes, 2cell embryos and CCs. Tubulin in red, DAPI in blue. Scale bars = 20 µm. Bottom panel: Representative confocal images of FSHR (green) in mouse ovary and skeletal muscle tissues. Actin in red, DAPI in blue. Scale bars = 20 µm. B) Representative confocal image of GV oocytes labeled for FSHR (green) and DAPI (blue) without permeabilization of cytoplasmic membrane. Scale bar = 20 µm.

Supplementary Figure 5. Quantities of global protein in FSH-treated/non-treated mouse oocytes and embryos. (A) Silver staining was used to display global protein levels in GV and MII DOs and 2cell embryos (left panel). (B) Quantification of silver staining intensity. Protein levels of GV non-treated oocytes were set as 100% (right panel). Means ± SEM, ANOVA, NS—not significant.

Supplementary Table 1. List of primary antibodies used for WB and ICC. Star displays the dilution factor used for ICC.

Supplementary Table 2. PCR primers used in the study.

Acknowledgement

We thank Jaroslava Supolikova and Marketa Hancova for excellent technical assistance with experiments.

Conflict of Interest

The authors have declared that no conflict of interest exists.

References

1. Combelles CMH, Cekleniak NA, Racowsky C, Albertini DF. Assessment of nuclear and cytoplasmic maturation in in-vitro matured human oocytes. *Hum Reprod* 2002; **17**:1006–1016.
2. Rybska M, Knap S, Jankowski M, Jeseta M, Bukowska D, Antosik P, Nowicki M, Zabel M, Kempisty B, Jaśkowski JM. Cytoplasmic and nuclear maturation of oocytes in mammals—living in the shadow of cells developmental capability. *Med J Cell Biol* 2018; **6**:13–17.
3. Sairam MR, Jiang LG, Yarney TA, Khan H. Follitropin signal transduction: alternative splicing of the FSH receptor gene produces a dominant negative form of receptor which inhibits hormone action. *Biochem Biophys Res Commun* 1996; **226**:717–722.
4. Simoni M, Gromoll J, Nieschlag E. The follicle-stimulating hormone receptor: biochemistry, molecular biology, physiology, and pathophysiology. *Endocr Rev* 1997; **18**:739–773.
5. Telikicherla D, Ambekar A, Palapetta SM, Dwivedi SB, Raju R, Sharma J, Prasad TK, Ramachandra Y, Mohan SS, Maharudraiah J, Mukherjee S, Pandey A. A comprehensive curated resource for follicle stimulating hormone signaling. *BMC Res Notes* 2011; **4**.
6. Heindel JJ, Rothenberg R, Robison GA, Steinberger A. LH and FSH stimulation of cyclic AMP in specific cell types isolated from the testes. *J Cyclic Nucleotide Res* 1975; **1**:69–79.
7. Dorrington JH, Armstrong DT. Effects of FSH on gonadal functions. In: *Proceedings of the 1978 Laurentian Hormone Conference*, vol. **1979**. Elsevier; 301–342.
8. Flores JA, Veldhuis JD, Leong DA. Follicle-stimulating hormone evokes an increase in intracellular free calcium ion concentrations in single ovarian (Granulosa) cells*. *Endocrinology* 1990; **127**:3172–3179.
9. Curtis D, Lehmann R, Zamore PD. Translational regulation in development. *Cell* 1995; **81**:171–178.
10. Latham KE. Mechanisms and control of embryonic genome activation in mammalian embryos. In: Jeon KW (ed.), *International Review of Cytology*, vol. **193**. Academic Press; USA, 1999: 71–124.
11. Nothias J-Y, Majumder S, Kaneko KJ, DePamphilis ML. Regulation of gene expression at the beginning of mammalian development. *J Biol Chem* 1995; **270**:22077–22080.
12. Keiper B. Cap-independent translation initiation in *Xenopus oocytes*. *Nucleic Acids Res* 1997; **25**:395–402.
13. Susor A, Jansova D, Cerna R, Danylevska A, Anger M, Toralova T, Malik R, Supolikova J, Cook MS, Oh JS, Kubelka M. Temporal and spatial regulation of translation in the mammalian oocyte via the mTOR–eIF4F pathway. *Nat Commun* 2015; **6**:1–12.
14. Romasko EJ, Amarnath D, Midic U, Latham KE. Association of maternal mRNA and phosphorylated EIF4EBP1 variants with the spindle in mouse oocytes: localized translational control supporting female meiosis in mammals. *Genetics* 2013; **195**:349–358.
15. Tomek W, Torner H, Kanitz W. Comparative analysis of protein synthesis, transcription and cytoplasmic Polyadenylation of mRNA during maturation of bovine oocytes in vitro. *Reprod Domest Anim* 2002; **37**:86–91.
16. Kastrop PMM, Bevers MM, Destree OHJ, Kruip TAM. Changes in protein synthesis and phosphorylation patterns during bovine oocyte maturation in vitro. *Reproduction* 1990; **90**:305–310.
17. Ding J, Moor RM, Foxcroft GR. Effects of protein synthesis on maturation, sperm penetration, and pronuclear development in porcine oocytes. *Mol Reprod Dev* 1992; **33**:59–66.
18. Susor A, Jelínková L, Karabínová P, Torner H, Tomek W, Kovárová H, Kubelka M. Regulation of cap-dependent translation initiation in the early stage porcine parthenotes. *Mol Reprod Dev* 2008; **75**:1716–1725.
19. Kochhar H, Wu B, Morris L, Buckrell B, Pollard J, Basrur P, King W. Maturation status, protein synthesis and developmental competence of oocytes derived from lambs and ewes. *Reprod Domest Anim* 2002; **37**:19–25.
20. Franciosi F, Manandhar S, Conti M. FSH regulates mRNA translation in mouse oocytes and promotes developmental competence. *Endocrinology* 2016; **157**:872–882.
21. Lu C-L, Wang T-R, Yan L-Y, Xia X, Zhu X-H, Li R, Zhao H-C, Yan J, Yin T-L, Jin H-Y, Zhang Y, Zhang W-X et al. Gonadotropin-mediated dynamic alterations during bovine oocyte maturation in vitro. *Biol Reprod* 2014; **9**:1–9.
22. Wetzels AMM, Artz MT, Goverde HJM, Bastiaans BA, Hamilton CJCM, Rolland R. Gonadotropin hyperstimulation influences the ^{35}S-methionine metabolism of mouse preimplantation embryos. *J Assist Reprod Genet* 1995; **12**:744–746.
23. Van der Auwera I. Superovulation of female mice delays embryonic and fetal development. *Hum Reprod* 2001; **16**:1237–1243.
24. Elmazar MMA, Vogel R, Spielmann H. Maternal factors influencing development of embryos from mice superovulated with gonadotropins. *Reprod Toxicol* 1989; **3**:135–138.
25. Guimarães ALS, Pereira SA, Leme LO, Dode MA. Evaluation of the simulated physiological oocyte maturation system for improving bovine in vitro embryo production. *Theriogenology* 2015; **83**:52–57.

26. Accardo C, Dattena M, Pilichi S, Mara L, Chessa B, Cappai P. Effect of recombinant human FSH and LH on in vitro maturation of sheep oocytes; embryo development and viability. *Anim Reprod Sci* 2004; **81**: 77–86.
27. Tetkova A, Hancova M. Mouse oocyte isolation, cultivation and RNA microinjection. *Bio-Protocol* 2016; **6**:1–8.
28. Holubcová Z, Kyjovská D, Martonová M, Páralová D, Klenková T, Otevřel P, Štěpánová R, Kloudová S, Hampl A. Egg maturity assessment prior to ICSI prevents premature fertilization of late-maturing oocytes. *J Assist Reprod Genet* 2019; **36**:445–452.
29. Saint-Dizier M, Malandain E, Thoumire S, Remy B, Chastant-Maillard S. Expression of follicle stimulating hormone and luteinizing hormone receptors during follicular growth in the domestic cat ovary. *Mol Reprod Dev* 2007; **74**:989–996.
30. Vigone G, Merico V, Redi CA, Mazzini G, Garagna S, Zuccotti M. FSH and LH receptors are differentially expressed in cumulus cells surrounding developmentally competent and incompetent mouse fully grown antral oocytes. *Reprod Fertil Dev* 2015; **27**:497.
31. Whitten WK, Bronson FH, Greenstein JA. Estrus-inducing pheromone of male mice: transport by movement of air. *Science* 1968; **161**:584–585.
32. Gangrade BK, Dominic CJ. Studies of the male-originating pheromones involved in the Whitten effect and Bruce effect in mice. *Biol Reprod* 1984; **31**:89–96.
33. Monti M, Zanoni M, Calligaro A, Ko MSH, Mauri P, Redi CA. Developmental arrest and mouse antral not-surrounded nucleolus oocytes. *Biol Reprod* 2013; **88**:2.
34. Houk MS, Epel D. Protein synthesis during hormonally induced meiotic maturation and fertilization in starfish oocytes. *Dev Biol* 1974; **40**:298–310.
35. Singh B, Meng L, Rutledge JM, Armstrong DT. Effects of epidermal growth factor and follicle-stimulating hormone during in vitro maturation on cytoplasmic maturation of porcine oocytes. *Mol Reprod Dev* 1997; **46**:401–407.
36. Skinner MK, Osteen KG. Developmental and hormonal regulation of bovine Granulosa cell function in the preovulatory follicle*. *Endocrinology* 1988; **123**:1668–1675.
37. Moor RM, Osborn JC, Cran DG, Walters DE. Selective effect of gonadotrophins on cell coupling, nuclear maturation and protein synthesis in mammalian oocytes. *Development* 1981; **61**:347–365.
38. Mattioli M, Bacci ML, Galeati G, Seren E. Effects of LH and FSH on the maturation of pig oocytes in vitro. *Theriogenology* 1991; **36**:95–105.
39. Sacchi S, Sena P, Degli Esposti C, Lui J, La Marca A. Evidence for expression and functionality of FSH and LH/hCG receptors in human endometrium. *J Assist Reprod Genet* 2018; **35**:1703–1712.
40. Chang C-C, Hsieh Y-Y, Hsu K-H, Lin C-S. Effects of α and β recombinant FSH (Gonal-F, Puregon) and progesterone upon human endometrial cell proliferation in-vitro: a preliminary study. *Gynecol Endocrinol* 2011; **27**:110–116.
41. Perrard MH, Saez JM, Dazord A. Effects of FSH on acidic nuclear protein synthesis in cultured pig Sertoli cells. *FEBS Lett* 1984; **168**:49–53.
42. Tung PS, Burdzy K, Fritz IB. Proteases are implicated in the changes in the Sertoli cell cytoskeleton elicited by follicle-stimulating hormone or by dibutyryl cyclic AMP. *J Cell Physiol* 1993; **155**:139–148.
43. Ben-Ze'ev A, Amsterdam A. In vitro regulation of granulosa cell differentiation. Involvement of cytoskeletal protein expression. *J Biol Chem* 1987; **262**:5366–5376.
44. Kranen RW, Overes HWTM, Kloosterboer HJ, Poels LG. The expression of cytoskeletal proteins during the differentiation of rat granulosa cells. *Hum Reprod* 1993; **8**:24–29.
45. Goldman S, Dirnfeld M, Abramovici H, Kraiem Z. Triiodothyronine and follicle-stimulating hormone, alone and additively together, stimulate production of the tissue inhibitor of metalloproteinases-1 in cultured human luteinized granulosa cells. *J Clin Endocrinol Metab* 1997; **82**: 1869–1873.
46. Patsoula E, Loutradis D, Drakakis P, Kallianidis K, Bletsa R, Michalas S. Expression of mRNA for the LH and FSH receptors in mouse oocytes and preimplantation embryos. *Reproduction* 2001; **121**:455–461.
47. Patsoula E. Messenger RNA expression for the follicle-stimulating hormone receptor and luteinizing hormone receptor in human oocytes and preimplantation-stage embryos. *Fertil Steril* 2003; **79**:1187–1193.
48. Méduri G, Charnaux N, Driancourt M-A, Combettes L, Granet P, Vannier B, Loosfelt H, Milgrom E. Follicle-stimulating hormone receptors in oocytes? *J Clin Endocrinol Metab* 2002; **87**:2266–2276.
49. Pandey A, Gupta SC, Gupta N. Effect of FSH and LH hormones on oocyte maturation of buffalo and gene expression analysis of their receptors and Cx43 in maturing oocytes. *Zygote* 2010; **18**:231–234.
50. Xie D, Chen C-C, Ptaszek LM, Xiao S, Cao X, Fang F, Ng HH, Lewin HA, Cowan C, Zhong S. Rewirable gene regulatory networks in the preimplantation embryonic development of three mammalian species. *Genome Res* 2010; **20**:804–815.
51. Pan H, O'brien MJ, Wigglesworth K, Eppig JJ, Schultz RM. Transcript profiling during mouse oocyte development and the effect of gonadotropin priming and development in vitro. *Dev Biol* 2005; **286**:493–506.
52. Kocabas AM, Crosby J, Ross PJ, Otu HH, Beyhan Z, Can H, Tam W-L, Rosa GJM, Halgren RG, Lim B, Fernandez E, Cibelli JB. The transcriptome of human oocytes. *Proc Natl Acad Sci USA* 2006; **103**:14027–14032.
53. Chakraborty P, Roy SK. Expression of FSH receptor in the hamster ovary during perinatal development. *Mol Cell Endocrinol* 2015; **400**:41–47.
54. Vannier B, Loosfelt H, Meduri G, Pichon C, Milgrom E. Anti-human FSH receptor monoclonal antibodies: immunochemical and immunocytochemical characterization of the receptor. *Biochemistry* 1996; **35**:1358–1366.
55. Long MJ, Sairam MR, Komar CM. Initiation of the expression of peroxisome proliferator-activated receptor gamma (PPAR gamma) in the rat ovary and the role of FSH. *Reprod Biol Endocrinol* 2009; **7**:145.
56. Potireddy S, Vassena R, Patel BG, Latham KE. Analysis of polysomal mRNA populations of mouse oocytes and zygotes: dynamic changes in maternal mRNA utilization and function. *Dev Biol* 2006; **298**:155–166.
57. Bhartiya D, Sriraman K, Gunjal P, Modak H. Gonadotropin treatment augments postnatal oogenesis and primordial follicle assembly in adult mouse ovaries? *J Ovarian Res* 2012; **5**:32.
58. Scarlet D, Walter I, Hlavaty J, Aurich C. Expression and immunolocalisation of follicle-stimulating hormone receptors in gonads of newborn and adult female horses. *Reprod Fertil Dev* 2016; **28**:1340.
59. Vu Hai-Luu Thi MT, Misrahi M, Houllier A, Jolivet A, Milgrom E. Variant forms of the pig lutropin/choriogonadotropin receptor. *Biochemistry* 1992; **31**:8377–8383.
60. Moore WT, Ward DN. Pregnant mare serum gonadotropin. An in vitro biological characterization of the lutropin-follitropin dual activity. *J Biol Chem* 1980; **255**:6930–6936.
61. Albertini DF, Wickramasinghe D, Messinger S, Mattson BA, Plancha CE. Nuclear and cytoplasmic changes during oocyte maturation. In: Bavister BD (ed.), *Preimplantation Embryo Development*. New York: Springer; 1993: 3–21.
62. Sakai C, Hoshino Y, Sato Y, Sato E. Evaluation of maturation competence of metaphase II oocytes in mice based on the distance between pericentriolar materials of meiotic spindle: distance of PCM during oocyte maturation. *J Assist Reprod Genet* 2011; **28**:157–166.
63. Sanfins A, Lee GY, Plancha CE, Overstrom EW, Albertini DF. Distinctions in meiotic spindle structure and assembly during in vitro and in vivo maturation of mouse oocytes. *Biol Reprod* 2003; **69**:2059–2067.
64. Sanfins A, Plancha CE, Overstrom EW, Albertini DF. Meiotic spindle morphogenesis in in vivo and in vitro matured mouse oocytes: insights into the relationship between nuclear and cytoplasmic quality. *Hum Reprod* 2004; **19**:2889–2899.
65. Bernstein LR, Mackenzie AC, Chaffin CL, Merchenthaler I. An FSH-lowering activin disrupting therapy prevents egg chromosome and spindle misalignments that predispose to aneuploidy, and increases fertility, in a mouse model of midlife reproductive aging. *Fertil Steril* 2015; **104**:e63.
66. Roberts R, Iatropoulou A, Ciantar D, Stark J, Becker DL, Franks S, Hardy K. Follicle-stimulating hormone affects metaphase I chromosome

alignment and increases aneuploidy in mouse oocytes matured in vitro. *Biol Reprod* 2005; **72**:107–118.
67. Xu Y-W, Peng Y-T, Wang B, Zeng Y-H, Zhuang G-L, Zhou C-Q. High follicle-stimulating hormone increases aneuploidy in human oocytes matured in vitro. *Fertil Steril* 2011; **95**:99–104.
68. Wei S, Shen X, Gong Z, Deng Y, Lai L, Liang H. FSHR and LHR expression and signaling as well as maturation and apoptosis of cumulus-oocyte complexes following treatment with FSH receptor binding inhibitor in sheep. *Cell Physiol Biochem* 2017; **43**:660–669.
69. Mayer S, Wrenzycki C, Tomek W. Inactivation of mTor arrests bovine oocytes in the metaphase-I stage, despite reversible inhibition of 4E-BP1 phosphorylation. *Mol Reprod Dev* 2014; **81**:363–375.
70. Jansova D, Koncicka M, Tetkova A, Cerna R, Malik R, del Llano E, Kubelka M, Susor A. Regulation of 4E-BP1 activity in the mammalian oocyte. *Cell Cycle* 2017; **16**:927–939.
71. Tomek W, Melo Sterza FA, Kubelka M, Wollenhaupt K, Torner H, Anger M, Kanitz W. Regulation of translation during in vitro maturation of bovine oocytes: the role of MAP kinase, eIF4E (cap binding protein) phosphorylation, and eIF4E-BP1. *Biol Reprod* 2002; **66**:1274–1282.
72. Alves VS, Motta FL, Roffé M, Delamano A, Pesquero JB, Castilho BA. GCN2 activation and eIF2alpha phosphorylation in the maturation of mouse oocytes. *Biochem Biophys Res Commun* 2009; **378**: 41–44.
73. Tosca L, Uzbekova S, Chabrolle C, Dupont J. Possible role of 5'AMP-activated protein kinase in the metformin-mediated arrest of bovine oocytes at the germinal vesicle stage during in vitro maturation. *Biol Reprod* 2007; **77**:452–465.
74. Kalous J, Tetkova A, Kubelka M, Susor A. Importance of ERK1/2 in regulation of protein translation during oocyte meiosis. *Int J Mol Sci* 2018; **19**:1–21.
75. Ellederová Z, Cais O, Susor A, Uhlírová K, Kovárová H, Jelínková L, Tomek W, Kubelka M. ERK1/2 map kinase metabolic pathway is responsible for phosphorylation of translation initiation factor eIF4E during in vitro maturation of pig oocytes. *Mol Reprod Dev* 2008; **75**:309–317.
76. Karabinova P, Kubelka M, Susor A. Proteasomal degradation of ubiquitinated proteins in oocyte meiosis and fertilization in mammals. *Cell Tissue Res* 2011; **346**:1–9.